Chest Radiology: A Resident's Manual

Johannes Kirchner

Thieme

Chest Radiology: A Resident's Manual

Johannes Kirchner, MD

Head Physician
Department of Diagnostic and Interventional Radiology
General Hospital Hagen
Hagen, Germany

630 illustrations
15 tables

Thieme
Stuttgart · New York

Library of Congress Cataloging-in-Publication Data
is available from the publisher.

This book is an authorized translation of the German edition published and copyrighted 2010 by Georg Thieme Verlag, Stuttgart.
Title of the German edition: Trainer Thoraxdiagnostik: Systematische kardiopulmonale Bildanalyse.

Translator: John Grossman, Schrepkow, Germany

Illustrator: Adrian Cornford, Rheinheim-Zeilhard, Germany

http://www.thieme.de
Thieme New York, 333 Seventh Avenue,
New York, NY 100001, USA
http://www.thieme.com

Cover design: Thieme Publishing Group
Typesetting by Ziegler + Müller, Kirchentellinsfurt, Germany
Printed in China by Everbest Printing Co Ltd, Hong Kong

ISBN 978-3-13-153871-0 1 2 3 4 5 6

For Esther-Maria,
Fridolin, and Amanda-Lioba

Preface

The study and management of disorders of the thoracic organs represent an essential part of the physician's work, and this necessarily involves an understanding of the plain chest radiograph as the routine imaging study. This has always applied to the diagnostic evaluation of the heart and great vessels. Yet even as pulmonary medicine has moved beyond its classic focus on tuberculosis, chest radiography has experienced a renaissance in clinical practice and research in the diagnosis of pulmonary disorders.

This book is the product of my daily work as learner and teacher alike and reflects the interactions with medical students, residents, and practicing clinicians. Its intent is to enable the reader to answer with confidence the most important questions associated with the plain chest radiograph that one encounters in everyday clinical practice. Diagnosticians are invariably forced to defend their evaluation against other preconceived notions. Nothing is more difficult than correcting preexisting erroneous opinions. Often this requires patient persuasion by objective analysis instead of "intuitive" interpretation of the radiograph.

The present volume on diagnostic chest radiology attempts to awaken the reader's awareness and appreciation of an interpretation strategy oriented to morphologic details. This is not to say that the more intuitive interpretation of radiographs is necessarily wrong. Yet that method requires extensive experience and many years of intensive guidance during training. The latter has become rare as jobs have been eliminated and specialists are now in short supply. One also notices a distinct lack of books on the subject that employ an incremental analytic approach. Current textbooks and manuals include extensive descriptions of etiology, pathophysiology, and clinical aspects whereas the actual radiographic signs (which findings are associated with this disorder?) are usually discussed only briefly.

The present book is thus intended as a supplement to more comprehensive textbooks of chest radiology. In a certain sense it represents a surrogate for those experienced supervising physicians under whose auspices we had the privilege of studying in the early 1990s in the Radiology Clinic of the Johann Wolfgang Goethe University Hospital in Frankfurt am Main, Germany, under its director at the time Professor Juergen Kollath, MD. Here I would like to express my gratitude to my academic instructors Professor Dieter Liermann, MD, Bochum, Germany; Associate Professor Ulrich Loercher, MD, Wiesbaden, Germany; and Professor Volkmar Jacobi, MD, Frankfurt am Main, Germany.

The structure of the book largely follows the proven design principle of the two-page spread. Descriptive text and explanatory graphic images appear opposite the actual figures on the facing page. Each chapter is concluded with several representative review cases intended to awaken readers' interest in researching or compiling their own case series. The reader will note that we have completely dispensed with literature citations. This was done intentionally. With Internet access now ubiquitous, the familiar search engines are in a far better position to provide more current and more comprehensive information to facilitate further study of the content presented than the most exhaustive bibliography could ever hope to do.

Although by their nature brief, the historical notes sparingly added to each chapter do more than simply break up the theoretical text and provide a memory aid. They are also intended as a conscious reminder to the reader of those who have gone before us and who have made our current knowledge possible.

One may criticize the gaps in the book, but limiting it to essentials appeared more important than attempting an encyclopedic treatment of the subject. An atypical pneumonia will be properly recognized when the radiologist has learned the fundamentals of shadowing typical of an infiltrate, even when he or she has not previously encountered rarities such as the pattern produced by Mucor pneumonia. Consequently, I have intentionally opted to leave out particularly spectacular cases (a decision that was painful at times) in an effort to do justice to more common everyday findings. It is precisely these common findings that often receive too little attention in scientific literature, and they deserve more comprehensive treatment. The various manifestations of the widespread disorder smoker's bronchitis are one example. There is a marked discrepancy between the frequency of the use of terms such as "peribronchitis," "signs of chronic bronchitis," "bronchitic shadowing," etc. in everyday radiologic practice and definitions of these key terms in published literature. Especially in light of the socioeconomic significance of such findings, I hope to have contributed to further clarifying these terms.

The studies leading to these results would not have been possible without close long-term cooperation with clinical colleagues. Here, I would like to express my gratitude to Professor Juergen Meier-Sydow, MD, former director of the Department of Pulmonary Medicine of the Frankfurt/Main University Hospital, whom I greatly admire. It was my privilege to assist him during my internist training on his private ward. Special thanks are also due to my dear wife Esther-Maria Kirchner, MD, who in her capacity as senior supervising physician in the Department of Hematology and Oncology at the Bochum/Herne University Hospital maintained the connection to internal medicine and without whose support and constant encouragement this book would never have been possible.

Finally I would like to thank the employees of Thieme Verlag, especially Dr Christian Urbanowicz; Susanne Huiss, MA, and Rolf Zeller for their enthusiastic acceptance of the original concept and their affectionate and professional support of the project, which they moved forward with great dedication. Last but not least, my particular thanks go to publisher Dr Albrecht Hauff, who bore the entrepreneurial risk and who made it possible to publish the book in large format with a very generous layout.

Johannes Kirchner

Contents

To access additional material or resources available with this e-book, please visit http://www.thieme.com/bonuscontent. After completing a short form to verify your e-book purchase, you will be provided with the instructions and access codes necessary to retrieve any bonus content.

1

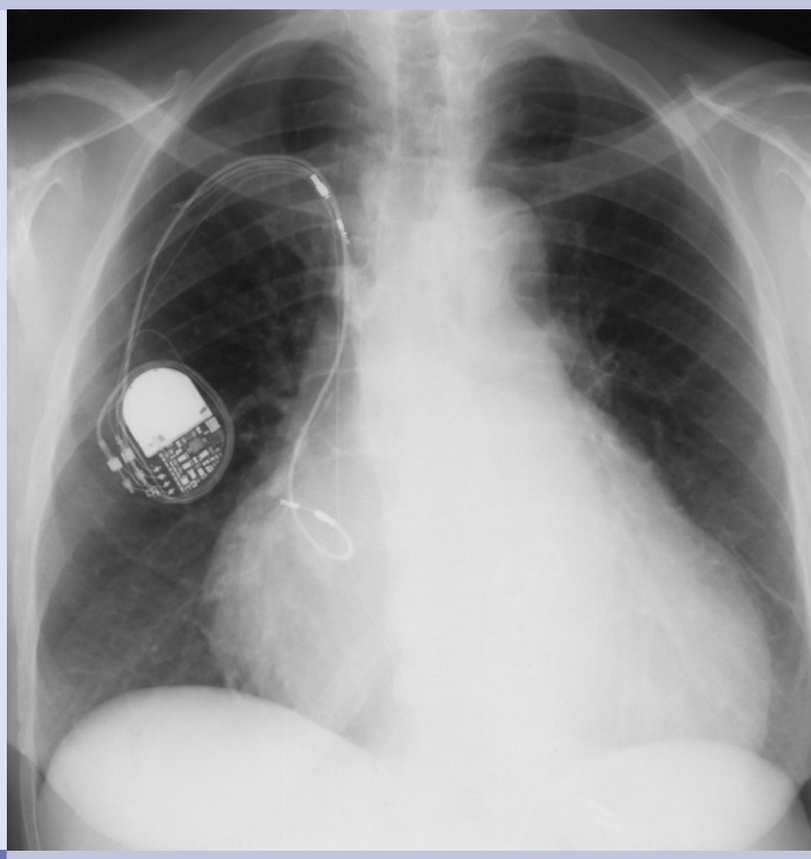

Heart Failure

General

Heart Size

Even a nonradiologist should be able to evaluate the chest radiograph and tell whether the heart shows signs of **enlargement (cardiomegaly)** or **weakness (heart failure).** In the latter case, one should also consider whether the condition predominantly involves insufficiency of the *right heart* with venous congestion (right heart failure) or of the *left heart* with pulmonary congestion (left heart failure).

Heart weight as an indicator of heart size depends on age, body weight, and physical fitness. With endurance training the heart can reach a physiologic weight of 500 g ("athlete's heart"). Heart weight less than 250 g is referred to as heart atrophy (senile atrophy or cachexia in the presence of a tumor, **Fig. 1.3**) and over 800 g is referred to as cor bovinum ("ox heart," **Fig. 1.4**).

In evaluating the heart on a plain chest radiograph, the rule is that the homogeneous projection of the cardiomediastinal shadow prevents evaluation of the ventricles and major vessels except where these structures contribute to the border of the shadow. The right ventricle cannot be evaluated on the posteroanterior radiograph because it does not produce a physiologic border on the image. The frontal projection alone is not sufficient to definitively exclude enlargement of the heart. This requires at least one additional view (lateral or oblique film).

Groedel described a simple rule for evaluating heart size: The long axis of the physiologic heart should fit within half the diameter of the chest (**Fig. 1.1**). The long axis of the heart is defined as the line connecting the base of the heart (center of the right atrial border) and the apex of the heart. The angle of inclination of this axis is not always easy to determine because the anatomic apex of the heart is often difficult to pinpoint precisely.

This measure should be used with caution where chest diameter is increased, as in the barrel chest associated with emphysema. Here an enlarged heart can appear to be of normal size.

A useful rule of thumb is that the clenched fist in the frontal projection should nearly cover the heart shadow (**Fig. 1.2**).

Franz Maximilian Groedel, * 1881 Bad Nauheim, Germany, † 1951 New York. Professor of Radiology, Frankfurt/Main; founder of the Kerckhoff Institute, Bad Nauheim, President of the German Radiography Society 1922; emigrated in 1933; cofounder of the American College of Cardiology. Defined the essentials of diagnostic evaluation of the heart in his *Atlas and Outline of Diagnostic Radiography in Internal Medicine*, published in 1909. The fifth edition could no longer be published in Germany in 1933 because Groedel was Jewish.

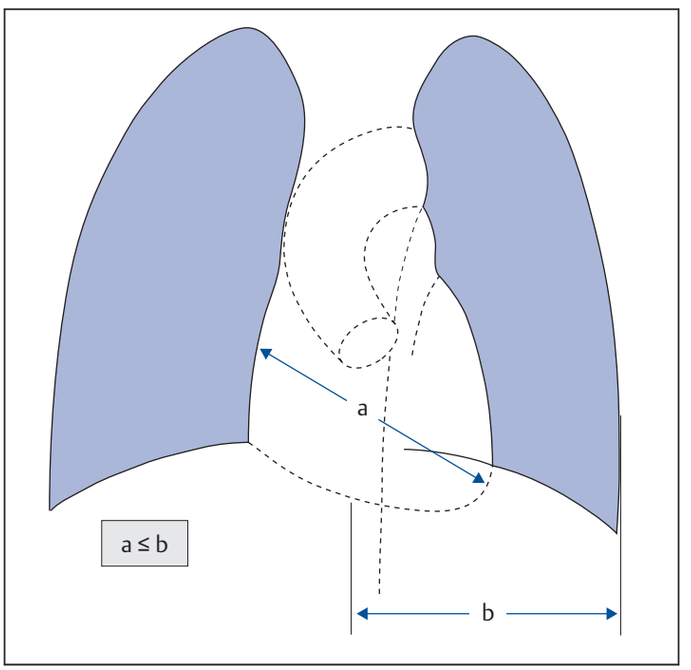

Fig. 1.1 Groedel method of estimating heart size. The length of the long axis of the heart (a) should not exceed the width of the left hemithorax (b).

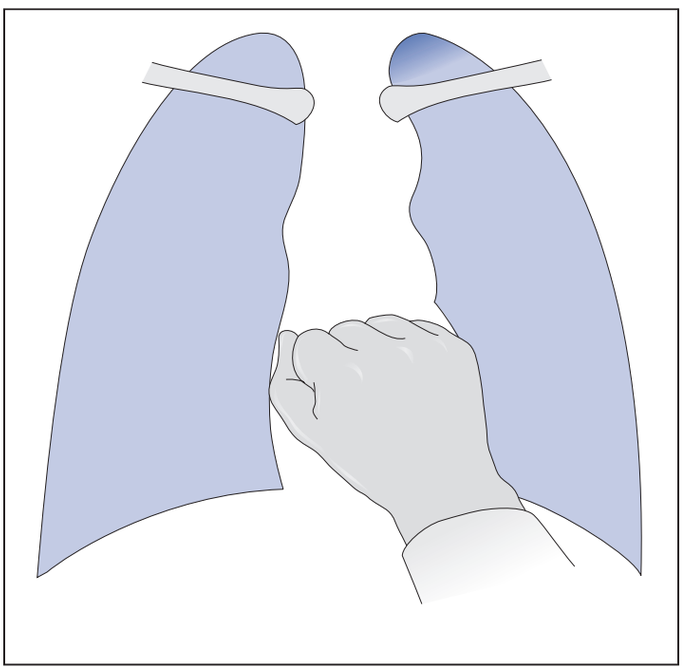

Fig. 1.2 Rule of thumb for estimating heart size. The clenched fist can cover the physiologic cardiac silhouette on the posteroanterior film.

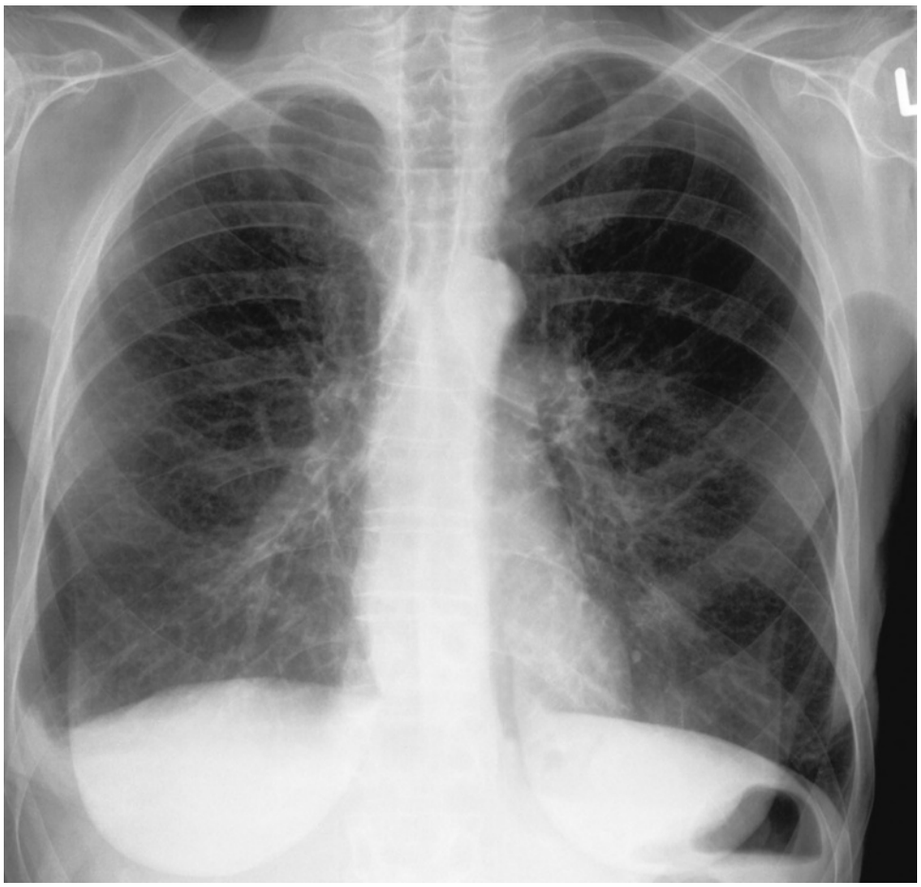

Fig. 1.3 Cardiac cachexia in a metastasizing carcinoma of the colon. The long axis of the heart is significantly shorter than the width of the left hemithorax. There is diffuse shadowing from bronchitis with a small effusion in the right costophrenic angle.

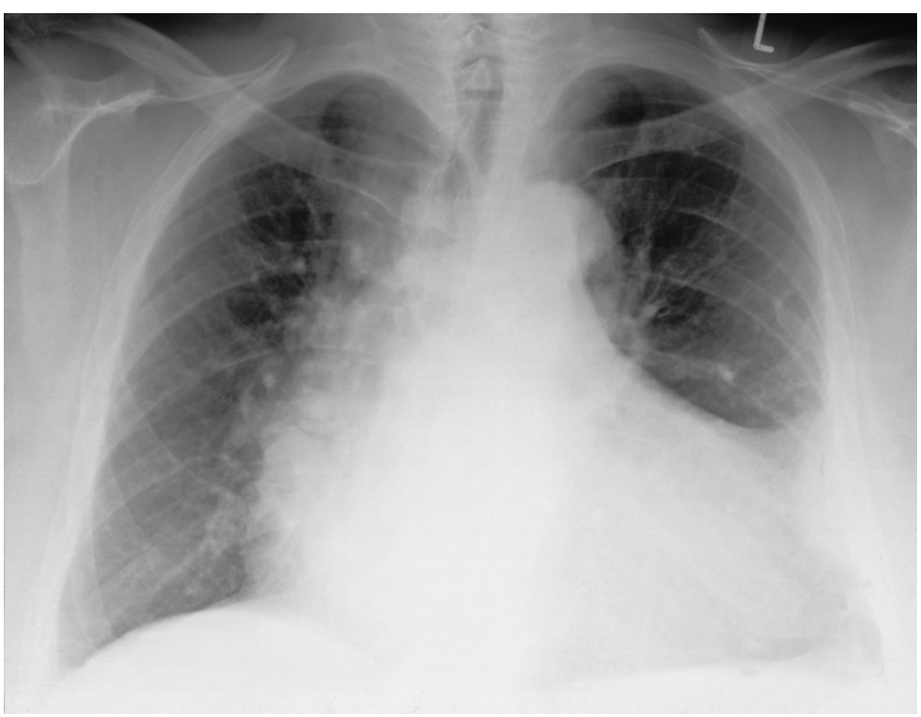

Fig. 1.4 Cardiomegaly without signs of decompensation. Massively expanded heart (cor bovinum) in a 59-year-old man with dilating cardiomyopathy. Pleural and pericardial calluses on the left side allow only a rough estimate of the length of the long axis of the heart, but it is undoubtedly longer than the width of the left hemithorax. There is no interstitial shadowing (Kerley lines), bronchial cuffing, or redistribution of pulmonary perfusion in the upper fields that would indicate decompensation.

Incorrect Imaging Technique

Decentering

Correct centering is particularly important for accurate evaluation of heart size on the plain chest radiograph. Evaluation is based on the level of the clavicles with respect to the spinous processes of the upper thoracic vertebrae. The spinous processes should be centered between the medial ends of the clavicles (**Fig. 1.5**).

Rotating the patient into the **left anterior oblique (LAO) position** reduces the size of the cardiac silhouette (**Fig. 1.9**), whereas rotating the patient into the **right anterior oblique (RAO) position** expands it (**Fig. 1.8**).

A good way to remember this is to think of the heart axis as the hull of a ship. Rotating the long axis of the heart to the left (RAO) shows us the ship's broadside; rotating it to the right (LAO) shows us its bow (**Fig. 1.6**).

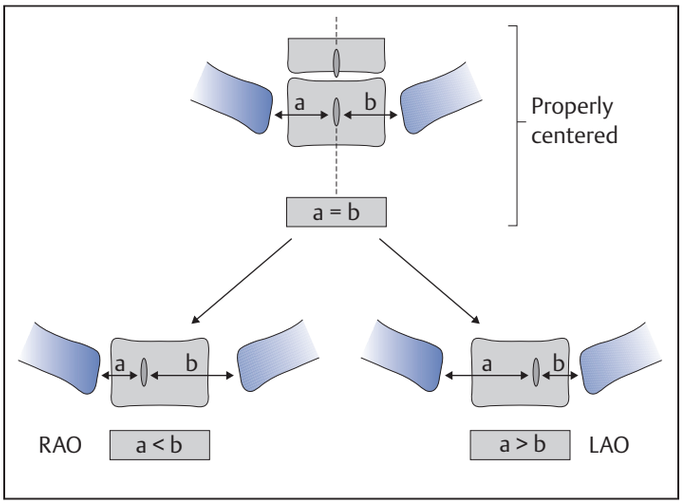

Fig. 1.5 Correctly centered posteroanterior view. The spinous processes should be centered between the medial ends of the clavicles.

Poor Inspiration

Poor inspiration is commonly observed in obese patients and patients with ascites but also in cases where there are communication problems. It can lead to overestimation of heart size, as the heart is in broad contact with the diaphragm (**Fig. 1.10**). In addition to counting of the ribs (the 9th or 10th rib should be visible in the right phrenicomediastinal recess), evaluation of the shape of the diaphragm is helpful in quickly recognizing poor inspiration. A diaphragm exhibiting a gull-wing shape (**Fig. 1.7**) is indicative of expiration. Impaction of the trachea (S shape) can occur in children.

Thoracic Deformity

Aside from incorrect imaging technique, anatomic anomalies such as pectus excavatum or flat back can lead to a reduction in the anteroposterior diameter of the thorax with displacement of the heart axis. The same applies to a high-riding left diaphragm (more common after bypass surgery), which leads to rightward rotation of the heart axis.

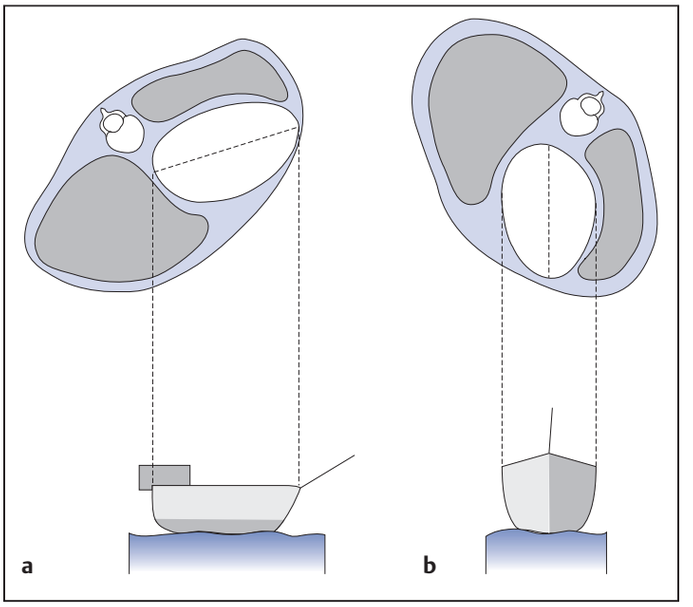

Fig. 1.6 a, b Effect of decentering on the cardiac silhouette. Rotating the patient into the RAO position enlarges the cardiac silhouette (creating a "broadside") and vice versa.

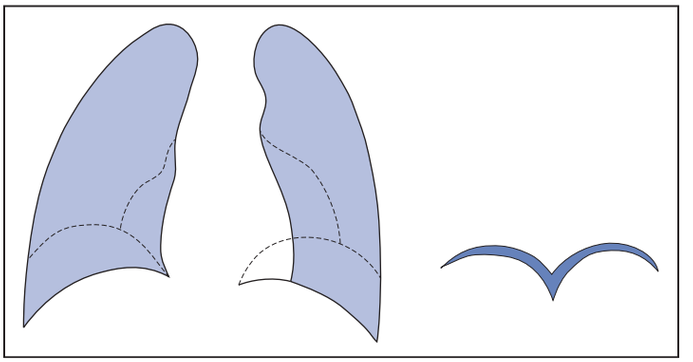

Fig. 1.7 Influence of poor inspiration. The reduction in the depth of inspiration can be estimated from the shape of the diaphragm, which shows increasing curvature. On expiration the diaphragm resembles a gull's wings.

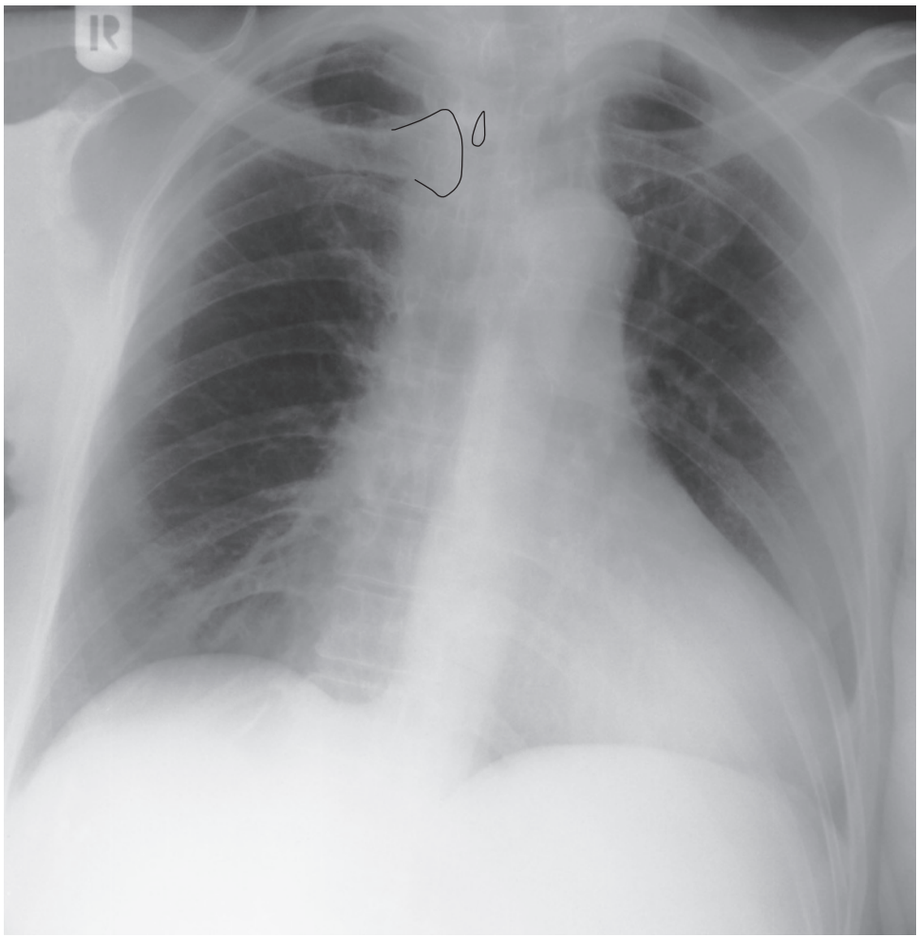

Fig. 1.8 Patient rotated into the RAO position. The right anterior oblique view shows what appears to be an enlarged cardiac silhouette.

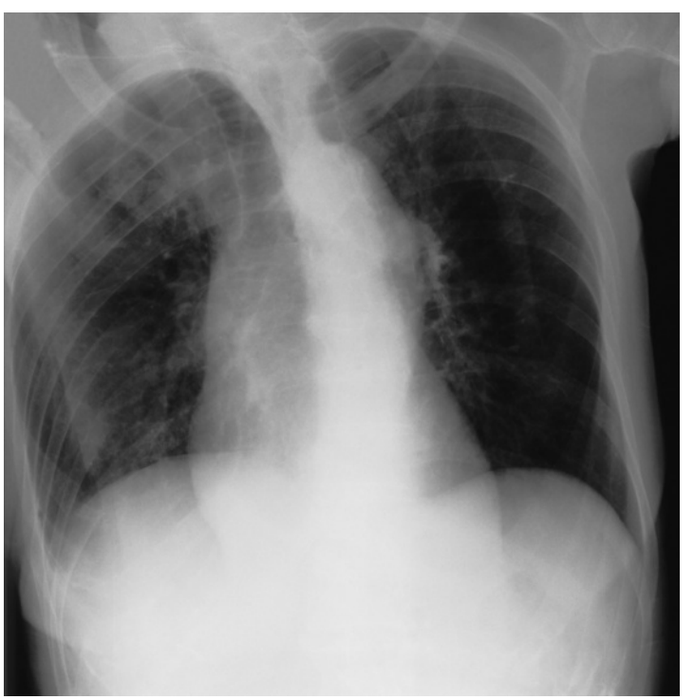

Fig. 1.9 Patient rotated into the LAO position. In the left anterior oblique view (the medial end of the clavicle is projected above the T3 spinous process), heart size appears normal and the left lung more transparent. Note the presence of senile emphysema and tracheobronchopathia calcarea.

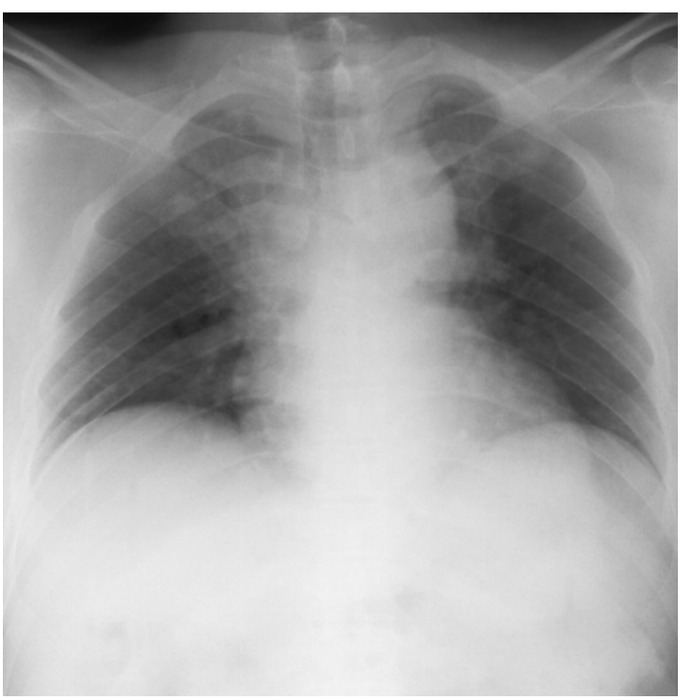

Fig. 1.10 Film with poor inspiration. Films obtained in a patient positioned supine due to ascites show a typical gull-wing shape of the high-riding diaphragm (the 7th rib is visible in the right phrenicomediastinal recess). The heart has broad contact with the diaphragm. The central vessels are foreshortened and the hilum is blurred.

Excursus: Radiographic Anatomy of the Heart

The following section presents a brief review of the radiographic anatomy of the cardiomediastinal silhouette, which is the basis for evaluating cardiomegaly or heart failure.

Posteroanterior Projection

The plain chest radiograph of a healthy patient (**Fig. 1.13)** shows the following contours within the cardiomediastinal shadow (clockwise starting at the 12-o'clock position):

- The prominent convexity of the mediastinum between the 1-o'clock and 2-o'clock positions corresponds to the aortic arch; the further course of the retrocardiac descending aorta can be traced caudally as a broad paravertebral band shadow (**Fig. 1.11**).
- The shape of the aortic arch depends significantly on its position in the projection: In leftward rotation (decentering in RAO, pectus excavatum, etc.), the aperture of the aortic arch is reduced; in rightward rotation (decentering in LAO, left hypertrophy, etc.), its aperture is increased (**Fig. 1.12**).
- The indentation adjacent to the aortic arch is referred to as the aortopulmonary window. It is typically concave; any convex protrusion at this location must be interpreted as a suspected mass.
- The protrusion lying caudal to the notch of the aortopulmonary window is formed by the main pulmonary trunk (main segment of the pulmonary artery) or by the left main branch of the pulmonary artery. This notch will spread open to a varying degree depending on the degree of rotation into the LAO position.
- Alternatively, a less pronounced concavity may be followed by a slight protrusion produced by the left atrial appendage.

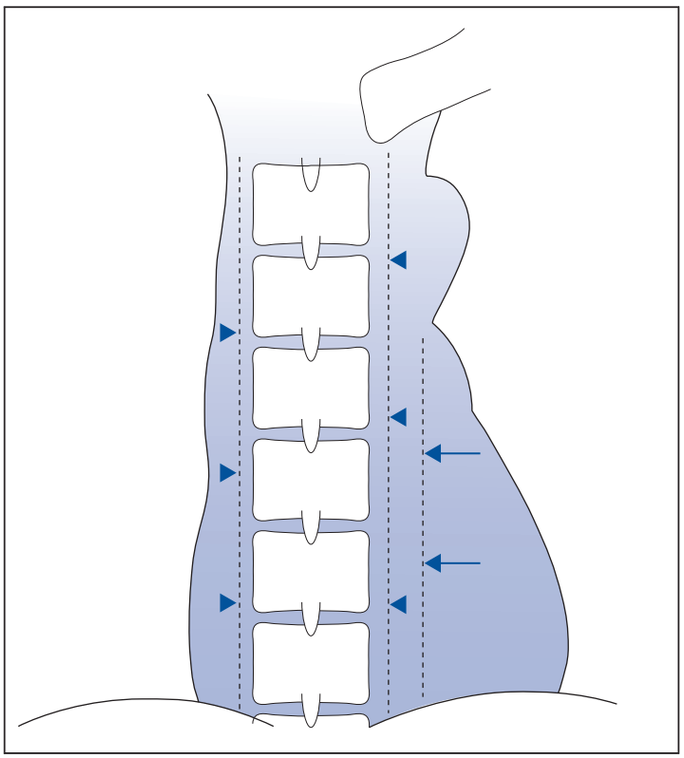

Fig. 1.11 Course of the thoracic aorta. The retrocardiac descending aorta can be traced as a paravertebral band shadow (arrows). This should be distinguished from the paravertebral secondary shadow (arrowheads).

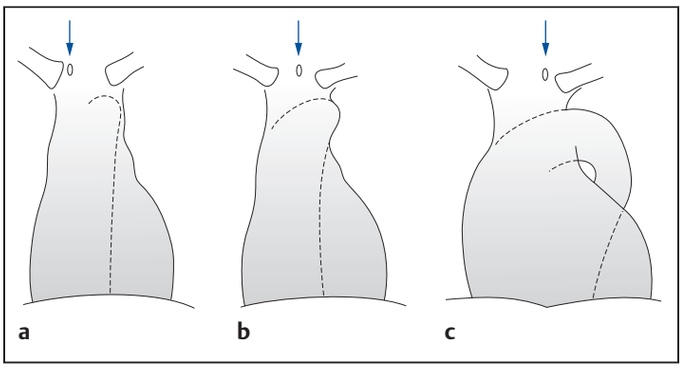

Fig. 1.12a–c Shape of the aortic arch. Depending on the rotation of the film or the degree of elongation (as in hypertension), the projection of the aortic arch is perpendicular or oblique to the imaging plane.

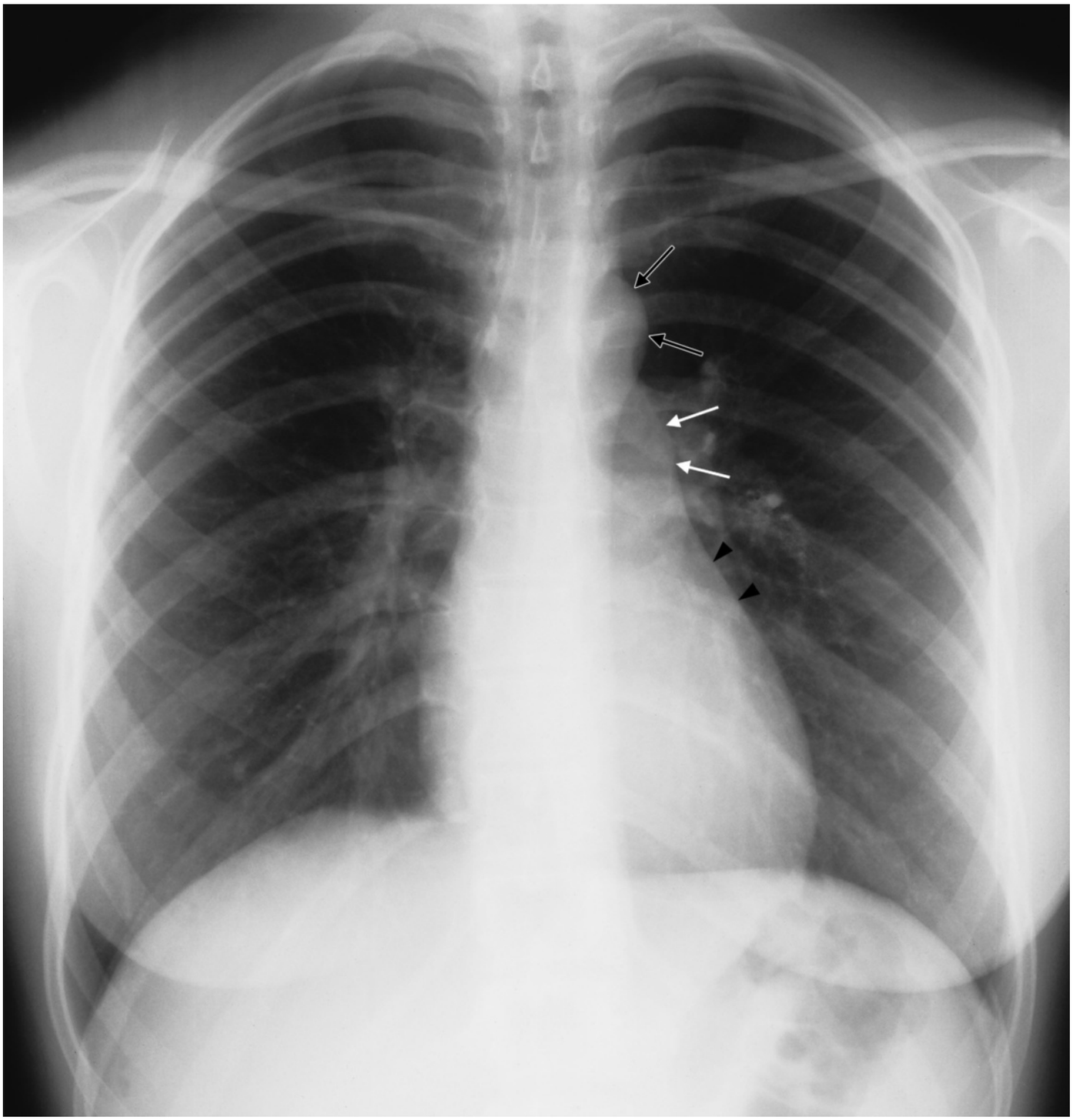

Fig. 1.13 Plain posteroanterior chest radiograph in a 22-year-old woman (examination following contact with tuberculosis patients). Typical cardiopulmonary findings for this age group. The upper margin of the left cardiomediastinal silhouette is formed by the aortic arch (black arrows), the left pulmonary artery (white arrows), and the atrial appendage (black arrowheads).

- The farthest caudal arc of the left cardiac border, extending as far as the diaphragm (**Fig. 1.17)**, is produced by the left ventricle. In right heart strain the right ventricle may occasionally contribute to this contour as well. To differentiate between these two cases, a lateral view must be obtained in the same session. A right ventricle which is of normal size on the lateral film cannot contribute to the left cardiac border on the frontal view.
  Note that the terminal segment of the left cardiac border above the diaphragm is often ill-defined (**Fig. 1.14**). This is due to the calluses or epicardial fat or connective tissue found here (**Fig. 1.15**). Large fat pads can simulate enlargement of the heart or an apical cardiac aneurysm. CT demonstrates the fat content clearly (**Fig. 1.16**).
- In a healthy person, the left contour of the diaphragm is visible through the medial heart shadow as far as the paravertebral shadow. This is due to the difference in absorption at the interface between the air-filled lower lobe and the diaphragm, which has soft-tissue density (see silhouette sign, Chapter 3).

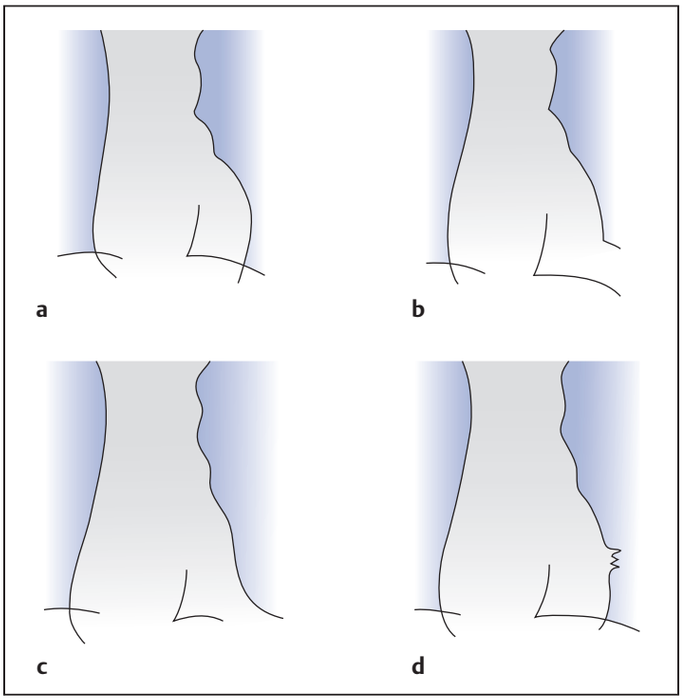

Fig. 1.14a–d Ill-defined border of the left cardiac apex. The part of the left cardiac border adjacent to the diaphragm is often difficult to evaluate due to the projections of the pericardial fatty tissue (**b**) or calluses (**c, d**) located here.

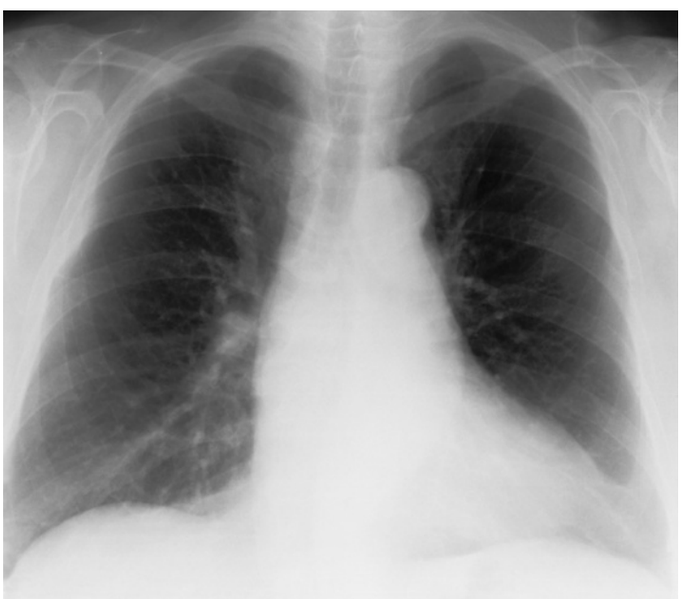

Fig. 1.15 Ill-defined cardiac border with a pleuropericardial callus on the left side. Moderately enlarged left heart without signs of decompensation with slight shadowing in chronic emphysematous bronchitis. The cardiac silhouette is obliterated at the typical locations.

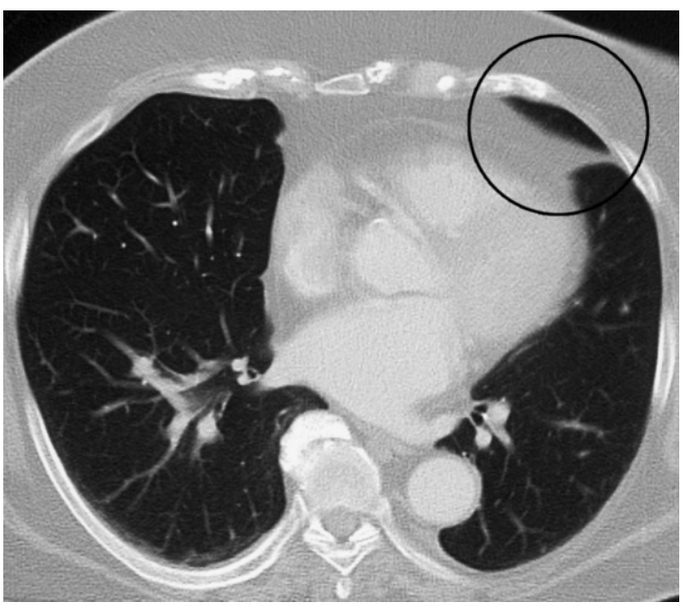

Fig. 1.16 CT image (detail enlargement) of a pleuropericardial callus. Narrow projection of pericardial fatty tissue with normal adjacent lung tissue.

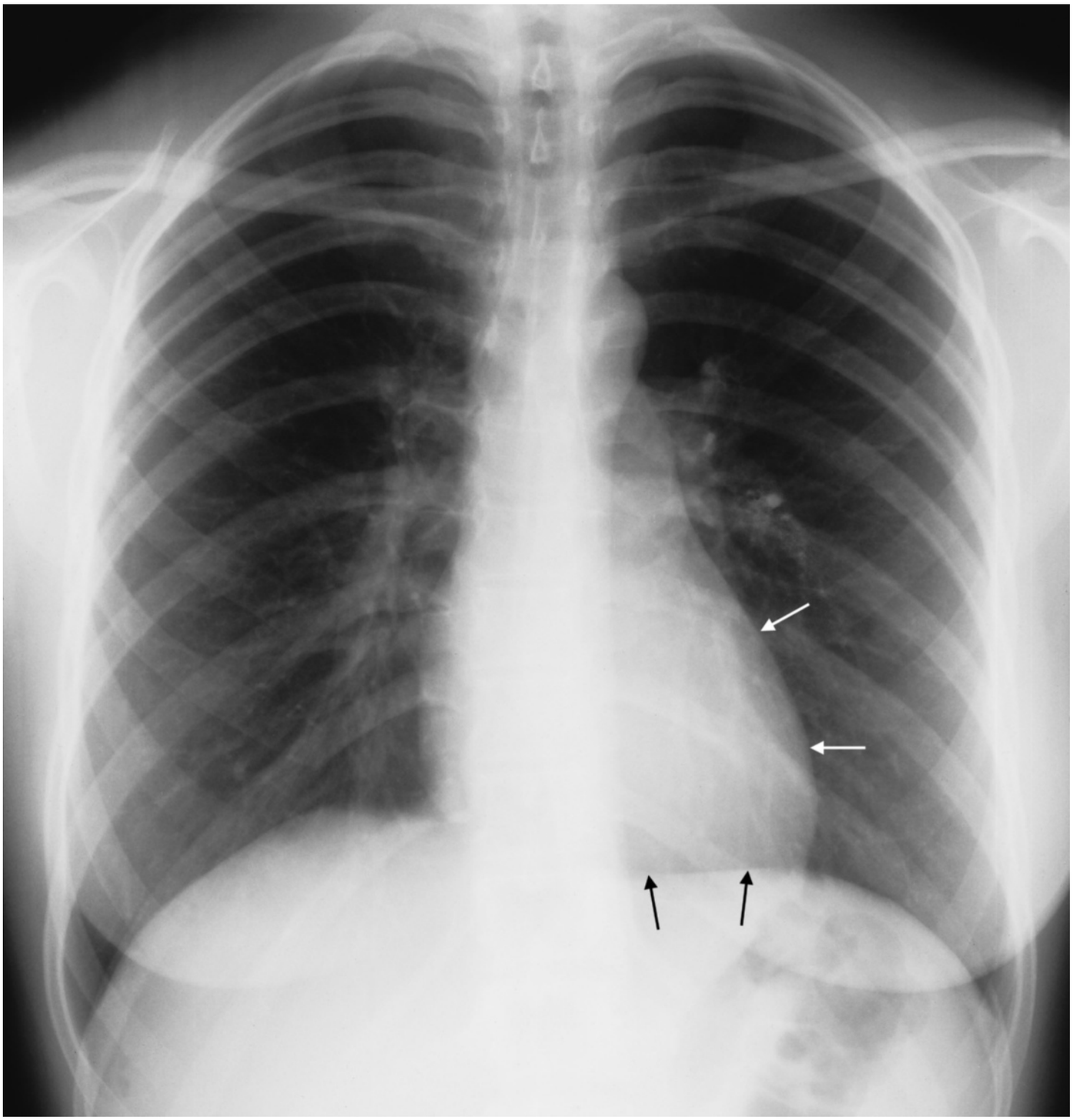

Fig. 1.17 Plain posteroanterior chest radiograph in a 22-year-old woman (examination following contact with tuberculosis patients). Typical cardiopulmonary findings for this age group. The lower part of the left cardiomediastinal silhouette is usually formed by the left ventricle (white arrows). The left contour of the diaphragm is visible through the heart shadow as far as the paravertebral shadow (black arrows).

- The right cardiac border in adults is produced by the right atrium and ascending aorta (**Fig. 1.18, Fig. 1.21).** The various anatomic structures that produce the right border of the cardiomediastinal shadow are often difficult to distinguish from one another. Nevertheless, especially in elderly hypertensive patients with a pronounced aortic segment, these structures can occasionally be differentiated by the notches they produce.
  The width and convexity of the right atrial segment decreases as the patient is rotated to the left (RAO, pectus excavatum, etc.). As leftward shift of the heart axis is also seen in right heart strain, the resulting enlargement of the right heart can be partially masked by leftward rotation. The distance between the right cardiac border and the midsagittal line should be a maximum of one-third of the right hemithorax (**Fig. 1.19**).
- The protrusion of the right cardiac border merges with the superior vena cava cranially at the 10-o'clock position.
- Farther cranially, the cardiomediastinal shadow widens into a funnel shape. Its right border is formed by the brachiocephalic trunk and its left border by the subclavian artery arising from the aortic arch. The Milne method determines the width of the mediastinal vascular band by comparing two distances: (1) the distance from the intersection of the superior vena cava and right main bronchus to the midline, and (2) the distance from the origin of the left subclavian artery to the midline. The total width at this site should be less than 5 cm (**Fig. 1.20**).

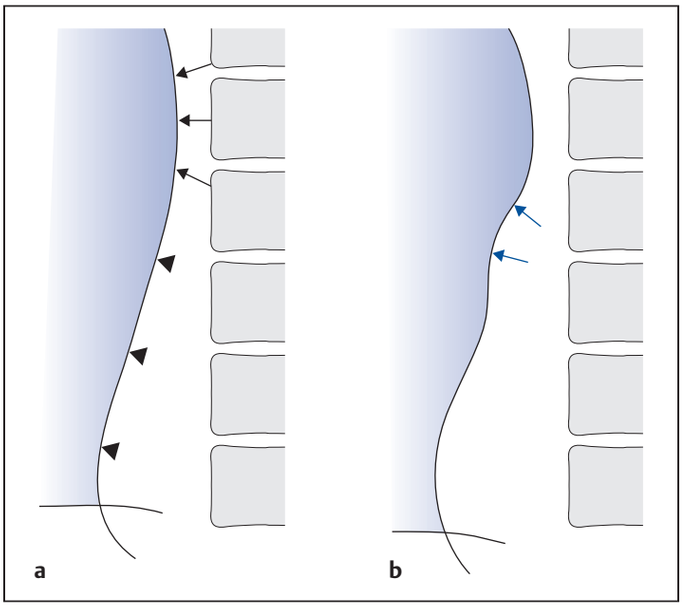

Fig. 1.18 a, b The right cardiac border.
a Variant with a smooth transition between the atrial shadow (arrowheads) and the upper mediastinum, i.e., the margin of the superior vena cava.
b Form observed especially in hypertensive patients with protrusion of the ascending aorta (blue arrows).

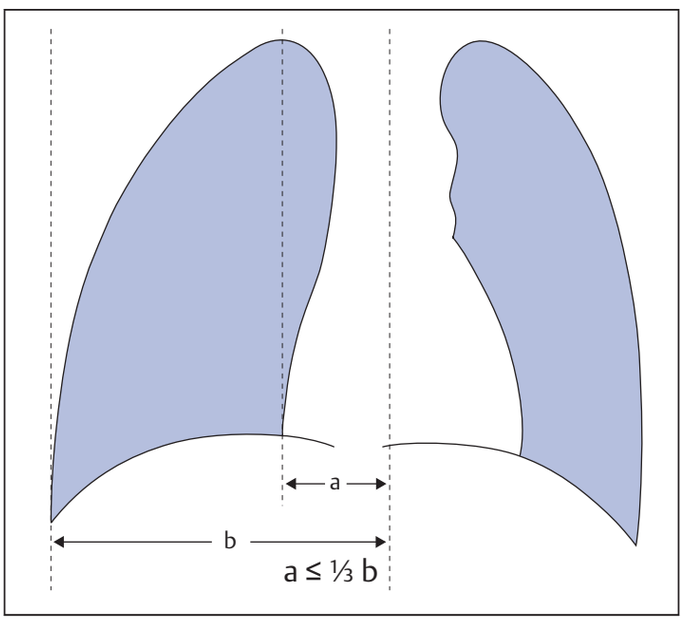

Fig. 1.19 Evaluation of the size of the right atrium. The distance between the lateral atrial border and the midsagittal line (a) is less than one-third of the right hemithorax (b).

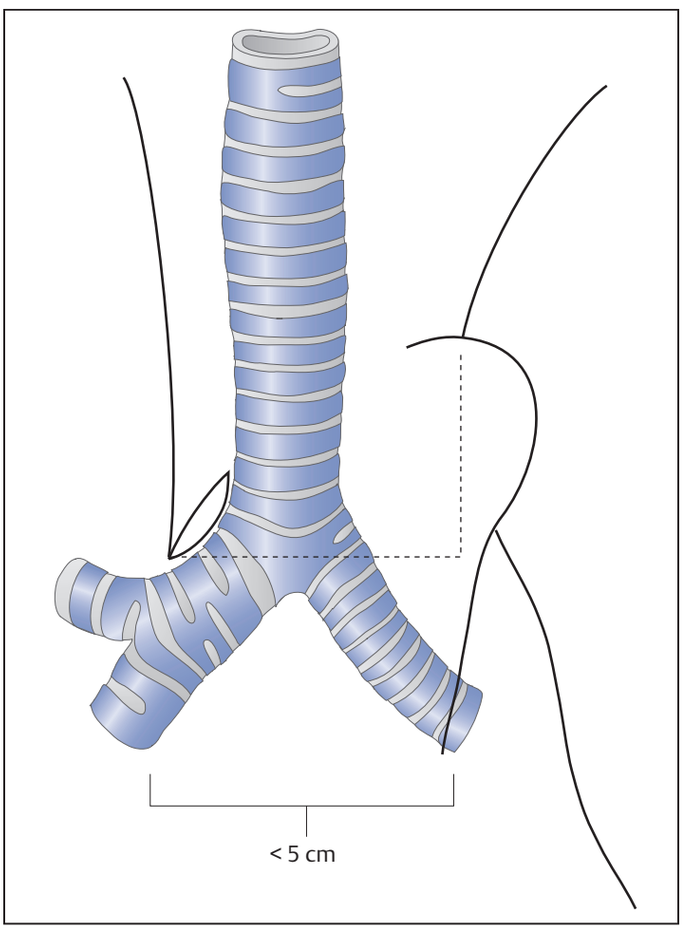

Fig. 1.20 Mediastinum according to Milne. The distance of the intersection of the superior vena cava and right main bronchus from the vertical extension of the origin of the left subclavian artery should be less than 5 cm.

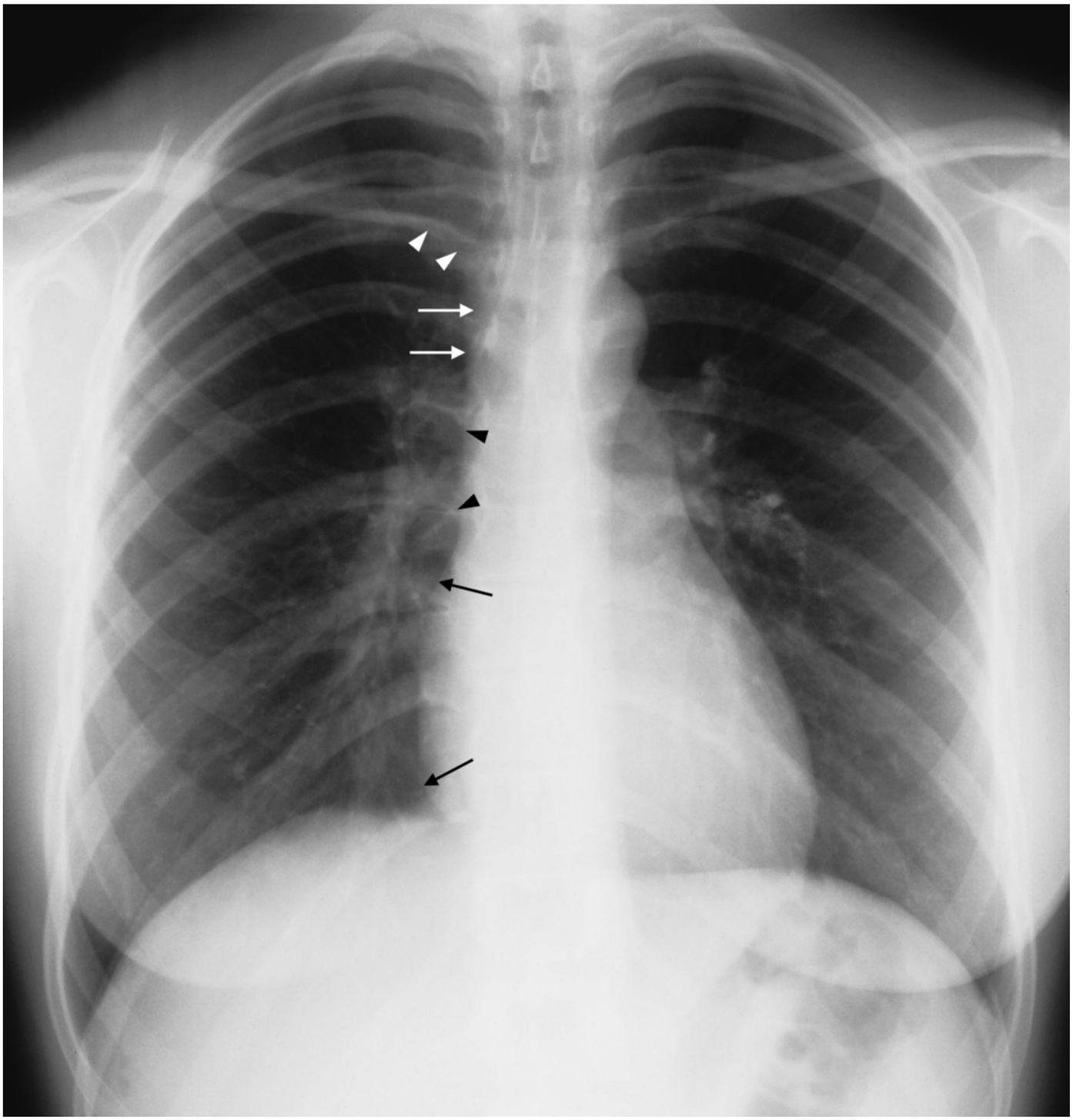

Fig. 1.21 Plain posteroanterior chest radiograph in a 22-year-old woman (examination following contact with tuberculosis patients). Typical cardiopulmonary findings for this age group. The right border of the cardiomediastinal shadow is formed by the right atrium (black arrows), ascending aorta (black arrowheads), and superior vena cava (white arrows). Farther cranially the cardiomediastinal shadow widens into a funnel shape, where its right border is formed by the brachiocephalic trunk (white arrowheads).

Lateral View

- The anterior cardiac border along the posterior aspect of the sternum is produced by the right ventricle (**Fig. 1.23).** The anterior surface of the right ventricle is in contact with the sternum along less than one-third of its craniocaudal length (**Fig. 1.22**).
- The cranial heart shadow usually forms a continuous arc with the aortic root and arch; occasionally a discrete notch demarcates the aorta.
- The cranial border of the middle mediastinal shadow is defined by the shadow of the aortic arch. This arch is interrupted by the radiolucent band of the trachea and main bronchi.

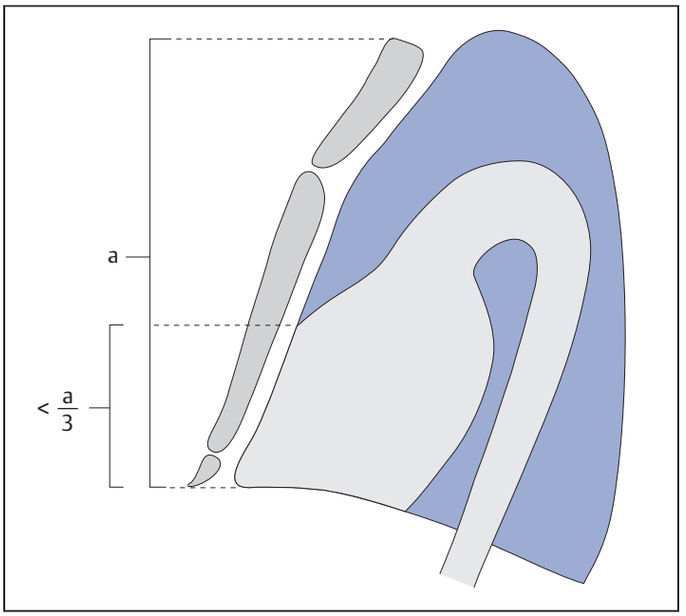

Fig. 1.22 **Area of contact between the anterior right ventricle and posterior sternum.**

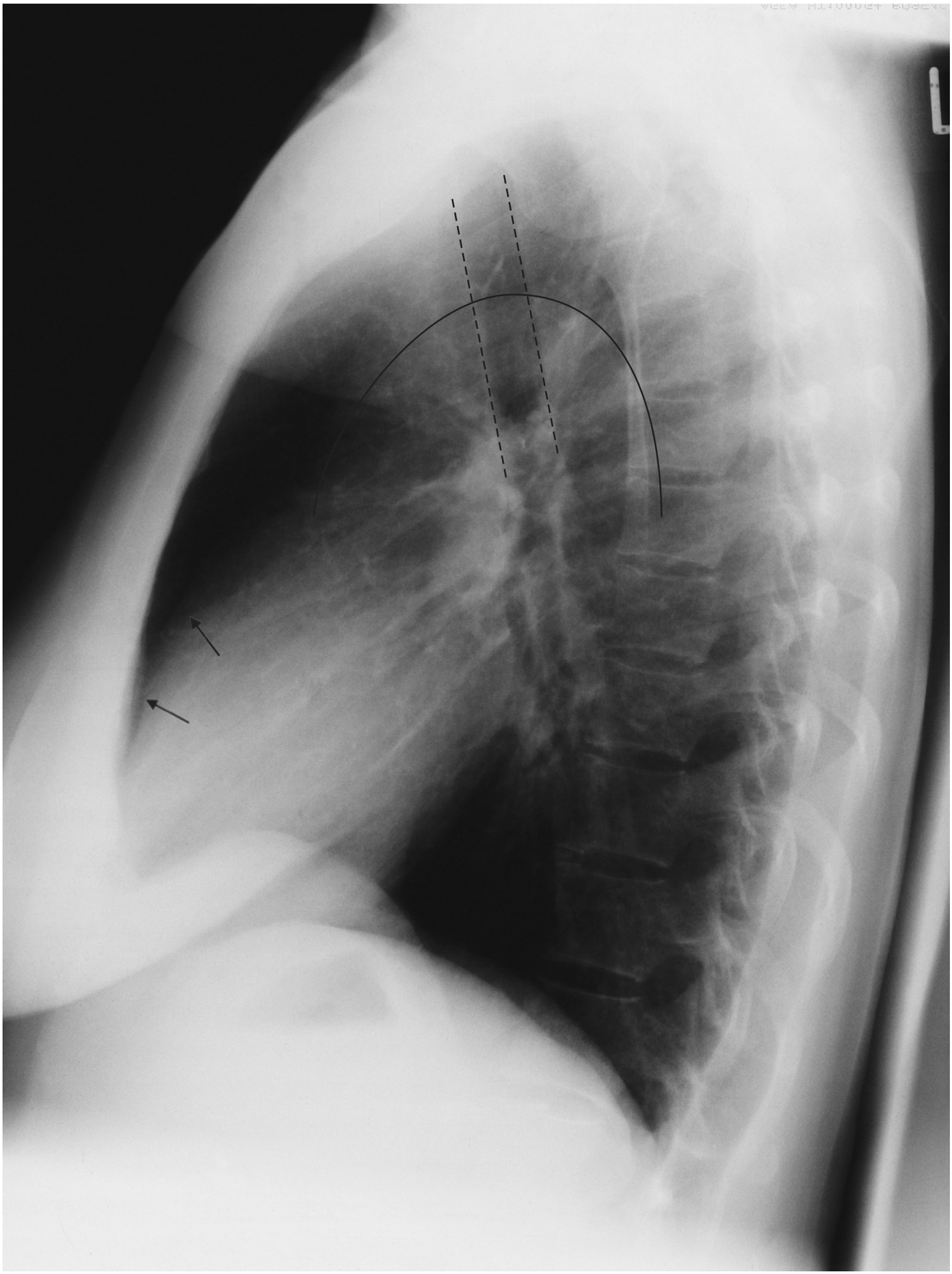

Fig. 1.23 Lateral chest radiograph of a 44-year-old woman obtained in tumor staging (normal findings). The anterior cardiac border corresponds to the anterior surface of the right ventricle and pulmonary outflow tract, respectively (black arrows). The aortic arch (continuous line) and the tracheal shadow (dashed lines) divide the central mediastinum.

- The posterior border of the heart shadow is formed by the protrusions of the left atrium and ventricle (**Fig. 1.26).**
  The space between the posterior cardiac border and the spine is known as the retrocardiac space of **Holzknecht.** The retrocardiac space is an important landmark for evaluating left ventricular hypertrophy. A thoracic deformity such as pectus excavatum or the decreased sagittal depth of the chest in flat back (**Fig. 1.24**) can reduce the size of this space or even obliterate it completely.

Enlargement of the left ventricle leads to protrusion in the lower portion of the posterior cardiac border. Enlargement of the left atrium (see below) leads to protrusion of the upper portions of the posterior cardiac border.

- A pale triangular shadow (triangle of the vena cava) is occasionally visualized at the caudal end of the posterior border directly above the diaphragm. This triangular figure represents the entry of the inferior vena cava into the right atrium. The posterior cardiac border usually intersects the diaphragm at an acute angle with an anterior apex (**Fig. 1.25**). The border of the left ventricle extends posteriorly beyond the posterior border of the inferior vena cava 2 cm above its intersection by less than 1.8 cm. This is known as the Hoffman–Rigler sign (see also **Fig. 1.39, Fig. 1.40**).

Guido Holzknecht, * 1872, † 1931. Austrian radiologist, founder of the Central Institute of Radiology at Vienna General Hospital and an important teacher of the new specialty. Severe radiation injury to his right hand began to manifest itself in 1910.

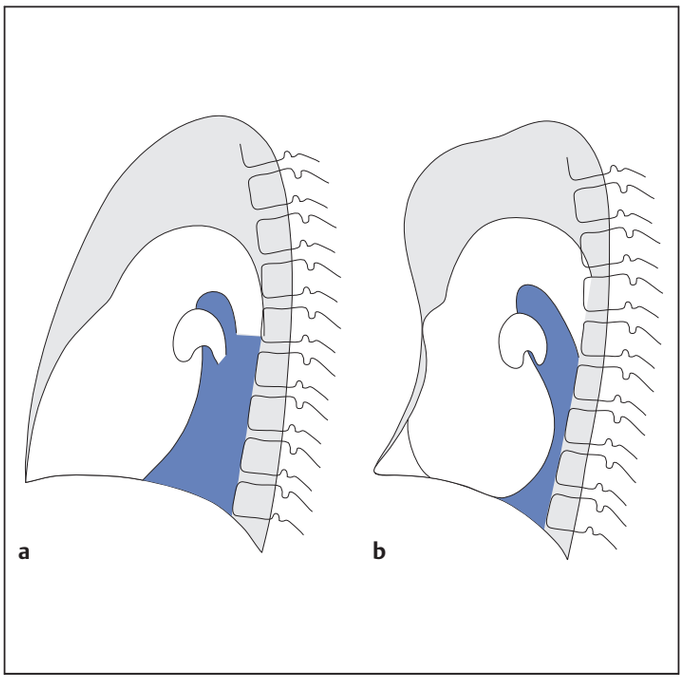

Fig. 1.24 a, b Change in the retrocardiac space in pectus excavatum.
a Normal.
b The heart is shifted posteriorly in pectus excavatum, compressing the retrocardiac space.

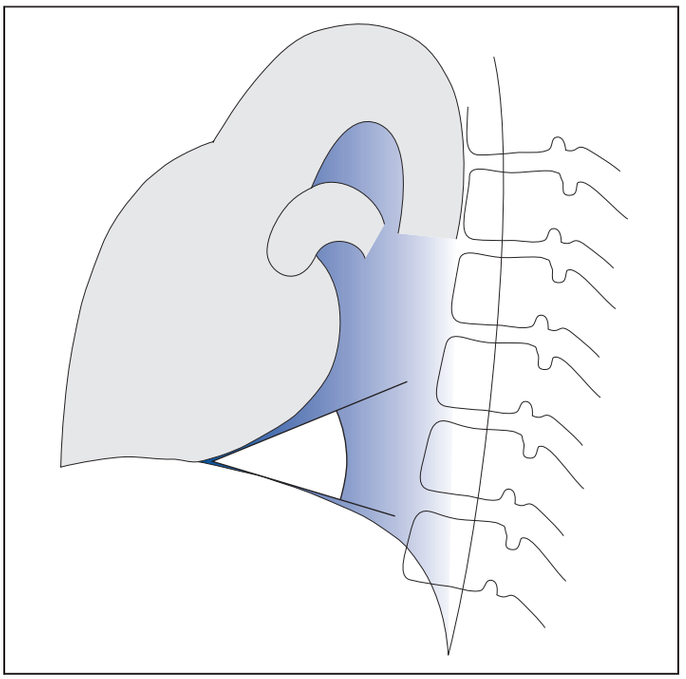

Fig. 1.25 Physiologic angle between the cardiac border and diaphragm.
The posterior border of the left ventricle crosses the diaphragm at an acute angle.

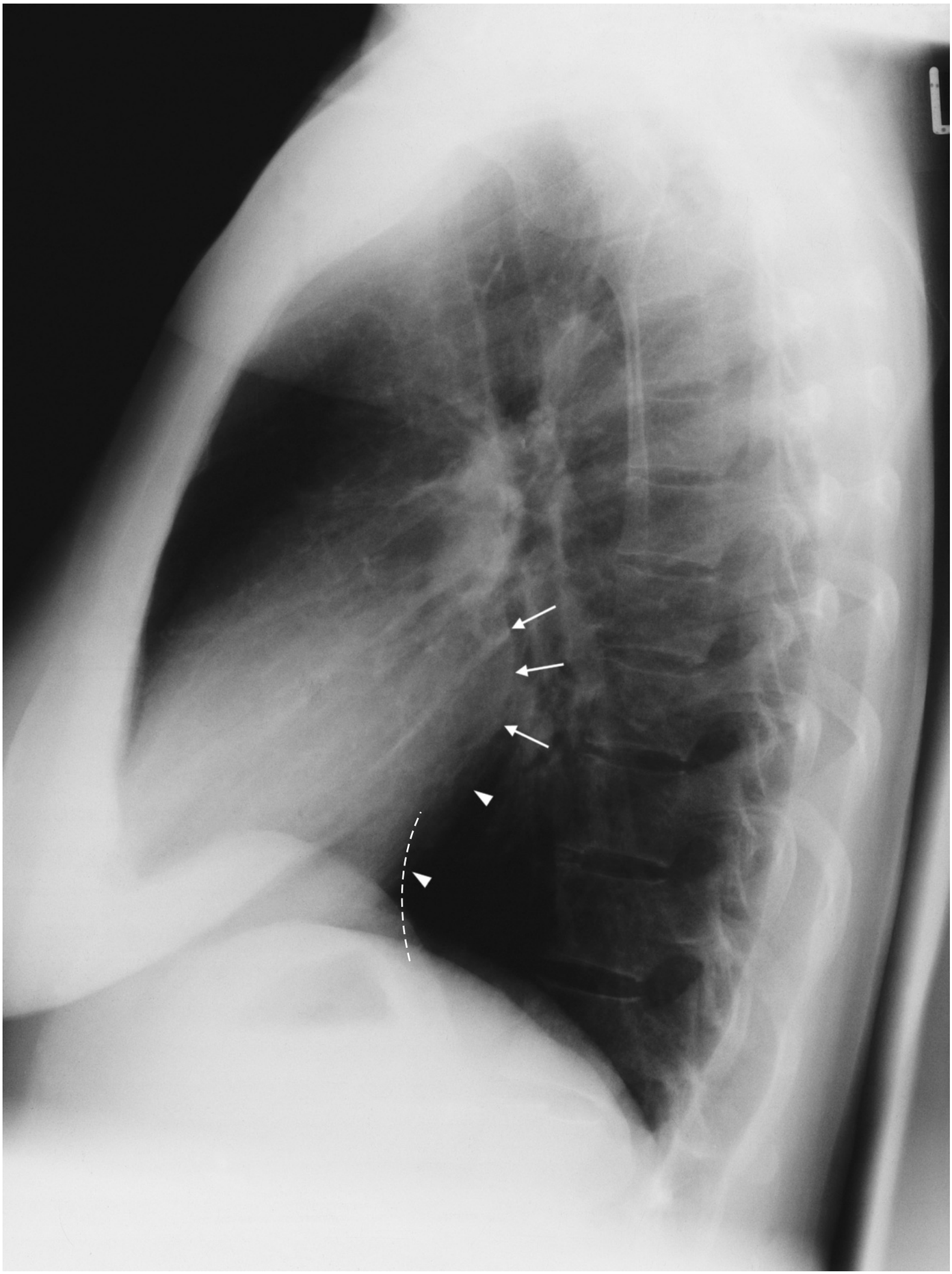

Fig. 1.26 Lateral chest radiograph of a 44-year-old woman obtained in tumor staging (normal findings). The posterior border of the heart shadow is formed by the left atrium (white arrows) and ventricle (white arrowheads).

Computed Tomography

Computed tomography (CT) imaging permits unobscured visualization of the heart and with intravenous contrast can clearly differentiate its various chambers. Further evolution of the technology to multislice helical CT and multidetector systems has made it possible to obtain whole-volume images of the coronary vessels as well. However, systems with these capabilities are not routinely used in clinical practice due to their cost and complexity and the fact that they still provide less diagnostic information than invasive modalities.

This book on diagnostic chest radiography cannot purport to be a textbook of cardiac CT. Our intent here is to alert the reader to findings that may be recognized on CT images of the chest obtained because of other indications. Here one should routinely evaluate the following parameters:

- Heart size
- Presence of circumscribed enlargement (such as right heart hypertrophy)
- Presence of signs of congestion
- Presence of coronary calcification
- Presence of other pathology (aneurysm or pericardial effusion)

Normal Findings

The right atrium and ventricle lie in a right anterior location, the left atrium and ventricle in a left posterior location (**Fig. 1.27**).

As on the plain chest radiograph, the normal heart exhibits a long axis of which the length should not exceed half of the transverse diameter of the chest. Selecting an imaging plane close to the base can visualize all four cardiac chambers as well as the mitral and tricuspid valves for a "four-chamber" view. Wall thickness and volume of the right and left ventricles should be compared in this plane. The walls of the right ventricle should be nearly invisible, the walls of the left ventricle up to 13 mm thick; volume should be about one-third in the right ventricle and two-thirds in the left.

The aortic valve is visualized in a farther-cranial imaging plane and in the coronal reconstruction (**Fig. 1.28**). The pulmonary valve is more difficult to identify. Any presence of coronary calcifications should be mentioned so that further cardiologic diagnostic studies may be performed where indicated. It is possible to identify their location within the main trunk, anterior interventricular artery, left circumflex coronary artery, and right coronary artery (**Fig. 1.29, Fig. 1.30**).

Visualization of the veins draining into the left atrium is important for CT evaluation of possible left ventricular congestion (**Fig. 1.31**). These veins have a diameter up to 10 mm at the point of entry.

The normal pericardium appears as a fine radiodense line surrounded by epicardial and pericardial fatty tissue (**Fig. 1.32**).

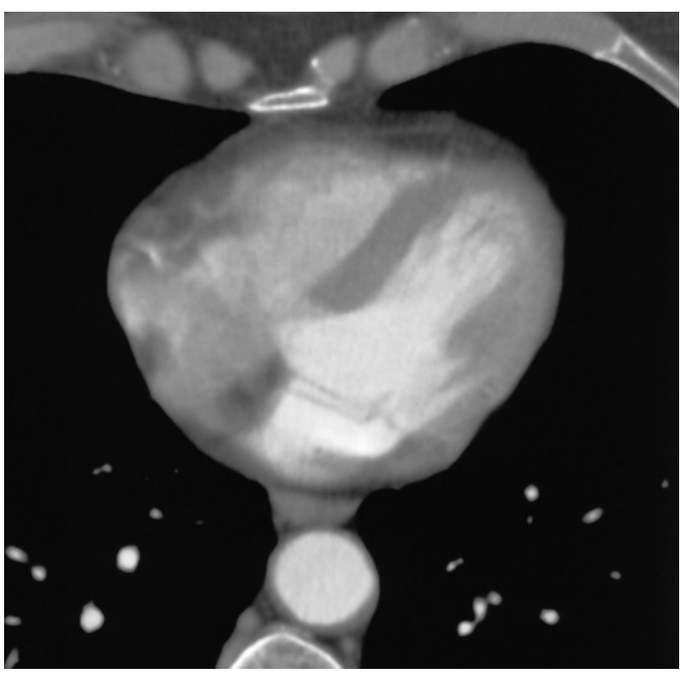

Fig. 1.27 Visualization of the cardiac chambers on CT. The image clearly demonstrates the physiologic mismatch between the thick wall of the left ventricle and the fine wall of the right ventricle, which is normally practically invisible.

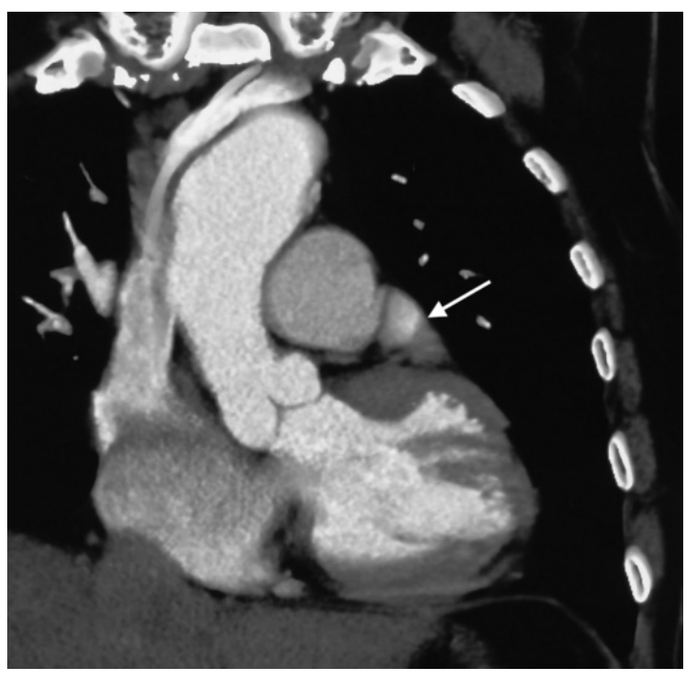

Fig. 1.28 Visualization of the aortic root on CT. Paracoronal reconstruction of the left ventricular outflow tract with the aortic valve and aortic bulb. Both the heart as a whole and the left atrium are enlarged (atrial appendage; white arrow).

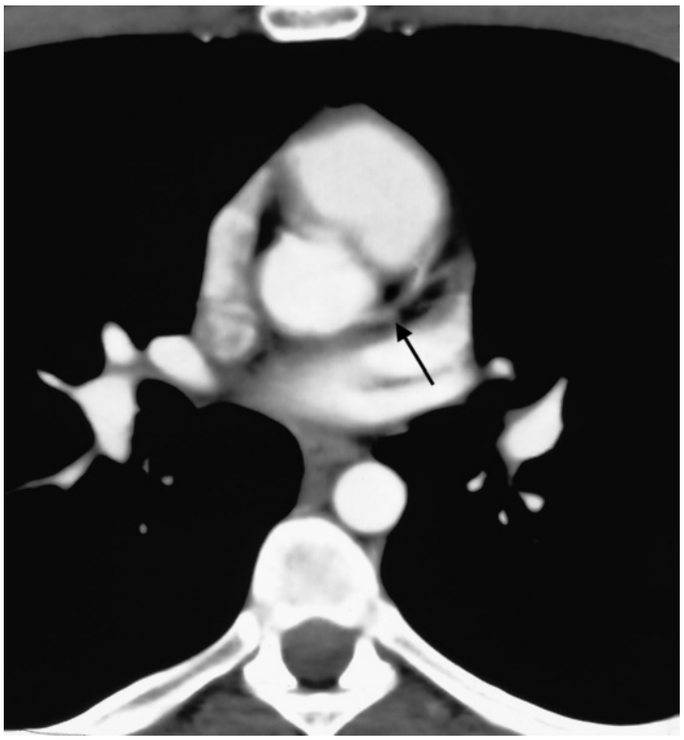

Fig. 1.29 Visualization of the left coronary artery. The image clearly demonstrates the origin of the left coronary artery arising from the aortic root (black arrow). No detectable calcifications.

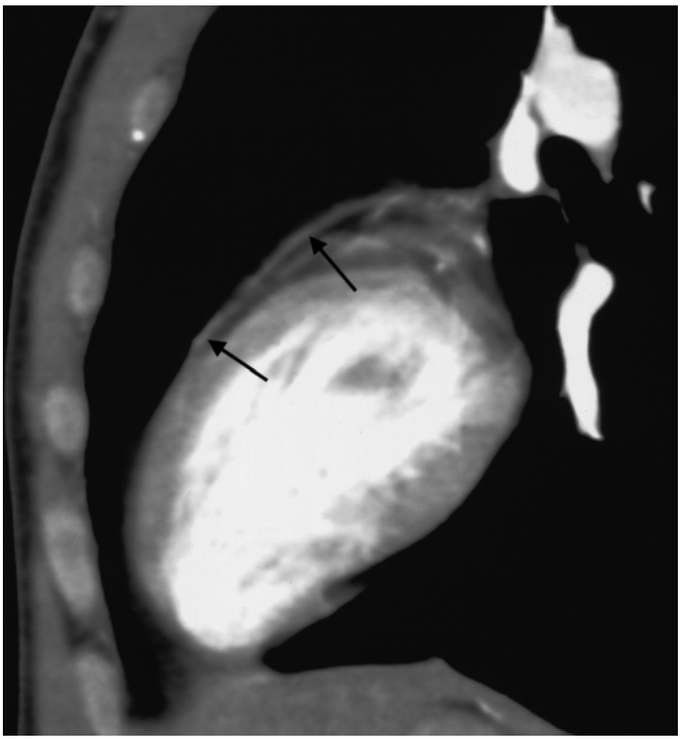

Fig. 1.30 Visualization of the course of the anterior interventricular artery on a sagittal reconstructed plane in chest CT. The long course of the artery (black arrows) is visualized on the sagittal reconstruction.

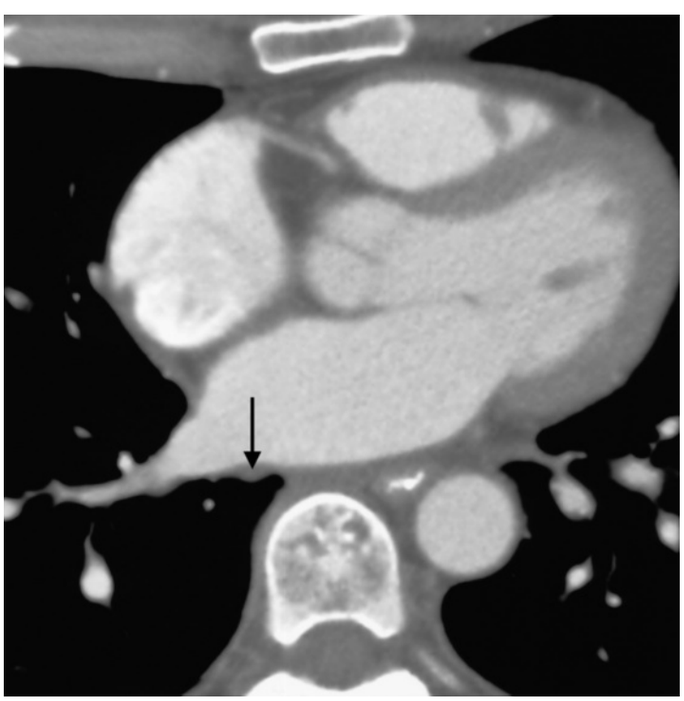

Fig. 1.31 Veins draining into the left atrium. The entry of the right inferior pulmonary vein into the left atrium is visualized with a width of 13 mm. A small pericardial projection (black arrow; see also **Fig. 4.21, Fig. 4.24**) is faintly demonstrated.

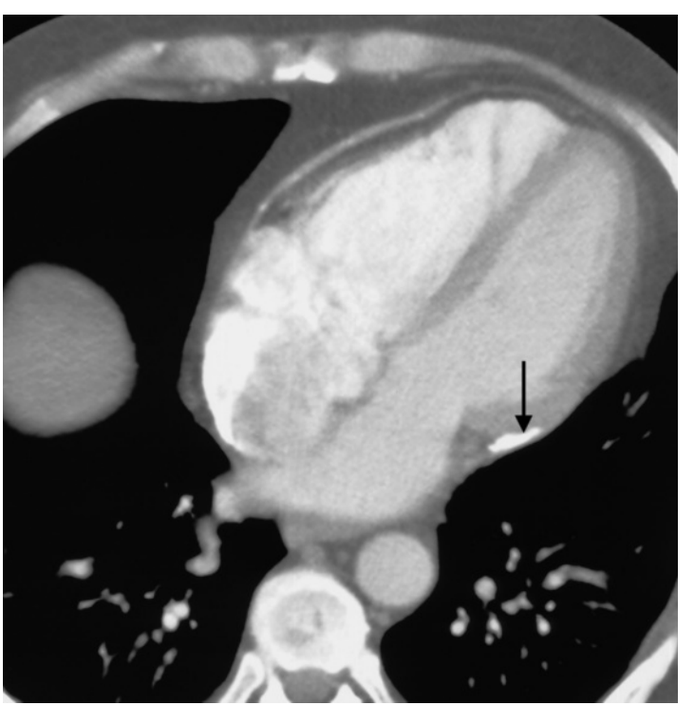

Fig. 1.32 Pericardial thickening in constrictive pericarditis. The pericardium anterior to the cardiac apex shows normal thickness, but significant thickening is observed anterior to the right ventricle. Posterior calcifications (black arrow) are included in the slice.

Left Heart Enlargement

Left Ventricle

Left heart enlargement occurs in response to left heart strain due to increased pressure and volume in the aorta or left ventricle and atrium. Causes include (**Table 1.1**):

- Impeded blood flow (valve lesions)
- Volume overload (septal defects, mitral valve insufficiency, etc.)
- Increased volume of residual blood (left heart failure)

Left ventricular enlargement exhibits the following signs on the posteroanterior radiograph:

- Rounding of the cardiac apex and more pronounced rounding of the left cardiac border
- Leftward elongation of the heart axis with a corresponding increase in transverse cardiac diameter
- Unchanged or deepened pulmonary bay

Hypertensive Configuration

The resulting heart deformation is characteristic of isolated left ventricular enlargement and is referred to as aortic configuration (**Fig. 1.33**). In severe cases the heart shadow can extend as far as the left chest wall. Except in tetralogy of Fallot, this enlargement of the left heart shadow with an intact pulmonary bay is typical of left ventricular enlargement. In right ventricular enlargement (see below) with leftward widening of the heart shadow, the pulmonary bay is obliterated.

The hypertensive configuration is typically associated with elongation and widening of the aorta. The aorta then forms the right border as an arc-shaped protrusion above the atrial shadow, extending cranially as far as the medial end of the left clavicle. It often exhibits calcifications (**Fig. 1.34**).

Table 1.1 Causes of left heart enlargement

Site	Valves	Shunt	Other
Left ventricle	Mitral stenosis	ASD	AF Left heart failure
Left ventricle	Mitral insufficiency Aortic insufficiency Aortic stenosis Supravalvular stenosis	VSD Ductus arteriosus Botalli apertus	Left heart failure Hypertension
Aorta	Aortic insufficiency Aortic stenosis (poststenotic dilatation) Coarctation of the aorta		Hypertension

AF, atrial fibrillation; ASD, atrial septum defect; VSD, ventricular septal defect.

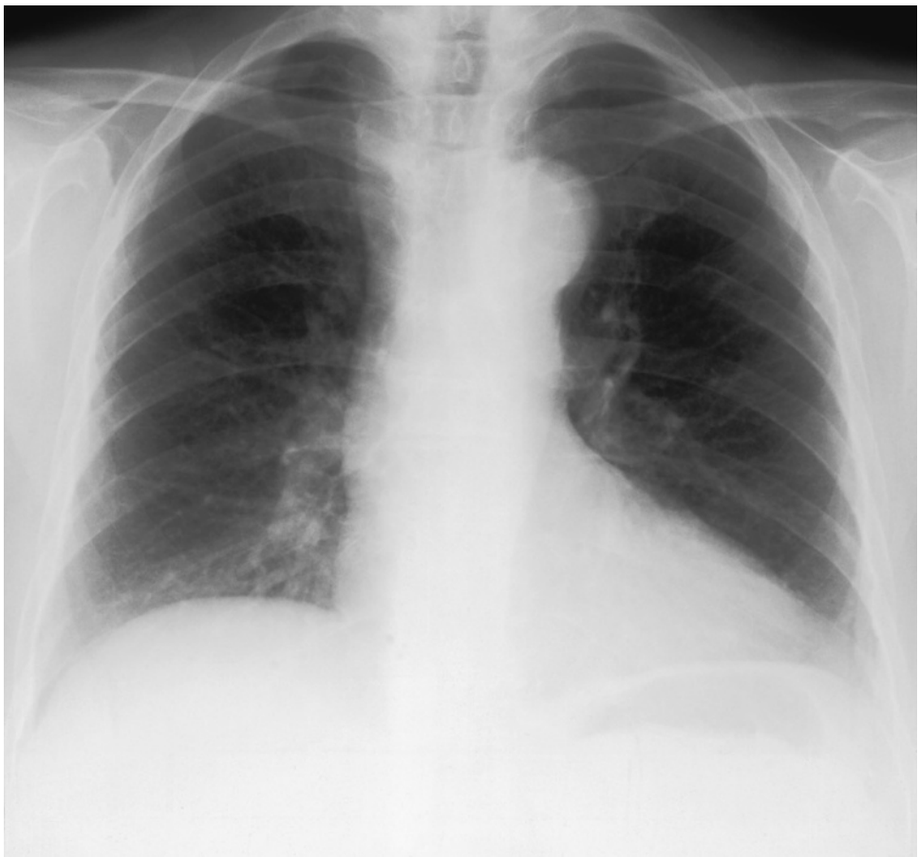

Fig. 1.33 Elongation of the aorta in hypertension. The aortic arch is significantly elongated, extending cranially as far as the clavicle. The left heart is moderately enlarged with a pronounced waist. There are no signs of decompensation.

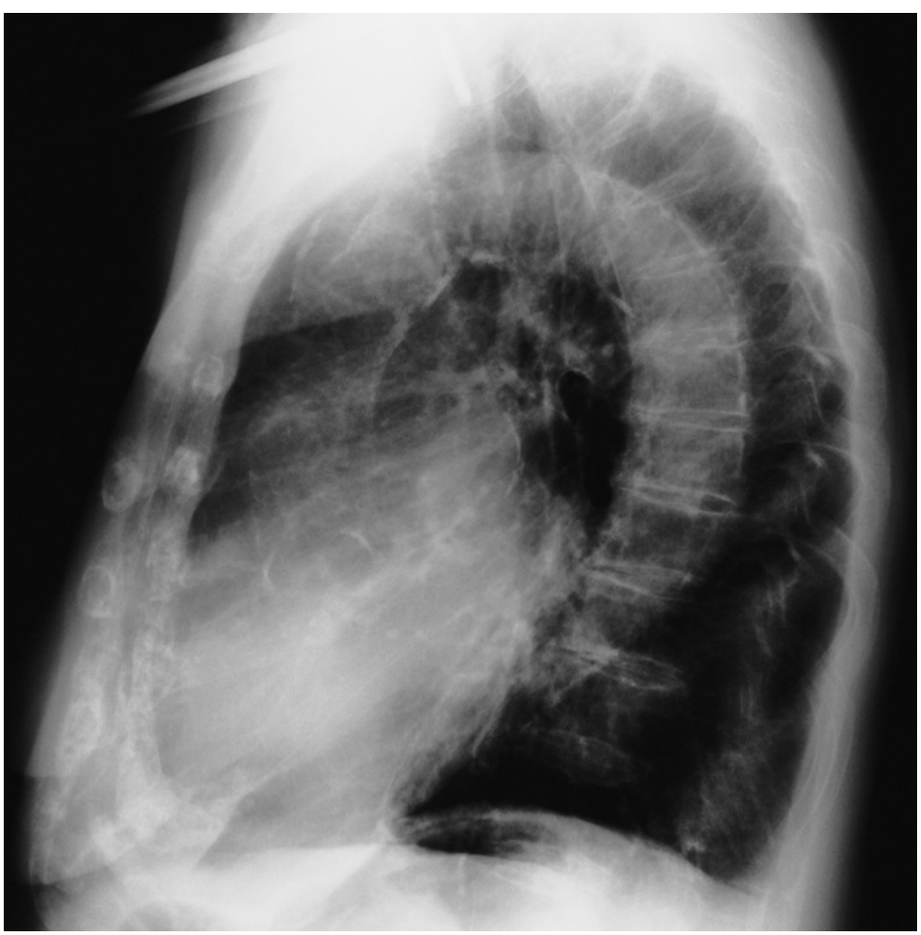

Fig. 1.34 Elongation of the aorta and calcification. The greatly elongated and moderately dilated thoracic aorta shows severe calcification. The entire course of the aorta including the valve level and the origins of the supra-aortic arteries appears almost as it would on an angiogram in this 93-year-old woman. Note the presence of senile emphysema.

Pressure Overload versus Volume Overload (Fig. 1.35)

A pressure overload (arterial hypertension, aortic stenosis) leads to concentric hypertrophy (**Fig. 1.36**), a significant increase in weight with thickening of the wall (up to 20 mm), a narrowed lumen, and a tapered cardiac apex ("Gothic arch"). Volume overload (aortic insufficiency or mitral valve insufficiency) quickly leads to enlargement of the heart (**Fig. 1.37**) with expansion of the ventricular lumen and rounding of the cardiac apex ("Romanesque arch"). For the sake of completeness, we should also mention global heart dilatation (acute myocardial infarction, myocarditis). Where there is only moderate hypertrophy of the cardiac wall the chambers will be grossly dilated.

CT directly visualizes thickening of the left ventricular wall (**Fig. 1.36**).

The term "coeur en sabot" should be used with caution. This term describes the enlargement of the left heart shadow with an intact pulmonary bay (which also includes an aortic configuration). Historically, however, it has been reserved for tetralogy of Fallot, where the enlargement of the left heart is caused by right-heart hypertrophy.

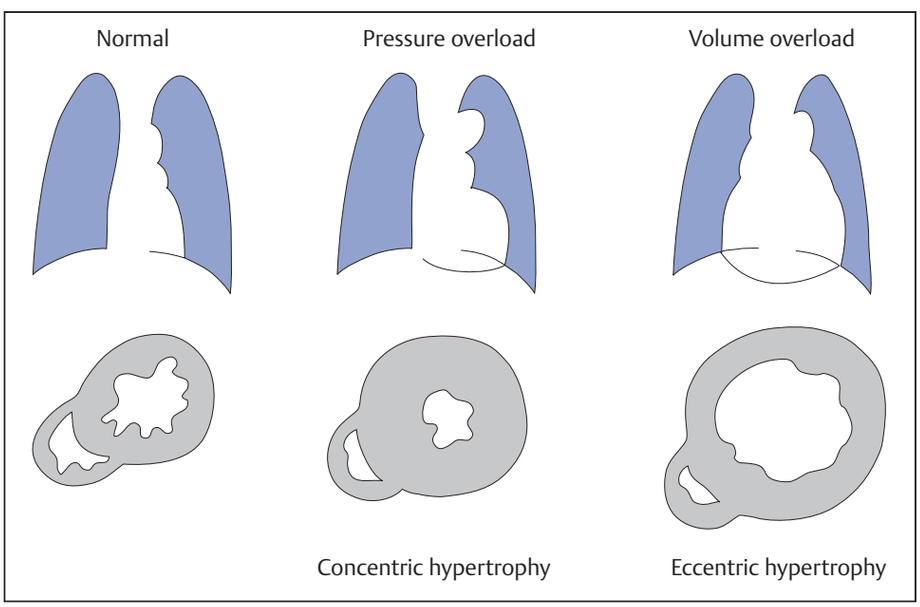

Fig. 1.35 Pressure overload versus volume overload.

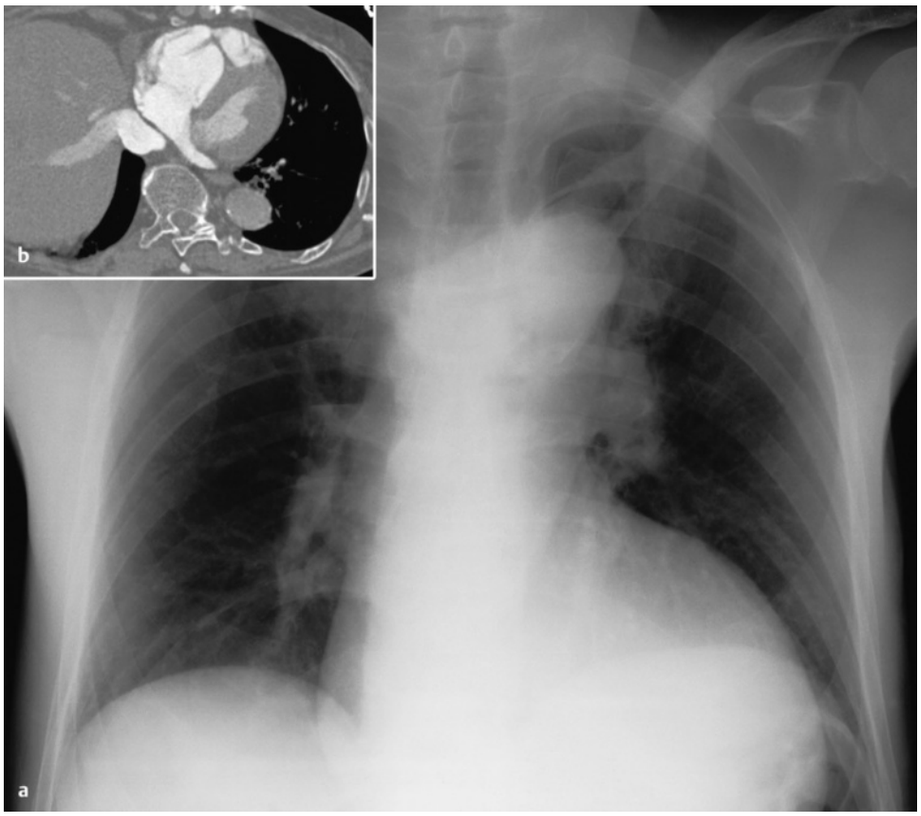

Fig. 1.36 a, b Pressure overload in severe hypertension. Significantly enlarged left heart with pronounced elongation of the aorta along the right cardiac border. There are no signs of decompensation. Deep cardiac waist (**a**). CT demonstrates hypertrophy of the left ventricular wall (**b**). Note the significant congestion in the hepatic veins indicative of left heart failure.

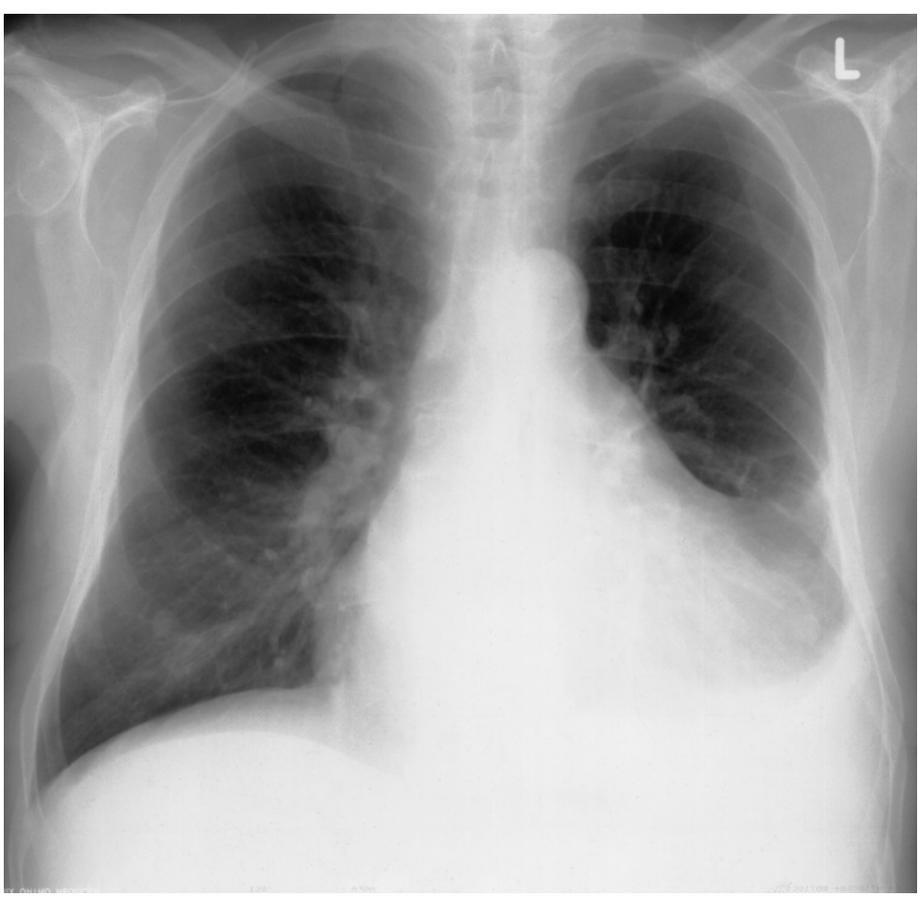

Fig. 1.37 Left heart volume overload in aortic insufficiency. This 81-year-old patient shows a significantly enlarged left heart with a moderately dilated and calcified aorta forming the right cardiac border, an obliterated cardiac waist, and a generally rounded heart. Pleural callus is visible on the left.

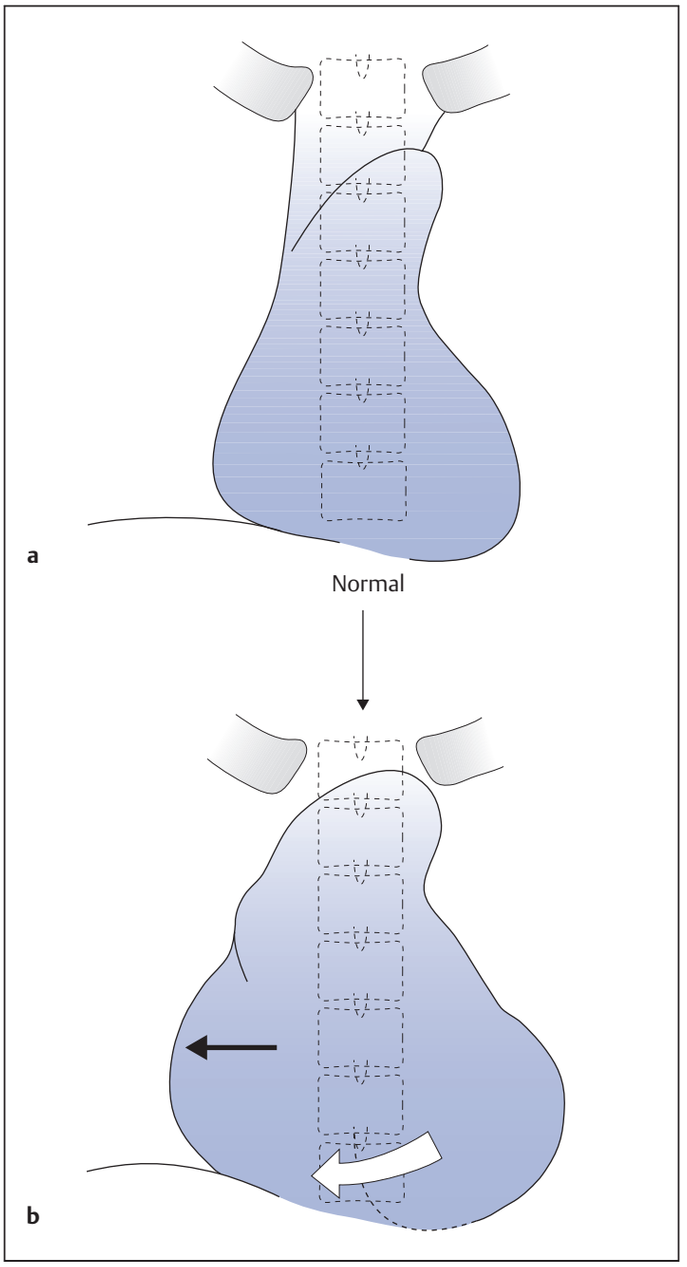

Fig. 1.38 a, b **Rotation creating the impression of generalized enlargement.**

The enlargement of the left ventricle leads to rightward rotation of the heart axis. This simulates enlargement of the right atrium and is thus often misdiagnosed as global enlargement of the heart (**Fig. 1.38**).

Enlargement of the left ventricle is identifiable on the **lateral radiograph** as:

- Protrusion of the posterior inferior contour
- Obtuse angle between the cardiac border and diaphragm
- Narrowing of the retrocardiac space
- Positive Hoffman–Rigler sign
- Contact with the spine

Left ventricular enlargement is characterized on the lateral radiograph by the protrusion along the caudal segment of the posterior cardiac border.

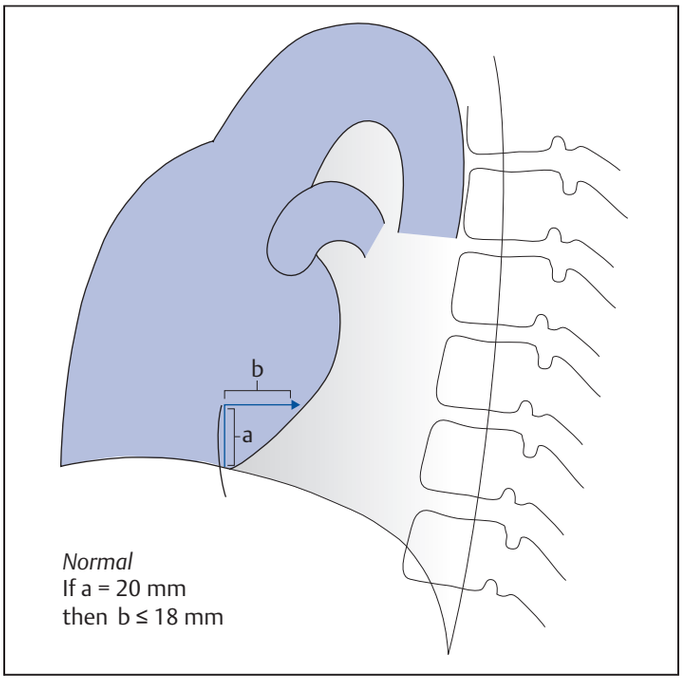

Fig. 1.39 **Hoffman–Rigler sign.** The unenlarged left ventricle projects beyond a perpendicular 2 cm above the intersection with the triangle of the vena cava by less than 1.8 cm.

This sign was deemed so important that a lateral chest radiograph to determine the precise position of the posterior cardiac border was often obtained only after a barium swallow.

In addition to this, the triangle of the vena cava is obscured by the heart and the caudal retrocardiac space is narrowed or obliterated. The angle between the cardiac border and diaphragm becomes obtuse and the Hoffman–Rigler sign is positive (**Fig. 1.39, Fig. 1.40**). In severe cases, the posterior border can extend as far as the spine or even obscure it (**Fig. 1.41**). Left ventricular enlargement is characterized by anteroinferior narrowing of the retrocardiac space. However, severe right ventricular enlargement can lead to posterior displacement of the left ventricle even in the absence of any enlargement of that chamber.

Enlargement of the left ventricle leads to protrusion in the lower portion of the posterior cardiac border. Enlargement of the left atrium (see below) leads to protrusion of the upper portions of the posterior cardiac border.

Obstruction

Caution is required where chest volume is increased (emphysema chest or increased kyphosis). Here the retrocardiac space can still appear relatively broad despite significant enlargement of the left ventricle.

The same applies to the posteroanterior projection in the case of an enlarged chest diameter. Here one should be alert to the steeper inclination of the heart axis, which may even include "drop heart."

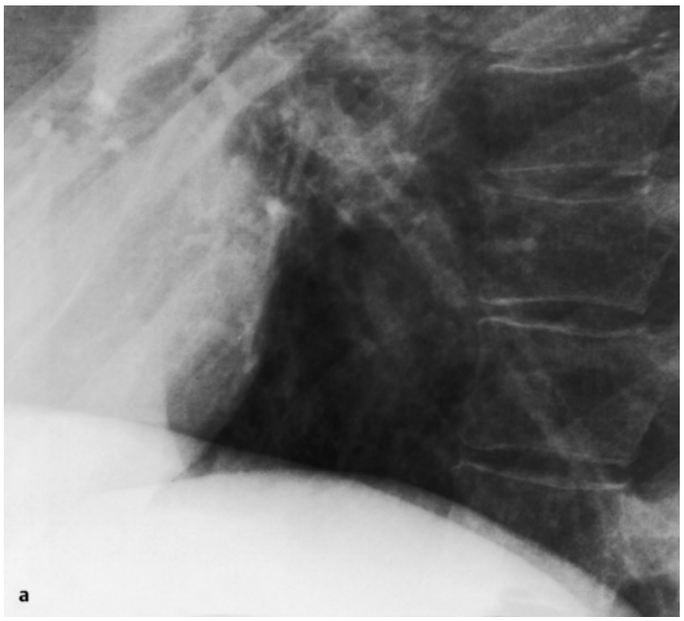

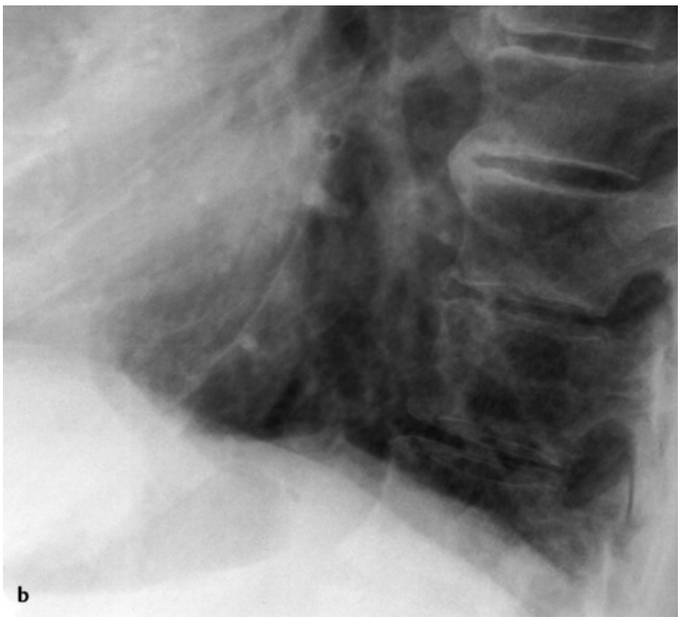

Fig. 1.40 a, b **Positive Hoffman–Rigler sign.**
a Normal posterior protrusion of the left ventricle.

b Enlarged left ventricle with positive Hoffman–Rigler sign.

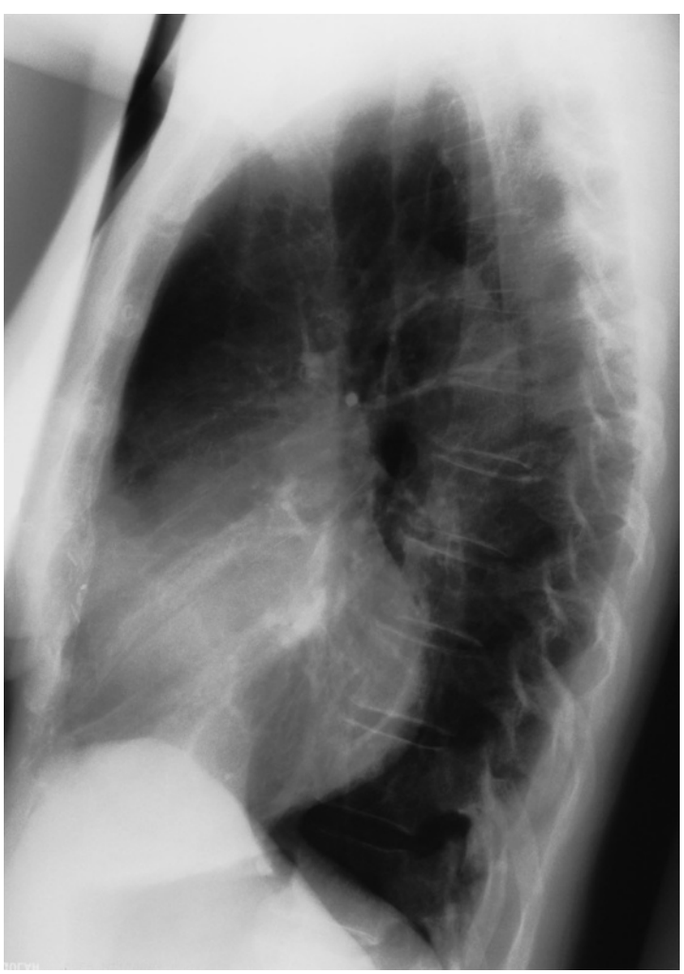

Fig. 1.41 **Left heart enlargement with obliterated retrocardiac space.** The left heart is significantly enlarged and its posterior border overlaps the anterior border of the spine in a chest with a relatively small sagittal diameter. No decompensation.

Left Atrium

Left atrial enlargement is characterized by the following features on the **posteroanterior radiograph**:

- Visualization of an atrial double shadow
- Protrusion in the pulmonary bay (enlarged left atrial appendage)
- Splaying of the carina resulting from cranial displacement of the left main bronchus
- Protrusion of the right (!) cardiac border
- Displacement of the esophagus (barium swallow)

Atrial Double Shadow

A cranial double contour is visualized within the right paravertebral cardiac shadow (normally produced by the right atrium). This double shadow is caused by bulging of the left atrium in its posterosuperior location (**Fig. 1.42**). This visualization of the left atrium as a double contour within the cardiomediastinal shadow is in itself a sign of atrial enlargement.

The double shadow is particularly apparent in mitral stenosis with a normal-sized left ventricle (**Fig. 1.44**).

Protrusion of the Atrial Appendage

Even in the normal heart, the left atrial appendage is occasionally visible as a protrusion of the left cardiomediastinal silhouette. Accordingly, increased prominence of this protrusion in the absence of other findings is not a sign of atrial enlargement (**Fig. 1.45**).

Splaying of the Carina

Splaying of the carina resulting from cranial displacement of the left main bronchus is a definite sign of left atrial enlargement (**Fig. 1.44**). The physiologic angle between the two main bronchi is 56°. An angle of 71° or more must be regarded as abnormal (**Fig. 1.43**).

The left atrium forms the cranial portion of the posterior cardiac border on the lateral radiograph and accounts for the greater part of that contour. Accordingly, left atrial enlargement leads to compression of the posterior mediastinum and anterosuperior narrowing of the retrocardiac space. The enlarged left atrium can extend as far as the spine (**Fig. 1.46**).

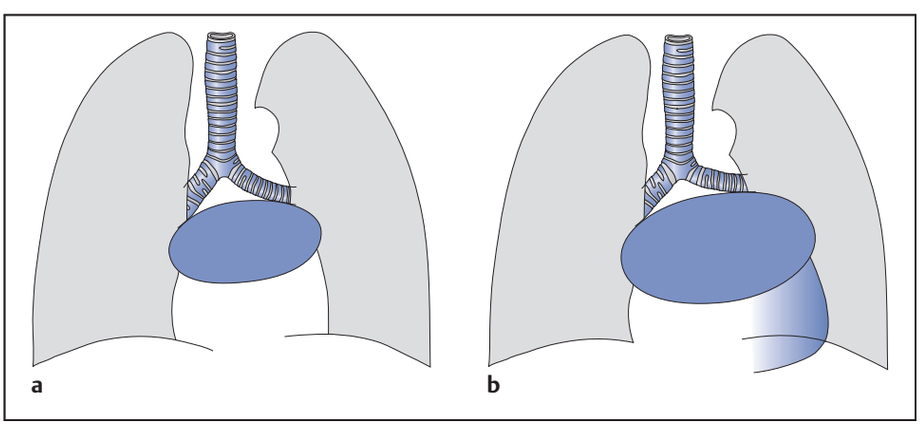

Fig. 1.42 a, b Schematic diagram of the atrial double shadow.
a Mitral stenosis.
b Mitral insufficiency.
Mitral stenosis produces a particularly prominent atrial appendage because of the normal size of the left ventricle.

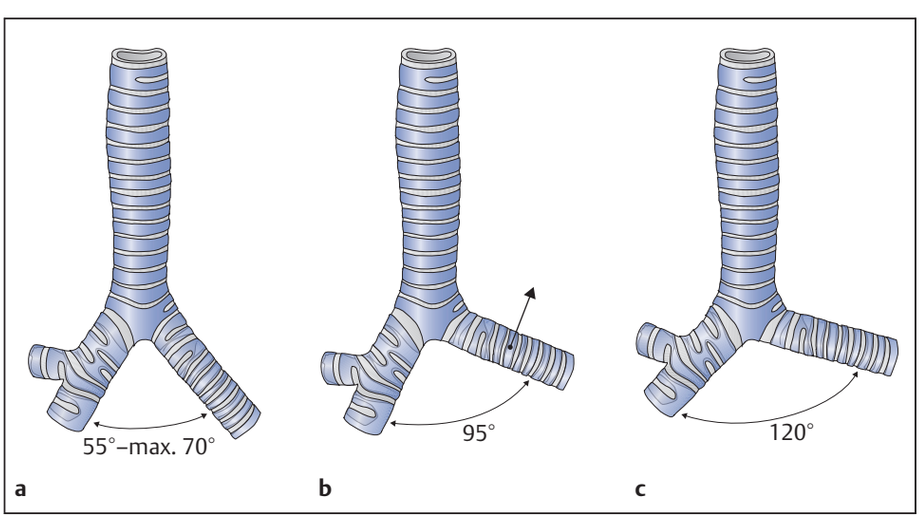

Fig. 1.43 a–c Schematic diagram of the normal (a) and abnormally widened tracheal bifurcation (b, c).

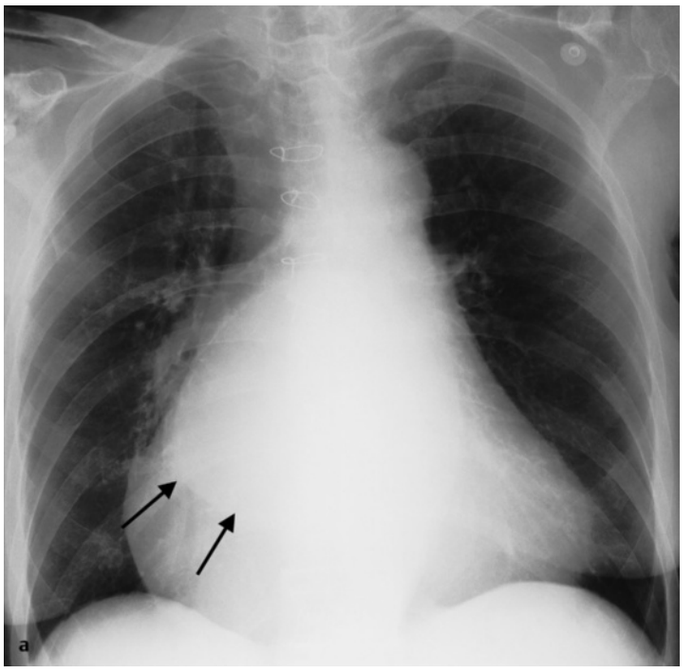

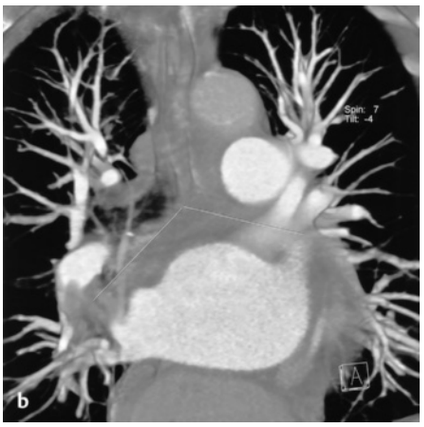

Fig. 1.44 a, b **Atrial double shadow after surgical correction of a mitral valve defect.** Massively enlarged left atrium in generalized enlargement of the heart. The tracheal bifurcation is widened and an atrial double shadow (black arrows in **a**) is visible. No decompensation. Sternal wire cerclage after mitral valve replacement. Findings include tracheobronchopathia calcarea and barrel chest indicative of chronic obstructive pulmonary disease. The coronal view of the 3D CT (**b**) reconstruction of the tracheobronchial tree shows a massively widened bifurcation angle measuring 120°.

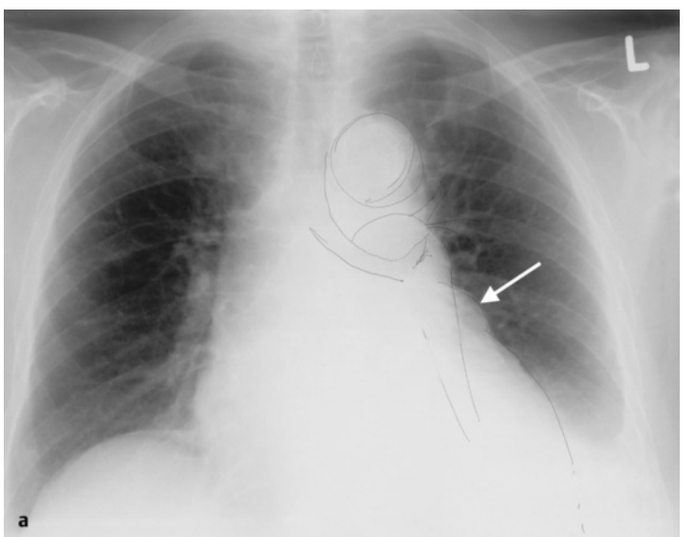

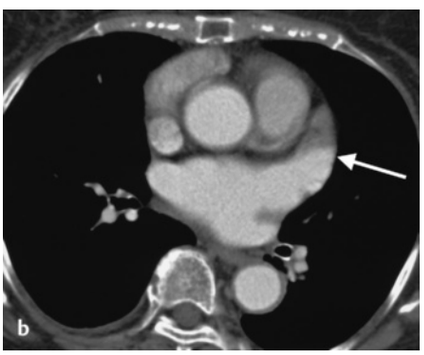

Fig. 1.45 a, b **Pronounced left atrial appendage in atrial enlargement.** The posteroanterior view (**a**) shows protrusion of the left pulmonary bay (white arrow) through the enlarged left atrium (atrial appendage). CT (**b**) shows circumscribed enlargement of the atrial appendage (white arrow).

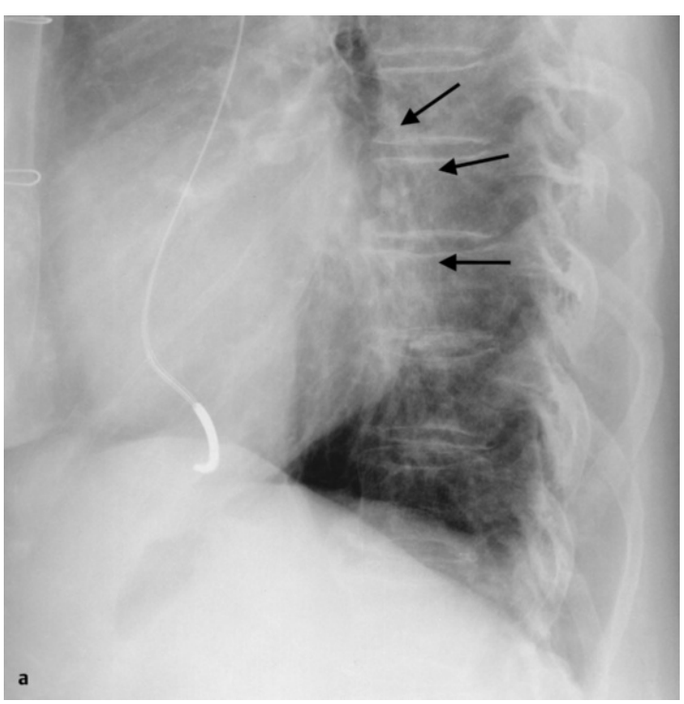

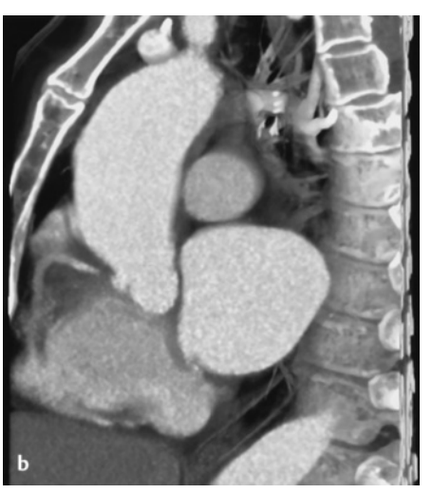

Fig. 1.46 a, b **Enlarged left atrium protruding into the posterosuperior cardiomediastinal shadow.** Generalized enlargement of the heart, particularly pronounced at the level of the left atrium (black arrows) and right ventricle (after placement of three prosthetic valves). CT (**b**) demonstrates the posterosuperior protrusion.

Right Heart Enlargement

Right heart enlargement is caused by pressure or volume overload of the right atrium or ventricle. Causes include (**Table 1.2**):

- Obstructions in the right ventricular outflow tract (acquired or congenital defects)
- Changes in pulmonary circulatory pressure (pulmonary arterial hypertension, left heart failure)
- Presence of shunt or regurgitant blood (septal defects, valve lesions)

Isolated enlargement of the right ventricle is very rare.

Right Ventricle

Right ventricular enlargement exhibits the following signs on the **posteroanterior radiograph**:

- Enlargement of the left heart shadow
- Obliterated cardiac waist (**Fig. 1.48**)
- Pronounced pulmonary segment in some cases

Demonstration of right ventricular enlargement is difficult because the physiologic right ventricle does not contribute to the cardiac border on the posteroanterior radiograph. Incipient enlargement is characterized by dilatation of the outflow tract leading to elongation of the long axis of the heart with cranial displacement of the pulmonary artery ostium. In the frontal projection this can lead to a prominent pulmonary segment as in children. Further enlargement of the right ventricle leads to transverse widening of the heart, primarily in a leftward direction. Then the right ventricle contributes to the left cardiac border. This occurs especially in volume overload of the right ventricle. In some cases the cardiac shadow can extend to the left wall of the chest.

Examination of the **lateral film** is crucial for the final determination of whether predominantly the left or right ventricle is enlarged. Signs include:

- Increased contact between ventricle and sternum (**Fig. 1.49**)
- Increase in the size of the heart shadow above an imaginary line between the main bronchus and the apex of the heart

A right ventricular outflow tract that narrows the retrosternal space is a sign of right ventricular enlargement. One should assume the right ventricle is enlarged if its anterior surface is in contact with the sternum over more than one-third of its craniocaudal length.

On CT, right ventricular enlargement is evident from the shift in the physiologic proportion between the smaller right ventricle and the larger left ventricle. Measurable wall thickness is proof of right heart strain.

The plain chest radiograph does not allow definitive evaluation of the posterior border of the right ventricle. An approximate method may be useful in certain cases. An imaginary line is drawn between the left main bronchus and the apex of the heart. The portion of the shadow above the line belongs to the right ventricle, the portion below it to the left ventricle (**Fig. 1.47**).

Table 1.2 Causes of right heart strain

Site	Valves	Shunt	Other
Right ventricle	Tricuspid stenosis	ASD	AF
	Tricuspid insufficiency		Right heart failure
	Ebstein anomaly		
Right ventricle	Pulmonary insufficiency	ASD	Left heart failure
	Pulmonary stenosis	VSD	
	Tricuspid insufficiency	Tetralogy of Fallot	
	Mitral stenosis		
Pulmonary artery	Pulmonary insufficiency	ASD	Pulmonary arterial hypertension
	Pulmonary stenosis	VSD	Embolism
			COPD

AF, atrial fibrillation; ASD, atrial septum defect; COPD, chronic obstructive pulmonary disease; VSD, ventricular septal defect.

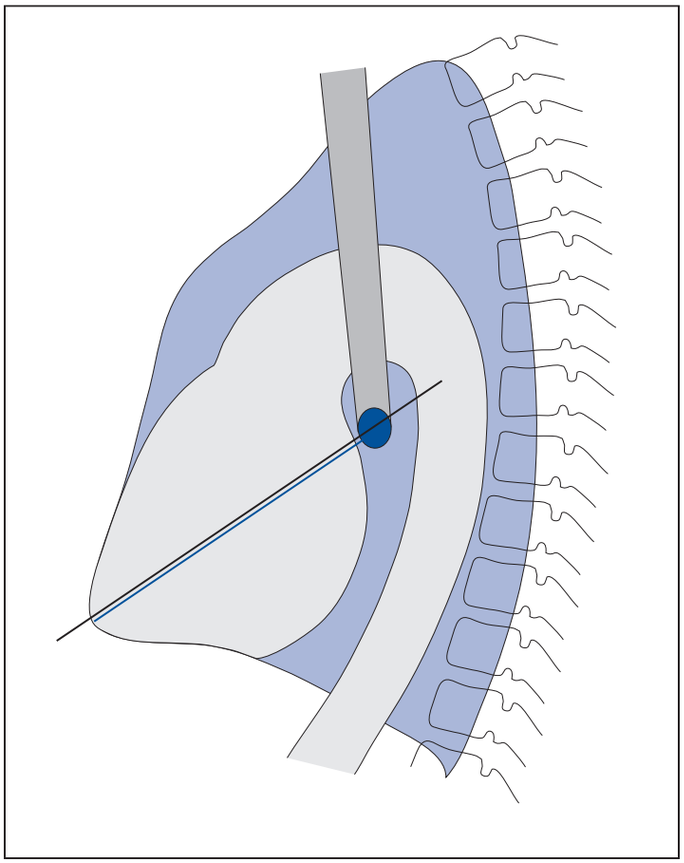

Fig. 1.47 Method for approximating the size of the right and left heart. The right heart lies above an imaginary line between the left main bronchus and the apex of the heart, while the left heart lies below it.

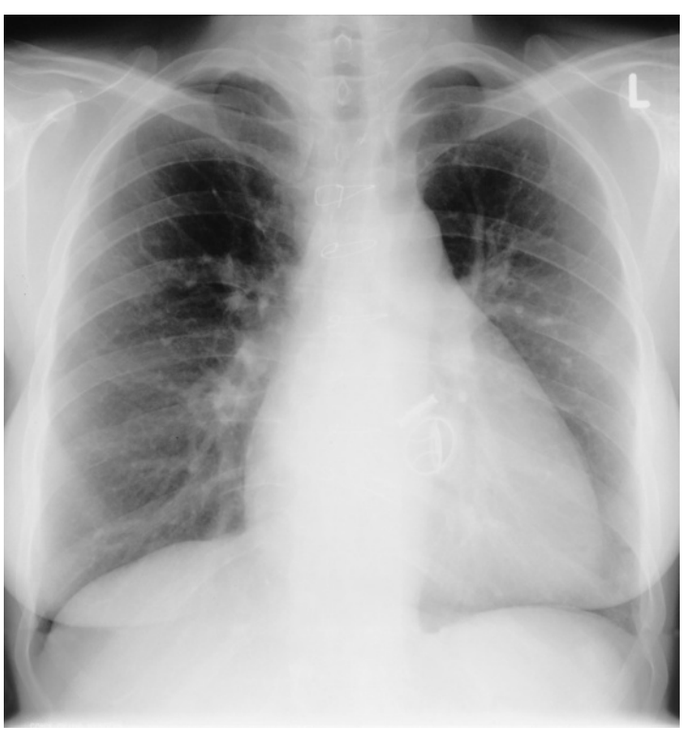

Fig. 1.48 Right ventricular hypertrophy with obliterated cardiac waist. The right ventricle and atrial level in particular are enlarged following placement of prosthetic aortic, mitral, and tricuspid valves. No decompensation.

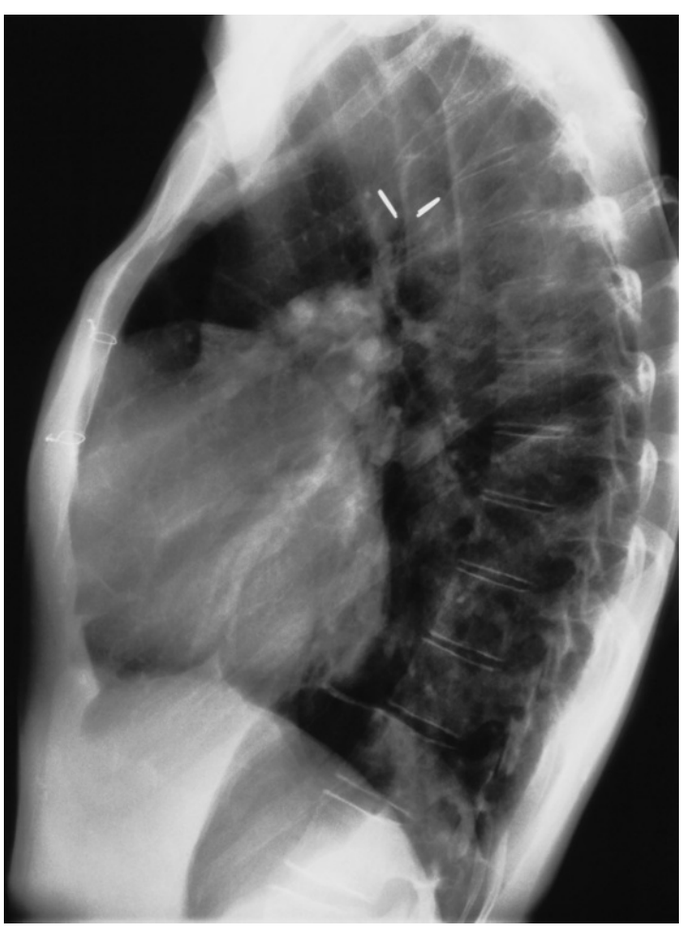

Fig. 1.49 The area of contact between the ventricle and posterior sternum is massively enlarged. The patient is a 28-year-old woman who underwent surgical correction of tetralogy of Fallot as a child. The right ventricle is now massively enlarged and is in contact with the sternum over three-fifths of its area. The sternum shows pronounced sagittal curvature.

Right Atrium

Enlargement of or increased pressure in the right atrium exhibits the following signs on the **posteroanterior radiograph**:

- Rightward widening of the heart shadow
- Craniocaudal elongation of the right arc of the heart
- Dilatation of the superior vena cava with widening of the mediastinal vascular band
- Dilatation of the azygos vein (see signs of right heart failure, p. 44)

In the normal heart, the right atrium forms the lower portion of the right mediastinal shadow, which merges cranially with the right mediastinal vascular band (right border of the superior vena cava). Enlargement of the right atrium causes the right cardiac border to project more prominently with increased rounding or craniocaudal elongation of the right arc of the heart (**Fig. 1.50, Fig. 1.52**). It would seem that conditions would be favorable for evaluating the size of the right atrium. However, this is in fact more difficult than with the other chambers of the heart, because there is no way to distinguish the relative contributions of the right atrium and ventricle in forming the abnormally expanded right cardiomediastinal shadow. Additionally, it is not easy to evaluate when exactly such a rightward shift of the cardiac border exceeds normal limits. The rule of thumb is that the distance between the right cardiac border and the midsagittal line should not exceed one-third of the right hemithorax (**Fig. 1.19**).

Atrial enlargement can be masked by leftward rotation due to right heart strain with hypertrophy of the right ventricle.

Isolated enlargement of the right atrium is rare because acquired tricuspid stenosis is extremely rare compared with mitral stenosis. Congenital tricuspid stenosis is nearly invariably accompanied by an atrial septal defect that prevents greater enlargement of the right atrium. This means that isolated enlargement of the right atrium is most commonly observed in Ebstein anomaly (**Fig. 1.51, Fig. 1.53**), a condition that will rarely not have been diagnosed before the patient is referred to the radiologist.

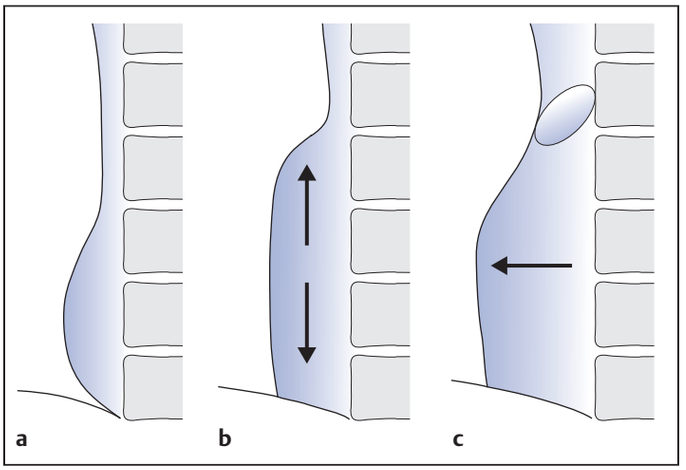

Fig. 1.50 a–c **Variations in atrial shape.** Whereas the normal atrial contour is a smooth arc (**a**), atrial enlargement manifests itself as either cranial elongation of the atrial shadow (**b**) or as rightward widening of the cardiomediastinal shadow (**c**).

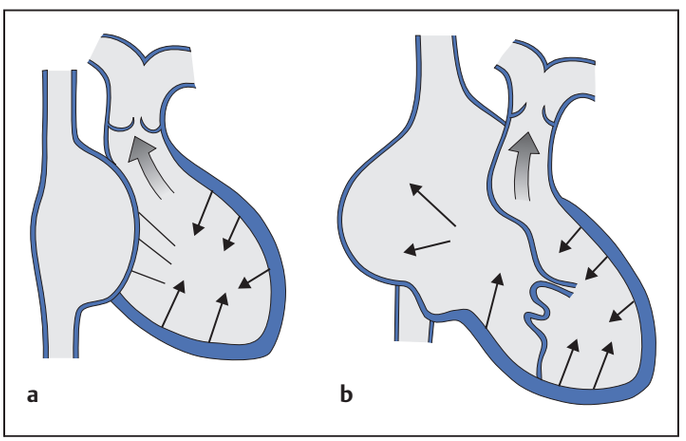

Fig. 1.51 a, b **Schematic diagram of the Ebstein anomaly.**
a In a normal heart, blood is pumped into the pulmonary trunk during ventricular systole after the tricuspid valve closes.
b Because of the displacement of the valve components in Ebstein anomaly, contraction of the right ventricle creates a pressure overload in the right atrium.

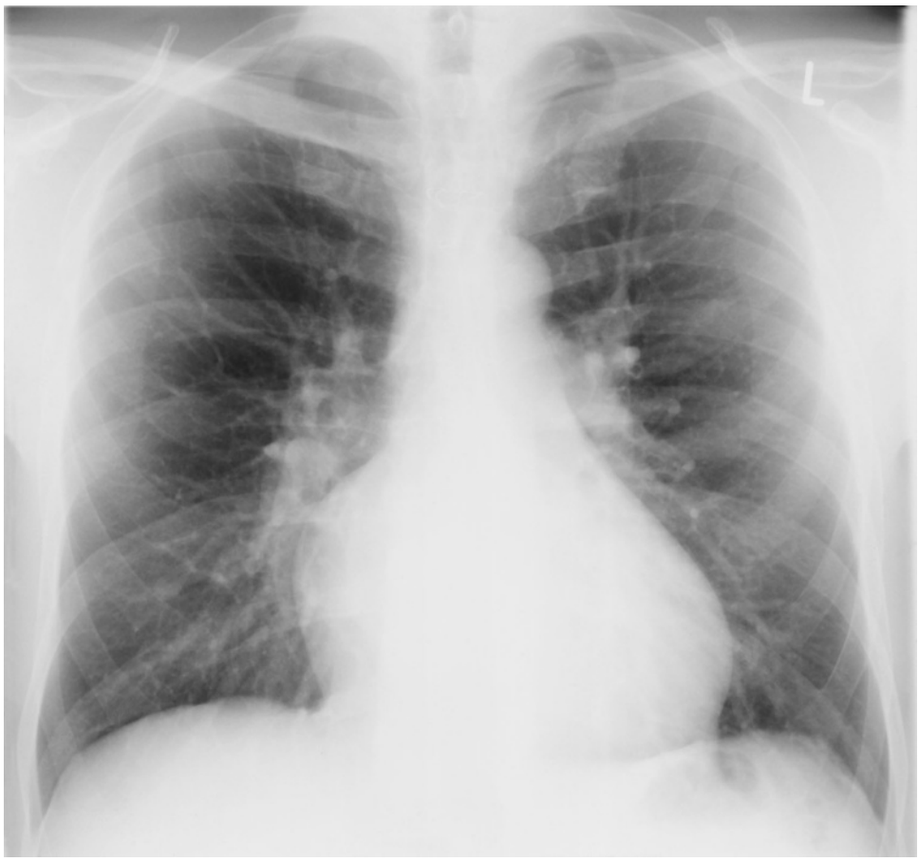

Fig. 1.52 Cranial elongation of the atrial segment in right atrial enlargement. In addition to the increased distance between the right cardiac border and the midsagittal line, there is significant cranial elongation. No signs of decompensation. Signs of chronic bronchitis.

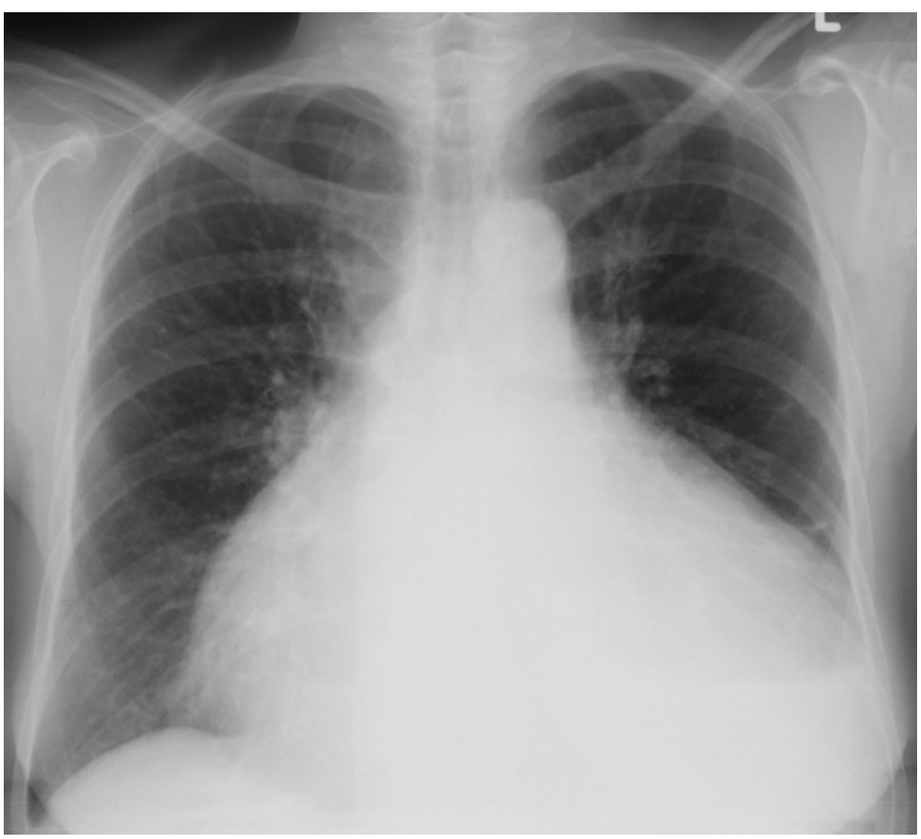

Fig. 1.53 Right atrial enlargement in Ebstein anomaly. The distance between the right cardiac border and the midsagittal line is significantly longer than half of the right hemithorax. Left heart enlargement without signs of decompensation.

A finding far more common than isolated enlargement of the right atrium is the combined enlargement of the right atrium and ventricle. This may be observed in secondary tricuspid insufficiency due to congestion in cor pulmonale. In these cases enlargement of the right heart silhouette is due to both the hypertrophic right ventricle and the enlarged right atrium. More often combined left and right atrial enlargement will occur, as is the case with atrial fibrillation (**Fig. 1.54, Fig. 1.55**).

Processes that can lead to rightward enlargement of the mediastinal shadow without atrial or ventricular enlargement must be excluded. These include (**Fig. 1.56, Fig. 1.57**):

- Pectus excavatum
- Pericardial effusion or cysts
- Most often: pleuropericardial calluses

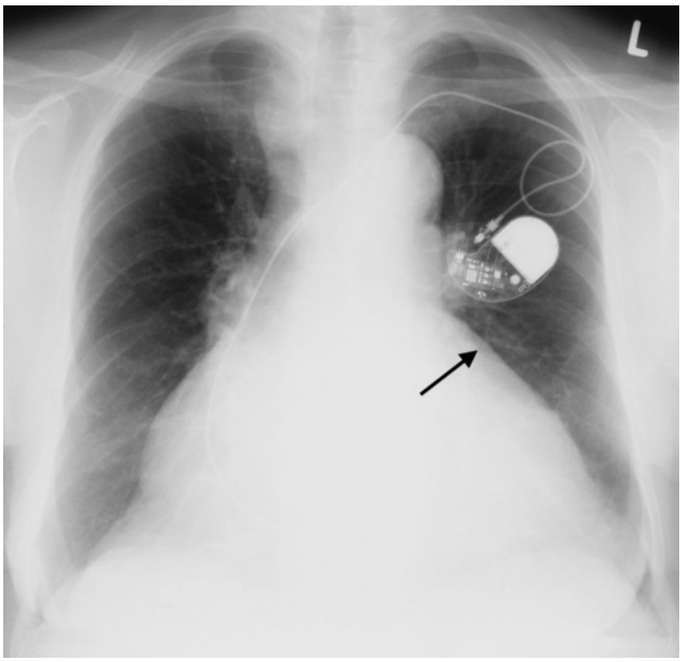

Fig. 1.54 Enlargement of both atria in atrial fibrillation. Significant right atrial enlargement and lesser left atrial enlargement (atrial appendage, black arrow). Despite concomitant aortic ectasia and arteriosclerosis, the left ventricle is only slightly enlarged. No decompensation.

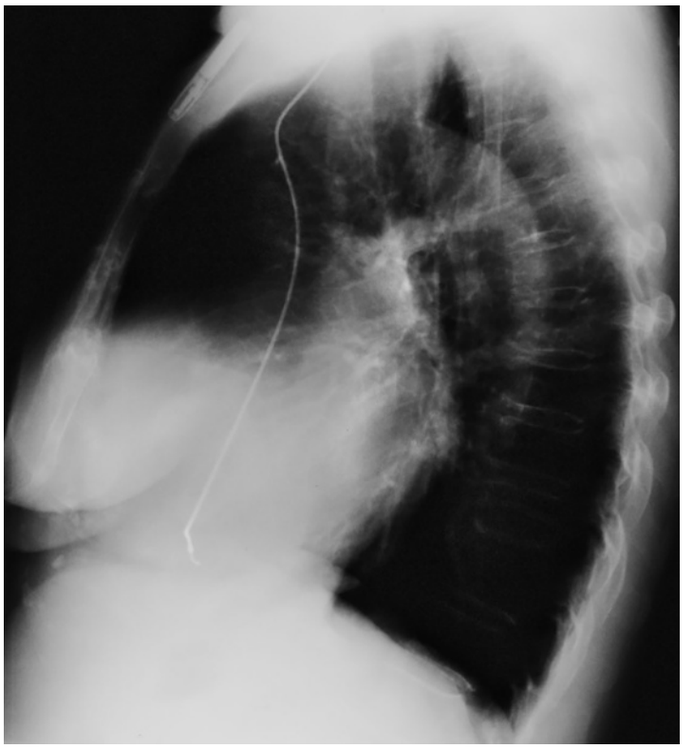

Fig. 1.55 Atrial enlargement in atrial fibrillation (lateral view of Fig. 1.54). Borderline enlargement of the right ventricle (in contact with the sternum over about one-third of its area) is seen. Protrusion into the posterosuperior cardiac shadow is indicative of left atrial enlargement.

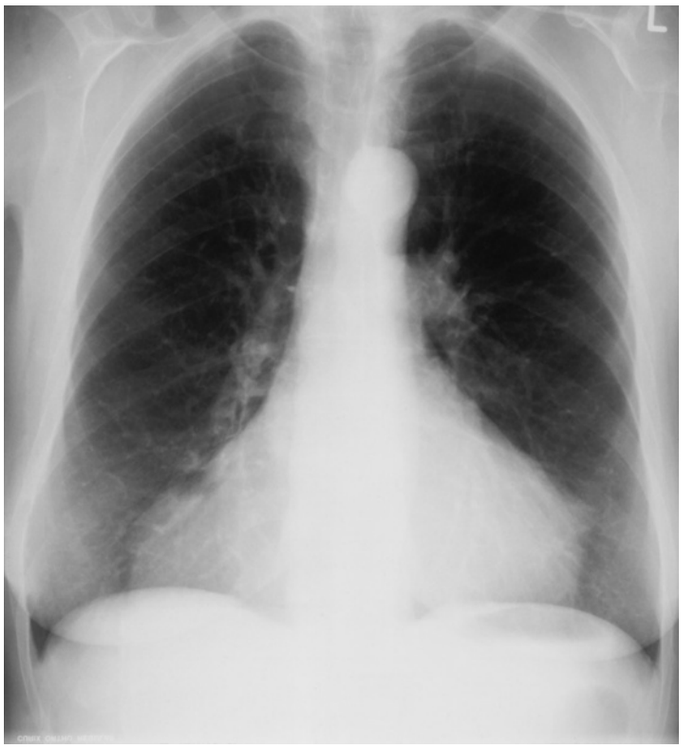

Fig. 1.56 A right epicardial fat pad simulates right ventricular enlargement. Hypertensive configuration without signs of decompensation. No infiltrates in obstructive barrel chest. There is rightward widening of the cardiomediastinal shadow.

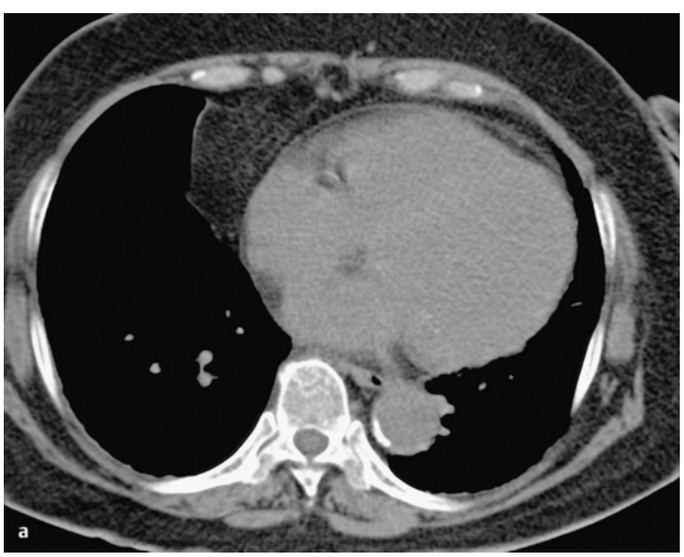

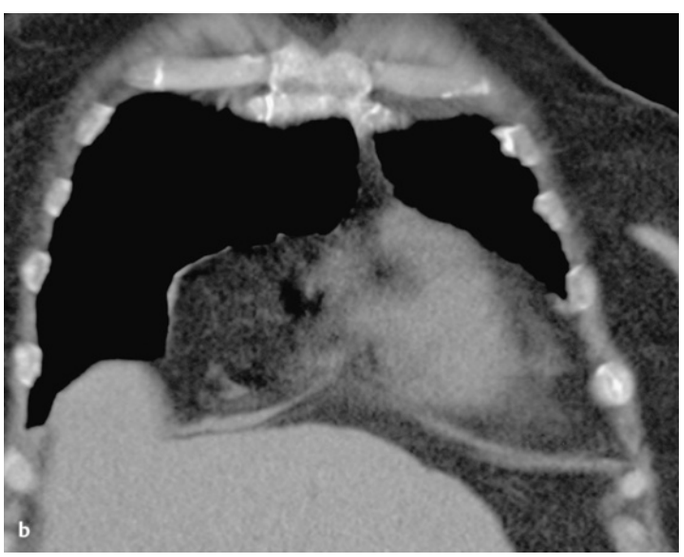

Fig. 1.57 a, b CT visualization of a right paramediastinal fat pad (same patient as in Fig. 1.56). Rightward widening of the pericardial fatty tissue.

Left Heart Failure

Excursus: Pathophysiology

The terms left heart failure and pulmonary congestion are often used rather loosely in clinical practice (**Table 1.3**).

Table 1.3 Terminology of pulmonary congestion in the presence of an increased volume of blood in the pulmonary vessels

Active congestion	Passive congestion
Increased pulmonary blood flow in the capillaries:	Increased pressure in the venous capillaries:
▶ Left-to-right shunts	▶ Left heart failure
▶ Thyrotoxicosis	▶ Constrictive pericarditis
▶ Increased blood volume	▶ Mitral valve defect
▶ CNS dysregulation	▶ Left atrial thrombosis
	▶ Endocardial fibroelastosis

Sources of Error

Underexposure, especially in obesity, or poor inspiration often simulate congestion (**Fig. 1.59, Fig. 1.60**). The combination of underexposure and poor inspiration makes the radiograph disproportionately more difficult to interpret with respect to possible congestion. In such cases, it can be helpful to compare the posteroanterior and lateral films. A degree of "learning effect" with deeper inhalation is apparent on the second radiograph when the patient is requested to inhale.

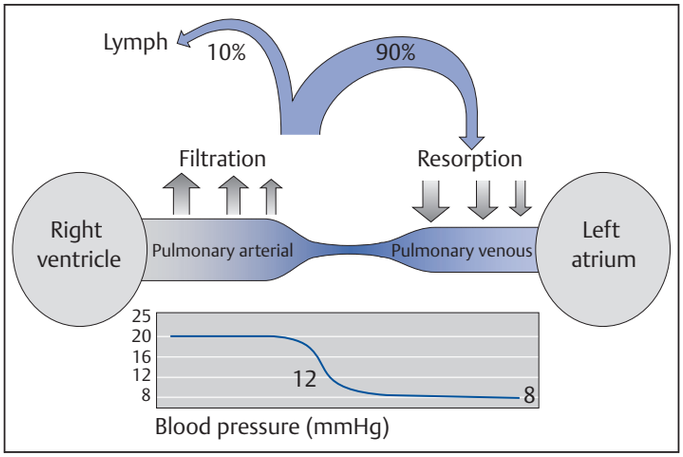

Fig. 1.58 Starling's hypothesis. Pulmonary arterial filtration and oncotic resorption in the postcapillary venules are nearly in equilibrium (10% of the volume drains through the lymphatic system). This equilibrium may be disturbed, for example, by an increase in intracapillary pressure on the venous side (left heart failure).

Notes on Physiology and Clinical Findings

Starling's model of capillary fluid exchange is fundamental to an understanding of the radiologic symptomology of left heart failure (**Fig. 1.58**). According to this hypothesis, the hydrostatic and oncotic pressure gradients between the interior of the capillaries and their surroundings decisively influence filtration (precapillary arterioles) and absorption (postcapillary venules). The relatively thin walls of the capillaries have pores of ~ 8 nm that permit the passage of substances dissolved in the plasma together with water, whereas blood cells and large protein particles remain within the vascular lumen. On the venous side of the capillary network, the intracapillary oncotic pressure due to water loss promotes resorption. However, ~ 10% of the filtered water is not absorbed but remains in the tissue and only rejoins the circulatory system indirectly via the lymphatic system. This model provides a simple explanation for the mechanism underlying pulmonary edema in decompensation of the left heart (increase in intracapillary pressure on the venous side). It also explains the development of other pulmonary edemas from causes unrelated to heart disease (changes in blood pressure on the arterial side, changes in blood pressure on the venous side, increased permeability for proteins, reduced lymph drainage, etc.).

Causes of left heart failure include:

- ▶ Acute hypertensive crisis
- ▶ Defects (aortic stenosis, mitral valve insufficiency, aortic insufficiency)
- ▶ Myocardial damage (ischemic, infectious, toxic, metabolic)

Left heart failure manifests itself as:

- ▶ "Forward" failure with weakness and oliguria
- ▶ "Backward" failure with abnormal filling of the pulmonary capillaries

The symptoms of backward failure predominate in the clinical picture with:

- ▶ Dyspnea during physical exertion
- ▶ Orthopnea
- ▶ Paroxysmal dyspnea (usually at night)

The constriction of peripheral vessels required for maintaining blood pressure and the resulting ischemia is less clinically apparent.

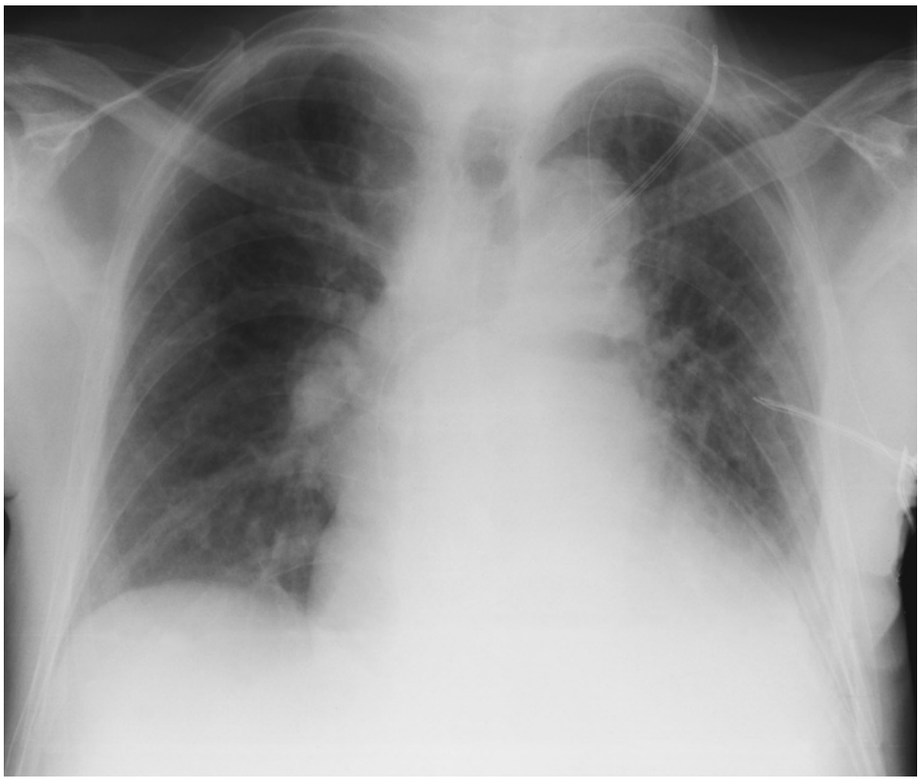

Fig. 1.59 Influence of inspiration on signs of congestion. Postoperative radiograph of an 80-year-old woman to verify proper catheter position. With poor inspiration, the film shows what appears to be left heart enlargement and broad contact with the diaphragm. A minor effusion is present on the left side. It is not clear whether infiltrates are also present.

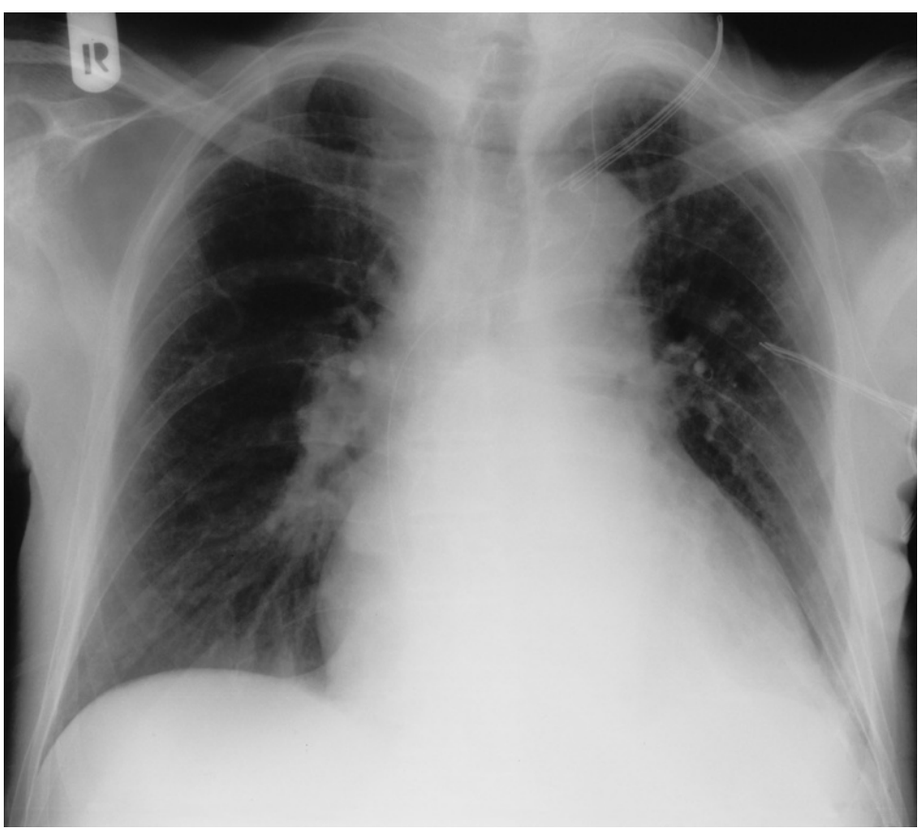

Fig. 1.60 Same projection as in Fig. 1.59 repeated with improved inspiration. The film now shows left heart enlargement without signs of decompensation. Infiltrate is present in the left lower lobe with minor associated effusion.

Acute left heart failure is most commonly caused by a hypertensive crisis. Radiographic signs on the plain chest radiograph obtained with the patient standing include:

- Redistribution of pulmonary perfusion
- Presence of interstitial patterns (Kerley lines, peribronchial cuffing)
- Alveolar densities with indistinct vascular structures (advanced stage)
- Pleural effusions

All of these signs are essentially attributable to increased fluid content in the abnormally heavy "wet" lung. The fluid accumulation follows gravity.

Redistribution

Changes in perfusion indicative of left heart weakness involve redistribution from the basal segments into the apical segments of the lungs. These changes can be diagnosed on the radiograph before the diagnosis of left heart failure can be made by auscultation. Lung perfusion in the erect patient is physiologically more pronounced in the basal segments than in the upper lobes (**Fig. 1.61**). The plain chest radiograph obtained with the patient standing shows that both the pulmonary arteries and the pulmonary veins in the basal segments lie closer together and exhibit greater diameter than those of similar size in the apical segments.

When you check laundry drying on a clothesline, you always feel the lower end. This is where the socks take longest to dry.

The capacity for diffusion is initially decreased in the flooded basal segments where the fluid accumulation begins. As a result, what is known as the Euler–Liljestrand mechanism reduces the normally greater basal perfusion in favor of the better-ventilated apical segments. This leads to greater prominence of the upper field vessels. As it is not easy to determine size on the plain chest radiograph, pragmatic compromises may be considered:

- Compare pulmonary vessels that are equidistant to a central point in the respective hilum.
- Compare the diameter of a random easily identifiable superior lobe artery (often the anterior segmental artery is most easily identifiable) with the diameter of the corresponding ipsilateral bronchus (**Fig. 1.62**).

As the pulmonary artery and corresponding ipsilateral bronchus are normally of precisely equal diameter, a larger arterial diameter is indicative of redistribution of perfusion (**Fig. 1.63**). The diagnostic criteria of caudal-to-cranial redistribution cannot be evaluated on radiographs obtained in the supine patient. This is another argument in favor of comparing the calibers of the pulmonary artery and the ipsilateral bronchus. The physiologic redistribution from posterior to anterior on the supine radiograph necessarily involves a caliber increase in the anterior segmental artery compared with the ipsilateral bronchus.

Expansion of the pulmonary artery in beginning pulmonary arterial hypertension (as in chronic obstructive pulmonary disease [COPD]) can simulate the redistribution of pulmonary perfusion. The decisive diagnostic criterion is such cases is the comparison with farther peripheral vessels that tend to be narrowed in pulmonary arterial hypertension (**Fig. 1.64**). Here, as always in such cases, the comparison should be made between arteries of the appropriate order in the vascular tree. For example, it would be a serious diagnostic error to compare a subsegmental artery with a segmental artery.

Redistribution can be absent in apical emphysema (**Fig. 1.65**).

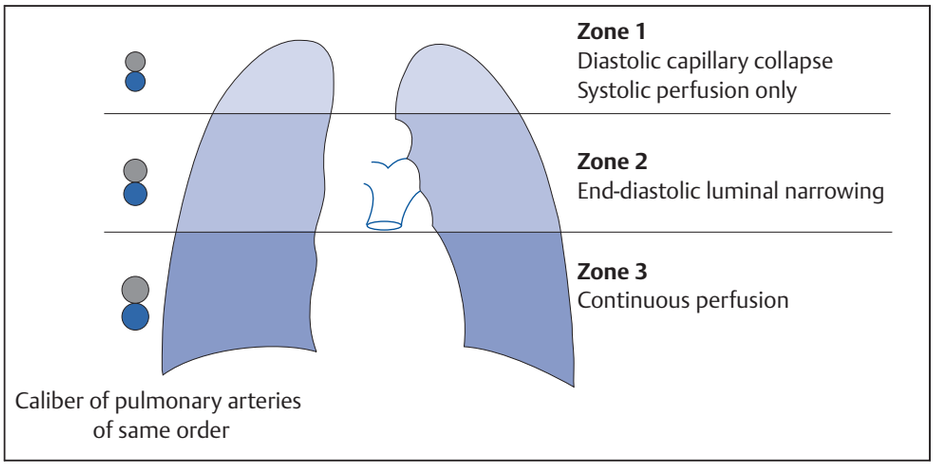

Fig. 1.61 Theory of pulmonary perfusion. Bjure and Laurell described the reduced vascular filling in the apical lung segments compared with the base of the lung as early as 1927. This increased basal perfusion is attributable to the hydrostatic pressure (approx. 12 mmHg), which is added to the blood pressure (systolic 25 mmHg, diastolic 8 mmHg).

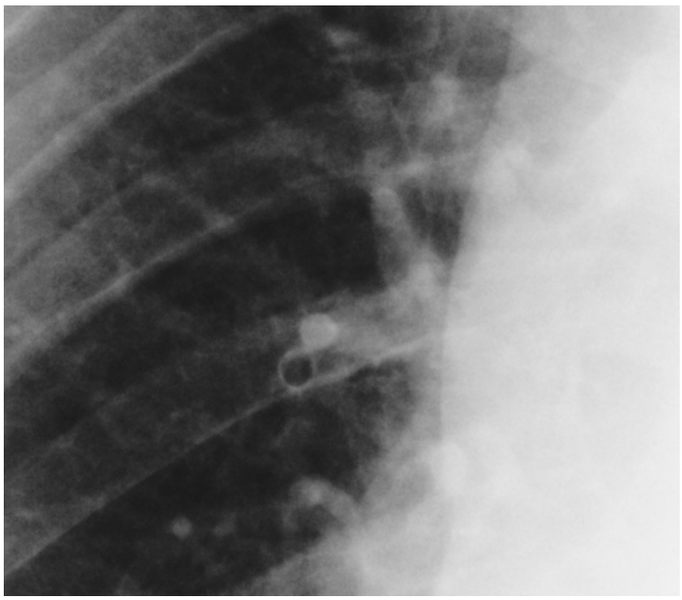

Fig. 1.62 Identical diameter of the anterior segmental artery and the accompanying bronchus (detail).

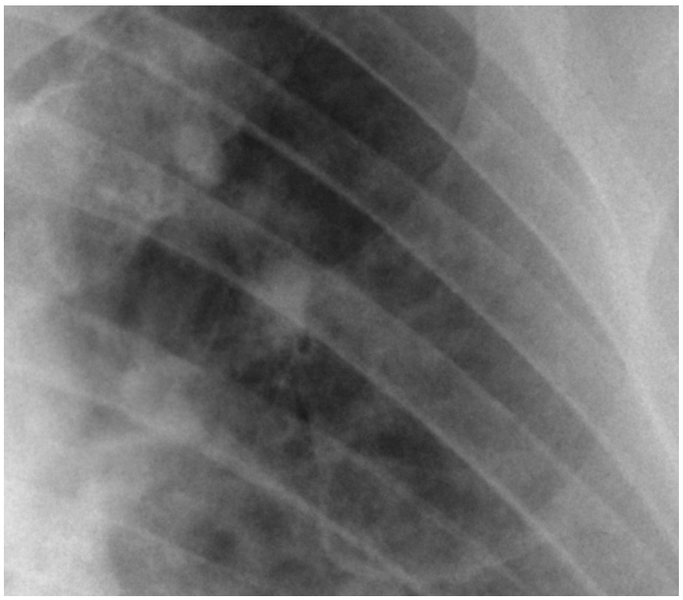

Fig. 1.63 Redistribution of pulmonary perfusion indicative of left heart failure. The detail shows a mismatch between the diameter of the slightly blurred segmental artery and the anterior upper lobar bronchus with wall thickening.

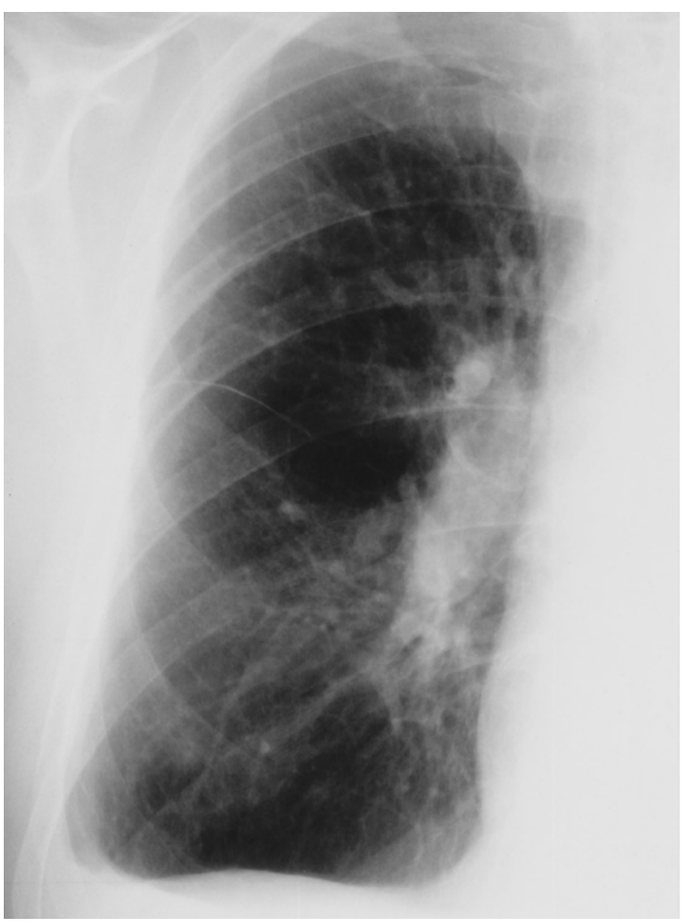

Fig. 1.64 Mismatch between the bronchial lumen and the accompanying artery in COPD. The relative increase in the size of the pulmonary artery compared with the bronchus results from the increased pulmonary arterial pressure and not from redistribution. Barrel chest in emphysema.

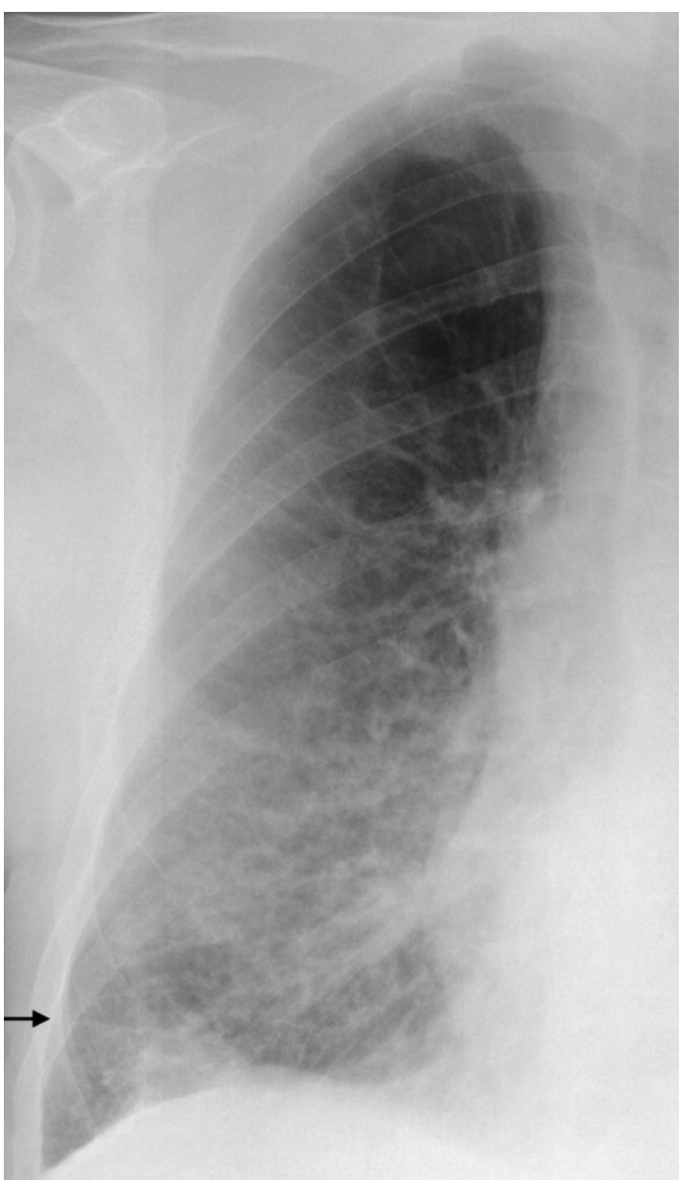

Fig. 1.65 Lack of redistribution in apical emphysema. Obstructive barrel chest in apical emphysema. Hypertensive configuration with definitive signs of congestion with Kerley lines (black arrow) and the onset of central blurring. Redistribution cannot develop due to emphysematous remodeling. ▶

Interstitial Edema

Increasing accumulation of intrapulmonary fluid leads to development of an interstitial edema (**Fig. 1.67**). The edematous fluid saturates the pulmonary interstitium, and the lymphatic system at this site is filled with hypocellular fluid and greatly dilated. Interstitial pulmonary edema can represent the onset of or a residual finding in edematous exudation of the lung.

Radiologic signs of interstitial pulmonary edema include:

- Thickened lymph vessels in the interlobular septa (**Kerley lines**)
- Peribronchial cuffing due to dilated lymph vessels coursing in the edematous wall of the bronchi

Kerley Lines (Fig. 1.66)

The most important sign of interstitial pulmonary edema is fine horizontal lines located primarily in the lower lung fields. Not always discernible on textbook images, these lines were first described by Kerley in conjunction with mitral stenosis and the resulting increased pressure in the pulmonary venous system. Named after him, these lines (**Fig. 1.66**) are initially visible as horizontal line shadows in the costophrenic angles of the lower lung fields (Kerley B lines). They measure up to 3 cm in length and 1–2 mm in width. Kerley B lines are distinguishable from discrete plate atelectasis by their typical stacked configuration (**Fig. 1.67**).

Kerley **B** lines occur primarily in the basal segments and course horizontally to the pleura, where they lead to pleural effusion. Remember: "Kerley **B** lines → **B**leura."

Kerley distinguished a second type of line from the B lines. These A lines course from the hilum to the periphery. These lines are attributable to edematous perivascular or peribronchial lymphatic channels (**Fig. 1.67**). C lines do not correspond to strictly linear changes but form a network of fine stripes (**Fig. 1.67**). Retrosternal Kerley lines coursing vertically are occasionally observed on the lateral radiograph. They are referred to as Kerley D lines but are essentially the same as Kerley B lines.

Peribronchial Cuffing

Edematous thickening of the bronchial wall due to lymphatic congestion is visualized on the posteroanterior radiograph as a well-defined ring structure, again usually in the vicinity of the anterior segmental artery (**Fig. 1.67**). In fact, a term like "donut" would be more informative than the ususal term peribronchial "cuffing". The thickening of the bronchial wall due to lymphatic congestion must be differentiated from bronchial wall thickening from other causes such as chronic bronchitis (mucosal edema, muscle hypertrophy). The presence of isolated peribronchial cuffing must not be interpreted as a sign of lymphatic congestion.

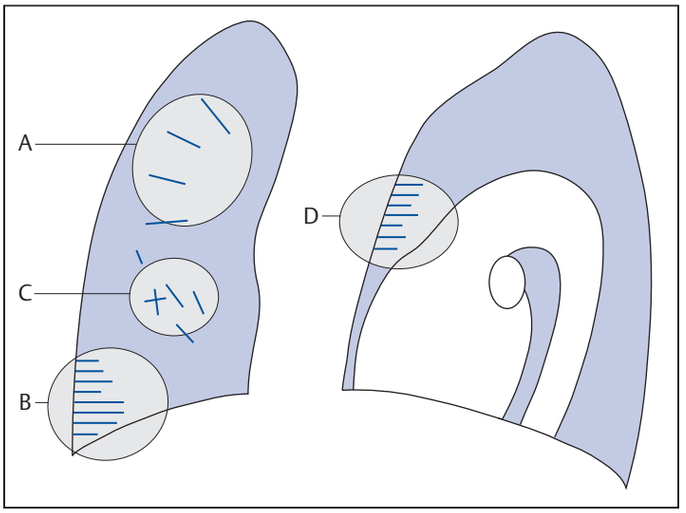

Fig. 1.66 Schematic diagram of the terminology of Kerley lines.

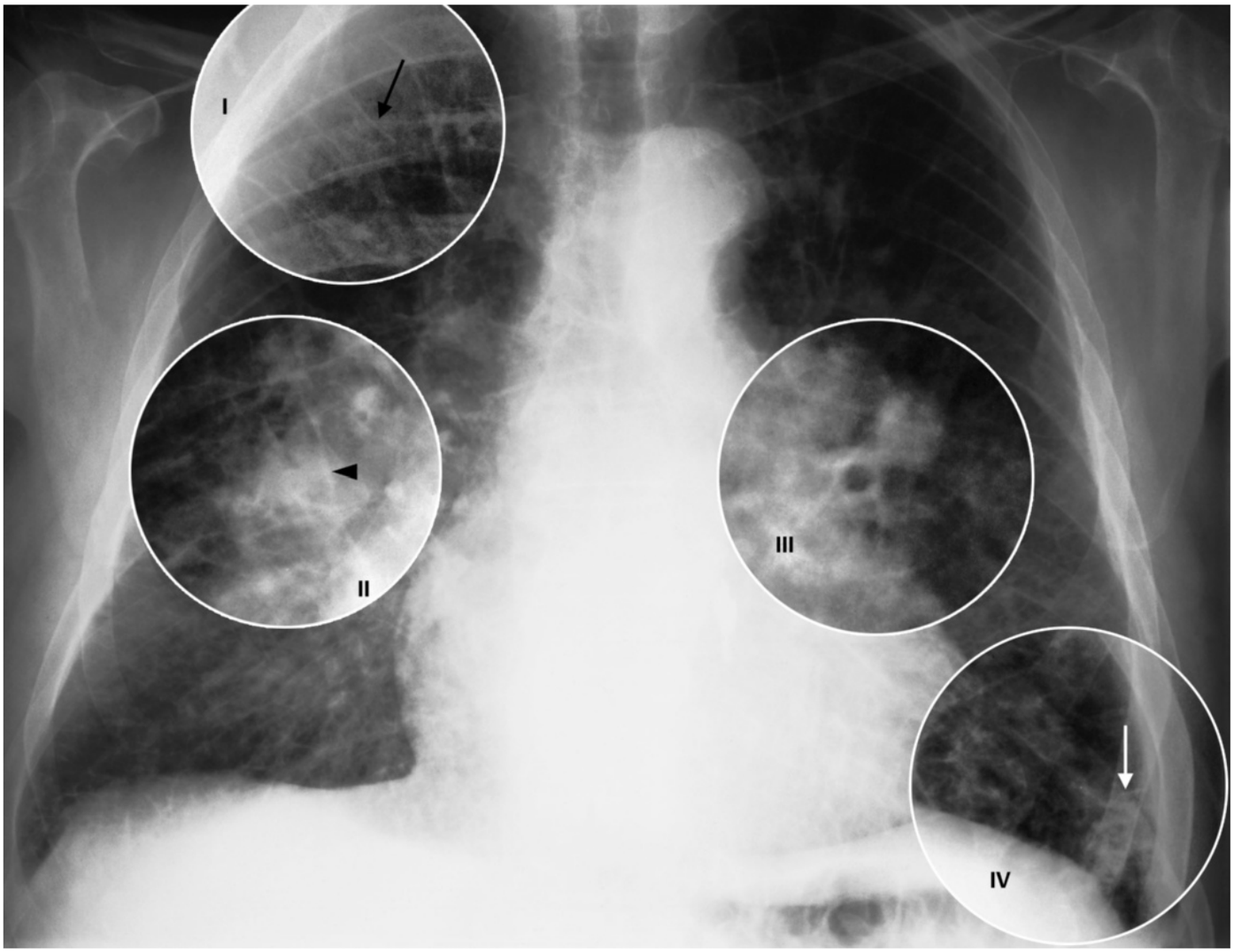

Fig. 1.67 Various examples of Kerley lines.
Pulmonary interstitial edema. Left heart enlargement is accompanied by findings of redistribution and significant septal thickening with Kerley lines. Bilateral effusions in the costophrenic angles. Initial blurring of vascular structures is seen in the right central region.

(I) Kerley A lines. The dilated lymph vessels coursing toward the hilum (black arrow) appear as radial streaky densities 1–2 cm long and less than 1 mm wide.

(II) Kerley C lines (detailed view of right middle lung field). Interstitial lines coursing neither radially nor horizontally to the pleura (black arrowhead).

(III) Peribronchial cuffing. Thickening of the bronchial wall appears as a ring when visualized end-on and resembles a tram line when visualized tangentially.

(IV) Kerley B lines. The fine, nearly horizontal line measuring 1 cm (white arrow) can be traced to the visceral pleura. The pleura is already slightly shifted away from the chest wall. An effusion is developing here in the costophrenic angle.

Alveolar Edema

Alveolar edema can develop gradually from interstitial pulmonary edema, or it can occur as an acute condition. The latter may often be observed in younger patients with no prior history of heart failure, for example in the first heart attack with cardiogenic shock.

Radiologic signs of interstitial alveolar edema include:

- Blurring of anatomic structures
- Acinar patches
- Cloudy opacities

The increased radiodensity of the pulmonary parenchyma initially manifests itself as blurring of the hilar shadow with ill-defined contours and broadening of the central vessels (**Fig. 1.69**).

Back in the days when chalkboards were used in lecture halls, it was easier for instructors to explain these radiographic signs. All they had to do was to smear the chalk sketch of the pulmonary vessels with their hand.

The loss of definition is due to the reduced difference in absorption between the visible lung structures (essentially blood vessels and large bronchi) and the normally invisible air-filled spaces. As the fluid content of the alveolar air spaces increases, the other structures become less distinct.

Aside from formation of small acinar patches (acinar pattern, **Fig. 1.70**) an increasing alveolar edema blurs the contours of anatomic structures. Confluent patches can coalesce into extensive shadows that vary depending on patient positioning (**Fig. 1.71**).

As the condition progresses further, cloudy opacities begin to appear in the basal lung segments. These can later form large, confluent area densities (**Fig. 1.68**). These patches occasionally spread out in a “butterfly” or “bat’s wing” pattern from the hila to the periphery of the lungs.

The alveolar densities of pulmonary edema are essentially indistinguishable from pneumonic exudate. Differential diagnosis is made on the basis of clinical findings and the course of the disorder. Additionally, the alveolar densities do not necessarily affect both lungs to the same extent. Note whether the patient prefers to lie in a lateral position. In addition to these mechanical influences, preexisting areas of induration or emphysematous segments also contribute to uneven distribution of alveolar pulmonary edema (**Fig. 1.76**). Especially where it exhibits an uneven focal distribution, edema is distinguishable from focal patches of pneumonia only by observing the clinical course of the disorder.

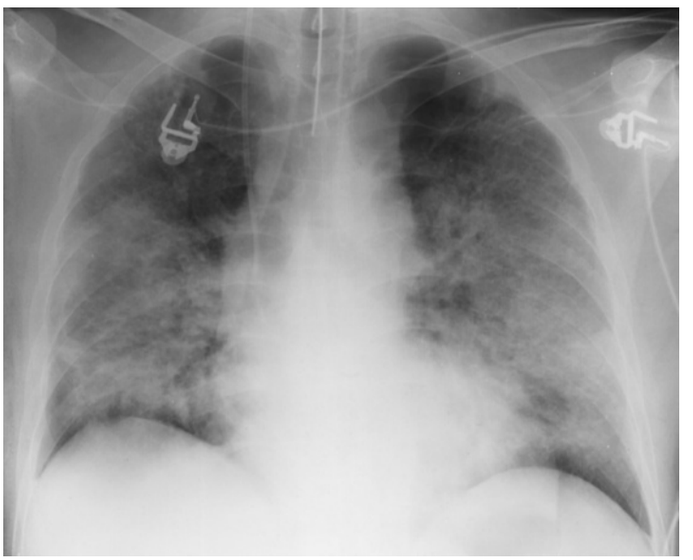

Fig. 1.68 Butterfly edema in cardiac decompensation. Symmetrical area shadowing is seen in the central region of both lungs. Left heart enlargement with apical bullous emphysema. An endotracheal tube is in place.

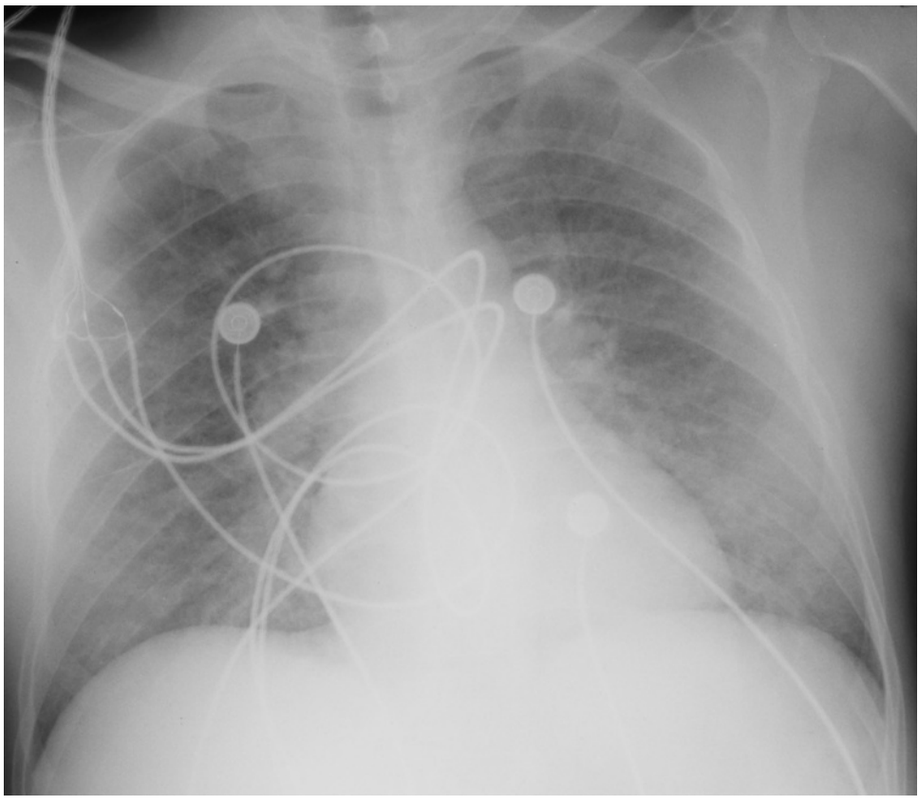

Fig. 1.69 Cardiogenic shock following an initial massive myocardial infarction. The patient is a 48-year-old man with acute coronary syndrome. Findings include a severe alveolar pulmonary edema with only a moderately enlarged heart. Vascular structures are blurred. No effusion. The patient died 3 hours after the radiograph was obtained.

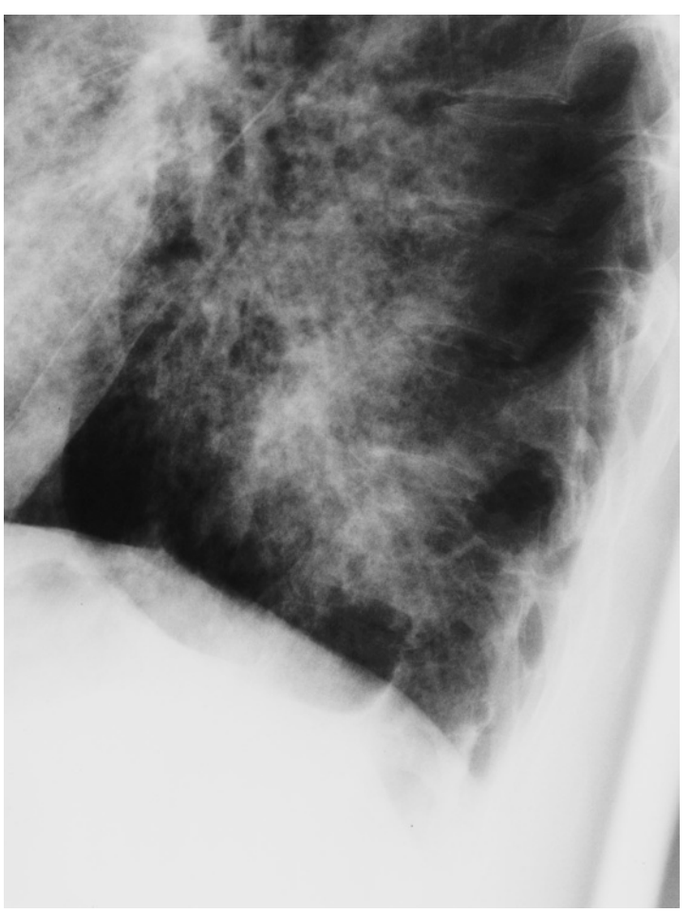

Fig. 1.70 Acinar pattern in alveolar pulmonary edema primarily involving the central lung. Multiple, partially confluent round patches measuring 2–5 mm in diameter. Interstitial shadowing is largely absent.

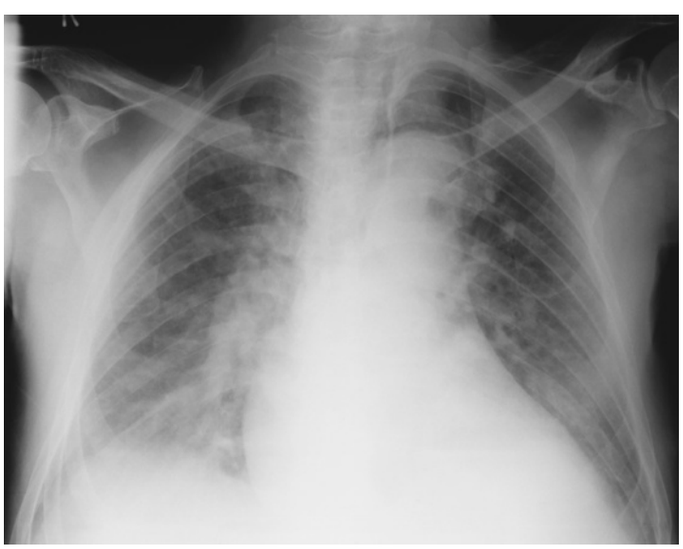

Fig. 1.71 Alveolar pulmonary edema showing beginning consolidated areas. Findings include significant left heart enlargement with massive congestion in the pulmonary veins, peribronchial cuffing, and pleural effusions. Central vascular structures are blurred and there are consolidated areas in the lower lung fields.

Computed Tomography

CT signs of interstitial edema in left heart failure include (**Fig. 1.73**):

- Thickening of the posterior basal interlobular septa
- Prominence of other intralobular septa

The thickened interlobular septa in the peripheral regions close to the pleura represent the Kerley B lines.

Alveolar fluid accumulations produce widely varied patterns on CT images. Occasionally these patterns can be seen to blend and can occur in various combinations. They include:

- Symmetrical distributions of ground-glass opacities in the dependent part of the lung
- Symmetrical "bat's wing" or "butterfly" edema centered on the perihilar region
- Finely nodular centrilobular patches
- Disseminated irregular nodular pattern of ground-glass opacities
- Rapid, dynamic development

What is referred to as an acinar pattern on the conventional radiograph with a diffuse distribution of fine patches, appears on CT as a diffuse centrilobular pattern (**Fig. 1.74**). It is significantly less common than the faint gravity-dependent and therefore primarily basal shadows that are described as having a ground-glass appearance. Ground-glass opacities are defined as areas of increased attenuation that preserve the underlying anatomic structure (secondary lobule with central artery and border). On the plain chest radiograph the shadows are located in the central and basal regions. However, on CT they appear to vary with posture. This means that the shadows increase from anterior to posterior (**Fig. 1.75**). Typically, they increase only as far as each interlobar fissure and then begin again (**Fig. 1.72**).

Additionally, fluid accumulations will typically occur bilaterally and symmetrically in lungs without any preexisting pathology. The "butterfly" edema is a special case. Ground-glass opacities limited strictly to secondary lobules, which occur irregularly, primarily in the upper lung fields, and simultaneously with irregular lung perfusion (as in emphysema patients) represent a formidable diagnostic challenge for both conventional radiography and CT (**Fig. 1.76**). Such cases can often be diagnosed only in conjunction with the clinical course. Rapid, dynamic development is a common feature of all patterns of fluid accumulation.

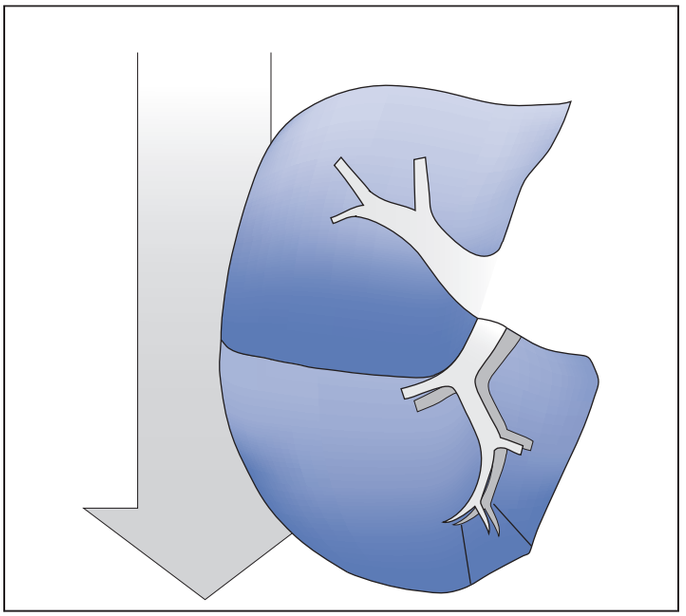

Fig. 1.72 **The ground-glass patterns show postural movement.**

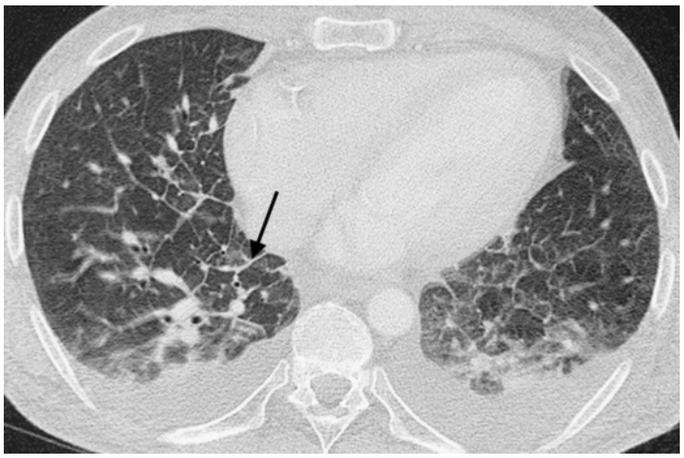

Fig. 1.73 Interstitial pattern on CT. Thickening of the interlobular septa (black arrow). Findings include bilateral pleural effusions with reduced ventilation in the posterobasal segments and an alveolar edema beginning in the left posterior region.

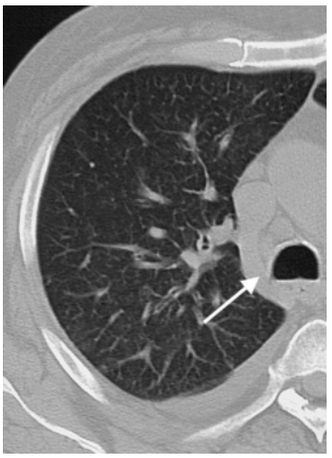

Fig. 1.74 CT in overhydration. Diffuse, finely nodular, and septal shadowing. Prominent azygos vein (white arrow) and effusion in the costophrenic angle. Note that individual mediastinal lymph nodes are enlarged.

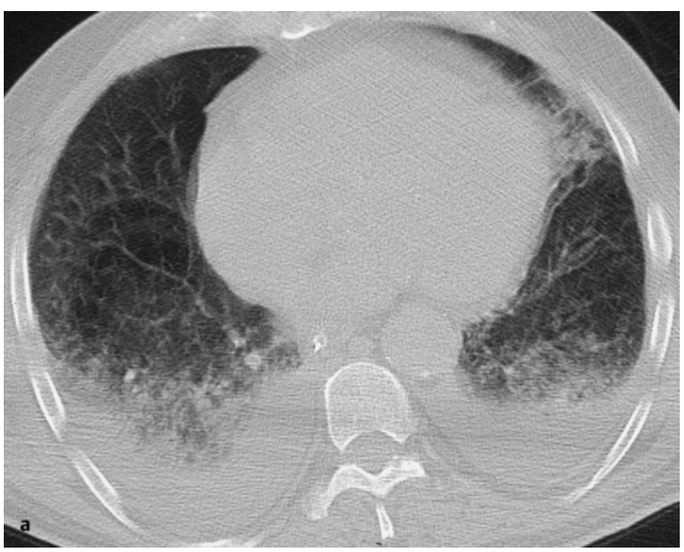

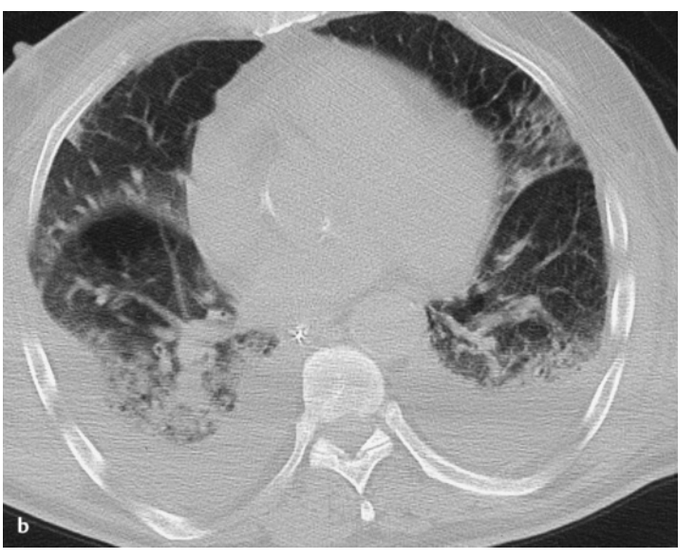

Fig. 1.75 a, b Pulmonary edemas show postural movement on CT.

a Posteriorly increasing ground-glass opacities and bilateral effusions.

b The opacities increase as far as each interlobar fissure, then they begin again.

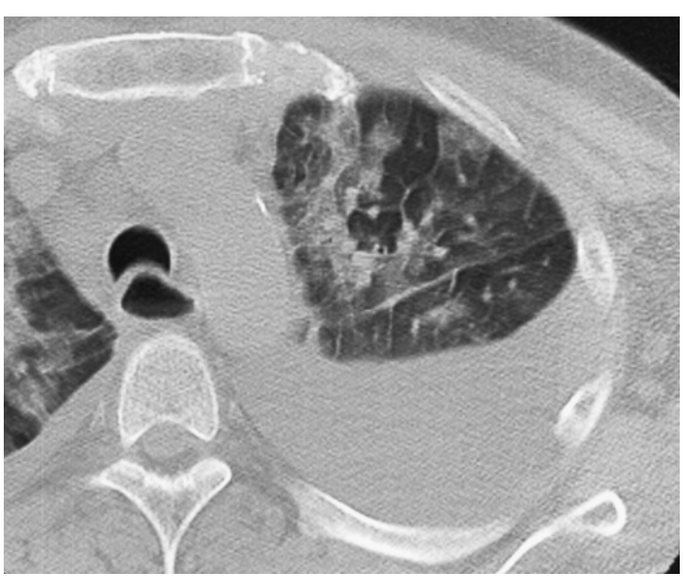

Fig. 1.76 Uneven distribution of the intrapulmonary fluid accumulation in a lung with preexisting pathology. This emphysematous lung exhibits a highly irregular pattern of fluid accumulation in alveolar edema.

Resolution and Chronic Congestion

Resolution of Congestion

The faint shadows can often resolve within a very short time as the edema is resorbed (**Fig. 1.78, Fig. 1.79**). The reticular densities of interstitial pulmonary edema then reappear. This is occasionally misinterpreted as an increasing interstitial edema.

Note that as the signs of congestion resolve (lumen of the anterior segmental artery again matches that of the accompanying segmental bronchus; Kerley lines resolve as the interlobular septa return to normal size), a corresponding increase in pleural effusions can initially occur (**Fig. 1.77**). This must not be interpreted as a sign of increasing congestion, as it is indicative of the repair process still in progress. Fluid from the interlobular septa collects in the pleural space, draining there via the Kerley B lines in particular.

In this context, Milne referred to the pleural space as the "vacuum cleaner bag" of the lymphatic cleaning crew. Once the apartment is halfway dry again, the bags will be well filled.

Chronic Congestion: Residual Findings

Whether compensation has been completely reestablished in the presence of signs of chronic congestion is a very difficult question. It is often answered only by observing the clinical course of the disorder (**Fig. 1.80, Fig. 1.81**). Radiologic sequelae of left heart failure include:

- Increased interstitial shadowing
- Very finely nodular opacities
- Peribronchial cuffing

One should meticulously compile and evaluate a synopsis of all findings including clinical data. Do not paint yourself into a diagnostic corner in those cases where everything is "simply bone dry." Diagnostic radiography is not always as definitive as it appears. Ask the following questions:

- Are inspiration and exposure sufficient?
- Is the heart really enlarged and if so, where?
- Is there redistribution?
- Or are signs of chronic bronchitis with pulmonary arterial hypertension present?
- Is additional fibrotic shadowing present that would indicate chronic emphysematous bronchitis?

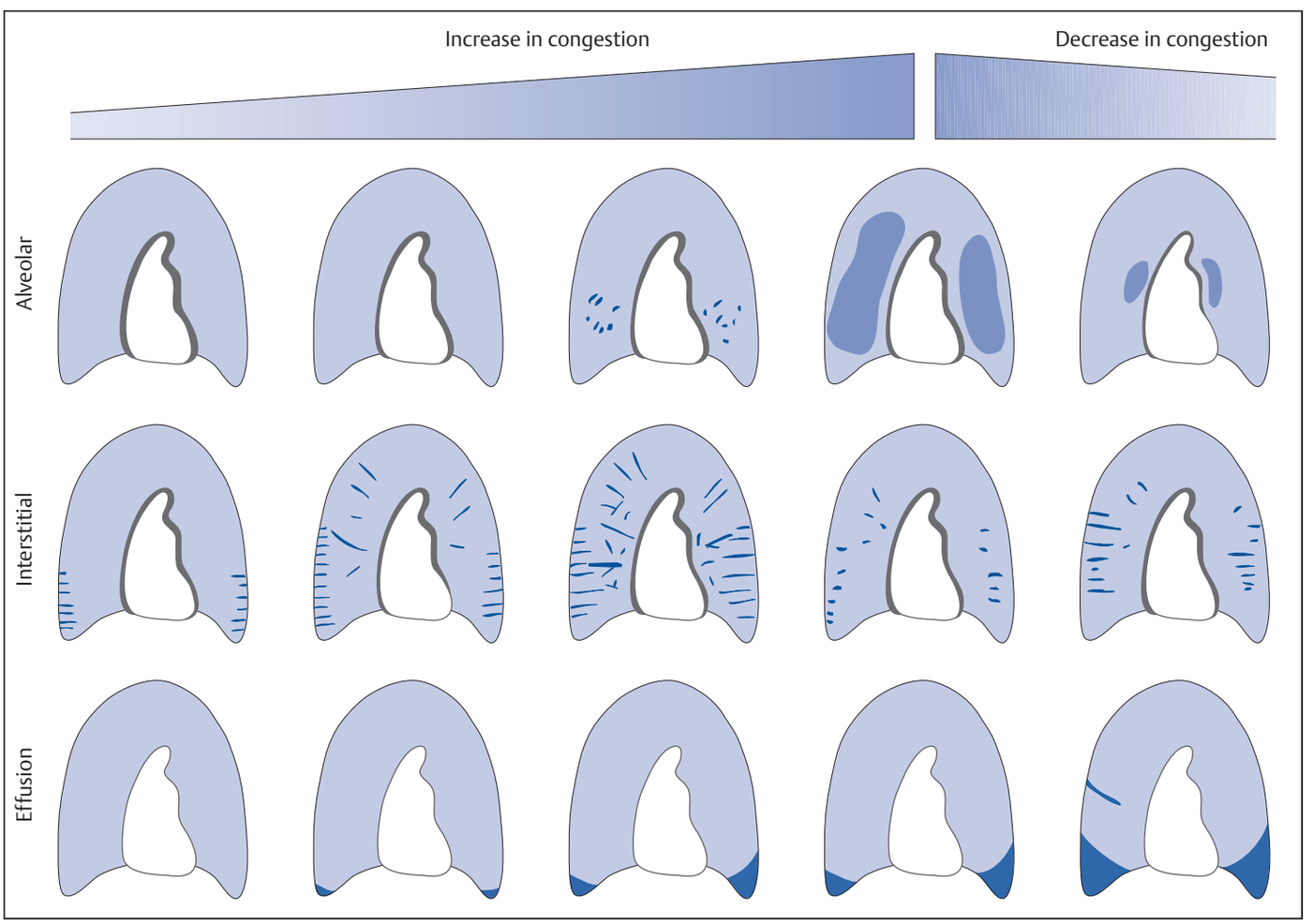

Fig. 1.77 Radiologic signs of congestion in decompensation and reestablishment of compensation. With increasing congestion, the first signs to appear are those of interstitial edema. These signs become less distinct as the alveolar pattern emerges and more distinct again as the alveolar edema resolves. Effusions can increase as congestion resolves.

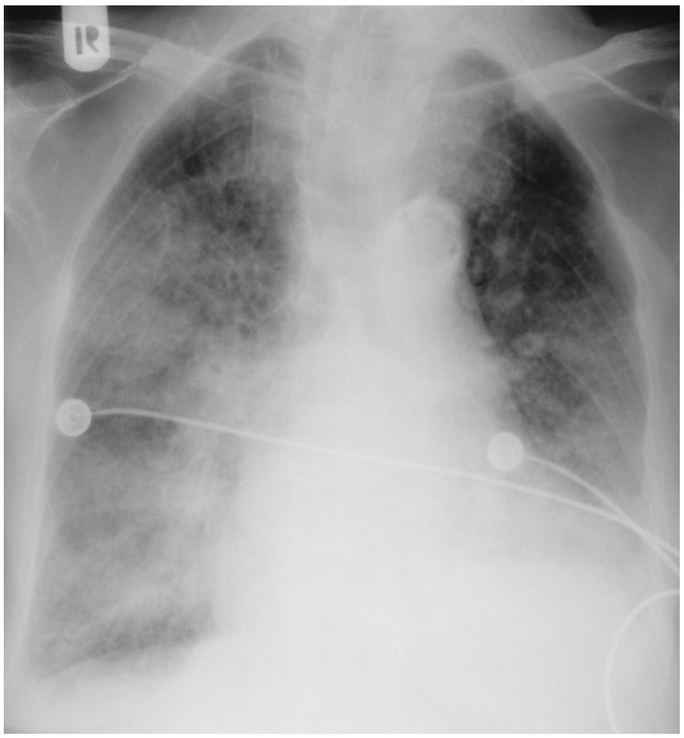

Fig. 1.78 Follow-up of resolving alveolar edema in left heart decompensation. Findings in left heart enlargement include significant decompensation with congested veins, redistribution, and alveolar area densities in circumscribed locations in the presence of senile emphysema.

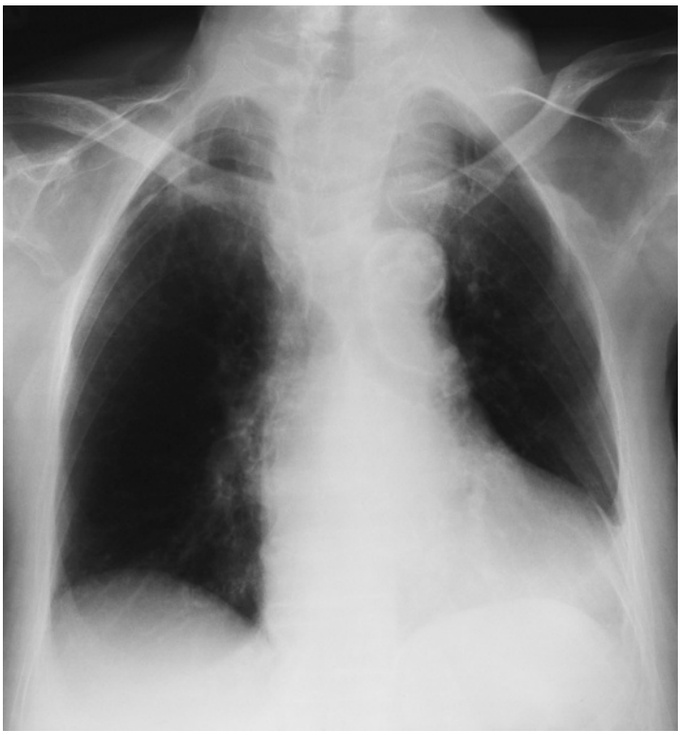

Fig. 1.79 Follow-up examination after 4 days of diuresis. The pulmonary edema has completely resolved. Findings now include left heart enlargement without signs of decompensation.

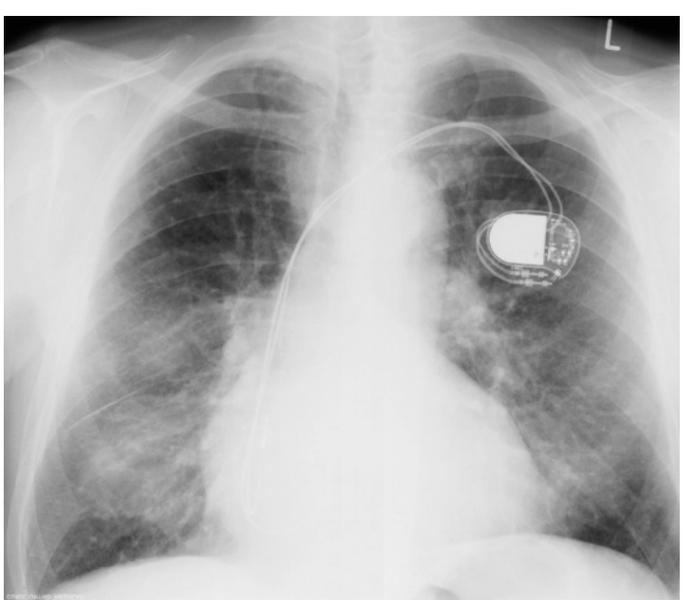

Fig. 1.80 Course of an interstitial edema with residual bronchitis from congestion. Findings include left heart enlargement, redistribution of pulmonary perfusion into the upper fields, interstitial shadowing with Kerley B lines (right costophrenic angle), pronounced right horizontal fissure. Diffuse, finely nodular shadowing.

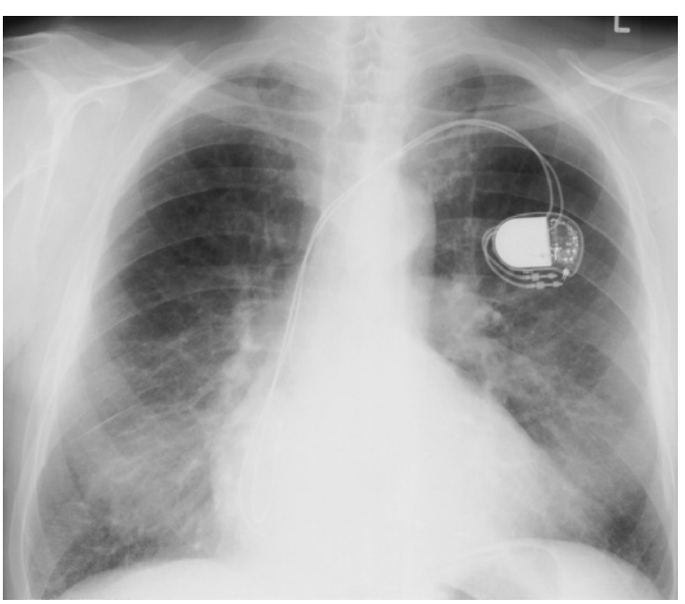

Fig. 1.81 Residual findings after resolution (follow-up of the patient in Fig. 1.80). After 6 days of therapy, the left heart is still enlarged but the redistribution (the active component of congestion) has resolved. Residual findings now include finely nodular shadowing, Kerley B lines, and the pronounced horizontal fissure in the right lung consistent with chronic bronchitis from congestion.

Right Heart Failure

Causes of right heart failure include:
- Preexisting left heart failure
- Pulmonary arterial hypertension (COPD, idiopathic, Eisenmenger reaction)
- Defect (pulmonary or tricuspid valve)

The most common situation is right heart failure as a sequela of chronic left heart failure ("congestive heart"). The "backward" failure of the right heart manifests itself in dilatation of the central veins (vena cava and azygos vein, **Fig. 1.85, Fig. 1.86**) with congestion of the peripheral veins and edema in dependent parts of the body, congested liver, and anasarca including ascites.

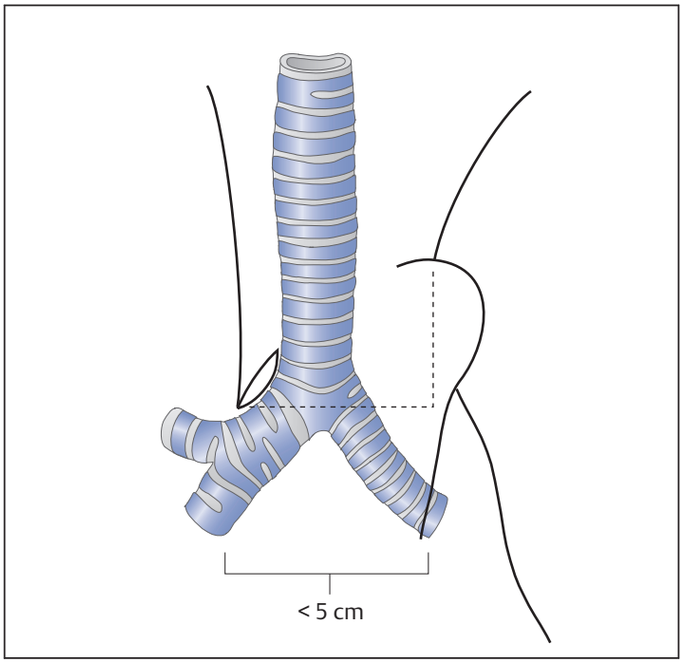

Fig. 1.82 **Mediastinal vascular band described by Milne.**

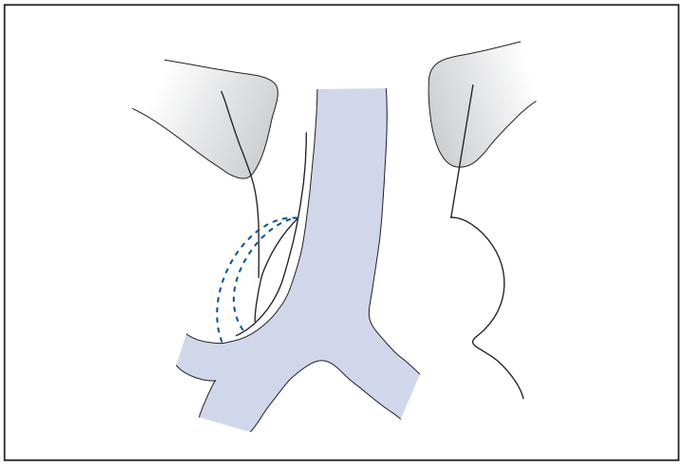

Fig. 1.83 **Schematic diagram of the azygos vein.**

Hence, radiologic signs of right heart failure include:
- Right atrial enlargement
- Dilatation of the vena cava
- Dilatation of the azygos vein
- Reduced pulmonary perfusion in some cases

Right Atrial Enlargement

Enlargement of the right atrium is present where the distance between the right cardiac border and the midsagittal line exceeds one-third of the right hemithorax (**Fig. 1.19**).

Widening of the Vascular Band

The lack of valves at the entry of the inferior and superior vena cava into the right atrium means that there is no pressure gradient between these structures. Accordingly, the increased pressure resulting from right heart failure is detectable as widening of the mediastinal vascular band. Milne demonstrated the close correlation between pressure gradients and the width of the vascular band (**Fig. 1.82**).

Dilatation of the Azygos Vein

The azygos vein lies in the angle between the right main bronchus and trachea. It drains into the superior vena cava and, like that vessel, lacks a valve at its point of entry. As a result, the azygos vein provides a good measure of increased central venous pressure (**Fig. 1.83**). The azygos vein appears spindle-shaped on conventional radiographs. CT images (**Fig. 1.84**) reveal that the vein is round and its apparent spindle shape comes from accompanying connective tissue.

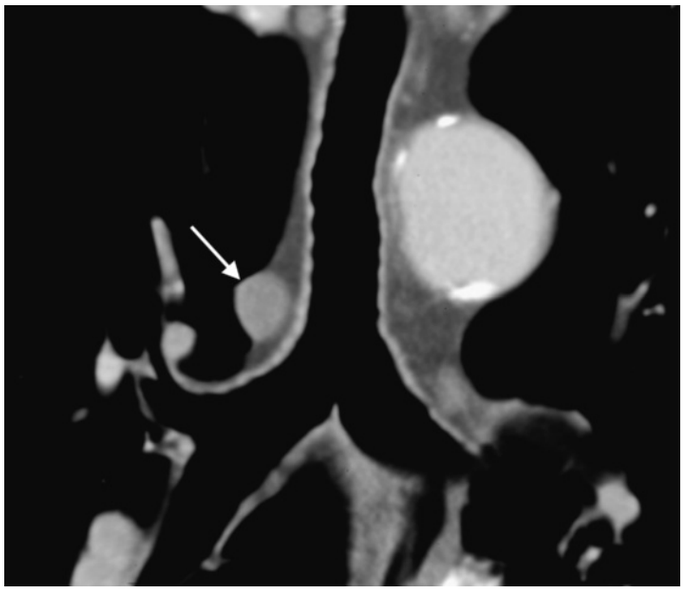

Fig. 1.84 **Position of the azygos vein.** CT reconstruction of the azygos vein (white arrow) in the coronal projection.

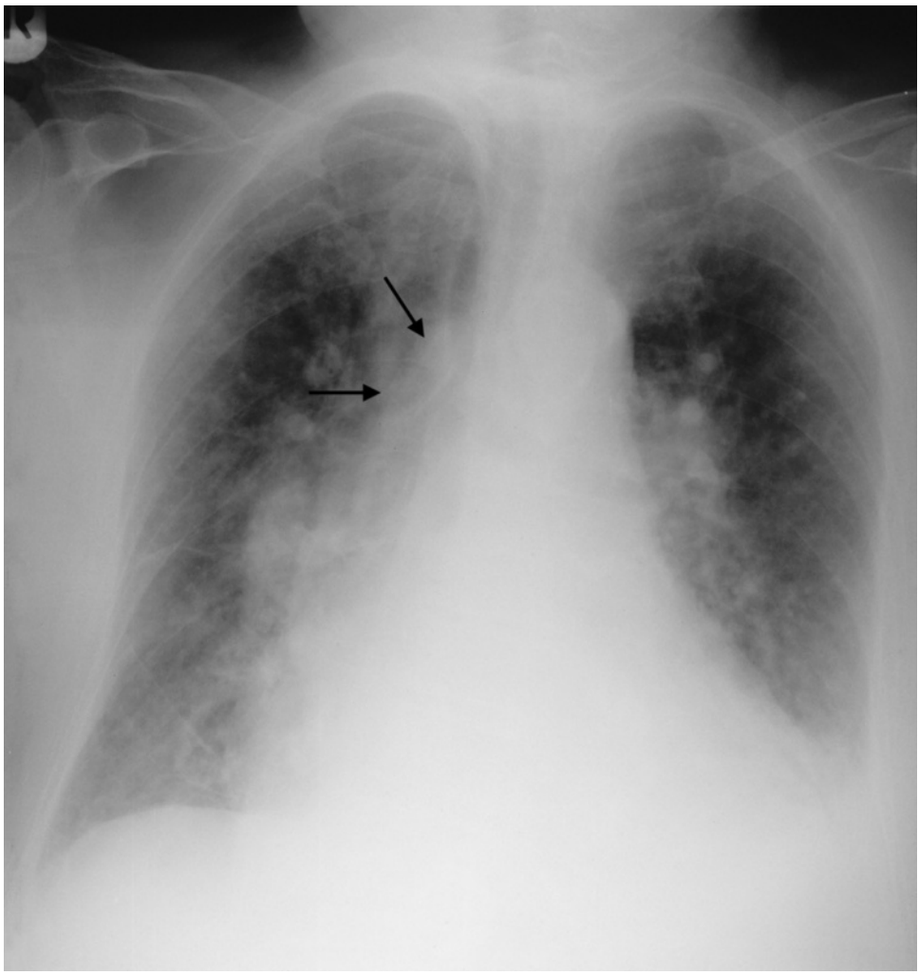

Fig. 1.85 "Backward" failure of the right heart in left heart failure. The heart is globally enlarged with redistribution and interstitial pulmonary edema. Dilated azygos vein (black arrows) with a widened mediastinal vascular band.

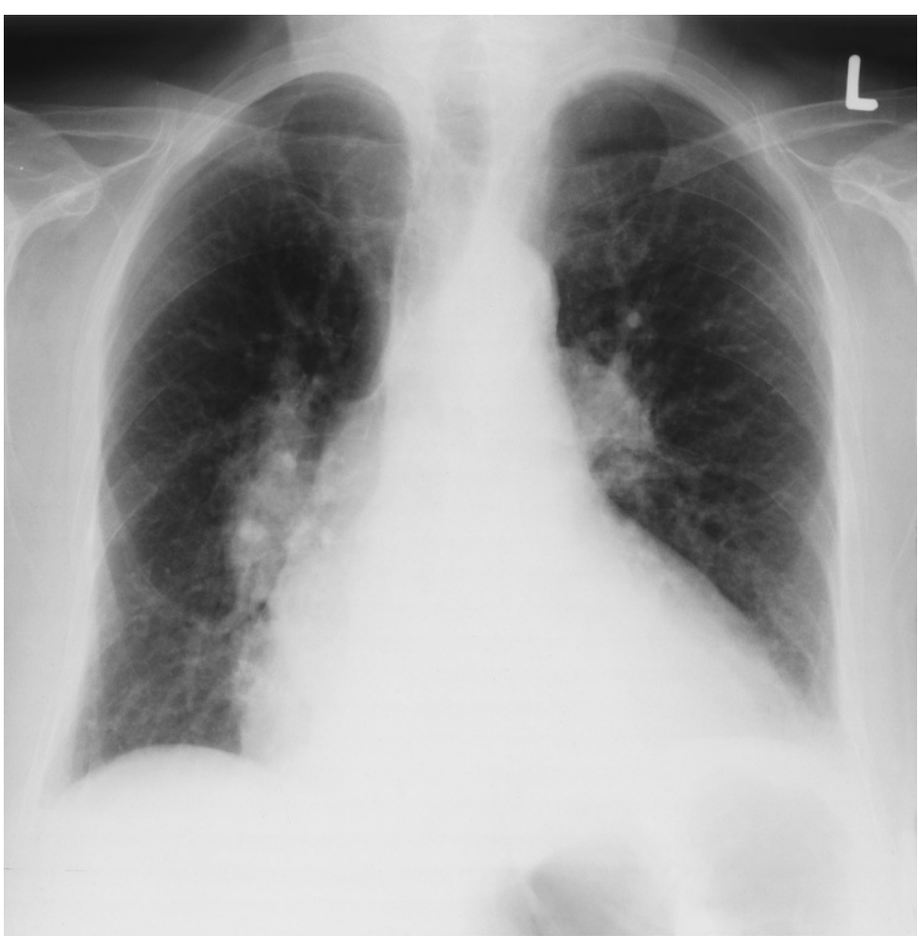

Fig. 1.86 Follow-up examination after reestablishment of compensation. The radiograph obtained 3 days later still shows a significantly enlarged heart but without signs of decompensation. The caliber of the azygos vein is now significantly smaller.

Decreased Pulmonary Congestion

Notably, the signs of pulmonary congestion can be less pronounced in combined right and left heart failure. Although left heart failure frequently precedes right heart failure, right heart failure involves less obvious congestion in the lungs. This is because it also manifests itself as "forward" failure with lesser pulmonary perfusion and reduced volume of the left heart chambers (**Fig. 1.87**).

CT Examination

In the diagnostic work-up of left heart enlargement, CT studies can only confirm findings already visualized on the plain chest radiograph. However, only the unobscured visualization of the cross-sectional image makes it possible to precisely delineate the right atrium and ventricle and compare them with the structures of the left heart.

CT signs of **right heart strain** include:
- Mismatch between structures of the right and left heart
- Visible right ventricular wall

CT signs of **right heart failure** include:
- Stasis of contrast agent in the cervical and thoracic veins (**Fig. 1.88**)
- Dilated azygos vein (**Fig. 1.89**)
- Dilated hepatic veins (**Fig. 1.90**)
- Peripheral edema (anasarca, ascites, lymphedema)

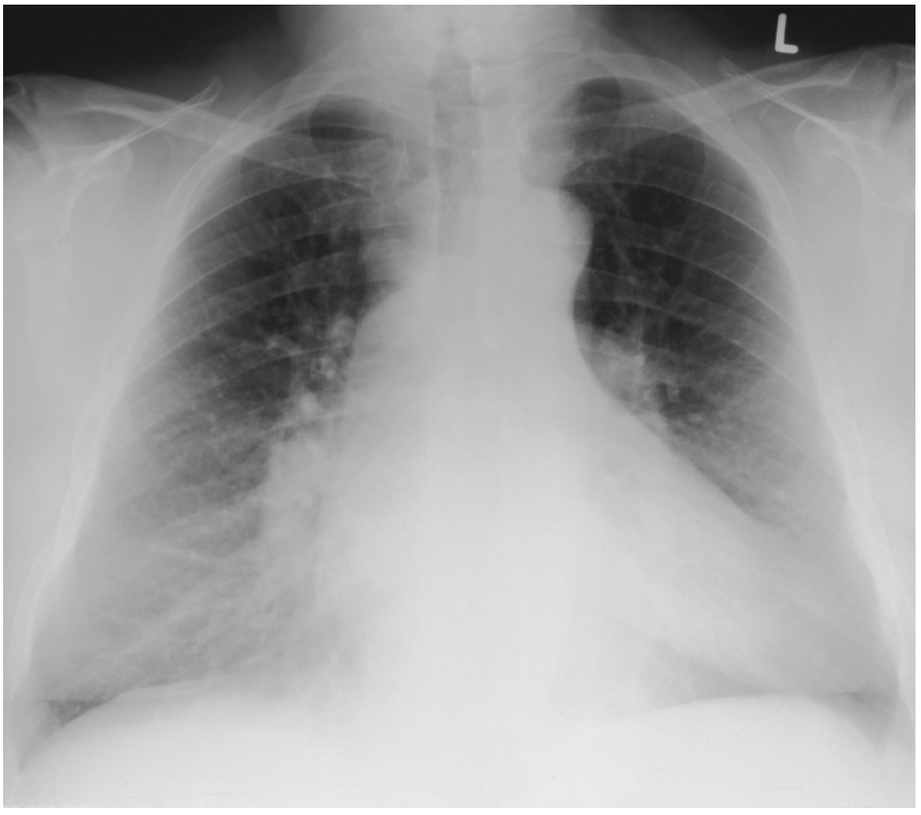

Fig. 1.87 Global failure with slight left congestion due to "forward" failure. In the setting of global heart enlargement with signs of pulmonary arterial hypertension and obstructive barrel chest, findings include widening of the mediastinum with dilatation of the azygos vein. No congestion in the pulmonary veins, redistribution, or shadowing.

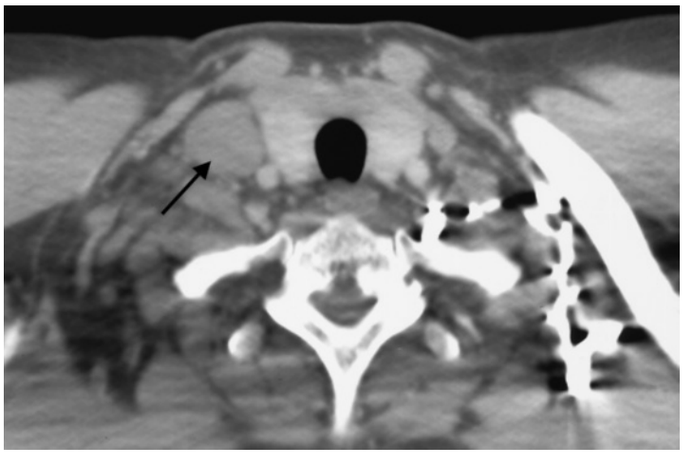

Fig. 1.88 Cervical venous congestion in constrictive pericarditis. After stasis of the contrast agent injected into the left arm occurred in the shoulder region, the right jugular vein (black arrow) and numerous smaller cervical veins appear dilated.

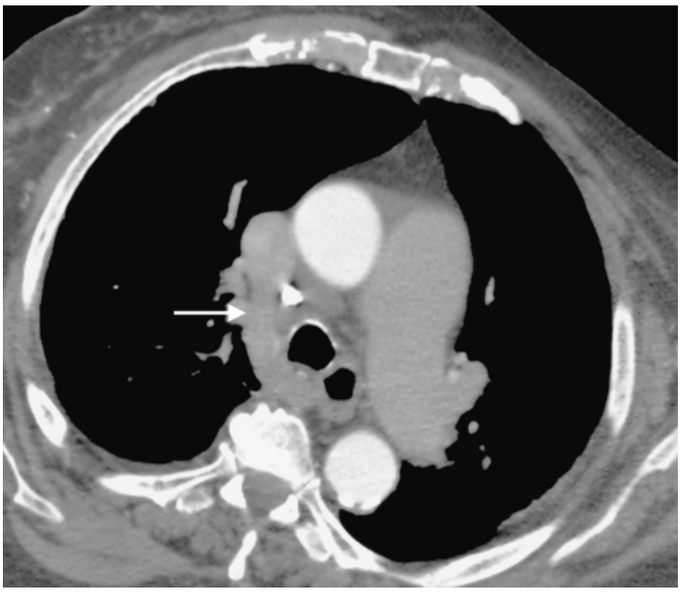

Fig. 1.89 Congestion in the azygos vein. Significantly dilated azygos vein (white arrow) in overhydration.

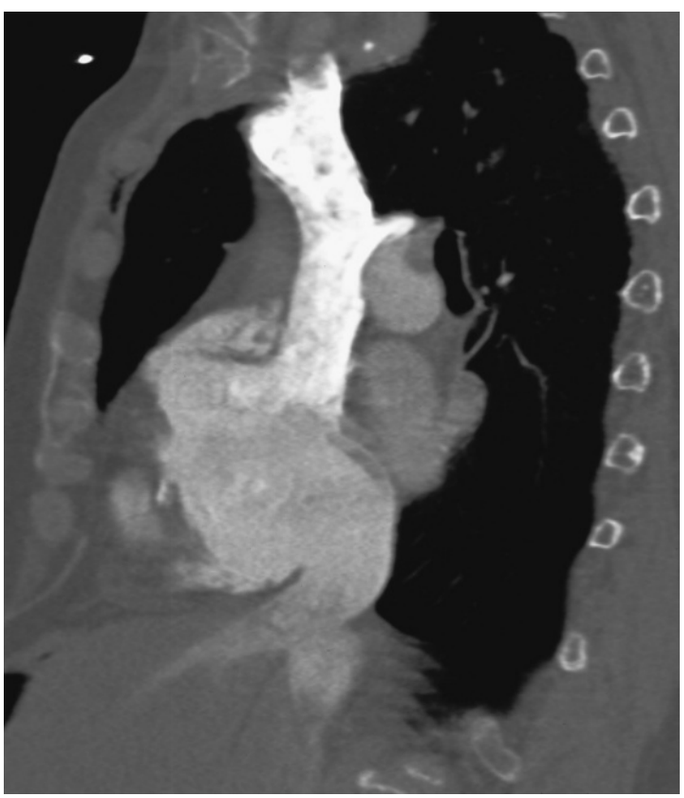

Fig. 1.90 Dilated hepatic veins in right heart failure. In addition to significant dilatation of the superior vena cava, the sagittal reconstruction shows significant congestion in the hepatic veins.

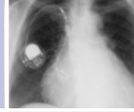

Review Case 1

The patient is a 71-year-old woman presenting for follow-up examination after placement of a pacemaker (Fig. 1.91). Clinical findings are normal.

Question 1

Evaluate the cardiac status after placement of the pacemaker: Do you see signs of cardiac decompensation?

Question 2

The patient previously underwent surgery. Can you see why? Which parts of the heart seem abnormal?

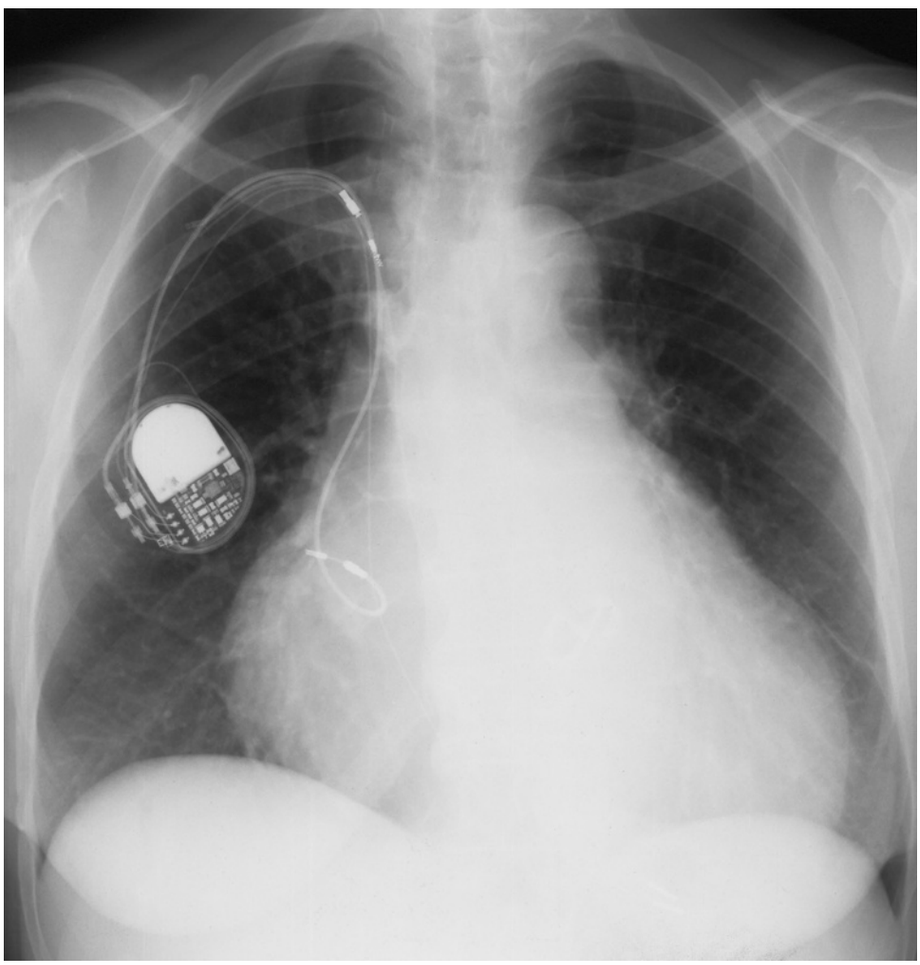

Fig. 1.91 Pacemaker follow-up study. Status post heart surgery several years previously.

Answer

The electrodes are projected over the enlarged right atrium and ventricle; an additional ventricular electrode remains in place (its end lies just below the clavicle). The protrusion of the atrial appendage and splaying of the tracheal bifurcation are indicative of left atrial enlargement. Well visualized in **Fig. 1.92**, the prosthetic mitral valve is barely visible on the slightly underexposed posteroanterior radiograph. The right ventricular enlargement is apparent from the enlarged area of contact between the ventricle and posterior sternum. Findings include neither redistribution nor signs of interstitial congestion. No effusion. Obstructive barrel chest. Narrow upper mediastinum.

Evaluation: Status post surgical correction of mitral valve defect without signs of congestion. Signs of right heart strain without decompensation.

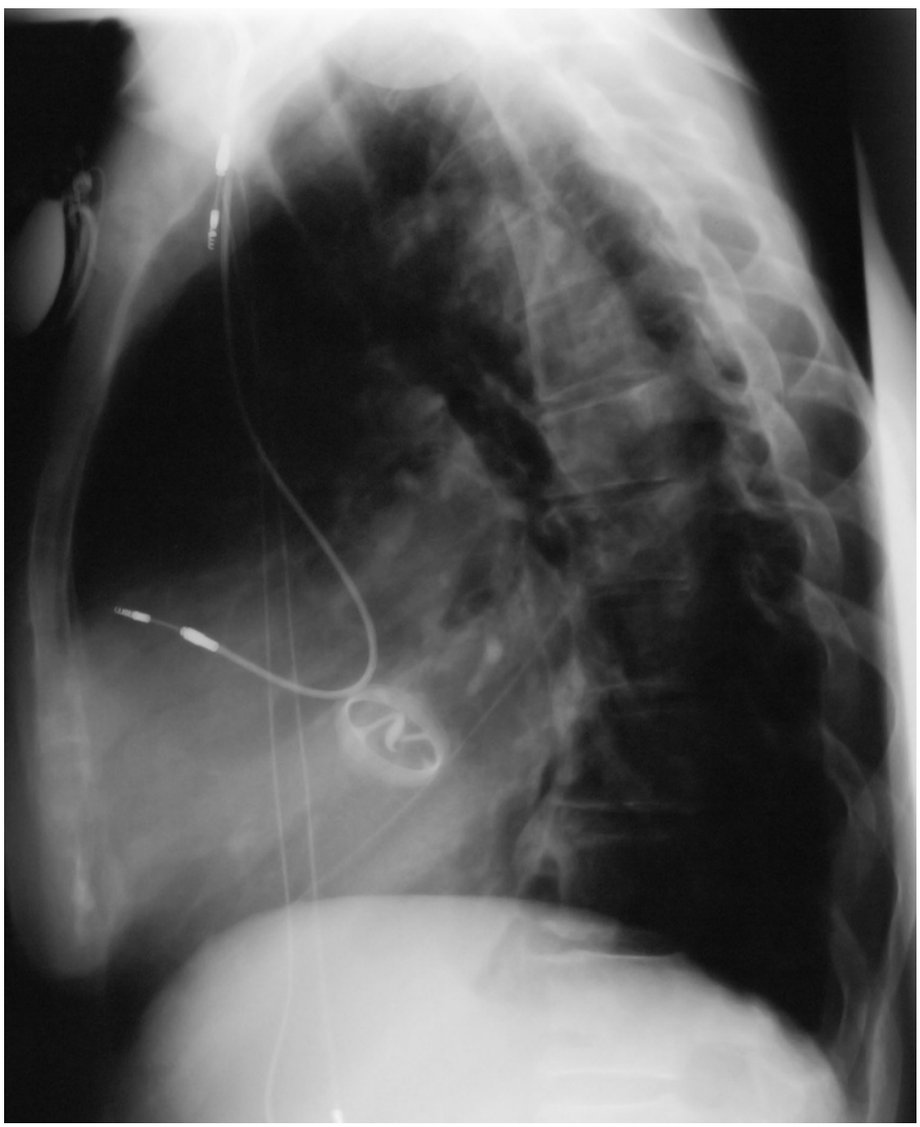

Fig. 1.92 Status post mitral valve replacement. The heart is enlarged at the level of the left atrium and right ventricle but shows no signs of decompensation.

Review Case 2

The patient is a 46-year-old woman presenting for follow-up examination after correction of a congenital heart defect (Fig. 1.93). The patient is clinically asymptomatic.

Question 1

How do you evaluate heart size? Are there signs of decompensation or other pathology?

Question 2

What findings are suggestive of the heart defect and the treatment performed?

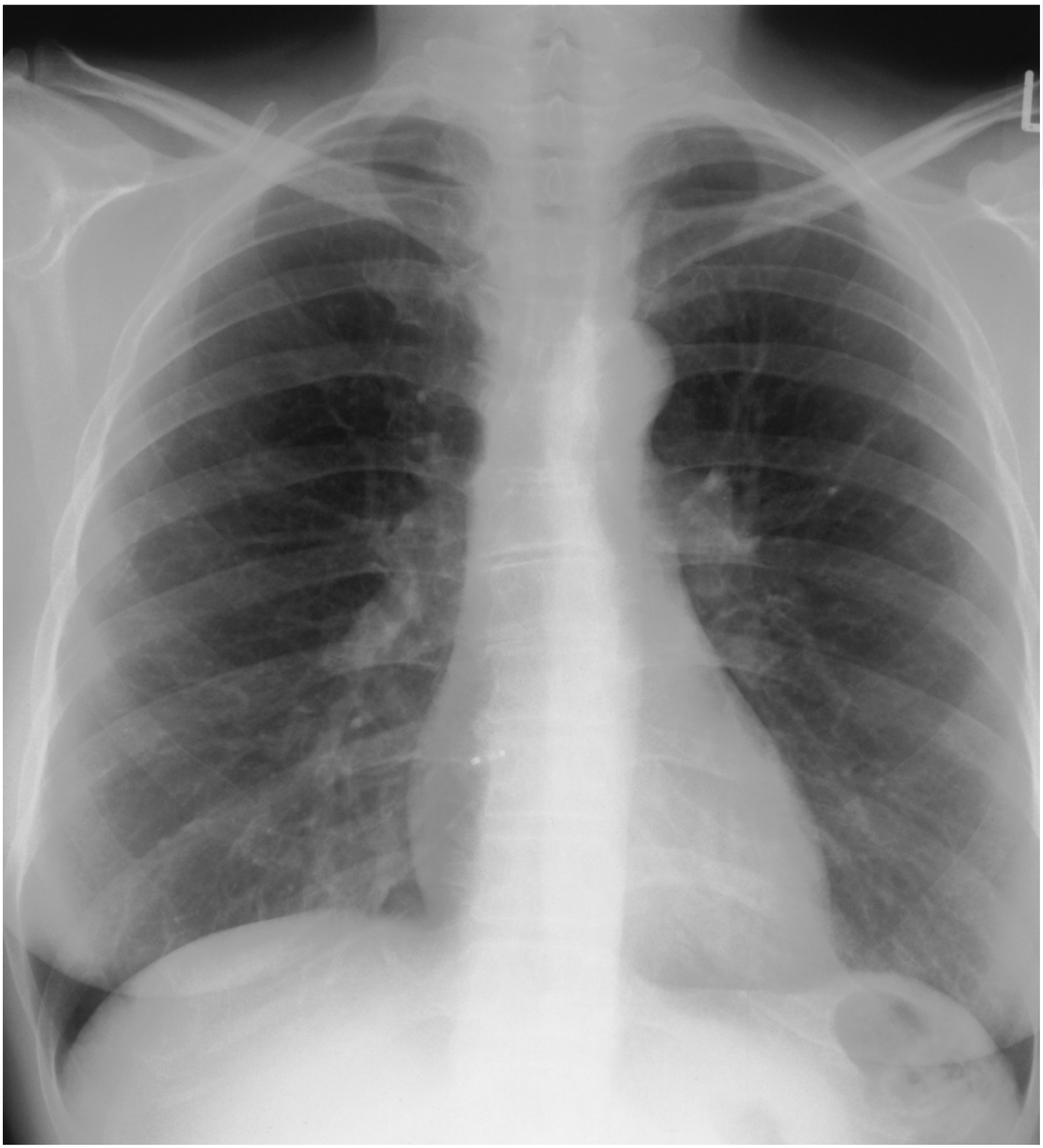

Fig. 1.93 Status post correction of a congenital heart defect.

Answer

Normal cardiac configuration following interventional closure of an atrial septal defect (**Fig. 1.94**). The umbrella occluder projected over the atrial septum in both imaging planes was placed angiographically. The right ventricle is of normal size (the distance between the right cardiac border and the midsagittal line is significantly shorter than one-third of the right hemithorax), as is the left atrium. There is currently no pulmonary hypervolemia, and the diameter of the intermediate artery is 15 mm.

Figure 1.95 shows an uncorrected atrial septal defect in the late stages. Significant global heart enlargement is seen here. The splayed tracheal bifurcation indicates an enlarged atrium, rightward widening of the cardiac border, and an enlarged ventricle. There is massive hilar thickening with pulmonary hypervolemia.

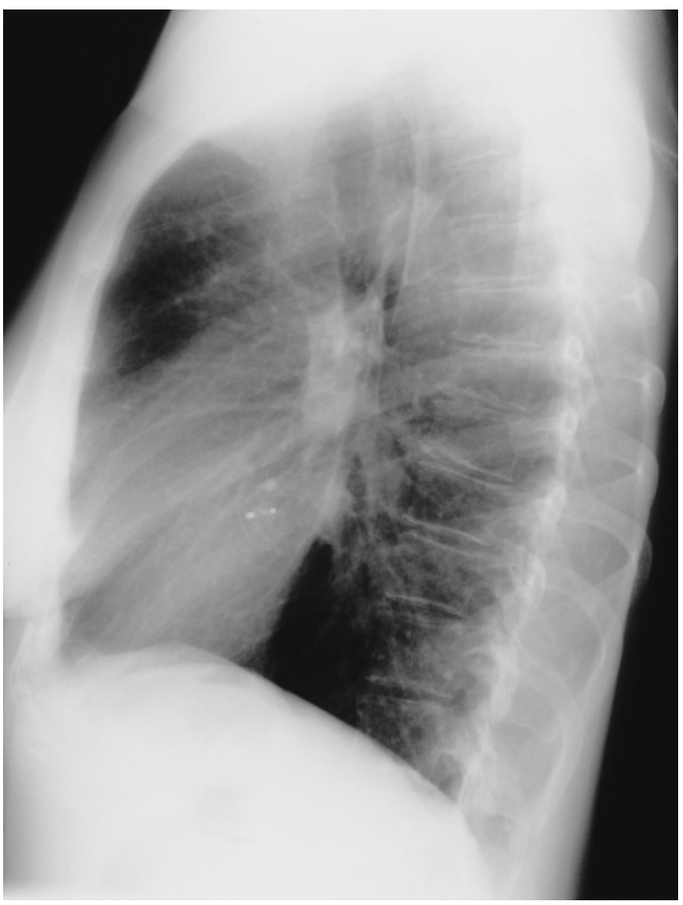

Fig. 1.94 Normal cardiopulmonary findings after interventional closure of an atrial septal defect.

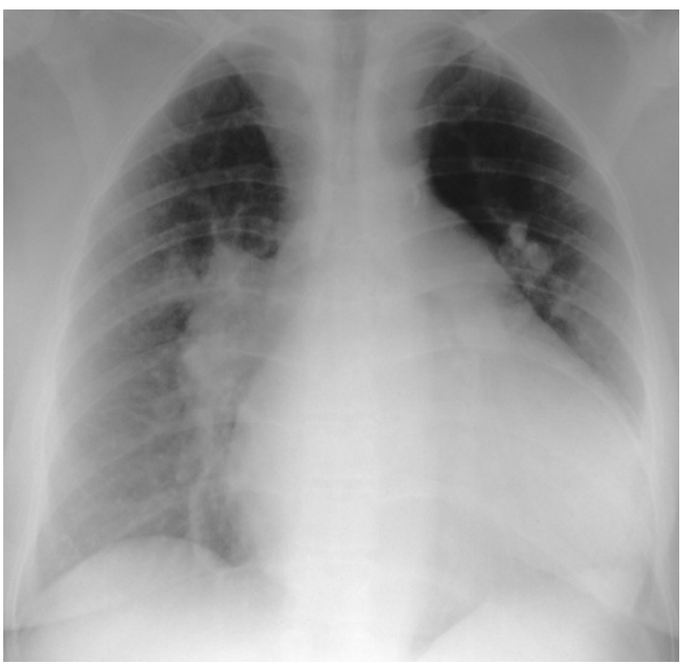

Fig. 1.95 Late stage of an uncorrected atrial septal defect: cardiomegaly, pulmonary arterial hypertension.

Review Case 3

The patient is a 46-year-old man admitted to the hospital with orthopnea and severe productive cough. Laboratory findings show no sign of infection. The patient has a history of dilated cardiomyopathy (Fig. 1.96).

Question 1

How do you evaluate heart size, especially with respect to the question of whether primarily the right or left heart is enlarged?

Question 2

What conclusion can you draw about cardiac function?

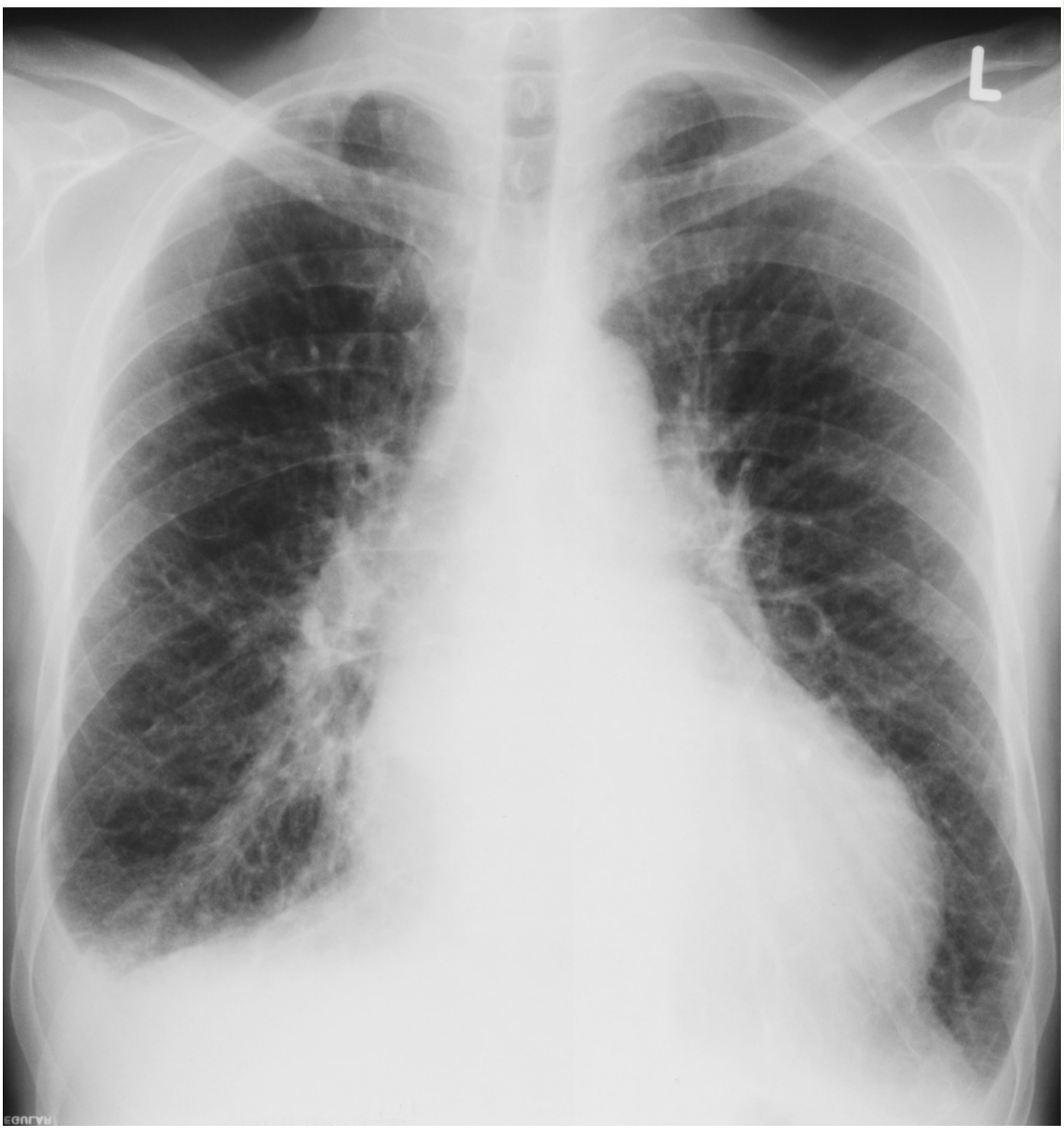

Fig. 1.96 Recurrence of an episode of severe orthopnea with a known heart condition.

Answer

The long axis of the heart is significantly longer than the width of the left hemithorax. The tracheal bifurcation is splayed, and the left atrial appendage is faintly visible. The redistribution of pulmonary perfusion is difficult to evaluate as no pulmonary artery with its matching segmental bronchus has been visualized end-on. However, a few vessels in the upper fields exhibit larger diameters than comparable vessels in the lower fields (white arrow in **Fig. 1.97**). Kerley B lines (white arrowhead) are visible in the basal region. Bilateral effusions in the costophrenic angles are present, and the basal and central vascular structures are beginning to blur.

Evaluation: The heart is significantly enlarged at the level of the left ventricle, less so at the atrial level. Other findings include interstitial and alveolar pulmonary edema beginning in the basal region.

The fateful course of cardiomyopathy in this relatively young patient is documented by comparison with an earlier radiograph obtained 2.5 years previously (**Fig. 1.98**). That image shows only normal age-related cardiac findings with signs of chronic bronchitis.

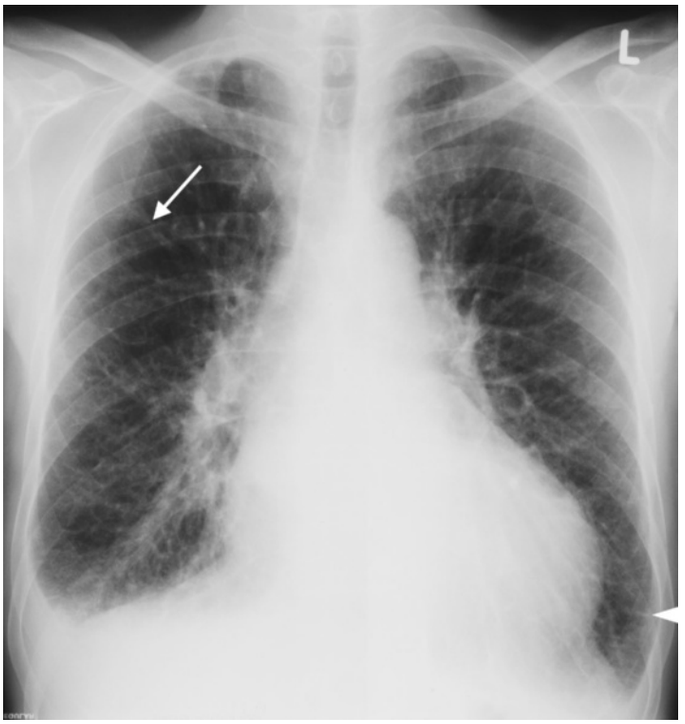

Fig. 1.97 Decompensated cardiomyopathy with interstitial and alveolar pulmonary edema beginning in the basal region, and bilateral pleural effusion.

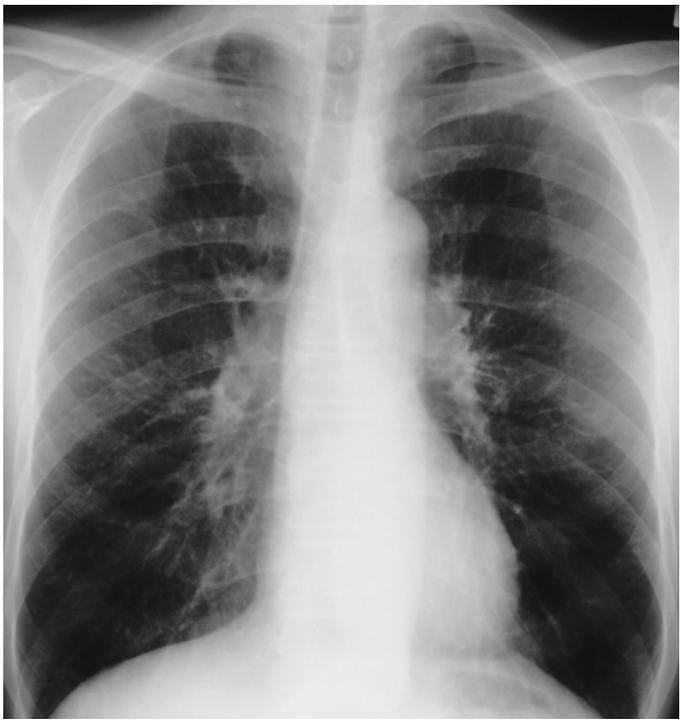

Fig. 1.98 Earlier radiograph of the same patient 2.5 years previously. Signs of chronic bronchitis are present with obstructive barrel chest. Heart size is normal and there are no signs of decompensation.

Review Case 4

The patient is a 77-year-old man admitted to the emergency room. Hypertensive derangement (Fig. 1.99, Fig. 1.100).

Question 1

Describe the heart configuration.

Question 2

Are there signs of decompensation or other pathology?

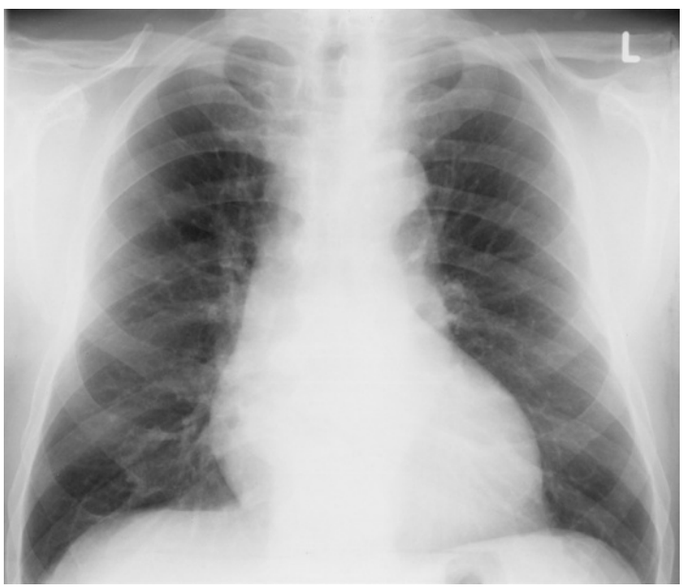

Fig. 1.99 Hypertensive derangement

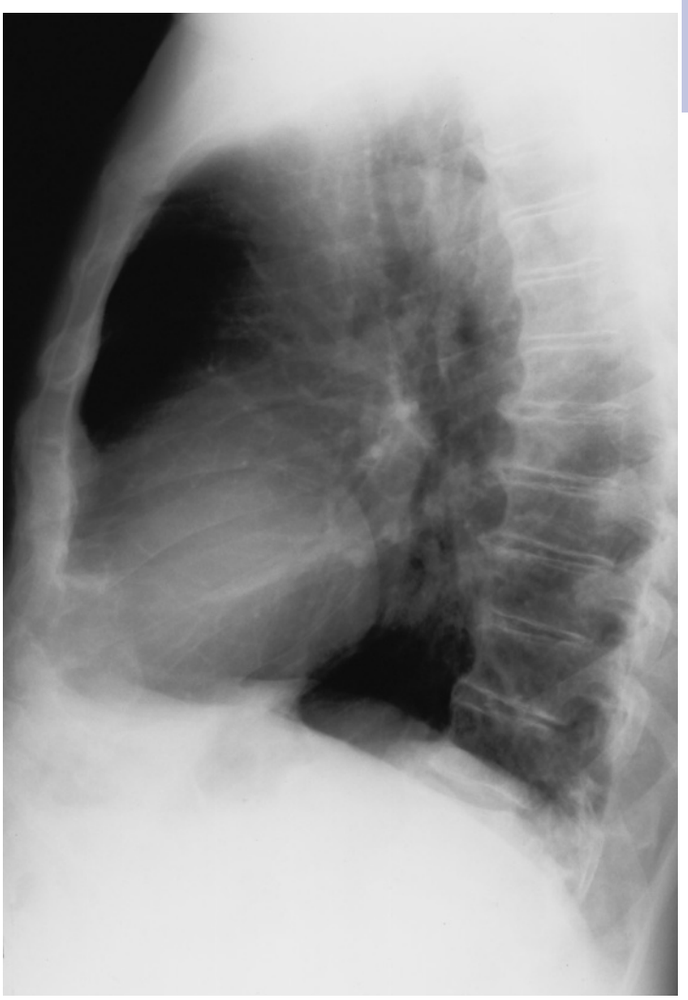

Fig. 1.100 Lateral view of Fig. 1.99.

Answer

The heart is enlarged at the level of the left ventricle (the long axis of the heart is longer than the width of the left hemithorax, and there is posteroinferior protrusion). The elongated aorta forms the right cardiac border (black arrow, **Fig. 1.101**). Findings are consistent with a hypertensive configuration. There is no redistribution, no Kerley lines, and no effusion, and therefore nothing suggesting cardiac decompensation. Finely nodular shadowing consistent with chronic smoker's bronchitis is present, appropriately accompanied by obstructive barrel chest (enlarged retrosternal space, **Fig. 1.102**). Additional findings include degenerative changes in the thoracic spine.

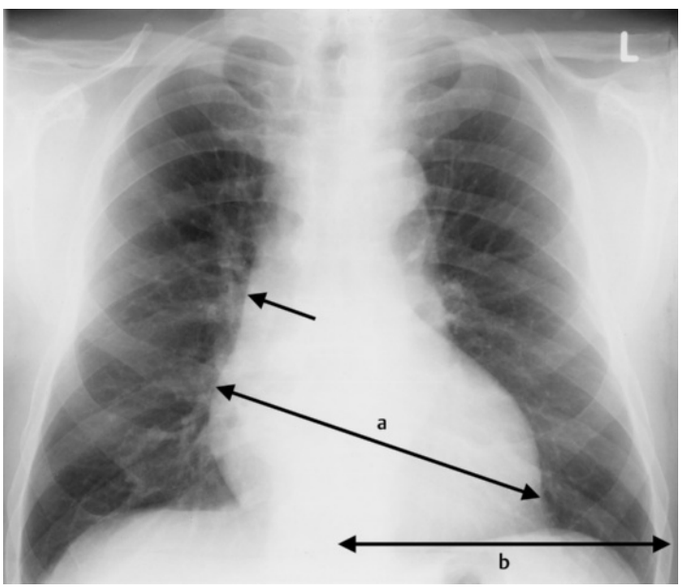

Fig. 1.101 Left heart enlargement and elongation of the aorta without signs of decompensation. The long axis of the heart (a) is longer than the width of the left hemithorax (b).

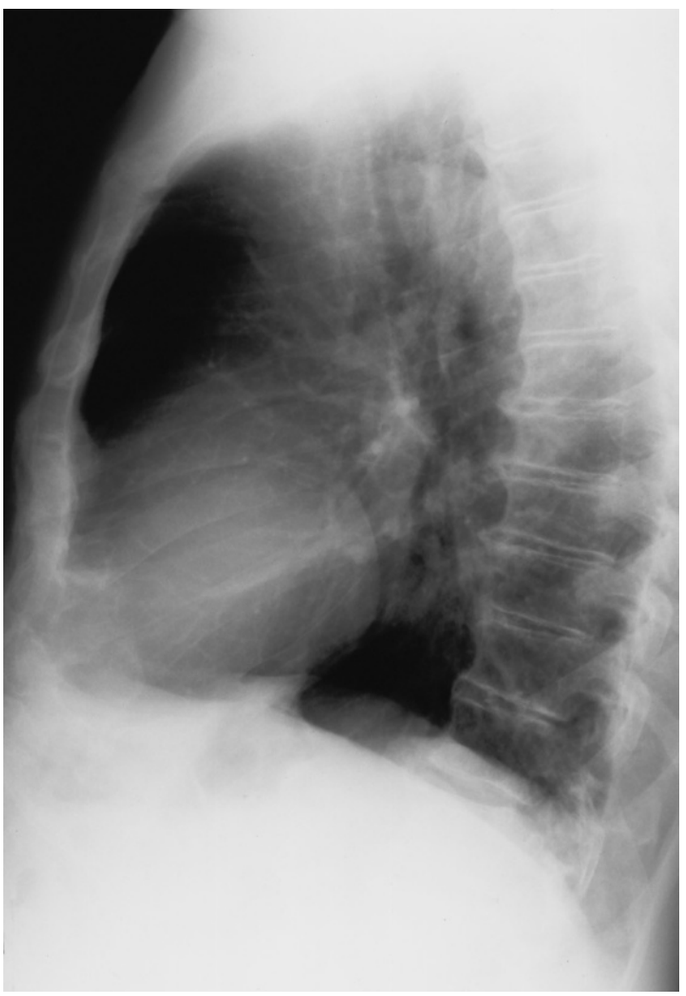

Fig. 1.102 Positive Hoffman–Rigler sign and narrowing of the retrocardiac space. The retrosternal space is widened, indicative of obstructive pulmonary disease.

Review Case 5

The patient is a 75-year-old man with a history of many years of chronic obstructive pulmonary disease and heart failure with underlying ischemic cardiomyopathy (Fig. 1.103). A cardiac pacemaker has been implanted. The current radiograph has been obtained in a patient with dyspnea at rest and fever as high 39°C.

Question 1

How do you evaluate heart size and cardiac output?

Question 2

Do you think a pulmonary infiltrate is present?

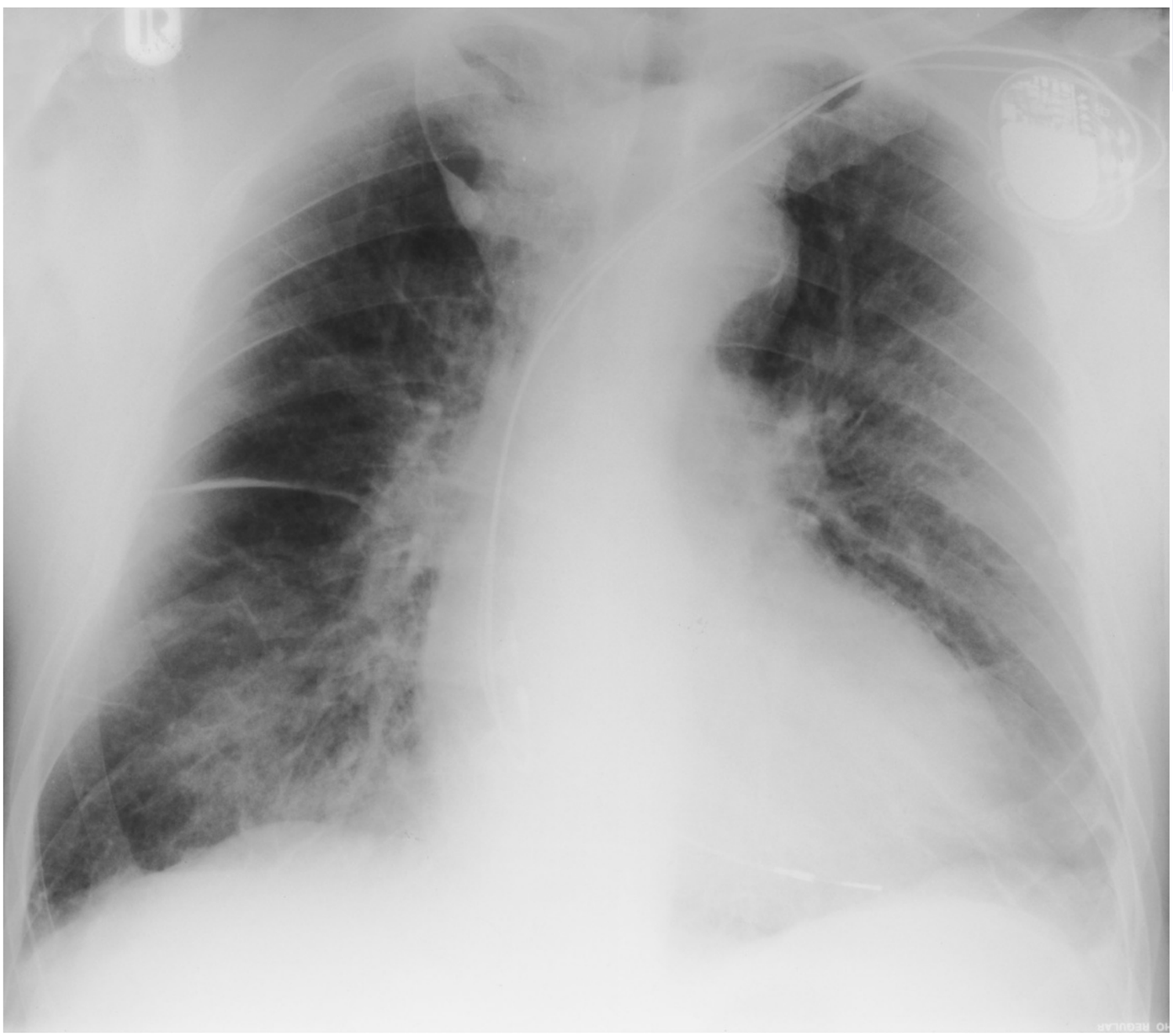

Fig. 1.103 Radiograph in a patient with dyspnea at rest and fever in the presence of known COPD and implanted cardiac pacemaker.

Answer

In the setting of a globally enlarged heart characterized by left heart enlargement in particular, there is significant left heart decompensation with Kerley lines (black arrows, **Fig. 1.104**), a small effusion radiating into the right interlobar fissures, and blurring of vascular structures beginning in the basal region. The dilated azygos vein in the azygos lobe (black arrowhead) indicates the presence of right heart failure as well.

Diagnosis: Congestive left and right heart failure with interstitial and alveolar pulmonary edema beginning in the basal region.

Evaluation: The question of whether an additional infiltrate is present can be answered only by observing the further course of the disorder. A follow-up examination 3 days later is helpful in such cases (**Fig. 1.105**).

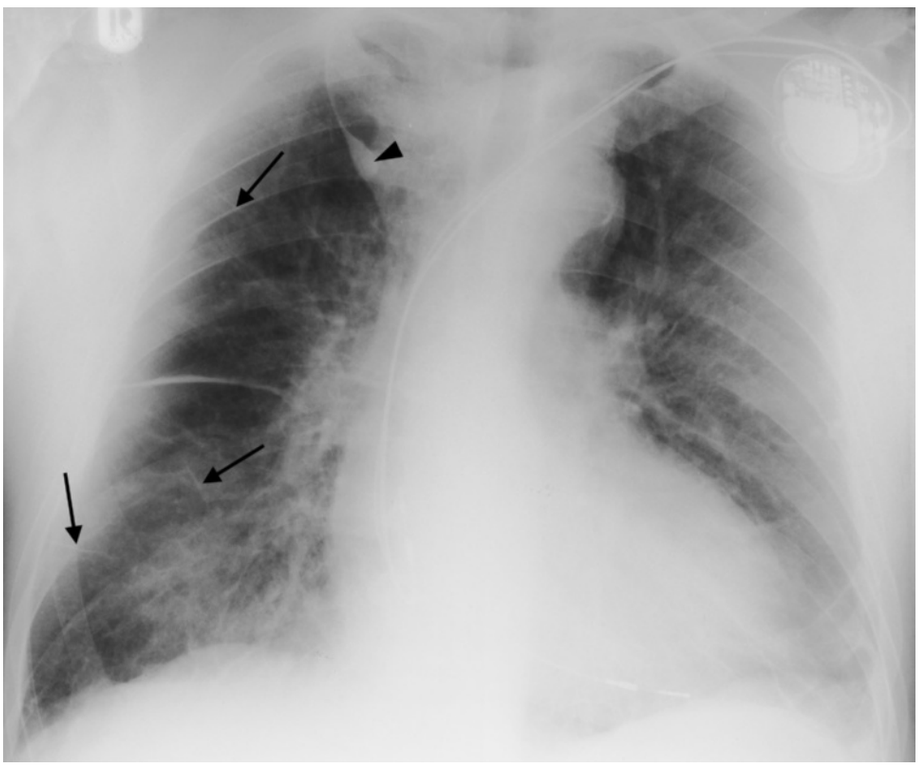

Fig. 1.104 Cardiac decompensation with interstitial and alveolar pulmonary edema and signs of right heart failure. The arrows demonstrate Kerley lines. Black arrowhead shows dilated azygos vein.

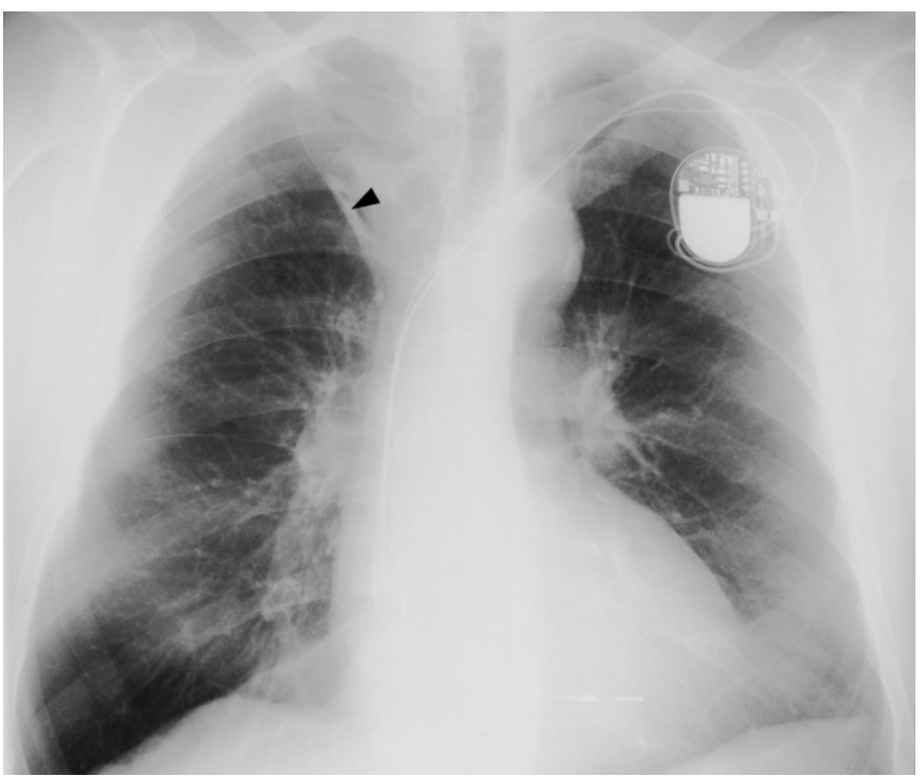

Fig. 1.105 Signs of cardiac decompensation have completely resolved. Azygos vein (black arrowhead) has returned to normal. Signs of COPD and obstructive barrel chest are present, no infiltrate.

2

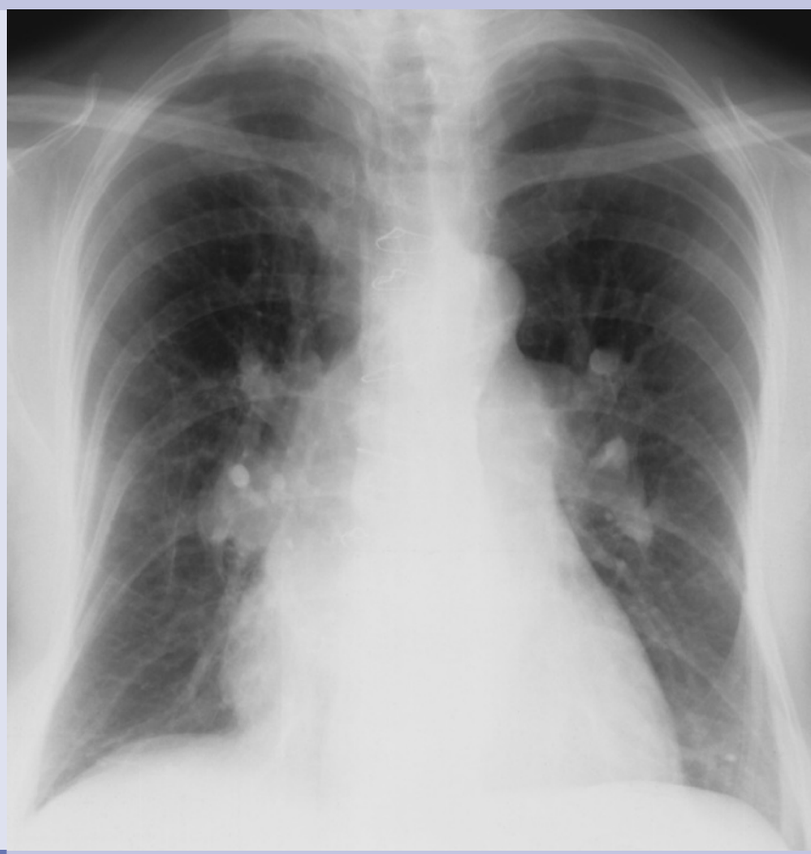

Bronchitis

General

Inflammatory lung disease can be acquired via respiratory, hematogenous, or lymphatic spread. Most often, noxious agents enter via the tracheobronchial tree. Depending on the depth of invasion, they lead to tracheitis, bronchitis or bronchopneumonia, bronchiolitis, or alveolitis (**Fig. 2.1**).

The portions of the tracheobronchial tree visible on the plain chest radiograph include:

- Trachea
- Bifurcation and carina
- Main bronchi (left more clearly visualized than right)
- Right middle lobar bronchus
- Segmental bronchi visualized end-on

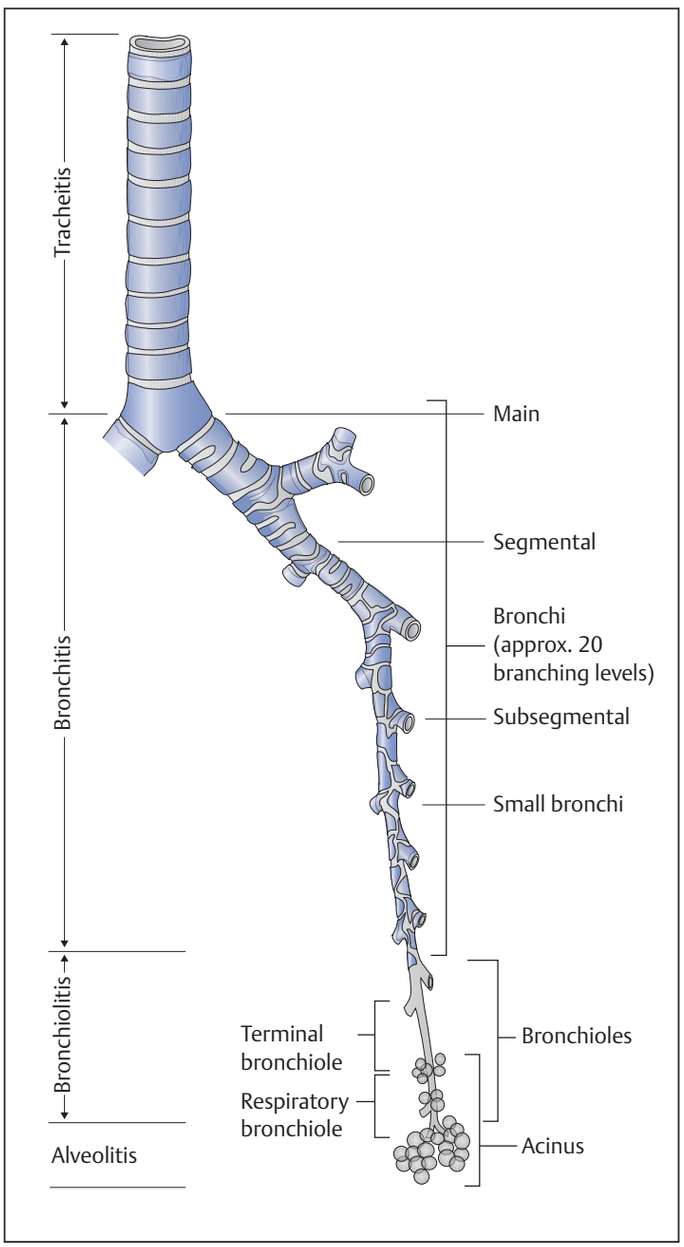

Fig. 2.1 Inflammatory reactions of the tracheobronchial tree acquired via respiration. Depending on their penetration depth, extrinsic noxious agents will produce different clinical pictures.

The vocal cords are occasionally visualized on high chest radiographs or images of the cervical spine.

The trachea appears as a radiolucent band as thick as the thumb. It is usually readily identifiable (**Fig. 2.3**). The tracheal bifurcation normally exhibits an angle of approximately 60°.

The radiolucent band of the normal trachea on the coronal projection is bordered by a linear shadow only a few millimeters wide. This is a normal finding; where abnormal thickening is present (as in severe chronic inflammation or, rarely, amyloidosis) or there is a change in its structure (calcification), it will appear more prominent (**Fig. 2.5**).

The left main bronchus is usually more readily identifiable than the right one. Its course is more horizontal, whereas the right main bronchus courses more steeply caudad.

The tracheal bifurcation and the main bronchi are usually better identifiable on the plain chest radiograph when it is viewed from an oblique inferior stress view.

The visible segmental bronchi physiologically exhibit the same diameter as the segmental arteries that accompany them (**Fig. 2.2**). They resemble a slender bracelet (**Fig. 2.4**). If the bronchi exhibit obvious cuffing when visualized end-on, then abnormal changes are present. This can occur in processes such as chronic bronchitis or fluid accumulations (**Fig. 2.6**).

CT reveals changes in the trachea and bronchi earlier than the plain chest radiograph and can differentiate them more clearly.

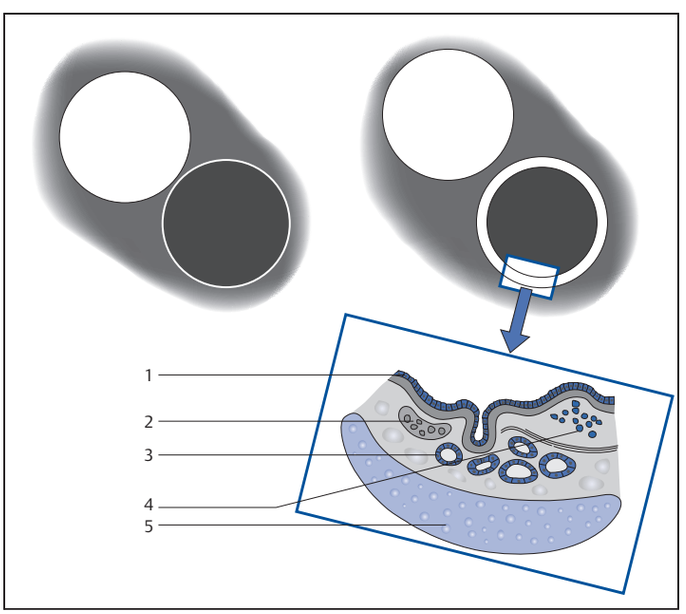

Fig. 2.2 Relative sizes of the segmental bronchus and accompanying artery. The pulmonary artery and accompanying bronchus are physiologically of identical diameter. The bronchus resembles a slender bracelet. Abnormal thickening of the wall results from chronic inflammatory processes. 1, Squamous metaplasia; 2, hyperemia; 3, mucous gland hyperplasia; 4, inflammatory infiltration; 5, cartilage.

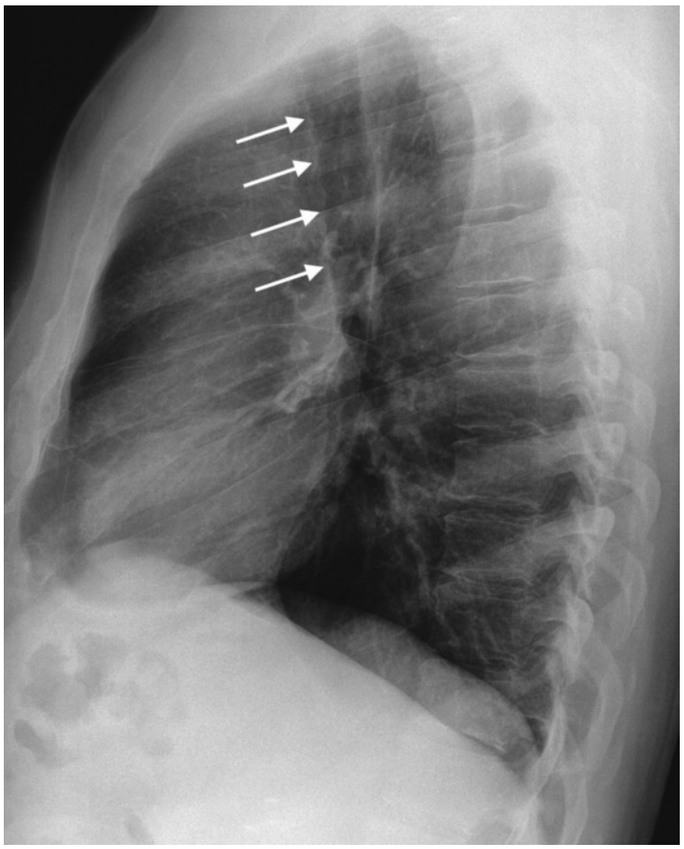

Fig. 2.3 **Lateral view of the trachea (white arrows).**

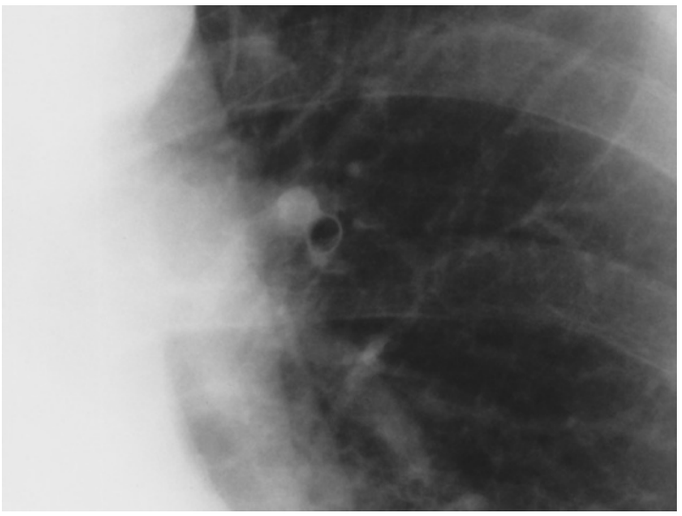

Fig. 2.4 **Detailed view of the left S3 bronchus (anterior upper lobe segment).** The normal bronchus, in close proximity to the accompanying pulmonary artery, resembles a slender bracelet.

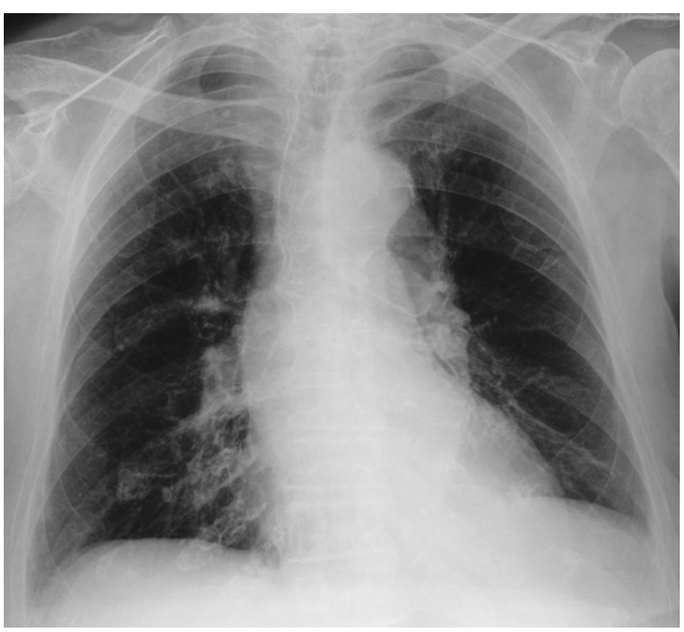

Fig. 2.5 **Calcification of the tracheal and bronchial wall in tracheobronchopathia calcarea.** The patient is a 95-year-old woman with senile emphysema. Significant calcification of the trachea and main and segmental bronchi, here partially obscured by calcified rib cartilage. Hypertensive configuration.

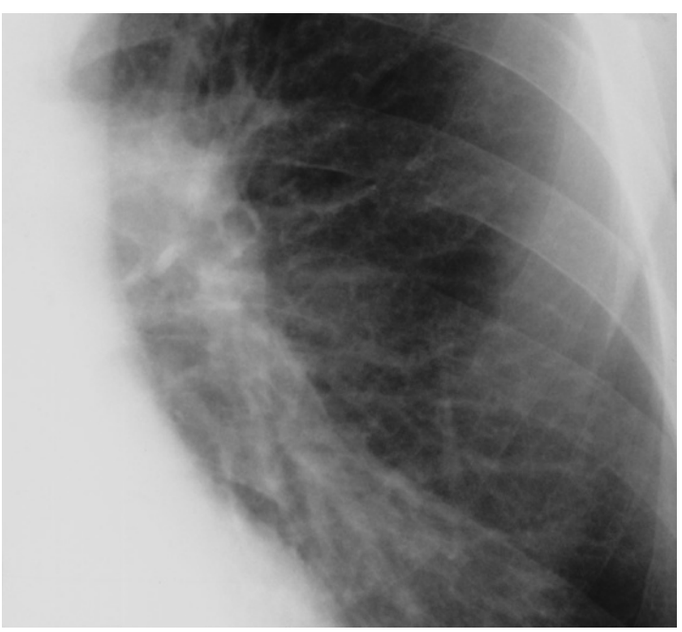

Fig. 2.6 **Thickening of the wall of the left S3 bronchus.** The bronchial wall thickening from chronic bronchitis appears as cuffing. The accompanying pulmonary artery is thickened as a result of pulmonary arterial hypertension.

Trachea

The wall of the normal trachea is 1–2 mm thick on CT images. It has a faintly oval cross-section that is slightly flattened posteriorly (**Fig. 2.7**). Thickening of the tracheal wall is usually observed in chronic irritation (chronic bronchitis), which is often associated with calcifications (tracheobronchopathia calcarea, **Fig. 2.9**). Rarely, significant wall thickening may also occur in other disease processes such as amyloidosis (**Fig. 2.10**). Marked deformation is often encountered in patients with chronic respiratory tract disease. The cross-section of the laterally narrowed trachea then increasingly assumes a keyhole shape (**Fig. 2.11**). Another variant indicative of chronic inflammatory processes is the instability of the posterior tracheal wall with transverse scimitar-like deformation (in contrast to the longitudinal compressive deformation in a goiter **Fig. 2.12**).

Bronchi

The width of bronchial lumen and the width of the accompanying pulmonary arteries are more easily compared on CT images than on the plain chest radiograph. As on the radiograph, the wall should resemble a slender bracelet (**Fig. 2.13**). Additionally, the course of the bronchi can be traced significantly farther into the periphery. Here, air-filled spaces detected in the outer mantle of the lung beyond a distance of 3 cm from the pleura should be regarded as a sign of pathologic change in the respective peripheral airway (widened lumen and/or thickened wall; see also **Fig. 2.21**).

In addition to thickening of the wall or widening of the lumen, tracheal deformation, i.e., loss of the normal round cross-section, is a significant sign of pathology. The most impressive example of this is the massive narrowing that can occur in bronchomalacia (**Fig. 2.14**).

Bronchioles and Terminal Bronchiole

CT visualizes the divisions of the healthy tracheobronchial tree as far as the branchings of the subsegmental bronchi. CT occasionally visualizes the airway tree as far as the bronchioles in cases of chronic inflammation with dilatation of the small airways or within patchy alveolar densities. Knowledge of the structure of the secondary lobule provides indirect information about the condition of the centrilobular terminal bronchiole (**Fig. 2.8**).

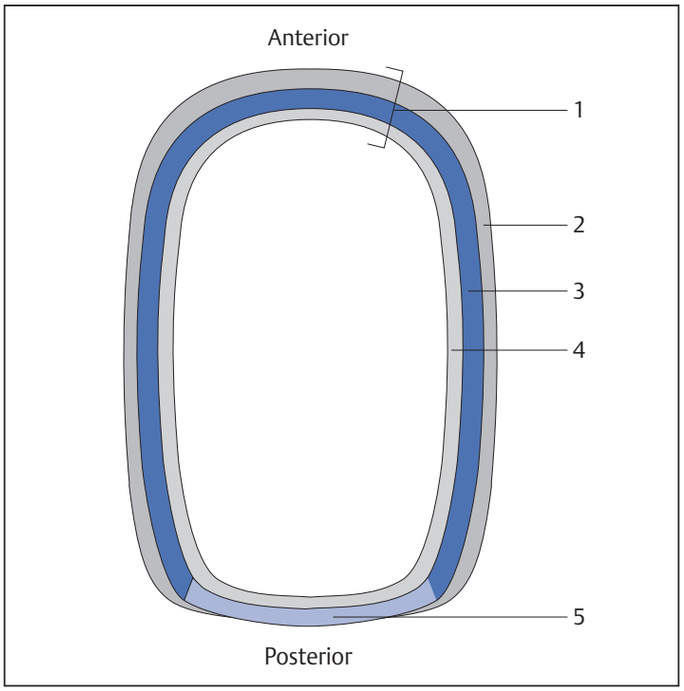

Fig. 2.7 Schematic diagram of the structure of the tracheal wall.
1 Normal thickness 2 mm
2 Adventitia
3 Cartilage
4 Mucosa
5 Posterior tracheal membrane

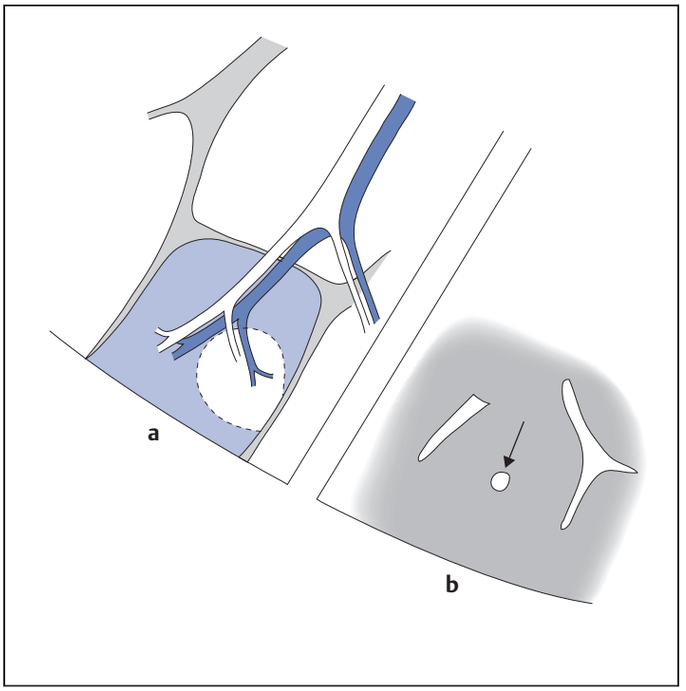

Fig. 2.8 a, b Schematic diagram of the structure of the secondary lobule. The secondary lobule consists of ca. 20 acini. It is demarcated by interstitial bundles containing centripetally coursing venules and centrifugally coursing lymph vessels (arrow). The centrilobular artery appears in CT as a punctate shadow in the center of the secondary lobule. The accompanying terminal bronchiole and the alveolar walls are not visible.
a Anatomic diagram.
b CT pattern.

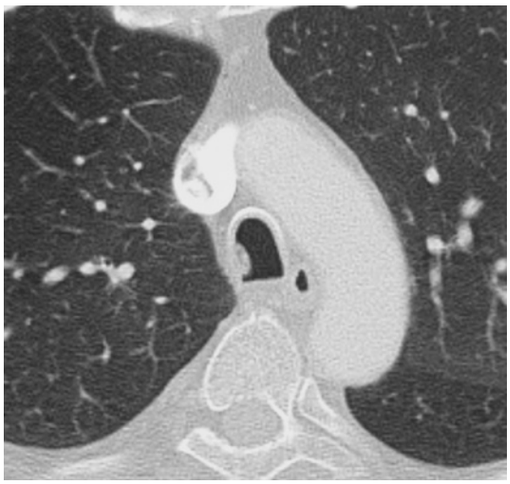

Fig. 2.9 Tracheobronchopathia calcarea. Signs of chronic bronchitis include accumulations of mucus in the trachea as well as calcification of the tracheal wall.

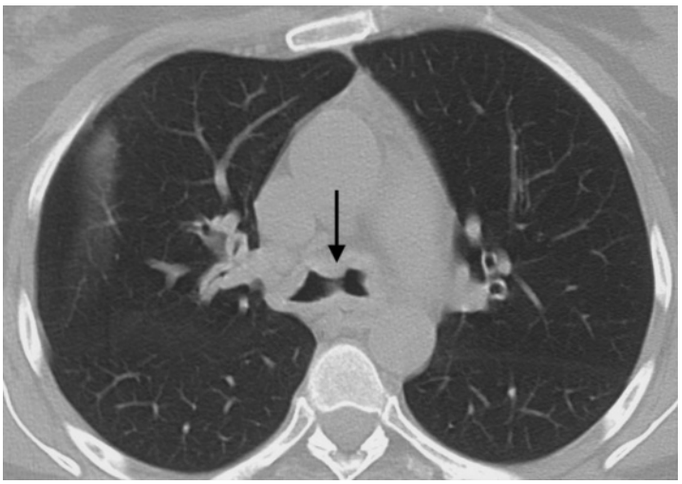

Fig. 2.10 Massive thickening of the tracheal wall at the bifurcation (black arrow) in amyloidosis.

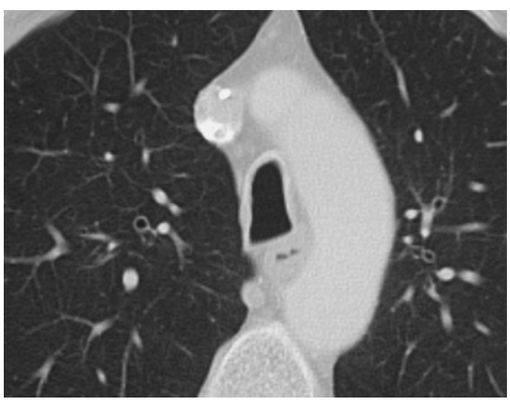

Fig. 2.11 "Keyhole" trachea. The keyhole deformation of the trachea is a sign of instability of the tracheal wall resulting from chronic inflammation.

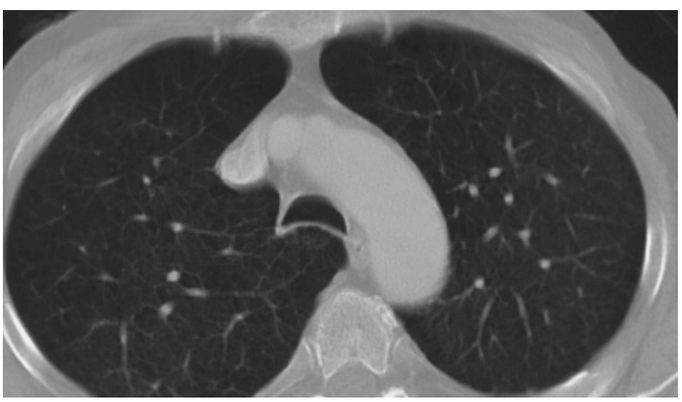

Fig. 2.12 Tracheomalacia. Protrusion of the noncartilaginous posterior tracheal wall is a sign of instability.

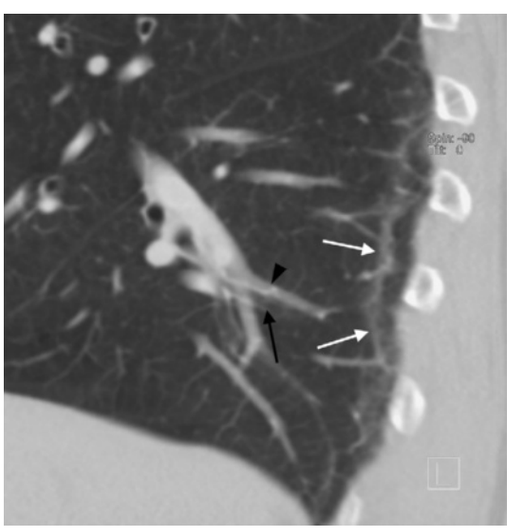

Fig. 2.13 Pulmonary periphery: pulmonary artery and accompanying bronchi. Bronchus (black arrow) and pulmonary artery (black arrowhead) are clearly visualized in cross-section and longitudinally. Here, only moderate thickening of the bronchial wall is present in bronchi that can be traced far into the periphery. Subpleural fibrotic strand (white arrows).

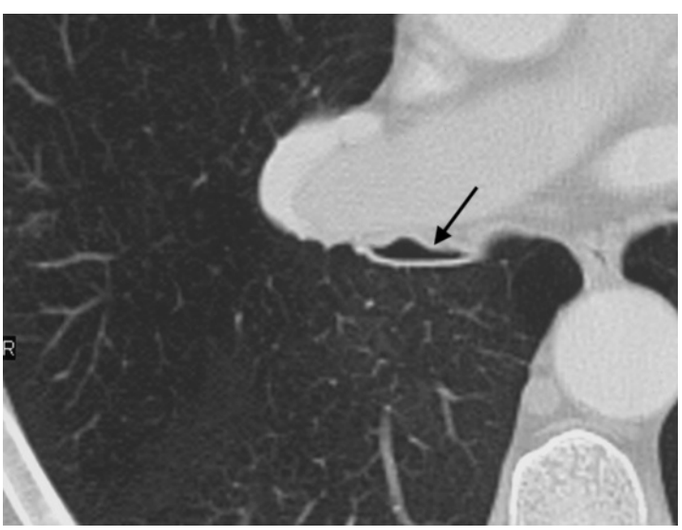

Fig. 2.14 Bronchomalacia of the right bronchus intermedius. Subtotal collapse of the right bronchus intermedius (black arrow) is seen with signs of chronic bronchitis including thickened bronchial wall. Signs of pulmonary arterial hypertension.

Acute Bronchitis

In principle, the role of conventional radiography is not to diagnose tracheitis, tracheobronchitis, and acute bronchitis but to exclude other findings in the presence of definitive clinical findings. Even the lack of patchy shadows on the radiograph is part of the clinical definition because auscultatory findings (wheezing and rattling) may be present in severe cases of acute bronchitis in addition to cough and pain. Bronchitis, for example, is defined as productive cough without radiologic evidence of pulmonary infiltrates.

Bronchitis = cough + sputum.

Acute bronchitis is caused by viral agents in 90% of all cases. It is one of many symptoms of inflammatory changes in the upper respiratory tract and is usually associated with rhinotracheitis. It is primarily a disorder of the large and middle bronchi. Acute bronchitis can persist for weeks and then give cause for radiologic examination (**Fig. 2.16, Fig. 2.17**).

There is a marked discrepancy between the frequency with which radiologic terms such as "bronchitic shadowing," "signs of chronic bronchitis," etc. are used in daily practice and the often harsh rejection of such usage in the published literature. "The radiographic diagnosis of bronchitis on the basis of a pronounced striped pattern must be rejected as untenable and unsubstantiated" (according to Huszly). Yet this raises the question: "What then do we see?"

We feel it is important to be able to categorize the changes that are actually detectable. Otherwise we would have no choice but to incorrectly refer to such findings as "normal."

Reactive hyperemia of the bronchial arteries and the inflammatory mucosal swelling of the bronchi in acute bronchitis lead to nonspecific overall increase of lung markings on the plain chest radiograph. We occasionally encounter such pictures as incidental findings on CT images of the chest. Such findings in adults are either indistinguishable from corresponding changes in chronic bronchitic irritation or distinguishable only by observing the course of the disorder. The situation is different in children. Significant, primarily central hyperemia is usually associated with detectable peripheral obstruction.

We can therefore regard the following findings as radiographic signs of acute bronchitis (**Fig. 2.15**):

- Central blurring (hyperemia)
- Absence of diffuse infiltrates
- Obstruction in certain cases

We should note that in a large percentage of infants acute bronchitis is probably evaluated as central obstructive bronchopneumonia.

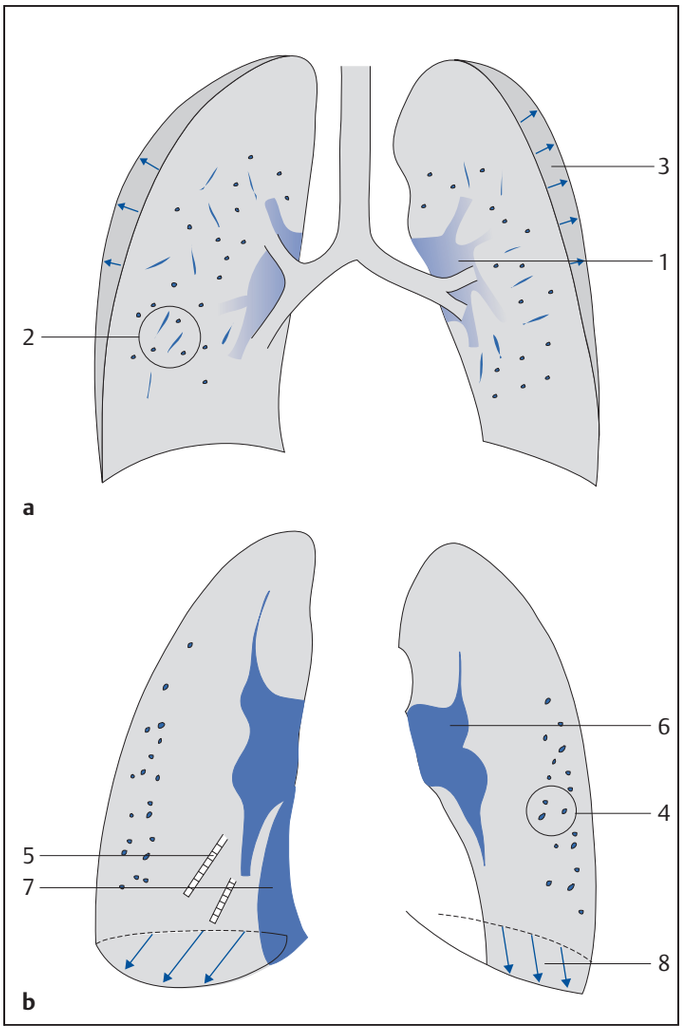

Fig. 2.15 a, b Comparison of radiographic signs of acute and chronic bronchitis.

a Acute bronchitis is characterized by blurring of the dilated hyperemic central vessels (1), diffuse interstitial shadowing (2), and occasionally peripheral obstruction (3).

b Signs of advanced chronic bronchitis include diffuse interstitial (4) and peribronchial shadowing that may even include "tramline" shadows (5), pulmonary arterial hypertension (6), and right heart enlargement (7) with emphysematous barrel chest (8).

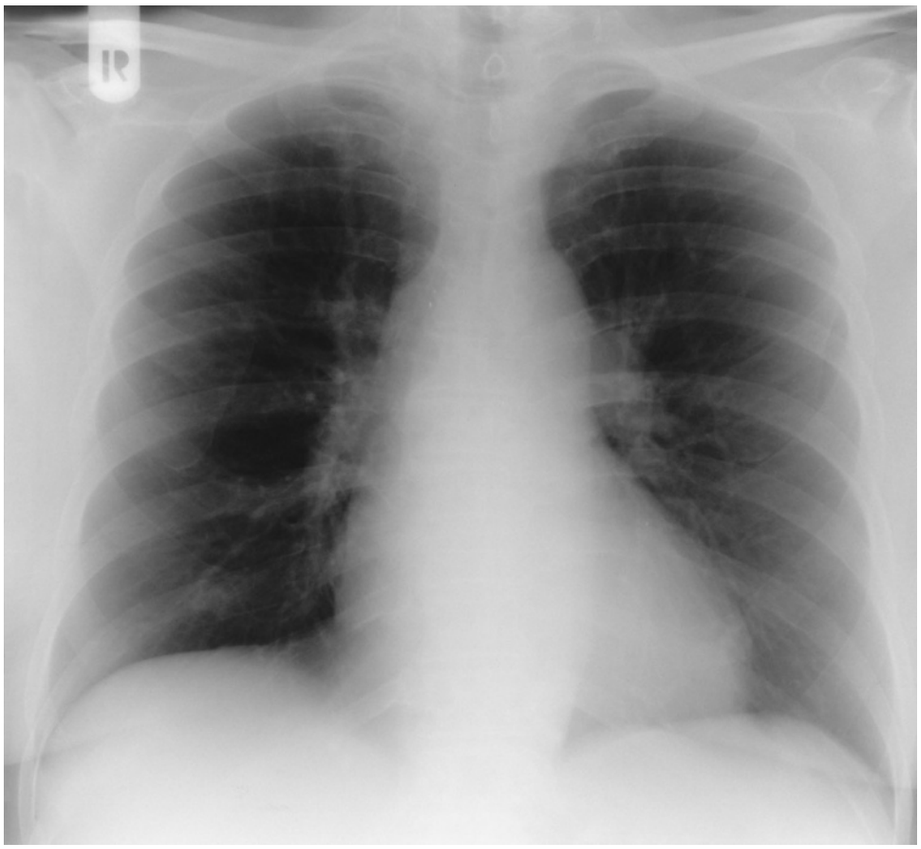

Fig. 2.16 Initial findings on a preoperative radiograph of a 73-year-old woman. Heart size is still within normal limits. The pulmonary segments appear slightly pronounced but without shadowing.

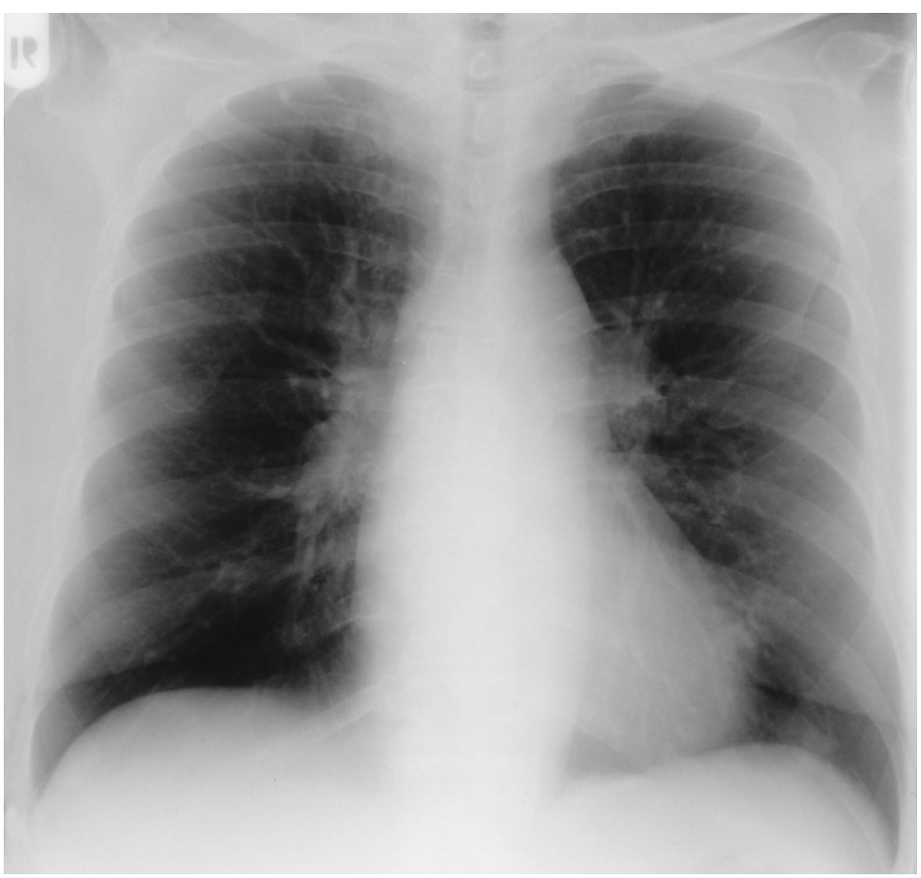

Fig. 2.17 The same patient presenting 6 months later. Clinical findings include productive cough. Heart size remains unchanged and within normal limits. However, now there is significant central hyperemia and diffuse interstitial shadowing consistent with acute bronchitis.

Chronic Bronchitis

In the case of chronic bronchitis we can expand the clinical definition of bronchitis as follows:

Chronic bronchitis = cough + sputum > 3 months.

Changes in the setting of chronic bronchitis are among the most common abnormal findings on a plain chest radiograph. They are so common that the evaluating physician is often inclined to dismiss them as "normal age-related findings." This raises the question of what is "normal." Perhaps it is no longer "normal" to have a lung that does not exhibit bronchitic pathology. Even published literature cites the prevalence of chronic bronchitis with normal radiographic findings as high as 50%. We strongly disagree.

Radiologic Changes after Years of Smoking

The often seemingly inevitable cascade of radiologic findings over the course of a smoker's life includes:

- *Peribronchial changes* (peribronchial cuffing, occurrence of parallel tubular "tramline" shadows in the lower fields with a pronounced striped pattern)
- Occurrence of a diffuse peripheral pattern of *very finely nodular densities*
- Development of obstructive barrel chest
- Pulmonary emphysema and pulmonary arterial hypertension

According to Fritz Ball, the strictest definition of the presence or absence of interstitial shadowing is expressed by the statement: "Pulmonary shadowing is nothing more than a low-contrast angiogram." We should qualify this by noting that segmental bronchi visualized end-on and identifiable as fine ring shadows do not represent abnormal shadowing.

The first stage of bronchitic shadowing and intrinsically the most difficult to identify is characterized by excessive visualization of lung tissue in regions that are often overexposed. In this sense, the smoker's lung demonstrates pulmonary anatomy "better" than normal findings (**Fig. 2.18**). Here one should consider whether the shadowing is caused by blood vessels alone or by the disproportionate prominence of other structures.

Extreme variants of chronic bronchitis (**Fig. 2.19**) lead to severe changes in pulmonary architecture that can complicate the evaluation of other pathologies such as pneumonia, overhydration, and tumor or even mask them completely.

Definition of Chronic Bronchitis

Chronic bronchitis is defined as productive cough persisting over a period of at least 3 months in two successive years. Other reasons for chronic cough such as neoplasms or chronic congestion must be excluded. The common mixed clinical picture of chronic obstructive bronchitis in combination with emphysema is referred to as **chronic obstructive pulmonary disease (COPD).** It is defined as a chronic irreversible obstruction of the airways developing over a period of years and resulting from pathologic reactions of the lungs to inhaled noxious agents. However, it is not bronchitis but secondary bronchiolitis in the setting of chronic bronchitis that causes the obstructive emphysema. Accordingly, Kartagener stated that there is no such thing as obstructive bronchitis because what is meant by this term is actually chronic bronchiolitis.

Yet what is meant by "diffuse shadowing as in chronic smoker's bronchitis" is immediately clear to every physician. Although this characterization has often been criticized as imprecise, it remains firmly entrenched because in a certain sense it aptly describes the findings. It is difficult to arrive at a more precise characterization. Published literature offers nothing that could provide the basis for a classification system in a manner analogous to the ILO classification of the pneumoconioses based on comparative radiographs. Interstitial shadowing is nonspecific and necessarily involves a broad spectrum of entities that must be considered in a differential diagnosis.

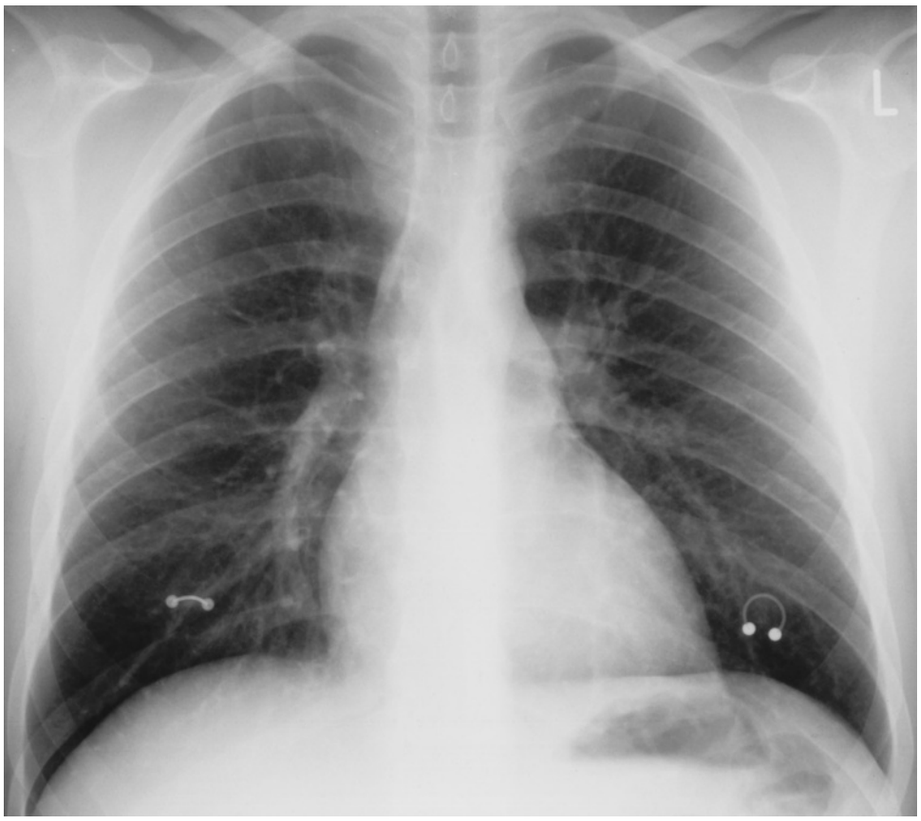

Fig. 2.18 Severe smoker's bronchitis with diffuse, finely nodular shadowing. The patient is a 23-year-old man with a history of drug use and many years of cigarette smoking. Heart size is normal. No patchy infiltrates are detectable; however, there is considerable increase of overall lung markings. Bilateral nipple piercing.

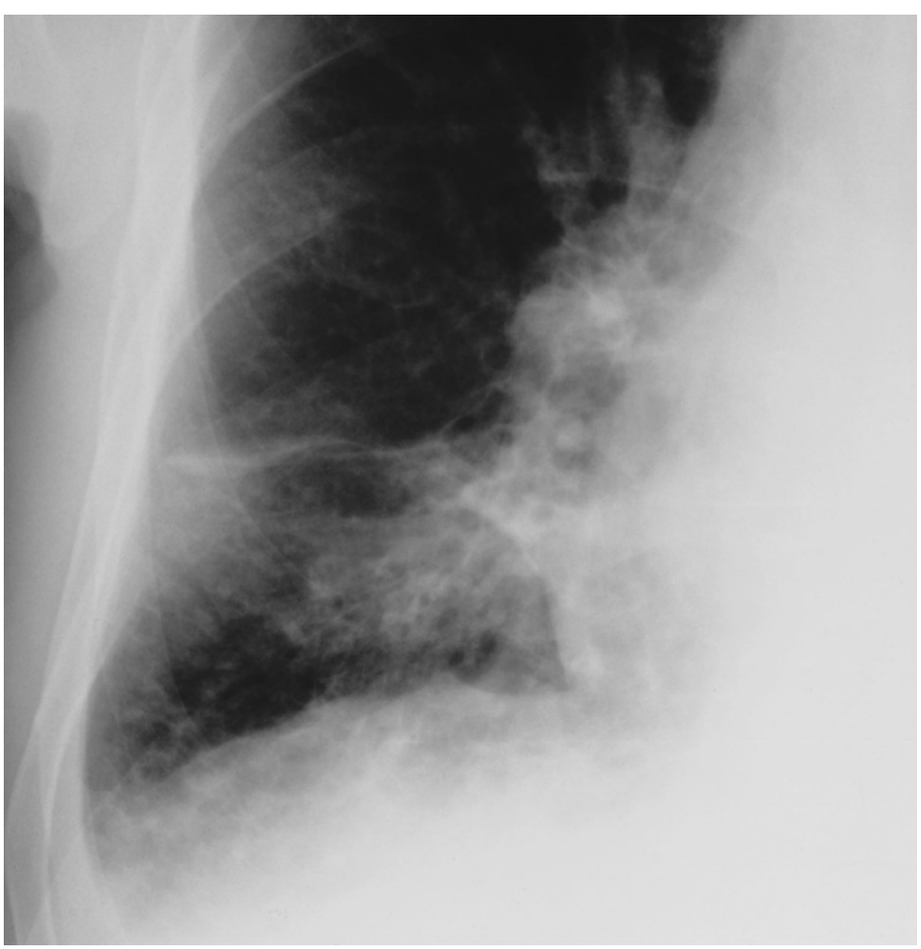

Fig. 2.19 Extreme form of chronic bronchitis (detail). Massive interstitial shadowing in a 77-year-old man with a history of many years of cigarette smoking, radiograph obtained prior to placement of a cardiac catheter. Diffuse septal and peribronchial shadowing. The changes largely mask the normal vascular markings (analogous to ILO 3/2).

Peribronchial Shadowing

Chronic inflammatory processes in the bronchial walls lead to thickening of the wall with:
a) Peribronchial cuffing
b) "Tramline" shadows

Both signs are produced by the same pathologic correlate, (a) viewed end-on (see **Fig. 2.6**) and (b) viewed tangentially (**Fig. 2.20**). Obviously (b) is less clearly visualized and therefore is observed less often or only in advanced cases. Known as the "tramline" sign, this peribronchial shadowing is most clearly visualized in the right paramediastinal region on the posteroanterior radiograph and in the posterobasal region on the lateral film.

On CT studies, a decisive finding in addition to bronchial wall thickening is that the course of the bronchi can be traced far into the periphery (**Fig. 2.21**).

Micronodules

Published literature to date has made little mention of the *occurrence of micronodules*. However, these findings are virtually diagnostic of chronic smoker's bronchitis. In their morphology, micronodules resemble small blood vessels imaged end-on and indeed are virtually indistinguishable from them. Crucial to the diagnosis is the number of such tiny structures in any one section of the image (**Fig. 2.22**). It is impossible to define which of the tiny shadows corresponds to the peripheral arteriole, but in any case too many such shadows are present. The small nodular shadows correspond to p shadows in the ILO classification of the pneumoconioses. The CT correlates of these micronodular changes are ill-defined peripheral parenchymal micronodules measuring 1–2 mm in diameter (**Fig. 2.23**).

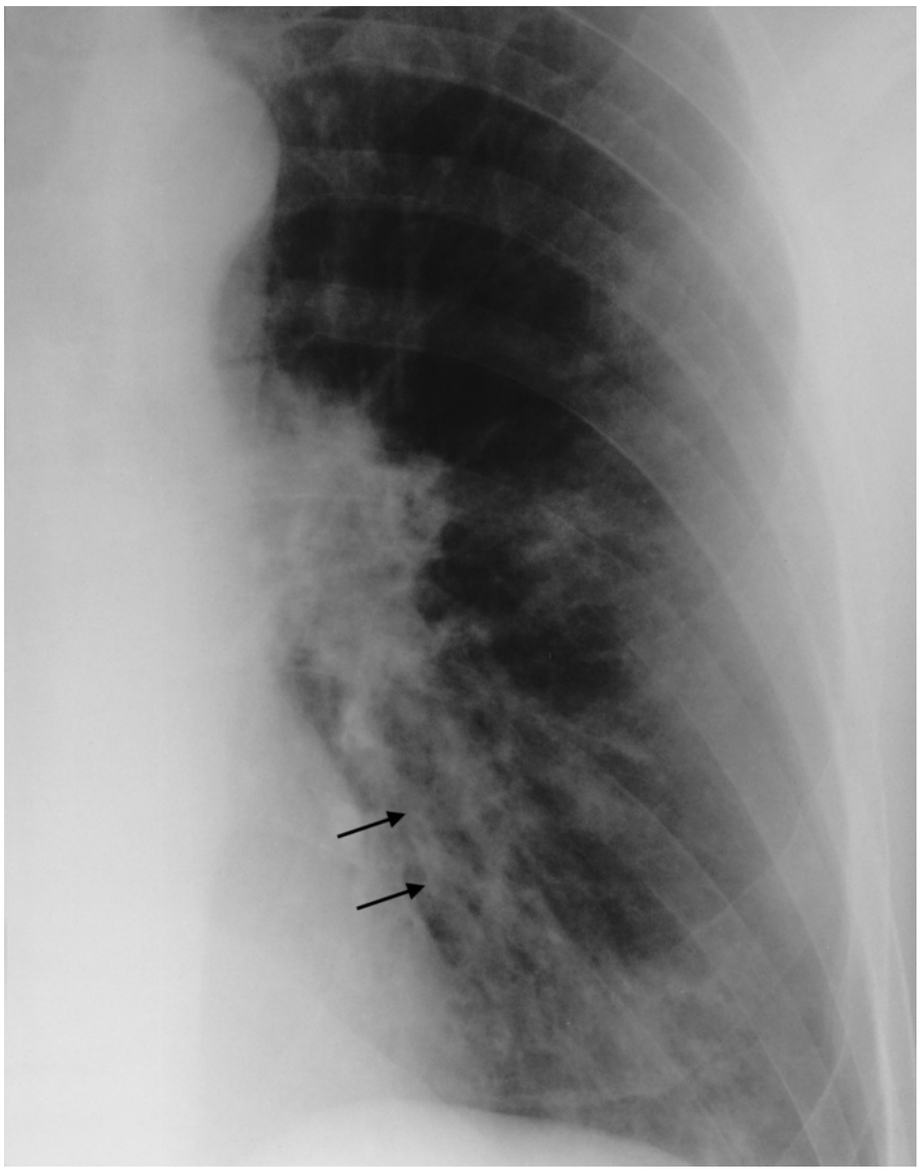

Fig. 2.20 "Tramlines" as a sign of bronchial wall thickening. The patient is a 61-year-old man with a history of many years of chronic bronchitis. "Tramline" shadowing (black arrows) is visible in the left paracardiac region.

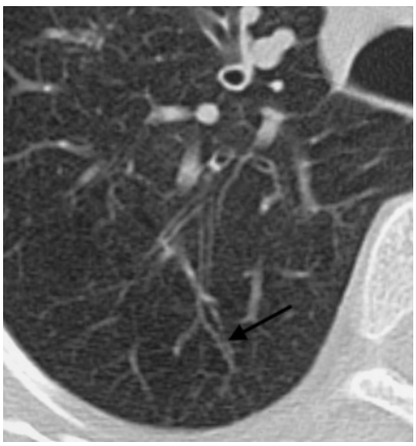

Fig. 2.21 The course of the bronchi can be traced far into the periphery (black arrow). This is a sign of chronic bronchitis with thickening of the bronchial wall.

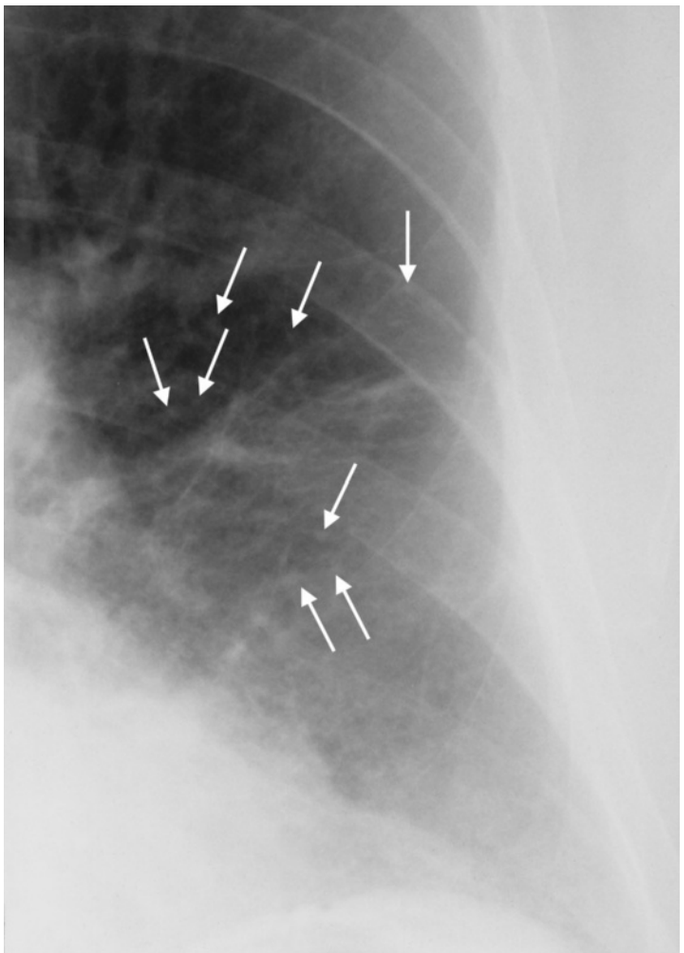

Fig. 2.22 Peripheral micronodular changes in severe chronic bronchitis (detail). Finely nodular shadowing (arrows) exceeding the possible number of peripheral blood vessels coursing through this region.

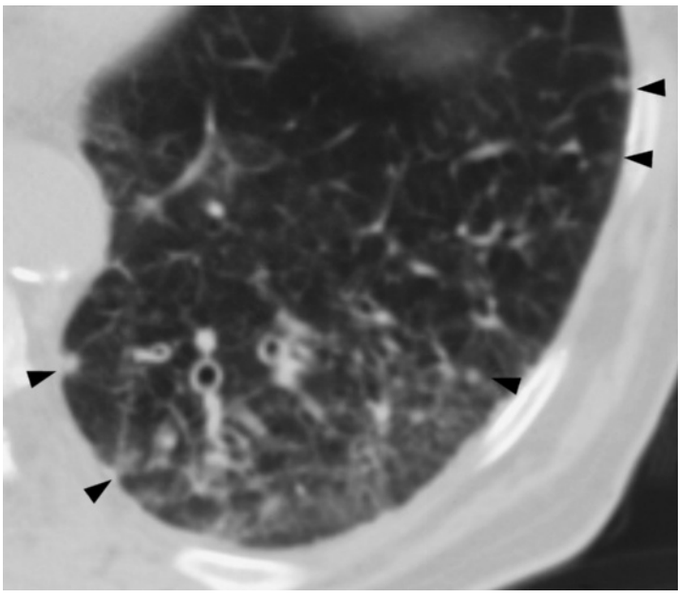

Fig. 2.23 CT image of Fig. 2.22 (enlarged). CT findings include diffuse interstitial shadowing with several subpleural micronodules (black arrowheads). Severe bronchial wall thickening.

Obstructive Barrel Chest

Chronic bronchitis and emphysema often occur together in the clinical picture of COPD.

Patients with chronic bronchitis are divided into two clinical and radiologic subtypes:

- More bronchitic, less obstructive with signs of right heart failure ("blue bloater")
- Highly obstructive ("pink puffer")

Usually overweight patients, the **"blue bloaters"** exhibit a productive cough, frequent episodes of worsening with infections and bronchospasm and severe changes in blood gas levels (hypoxia and hypercapnia). In contrast to the "pink puffers" the patient appears to succumb to the disease with slight shortness of breath. The latent hypoventilation leads to a pale appearance with cyanotic blue mucous membranes. These patients tend to develop pulmonary hypertension and cor pulmonale (**Fig. 2.24**). Accordingly, findings frequently include right heart failure with peripheral edema.

The predominant feature of the disease in **"pink puffers"** is emphysema (**Fig. 2.25**). They exhibit early dyspnea with nonproductive cough and normal blood gas values at rest. These patients are thin or even emaciated with a bony barrel chest and prominent pectoralis muscles (which aid in respiration). "Pink puffers" are fighters who work against the shortness of breath. Their skin color tends to be pinkish due to slight hyperventilation.

The signs of chronic obstruction are discussed in the section on emphysema (see p. 80 ff).

Pulmonary Arterial Hypertension

For a discussion of the signs of pulmonary emphysema and pulmonary arterial hypertension secondary to chronic bronchitis, see page 84.

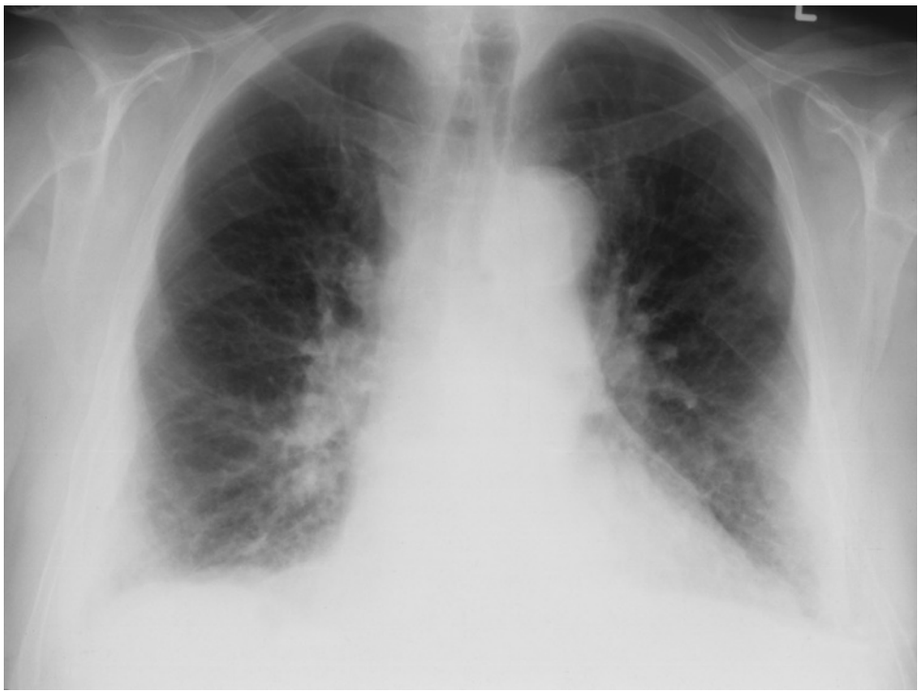

Fig. 2.24 Plain chest radiograph of a "blue bloater." The patient is a 77-year-old man with clinical findings of COPD (routine preoperative radiograph). With poor inspiration, the film shows what appears to be global heart enlargement without signs of decompensation. Findings also include reduced ventilation in the basal segments. Massive, primarily finely nodular shadowing with thickened and blurred hila and a relatively wide upper mediastinum indicative of right heart failure are observed.

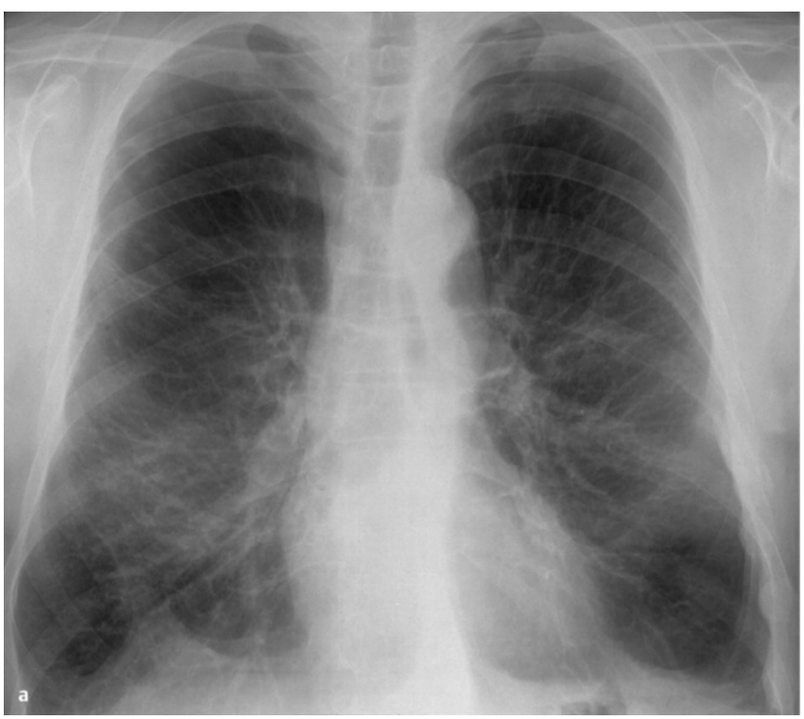

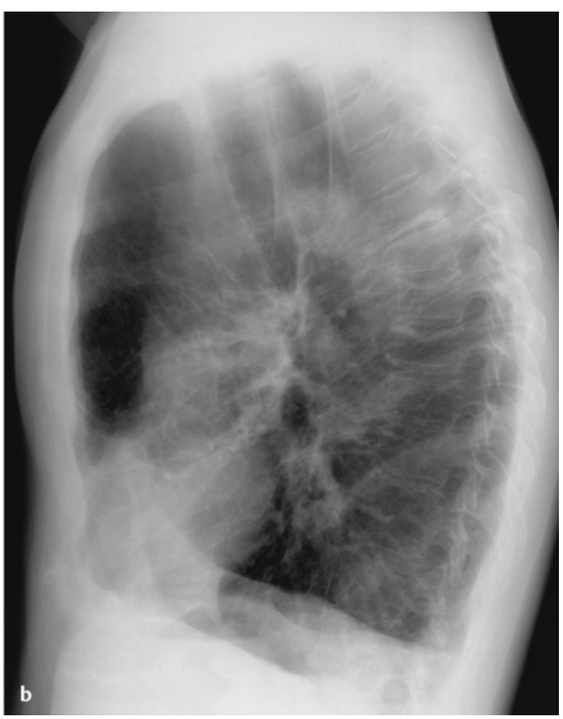

Fig. 2.25 a, b Plain chest radiographs of a "pink puffer" in two planes. The patient is a 50-year-old man with very severe smoker's bronchitis, alcohol abuse, and arterial hypertension.

a Diffuse interstitial and peribronchial shadowing. The posteroanterior view shows significantly diminished vascularity in the apical lung.

b The lateral view shows a significantly enlarged retrosternal space with faint sagittal curvature of the sternum. Other findings include old rib fractures and thoracic vertebral impression fractures.

Bronchiolitis

Inflammatory processes of the tracheobronchial tree produce spirometric changes (increased vital capacity, reduced Tiffeneau test values) only where there is bronchiolar involvement. Because there are no mucus-secreting cells at the level of the terminal and respiratory bronchioles, the clinical picture of isolated bronchiolitis without bronchitis lacks the sputum characteristic of the latter. However, severe dyspnea is the predominant symptom. Caused primarily by viral agents and usually affecting children, acute bronchiolitis often occurs in epidemics.

Bronchiolitis = cough + shortness of breath.

Bronchiolitis occurs in several distinct forms that are distinguishable both on the plain chest radiograph and on CT images (**Fig. 2.26**):

- Severely obstructive form
- Proliferative form with miliary pattern
- Bronchiolitis with organizing pneumonia

Obstructive Form

On the plain chest radiograph, the obstructive form of bronchiolitis is characterized by significant peripheral hyperinflation with central peribronchial shadowing (**Fig. 2.28**). Here, hyperinflation is observed with a low diaphragm and hypovascularity. It has occasionally been said that normal findings do not exclude bronchiolitis; this is based on observation of less severe forms of the obstructive form of bronchiolitis. The statement that severe shortness of breath without an adequate correlate on the chest radiograph is a clinical symptom of bronchiolitis should be regarded similarly.

Proliferative Form

Infiltration and thickening of the bronchiolar wall usually appears on the summation image of the chest radiograph as nonspecific reticulonodular shadowing. Obstruction of the smallest airways, whether from mucosal swelling or formation of granulation tissue (bronchiolitis obliterans), is visualized on both the plain chest radiograph and CT (**Fig. 2.29**) as miliary shadowing. CT can clearly differentiate miliary shadowing in bronchiolitis from nonspecific shadowing. Findings include (**Fig. 2.27**):

- Faint centrilobular opacities resembling cotton-wool balls
- Centrilobular "Mercedes star" patterns
- "Tree-in-bud" sign

Linear densities that either follow the bronchovascular bundle and course largely perpendicular to the pleura or are aligned parallel to it, are consistent with plate atelectases and are caused by complete occlusion of the bronchiolar lumen.

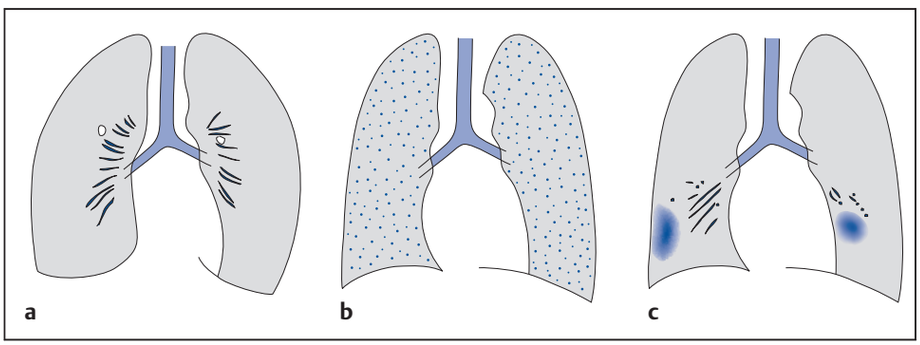

Fig. 2.26 a–c Various forms of bronchiolitis.
a Severely obstructive form with hyperinflated chest.
b Finely nodular form with miliary pattern.
c Locally limited form with circumscribed densities indicative of organizing pneumonia.

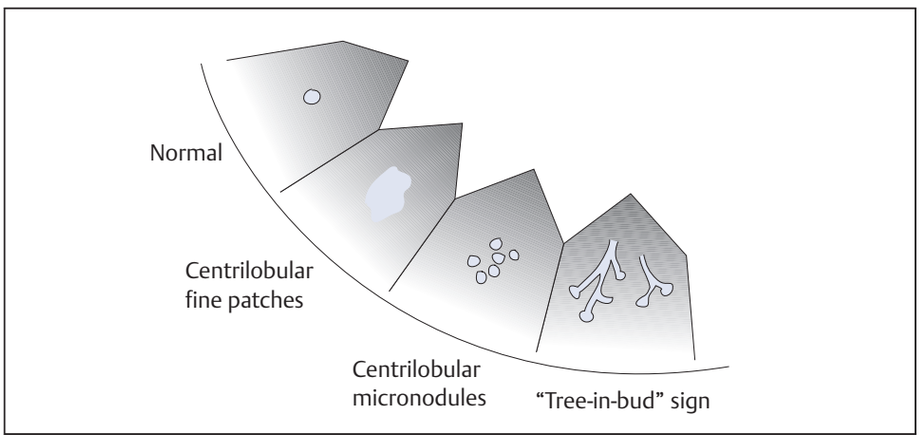

Fig. 2.27 CT signs of bronchiolitis. Aside from centrilobular finely patchy shadows there are also centrilobular micronodules or branchlike shadows in the secondary lobule, some of which have a "Mercedes star" appearance.

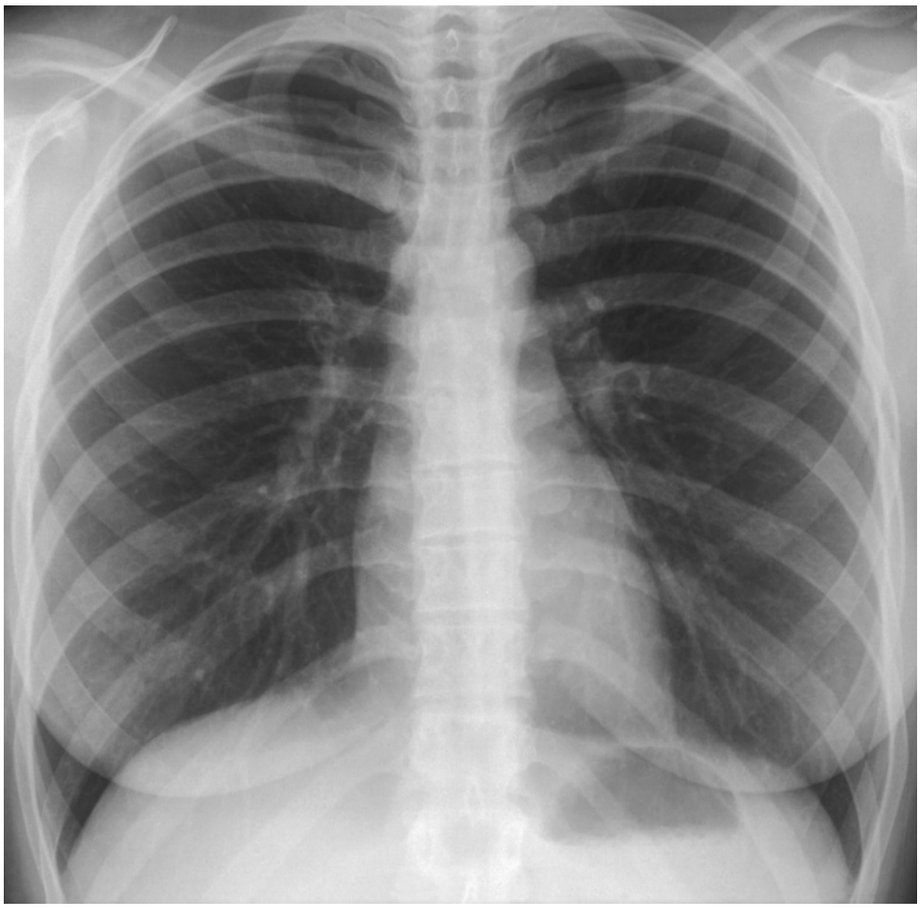

Fig. 2.28 Obstructive form of bronchiolitis. Primarily central peribronchial shadowing with significant peripheral obstruction in a 24-year-old woman with massive dyspnea during a "cold."

Fig. 2.29 a–c Proliferative form of infectious bronchiolitis with miliary picture. The patient is a 65-year-old man with COPD; radiograph obtained in acute disease with severe dyspnea and dry cough. Aortic configuration of the heart without signs of decompensation or area consolidation.

a Severe, diffusely distributed finely nodular pattern involving primarily the middle and lower lung fields.

b The detail shows a speckled acinar pattern.

c The CT image shows a "tree-in-bud" pattern in several adjacent secondary lobules of segment 9 in the left lung (black arrow). The other areas of the lung included in the image show finely nodular, primarily centrilobular shadowing.

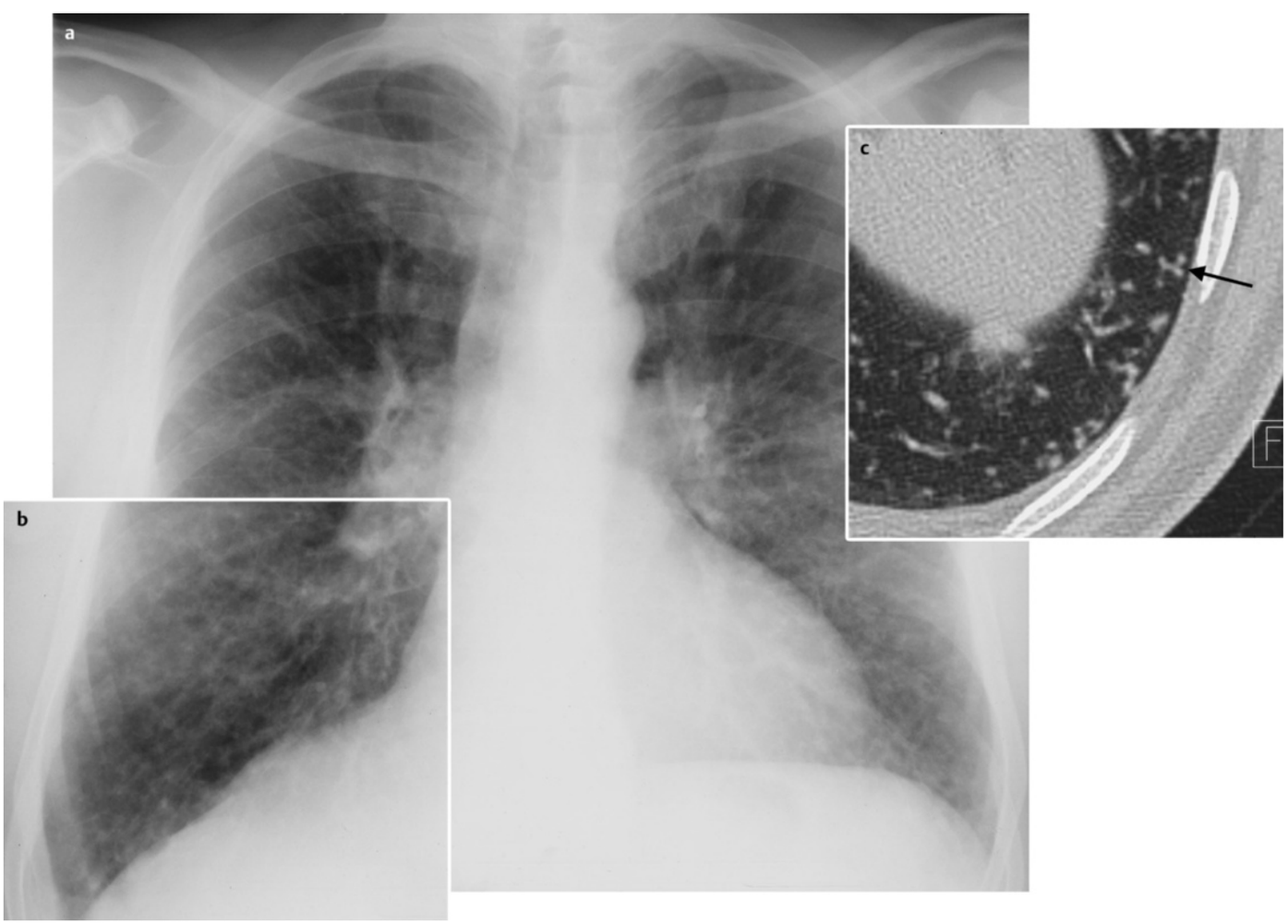

Bronchiectasis

Irreversible dilatation of the middle and small bronchi is referred to as bronchiectasis. The former classification of bronchiectasis as congenital (primitive) or acquired seems rather pointless. Most of the forms earlier referred to as "congenital" are also caused by early childhood infections with bronchiolitis. Special cases include:

- Bronchiectasis in cystic fibrosis (**Fig. 2.31**)
- Kartagener syndrome (bronchiectasis and situs inversus)
- Immotile cilia syndrome

Kartagener demonstrated that these forms in particular are hereditary and congenital.

Three morphologic types of bronchiectasis are differentiated (**Fig. 2.30**):

- Cylindrical
- Varicose
- Cystic or saccular

Radiographic signs suggestive of bronchiectasis include:

- Circumscribed shadowing with blurring of vascular structures
- Parallel streaky densities extending far into the periphery without tapering
- Changing patches
- Small fluid levels

Localized shadowing due to congestion of secretions within the bronchiectatic area is a nonspecific finding. The same applies to the blurring and bundling of the vascular band in these areas caused by peribronchial fibrosis (**Fig. 2.32**).

Thickened bronchial walls distinguishable as parallel linear densities are described as typical findings on the plain chest radiograph. Viewed end-on, the bronchiectatic areas appear as ring-like air-filled radiolucencies 5–20 mm in diameter (**Fig. 2.33**). Bronchiectatic areas completely occluded by mucus (mucoceles) appear as round nodules. Where they are incompletely occluded, they form fluid levels that must be differentiated from abscesses. Where the mucoceles are visualized over a longer distance, one will rarely observe linear shadow bands that split into V or Y figures and extend toward the periphery. These round nodules formed by retention of secretions can change rapidly. The nodules may be visible in the morning and have been coughed up by evening. In protracted chronic cases, signs of pulmonary hypertension or cor pulmonale may be detectable as well.

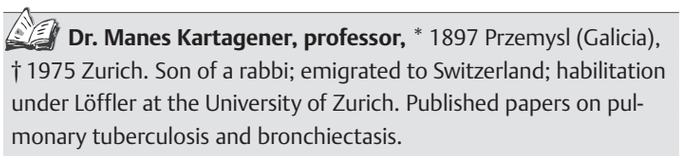

Dr. Manes Kartagener, professor, * 1897 Przemysl (Galicia), † 1975 Zurich. Son of a rabbi; emigrated to Switzerland; habilitation under Löffler at the University of Zurich. Published papers on pulmonary tuberculosis and bronchiectasis.

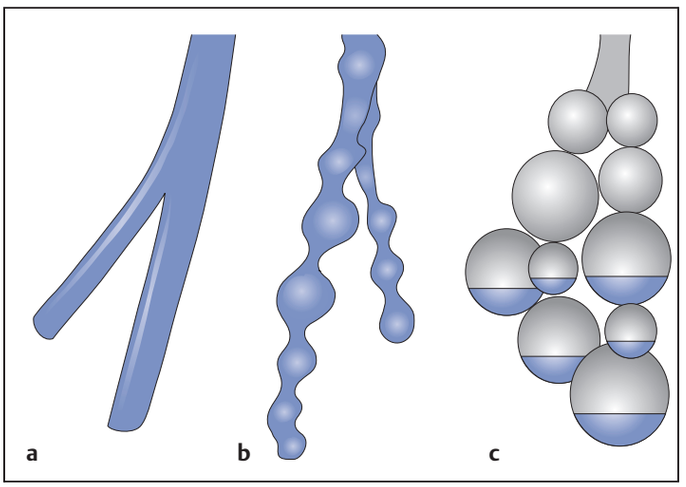

Fig. 2.30 a–c **Types of bronchiectasis.** Bronchiectasis belongs to one of three schematic types: cylindrical bronchiectasis with no taper and usually ending abruptly (**a**), varicose bronchiectasis with a meandering appearance due to intermittent widening of the bronchial lumina (**b**), or cystic bronchiectasis exhibiting circumscribed "clusters of grapes" (**c**).

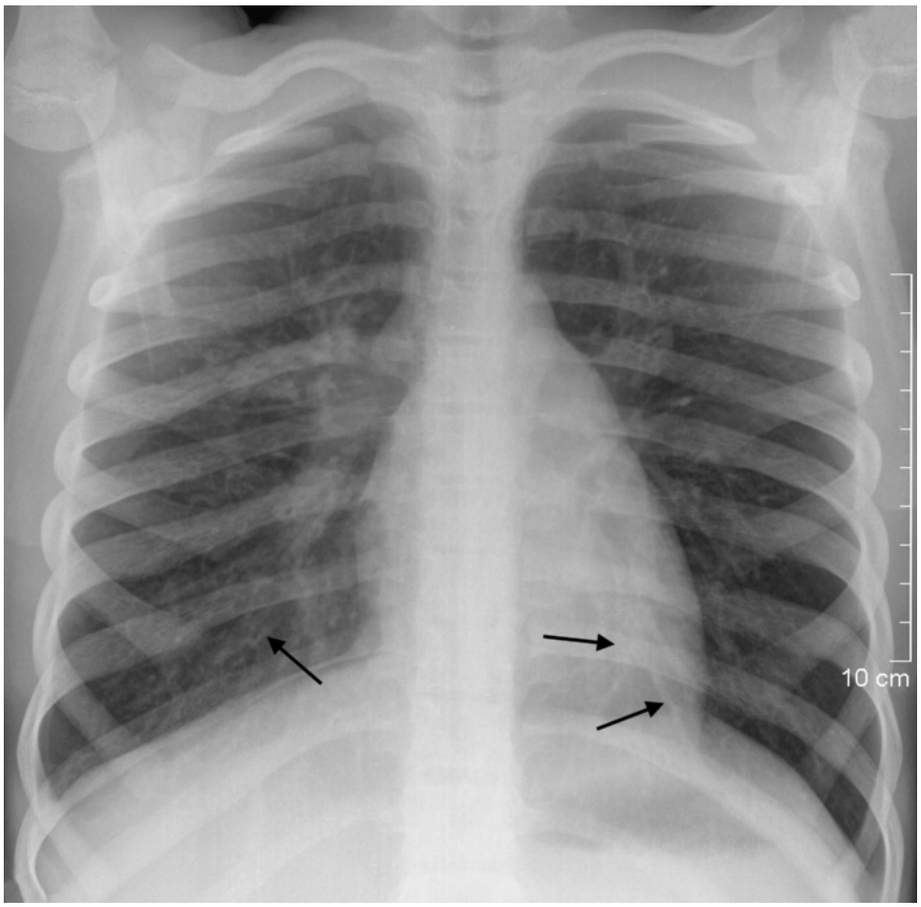

Fig. 2.31 **Cystic fibrosis.** The patient is an 8-year-old boy with cystic fibrosis; follow-up radiograph in *Pseudomonas* pneumonia. Significant hyperinflation in the peripheral chest with primarily central peribronchial shadowing and diffuse nodular pattern of opacities. Dilated bronchi are presumably present in both lower lobes (black arrows). Residual infiltrate in the right perihilar region.

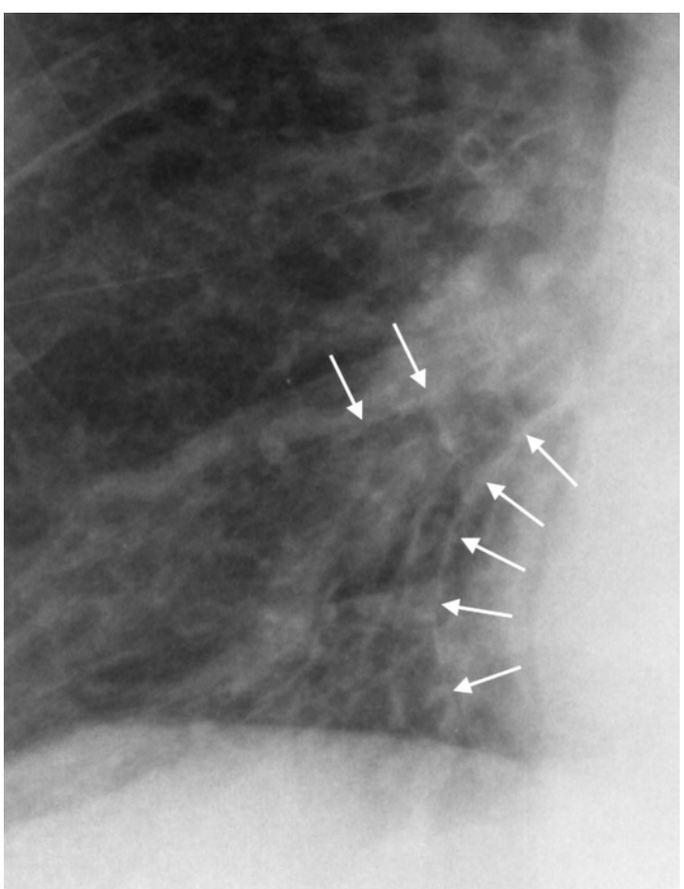

Fig. 2.32 **Streaky densities in bronchiectasis (detail).** In addition to diffuse nodular interstitial shadowing, findings include parallel streaky densities (white arrows) representing thickened bronchial walls in dilated bronchi. The structures of the vascular bundle appear blurred due to peribronchovascular fibrosis.

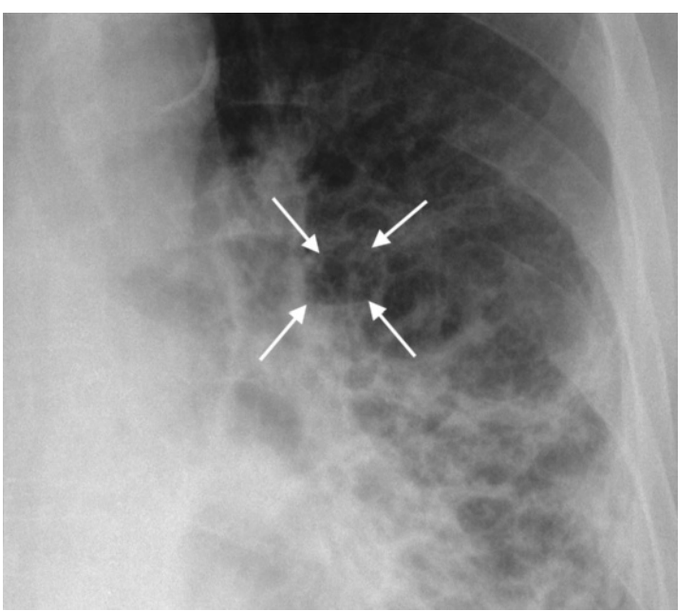

Fig. 2.33 **Fluid level in bronchiectasis (detail).** Several ring structures with diffuse densities in the lingular region corresponding to the cystic bronchiectasis found there. A visible fluid level in a larger cavity (white arrows).

Computed Tomography

CT allows the reliable detection and classification of bronchiectasis. CT signs of bronchiectasis include:

- Airways that extend into the periphery without tapering
- "Signet ring" sign (bronchial diameter exceeds the diameter of the accompanying pulmonary artery)
- Thickening of the wall and meandering course
- Thickening of the wall with "cysts"

Bronchial structures cannot normally be demonstrated in the outer subpleural segments of the lung. Visualization of bronchi extending into the pulmonary periphery is therefore evidence of their abnormal dilatation (**Fig. 2.35**). Absence of peripheral tapering supports the diagnosis.

Although it is not possible to establish normal values for the width of the respective bronchus, bronchial dilatation can be readily demonstrated by comparing its diameter to that of the accompanying artery, which is normally of identical diameter. A bronchus that is wider than the artery is abnormally dilated. Together with the artery it can form a "signet ring" sign (**Fig. 2.36**).

CT can reliably differentiate the following three types of bronchiectasis (**Fig. 2.34**):

- Cylindrical
- Varicose
- Cystic or saccular

Cylindrical bronchiectasis can be identified as bronchi that extend into the periphery without tapering. The bronchi exhibit homogeneous wall thickening, are smoothly demarcated, and usually end abruptly (**Fig. 2.35, Fig. 2.36**).

In varicose bronchiectasis the bronchus usually exhibits a meandering course. Its longitudinal contours are narrowed, creating a "string of pearls" sign (**Fig. 2.37**).

Cystic bronchiectasis (**Fig. 2.38**) shows the most severe changes. The airways are distended like balloons. Individual bronchi can no longer be clearly identified. Instead one sees only clustered cystic masses. These "cysts" exhibit a segmental arrangement, increase toward the periphery, and extend from the hilum into the subpleural region.

On CT images, mucoceles (**Fig. 2.39**) appear as smoothly demarcated masses that must be differentiated from a tumorous process. The decisive diagnostic criteria here are bifurcations demonstrated within the mucocele. Three-dimensional reconstructions are very helpful in this regard (**Fig. 2.40**).

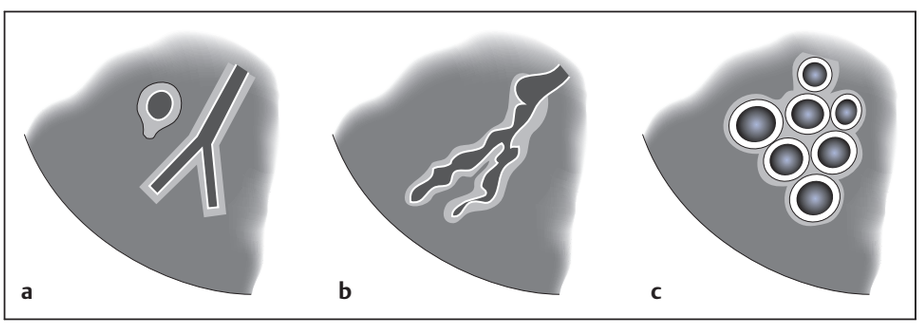

Fig. 2.34 a–c Appearance of the three types of bronchiectasis on CT.

a Cylindrical bronchiectasis imaged end-on appears as a "signet ring" sign with moderate thickening of the wall and absence of tapering.

b Varicose bronchiectasis is often found within densities and exhibits a meandering course.

c Cystic bronchiectasis in circumscribed areas appears as a conglomerate of air-filled and fluid-filled cavities.

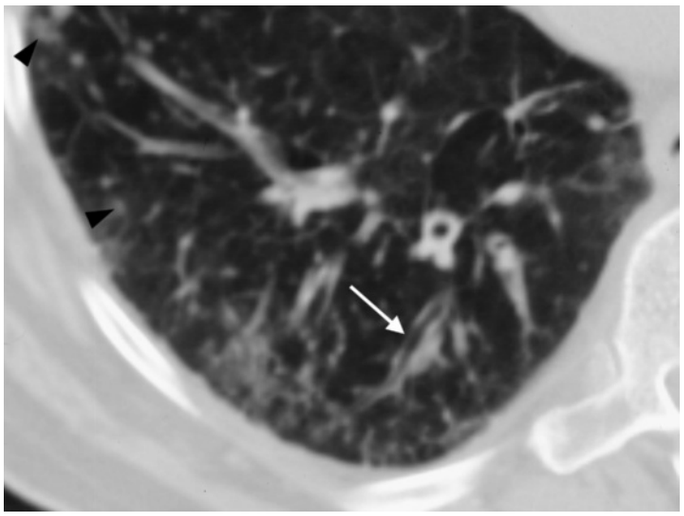

Fig. 2.35 Absence of tapering in cylindrical bronchiectasis. The abnormally dilated bronchus can be traced far into the periphery and does not taper (white arrow). Significant peribronchial cuffing and isolated micronodules (black arrowheads) are indicative of chronic respiratory bronchiolitis-interstitial lung disease (RB-ILD).

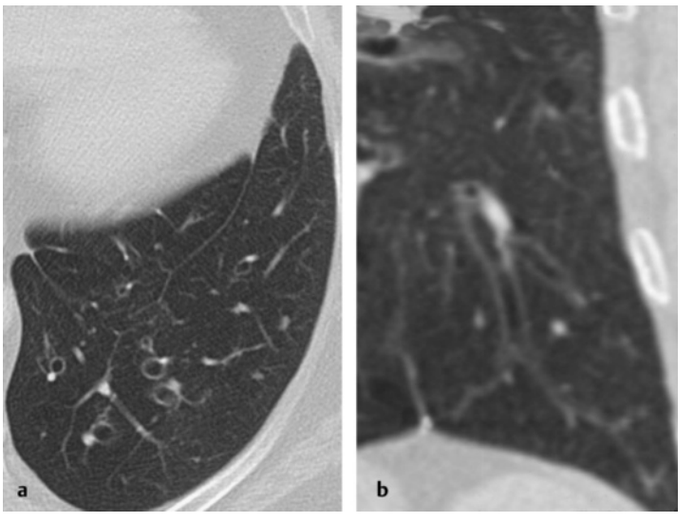

Fig. 2.36 a, b "Signet ring" sign in bronchiectasis.
a Several bronchi in segment 10 of the left lower lobe are dilated in comparison with the respective accompanying arteries.
b The coronal reconstruction demonstrates the cylindrical configuration.

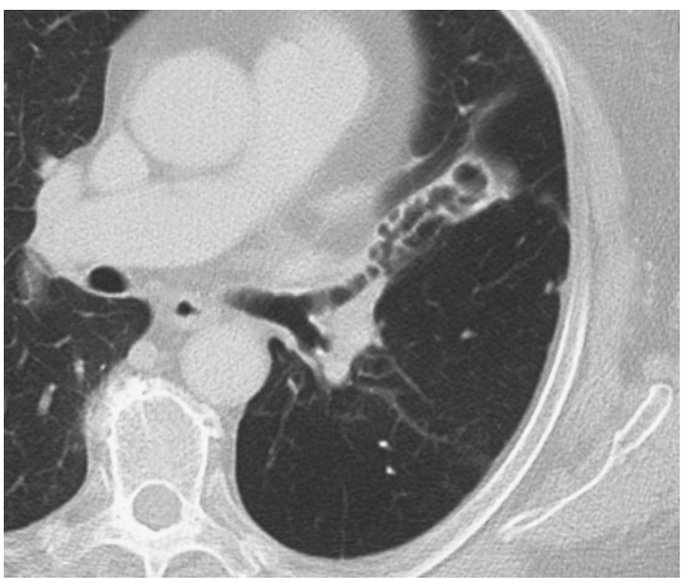

Fig. 2.37 Varicose bronchiectasis in an area of scarring. Diagnostic investigation of an uncertain shadow in the absence of clinical signs of pneumonia. Massive dilatation of the lingular bronchi with pronounced meandering. The thickened wall cannot be distinguished from the surrounding shrunken fibrotic tissue.

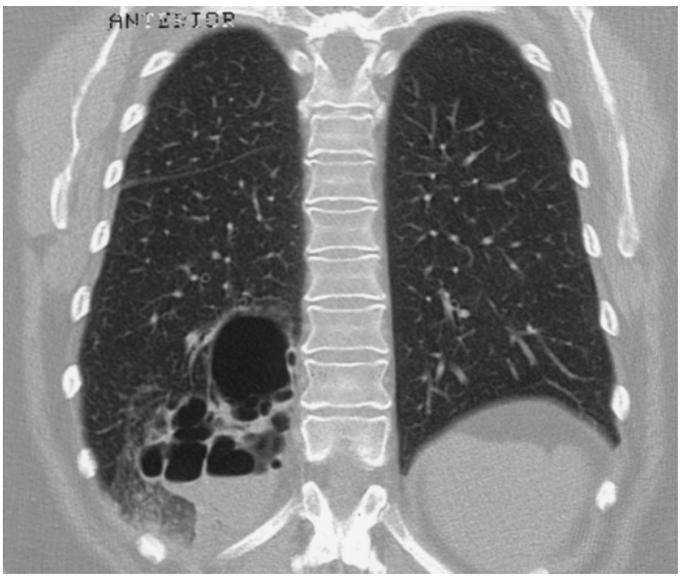

Fig. 2.38 Cystic bronchiectasis in the lower lobe. The coronal sequence shows clearly discernible circumscribed areas of cystic bronchiectasis appearing as "clusters of grapes" with fluid levels.

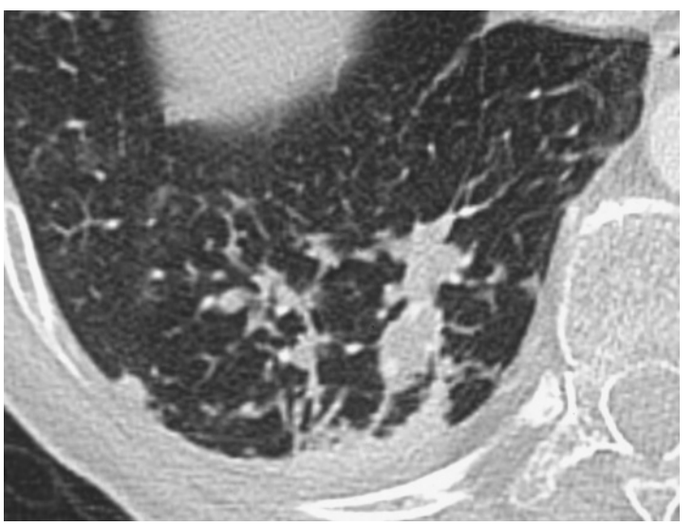

Fig. 2.39 Mucoceles in cylindrical bronchiectasis. The axial image shows an irregularly shaped shadow resembling a mass in segment 10 in addition to mucus-filled small airways, some with bizarre branching patterns.

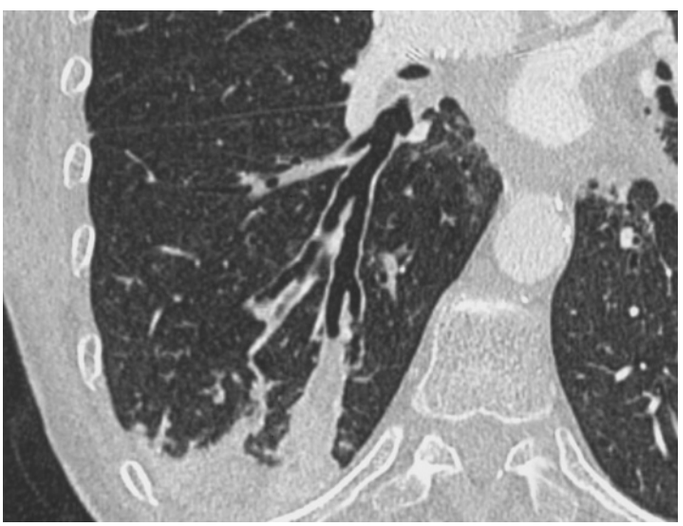

Fig. 2.40 CT reconstruction. The paraxial CT image clearly shows the cause of the circumscribed shadow visualized in **Fig. 2.39**. Massive swelling of the subsegmental bronchi with peripheral mucus filling consistent with a mucocele.

Pulmonary Emphysema

Chronic bronchitis and pulmonary emphysema are distinct disease entities but usually occur in combination. Emphysema (Greek εμφυσειν, emphysein, to blow into) in the strict sense is defined as an irreversible dilatation (i.e., one involving anatomic restructuring) of the air-filled spaces distal to the terminal bronchiole (**Fig. 2.41**).

Obstruction + alveolar wall destruction = irreversible dilatation

Forms of emphysema without significant obstruction include:
- Primary atrophic emphysema
- Senile atrophic emphysema
- Compensatory emphysema
- Emphysema occurring adjacent to scarring

A fundamental distinction should be made between emphysema and reversible enlargement of pulmonary air spaces without destruction of the pulmonary architecture. Such distension occurs in simple hyperinflation (volumen pulmonum auctum) such as can occur in an acute asthma episode. Rather confusingly, this has also been referred to as "acute emphysema" as distinct from chronic emphysema (i.e., emphysema in the strict sense).

The plain chest radiograph can reliably confirm or exclude severe forms of emphysema. Nonetheless, misdiagnoses of emphysema are hardly rare in daily clinical practice. Be alert to these diagnostic traps:
- Overexposed film
- Asthenic habitus (**Fig. 2.42**)

CT can readily detect even early forms of the disease and can reliably differentiate the various pathologic types.

"Acute Emphysema" (Volumen Pulmonum Auctum)

The picture of reversibly dilated air spaces (also called "volumen pulmonum auctum" [*auctum* from Latin *augmentare* = to augment, increase]) is occasionally encountered in patients examined during an acute asthma episode. Cursory examination of a radiograph obtained in a patient with no other complaints often leads to the misdiagnosis of normal findings. However, the increased radiolucency and chest volume should be obvious wherever previous imaging studies are available for comparison. These are direct but reversible signs of emphysema (**Fig. 2.43**). Massive hyperinflation of the lung due to bronchitis in an infant can occasionally be difficult to differentiate from pneumothorax.

Senile Emphysema

Atrophic senile emphysema (**Fig. 2.44**) is a result of the physiologic aging process and is not generally regarded as a disease. It is caused by the loss of alveoli with a compensatory increase in the size of the remaining structures. For this reason, both the radiologic findings and the underlying pathologic process in this condition resemble those in primary atrophic emphysema. In light of this pathophysiologic situation, one may expect to find fewer interstitial shadow patterns indicative of chronic bronchitis in patients with senile emphysema.

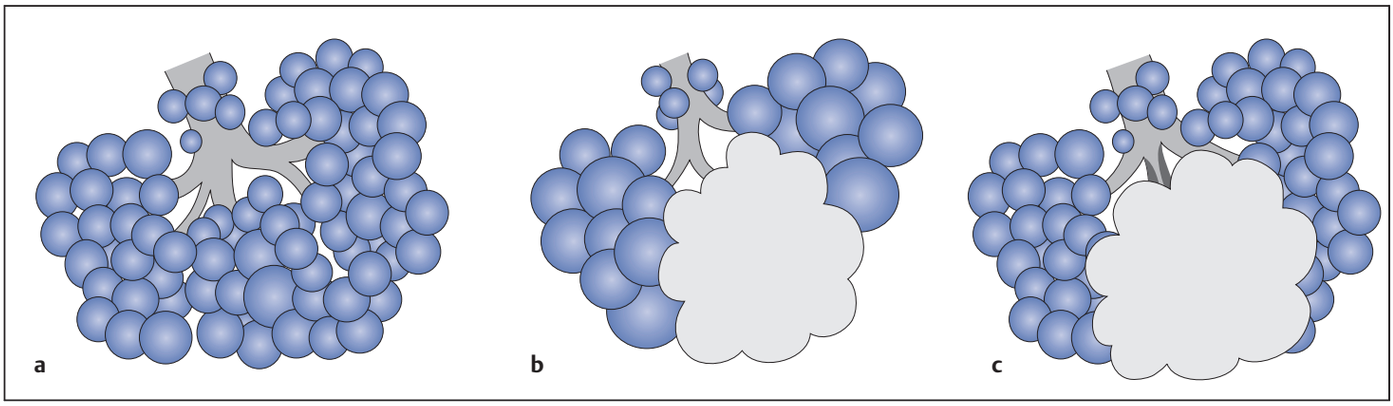

Fig. 2.41 a–c Schematic diagram of the various forms of emphysema.
a Unchanged secondary lobule.
b Primary emphysema exhibits homogeneous dilatation of all spaces with diffuse loss of alveolar walls.
c Obstructive emphysema begins in the center of the lobule with stenosis of the terminal bronchiole.

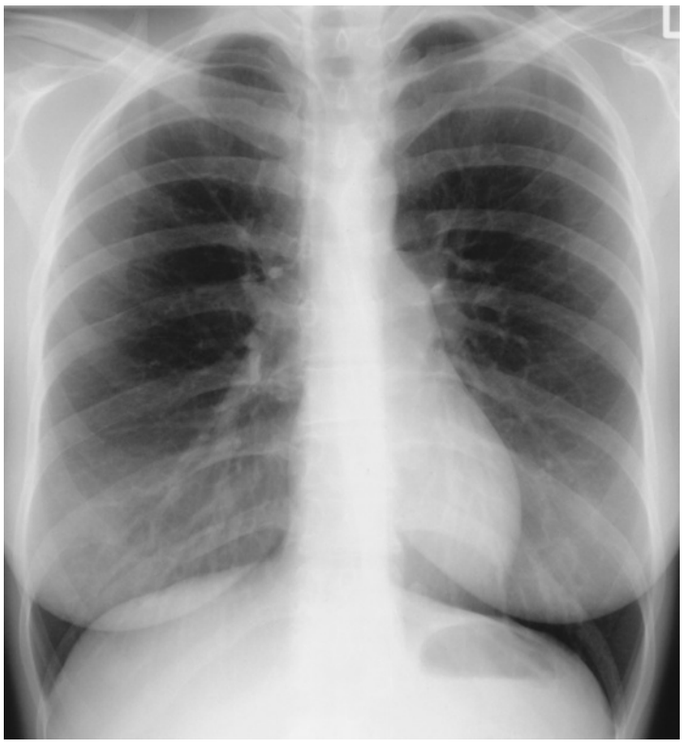

Fig. 2.42 Normal young adult habitus in a 22-year-old woman. Deep inspiration (the 10th rib is visible in the right medial costophrenic angle) should not be confused with acute obstruction or emphysema. Normal heart size without signs of decompensation, no signs of shadowing or infiltrates.

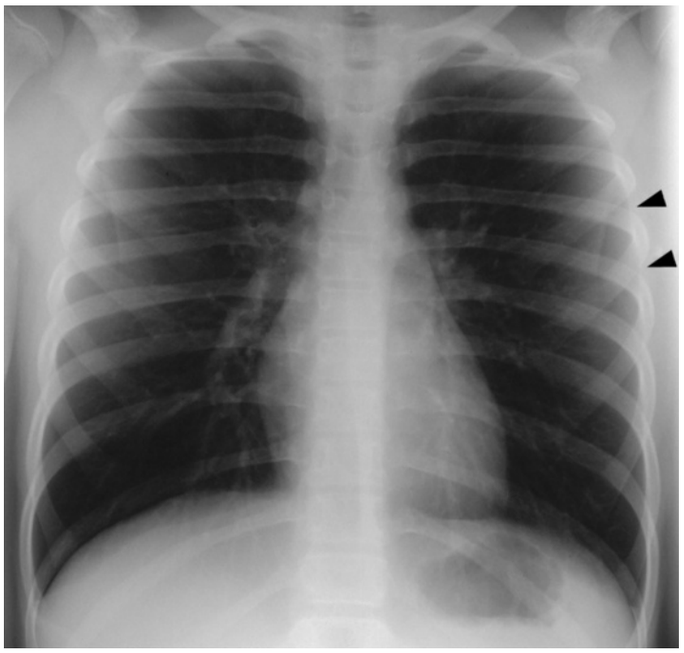

Fig. 2.43 "Acute emphysema" (volumen pulmonum auctum) in an acute asthma episode. The patient is a 10-year-old girl with significant dyspnea with known bronchial asthma. Acute hyperinflation of the chest with faint herniation of the pleura in the intercostal space (black arrowheads). Reduced peripheral vascularity.

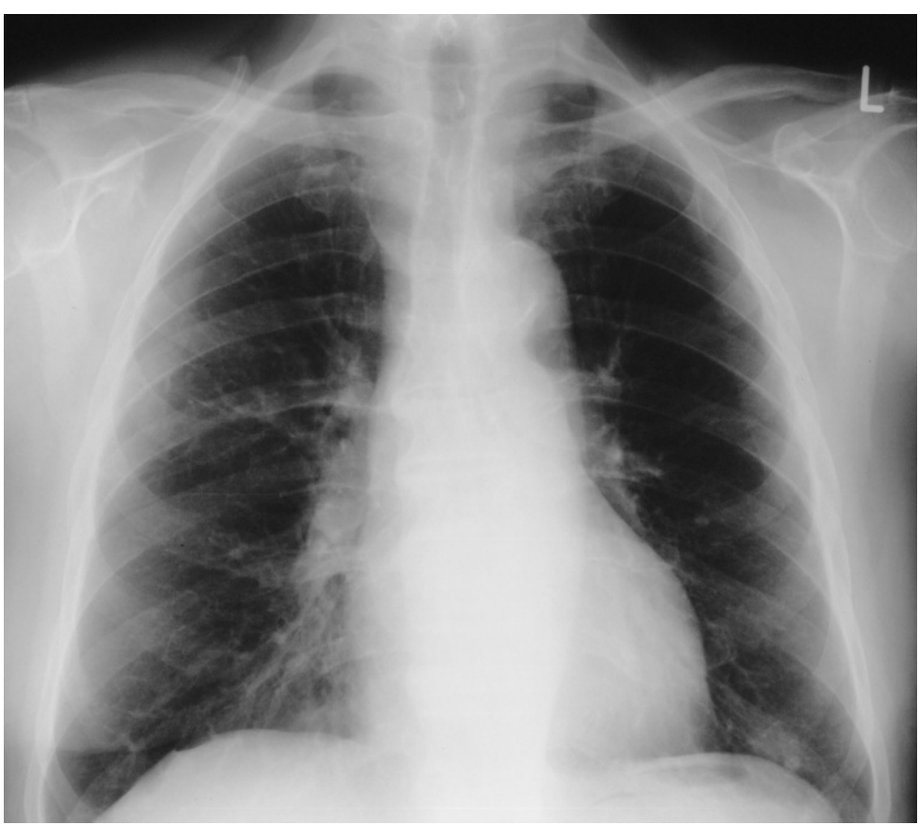

Fig. 2.44 Senile emphysema. Findings on a preoperative radiograph of a 90-year-old man. The 11th rib is just barely visible in the right phrenicomediastinal angle; findings are consistent with barrel chest. Vascularity is reduced in the apical region. There is no significant shadowing indicative of chronic bronchitis.

Emphysema in the Strict Sense

Signs of emphysema in the strict sense (**Fig. 2.45**) include:
- Increased lung volume
- Reduced vascularity
- Bullae

None of these signs is diagnostic. Increased volume can occur reversibly, or it can be associated with central airway obstruction. Reduced vascularity can occur in primary pulmonary arterial hypertension. A bulla can be the result of an inflammatory disorder. **Table 2.1** lists the radiographic findings that may be expected. These findings will be discussed in the following section.

Increased Volume

Increased lung volume in emphysema can be identified by the following criteria:
- Low diaphragm
- Flattened diaphragm
- Diaphragmatic digitations
- Increased intercostal distance
- Sagittal curvature of the sternum
- Barrel chest deformity

A low diaphragm is defined as depression of the diaphragm below the anterior end of the 7th rib in the right midclavicular line. A flattened diaphragm is present (a) when its highest point on the lateral film is less than 2.5 cm above a line drawn between the anterior and posterior costophrenic angles, or (b) when its highest point on the posteroanterior film lies less than 1.5 cm above a line drawn between the costophrenic and vertebrophrenic angles (**Fig. 2.46, Fig. 2.47**).

Tentlike diaphragmatic digitations are the result of visualization of diaphragmatic insertions normally obscured by the abdominal organs (**Fig. 2.46**).

The greater distance between the ribs, now coursing increasingly horizontally, is subjective. More important and more clearly identifiable is the enlargement of the retrosternal space resulting from the sagittal curvature of the sternum. Emphysema (like the early clinical finding of shortening of the distance between the jugular fossa and the cricoid cartilage) thus leads to protrusion of the sternum with a "kyphotic" sagittal angle. The further course of the disorder involves deformations of the entire thorax with development of a barrel chest and bell-shaped deformity and increased kyphosis of the thoracic spine. Fluoroscopy reveals a rigid chest with only slight respiratory excursion.

Little attention has been paid to changes in the intercostal space. Close observation reveals that pleural herniations occur here when lung volume is increased.

Table 2.1 Findings and radiologic criteria in pulmonary emphysema.

Radiographic sign	Measure
Decreased lung markings	▸ Distance from vessel to chest wall ▸ Retrosternal or retrocardiac overexposed areas ▸ Iris lamps required
Chest volume increase	▸ Low diaphragm ▸ Diaphragmatic digitations visible ▸ Flattened diaphragm ▸ Sagittal curvature of the sternum ▸ Increased intercostal distance ▸ "Drop heart" ▸ Rigid chest (on fluoroscopy)
Disorganized pulmonary architecture	▸ Ring structures = bullae ▸ Spider webs ▸ Honeycombing
Pulmonary hypertension	▸ Diameter of intermediate artery > 18 mm
Cor pulmonale	▸ Right ventricular enlargement ▸ Right atrial enlargement ▸ Widened mediastinum

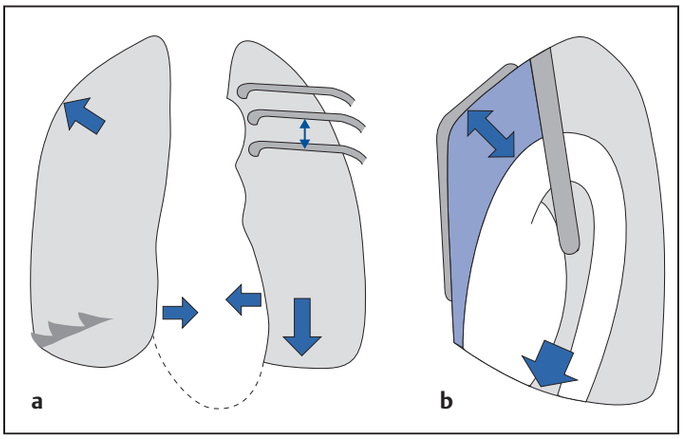

Fig. 2.45 a, b Diagram of volume increase.

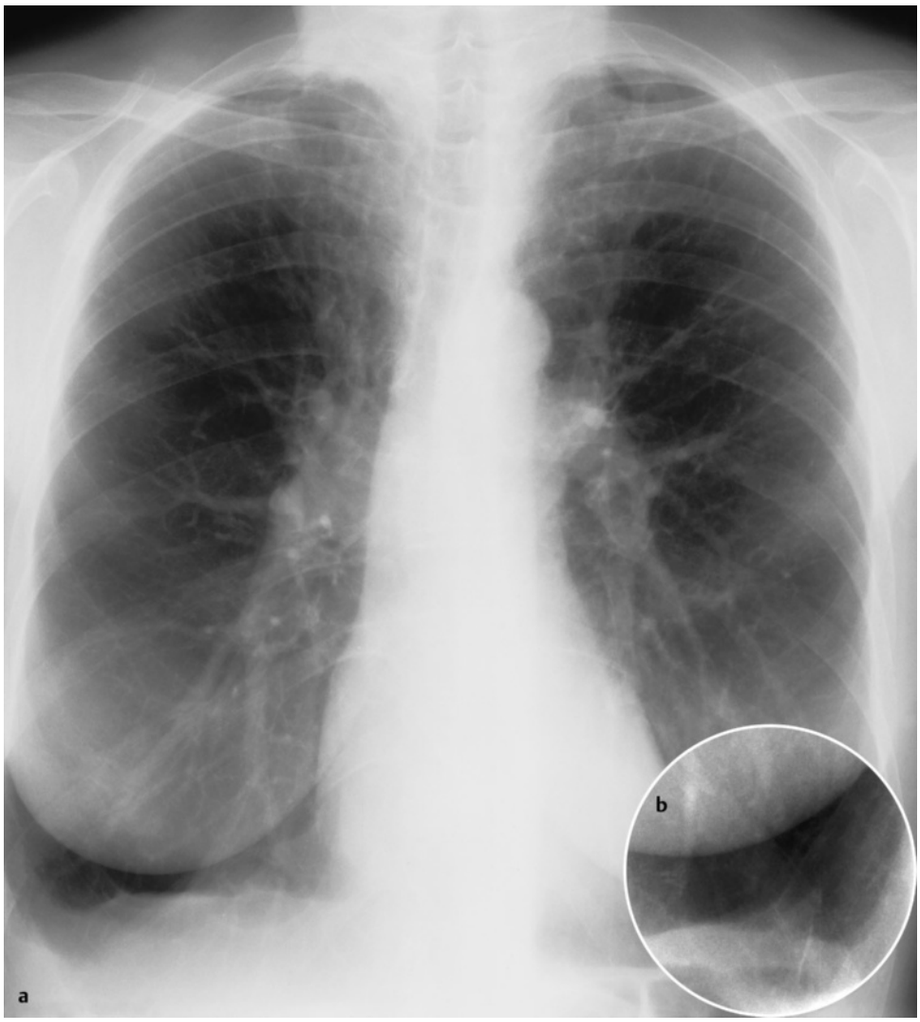

Fig. 2.46 a, b Increased volume in emphysema on the posteroanterior radiograph.

a The patient is a 63-year-old woman with a long history of COPD and pulmonary emphysema. Normal heart size. Hilar thickening is indicative of beginning pulmonary arterial hypertension. The 12th rib is identifiable in the phrenicomediastinal recess. The diaphragm is largely flattened.

b The detail shows a clearly visible diaphragmatic insertion in the left costophrenic angle.

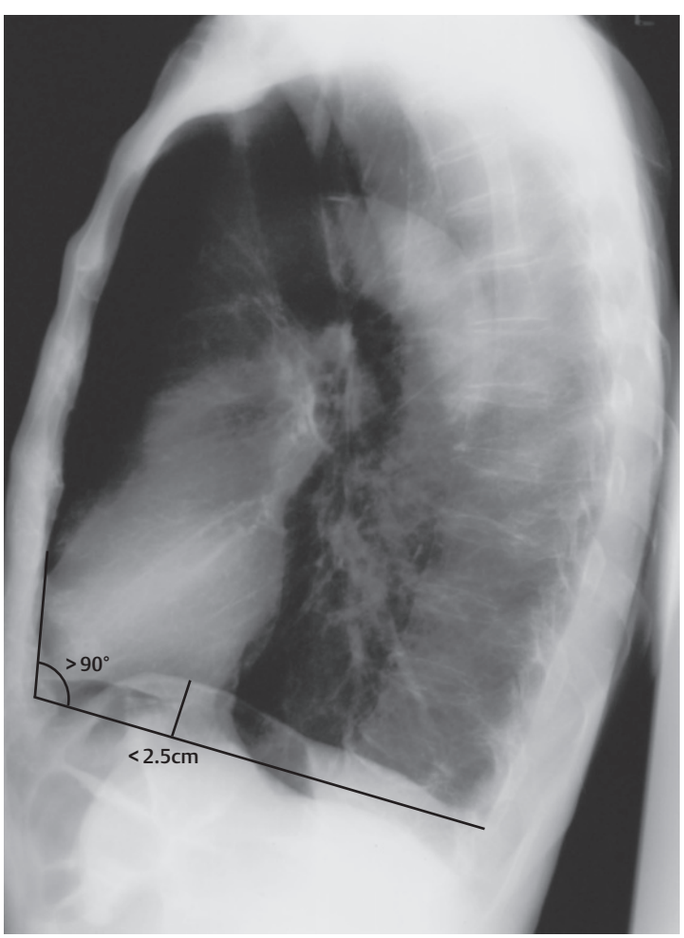

Fig. 2.47 Increased volume in emphysema on the lateral radiograph. Measurements for determining increased chest volume (which is significant in this 73-year-old "pink puffer") have been entered on the radiograph. The dome of the diaphragm is largely flattened. The angle between the sternum and costophrenic recess is increased, and the retrosternal space is enlarged.

Reduced Vascularity

The decrease in the number and caliber of pulmonary blood vessels, especially in the peripheral segments of the lung, is a crucial direct sign of emphysema. However, demonstrating emphysema in less severe cases is anything but straightforward. The vessels appear shifted and elongated with splayed bifurcations, occasionally producing a picture resembling a cobweb (**Fig. 2.49, Fig. 2.50**). In classic smoker's emphysema, the changes are most severe in the apical segments.

Bullae and loss of pulmonary architecture, which can produce a cobweb picture, are most pronounced in the apical segments. In any house, the thickest cobwebs will be found in the upper corners of the room. A long broomstick is needed to reach these cobwebs (**Fig. 2.48**).

Bullae

Bullae are other direct signs of emphysema that can be demonstrated on the plain chest radiograph (**Fig. 2.51**). They are often encountered in generalized emphysema and appear as avascular regions with hairline borders. Occasionally it can be difficult to differentiate severe subpleural bullae from *pneumothorax*. Where a bulla is present, the pulmonary parenchyma protrudes between it and the chest wall at an acute angle, whereas in pneumothorax the displaced lung tissue forms a shallow arc.

"In comes Hannchen with her broom to sweep the cobwebs from the room"
(W. Busch)

Fig. 2.48 Cobwebs are usually found high up on the wall. Broomsticks are long and thin.

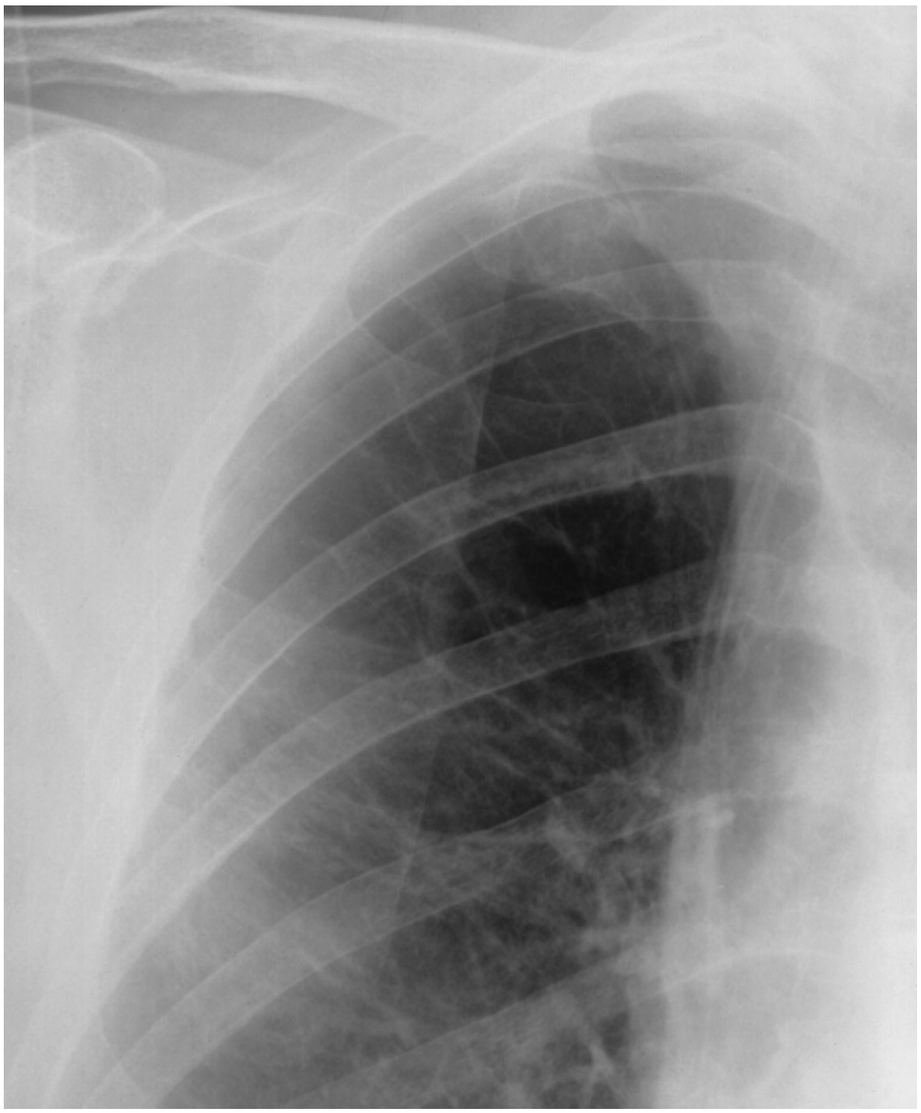

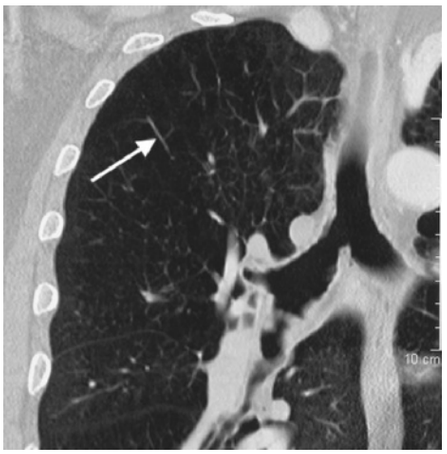

Fig. 2.50 **CT of Fig. 2.49.** Primarily apical smoker's emphysema with large "emptied" portions of the lung, reduced vascularity, and little branching in the elongated vessels (white arrow).

◀ **Fig. 2.49** **"Cobweb" pattern in apical emphysema (detail).** The patient is an 82-year-old man with advanced emphysema. The superior lobe arteries show thinning and abnormal elongation. They create a threadbare weblike pattern.

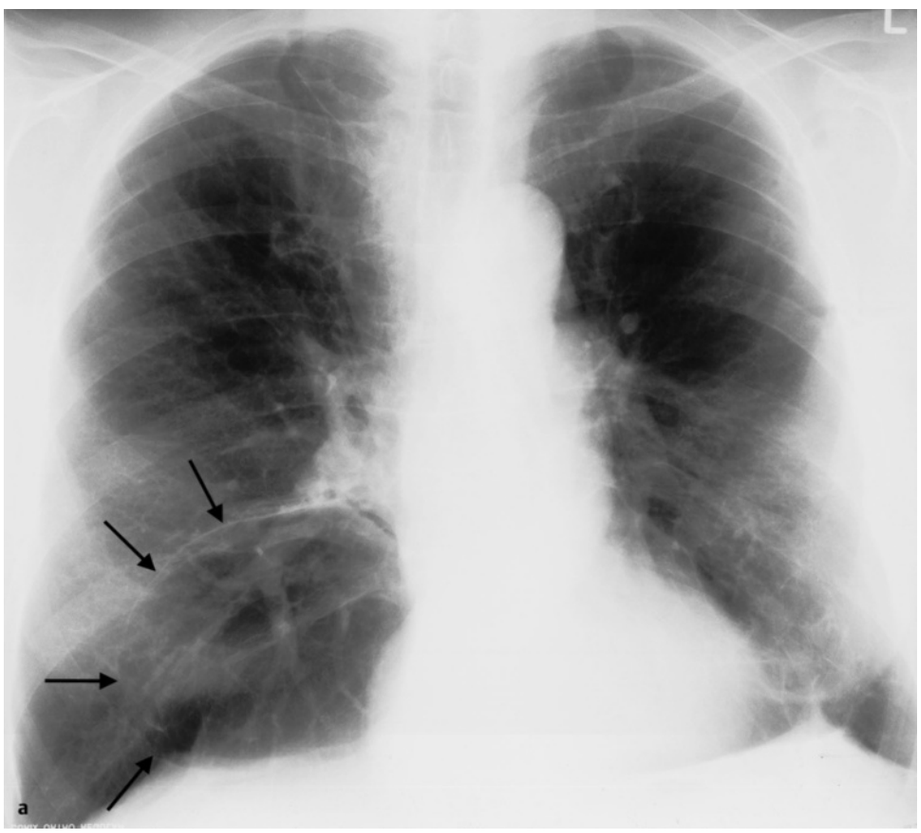

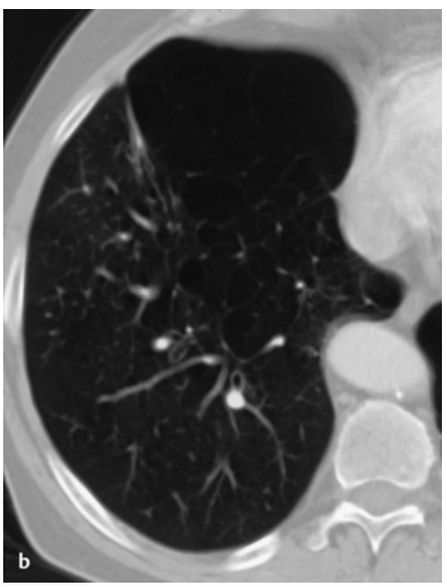

Fig. 2.51 a, b **Isolated bullae are visualized.** The patient is a 67-year-old man with destructive pulmonary emphysema. Primarily basal bullous destruction of pulmonary architecture with isolated, very large cavities (see also CT detail in **b**). Platelike areas of hypoventilation adjacent to the large inflated bullae (black arrows). Signs of pulmonary arterial hypertension. Heart and aorta show a hypertensive configuration.

Associated Phenomena

The increased *pulmonary arterial pressure* resulting from chronic emphysema leads to dilatation of the central pulmonary arteries and narrowing of the peripheral ones (**Fig. 2.53**). The diameter of the right intermediate artery at the level of the right intermediate bronchus has proven effective as an indicator of pulmonary hypertension. Its diameter should not exceed 16 mm (**Fig. 2.52**). A diameter exceeding 18 mm can be interpreted as clearly abnormal (**Fig. 2.54**).

Because of the increased chest volume and the steeper angle of the heart axis, the heart often appears elongated and therefore smaller ("drop heart"). This makes it nearly impossible to evaluate heart size or enlargement according to classic criteria. Here one should pay close attention to the lateral radiograph, where left ventricular hypertrophy reveals itself as a circumscribed protrusion in the basal portion of the posterior cardiac border.

Spontaneous pneumothorax can occasionally occur secondarily to paraseptal emphysema. Recurrent spontaneous pneumothorax is therefore an indication for CT examination of the lung (**Fig. 2.55**).

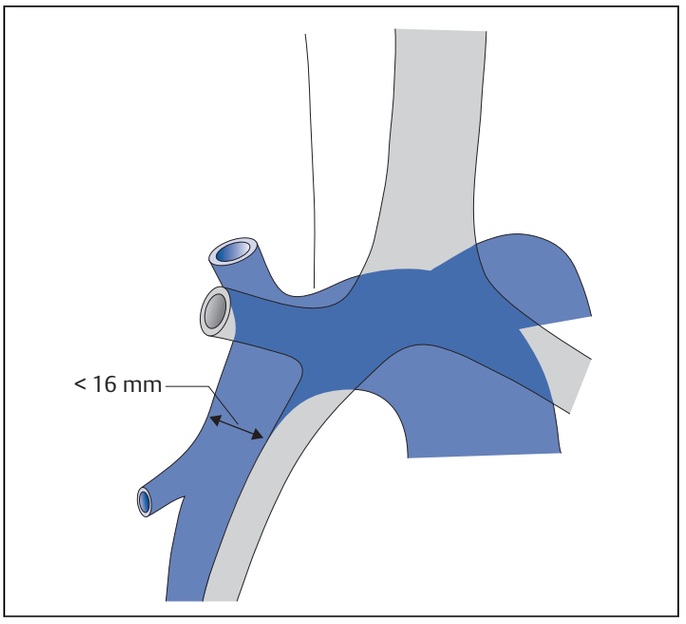

Fig. 2.52 Caliber of the intermediate artery as a measure of pulmonary arterial hypertension. The physiologic diameter of the right intermediate artery laterally overlying the intermediate bronchus is ca. 16 mm. Where this diameter exceeds 18 mm, it must be regarded as abnormally dilated.

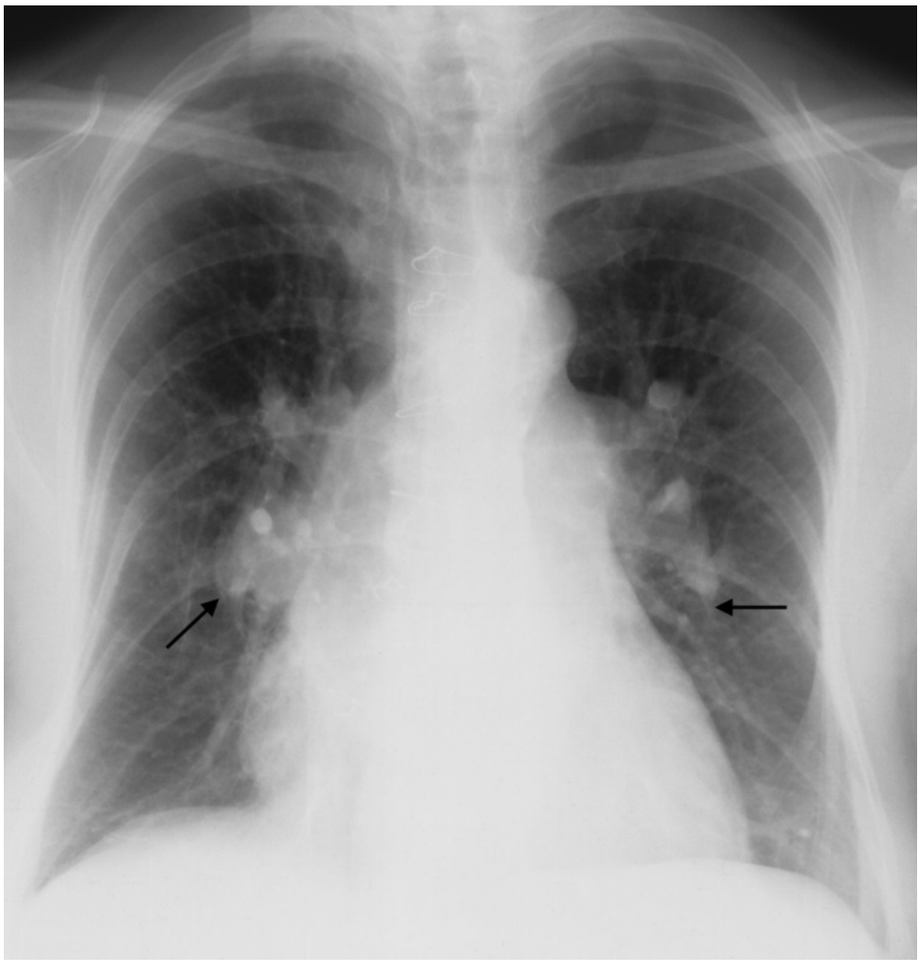

Fig. 2.53 Pulmonary arterial hypertension. The patient is a 75-year-old woman with coronary heart disease and status post aortocoronary venous bypass. History of chronic COPD with pulmonary arterial hypertension. Central vessels are thickened with a significant mismatch between the segmental arteries and accompanying bronchi and an abrupt reduction in caliber toward the periphery (black arrows).

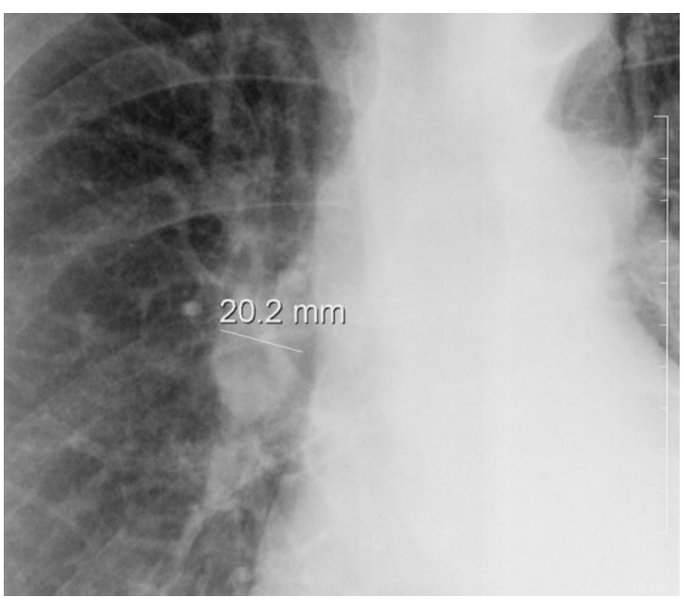

Fig. 2.54 Measuring the intermediate artery. The intermediate artery is significantly dilated to a diameter of 20 mm in this 78-year-old woman with advanced COPD, emphysema, and pulmonary arterial hypertension. There is an abrupt change in caliber toward the periphery.

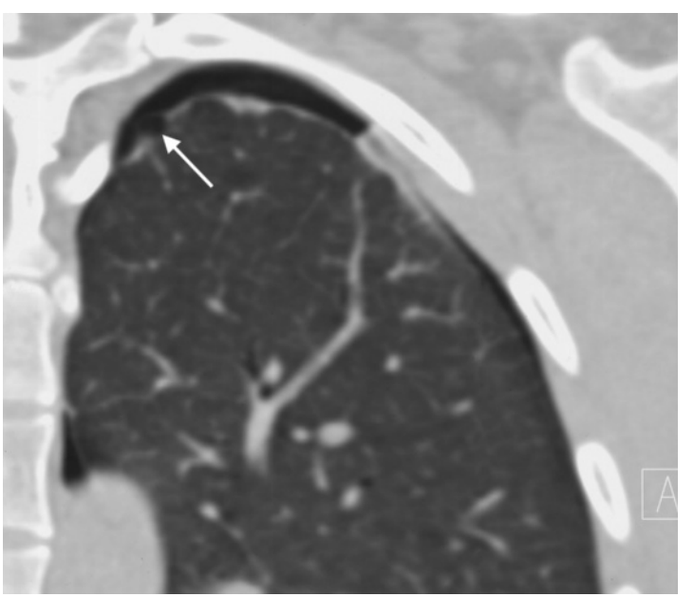

Fig. 2.55 Spontaneous pneumothorax with subpleural emphysematous bullae. The patient is a 27-year-old woman with spontaneous pneumothorax on the left side. CT shows tiny subpleural emphysematous bullae (white arrow) in addition to slight scarring of the apical pleura. These findings may be interpreted as discrete paraseptal emphysema.

Computed Tomography

The contribution of CT to the diagnosis of emphysema includes:

- Direct visualization of emphysematous tissue with less than − 900 HU
- Better detection of small bullae
- Identification of the specific type of emphysema

Lung tissue with a density of less than − 900 HU must be regarded as emphysematous. This means that, at a window setting of − 900 to − 1024 HU, CT can directly visualize emphysematous areas.

By visualizing the distribution of the emphysematous bullae in the secondary lobule, the CT study can differentiate centrilobular emphysema from panlobular emphysema (**Fig. 2.56**).

Centrilobular emphysema affects the respiratory bronchioles. It is characterized by relatively uniformly distributed small, round radiolucencies in the center of the secondary lobule (**Fig. 2.58**). The abnormal findings in the center of the lobule typically do not exhibit a wall, whereas actual bullae do.

In **panlobular emphysema** the entire lobule exhibits a homogeneous decrease in density. Often entire regions of the lung appear hypodense (**Fig. 2.59, Fig. 2.60**). Bullae rarely occur.

Paraseptal emphysema manifests itself primarily in the subpleural region or along the bronchovascular bundle (**Fig. 2.61**).

Notes on Pathology

The pathologic classification includes the following forms:

- Panlobular (panacinar) emphysema
- Centrilobular (centriacinar) emphysema
- Paraseptal emphysema
- Compensatory emphysema
- Emphysema associated with scarring

This classification is based on changes located in the respiratory lobule or acinus (**Fig. 2.57**). In panlobular emphysema, the entire lobule is involved. Here it is no longer possible to differentiate alveoli and alveolar ducts. The increasing destruction leaves only thin septa surrounding the blood vessels. The final stage of the disease is characterized by the picture of an "empty" lobule. It is the typical form of emphysema in nonsmokers, such as can occur in alpha$_1$-antitrypsin deficiency. Centrilobular emphysema is characterized by the form primarily occurring in the respiratory and terminal bronchioles. It is typically observed in smokers and in chronic bronchitis.

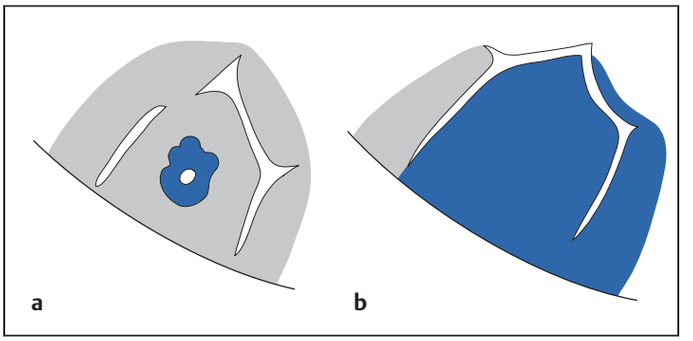

Fig. 2.56 a, b Schematic diagram of CT findings in centrilobular and panlobular emphysema.
a Hypodensities around a punctate centrilobular artery → centrilobular emphysema.
b Hypodensity of the entire lobule → panlobular emphysema.

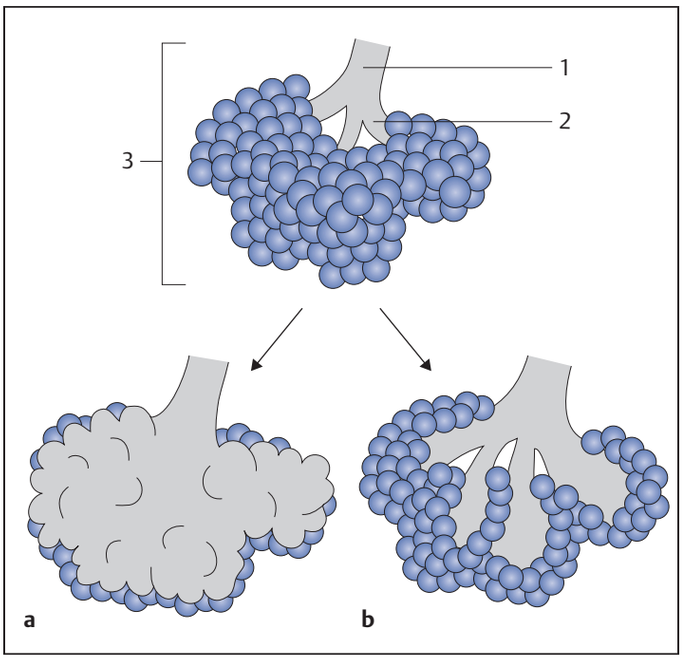

Fig. 2.57 Pathology of centrilobular and panlobular emphysema. In panlobular emphysema (**a**), the loss of alveolar walls involves the entire lobule; in centrilobular emphysema (**b**), the portions of the lobule around the central respiratory bronchioles are dilated.
1 Terminal bronchiole
2 Respiratory bronchiole
3 Secondary lobule

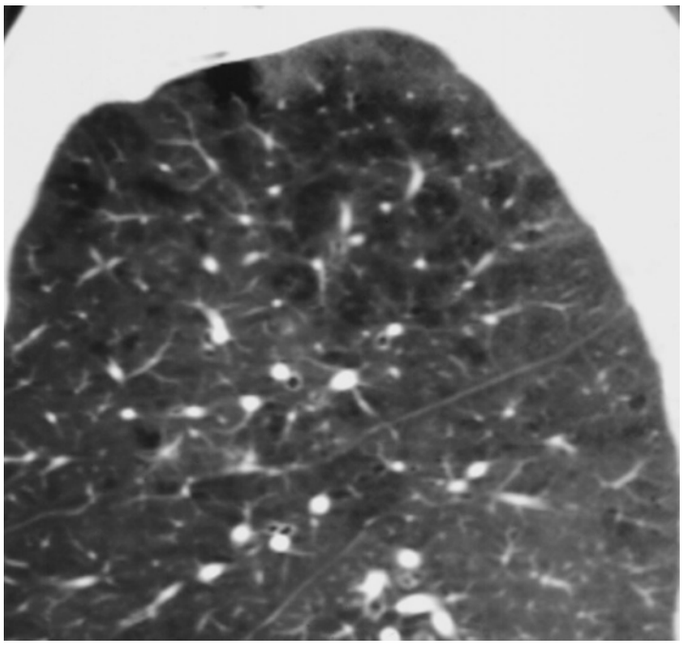

Fig. 2.58 CT image of centrilobular emphysema. The sagittal reconstruction shows emphysema beginning in the center of the secondary lobule with findings most pronounced in the apical lung. In some areas of advanced disease, entire lobules are involved.

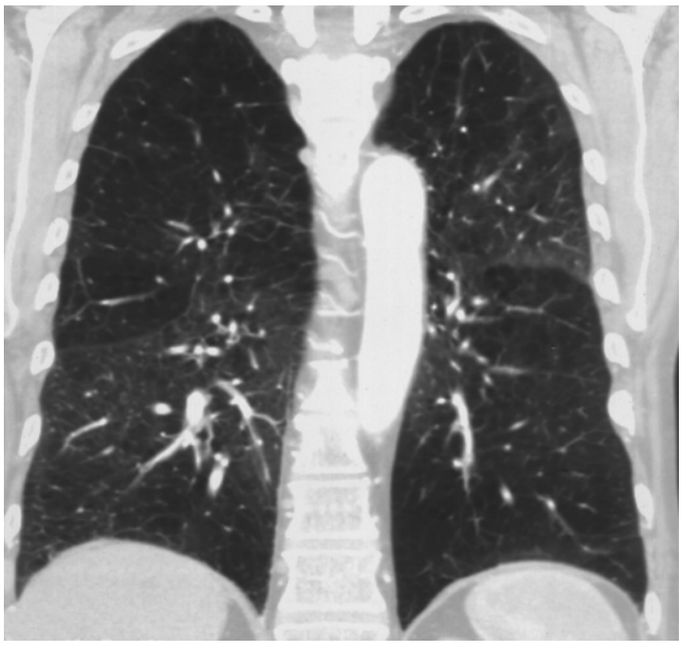

Fig. 2.59 CT image of panlobular emphysema. The coronal reconstruction clearly visualizes apical hypodensities in both lungs as well as in the entire left lower lobe. Changes show more area consolidation than in centrilobular emphysema.

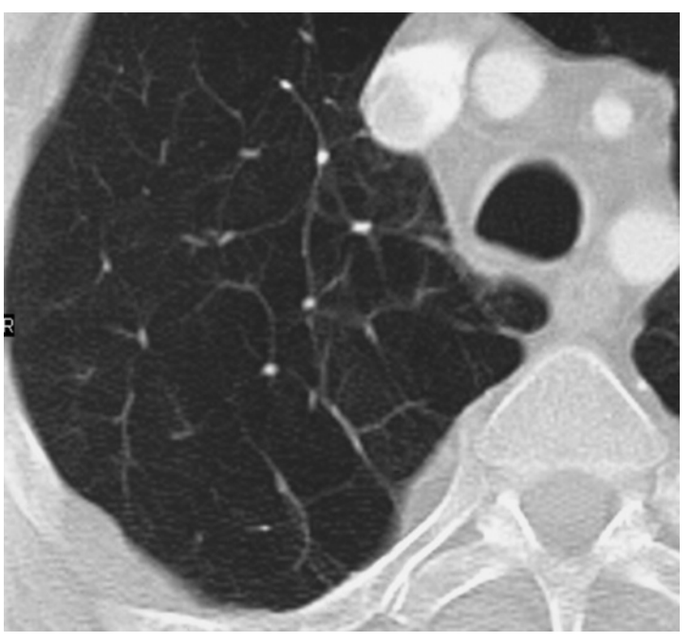

Fig. 2.60 Detail of panlobular emphysema. The hypodensities involve the whole secondary lobule. The lobule appears empty. Continuous tissue destruction is observed over larger areas.

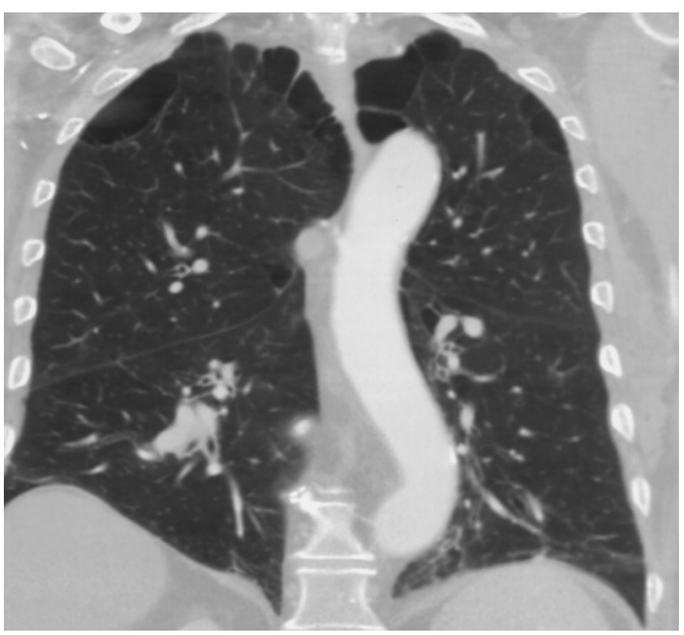

Fig. 2.61 CT image of paraseptal emphysema. The coronal reconstruction clearly shows large apical emphysematous bullae that typically occur along the pleura.

Special Cases

Special cases of pulmonary emphysema in the strict sense include:

- Emphysema associated with scarring
- Compensatory emphysema

Emphysema associated with scarring occurs adjacent to fibrotic processes. Fibrotic shrinkage stretches the alveolar walls, leading to irreversible dilatation of the air spaces. As a result it regularly occurs in pneumoconiosis (see **Fig. 5.44**). However, it often occurs as a mixed form in combination with panlobular emphysema. Localized emphysema with scarring (perifocal emphysema) can be an important criterion in the differential diagnosis of neoplasms, pulmonary masses, and changes due to scarring (see **Fig. 4.51**).

Compensatory emphysema occurs in:

- Atelectasis
- Pneumonectomy
- Thoracic deformity (kyphoscoliosis)

Here a portion of the lung expands to fill the resulting "vacuum." A clear nosologic distinction should be made between compensatory emphysema and emphysema associated with scarring, which is produced by traction. Compensatory emphysema is most commonly encountered after lobectomy (**Fig. 2.62**). Less often it occurs in the voluminous portions of the asymmetrical chest in severe scoliosis (**Fig. 2.63**). Localized compensatory emphysema on the plain chest radiograph can be an important indirect sign of masked hypoventilation.

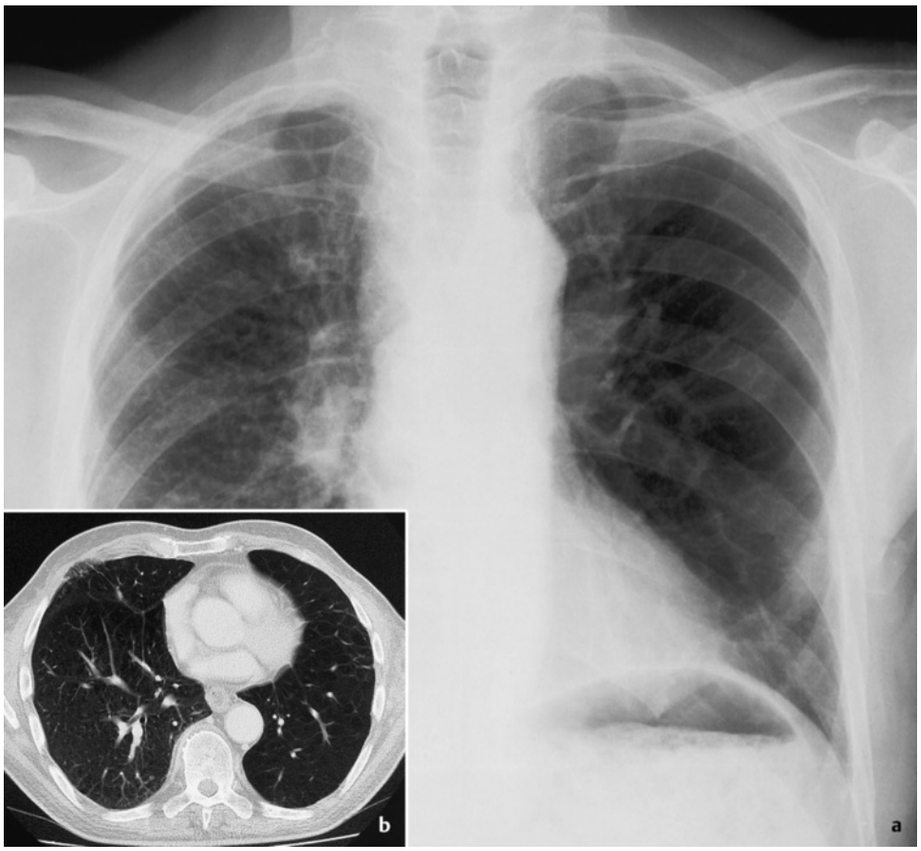

Fig. 2.62 a, b Compensatory emphysema following lobectomy. The patient is a 71-year-old man with status post left lower-lobe lobectomy.

a Significant hypertransparency of the left lung. Findings include a mass in the left central lung (local recurrence in the hilum) and significant shadowing in the right lung in the setting of severe chronic bronchitis.

b CT clearly demonstrates hyperinflation of the left upper lobe. The right lower lobe shows two small nodules (preexisting contralateral metastases) in addition to nonspecific interstitial shadowing.

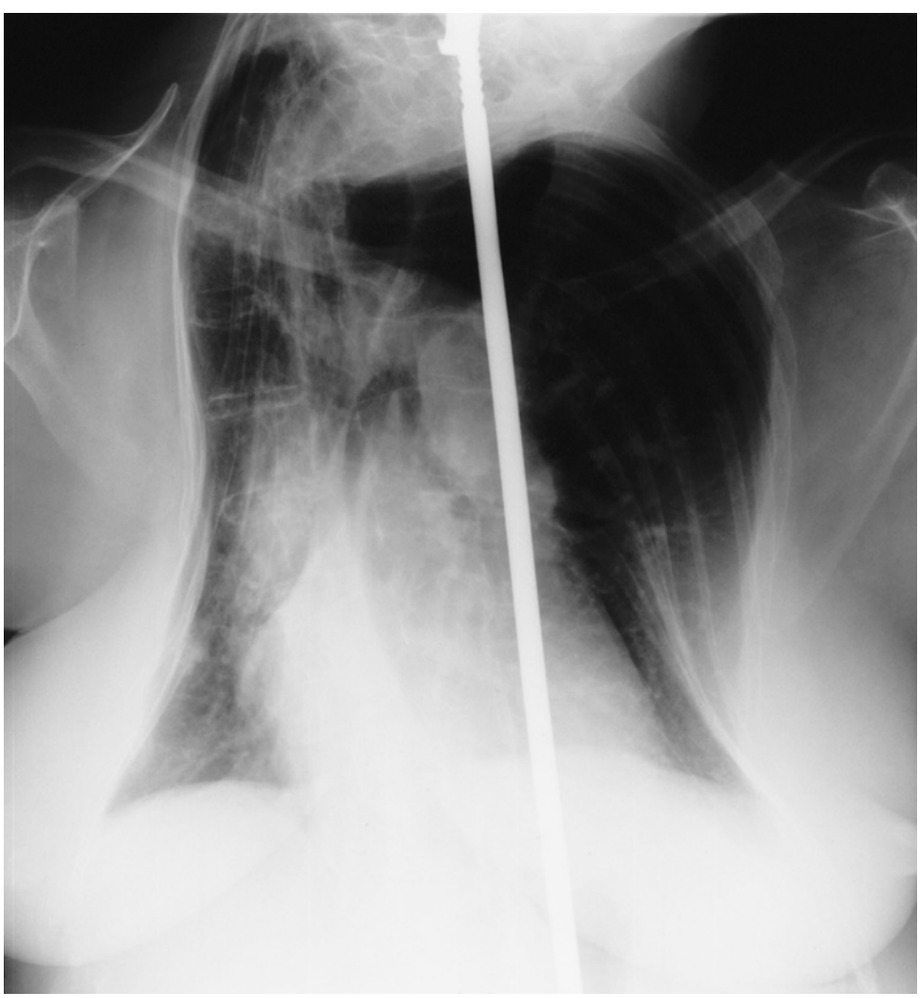

Fig. 2.63 Compensatory emphysema in thoracic deformity. Massive kyphoscoliosis stabilized with a Harrington rod and significant hyperinflation of the left lung consistent with compensatory emphysema.

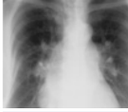

Review Case 1

The patient is a 46-year-old woman admitted to the emergency room with fever, cough, and general exhaustion. The patient has a history of many years of cigarette smoking. Chest radiography was performed to exclude pneumonia (Fig. 2.64, Fig. 2.65).

Question 1

How do you evaluate heart size and cardiac compensation? (Previously discussed in Chapter 1.)

Question 2

Which changes can you associate with a history of many years of cigarette smoking? (This chapter.)

Question 3

Are pulmonary infiltrates present? (This will be discussed in Chapter 3.)

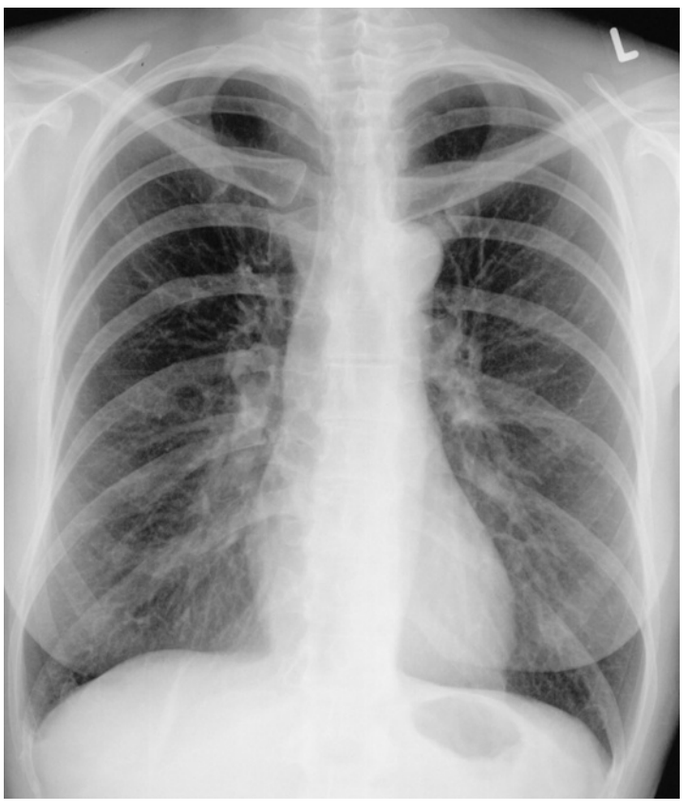

Fig. 2.64 Fever and cough with chronic cigarette smoking.

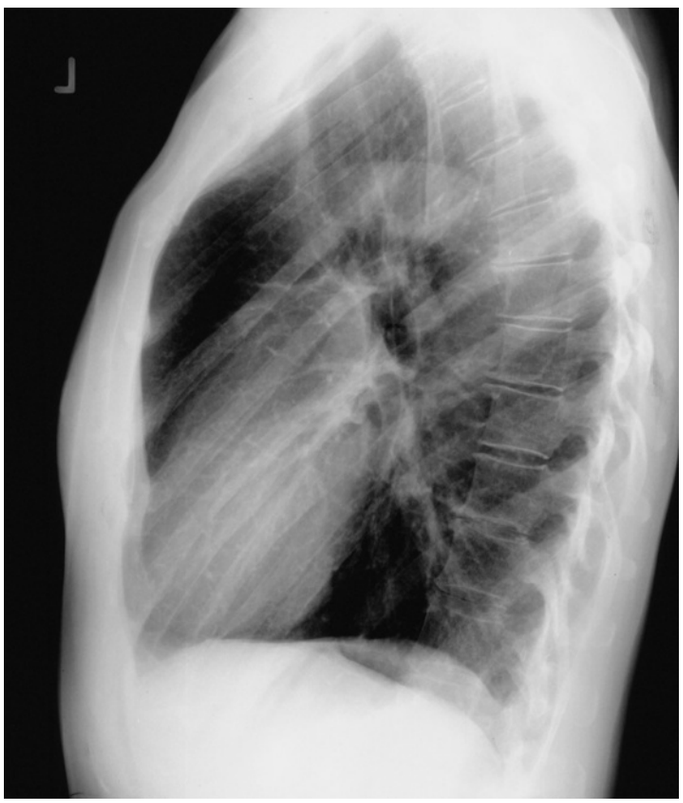

Fig. 2.65 Lateral view of the patient in Fig. 2.64.

Answer

Answer to question 1: Heart size is normal, although the aorta extends as far as the clavicle and forms the right cardiac border, meaning that one should assume that hypertension is present.

Answer to question 2: With reduced vascularity in the apical region, the very deep inspiration almost as far as the 12th rib, the significant expansion of the posterior horizontal portions of the disk interspaces (on the posteroanterior radiograph), and the widening of the retrosternal space are evidence of chronic obstruction with an increase in chest volume consistent with obstructive emphysema. Additionally, there is significant interstitial reticulonodular and peribronchial shadowing. An enlargement of the posteroanterior radiograph clearly demonstrates these latter changes, which are signs of chronic bronchitis (**Fig. 2.66**).

Answer to question 3: No patchy pulmonary infiltrates suggestive of pneumonia are detectable (the fever was attributable to a urinary tract infection).

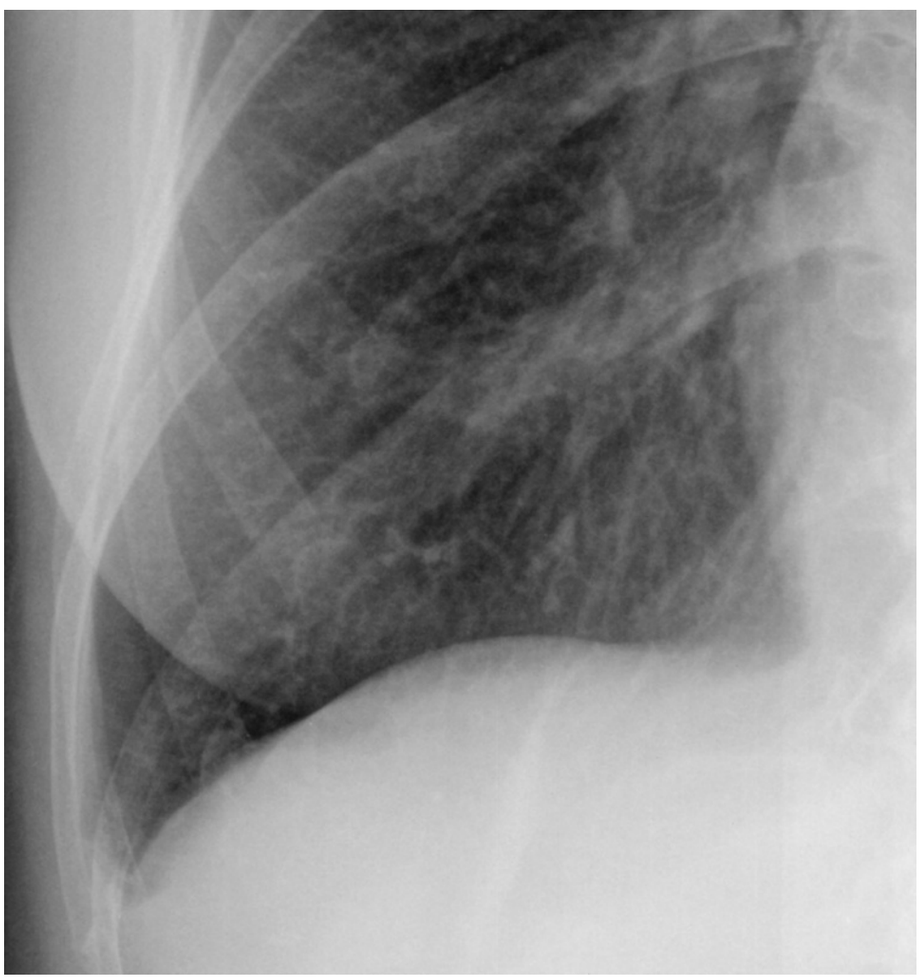

Fig. 2.66 **Severe smoker's bronchitis with no evidence of pneumonic infiltrates.**

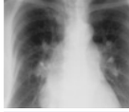

Review Case 2

The patient is an 80-year-old woman with known coronary heart disease. Preoperative radiographs obtained in a clinical state of good health (Fig. 2.67, Fig. 2.68). Known COPD.

Question 1

Are there signs of cardiac decompensation? (Previously discussed in Chapter 1.)

Question 2

Which signs suggest chronic bronchitis?

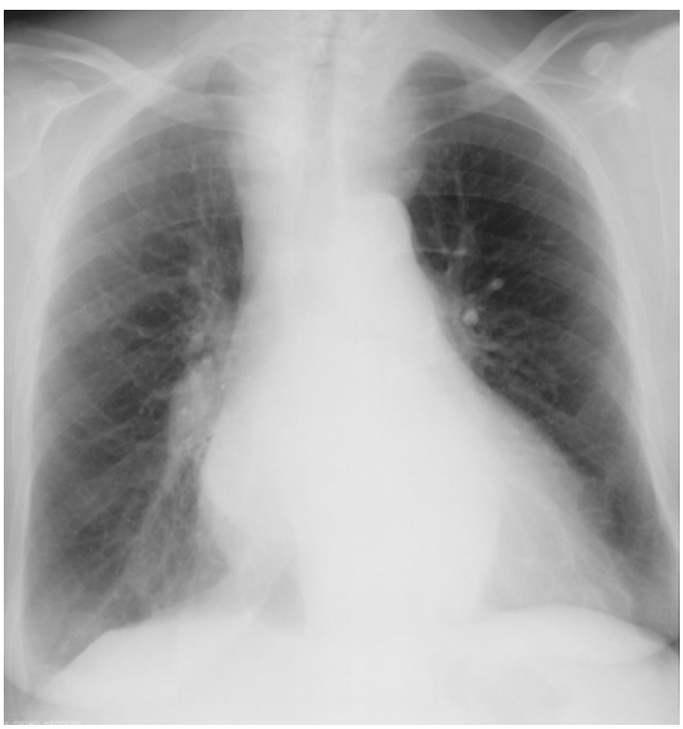

Fig. 2.67 Coronary heart disease, COPD, clinical state of good health.

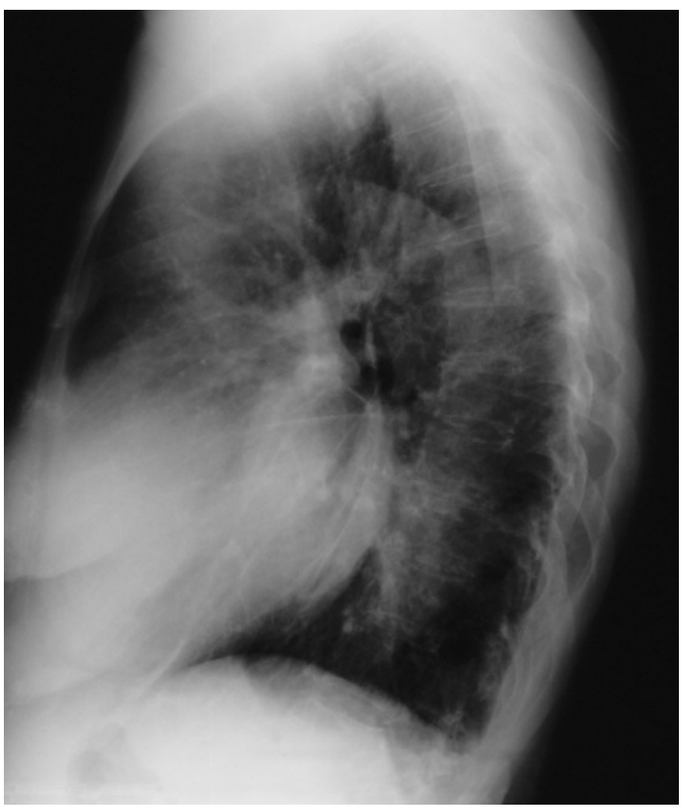

Fig. 2.68 Lateral view of the patient in Fig. 2.67.

Answer

Answer to question 1: The left heart is significantly enlarged (the long axis of the heart is longer than the width of the hemithorax, and the retrocardiac space is narrowed). Markedly thick Kerley B lines (white arrow) are observed in the right costophrenic angle, which appears to have lateral calluses (**Fig. 2.69**). However, the lines may be indicative of chronic congestion as there is no redistribution.

Answer to question 2: Signs of chronic bronchitis include obstructive barrel chest and evidence of pulmonary arterial hypertension (thickened hila, abrupt change in caliber of the pulmonary arteries [black arrow]). Additionally, there is significant bronchial wall thickening especially in the lower field of the right lung (black arrowheads).

Incidental findings include a widened upper mediastinum as in a goiter.

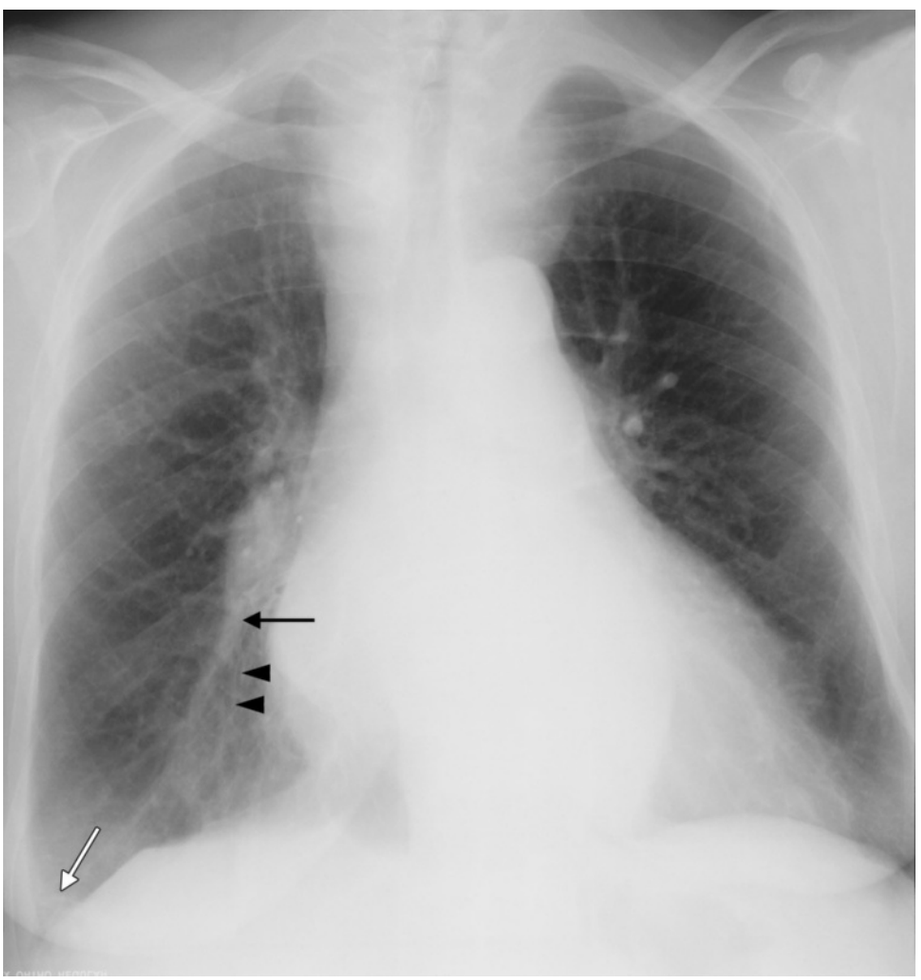

Fig. 2.69 Significant left heart enlargement without signs of decompensation. Signs of chronic bronchitis with pulmonary arterial hypertension.

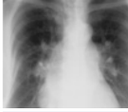

Review Case 3

The patient is a 27-year-old male smoker admitted to the emergency room with fever and productive cough (Fig. 2.70, Fig. 2.71). The patient reports having had an infection for a week, which has now worsened.

Question 1

Which changes are associated with chronic cigarette smoking?

Question 2

Which changes suggest acute bronchitis as well?

Question 3

Are there further changes consistent with pneumonia?

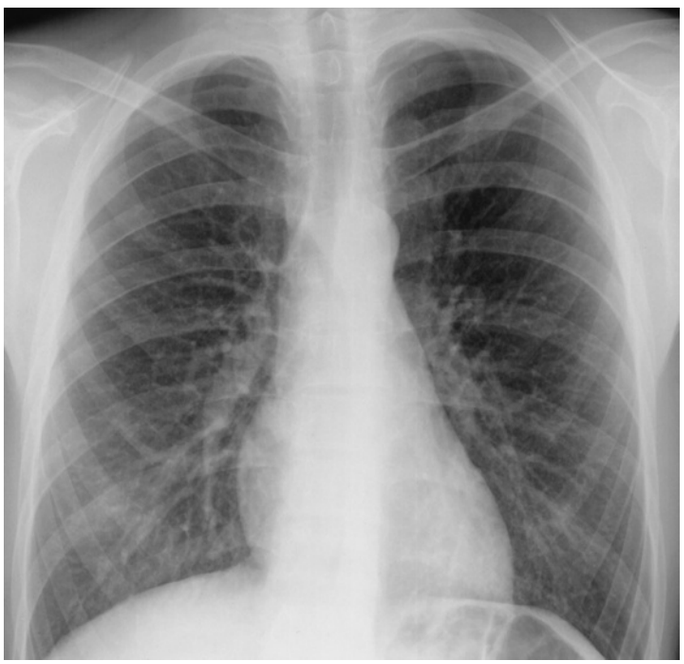

Fig. 2.70 Fever and productive cough with worsening general health.

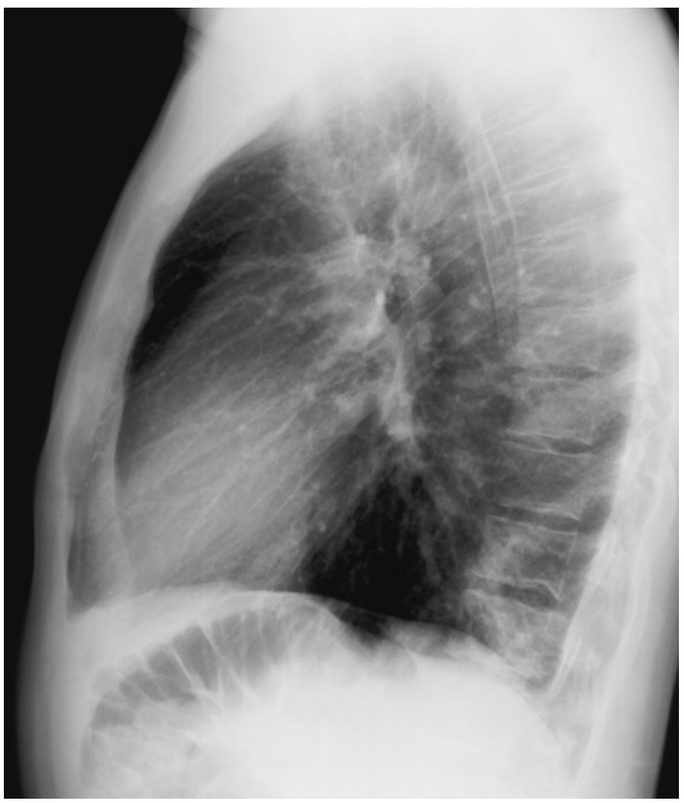

Fig. 2.71 Lateral view of the patient in Fig. 2.70.

Answer

Answer to question 1: The diffuse, finely nodular peribronchial shadowing suggests chronic bronchitis or respiratory bronchiolitis-interstitial lung disease.

Answer to question 2: The central vascular engorgement with pronounced hila can be interpreted as signs of clinically acute bronchitis. Incipient pulmonary arterial hypertension secondary to COPD is unlikely at this age. The most probable answer is therefore central hyperemia in acute inflammation.

Answer to question 3: An infiltrate is present in the posterobasal lower lobe, presumably in the right lung. Here (**Fig. 2.72**) the lower thoracic vertebrae appear blurred, whereas normally they are more clearly visualized than the middle and upper thoracic vertebrae (see Chapter 3).

Evaluation: Here we see a bronchopneumonic superinfection on top of preexisting chronic pathology and acute bronchitis.

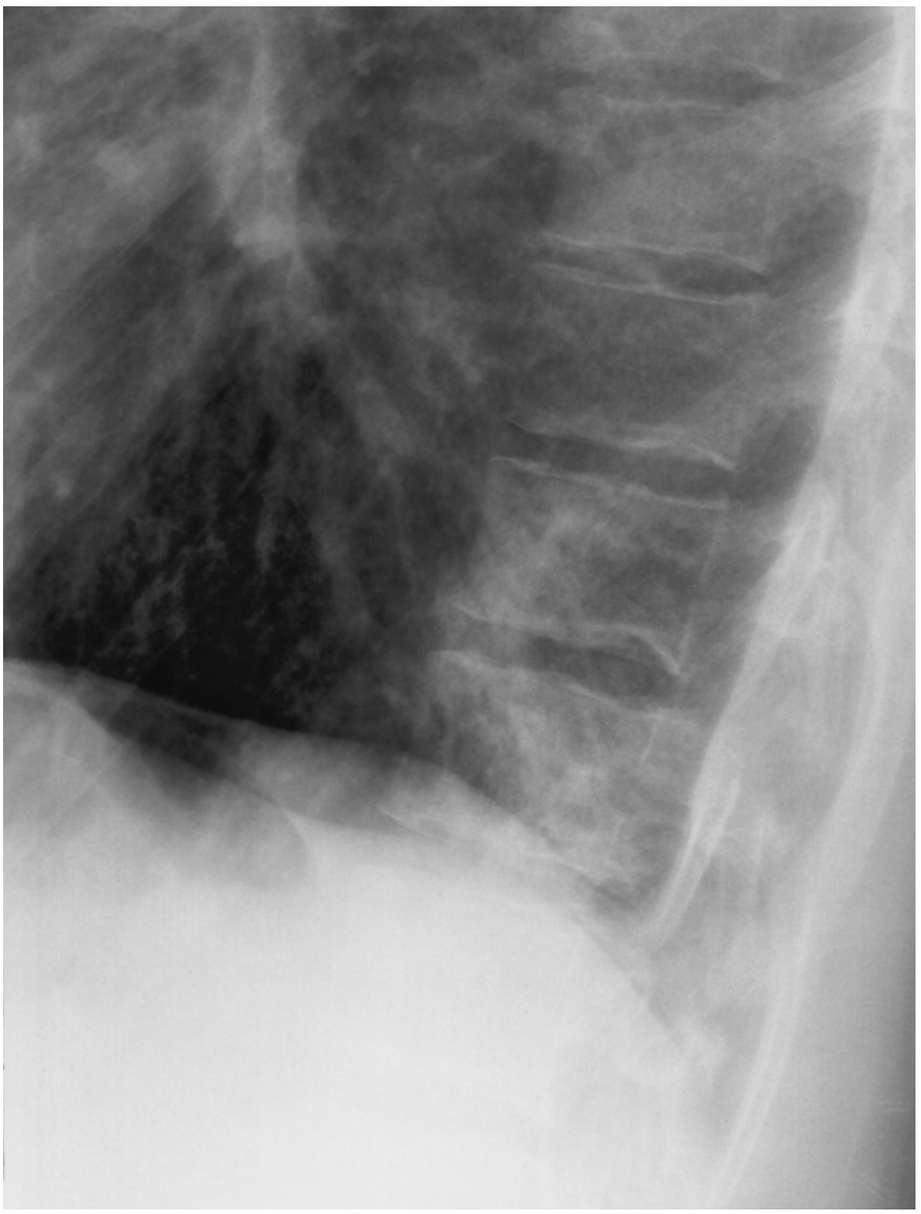

Fig. 2.72 Signs of chronic smoker's bronchitis with bronchopneumonia in the lower lobe.

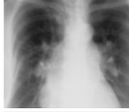

Review Case 4

The patient is a 53-year-old woman presenting with a persistent cough with known COPD and chronic recurrent pulmonary infections with fever and massive quantities of occasionally blood-tinged sputum.

Question 1

Which changes on the enlarged detail image of the right lower lobe (Fig. 2.73) suggest the clinically known chronic bronchitis?

Question 2

What additional change can you detect?

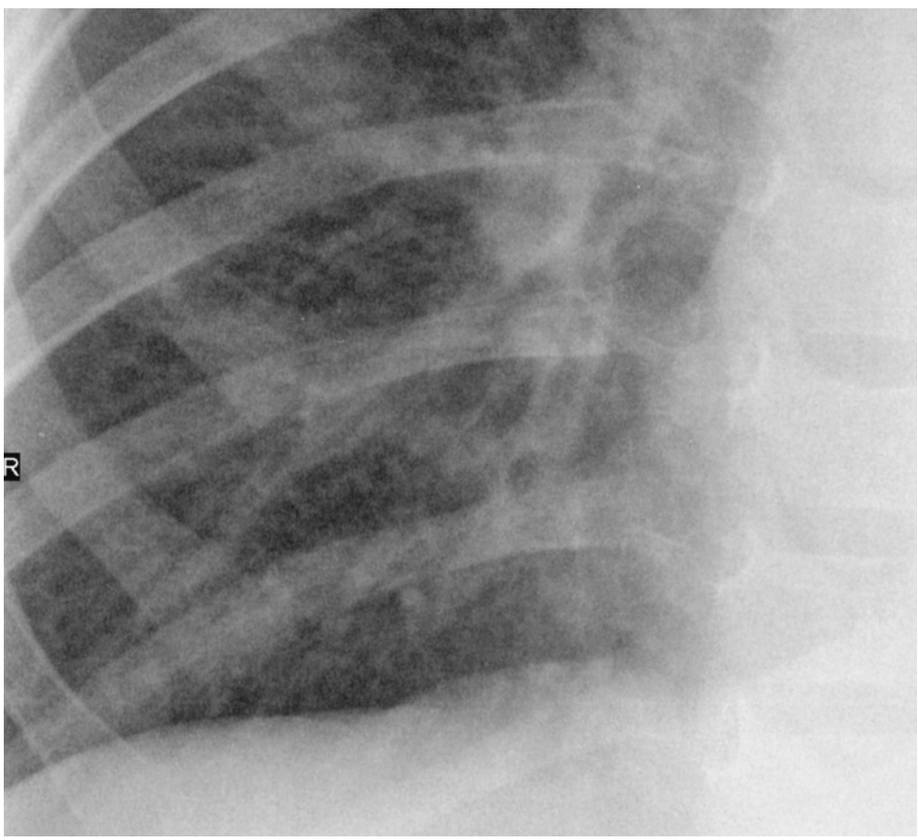

Fig. 2.73 Recurrent infections, occasionally with blood-tinged sputum.

Answer

Answer to question 1: Diffuse reticulonodular shadowing as a sign of chronic bronchitis is present with blurring of vascular structures.

Answer to question 2: Additional findings include significant dilation of the bronchial lumen with severe thickening of the bronchial wall (black arrows) (**Fig. 2.74**). The CT study that was then ordered (**Fig. 2.75**) confirmed the tentative diagnosis of bronchiectasis.

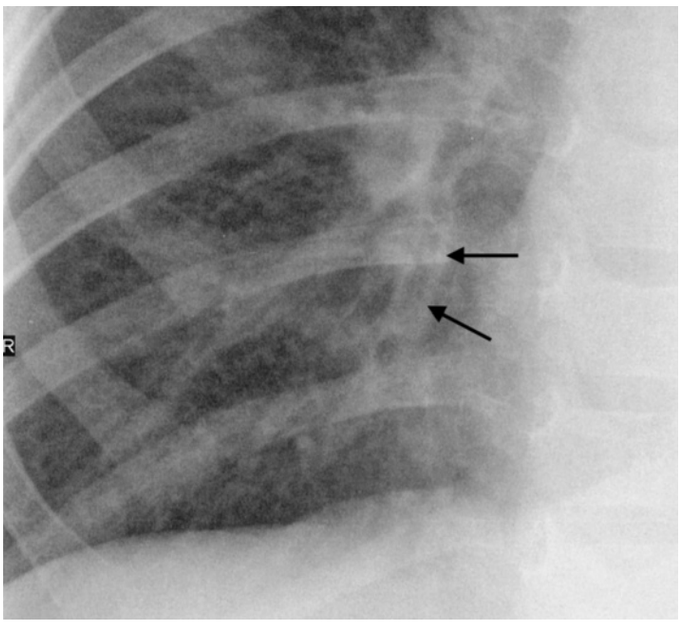

Fig. 2.74 Bronchiectasis (black arrows) in the right lower lobe.

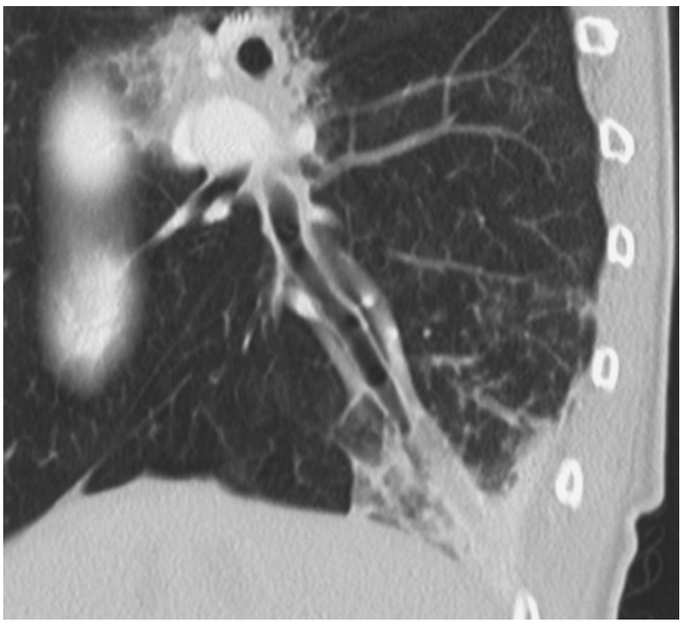

Fig. 2.75 Cylindrical bronchiectasis in the posterobasal lower lobe with peripheral mucus retention (mucocele) and beginning peribronchial infiltrate.

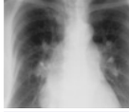

Review Case 5

The patient is a 61-year-old man with advanced chronic bronchitis now referred due to clinical suspicion of exacerbation from infection.

Question 1

Which changes on chest radiograph (Fig. 2.76) correlate with the clinical diagnosis of chronic obstructive pulmonary disease?

Question 2

Which changes do you evaluate as irreversible damage?

Question 3

How do you evaluate the central tracheobronchial tree on the lateral view (Fig. 2.77)?

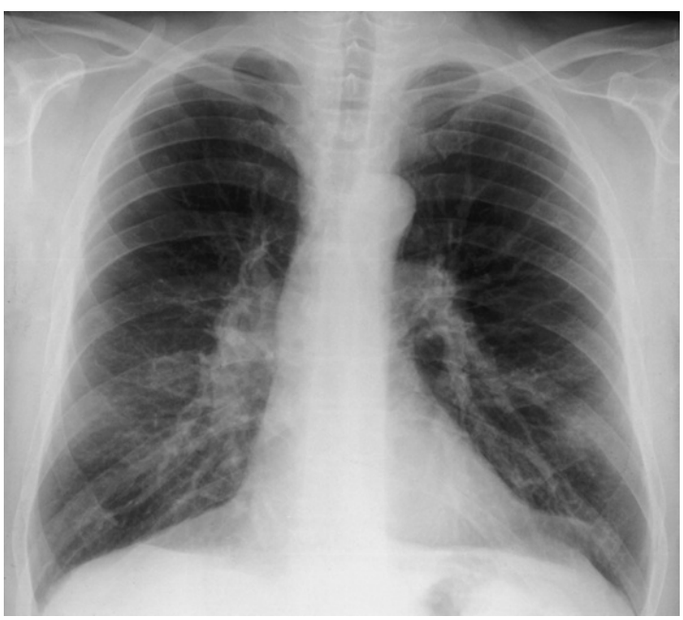

Fig. 2.76 COPD clinically exacerbated by infection.

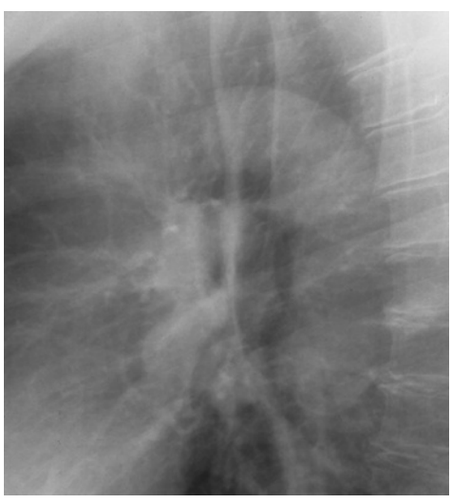

Fig. 2.77 Lateral view of the patient in Fig. 2.76.

Answer

Answer to question 1: As well as obstructive barrel chest there is diffuse interstitial and peribronchial shadowing, the latter visible primarily in the basal lungs as a “tramline” sign.

Answer to question 2: Thickened hila indicative of preexisting pulmonary arterial hypertension. Reduced apical vascularity especially in the right lung, indicative of apical emphysema.

Answer to question 3: The tracheal wall shows an undulating configuration. The left main bronchus is noticeably deformed and appears slit-shaped instead of round or oval (**Fig. 2.78**).

Because of the persistent symptoms a CT study was ordered to exclude a central mass. CT confirms the apical emphysema (**Fig. 2.79**) and demonstrates significant narrowing of the main bronchi from bronchomalacia and endobronchial mucus accumulations (**Fig. 2.80**).

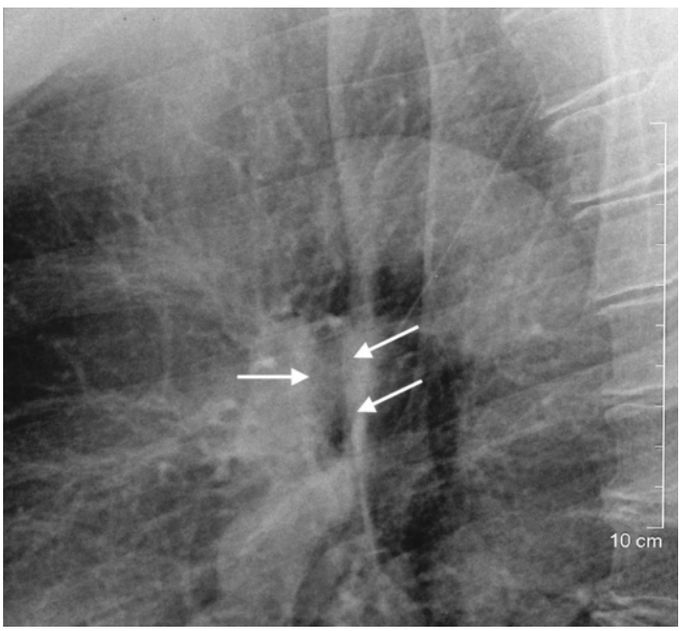

Fig. 2.78 Deformation of the left main bronchus (white arrows) in COPD.

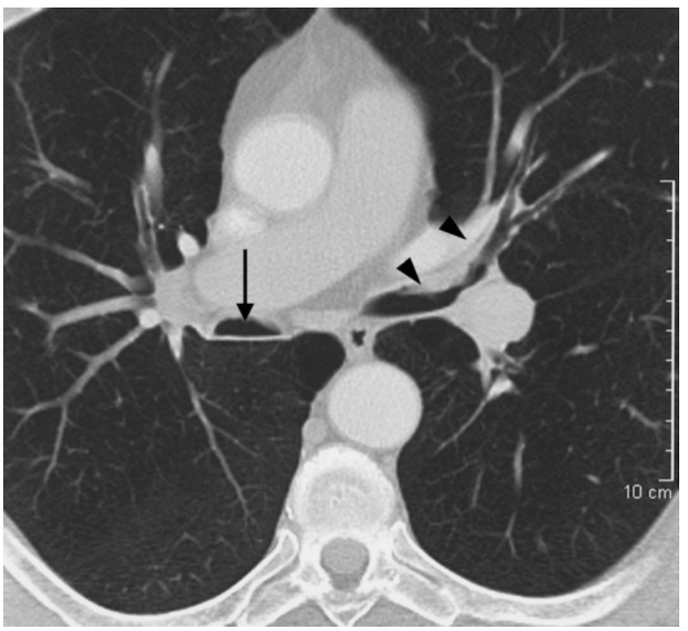

Fig. 2.80 Bronchomalacia (black arrow) and endobronchial mucus accumulation (black arrowheads).

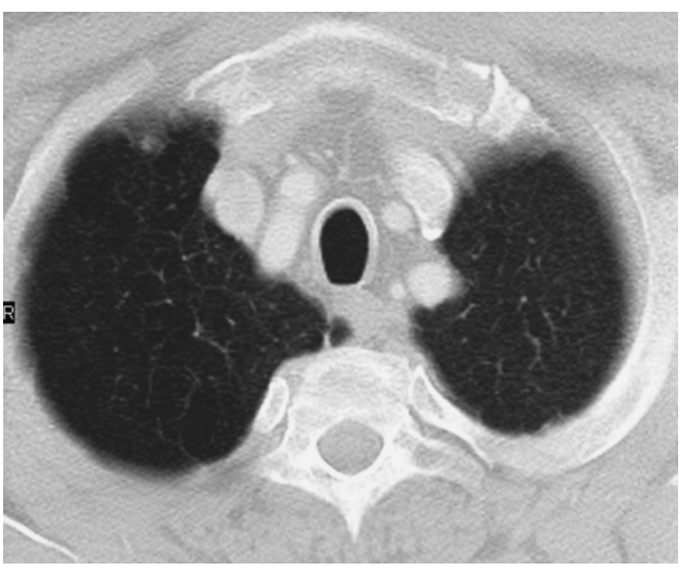

Fig. 2.79 Apical pulmonary emphysema

3

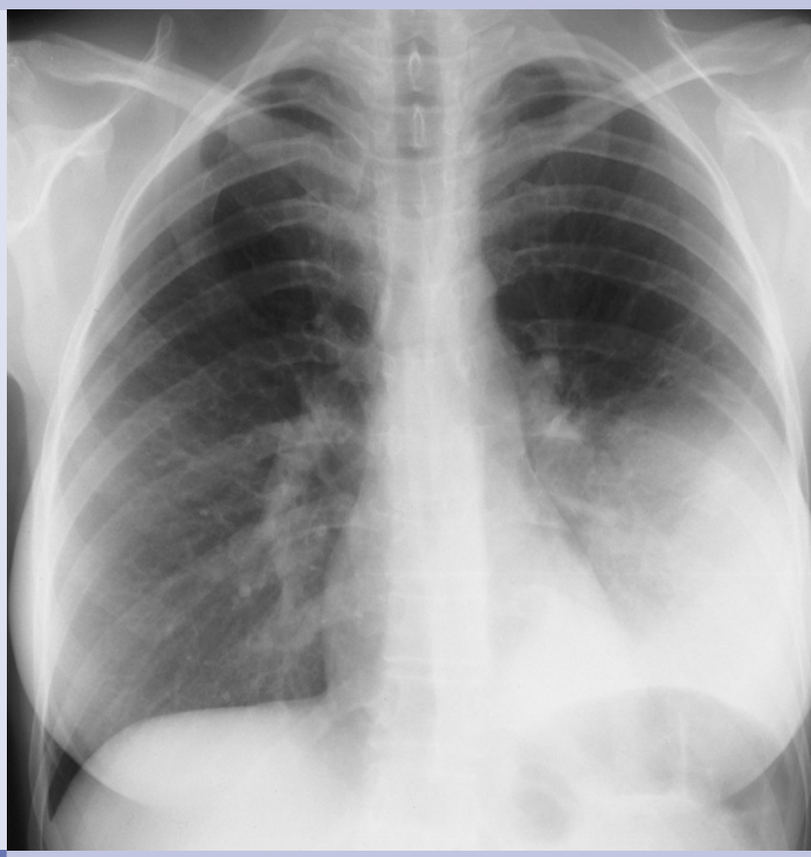

Pneumonia

General

The diagnosis of pneumonia is based on findings of:
- Circumscribed opacities, or
- Interstitial shadowing

Such findings must occur in cases of clinical suspicion and may not be attributable to technical causes (poor inspiration, overlapping, etc.) or other abnormal findings (chronic obstructive pulmonary disease [COPD], congestion, tumor). For example, occasionally the differential diagnosis between congestion and pneumonia can only be made by observing the clinical course of the disorder. The conclusion "local shadow = pneumonia" is not self-evident but requires careful differential diagnosis that must also consider imaging artifacts (**Fig. 3.1**).

The radiologic description follows the basic pathoanatomic distinction between alveolar pneumonia (expanded to include lobar, bronchopneumonic, and focal distribution patterns) and interstitial pneumonia. This basic distinction leaves ample room for considering signs of underlying noxious agents. Due to the distinctive features of their clinical course and history, the forms of pulmonary tuberculosis will be discussed separately. We differentiate:
- Lobar pneumonias (**Fig. 3.3**)
- Bronchopneumonias (**Fig. 3.4**)
- Focal pneumonias
- Interstitial pneumonias
- Opportunistic pneumonias
- Tuberculosis

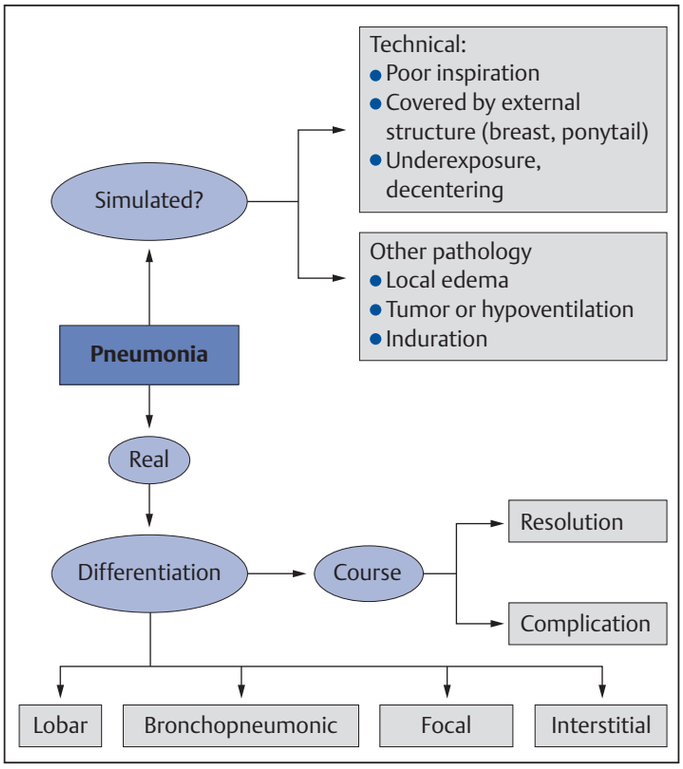

Fig. 3.1 **Diagnostic flowchart for pneumonia.**

Notes on Pathology and Epidemiology

Like tracheitis, bronchitis, and bronchiolitis, the pneumonias are also infectious diseases (caused by bacteria, mycoplasmata, viruses, and other pathogens) involving the pulmonary parenchyma. Pneumonias manifest themselves with exudates in the interstitium and alveolar space. In addition to the pathoanatomic classification in primarily alveolar and interstitial forms, pneumonias can also be classified according to clinical and epidemiologic criteria or according to the spectrum of pathogens (**Fig. 3.2**).

Classification of pneumonias. The advances in modern chemotherapy and antibiotic treatment have reduced the mortality of infectious pulmonary diseases in the generations since the Second World War. However, they have not led to a lower incidence of bronchitis or pneumonia. Accordingly, the annual incidence of new cases of pneumonia in Germany is 200 000, of which 100 000 represent hospital-acquired infections. The following classification should be observed with respect to the spectrum of pathogens:
- Community-acquired versus hospital-acquired (nosocomial)
- Secondary versus primary
- Presence versus absence of an underlying disorder

In cases of community-acquired pneumonia without an underlying disorder, even today pathogens include mainly pneumococci and *Haemophilus*. In 50 % of all cases the etiology remains unclear. Hospital-acquired pneumonia occurs in up to 70 % of all intensive care patients. These infections have a mortality of 10–20 %. The most common pathogens include:
- *Pseudomonas*
- *Staphylococcus aureus*
- *Enterobacter*

Viral pneumonias account for a share of less than 20 %.

Pathology	**Epidemiology**	**Microbiology**	**Radiology**
Alveolar	Community-acquired	Viral	Lobar
Interstitial	Hospital-acquired	Specific	Focal
		Bacterial	Broncho-pneumonic
			Interstitial

Fig. 3.2 **Classification of the pneumonias.** The pneumonias can be classified according to pathologic, epidemiologic, and radiologic criteria. As these criteria overlap, the terminology can be rather confusing.

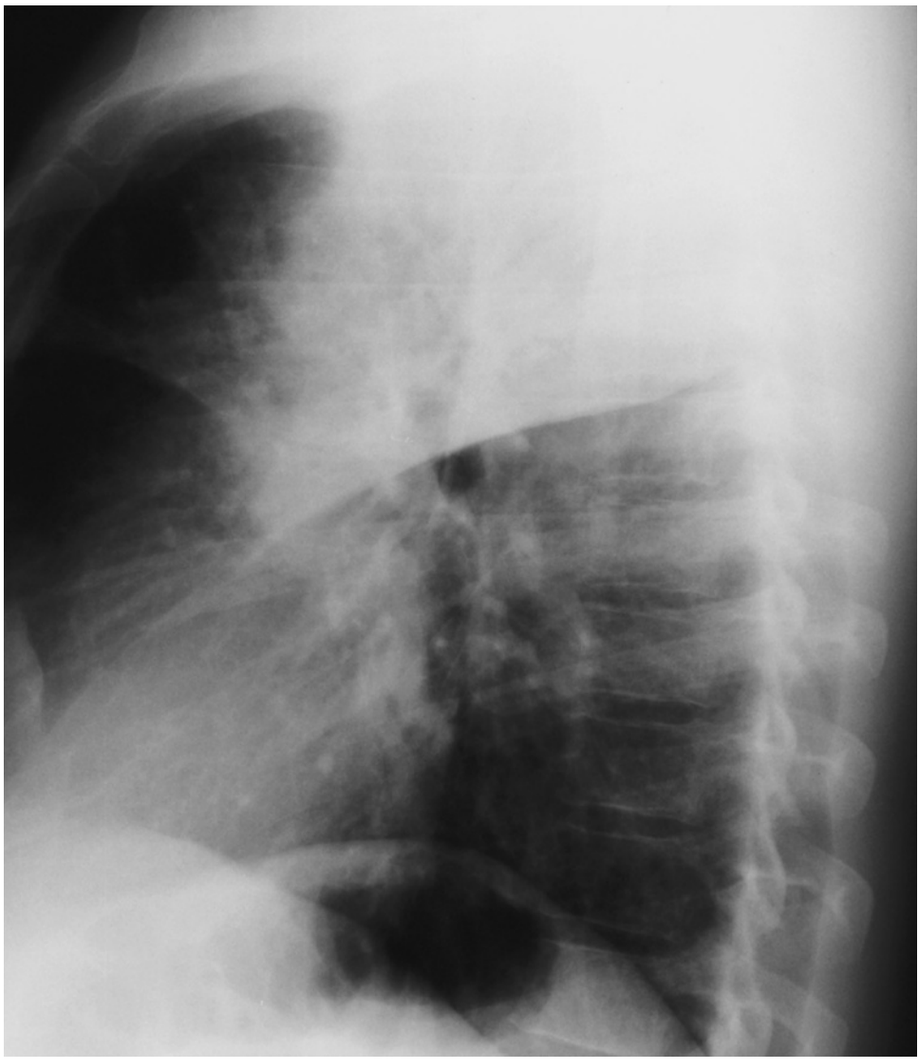

Fig. 3.3 Lobar pneumonia. The patient is a 30-year-old man presenting with sudden onset of severe malaise, cough, and fever. The right upper lobe shows a homogeneous consolidation that is most pronounced in the posterior segment.

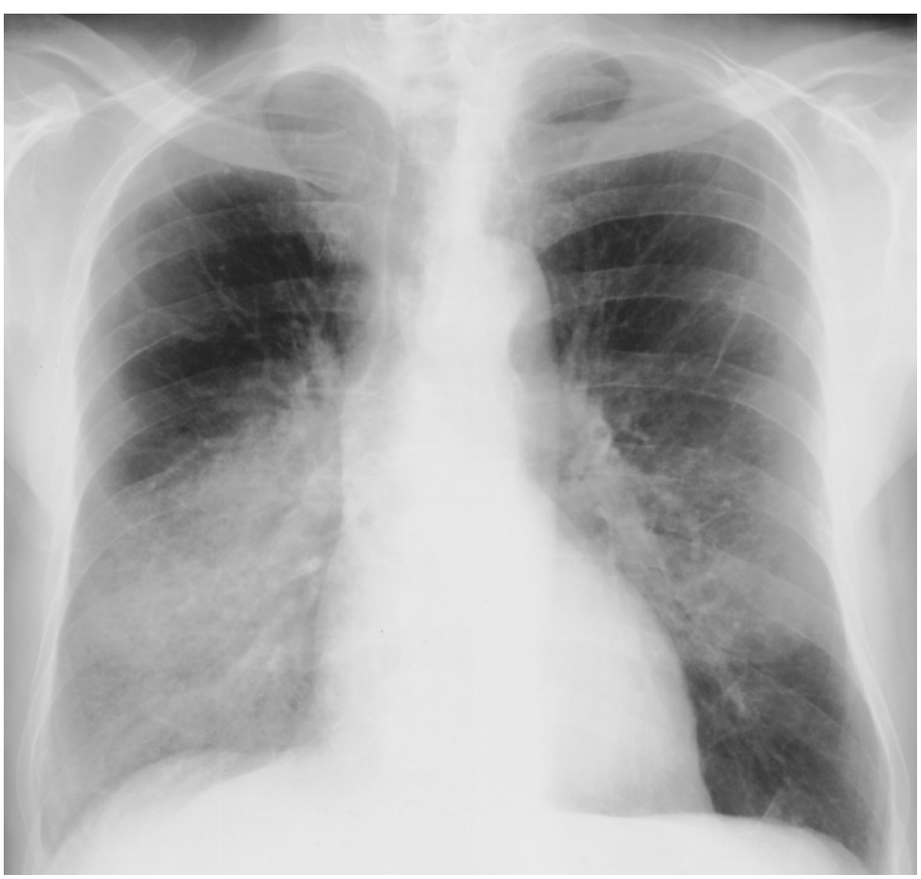

Fig. 3.4 Bronchopneumonia. The patient is a 75-year-old man with a long history of COPD. He presents here with acute exacerbation evidenced by significant dyspnea and productive cough. Signs of chronic bronchitis are present with diffuse shadowing and barrel chest with primarily apical emphysema. Peribronchial infiltrates are seen in the right middle and lower fields. The heart and aorta exhibit a hypertensive configuration.

Alveolar Pneumonia

Excursus: Alveolar Pattern

Alveolar pneumonias can be subdivided according to their distribution pattern as follows:
- Lobar pneumonia
- Bronchopneumonia
- Focal pneumonia

The following section will examine the basic "alveolar" pattern (**Fig. 3.5**). First, the radiologic term "alveolar shadow" requires some explanation. "Alveolar" describes changes leading to increased attenuation in the region of the alveoli or caused by disorders of the alveolar space. Causes include:
- Intra-alveolar edema (**Fig. 3.6**)
- Inflammatory alveolar congestion (**Fig. 3.8**)
- Other consolidation of the alveolar space such as proteinosis or tumor spread (**Fig. 3.7**)

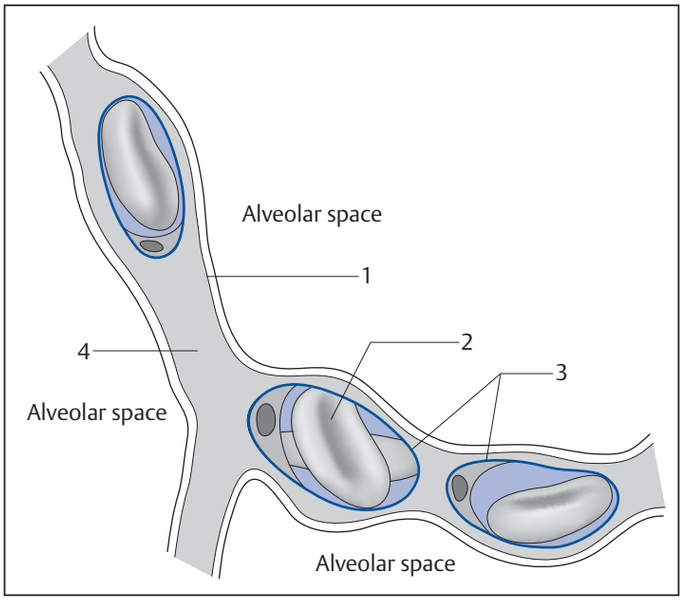

Fig. 3.5 Interstitial and alveolar compartments. The air-filled alveolar space is subdivided by the interstitium, a space filled with collagen connective tissue between blood and lymph vessels.
1 Surfactant
2 Erythrocyte
3 Vascular endothelium
4 Interstitium

Other causes of increased radiodensity in the alveolar space included under the term "alveolar shadow" with somewhat less justification include:
- Collapse of the alveoli
- Thickening of the alveolar wall in fibrosis

The **radiographic signs** indicative of increased alveolar radiodensity are rarely defined clearly and comprehensively, and they cause problems especially for the beginner. Radiographic signs of alveolar infiltrate (and of other alveolar processes) include:
- The classic acinar pattern
- Blurring of anatomic structures
- Ground-glass opacification
- Homogeneous area consolidation
- With or without air bronchogram

The most important **CT signs** of alveolar processes include:
- Ground-glass opacities
- Area consolidations

In defining these alveolar shadow signs one should consider, as in a differential diagnosis, findings that simulate alveolar patterns. The same applies to the CT patterns.

Acinar Pattern

Acinar pattern (**Fig. 3.9**) is the term used to describe the disseminated occurrence of tiny nodular shadows. This does not mean that individual consolidated lobules are directly visualized on the radiograph. They are too small and would escape detection. The radiographic sign is a summation effect produced by several superimposed lobules similar to the effect of vessel imaged end-on. The acinar pattern is difficult to distinguish from micronodular changes due to other causes (the most common of these is respiratory bronchiolitis-interstitial lung disease in chronic smoker's bronchitis).

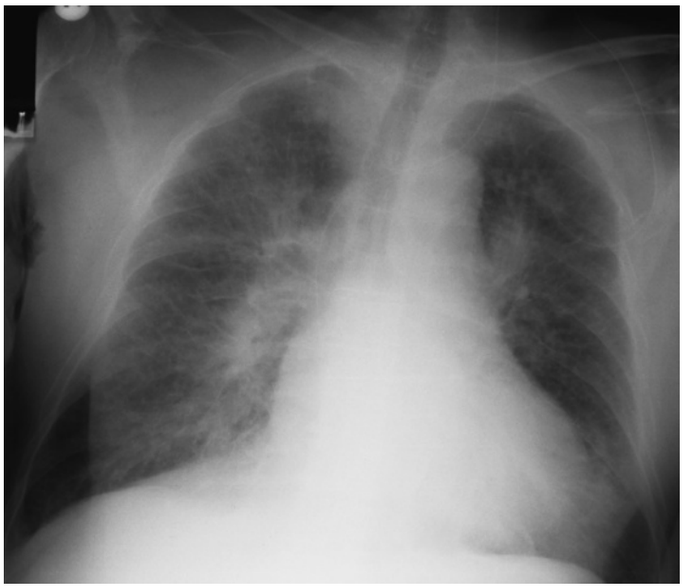

Fig. 3.6 Alveolar pulmonary edema in myocardial infarction and kidney failure. The patient is an 84-year-old man with an acute myocardial infarction and kidney failure. Both lungs show diffuse, faint opacification that is most pronounced in the central region of each lung.

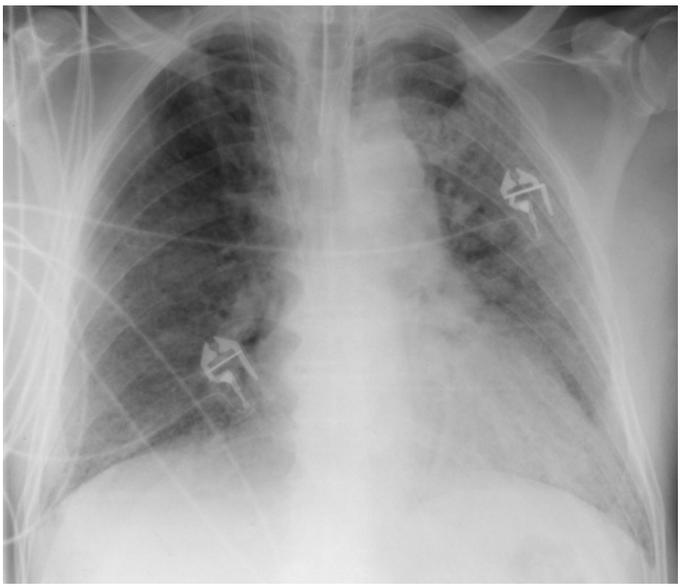

Fig. 3.7 Pattern of ground-glass opacities in alveolar proteinosis. The film shows extensive, partially confluent area densities, appearing as ground-glass opacities in the peripheral areas. Left heart enlargement without any significant effusion. Radiograph obtained after intubation.

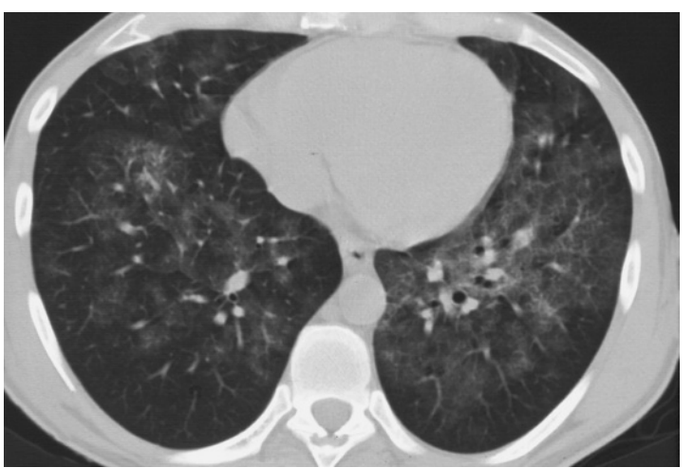

Fig. 3.8 Alveolar opacities in infection. Ground-glass opacities sparing the periphery of the lung and the bronchovascular spaces in *Pneumocystis carinii* pneumonia. The densities correlate with the increasing filling of the alveoli with foamy exudate and pathogens as the disease progresses.

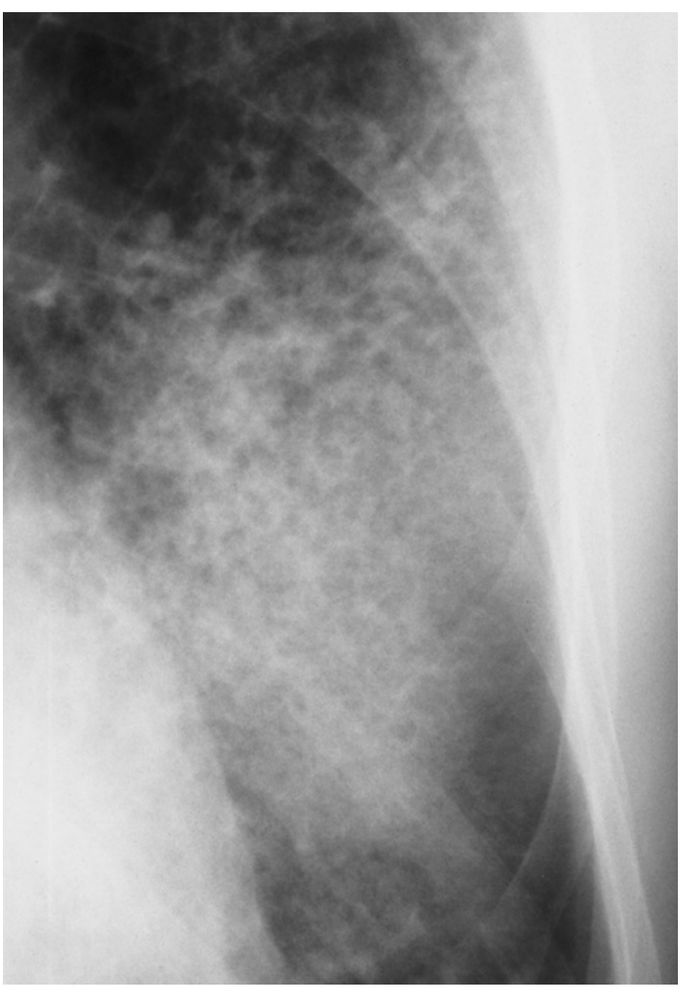

Fig. 3.9 Acinar pattern (detail). Alveolar edema in acute kidney failure. The edema is composed of myriad confluent small nodular shadows (acinar nodules).

CT Pattern

Shadow patterns to look for on CT can be classified as follows (**Fig. 3.10**):

- Area consolidation
- Nodular densities
- Streaky opacities
- Ground-glass opacities

Area consolidations with or without an air bronchogram (**Fig. 3.12**) and the ground-glass pattern are often evaluated as signs of an alveolar density (certain qualifications apply; see Chapter 5, "General").

In contrast to consolidated areas, a *ground-glass pattern* (**Fig. 3.11**) refers to a shadow through which the basic anatomic structure remains visible. Vascular structures, bronchi, and septa are recognizable, and the structure of the secondary lobule remains intact. A ground-glass pattern is caused by partial filling of the air spaces with substrate isodense to soft tissue (edema [**Fig. 3.13**], inflammatory cells, mucus, protein, fibrosis [**Fig. 3.14**], etc.) within the thickness of the CT slice.

Densities *simulating ground-glass patterns* can be caused by technical effects without actual partial filling of the air spaces. Such findings should be referred to as "ground-glass artifacts" (see **Fig. 3.11**). Such phenomena include:

- Partial volume effects
- Pulsation effects
- Respiratory artifacts
- Motion artifacts in general

The partial volume effect (**Fig. 3.15**) is the most important of these phenomena. The summation of a solid process lying partially within the slice thickness and an adjacent air-filled space within the slice thickness mimics a volume element of medium density. Pulsation and respiratory artifacts are attributable to a similar mechanism with respect to temporal resolution as opposed to spatial resolution.

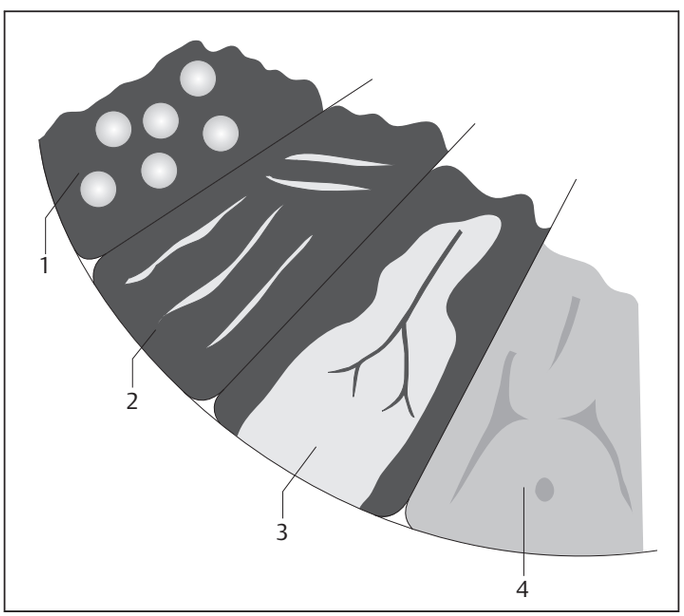

Fig. 3.10 Classification of the opacities on CT.
1 Nodular
2 Streaky
3 Area consolidation
4 Ground-glass

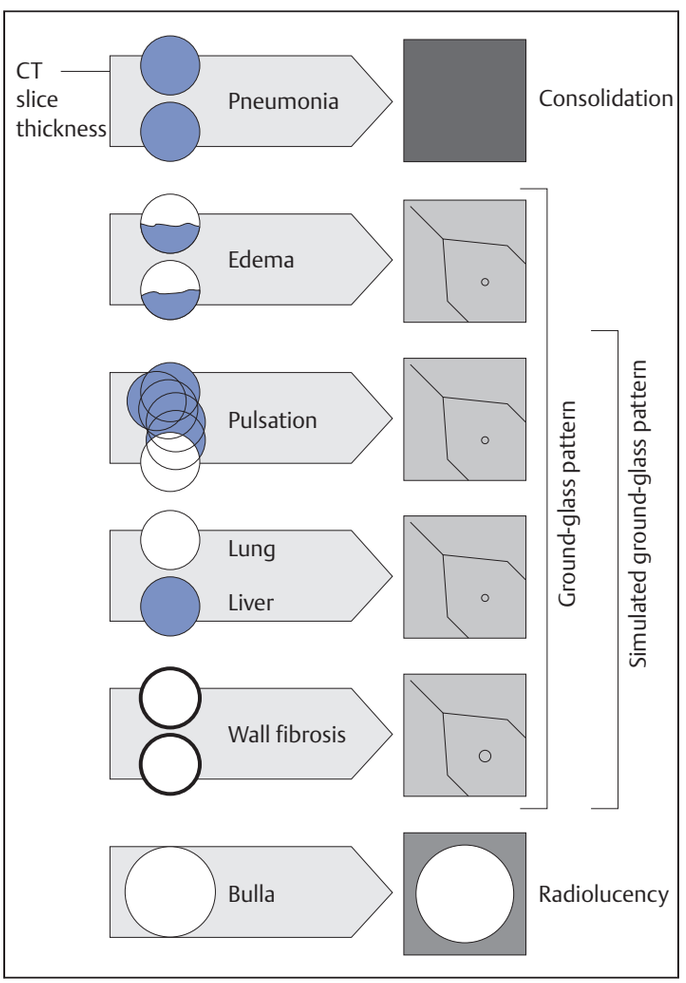

Fig. 3.11 Ground-glass pattern produced by partial filling. Processes of different densities are detected in the CT slice, simulating a volume element of medium density. This phenomenon can produce ground-glass opacities or artifacts resembling ground-glass opacities.

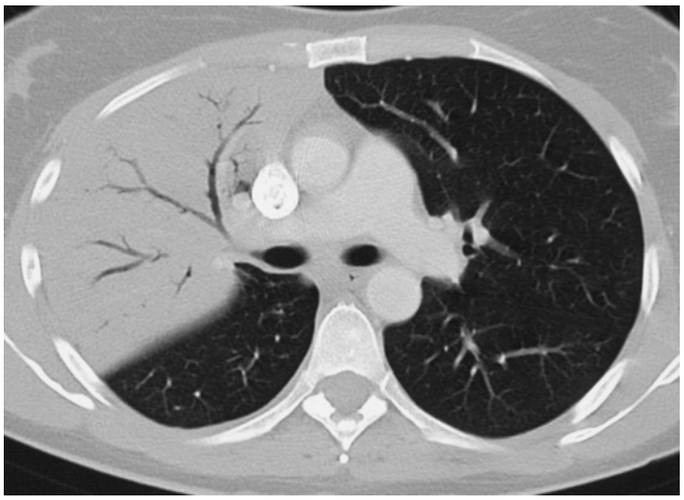

Fig. 3.12 Area consolidation with air bronchogram. Lobar pneumonia in the right upper lobe.

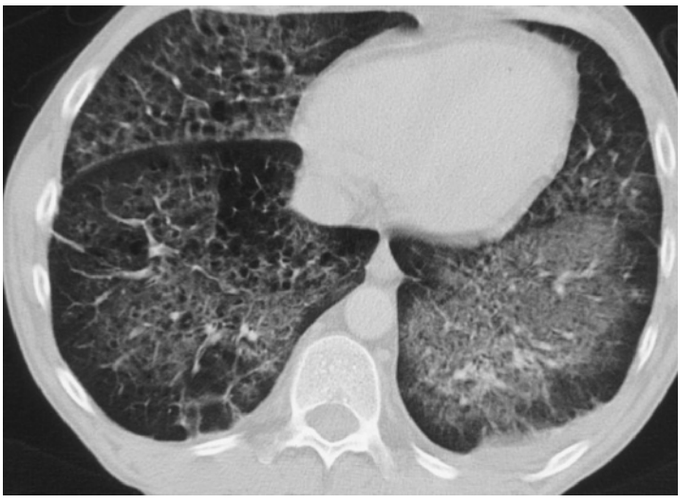

Fig. 3.13 Ground-glass opacity. Ground-glass opacities in the central region of both lungs in an alveolar pulmonary edema due to acute kidney failure. The basic structure of the lung (vascular structures and septa) remains visible through the opacity.

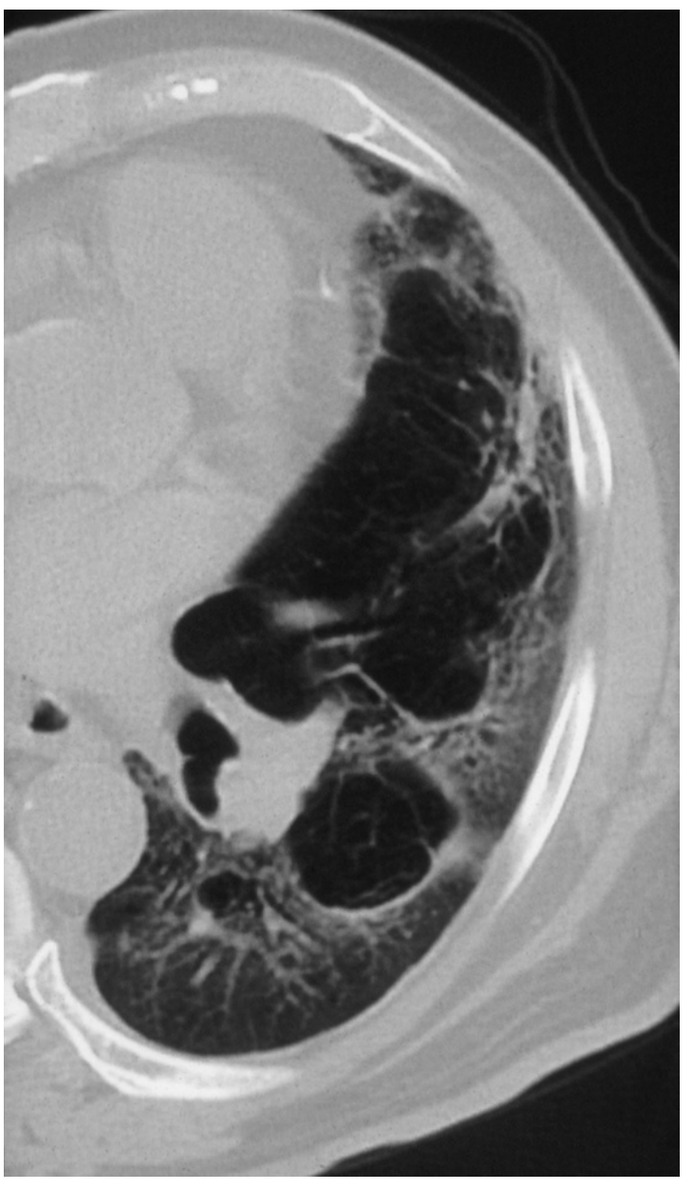

Fig. 3.14 Ground-glass pattern in alveolar fibrosis. Thickening of the alveolar walls in the setting of a fibrosing reaction (idiopathic pulmonary fibrosis) creates a ground-glass opacity. The central region of the lung appears hyperinflated due to the shrinkage occurring there.

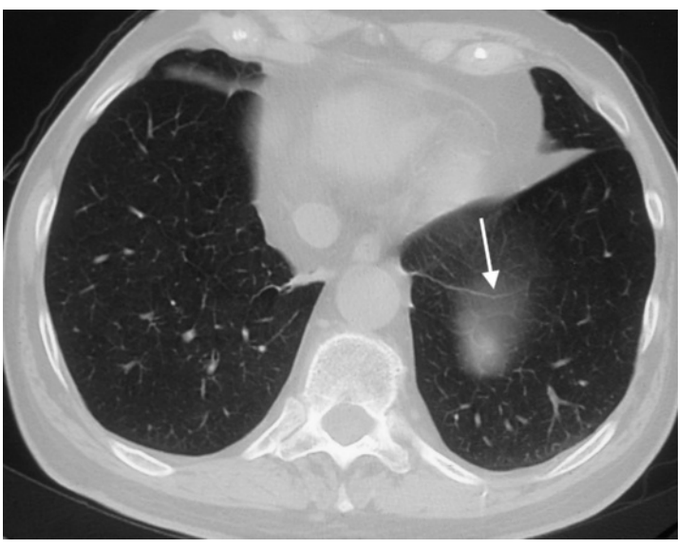

Fig. 3.15 Ground-glass artifact on the diaphragm as a result of a partial volume effect. The most common partial volume effects regularly occur on the dome of the diaphragm. Here the basal lung shows what looks like a circumscribed density. The structure of the lung beneath it remains visible (white arrow).

Lobar Pneumonia

With **pneumococcal pneumonia** as its classic example, lobar pneumonia produces typical pictures on the plain chest radiograph that reflect its respective pathoanatomic stages (see "Notes on Pathology and Epidemiology"):

- There is dense, homogeneous opacification of broad areas
- Borders of the shadow coincide with lobar or segmental boundaries
- It rarely crosses segmental boundaries
- Volume increases
- Air bronchogram is common

Congestion

In the initial phase of the disorder (congestion), the patient typically reports a sudden onset ("since yesterday afternoon") and severe malaise with fever and cough ("hit me like a ton of bricks"). Patients generally present as outpatients and are often young. Close examination of the plain chest radiograph reveals veil-like opacification of the pulmonary parenchyma. Pulmonary anatomy appears blurred as discussed above. The shadow is initially inhomogeneous, beginning at the hilum and extending with increasing density toward the periphery. In this stage, the typical picture of *lobar pneumonia* is not yet evident. However, an air bronchogram will occasionally be visible within ground-glass opacities (**Fig. 3.16**). The hilum of the affected segment initially appears thickened. During the further course of the disorder it is no longer distinguishable from the infiltrated area. However, there is no mediastinal shift (differential diagnosis should consider atelectasis).

Hepatization

The stage of red hepatization is typically characterized by homogeneous opacification developing within hours and covering the entire lobar parenchyma with convex protrusion of the lobar boundary. The shadow respects anatomic boundaries (**Fig. 3.17, Fig. 3.18**). Affected and non-affected areas are usually well defined. Although the term "lobar" implies involvement of the entire lobe, this need not be the case. One also refers to a "lobar" pattern where there is uniform involvement of an individual segment.

Notes on Pathology and Etiology

The first precise pathoanatomic descriptions of pneumonia go back to **Karl Freiherr von Rokitansky**, the founder of the New Vienna School of Medicine. His stages of lobar pneumonia provided the basis for the classification and clinical evaluation of the spread, course, and prognosis of this disorder for many decades. Why pneumonias occur as an alveolar lobar type or bronchopneumonic type has remained unclear. The relationship between the immune system and the virulence of the pathogens appears to be important. Pathogen-specific mediators and the influence of the central nervous system have been discussed. Pneumococcal pneumonia represents the prototype of lobar pneumonia. However, pneumococci can also cause bronchopneumonia. Findings in immunocompromised patients typically include diffuse bilateral pneumonia that produces the picture of bronchiolitis.

The histologic correlate of lobar pneumonia is a largely uniform spread of granulocytic exudate in the alveoli. The congestion phase (serous exudate in the alveoli) occurs in the first 24–28 h. The red hepatization stage between days 2 and 3 shows a marked increased in fibrin deposits in the alveoli that then form a solid mass. The gray hepatization stage (3–4 days) is characterized by reopening of the pulmonary vessels and leukocyte infiltration. The affected lung segment increases significantly in volume. The resolution stage on days 7–11 is characterized by breakdown of the fibrin, which is then removed via the lymph or coughed up.

The bronchial tree in lobar pneumonia shows only an associated inflammatory reaction with desquamation of the epithelium in the small bronchi.

Karl Freiherr von Rokitansky (* 1804 Königgrätz, † 1878 Vienna): professor ordinarius of pathologic anatomy; co-founder of the New Vienna School of Medicine; introduced the classification of the pneumonias and studied the pathologic basis of emphysema. Died of an acute asthma attack 3 years after being named emeritus professor.

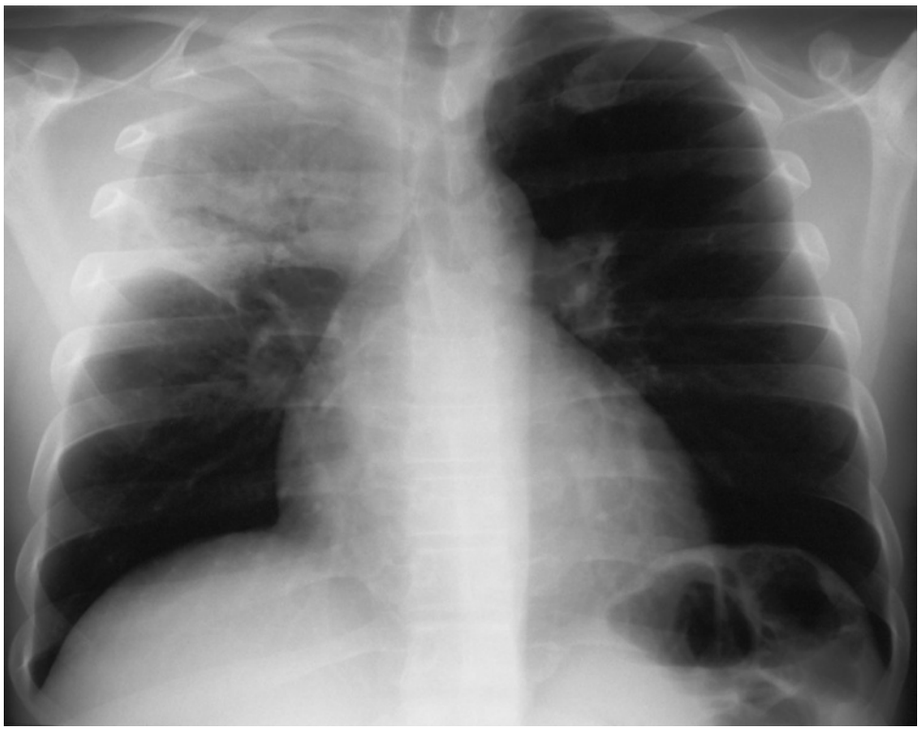

Fig. 3.16 Air bronchogram in lobar pneumonia in the right upper lobe. Homogeneous area consolidation of the right upper lobe with an air bronchogram. The patient is a 30-year-old man with normal heart size and no signs of chronic pulmonary damage.

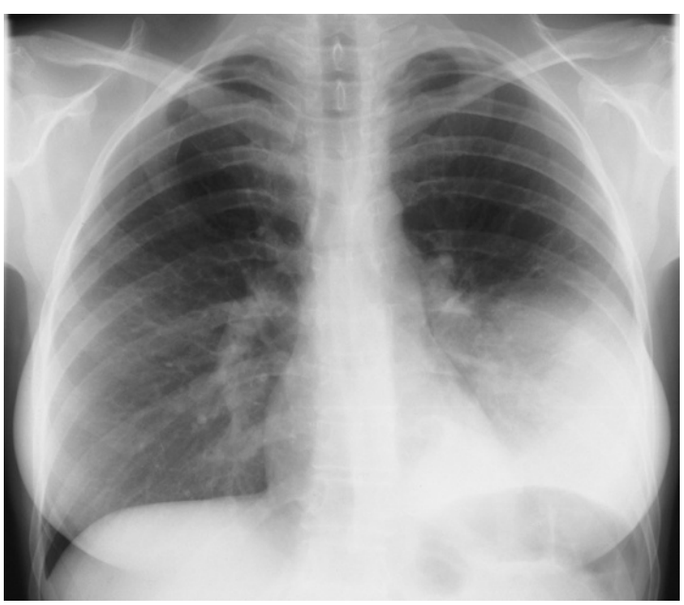

Fig. 3.17 Homogeneous shadowing of the left lower lung field. The patient is a 35-year-old woman with sudden severe malaise, cough, and fever. The posteroanterior radiograph shows a homogeneous area consolidation in the left lower lung field that obliterates the silhouette of the diaphragm.

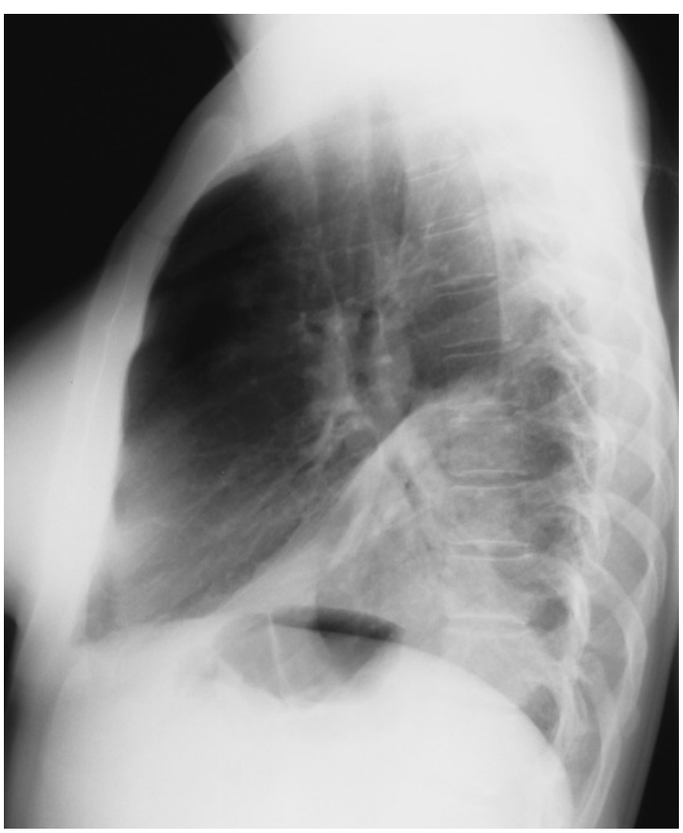

Fig. 3.18 Infiltrate is present in the lower lobe with a significant increase in volume. The lateral radiograph confirms the tentative diagnosis of lower lobe involvement. Marked protrusion of the oblique fissure indicative of increased volume. The findings respect the anatomic boundaries.

Silhouette Sign

Homogeneous Area Consolidation

The silhouette sign first described by Felson in 1950 is important for recognizing and **defining** area consolidation. A silhouette is a dark area that stands out against a light background. If structures of the same radiodensity cannot be separated, then they lie in the same plane. Where a natural boundary is no longer detectable and, for example, the left lower lobe, cardiac border, and diaphragm form a single continuous silhouette, then one may assume that an infiltrate is present. Isodense to soft tissue, the infiltrate gives these structures a uniform radiodensity, whereas normally they are distinguishable by their dissimilar radiodensities.

A positive silhouette sign refers to the loss of a radiographic border that is normally present. A negative silhouette sign refers to the occurrence of a border that is not normally visible.

The **diagnosis** of a "genuine" lobar shadow may be assumed where the plain chest radiograph shows an alveolar density with a silhouette sign.

A **differential diagnosis** should then consider the following entities:

- Infiltrate?
- Circumscribed edema (congestion in an emphysematous area)?
- Atelectasis?

Volume loss is often mentioned as the decisive criterion for ruling out atelectasis. At first glance this appears plausible. Unfortunately, it does not always apply, as completely infiltrated areas often exhibit dystelectasis due to mucus accumulation in the bronchi.

The presence or absence of a silhouette sign can be used to determine the precise anatomic location of the dense, well-demarcated infiltrates of lobar pneumonia on the plain chest radiograph.

Upper Lobes

In upper-lobe pneumonias (**Fig. 3.16**), involvement of the apical or posteroapical segment causes shadowing in the apex of the lung. However, such findings are rare in classic lobar pneumonia. If the apex of the lung remains clear, the infiltrate lies in the anterior segment of the upper lobe. Radiographs in two planes invariably visualize findings clearly.

Middle Lobe and Lingula

The classic example for a silhouette sign is the location of pneumonia findings in the middle lobe or lingula. In contrast to lower-lobe infiltrates, the silhouette sign here involves the respective mediastinal border (**Fig. 3.19**). The lateral view showing a triangular shadow with its apex at the hilum and its base along the chest wall is even more characteristic than the findings on the posteroanterior radiograph mentioned above.

Caution is required in the presence of pectus excavatum. This condition regularly obliterates the right cardiac border (**Fig. 3.21**).

Lower Lobes

Shadowing of the apical segment of the lower lobe is occasionally difficult to detect on the posteroanterior radiograph. An opacity is visualized in the middle field near the hilum. This shadow on the posterior chest wall below the horizontal fissure can occasionally be difficult to detect when overlapped by the thoracic spine. The infiltrate in the apical segment of the lower lobe is usually more clearly visualized on the lateral film. In contrast to middle-lobe or lingular infiltrates, infiltration of segments 8–10 produces a silhouette sign with the respective diaphragmatic crus (**Fig. 3.20**). The lateral view aids in evaluating the exact position of the shadow within the segment. Infiltrate in the anterior (anterior basal) segment of the lower lobe lies in the vicinity of the heart shadow beneath and posterior to the horizontal fissure, which sharply demarcates the infiltrate from the middle lobe or lingula. The posterior basal segment of the lower lobe leads to opacification of the posterior recess, obscuring the structures of the lower thoracic spine.

Etienne de Silhouette (*1709, † 1767): Finance minister of Louis XIV of France. Silhouette decorated the walls of his palace with paper shadow portraits he cut himself, an artistic reduction to basic essentials.

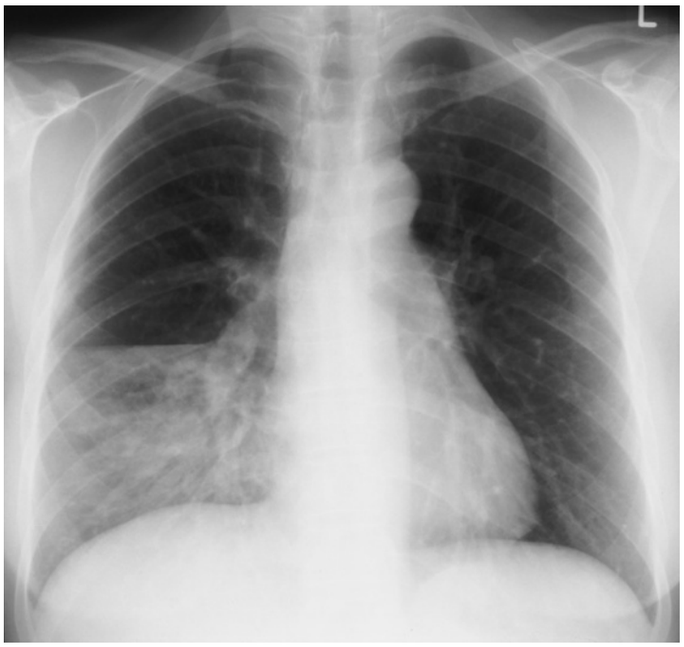

Fig. 3.19 Infiltrate in the middle lobe. The posteroanterior radiograph shows a rather homogeneous consolidation in the right lower lung field with a sharp horizontal cranial demarcation (this in itself defines middle lobe involvement). The right cardiomediastinal silhouette is obliterated. The silhouette of the diaphragm is preserved.

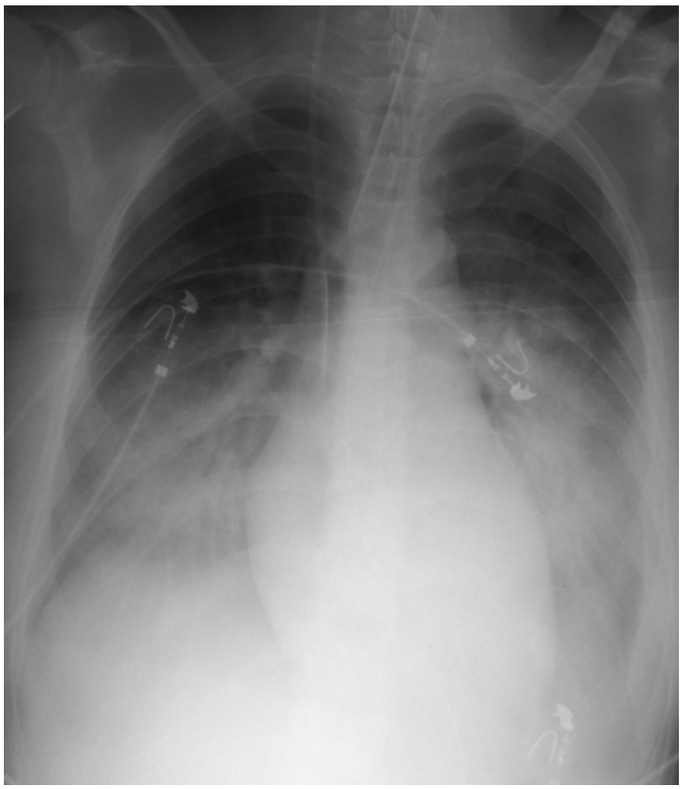

Fig. 3.20 Lobar pneumonia in both lower lobes. The silhouette of the diaphragm is obliterated bilaterally in this 28-year-old woman with normal heart function. The patient has been intubated for respiratory failure.

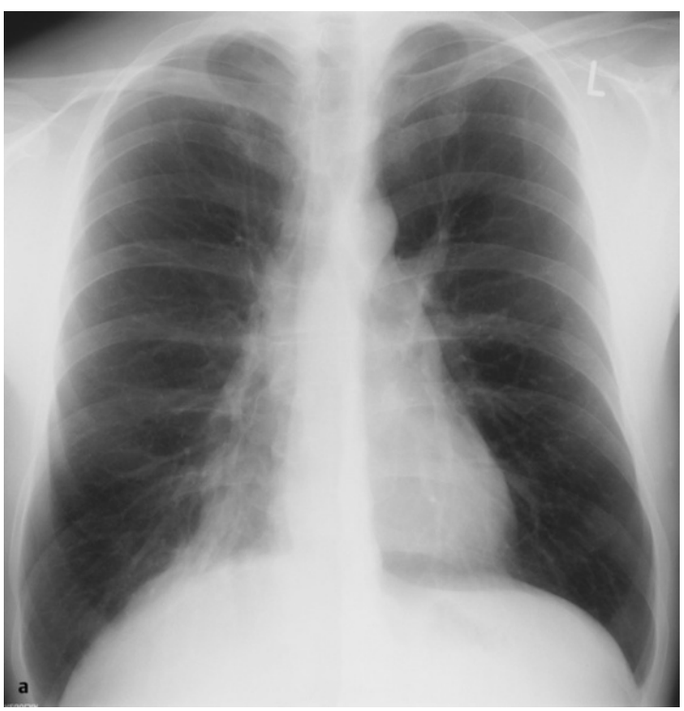

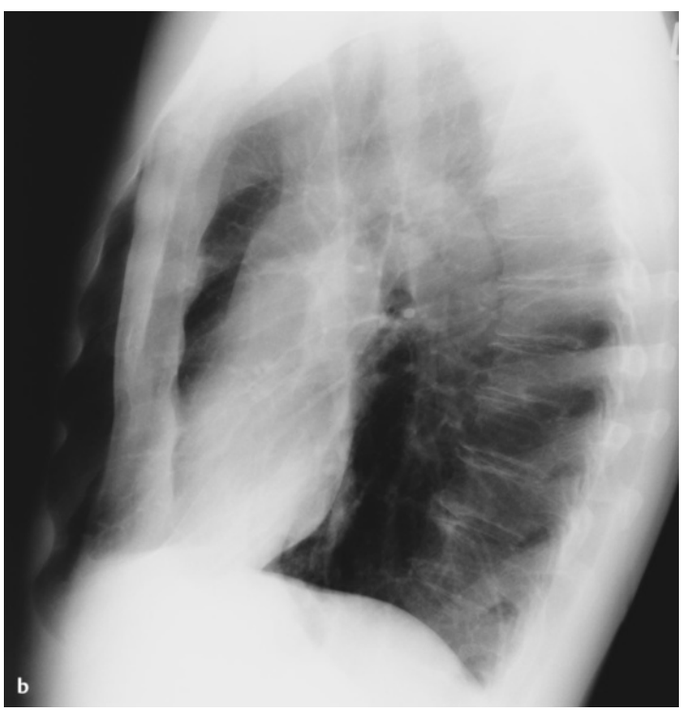

Fig. 3.21 a, b Pectus excavatum simulating infiltrate in the middle lobe.

a Posteroanterior view. Right cardiac border is obliterated and a right paramediastinal opacity is present.

b Lateral view. Severe pectus excavatum with no sign of increased attenuation.

Lysis

The shadows on the plain chest radiograph appear most intense on the third to fourth day, and on the eighth day the opacity begins to disappear, reflecting the beginning resolution process. In the stage of massive alveolar infiltration, the bronchial tree is often no longer visible because of mucus obstruction of the bronchi. This marks the beginning of the resolution stage.

Resolution

The infiltrate becomes more radiolucent as the air content of the alveolar space increases. The homogeneous shadow typical of lobar pneumonia changes into an inhomogeneous, patchy picture with peribronchial residues. Loss of volume in the affected lung segments suggests an abnormal resolution process with development of secondary atelectasis.

Follow-up Examinations

As the resolution process lasts up to 4 weeks, this stage is often characterized by a marked discrepancy between continued abnormal radiologic findings and clinical findings of restored health. Ignorance of this fact can lead to premature follow-up examinations and, as is seen every day, to great disappointment on the part of a clinician ready to discharge a patient.

In the first few days, radiologic findings may even worsen despite initiation of antibiotic treatment and improvement of clinical symptoms. This applies to lobar pneumonia as well as to bronchopneumonia (**Fig. 3.22, Fig. 3.23**).

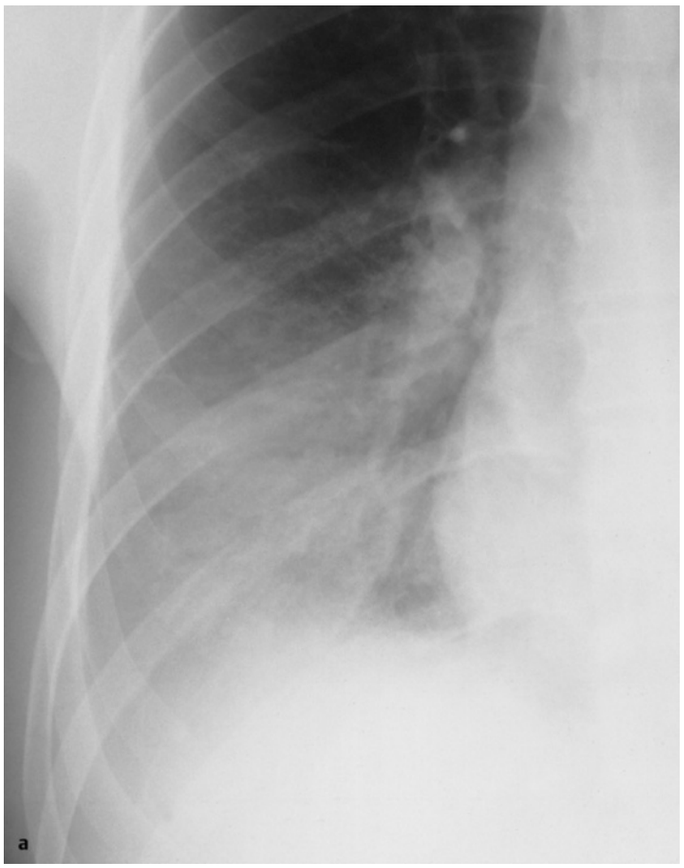

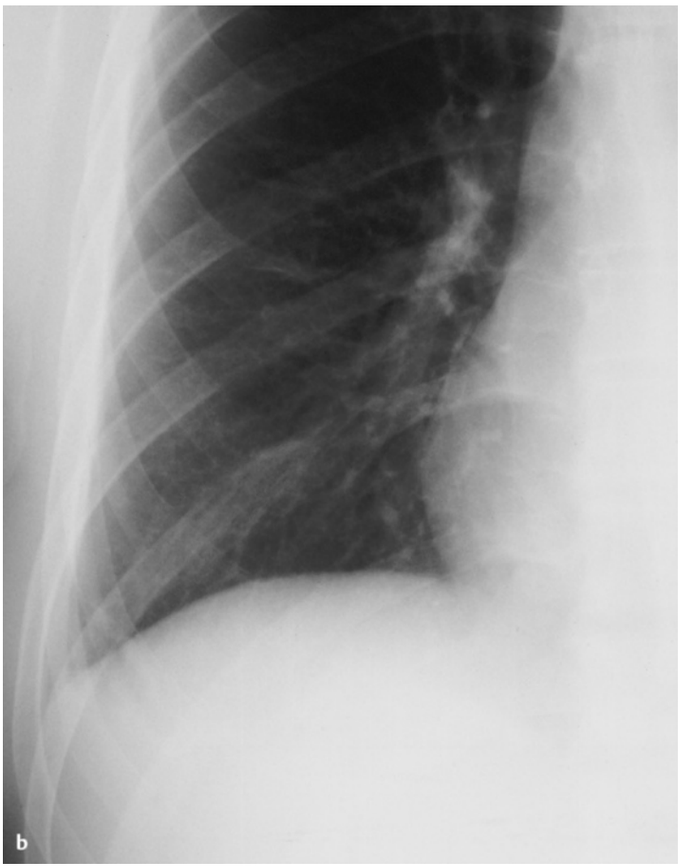

Fig. 3.22 a, b **Normal resolution of lobar pneumonia in the right lower lobe.**

a Detail of the right lower lung field. Homogeneous consolidation with obliteration of the contour of the diaphragm (sudden onset 3 days previously in a 38-year-old male self-employed contractor with chills and severe malaise).

b Follow-up examination 3 weeks later. Findings are completely normalized.

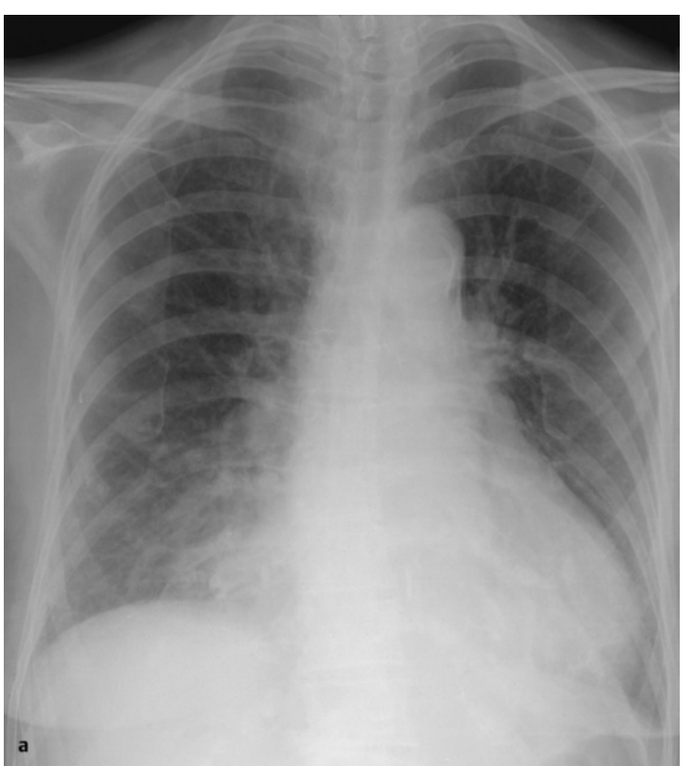

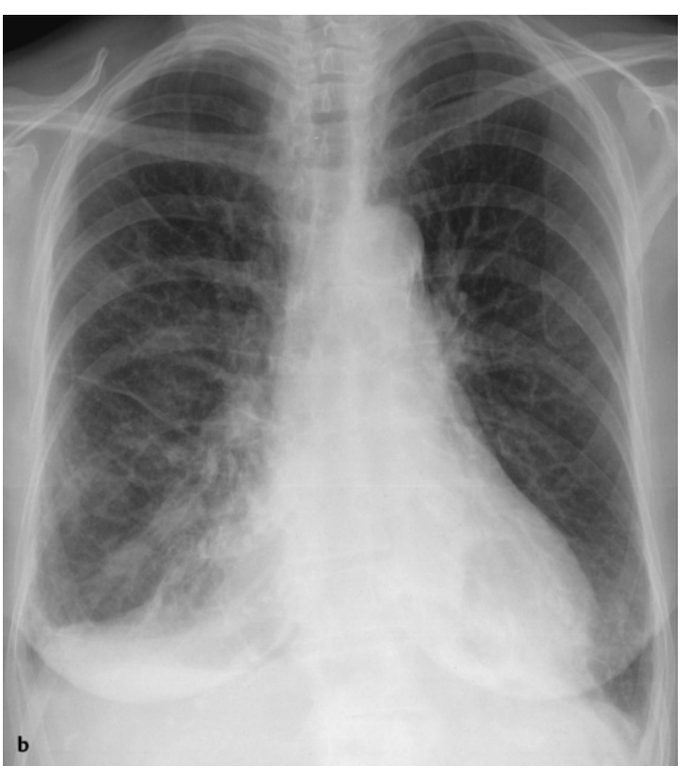

Fig. 3.23 a, b **Pneumonia**

a Premature follow-up examination in pneumonia. An 89-year-old woman with initial findings of bronchopneumonic infiltrate in the middle lobe. Left heart enlargement with slight congestion in the pulmonary veins.

b Follow-up examination 4 days later. The patient already shows marked clinical improvement. Compared with the previous study, the radiograph shows increasing consolidation in the right lower lung field and a small effusion in the costophrenic angle.

Computed Tomography

CT of the lung may seem superfluous in lobar pneumonia as an unequivocal diagnosis can be made by clinical examination in combination with conventional chest radiography. However, it is useful in cases where physical examination is difficult (intensive care patients), and it allows an earlier and more definitive diagnosis in immunocompromised patients. The CT examination also allows earlier detection of possible complications (**Fig. 3.24**).

CT findings in lobar pneumonia correspond to the signs on conventional radiographs, which themselves are largely unequivocal. The ground-glass opacities in pneumonic congestion do not lie in an area of reduced volume as they do in beginning hypoventilation. CT demonstrates the air bronchogram in the presence of area consolidation more clearly than does the plain chest radiograph.

In the classic resolution phase, the infiltrate thins and takes on more of a ground-glass appearance (**Fig. 3.25**). The air bronchogram can resolve or be largely obscured as mucus is expectorated. Resolving lobar pneumonia in this stage becomes increasingly difficult to distinguish from bronchopneumonia. The crucial criterion in a differential diagnosis is the strictly segmental and lobar distribution that respects anatomic boundaries.

CT can visualize complications in the form of:

- Liquefaction within the consolidation (pulmonary abscess)
- Increasing effusion with thickening of the visceral and parietal pleura (secondary pneumonic empyema)
- Residual patchy shadow, usually with volume loss (lack of resolution with consolidation or carnification)

Pulmonary abscess (**Fig. 3.26**) can be diagnosed early on CT from hypodensities within the infiltrate, which is isodense to soft tissue. Differential diagnosis of air accumulations must distinguish simple communication with the bronchus in coughing from gas gangrene. Use of intravenous contrast agents is often helpful in determining whether colliquation is present and in differentiating associated effusion from empyema. Characteristic signs include the strong, uniform hyperdensity of the hypervascular abscess wall and of the thickened pleura (**Fig. 3.27**) in empyema.

The lack of resolution later leads to volume loss from retraction of the dense infiltrate (**Fig. 3.28**). The shrinkage processes often lead to bronchiectasis within the scarred areas.

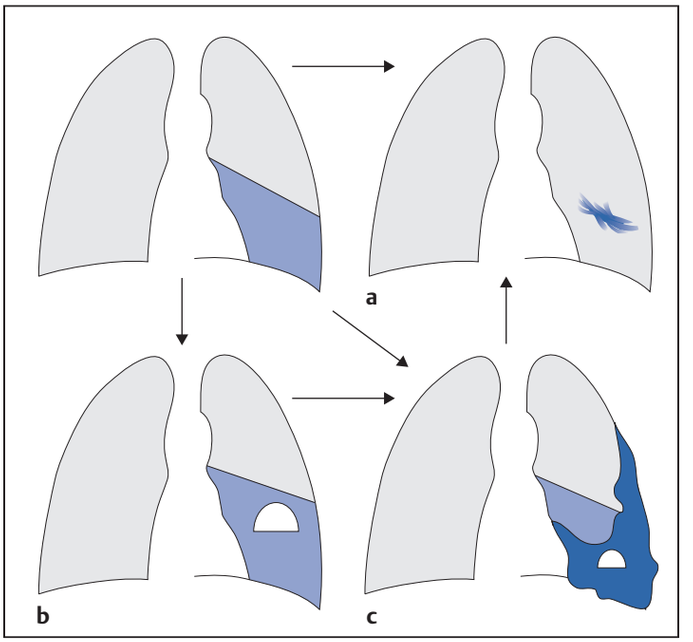

Fig. 3.24 a–c Schematic diagram of possible complications of lobar pneumonia. After a normal course with resolution and recuperation, regression will often be incomplete with extensive scarring and occasionally carnification (**a**), less often with tissue loss and a pulmonary abscess (**b**), or with spread of infection to the pleural space and development of an empyema (**c**).

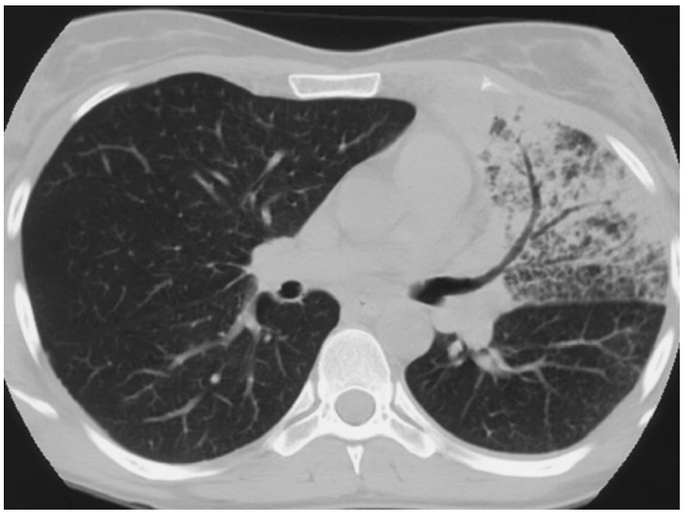

Fig. 3.25 Resolving lobar infiltrate in the upper lobe. An area consolidation in the left upper lobe is still visible but has already thinned out considerably. Loss of volume is already detectable while the air bronchogram is still visible. The pneumonia remains sharply demarcated from the unaffected lower lobe.

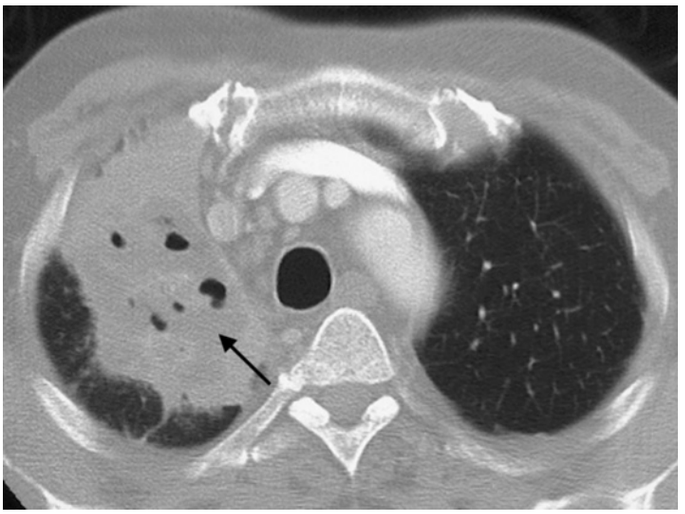

Fig. 3.26 Abscesses in lobar pneumonia. Area consolidation is seen in the right upper lobe, which already shows hypoventilation. Other findings include central hypodense areas (black arrow) and air inclusions.

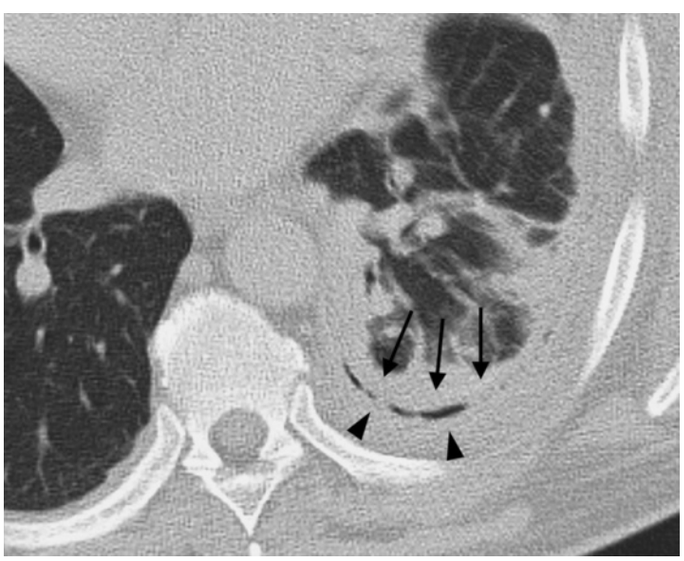

Fig. 3.27 Secondary pneumonic empyema. The infiltrate in the lower lobe has largely resolved. After repeated aspiration and drainage of an empyema, thickening of the visceral pleura (black arrows) and parietal pleura (black arrowheads) is still detectable.

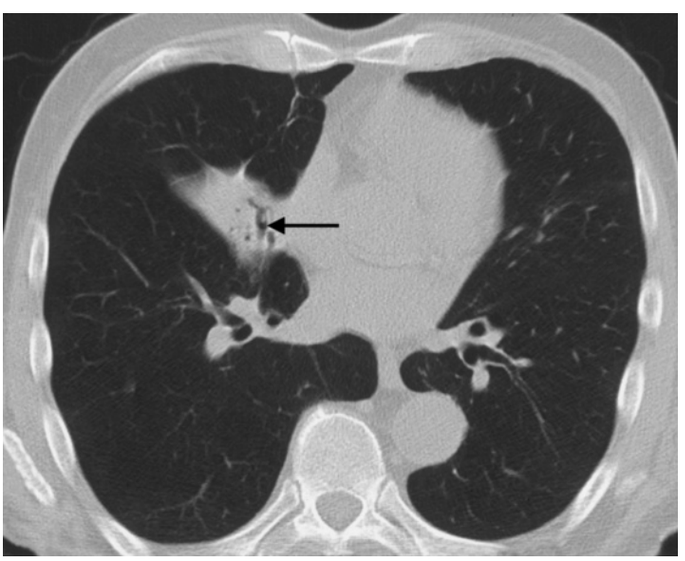

Fig. 3.28 Carnification of the middle lobe following lobar pneumonia. Severe shrinking of the middle lobe has occurred after lobar pneumonia. The bronchi (black arrow) in the consolidated area are dilated in response to the retraction processes.

Bronchopneumonia

The second form of alveolar pneumonia is known as focal pneumonia or bronchopneumonia. Today more common than lobar pneumonia, this form is limited to individual lobules in circumscribed areas. Whereas the virulence of the pathogen is the major causative factor in lobar pneumonia, bronchopneumonia often develops secondary to a bronchial infection or as a complication of other underlying disorders (heart failure, COPD, or in bedridden patients). Consequently, the spectrum of pathogens is far broader (**Fig. 3.29**).

In contrast to the homogeneous consolidation seen in lobar pneumonia, bronchopneumonia exhibits the following features on the plain chest radiograph:

- Streaky peribronchial opacities and/or
- Solitary or multiple ill-defined focal opacities (**Fig. 3.30**)

Bronchopneumonia is more difficult to identify than lobar pneumonia.

The same criteria of infiltration of the alveolar space apply as in lobar pneumonia, i.e., alveolar density with a silhouette sign.

Often the predisposing comorbidities are already identifiable on the plain chest radiograph based on findings such as:

- Diffuse shadowing (bronchitis in a flulike infection)
- Obstructive barrel chest (exacerbated COPD)
- Cardiomegaly (hypostatic pneumonia)
- Poor inspiration in a supine patient (orthostatic pneumonia)

Bronchopneumonia is mimicked by other conditions more often than lobar pneumonia.

Radiographic diagnosis is more difficult than in lobar pneumonia, often due to overlapping findings such as:

- Pleural effusion
- Basal edema
- Basal hypoventilation

In an emphysematous lung, a pulmonary fluid accumulation may occur at a location that masks simultaneous hypostatic pneumonia. The pneumonia can then be diagnosed only by observing the further course of the disorder in response to dehydration treatment.

An important criterion for the presence of lower-lobe infiltration is that the lower thoracic vertebrae appear less distinct than the upper thoracic vertebrae. Normally this is the other way around due to the thicker soft-tissue envelope of the upper thoracic spine (**Fig. 3.30**).

CT examination of the lung in the presence of bronchopneumonic infiltrates shows nodular to patchy densities in addition to an asymmetrical contour of the thickened ring structures. Despite their confluence, it is usually apparent that the densities are multifocal. The changes are usually identifiable even where edema is present.

Patients generally recover completely from bronchopneumonia. Rarely but increasingly, fibrosis of variable intensity can be observed where delayed leukocyte infiltration occurs as with antibiotic therapy. Rarely the disorder will resolve incompletely or not at all despite adequate treatment, and carnification will occur. Carnified pneumonia appears as a patchy density with broad pleural contact that remains unchanged over a period of weeks. Radiologic findings are indistinguishable from bronchiolitis obliterans with organizing pneumonia (BOOP).

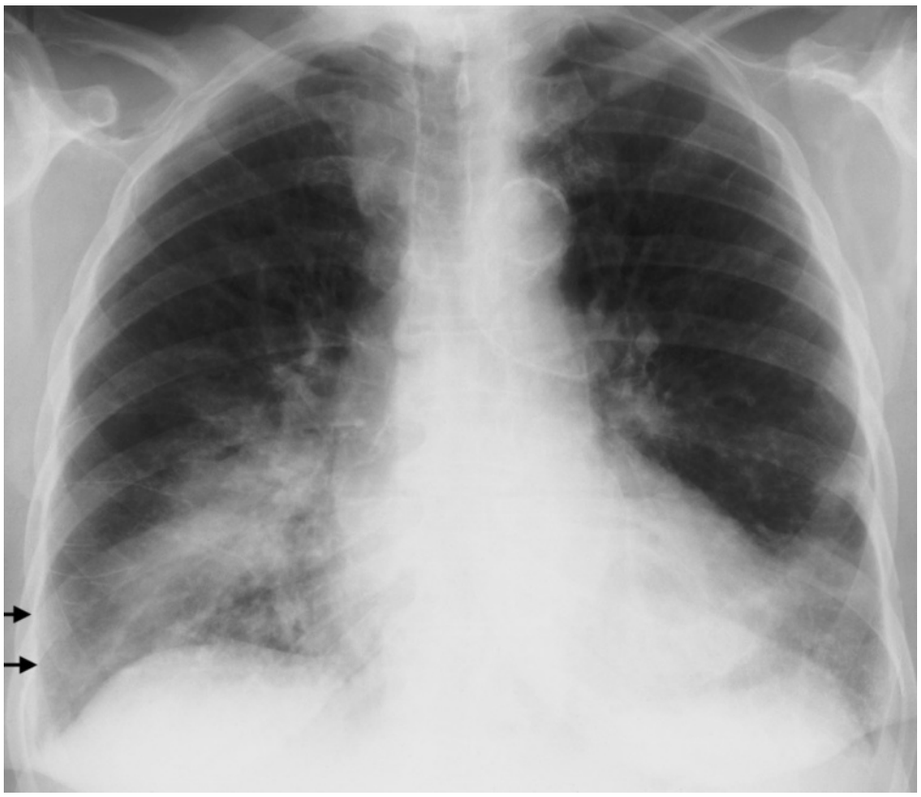

Fig. 3.29 Bronchopneumonia in an 89-year-old woman with known COPD and heart failure. The patient presented with severe dyspnea, fever, and productive cough. Findings include left heart enlargement with significant decompensation, redistribution of perfusion, and Kerley lines (black arrows). Circumscribed densities are seen in both lower lung fields. The patient was diagnosed with hypostatic pneumonia; the causative pathogen was *Enterobacter cloacae*.

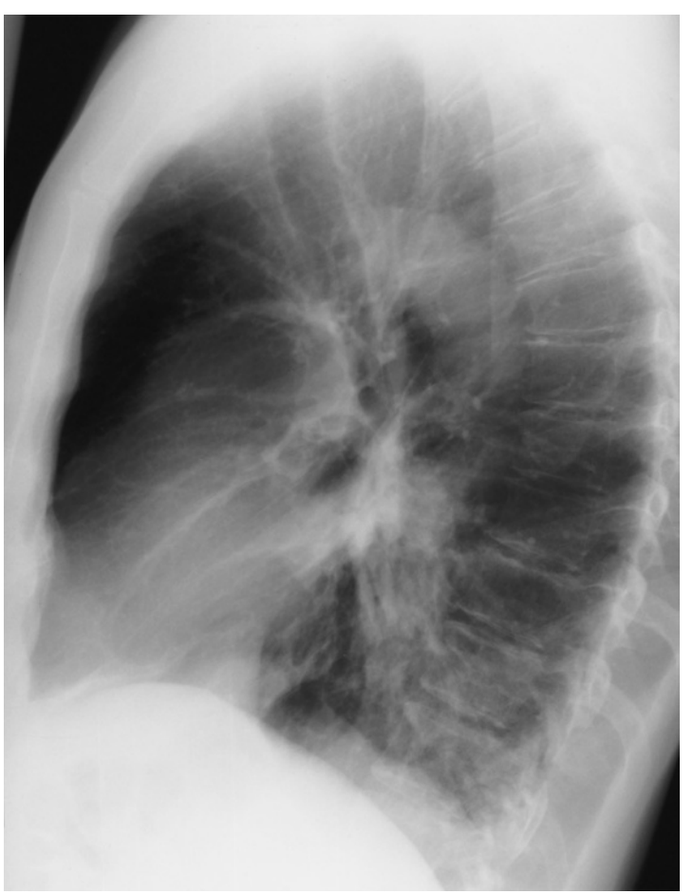

Fig. 3.30 Lower-lobe infiltrate on the lateral radiograph. The patient is a 43-year-old man with confirmed *Haemophilus influenzae* pneumonia. Findings include peribronchial shadowing and nodular-to-patchy opacities in the posterobasal lower lobes. The middle thoracic vertebrae are more distinct than the lower thoracic vertebrae because of the infiltrate.

Pitfalls

The blurring caused by the beginning bronchopneumonic infiltrate (congestion phase) is often difficult to distinguish from the findings listed below. Because of these diagnostic pitfalls, findings of blurring probably lead to more false-positive than true-positive diagnoses of pneumonic congestion.

Pitfall 1: Induration. Indurations often produce a silhouette sign. Classic misdiagnoses of these findings are incipient focal infiltrate in the middle lobe and lingula. The diagnostic key is the lateral film, which shows normal findings. Here the pleuropericardial callus appears as an entirely homogeneous shadow with a smooth transition to the adjacent heart shadow. Its cranial aspect usually exhibits narrow projections (see **Fig. 1.16**).

Pitfall 2: Poor inspiration. It bears repeating that many disorders (cardiomegaly, heart failure, atelectasis, and even infiltrate) can be simulated by expiration posture on the plain chest radiograph. This is particularly apparent, and unfortunately quite common, on radiographs of infants. The symmetry of the bilateral basal "infiltrates" should arouse suspicion (**Fig. 3.33, Fig. 3.34**). Evaluating depth of inspiration by counting the ribs confirms the expiration posture suggested by the gull-wing shape of the diaphragm. When in doubt, obtain a repeat film.

Your own extended hand provides a good model of the mechanism by which poor inspiration can influence lung shadows and simulate an infiltrate or overhydration. Bringing your fingers together creates a consolidated surface with which you can scoop up water (**Fig. 3.31**).

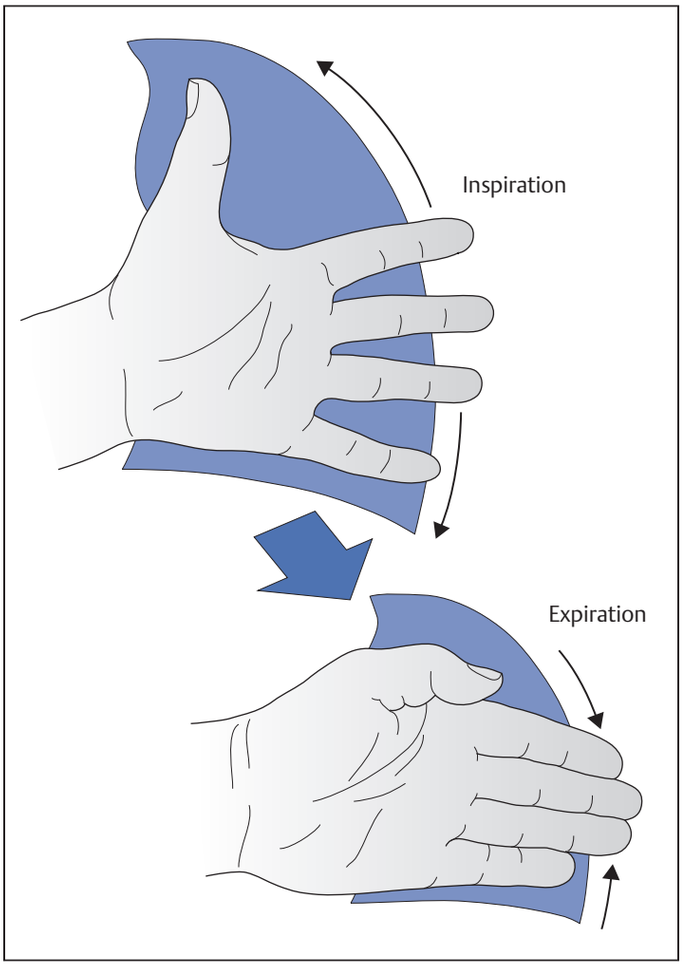

Fig. 3.31 Poor inspiration simulates a density. The closer proximity of vascular structures in poor inspiration can simulate area consolidation. The visual effect of respiration is like spreading the fingers of the extended hand and bringing them together.

Pitfall 3: Breast shadow. Particularly in women with large breasts, beginners typically misinterpret findings and ask whether there is congestion in the basal segments. A unilateral radical mastectomy can reinforce this impression. In addition to the typical appearance of uniformly increasing density within smooth contours as one moves caudally, the instructor can usually convince the skeptical student when part of the costophrenic angle is identifiable projecting caudally beyond the troublesome shadow (**Fig. 3.32**).

Pitfall 4: Decentering. Rotating the supine patient, especially into the right anterior oblique (RAO) position, optically shortens the contralateral hemithorax and creates an area of unilaterally increased attenuation. This can be misinterpreted as pneumonia.

Pitfall 5: Pleural effusion and vascular congestion. The incorrect assumption that a pneumonic infiltrate is present in addition to a pleural effusion or alveolar pulmonary edema is no longer trivial. Indeed, it represents an often insoluble problem of the conventional radiographic imaging technique. Here as in the other cases, CT can rapidly clarify findings. However, the goal and ambition of every diagnostic radiologist should be to minimize the number of such secondary imaging studies.

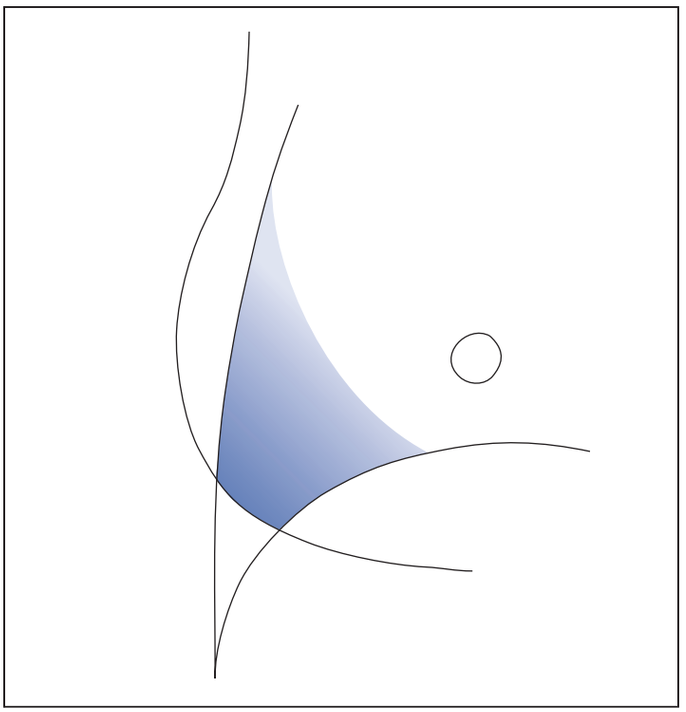

Fig. 3.32 Schematic of the area of increased attenuation created by the breast shadow.

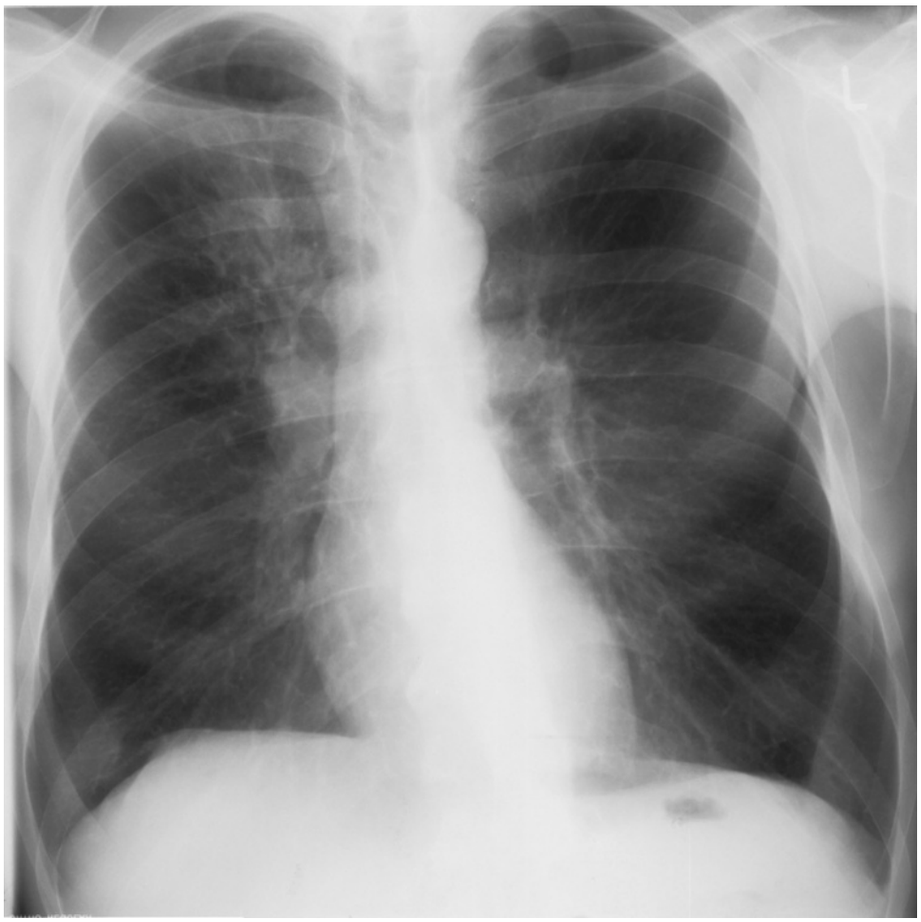

Fig. 3.33 Poor inspiration simulating bilateral infiltrates. The patient is a 59-year-old man with esophageal carcinoma. Findings include signs of smoker's bronchitis with obstructive barrel chest and a mass measuring 3.5 cm in the right upper lobe, partially obscured by the end of the first rib. The heart is of normal size with no signs of decompensation.

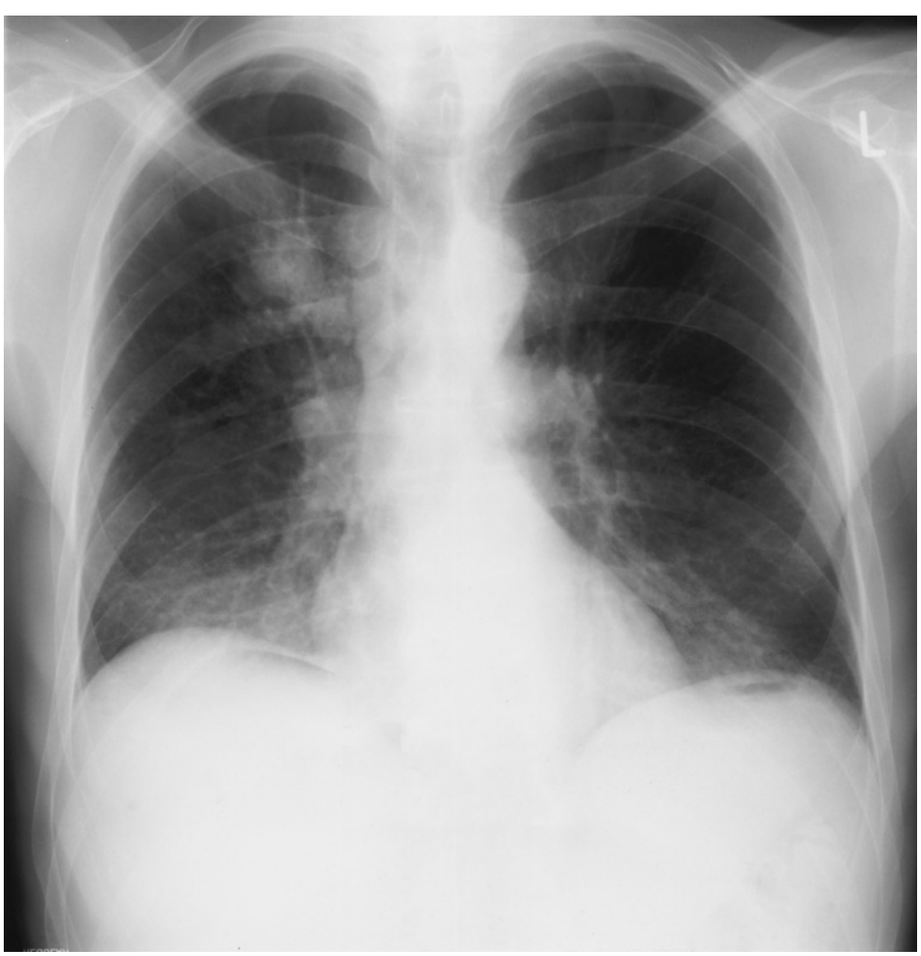

Fig. 3.34 Expiration film obtained after aspiration of the focal lesion in the right upper lobe (diagnosed as bronchial carcinoma) to exclude pneumothorax. There are no signs of pneumothorax but findings include symmetrical densities in both lower lobes. The crura of the diaphragm are well demarcated (no silhouette sign).

Staphylococcal Pneumonia

Recent decades have seen a significant increase in pneumonia caused by staphylococci such as *Staphylococcus aureus*. These mainly secondary pneumonias are often hospital-acquired infections. There are **two basic modes of infection:**

- *Airborne infection,* usually occurring as a superinfection over a primary viral infection. Findings include focal peribronchial infiltrates.
- *Hematogenous infection* in staphylococcal sepsis arising from skin lesions (decubitus ulcers), septic thrombophlebitis, and umbilical infection in newborns. This form of infection also involves other organs. Pulmonary findings include disseminated foci.

Onset of staphylococcal pneumonia is usually insidious, less often acute with severe malaise. The high fever is often due to sepsis. Dyspnea is accompanied by productive cough (purulent or bloody). Chest pain occurs where there is pleural involvement.

Increasing **resistance** to antibiotics has been observed. Infections with methicillin-resistant *Staphylococcus aureus* (MRSA) have a high mortality (30–40% despite specific therapy).

Radiographic signs suggestive of staphylococcal pneumonia (**Fig. 3.35**) include:

- Multiple focal infiltrates
- Liquefaction and occasionally cavitation
- Disseminated bronchiolitis
- Pleural involvement is common
- Pneumatoceles

The disease can produce a rather "colorful" picture (**Fig. 3.36**), particularly in intensive care patients with minimal expectoration.

The most important radiographic symptoms include pulmonary parenchymal findings indicative of the severe tissue destruction caused by the disorder. Focal pneumonia usually leads to necrosis, with liquefaction that CT demonstrates as lesions with central hypodensities (**Fig. 3.36b**). The liquefied lesions within the infiltrated area can often be identified after contrast administration. Where liquefaction has occurred at a site communicating with a bronchus, the cavity will typically be nearly empty due to the severe lytic effect of the disorder. No septa will be visualized (**Fig. 3.37**). The CT correlate of the perifocal pathology (serous alveolar exudate, severe hyperemia) is a broad hypodense halo. Hemorrhages may be observed in a fulminant course. Rapidly progressive pneumatoceles can occasionally occur where tissue destruction has created a valve mechanism (**Fig. 3.38**).

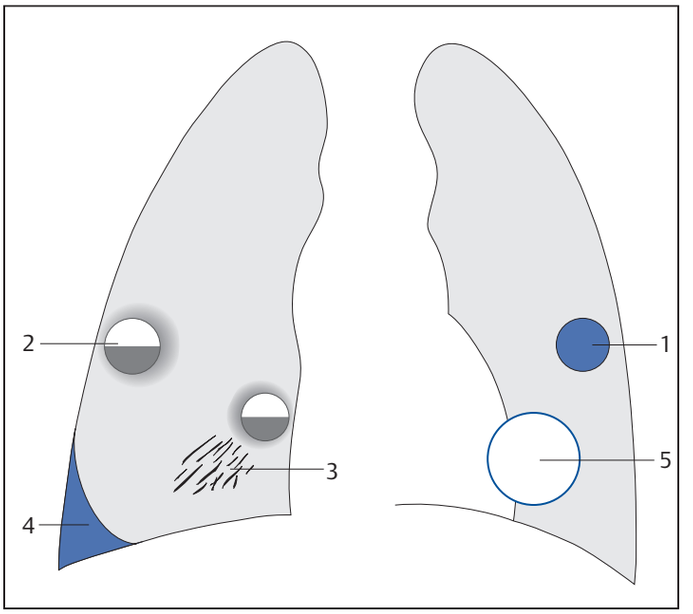

Fig. 3.35 Diagram of radiographic signs in staphylococcal pneumonia. Aside from usually numerous focal infiltrates (1) that often show liquefaction (2), findings include disseminated bronchiolitis (3), and pleural effusions (4). Pneumatoceles (5) are observed as late signs of resolved infection.

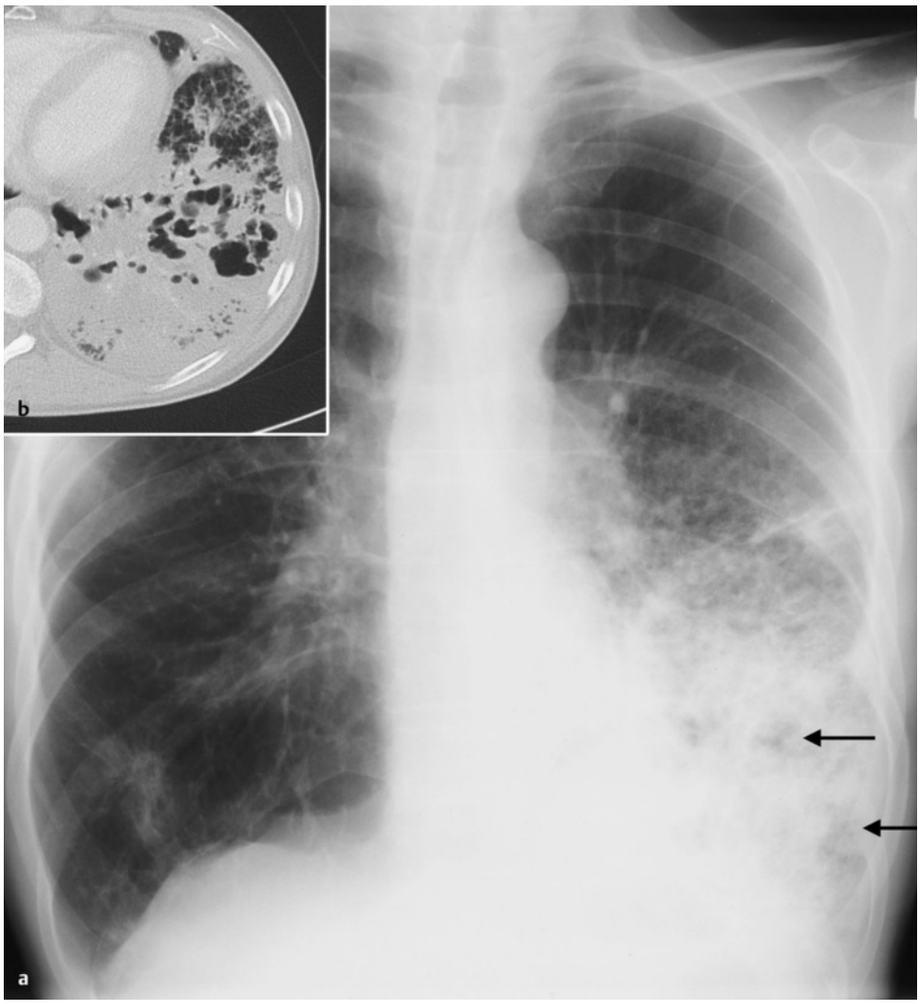

Fig. 3.36 a, b Staphylococcal pneumonia in the left lower lobe (detail).

a Massive infiltrates of the left lower lobe with very inhomogeneous density and isolated radiolucencies (black arrows). There is severe preexisting lung damage from chronic emphysematous bronchitis.

b CT shows numerous air inclusions within a large necrotic area of low radiodensity.

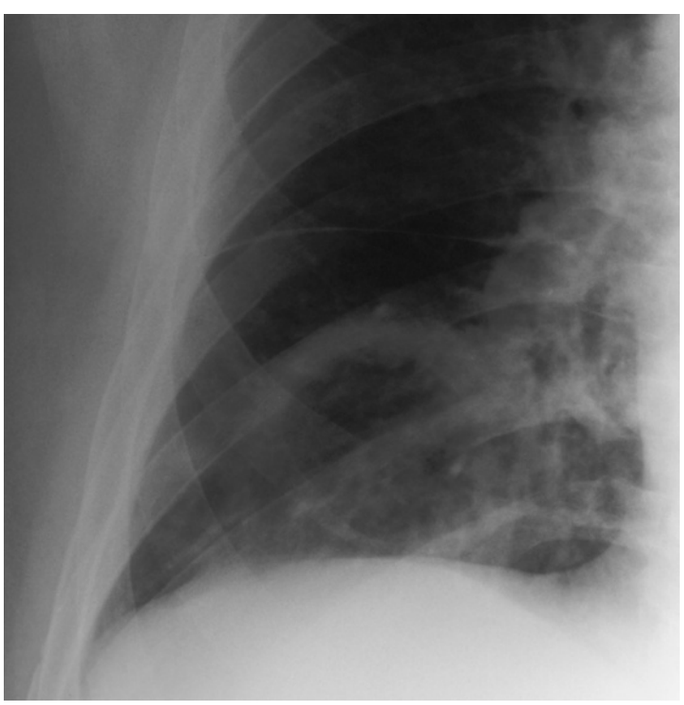

Fig. 3.37 Liquefaction of a focus of MRSA infection. The patient is a 76-year-old man with staphylococcal sepsis. A thick-walled liquefying focus 5 cm in diameter is seen in the right lower lung field.

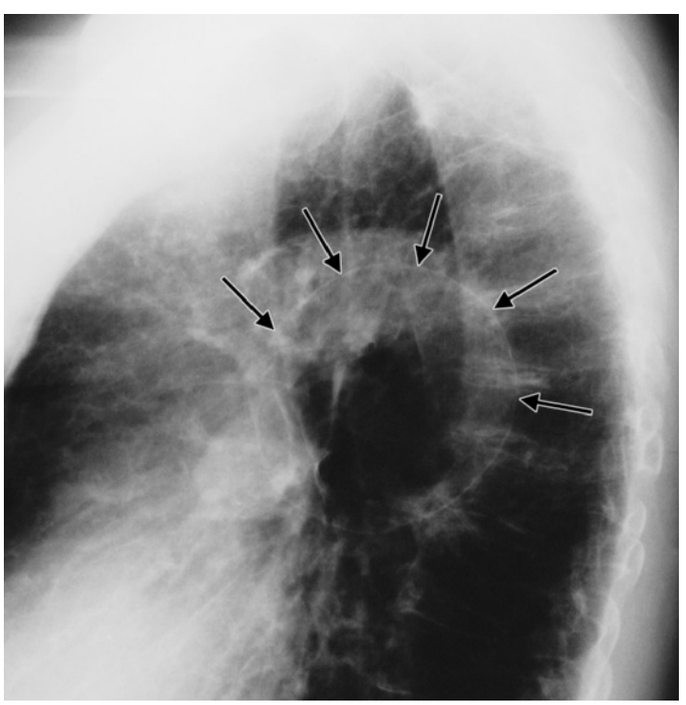

Fig. 3.38 Pneumatocele following resolution of staphylococcal pneumonia. The patient is an 86-year-old woman with COPD. Findings include a ring structure 7 cm in diameter projected on the middle mediastinum (black arrows).

Interstitial Pneumonia: Viral Pneumonia

Viral pneumonias are classified as interstitial pneumonias. These include disorders of the pulmonary parenchyma in which exudation occurs primarily in the interstitium. Many other noxious agents also cause interstitial pneumonias; such agents include radiation and toxins such as gases or drugs.

Notes on Terminology

The terminology of pneumonias caused by viruses is confusing. There are historical reasons for this. Before the existence of viruses was known, atypical lung infections characterized by negative bacterial cultures and unusual radiographic shadowing were observed during the great influenza epidemics. The term "atypical pneumonia" refers to forms of the disorder other than the common bacterial pneumonias.

The viral pneumonias caused by measles and varicella viruses are diagnosed on the basis of the typical clinical picture of the underlying disorder (typical viral exanthema in measles or chickenpox). Viral pneumonias begin with moderate pulmonary symptoms such as dry cough and slight dyspnea. There is a striking discrepancy between the minimal auscultatory findings and the significant changes on the radiograph. In varicella pneumonia the patient develops a high fever about one week after the skin rash occurs. This is accompanied by a painful dry cough, dyspnea, and chest pain. Severe symptoms with high fever and dyspnea suggest bacterial superinfection.

Radiographic signs of viral pneumonia (**Fig. 3.39**) include:

- Streaky or reticular densities that extend into the periphery
- Finely nodular picture
- Ground-glass opacities
- Dense, widened hilar structures
- Small dense focal lesions (late sequela)

The most common and consistent radiographic signs on the plain chest radiograph in interstitial pneumonia are a dense, widened hilar shadow and perihilar streaky densities extending into the periphery which can be seen to blend into a finely nodular pattern (**Fig. 3.40**). Aside from ground-glass opacities, one often sees the reticular patterns that prompted the name "interstitial pneumonia."

CT clearly demonstrates a mixed picture of inflammation of the interstitium and infiltration of the alveolar space. In addition to septal thickening, diffuse shadowing is seen with blurring of the margins between the veins and septa and patchy centrilobular densities consistent with minor alveolar hemorrhages (**Fig. 3.41**). In contrast to the plain chest radiograph, the lack of postural movement and the asymmetry of the densities are clearly demonstrated. This information is important for a differential diagnosis and excludes the various forms of alveolar edema.

Residues

More often one encounters findings indicative of previous viral pneumonia on other occasions, such as on a preoperative chest radiograph. Findings in such cases occasionally include a finely nodular pattern of myriad hyperdensities such as occur in pneumoconiosis (**Fig. 3.42**).

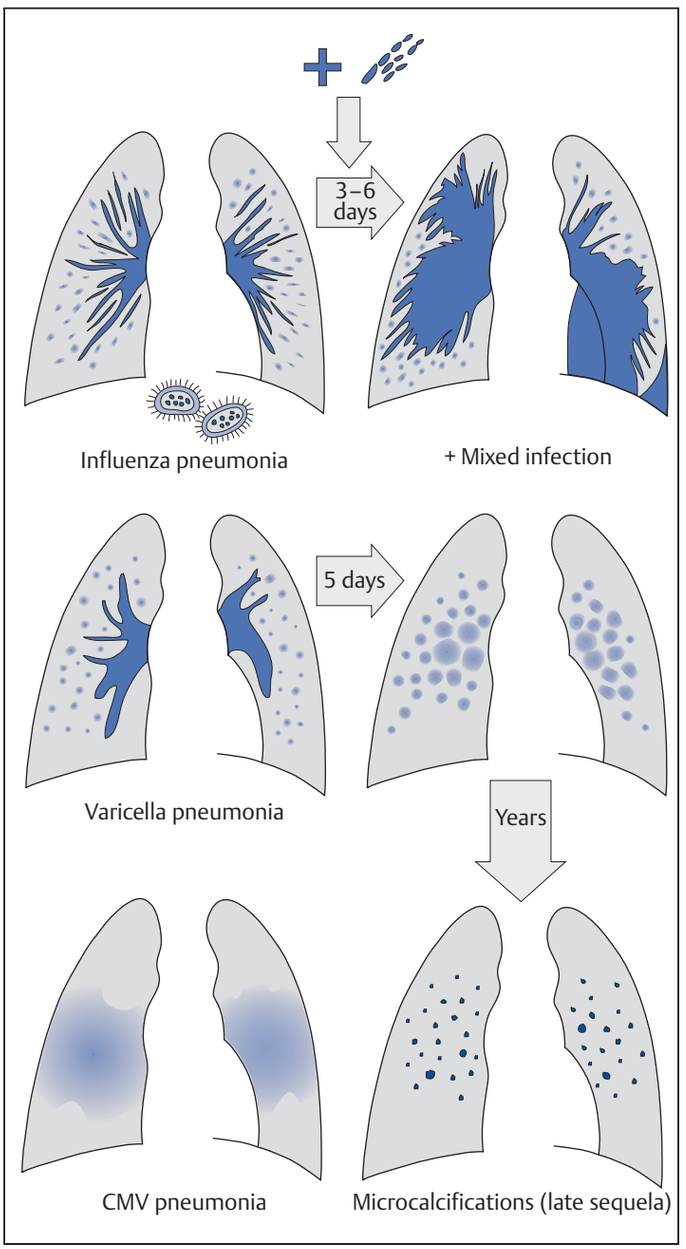

Fig. 3.39 **Schematic diagram of radiographic signs in viral pneumonia.**

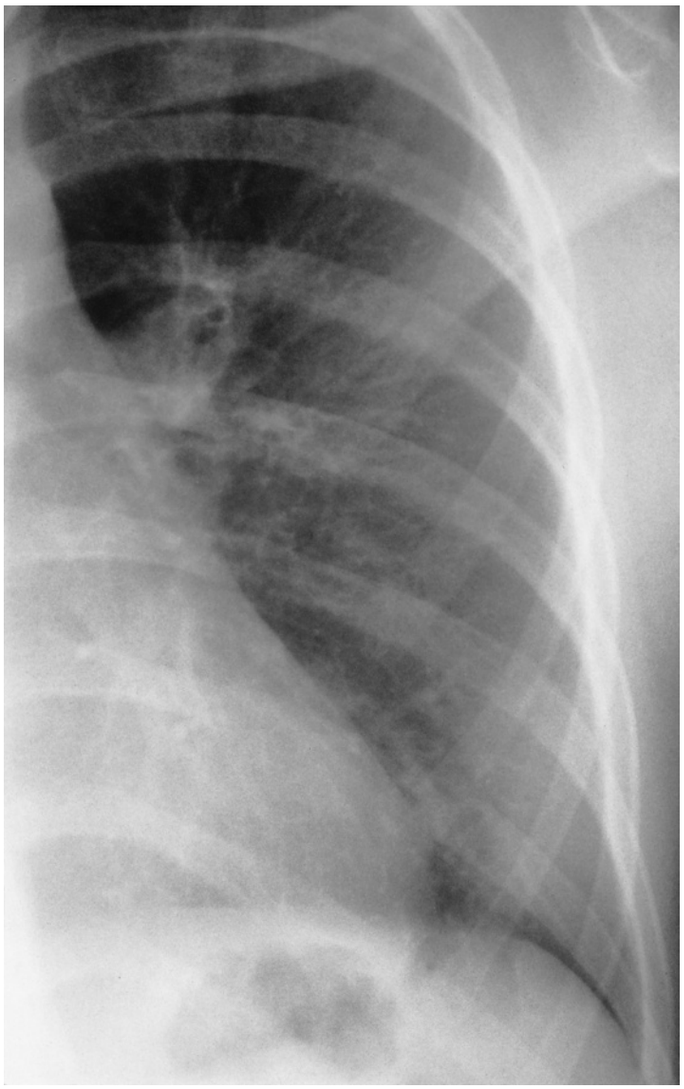

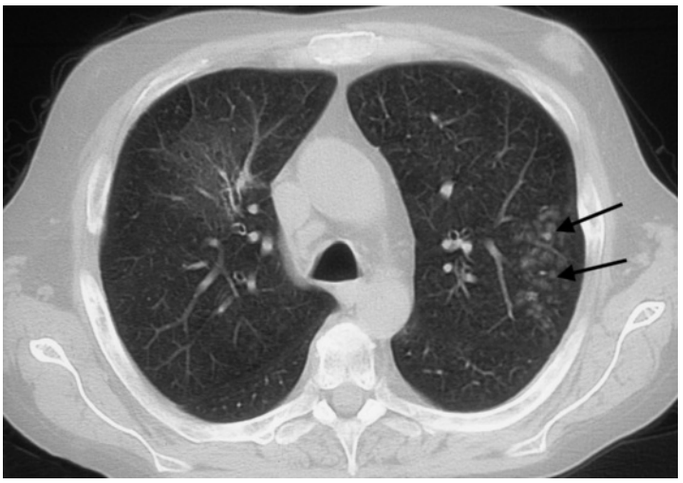

Fig. 3.41 **CT in viral pneumonia.** Ground-glass opacities indicative of the spread of inflammatory processes to the alveolar space and finely nodular focal lesions consistent with minor hemorrhagic exudates (black arrows).

◀ **Fig. 3.40** **Interstitial pneumonia in varicella infection.** The patient is a 10-year-old girl with chickenpox. For the last few days she has had a worsening dry cough; now she has dyspnea on exercise. Findings include streaky shadowing, blurred vascular structures, and peribronchial densities.

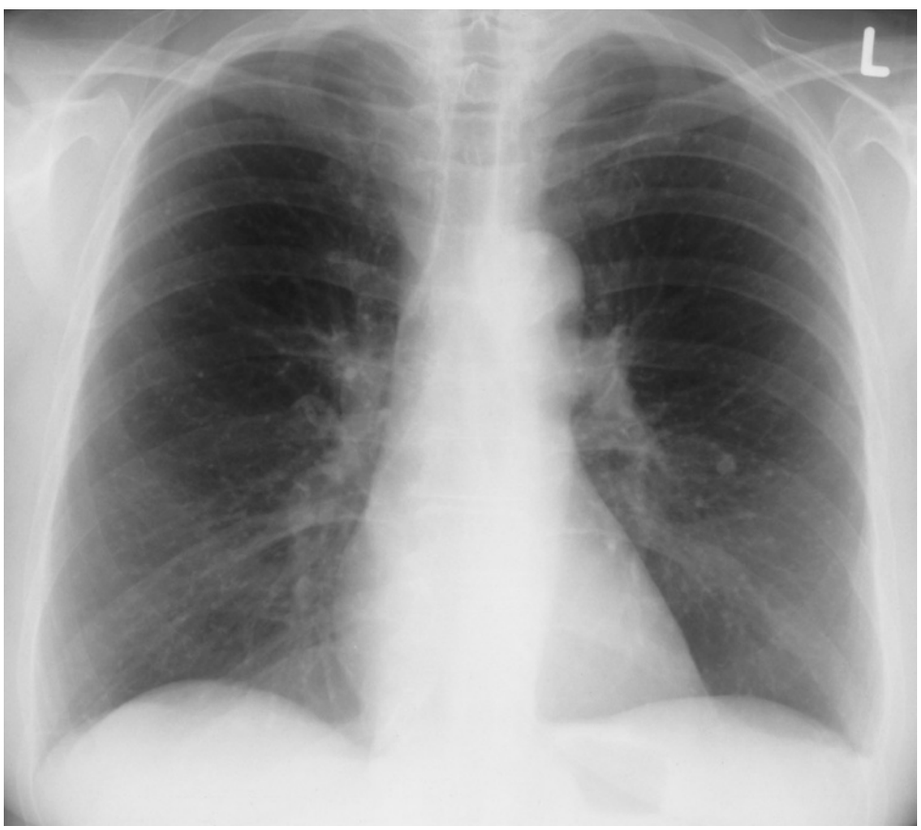

Fig. 3.42 **Status post viral pneumonia.** Diffuse distribution of calcification densities in a 63-year-old woman. Numerous small focal lesions, some of which measure 6–7 mm in diameter and correspond to q shadows in the ILO classification of the pneumoconioses (see Chapter 5, "Pneumoconiosis"). Status post varicella pneumonia at age 30.

Opportunistic Lung Infections

Pneumocystis carinii Pneumonia

Pneumocystis carinii pneumonia begins with an unproductive cough and early onset dyspnea on exercise. Symptoms develop insidiously and include general malaise, decreased exercise tolerance, and weight loss. Patients usually present in poor general health with preexisting dyspnea at rest. They appear pale and occasionally show cyanosis. This is marked contrast to their usually normal auscultatory findings. Analysis shows restricted pulmonary function.

In the initial phase of the HIV pandemic, patients' health generally deteriorated rapidly and respiratory insufficiency developed (**Fig. 3.43**). Mortality was approximately 90%. As knowledge of the clinical picture increased, early radiologic diagnosis became established, and treatment options such as high-dosage co-trimoxazole became available, mortality decreased. Today, these measures have successfully reduced mortality in the initial occurrence of *Pneumocystis carinii* pneumonia in HIV patients to less than 10%. Clinical symptoms normally resolve under therapy within 3 weeks.

Signs of *Pneumocystis carinii* pneumonia on the plain chest radiograph include:

- Reduced depth of inspiration
- Primarily basal reticulonodular shadowing
- Sparing of the periphery
- Alveolar ground-glass opacities
- Progression to a "white lung"

The only abnormal finding on the plain chest radiograph in the initial phase of the disorder is reduced depth of inspiration compared with films obtained prior to infection. As the patients at this time are already severely ill, there is a significant discrepancy between the clinical symptoms and conventional radiographic findings. In the further course of the disorder, interstitial shadowing is observed in the form of a reticulonodular densities more pronounced in the basal segments and sparing the periphery (**Fig. 3.43 c**). The vascular structures become increasing less distinct until findings degenerate into what is known as a "white lung" (**Fig. 3.44**). In this phase of the disorder, radiographs must usually be obtained with the patient supine. Pleural effusions are rarely observed. When therapy is initiated promptly, the changes will resolve completely. However, radiographic findings resolve only after a significant interval so that significant shadows may still be detectable even in a clinically asymptomatic patient.

Notes on Pathology

Since the beginning of the HIV pandemic, a special case of atypical interstitial plasma cell pneumonia first described by Feyrter in 1927 has become particularly important. In 1960 Goetz identified the protozoan *Pneumocystis carinii* as the causative pathogen. *Pneumocystis carinii* pneumonia often appears as the first manifestation of the full clinical picture of AIDS. Histologic findings in *Pneumocystis carinii* pneumonia include a foamy alveolar exudate. The alveoli are filled with masses of pathogens and inflammatory exudate. In contrast to this, interstitial involvement is relatively slight. Paradoxically, the picture this creates on conventional radiographs is usually referred to as an "interstitial pattern." Grocott and Giemsa stains are used to demonstrate the pathogen. The Grocott methenamine silver stain reveals typical staplelike structures.

The chronic course of *Pneumocystis carinii* pneumonia is now increasingly observed. It is characterized by more pronounced interstitial involvement with septal thickening.

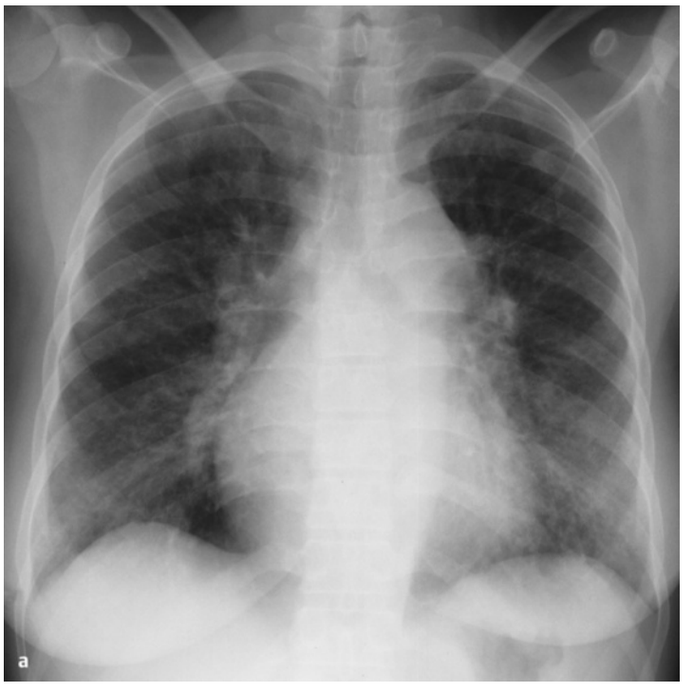

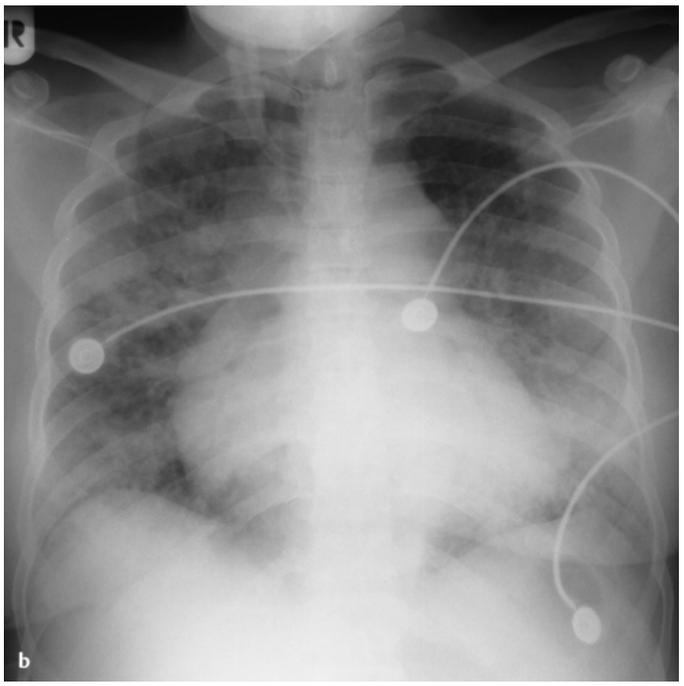

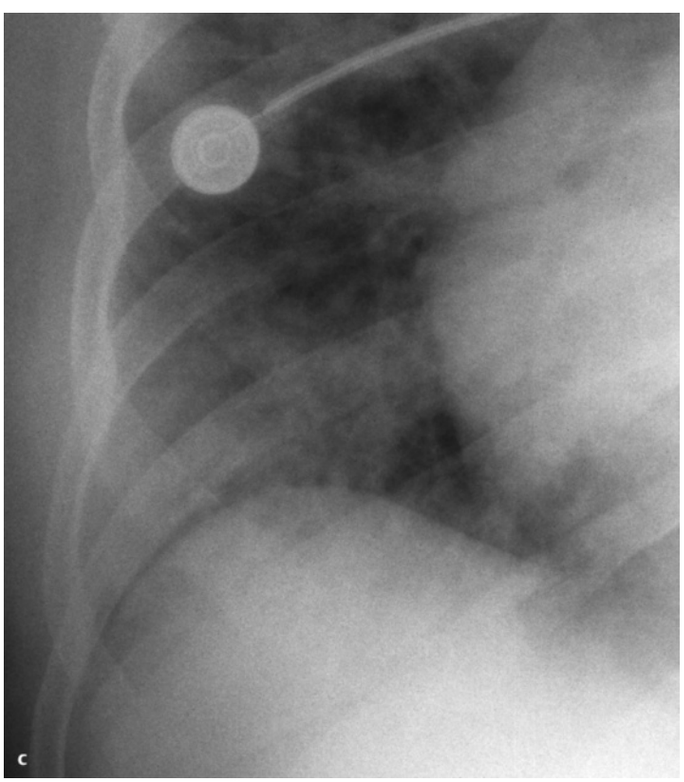

Fig. 3.43 a–c ***Pneumocystis carinii*** **pneumonia in AIDS.** The patient is a 38-year-old African woman presenting with massive dyspnea.

a Diffuse reticulonodular shadowing is seen with blurring of vascular structures. Marked thickening of the hila suggests a mediastinal lymphoma. Right atrial enlargement.

b Follow-up examination of **a.** Findings have continued to worsen; the patient now requires oxygen. Massively increasing areas of increased attenuation; depth of inspiration is markedly decreased.

c Ground-glass and finely nodular pattern sparing the periphery. The detail image of the right lower lung field shows sparing of the periphery with significant blurring of vascular structures and finely nodular opacities.

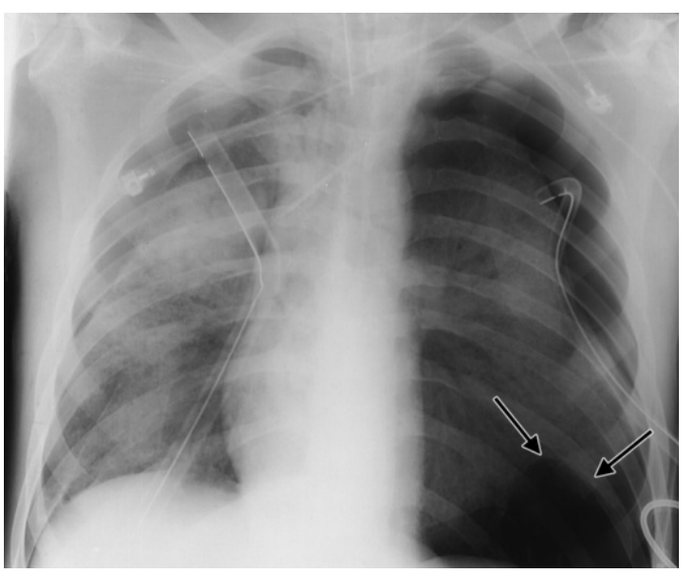

Fig. 3.44 **Terminal stage of** ***Pneumocystis carinii*** **pneumonia with tension pneumothorax.** The patient is a 23-year-old HIV-positive man with a repeat episode of *Pneumocystis carinii* pneumonia. Status post intubation and bilateral placement of pleural drains in pneumothorax from assisted ventilation. "White lung" with persistent left pneumothorax and a massive pulmonary fistula. The image partially includes an inflated bulla in the left basal region (black arrows). The patient died a few hours later.

Computed Tomography

As CT can demonstrate ground-glass opacities indicative of foamy alveolar exudate, it has high sensitivity for detecting *Pneumocystis carinii* pneumonia in its early stages. A tentative diagnosis can usually be made where findings on the plain chest radiograph are still negative.

In contrast to the primarily interstitial shadowing seen on the plain chest radiograph, alveolar findings predominate on CT. Here the cardinal symptom is ground-glass opacification with density values between − 400 and − 700 HU. The distribution pattern corresponds to findings on the plain chest radiograph, showing primarily basal and central ground-glass infiltrates. Classic CT findings include complete sparing of individual segments or subsegments (**Fig. 3.45**) and radiolucencies along the bronchovascular bundle (**Fig. 3.46**). These perivascular streaks of normal pulmonary density disappear only in the terminal stage of severe cases.

The ground-glass opacities of *Pneumocystis carinii* pneumonia are highly characteristic of immunosuppression and HIV-positive patients in particular. In differential diagnosis, it can be difficult to exclude extrinsic allergic alveolitis. Clinical findings are crucial in such cases.

Atypical Patterns of CT Findings in *Pneumocystis carinii* Pneumonia

Extensive therapeutic efforts in the last few years have increasingly altered what has come to be known as the classic CT appearance of *Pneumocystis carinii* pneumonia. This is primarily attributable to prophylaxis with inhaled pentamidine. The main radiographic symptoms still include ground-glass shadowing, although with an altered pattern of distribution. The disorder now primarily affects the upper lung fields (**Fig. 3.47**), as these are the areas least accessible to inhalational prophylaxis. The ground-glass opacities are accompanied by area consolidations with density values in the positive Hounsfield range. As these denser infiltrates tend to produce areas of liquefaction, a differential diagnosis must consider pulmonary tuberculosis. Some cases develop multiple bullae with distortion of pulmonary architecture (**Fig. 3.48**). Where these changes are progressive, they often lead to pneumothorax, especially in assisted ventilation. Understandably, complete recovery cannot be expected in such cases.

Chronic courses with only slight clinical symptoms have been observed with inhalational prophylaxis. Radiographic findings in these cases are atypical. There are only slight ground-glass infiltrates; interstitial changes predominate with septal thickening and strands of scar tissue.

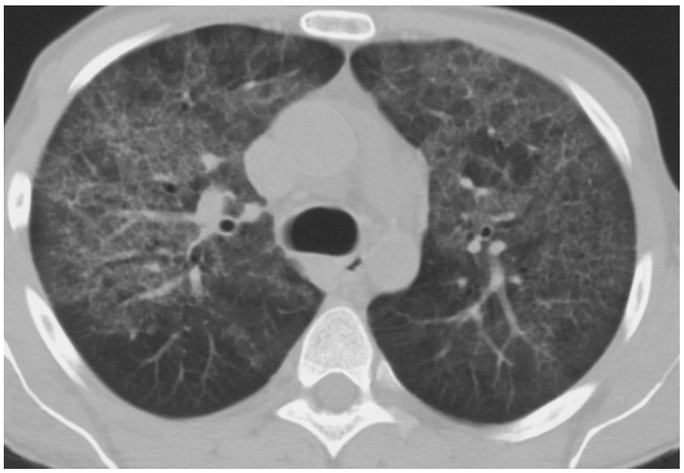

Fig. 3.45 ***Pneumocystis carinii*** **pneumonia with sparing of individual subsegments.** Findings show a predilection for the central region of the lung while certain subsegments and individual lobules remain unaffected.

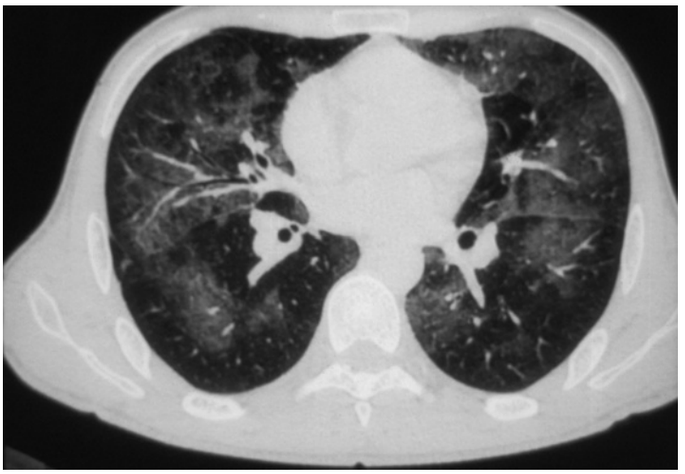

Fig. 3.46 **Classic picture of** ***Pneumocystis carinii*** **pneumonia.** CT clearly demonstrates the position of the ground-glass opacities in the central lung, sparing the periphery. There is also some sparing of the peribronchovascular region.

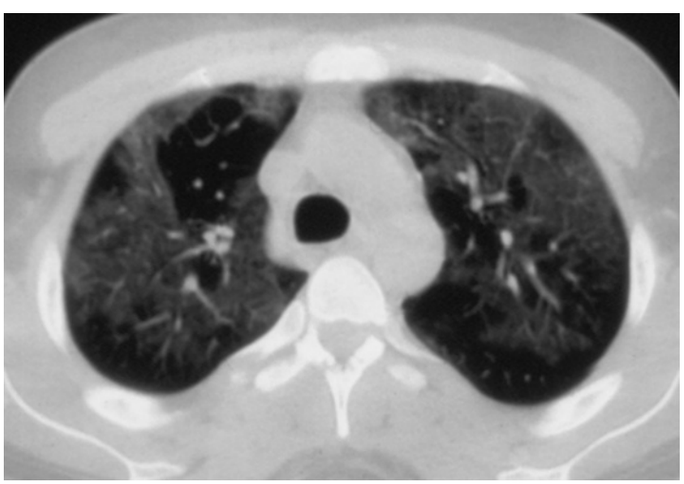

Fig. 3.47 **Involvement is primarily limited to the upper lungs fields with inhalational prophylaxis.** This patient receiving inhaled pentamidine shows extensive bilateral ground-glass opacities in the upper lung fields.

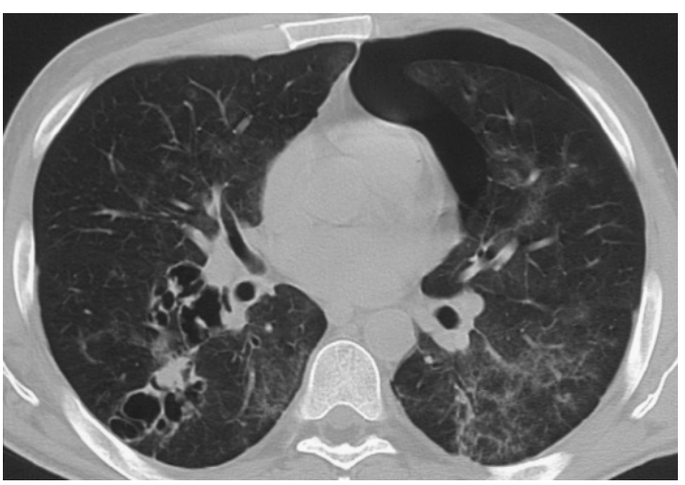

Fig. 3.48 **Atypical course of** ***Pneumocystis carinii*** **pneumonia.** The image shows multiple bullae, bronchiectasis, and traction bronchiectasis. Other findings include strands of fibrosis and distraction of the pulmonary architecture. Pneumothorax is seen on the left.

Pulmonary Aspergillosis

Fungal pneumonia represents a particularly severe pulmonary infection acquired via the respiratory tract. The inflammatory reaction caused by *Aspergillus*, the most common of these pathogens, can take one of three forms:

- Allergic aspergillosis
- Invasive pulmonary aspergillosis
- Primary and secondary aspergilloma

Notes on Epidemiology and Pathology

Aspergillus fungi are ubiquitous saprophytes found on dying tissue of plant, animal, and human origin. Their spores are spread by airborne transmission. Increased incidence of *Aspergillus* infections is observed during demolition and renovation work in hospitals (such as asbestos removal). The sun and high humidity of the summer months are conducive to growth.

Allergic bronchopulmonary aspergillosis is characterized by the picture of severe allergic bronchitis. Invasive pulmonary aspergillosis typically involves local thrombosis once the fungi have penetrated into the peribronchial connective tissue and the bronchial artery. The resulting infarction of pulmonary tissue with perifocal hemorrhaging is clearly visible on the macroscopic lung image. Shrinkage processes within the infarcted area can lead to air inclusions of variable size including cavitations (primary aspergilloma). Hematogenous dissemination can result from invasion of the pulmonary veins.

In aspergilloma or mycetoma, fungi colonize either preexisting cavities in pulmonary tissue (cavitation from previous disease or emphysematous bullae [secondary aspergilloma]) or an infarct cavity left by invasive pulmonary aspergillosis (primary aspergilloma). Histologic examination reveals a fungus ball composed of hyphae, spores, blood products, and cell detritus.

Invasive Pulmonary Aspergillosis

The cardinal symptom of invasive pulmonary aspergillosis is an antibiotic-resistant fever in an immunosuppressed patient. Because normal contamination often leads to false-positive sputum cultures, bronchial lavage, transbronchial biopsy, and diagnostic imaging become particularly important.

Conventional **radiographs** show uncharacteristic findings in the early stage of the disease. Findings include focal lesions with broad pleural contact as in infarction (**Fig. 3.49, Fig. 3.50**). Central radiolucencies consistent with liquefaction are occasionally observed within the shadows.

In contrast, **CT findings** are relatively characteristic and allow early specific diagnosis:

- Broad pleural contact
- Open bronchus
- Ground-glass halo
- Air inclusions

Measuring up to 3 cm in diameter and located in close proximity to the pleura, the infiltrates typically show an open bronchus (**Fig. 3.51**). They usually occur in several locations, although rarely more than 10 lesions are present at any one time. The focal lesions are usually surrounded by a ground-glass halo indicative of perifocal bleeding. The focal lesions tend to retract and create air inclusions (**Fig. 3.52**), forming a "bell sign," which is commonly presumed to be typical of a secondary aspergilloma. Larger septated cavities can also develop.

Refer to "Notes on Epidemiology and Pathology," and to **Fig. 3.53** and **Fig. 3.54** for information on pathophysiology.

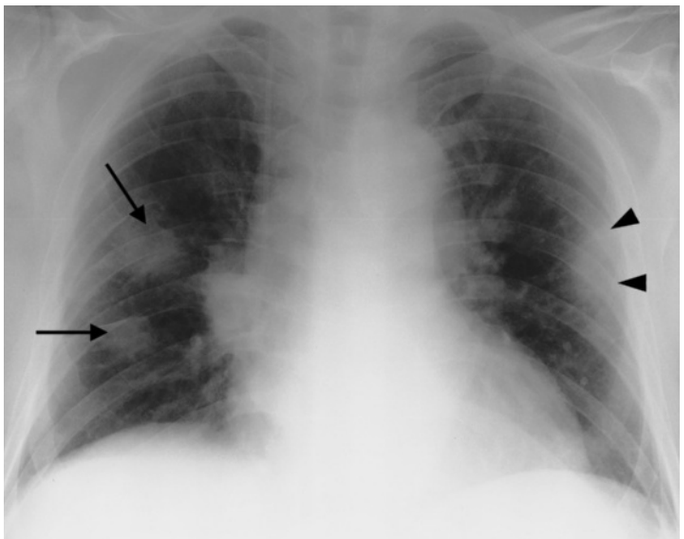

Fig. 3.49 Wedge-shaped infiltrate in invasive aspergillosis. The patient is a 57-year-old man with Wegener granulomatosis receiving immunosuppression therapy. He has an antibiotic-resistant fever. The radiograph shows focal infiltrates (black arrows) with broad pleural contact in the left upper lung field (black arrowheads).

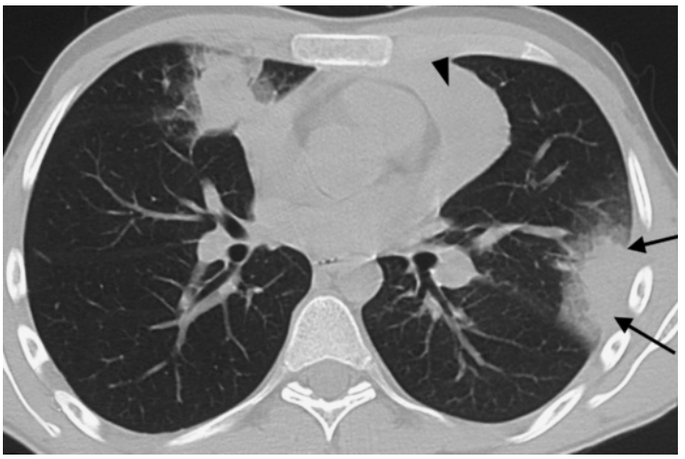

Fig. 3.50 Broad pleural contact and perifocal hemorrhage in aspergillosis. The patient is a 20-year-old man with AIDS, presenting with persistent fever and loss of strength. Opacities surrounded by ground-glass halo are seen in the middle lobes and lingula, here with broad pleural contact (black arrows). Note the severe pericardial effusion (black arrowhead).

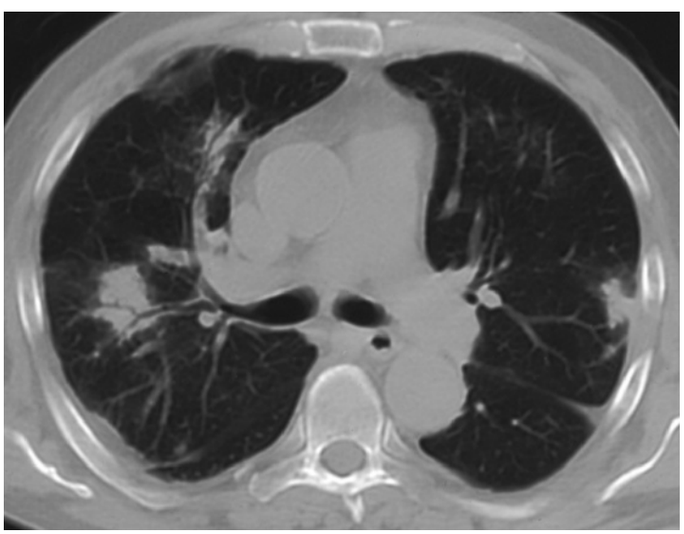

Fig. 3.51 Open bronchus in an *Aspergillus* lesion. Subsegmental bronchi coursing through the center of a lesion 3 cm in diameter located in the posterior segment of the right upper lobe (same patient as in **Fig. 3.49**).

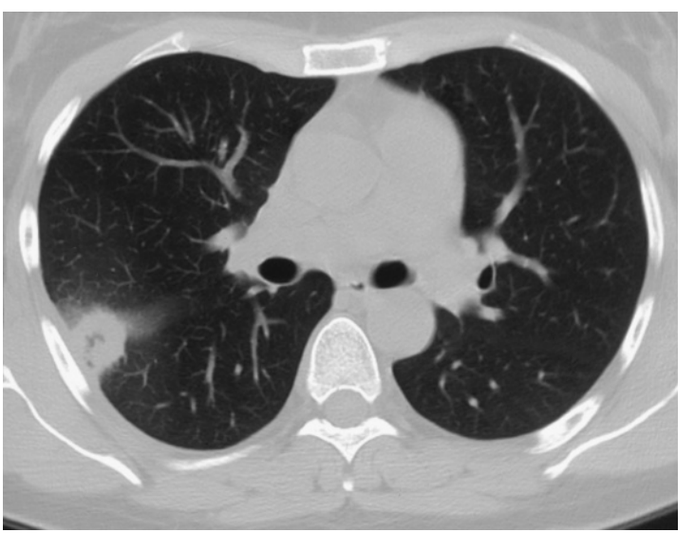

Fig. 3.52 Air inclusions in an *Aspergillus* lesion. The patient is a 42-year-old man with acute myeloid leukemia; nadir of induction therapy with antibiotic-resistant fever. In the posterior segment of the right upper lobe there is a lesion 3 cm in diameter showing a halo and central air inclusions.

Aspergilloma

Clinical terminology identifies two types of aspergilloma. To a lesser extent, this distinction also applies to radiologic findings, namely where imaging studies demonstrate the course of the disorder. These are (**Fig. 3.53**):

- Primary aspergilloma (terminal stage of invasive pulmonary aspergillosis)
- Secondary aspergilloma (colonization of a preexisting cavity by *Aspergillus*)

The characteristic **radiographic sign** of aspergilloma, detectable on a conventional radiograph, is a round shadow (fungus ball) within a radiolucency (preexisting cavity) with an air crescent above it (**Fig. 3.55**). This air crescent occasionally has the appearance of a bell on a fool's cap (**Fig. 3.54**). As the fungus ball is not adherent to the wall of the cavity, it shows postural movement.

On **CT** the immediate vicinity of the aspergilloma occasionally provides indirect signs of whether it is a primary or secondary lesion. Significant scarring around a preexisting tapered cavity suggests that a fungus ball found there represents secondary colonization (**Fig. 3.56**).

Occasionally a follow-up study of invasive pulmonary aspergillosis can directly visualize the development of a primary aspergilloma (**Fig. 3.57**).

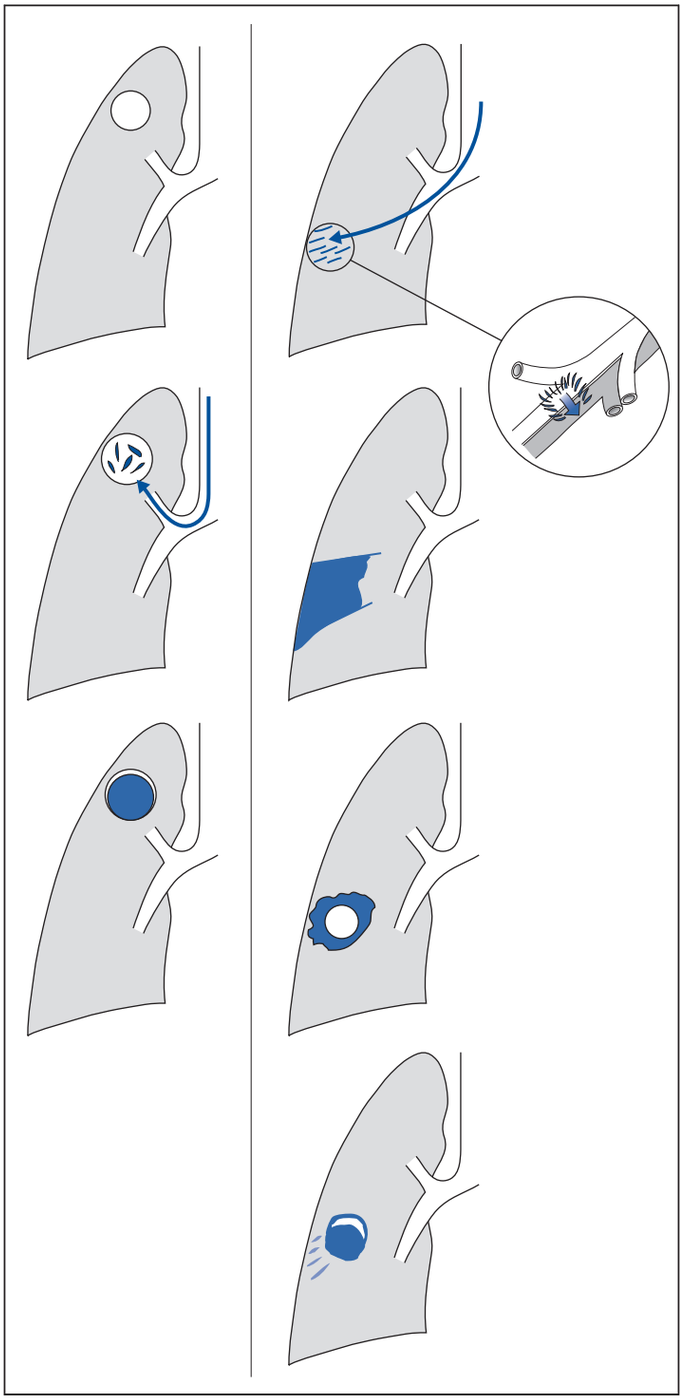

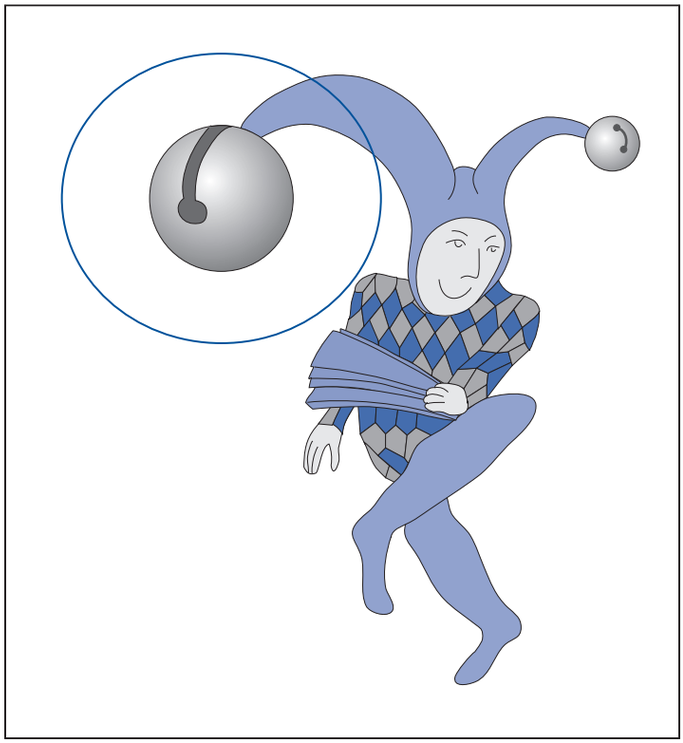

Fig. 3.54 **"Fool's cap bell" as a sign of aspergilloma.**

◀ **Fig. 3.53** **Pathophysiologic differentiation of primary and secondary aspergilloma.** In a primary aspergilloma (right diagrams), invasion of the pulmonary artery by hyphae leads to local infarction and cavitation. Here, hyphae later grow to the fungus ball. In a secondary aspergilloma (left diagrams), a preexisting cavity is colonized by hyphae.

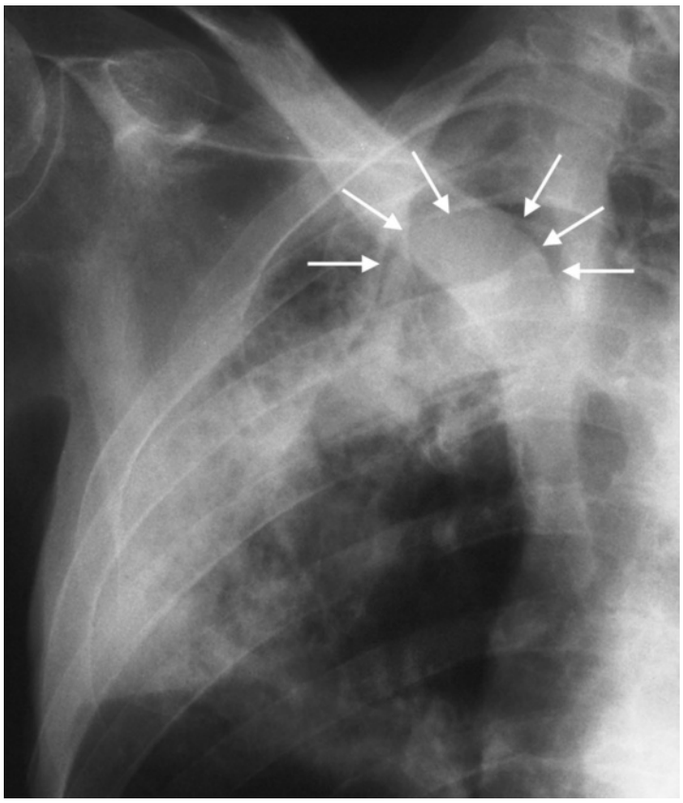

Fig. 3.55 "Fool's cap bell" in aspergilloma (detail). The patient is a 79-year-old man with severe COPD and emphysema, now presenting with dyspnea, fever, and productive cough. In addition to extensive bronchopneumonia of the right upper lobe, the radiograph also demonstrates a mass 4 cm in diameter with an apical air crescent (white arrows).

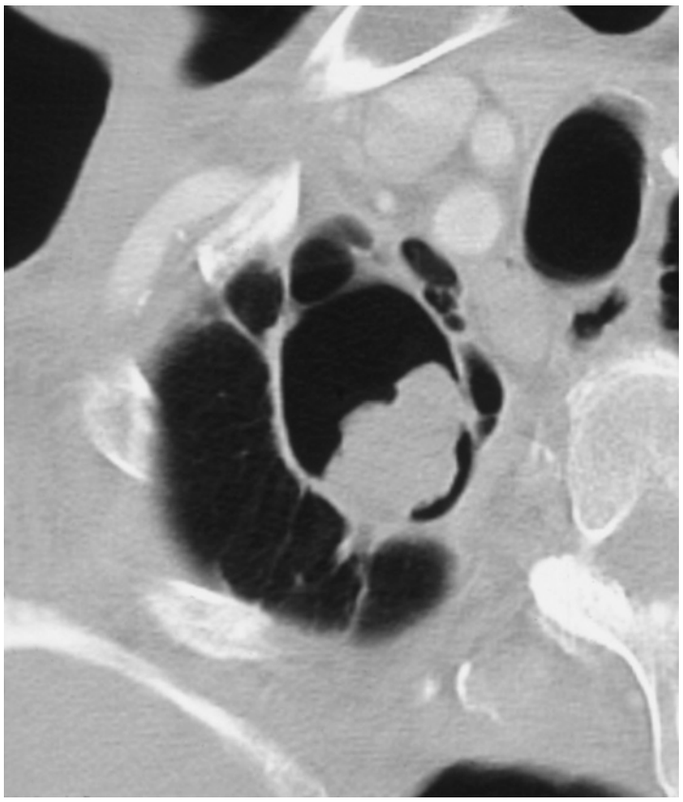

Fig. 3.56 Secondary aspergilloma (fungus ball in a preexisting cavity). The patient is a 76-year-old man with a history of many years of COPD. Status post pulmonary tuberculosis in the postwar years. Preoperative chest image in the presence of rectal carcinoma. A solid lobulated mass measuring 3 cm in diameter and largely surrounded by air is seen within a thin-walled cavity in the severely scarred right upper lobe.

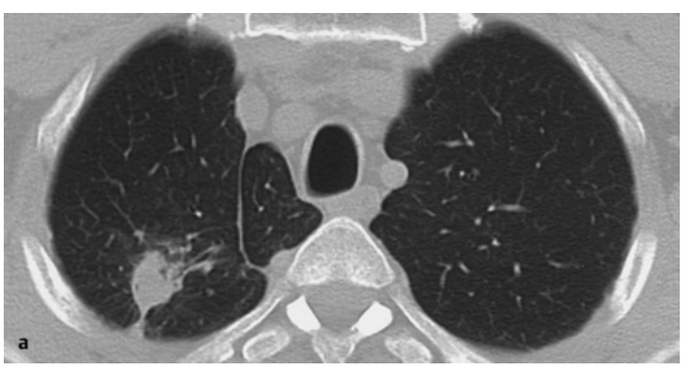

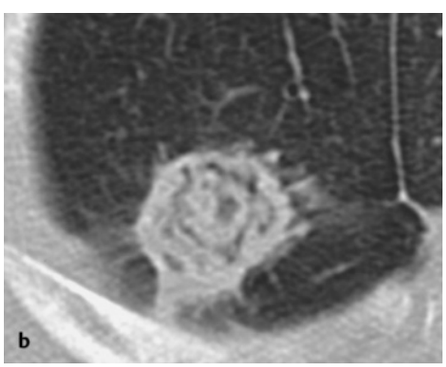

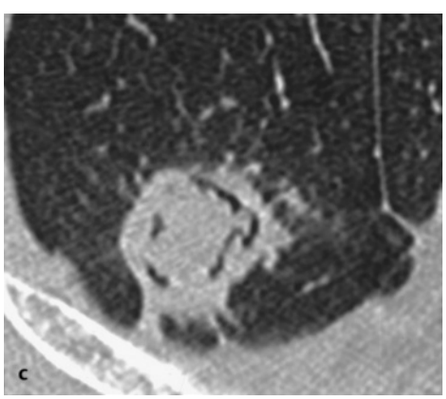

Fig. 3.57 a–c Development of a primary aspergilloma from invasive pulmonary aspergillosis. Initially there are minimal marginal air inclusions (**a**) within a lesion in the posterior segment of the upper lobe. Later the lesion is interspersed with crescentic air inclusions (**b**). In the final stages, there is significant marginal air accumulation as the central masses retract from the surrounding tissue (**c**).

Tuberculosis

After the dramatic drop in the incidence of new infections in the second half of the last century, a development not explainable solely by the use of modern antibiotics, pulmonary tuberculosis has recently acquired new significance. This is due to several factors. Major causes include adverse social trends in the course of globalization, with increased poverty among larger segments of the population, increasing alcoholism, and migration from endemic areas. Consequently, familiarity with radiologic findings in reactivated disease, often masked by the very comorbidities that promote them, has again become very important. Most importantly, do not forget to consider the possibility of tuberculosis (**Fig. 3.58**).

Because of the great importance of tuberculosis to medicine in the last century, extensive research results are available. Journals for phthisiology once filled entire departmental libraries and occasionally still do. The highly complex staging classification with all its names and mystique is now largely dispensable and makes it very difficult to work with radiologic problems.

The only practical classification of the various stages of the disease (**Fig. 3.60**) is as follows:

- Primary tuberculosis (initial infection)
- Progressive primary tuberculosis
- Postprimary tuberculosis (reactivation)
- Scarring stages

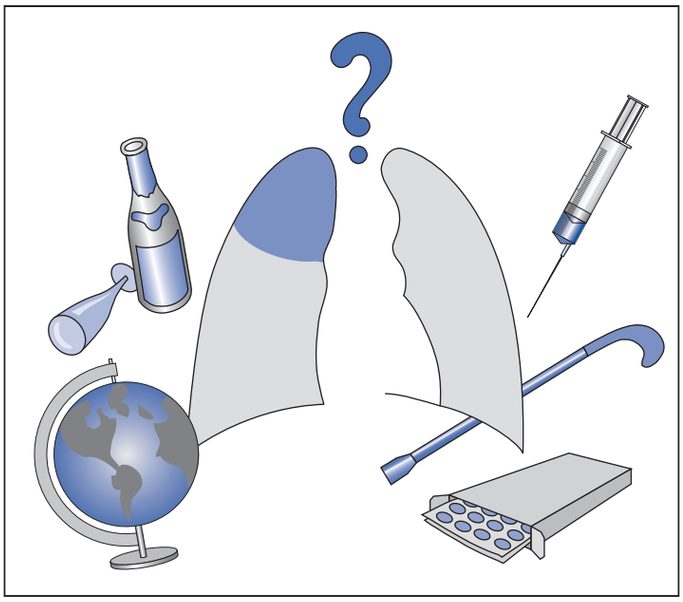

Fig. 3.58 **"It can also be tuberculosis."**

Notes on Epidemiology and Pathology

Known in the Middle Ages as "white plague" and still responsible for a high percentage of deaths among adolescents in modern times, tuberculosis is caused by the aerobic acid-resistant rod *Mycobacterium tuberculosis*, discovered by **Robert Koch.** In response to airborne infection, alveolar macrophages consume the mycobacteria, disintegrate, and form necrosis around which other macrophages and lymphocytes gather (exudative reaction). An immunocompetent host will successfully isolate the focus of infection behind a barrier of epithelioid cells (productive reaction; **Fig. 3.59**). In an immunocompromised host, CD8 lymphocytes destroy infected macrophages, leading to necrosis. Where the necrosis breaches the bronchial system (cavitation), the improved supply of oxygen triggers massive bacterial proliferation. This in turn leads to spread of infection via endobronchial dissemination.

Where the infection breaches the vascular system, the result is hematogenous dissemination in the form of miliary tuberculosis.

The mycobacteria in necrotic areas can be reactivated years later. The reactivated tuberculosis in the immunocompromised host (postprimary tuberculosis) is characterized by an accelerated reaction due to the residual immunity. Severity is variable, with more rapid formation of necrosis ("caseous pneumonia") and often several cavities. Typically there is no lymph node involvement.

Robert Koch (* 1843 Clausthal, † 1910 Baden-Baden, Germany): Physician and microbiologist; identified the anthrax pathogen in 1876; discovered the tuberculosis pathogen in 1882 and the cholera pathogen in 1884. Received the Nobel prize for medicine 1905.

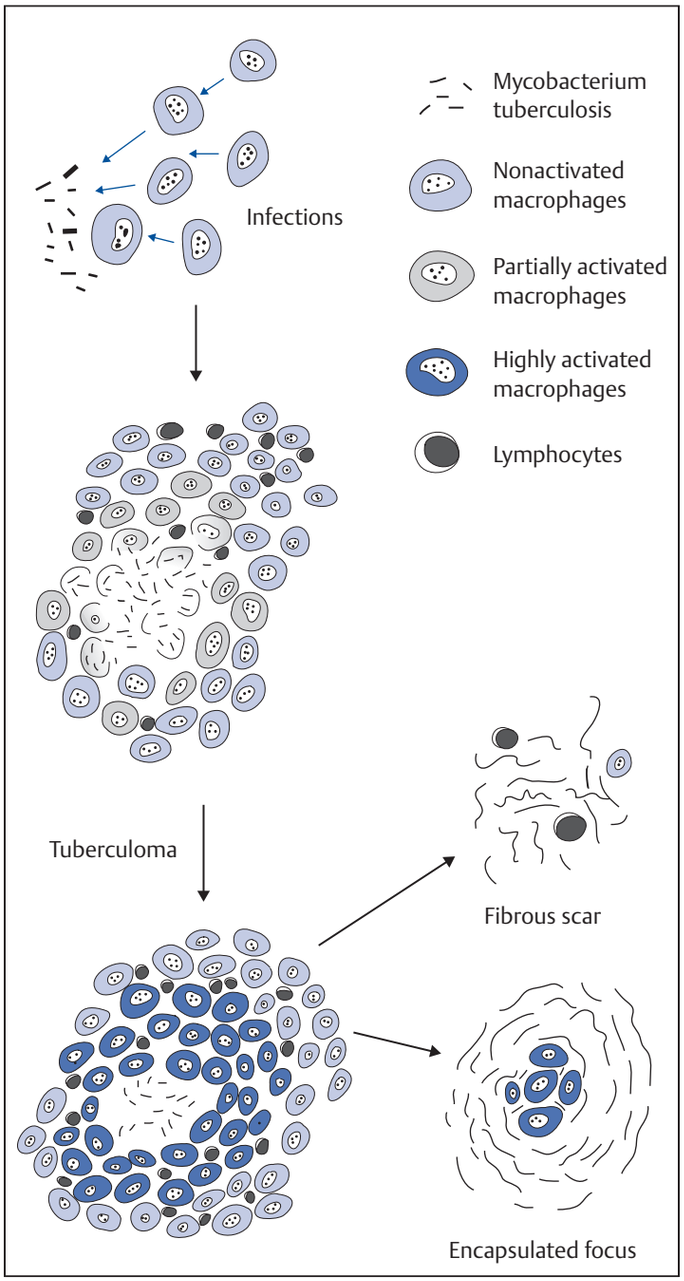

Fig. 3.59 Development of the epithelioid cell granuloma. After infection, disintegrated macrophages form a necrotic focus around which activated macrophages and lymphocytes gather. A thick wall of highly activated immune cells forms. This can heal to form a fibrous scar. On the other hand, the encapsulated focus bears the risk of reactivation because of the constant presence of infectious substrate.

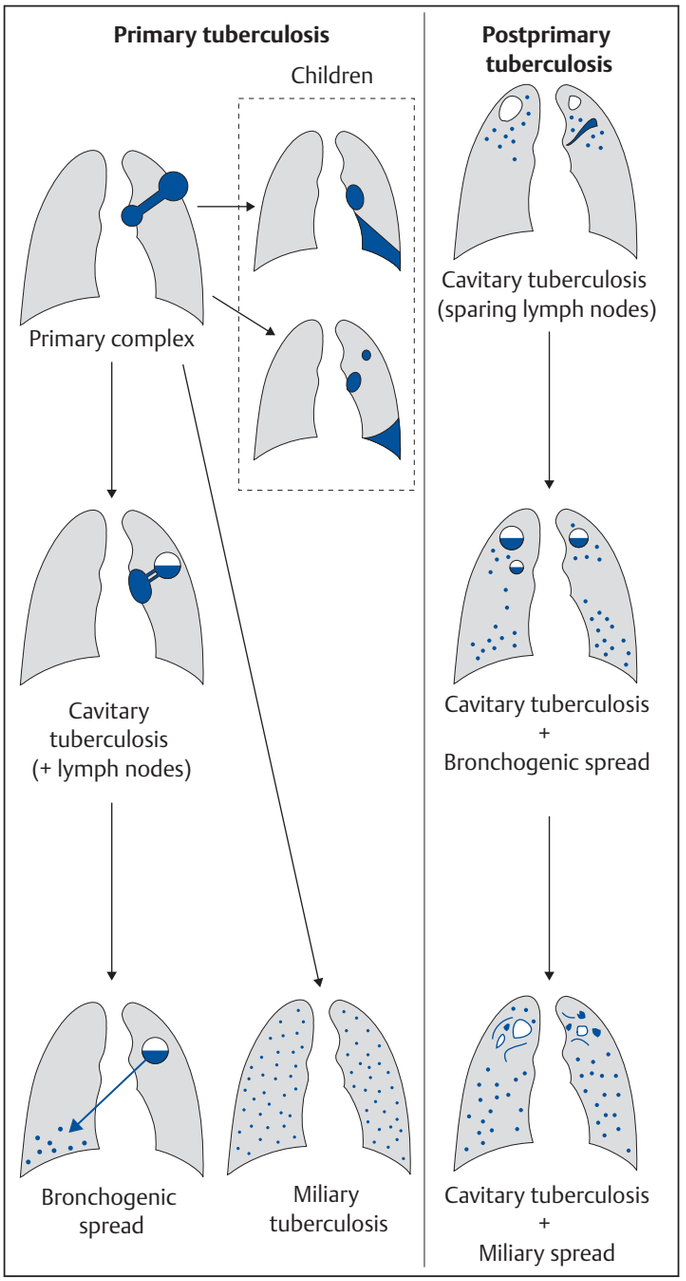

Fig. 3.60 Schematic diagram of simplified staging of pulmonary tuberculosis. In primary tuberculosis, the collapse of immune mechanisms leads to development of cavities with endobronchial spread, lymph node involvement with miliary spread, and often, in children, to atelectasis or pleural involvement. Postprimary tuberculosis arising from reactivation or renewed infection shows a mixed picture of various stages with noticeably slight lymph node involvement.

Primary Tuberculosis

Radiographic signs of primary tuberculosis (which in most cases will be clinically occult) include:

- Peripheral focus of consolidation
- Primarily in the upper and middle lung fields
- Increased shadowing toward the hilum
- Thickened ipsilateral hilum
- Associated effusion (rare)

Additional findings in children include:

- Hypoventilation caused by swollen lymph nodes (epituberculosis)
- Pleural reaction (common)

The peripheral focus of consolidation (Ghon complex) in primary tuberculosis is the product of an exudative reaction of macrophages and lymphocytes to the local proliferation of mycobacteria on the alveolar surface. An airborne pathogen, *Mycobacterium tuberculosis* tends to prefer the upper segments. This is because these parts of the lung are hyperventilated relative to their perfusion. The increased shadowing extending from the Ghon complex toward the center is caused by local lymphangitis, which can be traced as far as the local and regional lymph nodes. Evidence of involvement of a central lymph node is a definite sign that the pathology observed represents primary tuberculosis as opposed to the postprimary type.

The barbell-shaped combination of:

- Ghon complex
- Lymphangitis
- Central lymph nodes

is also referred to as a **primary complex** or Ranke complex (**Fig. 3.62**). The peripheral focus and central lymph nodes typically heal with calcifications (**Fig. 3.63**).

Further progression of the primary complex in an immunocompromised host can lead to cavitation communicating with the bronchus in the vicinity of the Ghon complex. Typically only one cavity is observed in progressive primary tuberculosis. Cavitation leads to bronchogenic spread (**Fig. 3.64**). Being a special case of infectious bronchiolitis, bronchogenic spread shows a relatively typical "tree-in-bud" sign (**Fig. 3.65**) and follows typical routes (**Fig. 3.61**). Hematogenous dissemination (miliary tuberculosis) arises where the infection breaches the vascular system, as can occur when the barrier of the central lymph node is compromised.

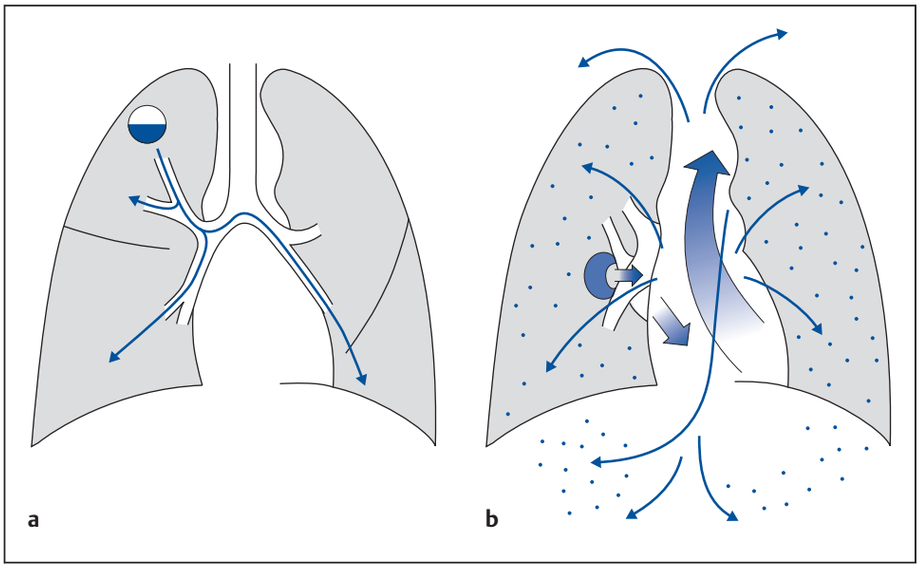

Fig. 3.61 a, b Schematic diagram of the spread of infection in pulmonary tuberculosis. Endobronchial dissemination (**a**): In addition to the classic endobronchial spread of infection from a cavity to the lower lung fields (often diagonally to the opposite lung), one more often encounters spread to the posterobasal segments of the upper lobes. Miliary dissemination (**b**): diffuse hematogenous spread of the pathogen results when an infected lymph node erodes into adjacent blood vessels.

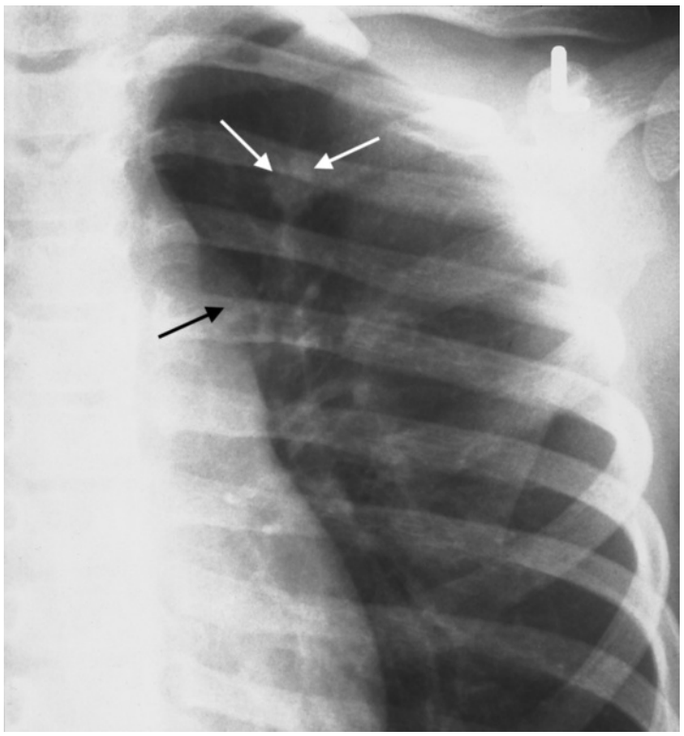

Fig. 3.62 Primary complex in the left upper lobe. The patient is a 6-year-old girl of African descent (screening examination because father has known pulmonary tuberculosis). A peripheral focus of consolidation (anterior end of the 2nd rib [white arrows]) is seen in combination with lymphangitic markings and thickened lymph nodes (black arrow) on the left side in the aortopulmonary window.

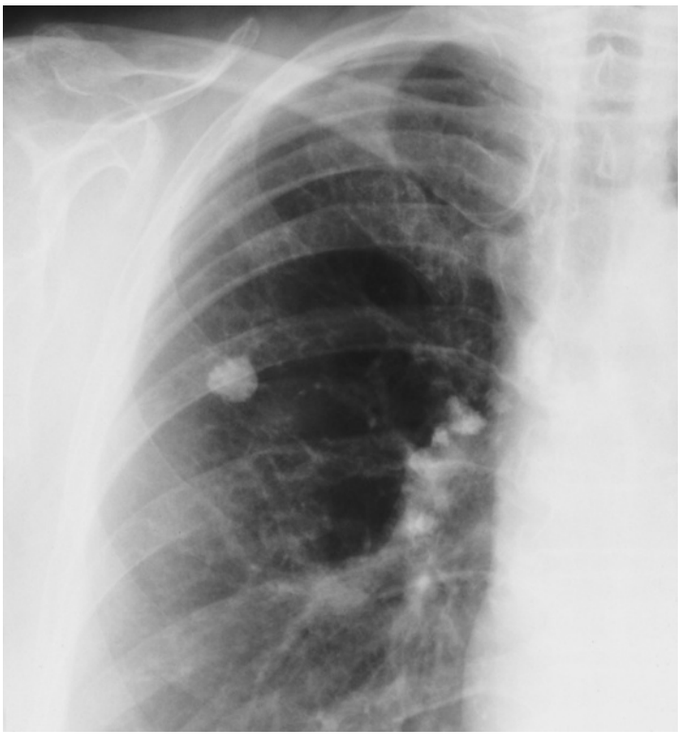

Fig. 3.63 Calcified Ghon complex. This is a routine preoperative chest radiograph of a 71-year-old woman with a history of chronic bronchitis and a known "shadow in the lung." Findings include a massively calcified focus 12 mm in diameter projected on the anterior 3rd right rib. Several calcified lymph nodes are present in the right anterior region.

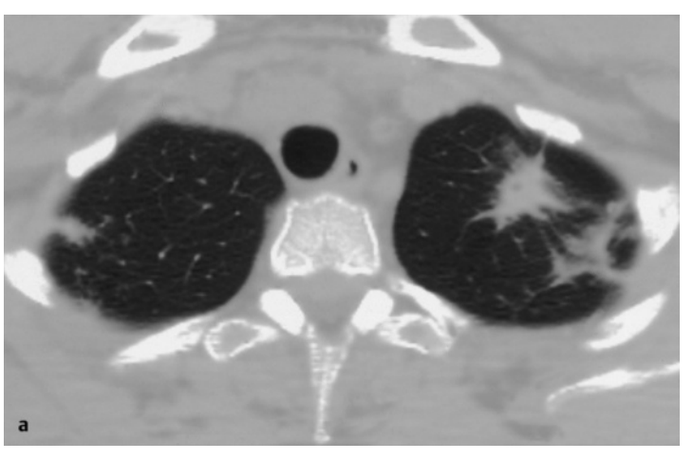

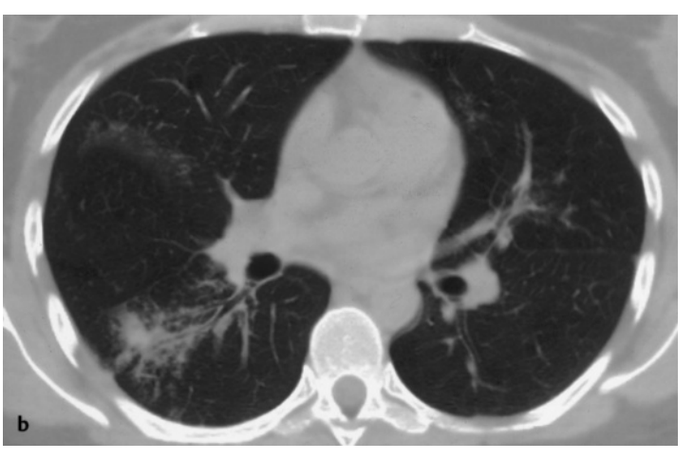

Fig. 3.64 a, b Primary tuberculosis with bronchogenic spread. The patient is a 31-year-old woman with newly diagnosed upper-lobe infiltrates (screening examination).

a Small areas of liquefaction are already visible in the left upper lobe.

b Simultaneous findings in the right lower lobe. These include bronchial wall thickening and incipient infiltrates. Mucus-filled small airways are faintly visible.

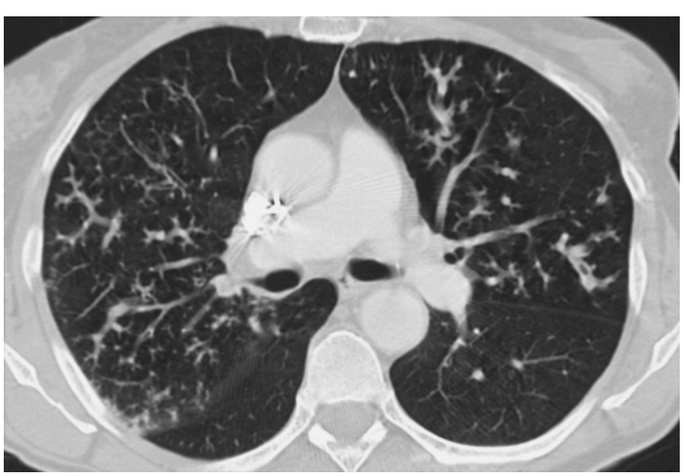

Fig. 3.65 "Tree-in-bud" sign in bronchogenic spread. The patient is a 65-year-old woman with massive bronchogenic spread of reactivated pulmonary tuberculosis. Centrilobular nodules in the right middle lung field, some with bizarre configurations, and individual nodules forming a "tree-in-bud" sign.

Miliary Tuberculosis

The diffuse finely nodular shadowing of miliary tuberculosis is a sign of the underlying hematogenous dissemination. Most affected patients have relatively slight clinical symptoms (in an analysis by Doerr, 50% of cases confirmed by autopsy had not been suspected clinically). However, the entity can quickly prove fatal in an immunocompromised host, especially in advanced age (Landouzy septicemia).

Radiographic signs of miliary tuberculosis on the plain chest radiograph include multiple, diffusely distributed, relatively sharply demarcated, uniform nodules measuring approximately 1–2 mm in diameter. Characteristic findings include myriad individual, absolutely uniform nodules that show no predilection for any particular area of the lungs (**Fig. 3.67**). Another striking feature is the lack of any interstitial septal pattern.

CT clearly demonstrates this markedly diffuse and apparently random distribution (**Fig. 3.66**) as well as the lack of any septal structures (**Fig. 3.68**).

A **differential diagnosis** need only consider severe hematogenous metastatic spread or sarcoidosis (**Table 3.1**).

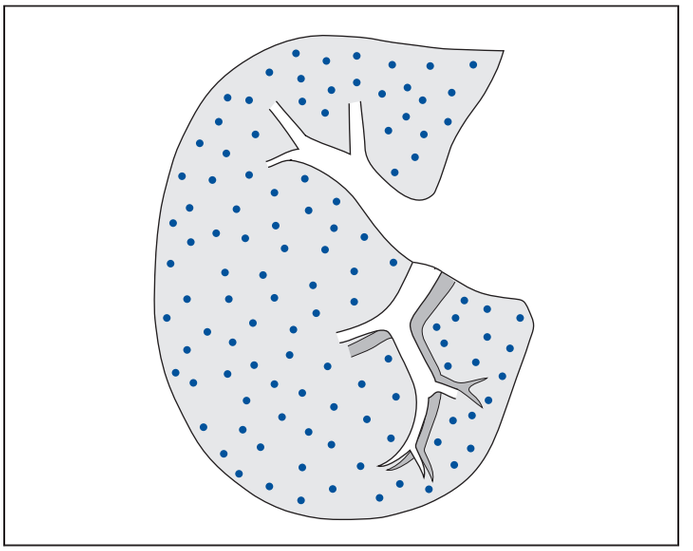

Fig. 3.66 Schematic diagram of the random nature of nodular shadowing. Lesions show a uniform distribution in all lung segments with no postural movement or predilection for specific compartments such as the bronchovascular bundle.

Table 3.1 Differential diagnosis of the distribution pattern of micronodules.

Random	Perilymphatic	Centrilobular
Miliary Tuberculosis	Sarcoidosis	Infectious bronchiolitis
Sarcoidosis	Lymphangitis	Pulmonary edema
		BOOP
Metastases	Silicosis	EAA
	Amyloidosis	Vasculitis
		Silicosis
		Alveolar carcinoma

BOOP, bronchiolitis obliterans with organizing pneumonia
EAA, extrinsic allergic alveolitis

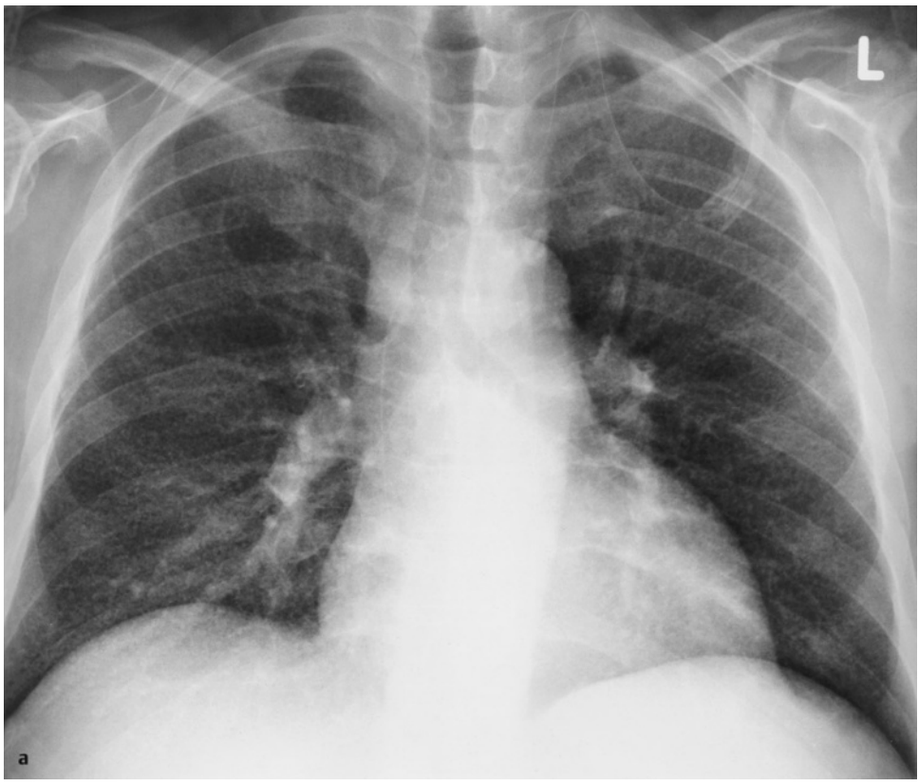

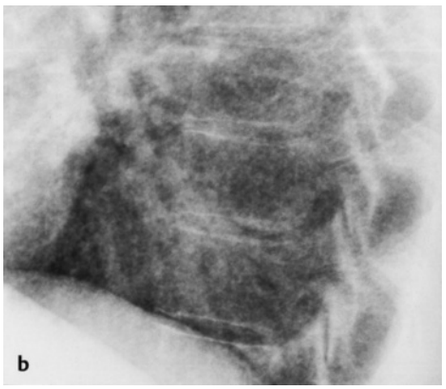

Fig. 3.67 a, b **Miliary tuberculosis**

a The patient is a 38-year-old-man suffering from a kidney disease with severe malaise and persistent mild fever. The plain chest radiograph shows diffuse, very finely nodular shadowing with myriad lesions. No pleural effusion. Left heart enlargement with a Demers catheter in place.

b The detail enlargement shows completely uniform, pin-sized focal lesions in almost completely uniform distribution in addition to tiny ring structures corresponding to the peripheral airways. Note the complete absence of any septal structures.

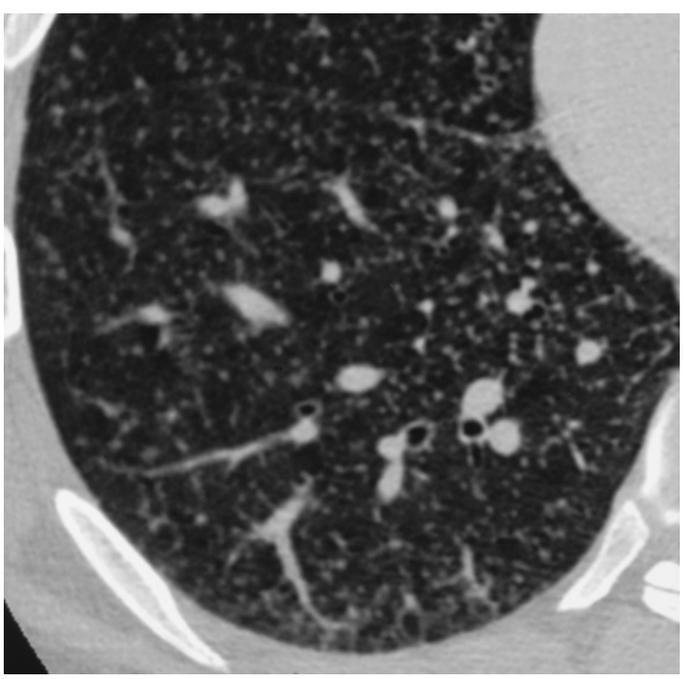

Fig. 3.68 **Miliary tuberculosis.** The patient is a 33-year-old South American man presenting in the emergency room with circulatory collapse. A CT scan was ordered to evaluate findings of finely nodular shadowing on the plain chest radiograph. CT impressively demonstrates the diffuse, completely uniform distribution without any postural movement or predilection for the bronchovascular bundle, central lung, or periphery. There is no associated effusion or area consolidation.

Reactivation

Postprimary Tuberculosis

The radiologic picture produced by reactivated pulmonary tuberculosis differs from that of primary tuberculosis due to residual partial immunity. The following signs are characteristic findings:

- More rapid reaction
- Polymorphism
- No lymph node involvement

Postinflammatory changes are invariably detectable. Where such findings occur (**Fig. 3.69**), the clinician's overriding question for the radiologist will be: "chronic or acute?"

Radiologic signs of **activity** include ill-defined "soft" or "cloudy" shadows, cavitation especially with fluid levels, increasing shadowing, and signs of spread. Cavitation and signs of spread are positive evidence; increasing shadowing is as well, although it can only be evaluated by observing the further course of the disorder. The signs of endobronchial or hematogenous dissemination are clearly identifiable earlier on CT (**Fig. 3.70**).

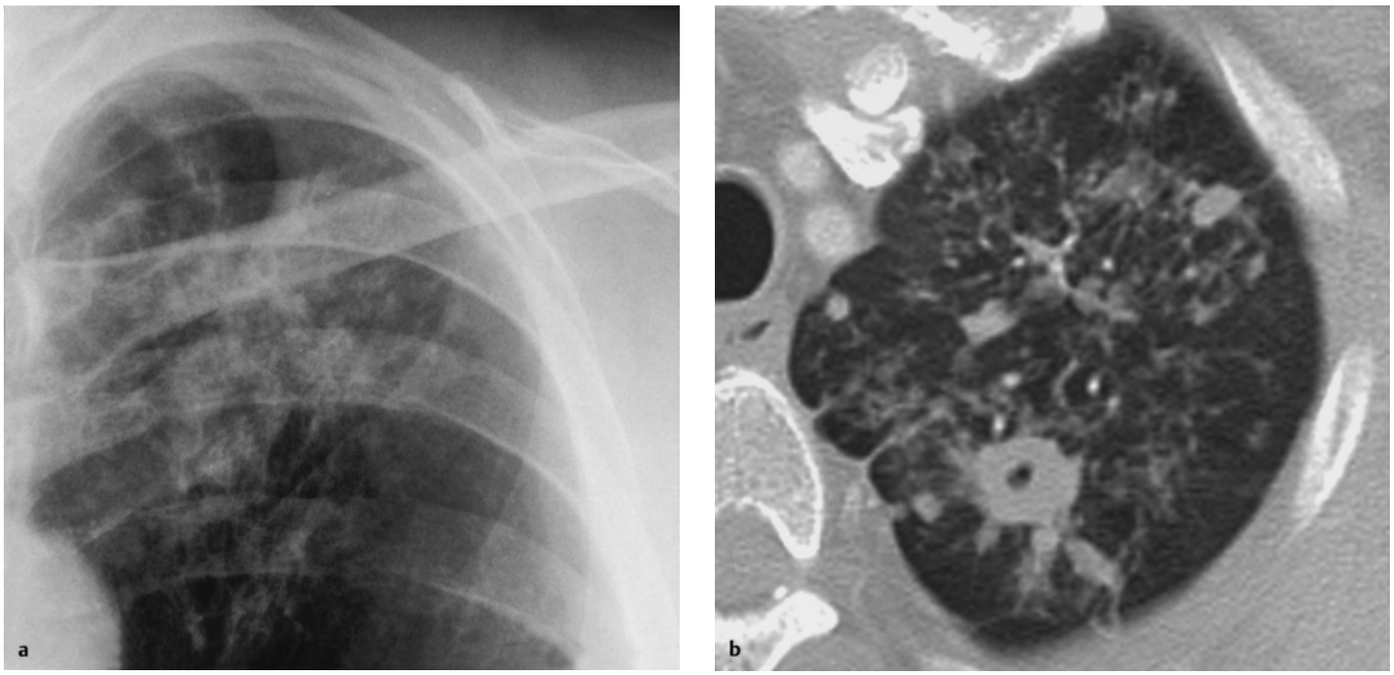

Fig. 3.69 a, b **Reactivated pulmonary tuberculosis.** The detail enlargement (**a**) shows faint cloudy densities with the clavicle shadow in addition to sharply defined linear shadows and nodules. CT (**b**) confirms reactivation by demonstrating liquefaction.

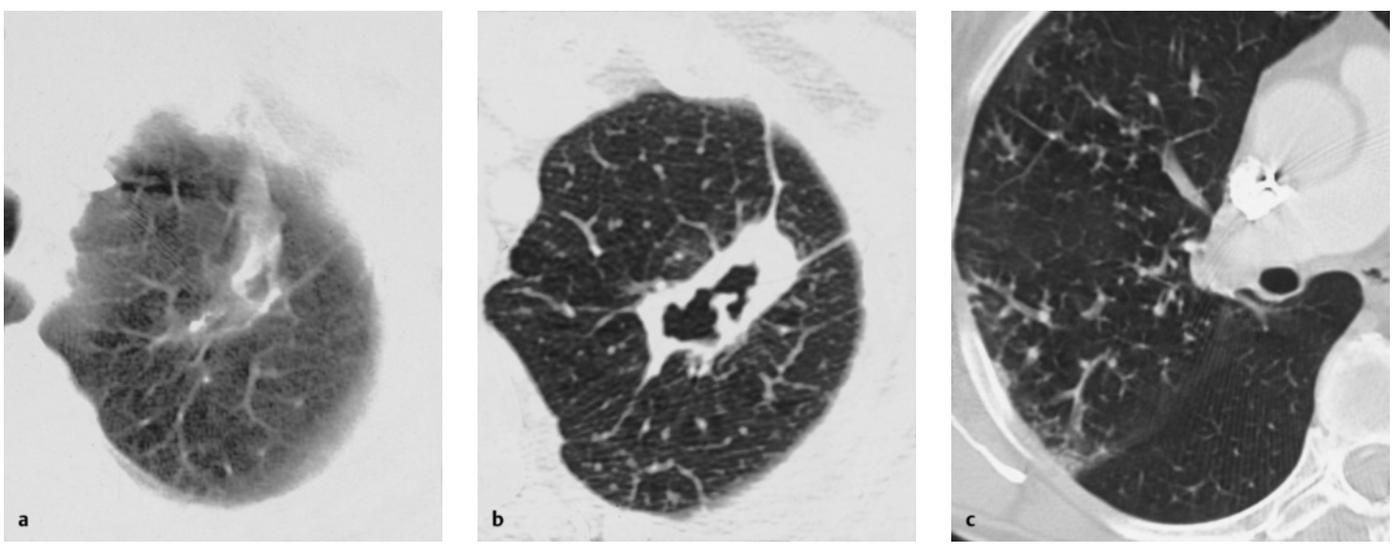

Fig. 3.70 a–c **Reactivation and cavitation.** The previous study (**a**) is difficult to evaluate, possibly for technical reasons, and shows what appears to be scarring consistent with a shrunken cavity. Three months later the process is clearly recognizable with a thick-walled cavity (**b**) and bronchogenic spread into the right middle lung field (**c**).

Healing

Radiologic signs of healing include:

- Increasing sharpness and density of the shadows
- Shrinking of the infiltrates
- Shrinking of the cavities

Increasing sharpness of the infiltrates observed is a sign of "productive conversion" of the exudative processes.

A specific process may be declared definitively *inactive* when all radiologic, laboratory, and bacteriologic findings have remained unchanged for 6 months.

Scarring Stage and Defects

There has been a marked shift in the importance of the knowledge of various pictures of tuberculosis. Today significantly greater emphasis is placed on the certain detection and classification of defects than on the signs of primary infection or reactivation. Classic defects that should be clearly detectable on the plain chest radiograph include:

- Postinflammatory focal calcifications
- Apical pleural thickening with cranial displacement of the hila and shrinkage of the upper lobes
- Calcified indurations after tuberculous pleuritis
- Status post plombage
- Status post thoracoplasty

These changes can mimic other pathologies (volume loss in cranial displacement of the hila, **Fig. 3.71**) or mask them (calcified indurations, **Fig. 3.72**).

Surgical treatment of tuberculosis calls to mind the bygone era of **Ferdinand Sauerbruch.** Such postoperative findings are rapidly disappearing, although they are still encountered on occasion. The less often postoperative findings after thoracoplasty (**Fig. 3.73**) and plombage (**Fig. 3.74**) are encountered, and the older and less communicative these patients become, the more such findings are viewed with doubt and incomprehension on the part of the examiner.

Ferdinand Sauerbruch (* 1875, † 1951): Professor ordinarius of surgery in Munich and Berlin, pioneer of thoracic trauma surgery. Introduced many new surgical methods in the 1920s as well as nonsurgical treatments for pulmonary tuberculosis.

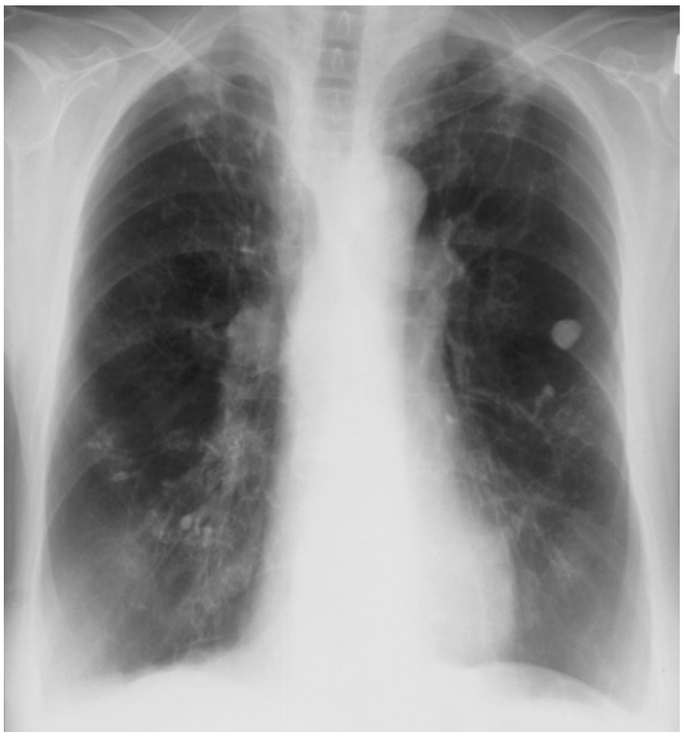

Fig. 3.71 Apical pleural thickening with cranially displaced hila. Severe post-inflammatory changes are seen in the apical segments of both lungs. The resulting shrinkage of the upper lobes has led to cranial displacement of the hila. A sharply demarcated focal calcification measuring 12 mm in diameter is visible in the left middle lung field.

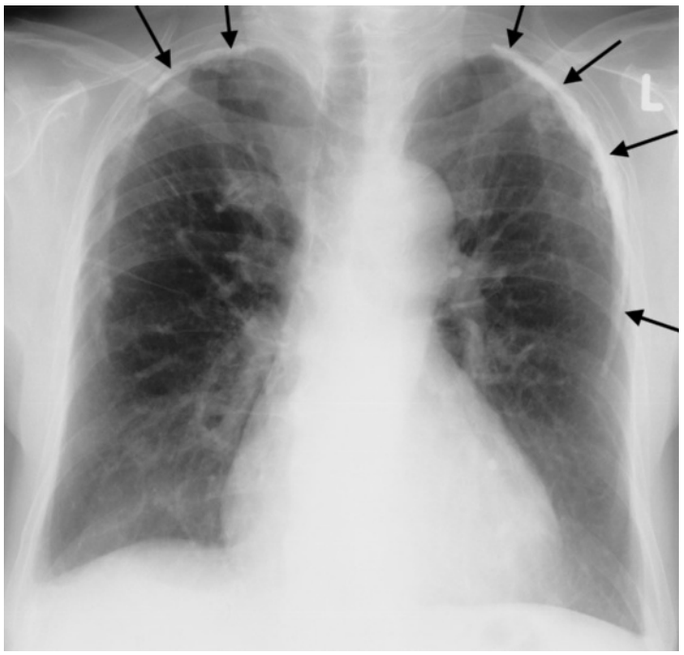

Fig. 3.72 Calcified induration in tuberculous pleuritis. Mantlelike calcifications are clearly visible (black arrows). When they are imaged in top view, such lesions produce only a faint density.

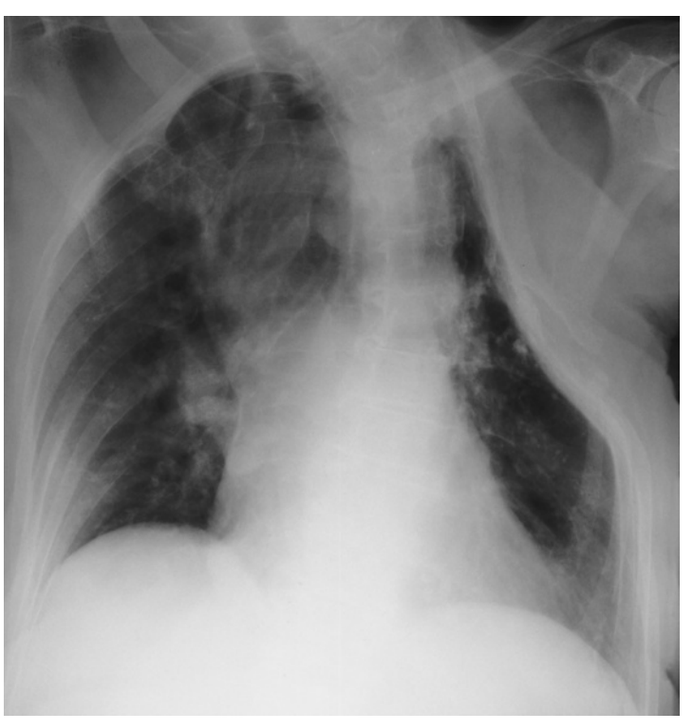

Fig. 3.73 Status post thoracoplasty in pulmonary tuberculosis. The patient is a woman who was 92 years old in 2001 when this preoperative chest radiograph was obtained prior to open reduction of a femoral neck fracture. Severe chest deformity is present following left thoracoplasty. Findings include extensive compression of the upper lobe and rightward upper mediastinal shift. Other findings include moderate senile emphysema with tracheobronchopathia calcarea and signs of pulmonary arterial hypertension. Heart size is normal. There is no infiltrate.

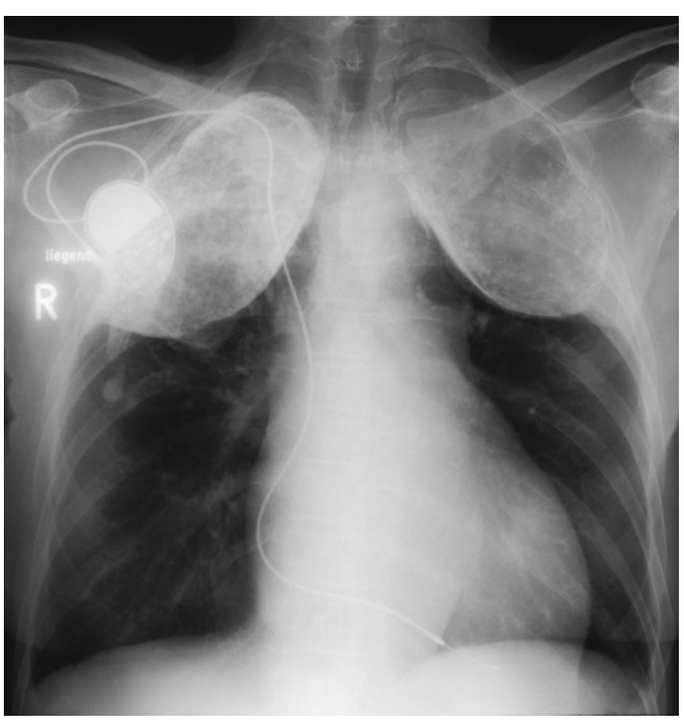

Fig. 3.74 Status post plombage in pulmonary tuberculosis. The patient is a woman born in 1927 (!) who underwent plombage in both upper lung fields. Isolated focal calcifications are visible in the right middle lung field. Left heart is enlarged with a pacemaker in situ and no signs of decompensation. There are no signs of florid infiltrates. Senile emphysema is present with obstructive barrel chest. There is marked destruction of the posterior portion of the 4th left rib. As this finding was identical on older films, it was evaluated as postoperative.

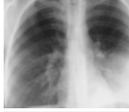

Review Case 1

The patient is a 71-year-old woman with chest pain of unknown cause (Fig. 3.75). She is presenting for coronary angiography following abnormal findings on exercise electrocardiogram with known hypertension. No fever. Slight cough, less than the chronic cough reported.

Question 1

How do you evaluate heart size and cardiac compensation? (Previously discussed in Chapter 1.)

Hints

Imaging technique?
Silhouettes?

Question 2

How do you evaluate the pulmonary parenchyma?
Are other noncardiac changes present? (This chapter.)

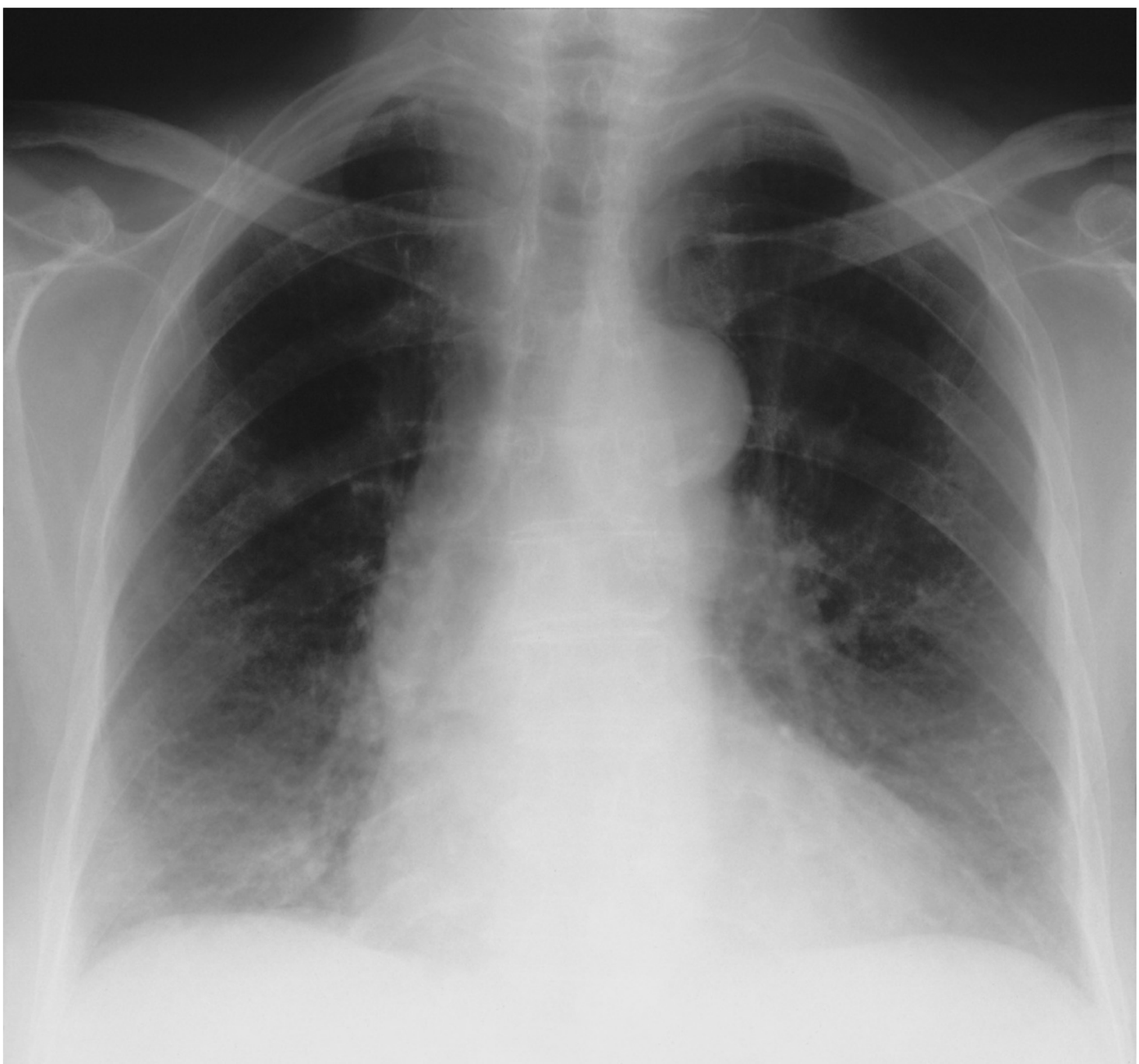

Fig. 3.75 Chest pain of unknown cause. Radiograph obtained prior to coronary angiography.

Answer

With signs of chronic obstruction and a barrel chest deformity, findings in moderate inspiration (faint gull-wing shape of the diaphragm) include a bilateral symmetrical basal opacity but a silhouette sign is absent. The long axis of the heart is significantly longer than the width of the left hemithorax. However, like the bilateral symmetrical opacification of the lower lung fields, this must be seen in the context of poor inspiration.

To substantiate this, we examine the lateral view (**Fig. 3.76**).

Evaluation: Poor inspiration simulating cardiomegaly and bilateral infiltrates.

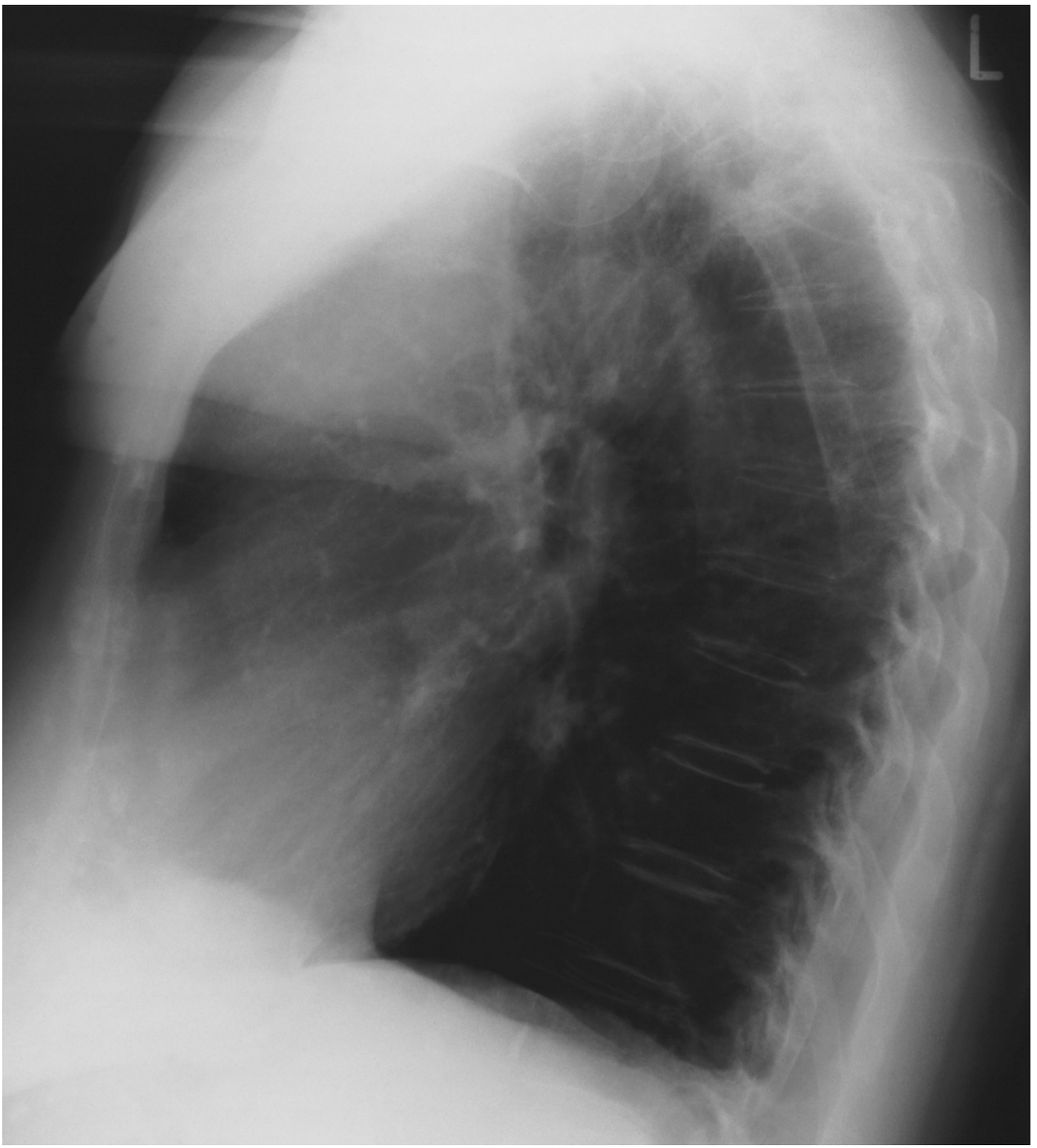

Fig. 3.76 Chronic obstruction with barrel chest. The obstructive barrel chest and sagittal curvature of the sternum are more clearly visualized with improved inspiration. The heart and aorta exhibit a hypertensive configuration without signs of congestion. No effusion. There are no signs of infiltrates.

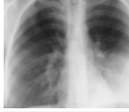

Review Case 2

The patient is a 38-year-old woman admitted to the emergency room with chest pain after a fall. Chest radiographs (Fig. 3.77, Fig. 3.78) were obtained to exclude pneumothorax.

Question 1

Is the lung completely expanded and/or does it show a sequela of trauma?

Question 2

How do you evaluate heart size and cardiac compensation?

Question 3

The right cardiac border cannot be identified. Is a pulmonary contusion present?

Hint

Lateral view.

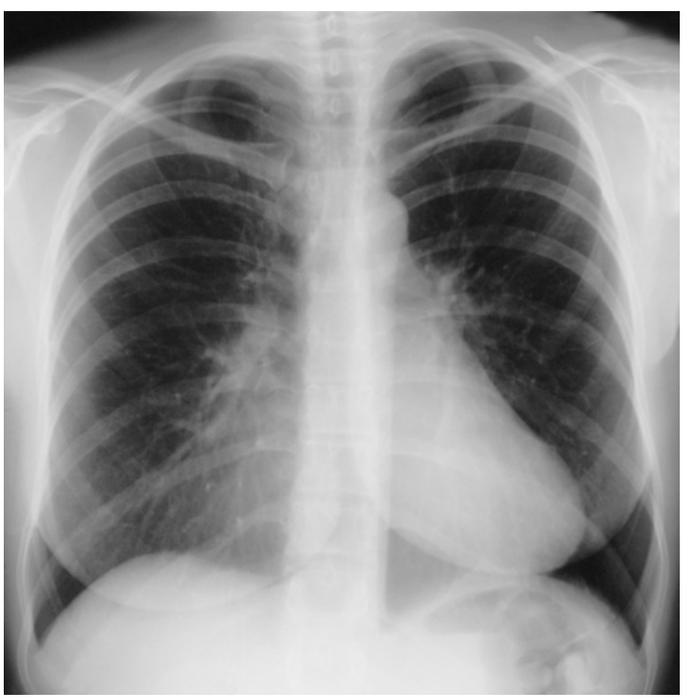

Fig. 3.77 Radiograph obtained in a patient with chest pain after a fall to exclude pneumothorax.

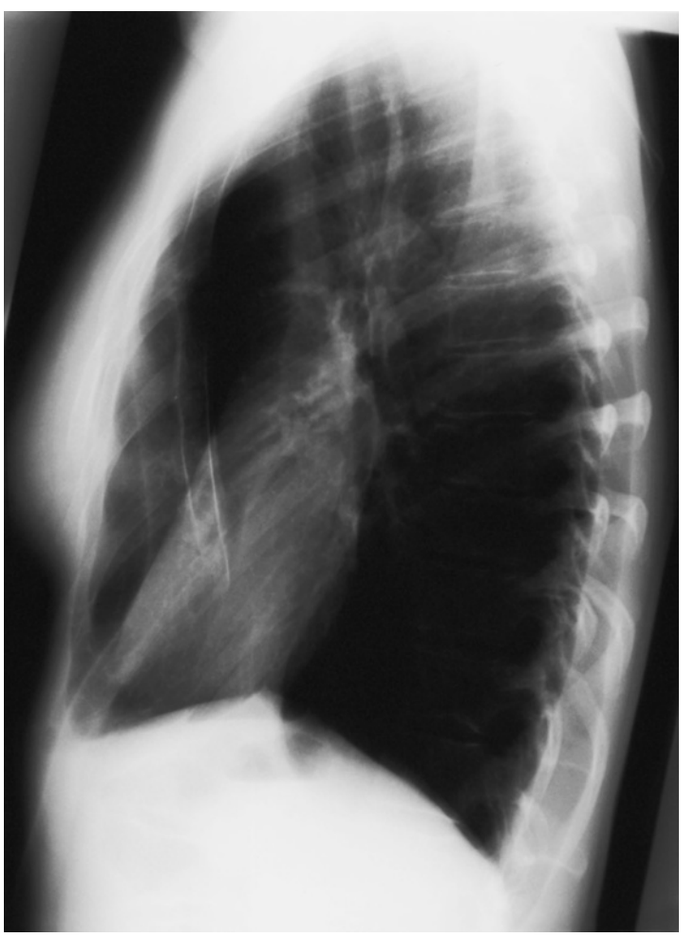

Fig. 3.78 Lateral view of the patient in Fig. 3.77.

Answer

Severe pectus excavatum simulates infiltrate in the middle lobe by obliterating the right cardiac border. The sternum is shifted far posteriorly but is not fractured. However, there is a fracture in the anterior part of the right 8th rib (**Fig. 3.79**). There is no evidence of pneumonic infiltrates, focal contusions, or pneumothorax.

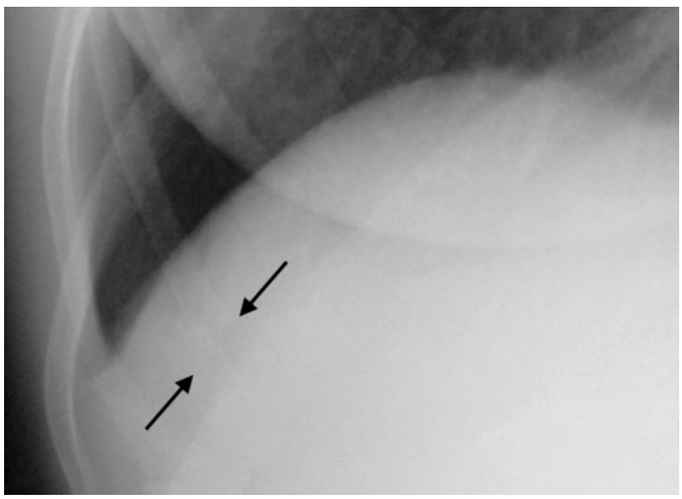

Fig. 3.79 Detail enlargement of the right hemithorax. Moderately displaced fracture of the right 8th rib (black arrows).

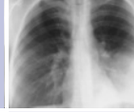

Review Case 3

The patient is a 76-year-old woman with advanced cervical carcinoma who had a venous port implanted. She now has an unexplained fever and a port infection is suspected (Fig. 3.80).

Question 1

How do you evaluate heart size and cardiac compensation? (Previously discussed in Chapter 1.)

Question 2

What else might be causing the pathology at the site where you suspect an infiltrate? (This chapter.)

Hints

What about the shape of the left cardiomediastinal border and central vascular structures?
Silhouette sign?

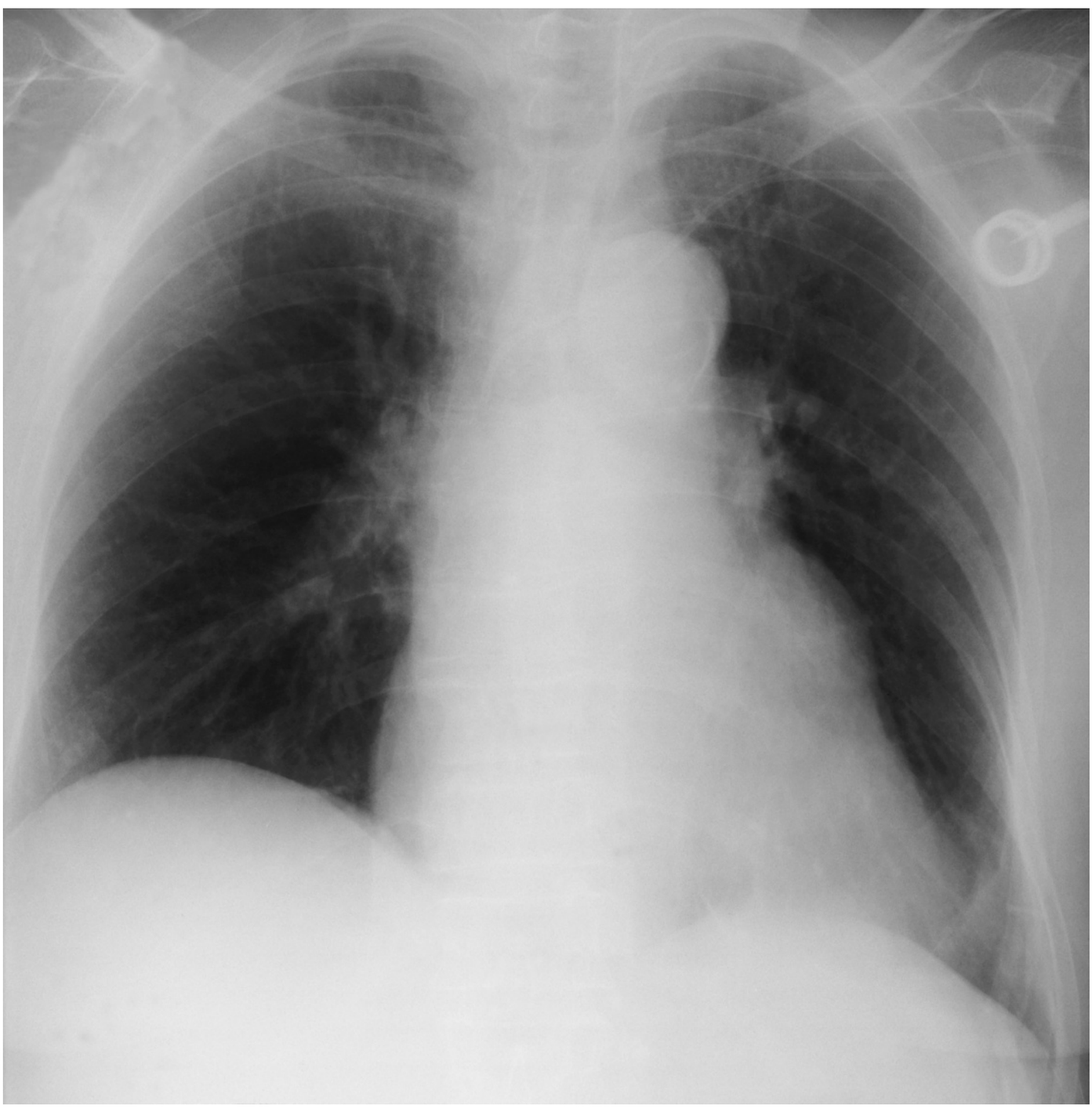

Fig. 3.80 Patient with cervical carcinoma and now fever. Radiograph to verify proper position of venous port.

Answer

The heart is enlarged, particularly at the level of the left atrium (atrial appendage), without signs of decompensation. With good depth of inspiration, the supine radiograph indicates the presence of COPD. The retrocardiac portion of the left diaphragmatic crus is blurred.

The follow-up study 5 days later (**Fig. 3.81**) supports the tentative diagnosis of incipient bronchopneumonia in the left lung.

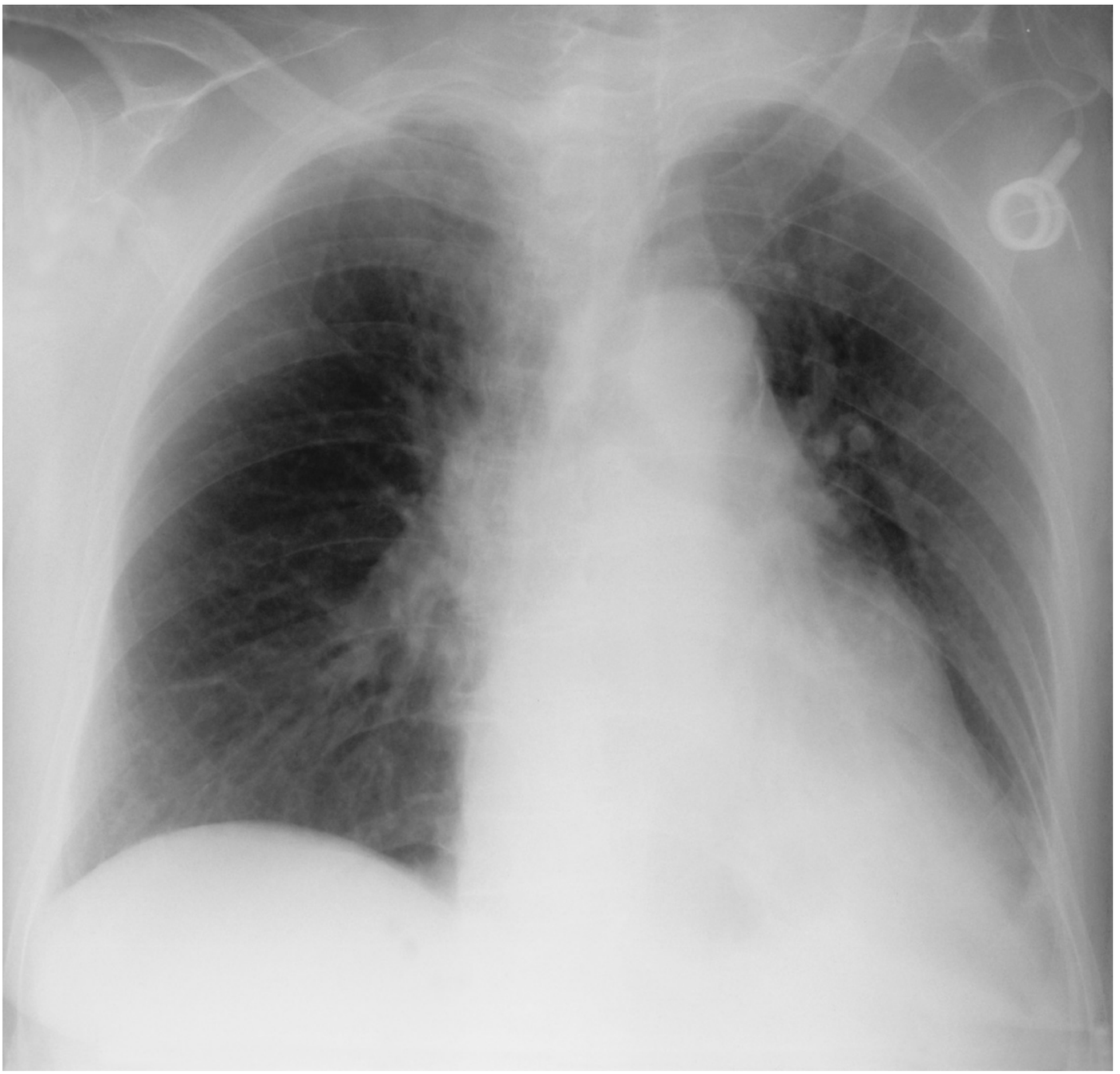

Fig. 3.81 **In addition to signs of significant central congestion (note the left anterior segmental artery), an infiltrate in the left lower lobe has obliterated the contour of the left diaphragm, producing a silhouette sign.**

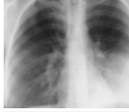

Review Case 4

The patient is a 70-year-old man with acute malaise, fever, and dyspnea on exercise (Fig. 3.82).

Question 1

Is the dyspnea on exercise caused by cardiac decompensation with left heart enlargement? (Previously discussed in Chapter 1.)

Question 2

Is there chronic preexisting lung damage? What changes suggest chronic bronchitis? (Previously discussed in Chapter 2.)

Question 3

What changes suggest pneumonia? (This chapter.)

Question 4

What type of infiltrate would you describe?

Hints

Pairing, redistribution?
Chest shape, central and apical vascular marking?
Local blurring and alveolar shadowing?

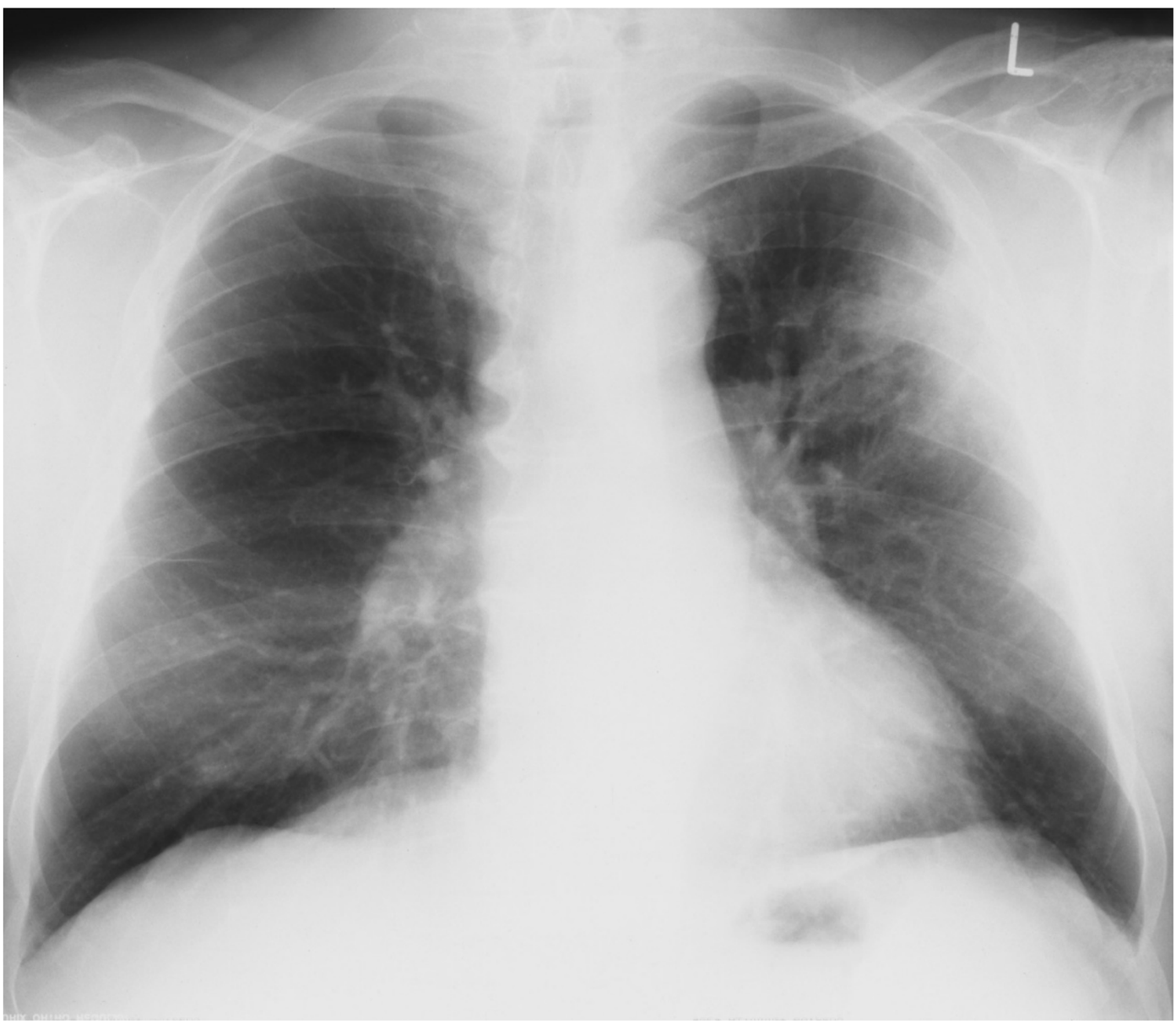

Fig. 3.82 Acute malaise, fever, and dyspnea on exercise.

Answer

Answer to question 1: The heart exhibits a clear aortic configuration; its long axis no longer fits in the hemithorax. However, the presence of emphysema masks the left heart enlargement. Although the right anterior segmental artery has a larger diameter than the accompanying bronchus, the total absence of Kerley lines indicates that there is no decompensation.

Answer to question 2: The thickening of the right anterior segmental artery is more likely attributable to pulmonary hypertension (width of the intermediate artery is 21 mm) in chronic obstructive airway disease with emphysema. The significant rarefaction of the apical vessels supports this interpretation. Moderate bronchial wall thickening is observed in the basal segments.

Answer to question 3: Congestion is seen in the left upper lobe with ill-defined ground-glass shadows in the peripheral regions increasing in density toward the periphery.

Answer to question 4: The ill-defined border independent of segmental boundaries and the preexisting lung damage suggest bronchopneumonia. However, the clinical evidence (sudden onset), the course (**Fig. 3.83**, **Fig. 3.84**) with increasing area consolidation of segments 2 and 3 of the left lung (greatly increased in volume), and the development of an air bronchogram all suggest lobar pneumonia.

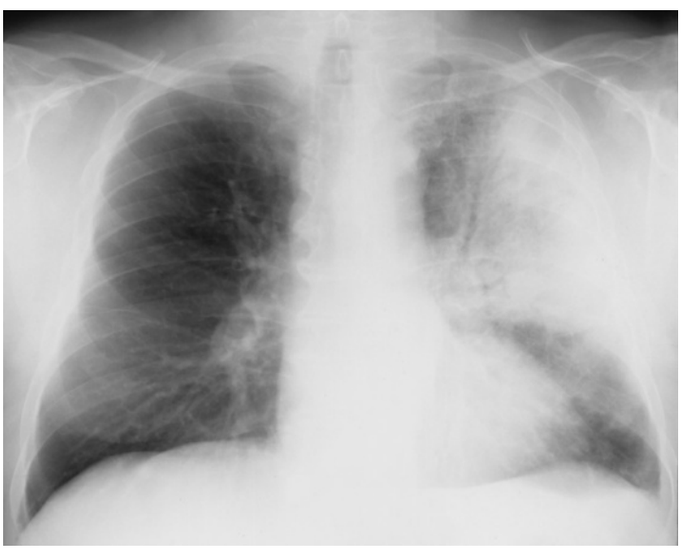

Fig. 3.83 **Four days later there is a severe lobar infiltrate in the left upper lobe with increased volume and an air bronchogram.**

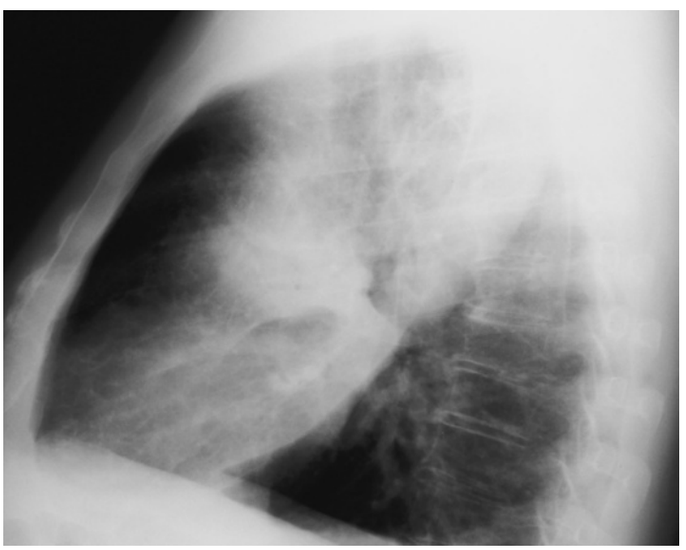

Fig. 3.84 **Lateral view obtained at the same time.** Significantly increased volume of the left upper lobe.

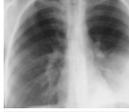

Review Case 5

The patient is an 85-year-old woman with progressive dyspnea for the past 3 months and worsening findings for the last week (Fig. 3.85). Employment history: farmer and housewife.

Question 1

How would you describe the pulmonary shadowing?

Question 2

Might the densities have cardiac causes?

Question 3

Are there signs of chronic bronchitis? Might the densities be related to chronic emphysematous bronchitis? If so, what explains the acute worsening of clinical symptoms? Is there an additional infiltrate in the left lower lobe?

Question 4

How do you interpret the shadowing in the posterobasal region on the lateral view (Fig. 3.86)?

Hints

Number of densities? Pattern of distribution?
Septal changes? Effusion?
Microlesions or larger?
Radiodensity? Pleural involvement?

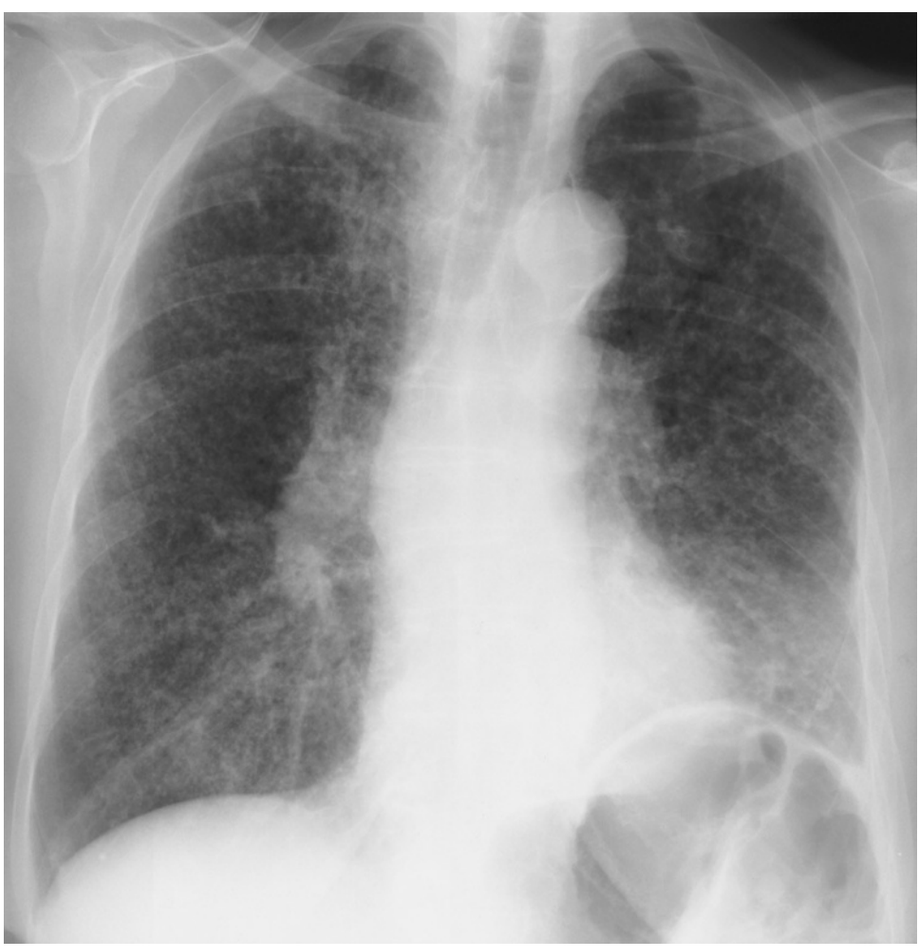

Fig. 3.85 The patient is an 85-year-old woman, a farmer with progressive dyspnea.

Answer

Answer to question 1: Given the uniformity (all look the same), size (pinhead size), and diffuse distribution (central and peripheral, no postural movement), this must be diagnosed as a miliary pattern.

Answer to question 2: No. In the presence of an aortic configuration there are no signs of interstitial edema. The changes show no postural movement. No effusion.

Answer to question 3: Chronic bronchitis or senile emphysema is certainly present (barrel chest and thickened hila indicative of preexisting pulmonary arterial hypertension). However, the individual densities are too uniform, too large, and too diffusely distributed for micronodules in bronchitis.

Answer to question 4: The shadow in broad contact with the pleura on the left side exhibits a pattern of thin calcification. It represents a chronic pleural induration consistent with tuberculous pleuritis.

Evaluation: Suspicion of miliary tuberculosis from reactivated pulmonary tuberculosis. The CT chest scan performed the same day (**Fig. 3.87**) confirms this suspicion.

Epicrisis: The patient died 7 days later despite immediate initiation of tuberculostatic therapy. The autopsy revealed massive miliary tuberculosis with reactivation in the vicinity of a calcified induration on the left side with local caseous pneumonia.

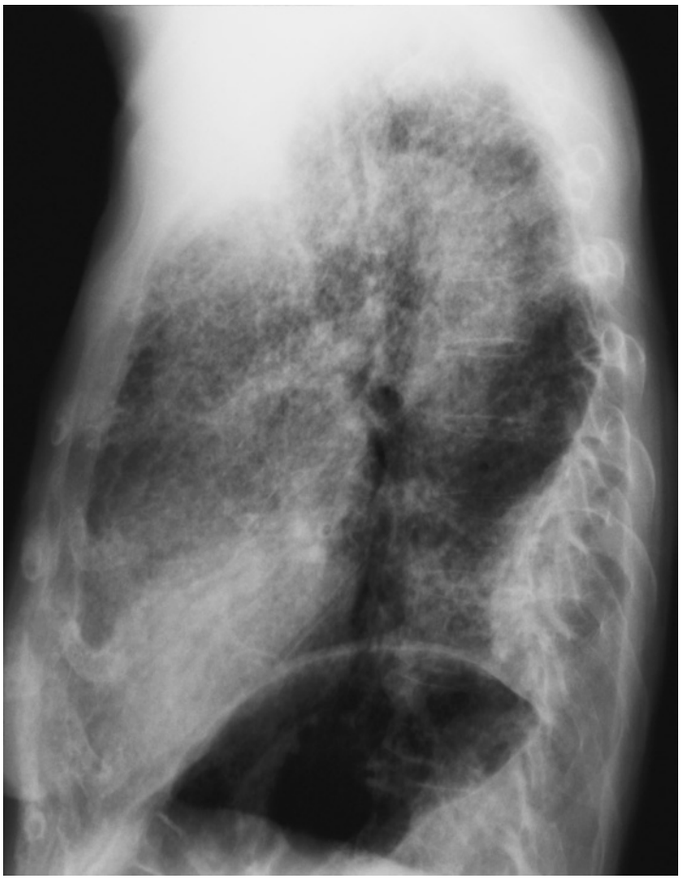

Fig. 3.86 **Lateral view of the patient in Fig. 3.85.**

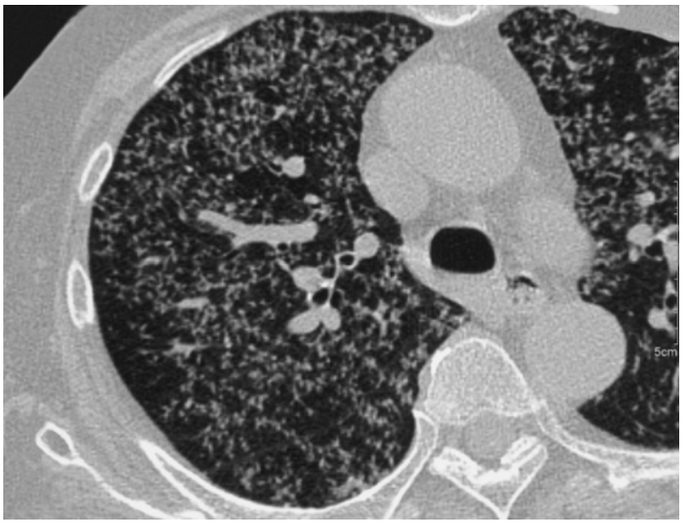

Fig. 3.87 **CT findings on the day of admission.** Pronounced random pattern of nodular shadowing. The morphology is consistent with sarcoidosis, but this is improbable given the patient's age. A report of previous findings mentioned no abnormalities, which eliminates pneumoconiosis. The tentative diagnosis is miliary tuberculosis (senile tuberculosis).

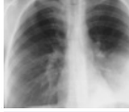

Review Case 6

The patient is an 84-year-old woman with known absolute arrhythmia presenting in the outpatient department with palpitations (Fig. 3.88). No fever or dyspnea. Nonsmoker.

Question 1

Insofar as this is possible in only one plane, describe the heart configuration. Which heart chamber is definitely enlarged? (Previously discussed in Chapter 1.)

Question 2

How do you evaluate chest shape? Is COPD present? (Previously discussed in Chapter 2.)

Question 3

How do you evaluate the changes in the upper lung fields and hila? Is any other pathology present that might be related to the next chapter (Chapter 4)?

Hints

Note the left cardiac border.
Note the patient's age.
The patient is a nonsmoker.

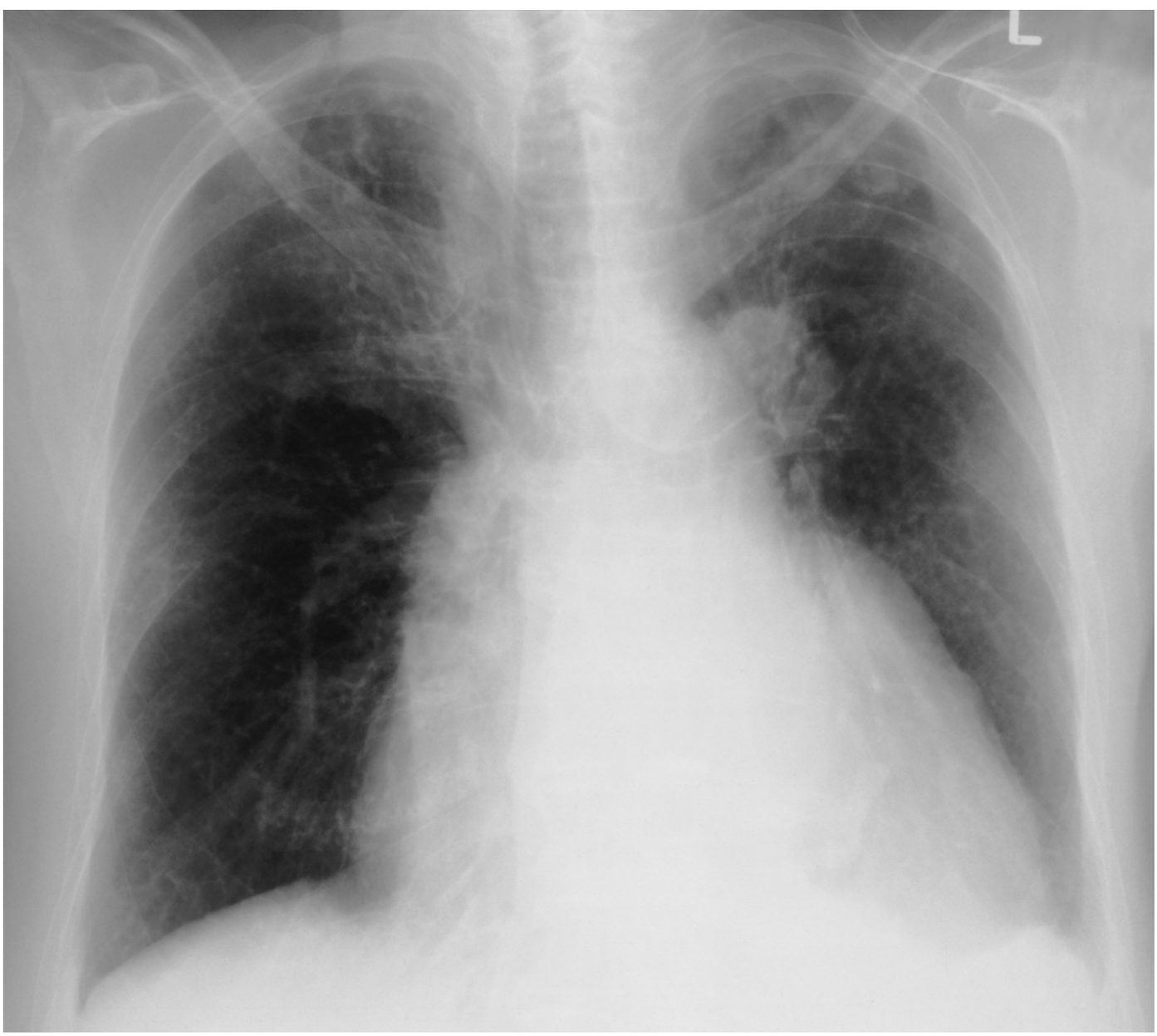

Fig. 3.88 Patient presenting for diagnostic evaluation of cardiac arrhythmia.

Answer

Answer to question 1: The left heart is significantly enlarged (the long axis of the heart is longer than the width of the hemithorax). The pronounced left atrial appendage (black arrows) and the splaying of the tracheal bifurcation suggest enlargement of the left atrium in particular (**Fig. 3.89**).

Answer to question 2: Emphysema chest, because of the slight interstitial shadowing and the lack of previous clinical findings such as senile emphysema.

Answer to question 3: Significant streaky shadowing in both upper lung fields with shortened, cranially displaced hila. There are some cloudy shadows indicative of calcifications. The left hilum is so deformed (drawn lines) that its shape could suggest the false-positive finding of a mass in the left central region.

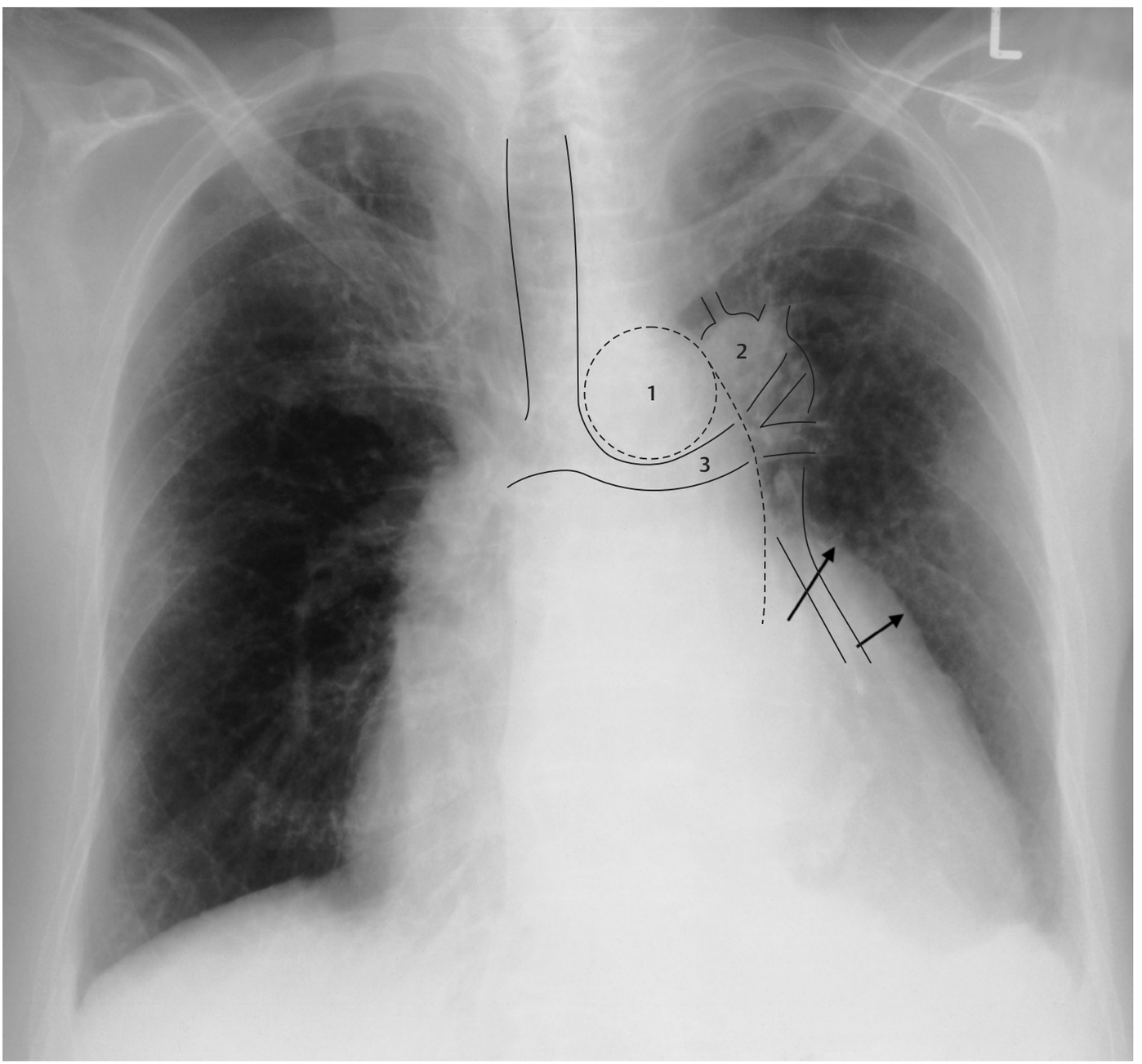

Fig. 3.89 **Cranially displaced hila with shrinkage of the upper lobes.**
1 Aorta
2 Left pulmonary artery
3 Left main bronchus

4

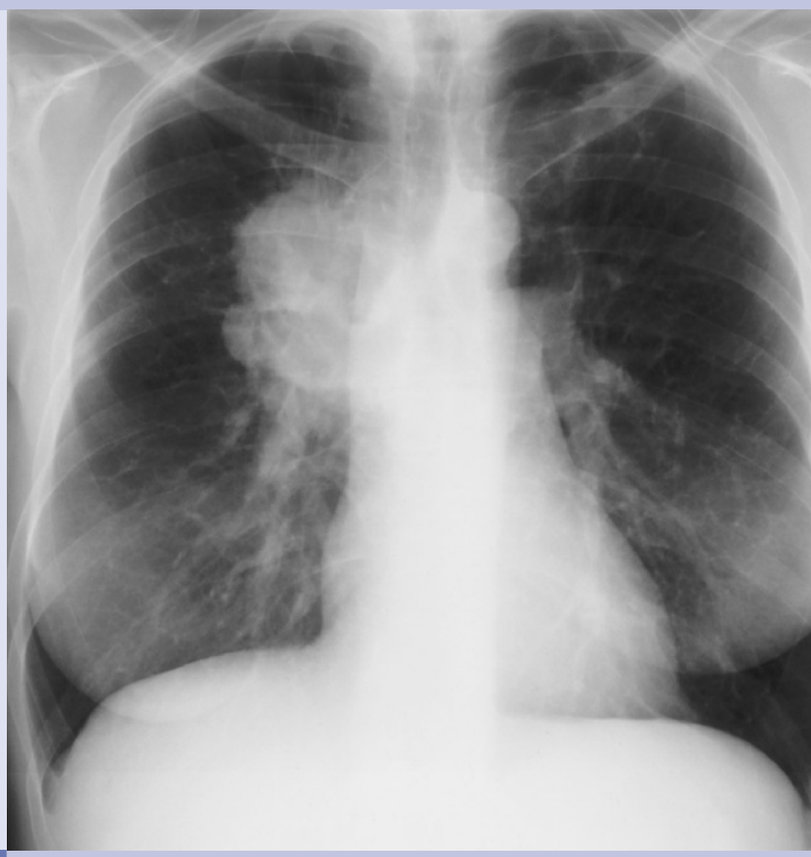

Bronchial Carcinoma

General

First described by **René T. H. Laennec**, cancerous disease of the lung was still a rarity in the early 20th century. Today bronchial carcinoma is a leading cause of death from tumorous disease. The dramatic increase in incidence has been attributed to the rapid increase in cigarette smoking especially in the period after the Second World War. The number and type of cigarettes (with or without filter) and the age at which the person began smoking are regarded as the main risk factors. Whereas the incidence of bronchial carcinoma in men stagnated at a high level in the 1980s, a rapid increase may still be observed in women.

Early diagnosis is crucial to improving survival times. The increasingly high number of cases diagnosed late and suspicious findings missed on earlier images may be attributed to several factors:

- Resignation on the part of the examiner ("Go ahead and do a CT instead," or "You can forget the chest radiograph")
- Lack of concentration in an overworked examiner ("I've got to get rid of the internists")
- Lack of practice and insufficient training
- Lack of published literature

Recent studies show that a focal lesion is more often misinterpreted ("That's healed") than overlooked ("No abnormal findings"). This chapter will focus on training the radiologist to detect lesions and then to evaluate them.

Radiographic signs of bronchial carcinoma depend on morphology and location (**Fig. 4.1**). Clinical evaluation and radiologic symptomology reflect the basic dichotomy of a **central form** (**Fig. 4.2**) and a **peripheral form** (**Fig. 4.3**) of bronchial carcinoma. This basic distinction is dependent on the underlying histology only insofar as adenocarcinoma primarily occurs at a peripheral location. However, both squamous cell and small-cell carcinomas can occur at both central and peripheral locations.

Notes on Pathology and Clinical Findings

The World Health Organization (WHO) distinguishes small-cell bronchial carcinoma from non-small-cell forms (adenocarcinoma, squamous cell, large cell, and adenosquamous carcinomas). The non-small-cell forms currently represent approximately 85% of all diagnoses of lung cancer. In the 1950s squamous cell carcinomas occurred 16 times more often than adenocarcinomas. Since then the balance has shifted, with adenocarcinomas now accounting for nearly 40% of cancers and squamous cell carcinoma for 30%. This striking change is attributed to the increasing proliferation of filter cigarettes with low nicotine content. The deeper inhalation with filter cigarettes increases exposure of the small airways. Consequently, these tumors tend to occur farther peripherally.

The share of small-cell bronchial carcinoma is approximately 15%. A particularly high percentage of smokers and ex-smokers contract this type of tumor. Because small-cell carcinoma shows early dissemination, it is regarded differently from other carcinomas and immediately classified as a generalized disorder at the time of diagnosis.

Clinical symptoms depend on the size and location of the tumor. Up to 20% of all cases are diagnosed as incidental findings, for example on routine preoperative radiographs. The cardinal symptom is a cough. However, the diagnostic significance of this finding is often masked in smokers, the main risk group, because smoking itself usually leads to a cough. The same applies to blood-tinged sputum. Hoarseness is an initial symptom in up to 18% of all cases. It indicates mediastinal involvement (lymph node involvement or tumor invasion). Pain (rib destruction) or dyspnea (atelectasis) should also be interpreted only as signs of advanced disease.

René Théophile Hyacinthe Laennec (*1781 Quimper, †1826 Kerlouarnec): Professor at the Collège de France; inventor of the stethoscope. Laennec introduced precise physical diagnostic examination of the lung into clinical practice. He popularized the diagnostic technique of percussion and auscultation devised by the Austrian physician Leopold Auenbrugger von Auenbrugg. Laennec was the first to describe bronchial carcinoma, which he did as part of his classification of airway disorders. He later contracted tuberculosis and died of the disease.

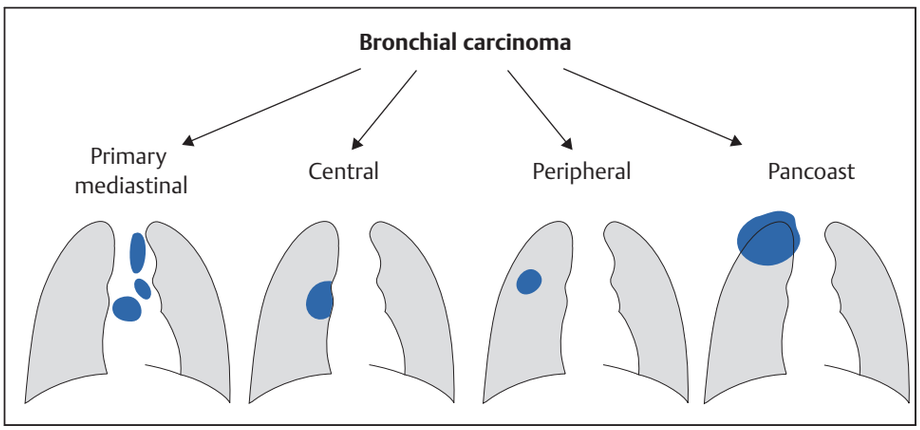

Fig. 4.1 Topographic classification of bronchial carcinoma.

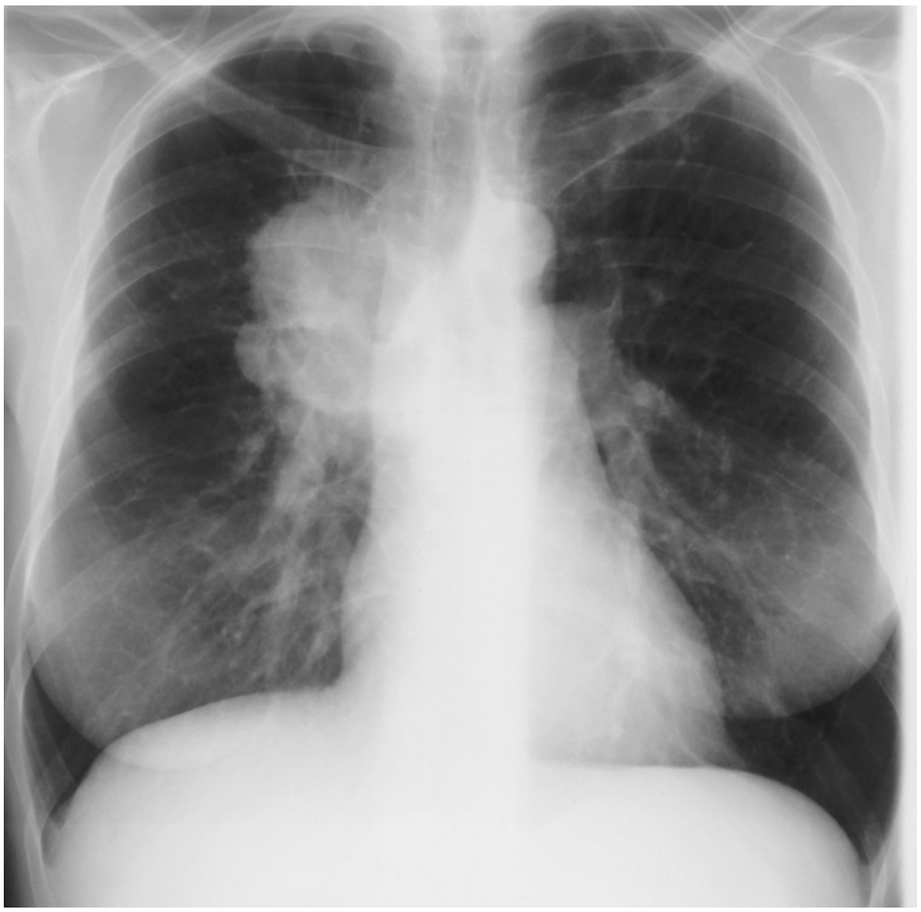

Fig. 4.2 Central bronchial carcinoma. A lobulated mass with a maximum size of 8 cm is present in the right central region at origin of the upper lobe. There is no significant atelectasis in the area peripheral to the mass. Signs of advanced chronic bronchitis are present with obstructive barrel chest and diffuse peribronchial shadowing. Postinflammatory scarring is seen in the apical segments of both lungs.

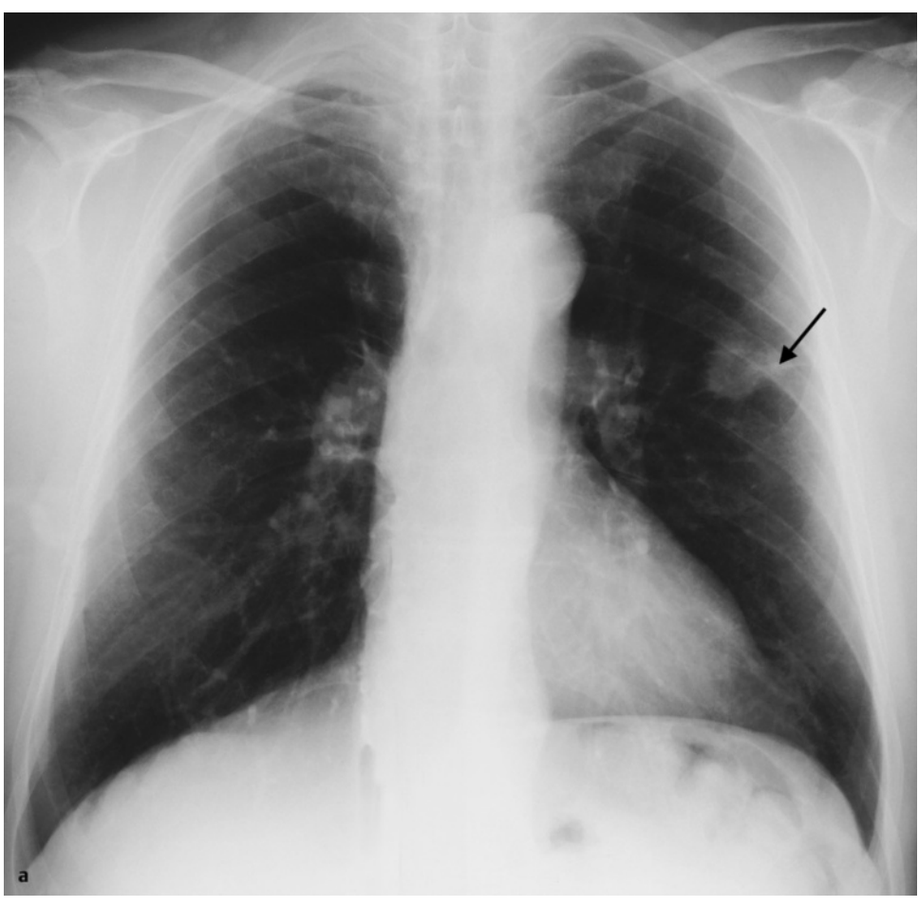

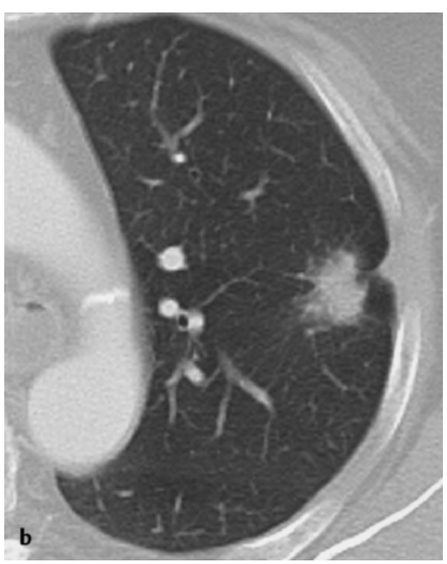

Fig. 4.3 a, b Peripheral bronchial carcinoma

a There is an ill-defined focal lesion measuring 2 cm × 2 cm in the middle region of the left lung with numerous small spicules and a clearly visible fingerlike pleural extension (black arrow). Bronchitic shadowing and a hypertensive configuration are present.

b CT demonstrates the corona radiata and fingerlike pleural lesion.

Central Bronchial Carcinoma

Radiographic findings in central bronchial carcinoma may be classified as direct or indirect signs caused by the tumor.

Indirect signs:

- Reduced perfusion
- Paradoxical hilum sign
- Hypertransradiancy
- Hypoventilation
- Displaced septa
- Mediastinal shift
- Dystelectasis or atelectasis
- Poststenotic pneumonia

Direct signs:

- Contour deformity due to hilar thickening, perihilar streaky densities, and central mass
- Bronchial or tracheal narrowing

For example, a central bronchial carcinoma with endobronchial growth will only be suggested by indirect signs on the plain chest radiograph. However, CT can directly visualize the lesion as a mass within the bronchus.

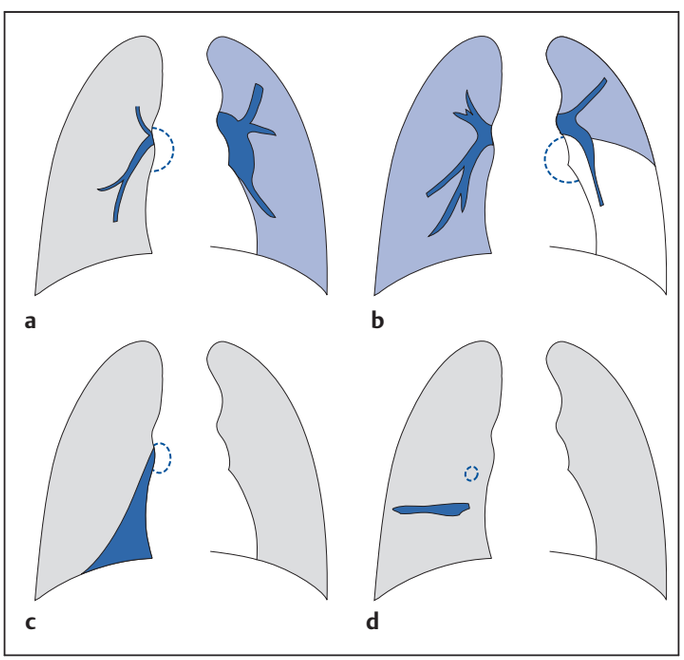

Fig. 4.4a–d **Schematic diagram of indirect signs.**
a Reduced perfusion and paradoxical hilum sign.
b Hypertransradiancy.
c Atelectasis.
d Local hypoventilation.

Indirect Signs (Fig. 4.4)

Bronchial narrowing from a carcinoma close to the hilum but undetectable on the plain chest radiograph can also be demonstrated indirectly by a reflexive reduction in perfusion. The ipsilateral hilum is reduced in size, whereas the contralateral hilum is thickened. Oeser described this as the **"paradoxical hilum" sign** (Fig. 4.5).

Hypertransradiancy of the affected area can be exacerbated by local hyperinflation due to a valve mechanism. This valve mechanism is similar to that observed in children presenting with chronic aspiration of a foreign body such as a peanut. Air is able to pass through the bronchial stenosis on inspiration but cannot escape on expiration (see Table 4.1 for differential diagnosis of local hypertransradiancy).

Table 4.1 **Causes of local hypertransradiancy**

- Pulmonary embolism?
- Pneumothorax?
- Local emphysema?
- Valve mechanism?
- Pneumatocele?
- Dystrophy?
- Soft-tissue defect?

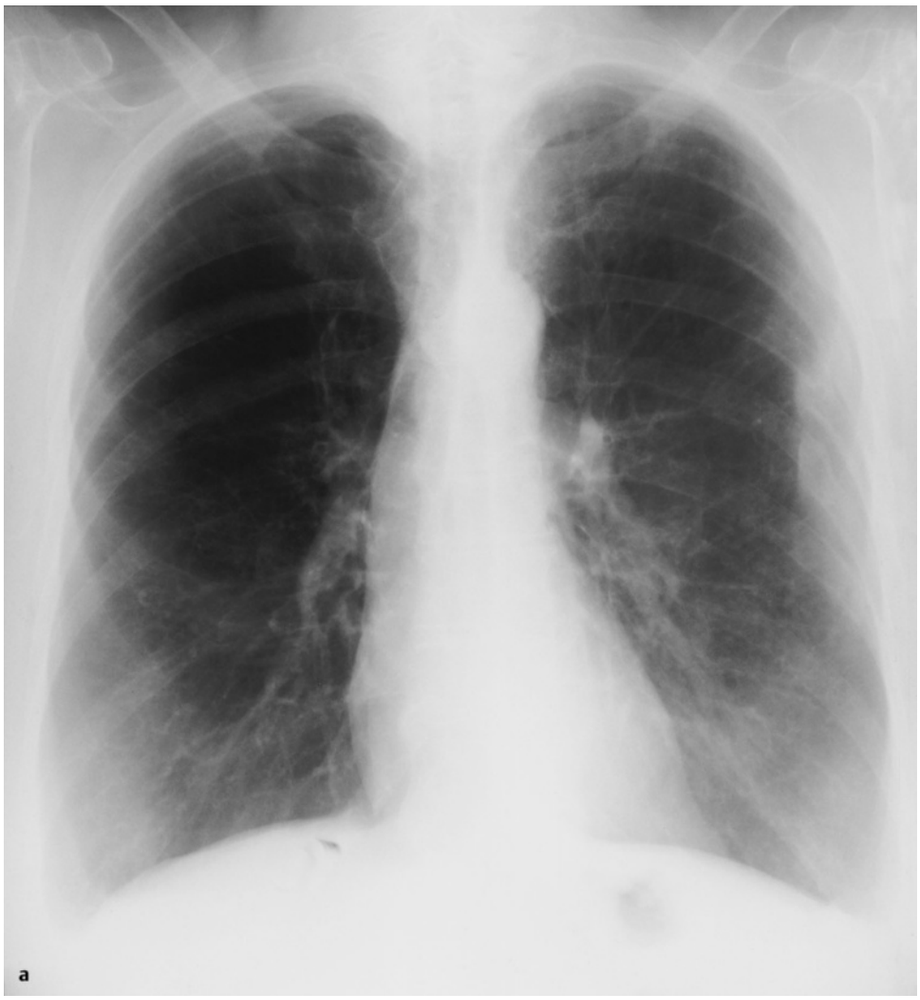

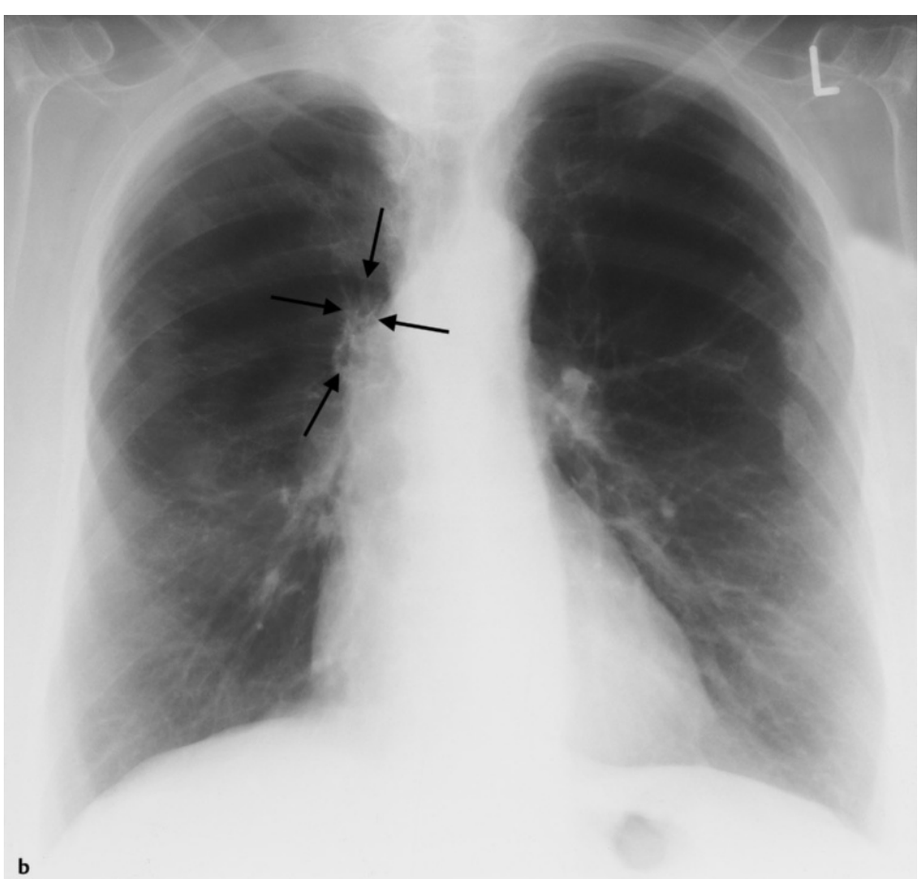

Fig. 4.5 a, b Oeser paradoxical hilum sign in a bronchial carcinoma in the right lung.

a Obstructive barrel chest with signs of chronic bronchitis. Heart size is normal with no signs of decompensation. The left hilum appears normal, whereas the right one is narrowed. The right upper lobe is hyperinflated and pulmonary emphysema is suspected. Status post serial rib fractures on the left side.

b Follow-up examination one year later. The right upper lobe still appears hyperinflated. There is now a mass 3 cm in diameter at the right upper lobar bronchus with streaky spicules radiating into the surrounding tissue (black arrows).

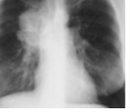

Congestion with mucus-filled bronchi distal to the airway obstruction can later progress to **poststenotic pneumonia** (**Fig. 4.6**). This pneumonia exhibits a segmental configuration despite its obvious peribronchial and bronchopneumonic nature. Early recurrence under antibiotics and atypical location (for example in the upper lobe) will require additional diagnostic studies (**Table 4.2**).

Computed tomography (CT) can demonstrate poststenotic mucus retention as an indirect sign of central bronchial carcinoma (**Fig. 4.6c**). CT can also demonstrate poststenotic pneumonia or hypoventilation (see below) that masks the tumor causing the obstruction or obscures its margins. However, the primary purpose of the CT examination is to demonstrate direct signs.

Table 4.2 Criteria of pneumonia due to tumor

- Early recurrence of pneumonia despite antibiotics
- Segmental bronchopneumonia
- Atypical location
- No other cause

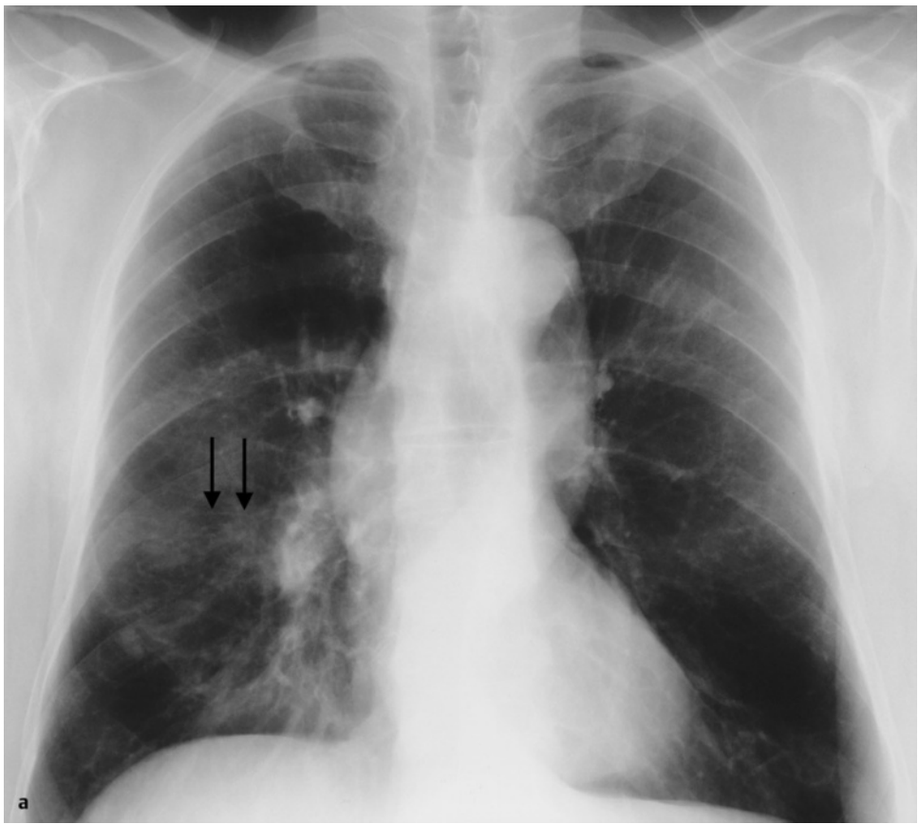

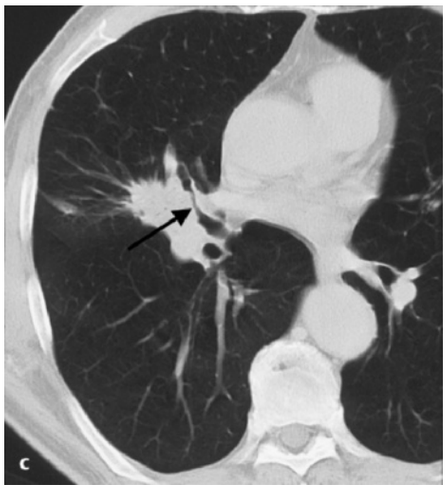

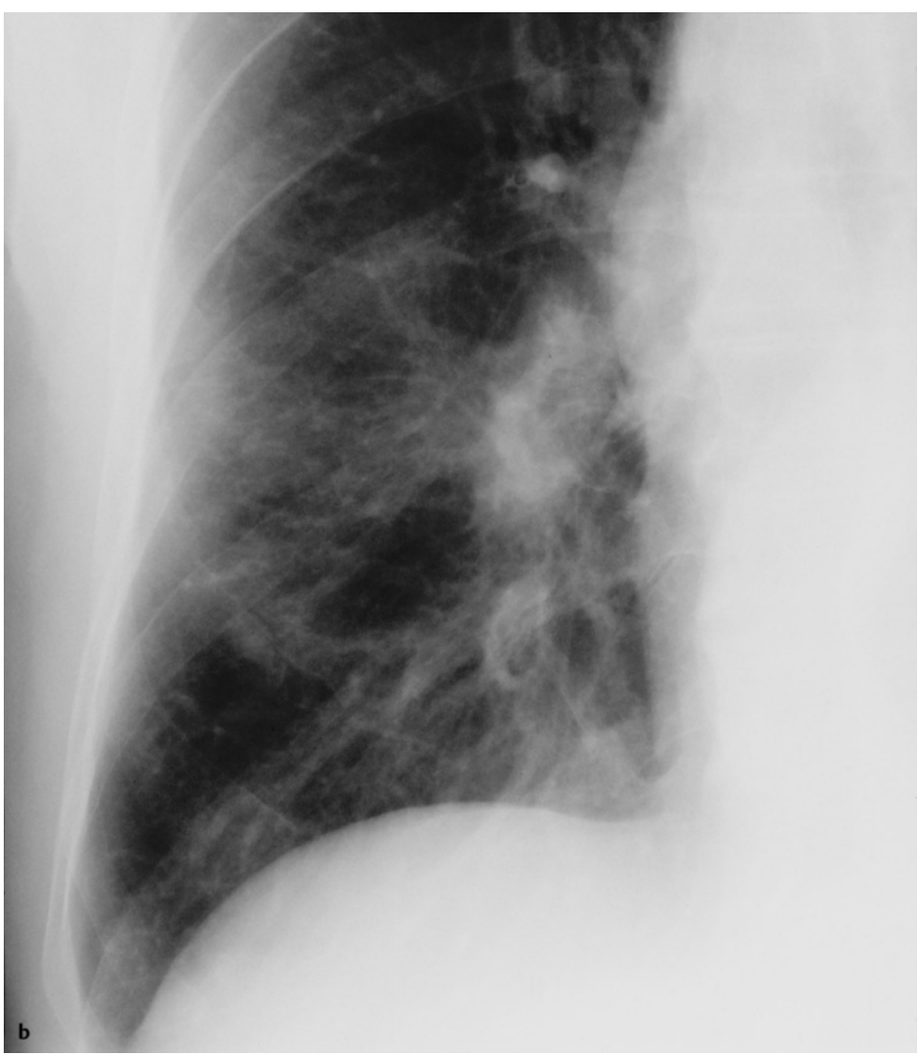

Fig. 4.6 a–c Right central bronchial carcinoma with poststenotic infiltrate.

a The patient is a 76-year-old man with a long history of COPD, now presenting with hemoptysis and fever. Signs of chronic bronchitis with barrel chest. Findings include a hypertensive configuration without signs of decompensation, peribronchial shadowing in the right lower lung field. A discrete caudal extension of the right horizontal fissure (black arrows) is observed, and the vascular structures located there appear closer together.

b Follow-up examination 2 months later reveals thickening of the right hilum where the right intermediate artery bifurcates into the lower and middle lobar arteries. There is also a spiculated reaction in adjacent tissue at this site.

c Visualization of the central mass on CT. The image shows a right central mass measuring 2.5 cm in diameter and compressing the middle lobar bronchus at its origin (black arrow).

Hypoventilation

Bronchial stenosis due to a tumor leads to hypoventilation. This initially appears as streaky densities (**dystelectasis** or "poor ventilation," **Fig. 4.10**) and in total occlusion as **area consolidation** with volume loss (**atelectasis** or "absent ventilation").

Atelectasis (**Fig. 4.9**) exhibits a concave border with the adjacent lung tissue. The trachea and other mediastinal structures may or may not be displaced. In the further course of the disorder, the atelectasis can shrink and appear to adhere to the mediastinum. The occasional total atelectasis of the upper lobe (**Fig. 4.11**) can exhibit a strange appearance, and beginners can easily miss it or misinterpret it as mediastinal widening. Total atelectasis of the middle lobe can also be difficult to recognize or distinguish from indurations. The key to CT diagnosis in this case is the careful analysis of the course of the bronchi.

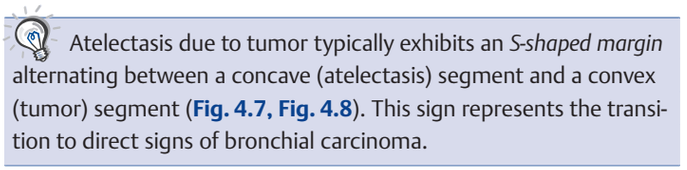

Atelectasis due to tumor typically exhibits an *S-shaped margin* alternating between a concave (atelectasis) segment and a convex (tumor) segment (**Fig. 4.7, Fig. 4.8**). This sign represents the transition to direct signs of bronchial carcinoma.

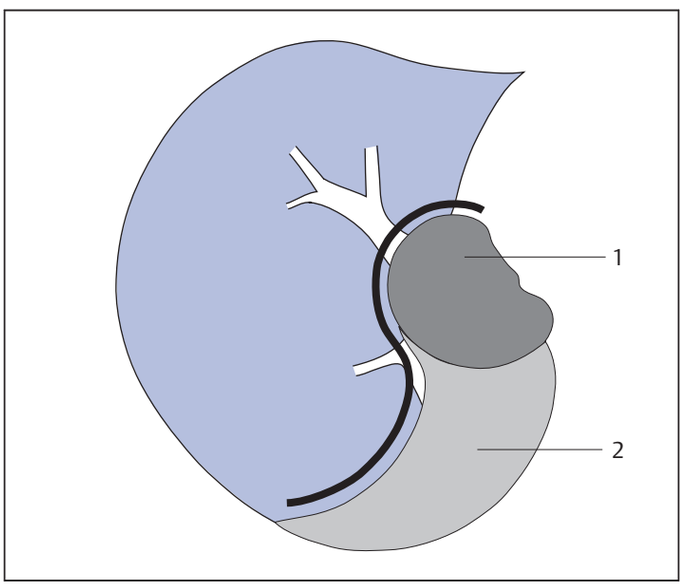

Fig. 4.7 "S" sign in atelectasis due to tumor. The "S" is formed by the combination of a convex (tumor) segment and a concave (atelectasis) segment of the shadow.
1 Tumor
2 Atelectasis

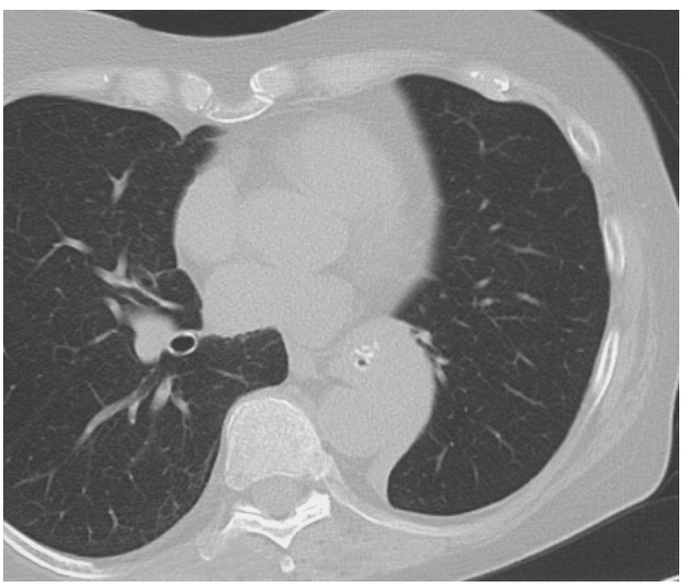

Fig. 4.8 The "S" sign on CT. The image shows a mass along the left lower lobar bronchus with lower lobar atelectasis peripheral to it. The walls of the segmental bronchi are calcified within the tumor. The left upper lobe shows compensatory emphysema.

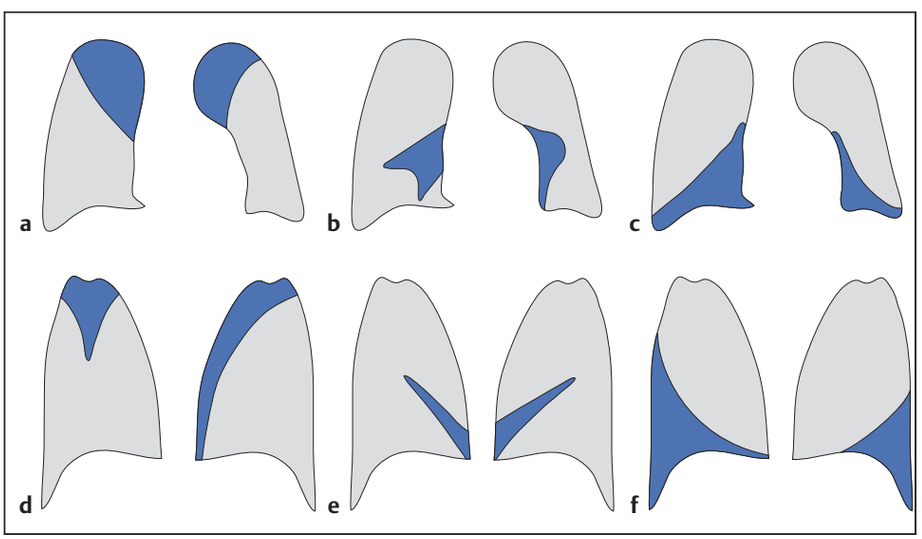

Fig. 4.9 a–f Forms of atelectasis. Figures **a–c** show findings on the posteroanterior projection; figures **d–f** show them on the lateral projection.
a, d Upper-lobe atelectasis.
b, e Atelectasis in the middle lobe and lingula.
c, f Lower-lobe atelectasis.

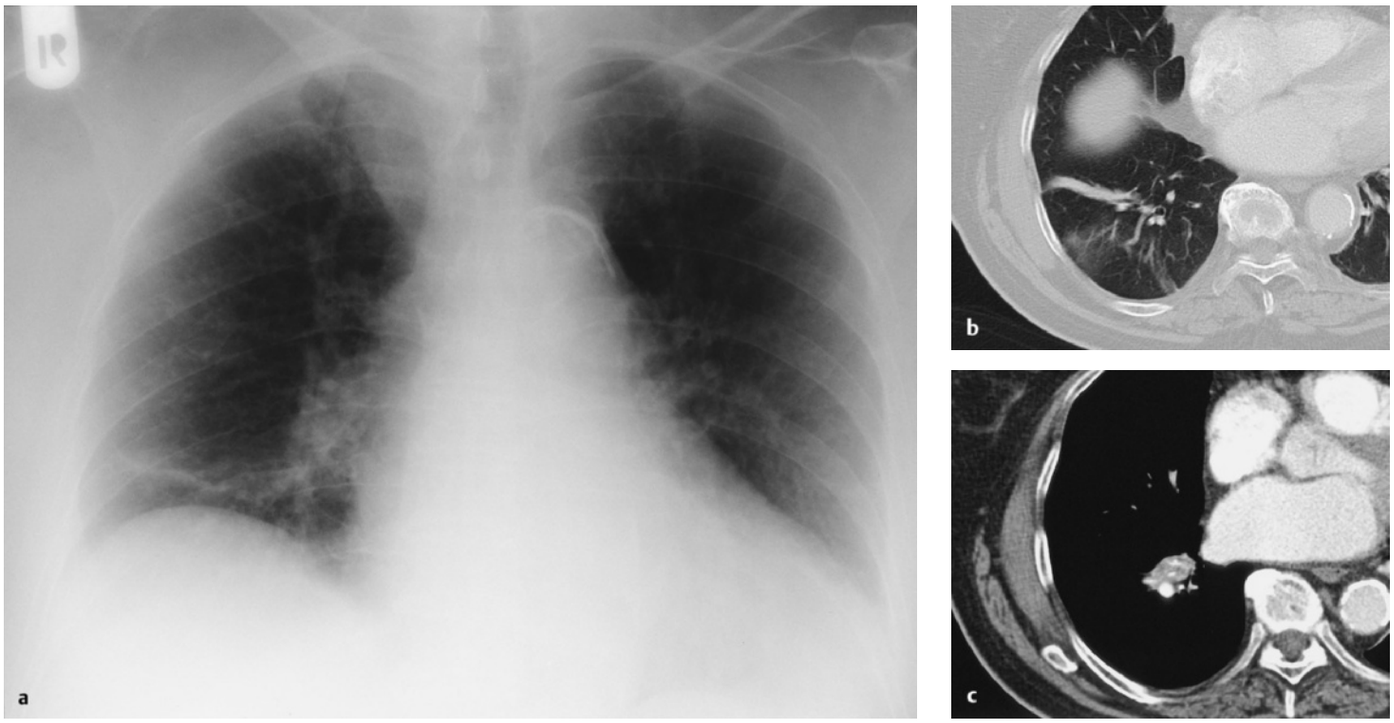

Fig. 4.10 a–c Dystelectasis as a warning sign of tumor. The patient is an 85-year-old woman with known coronary heart disease. She was admitted because of dyspnea. The heart shows global enlargement with moderate congestion in the pulmonary veins. There is aortic arteriosclerosis. Other findings include a relatively high-riding right diaphragm with platelike atelectasis in the right lower lung field (**a**). CT shows two areas of platelike atelectasis in segments 8 and 9 (**b**) with a 1.5-cm tumor at the bronchial bifurcation (**c**) showing marked partial enhancement.

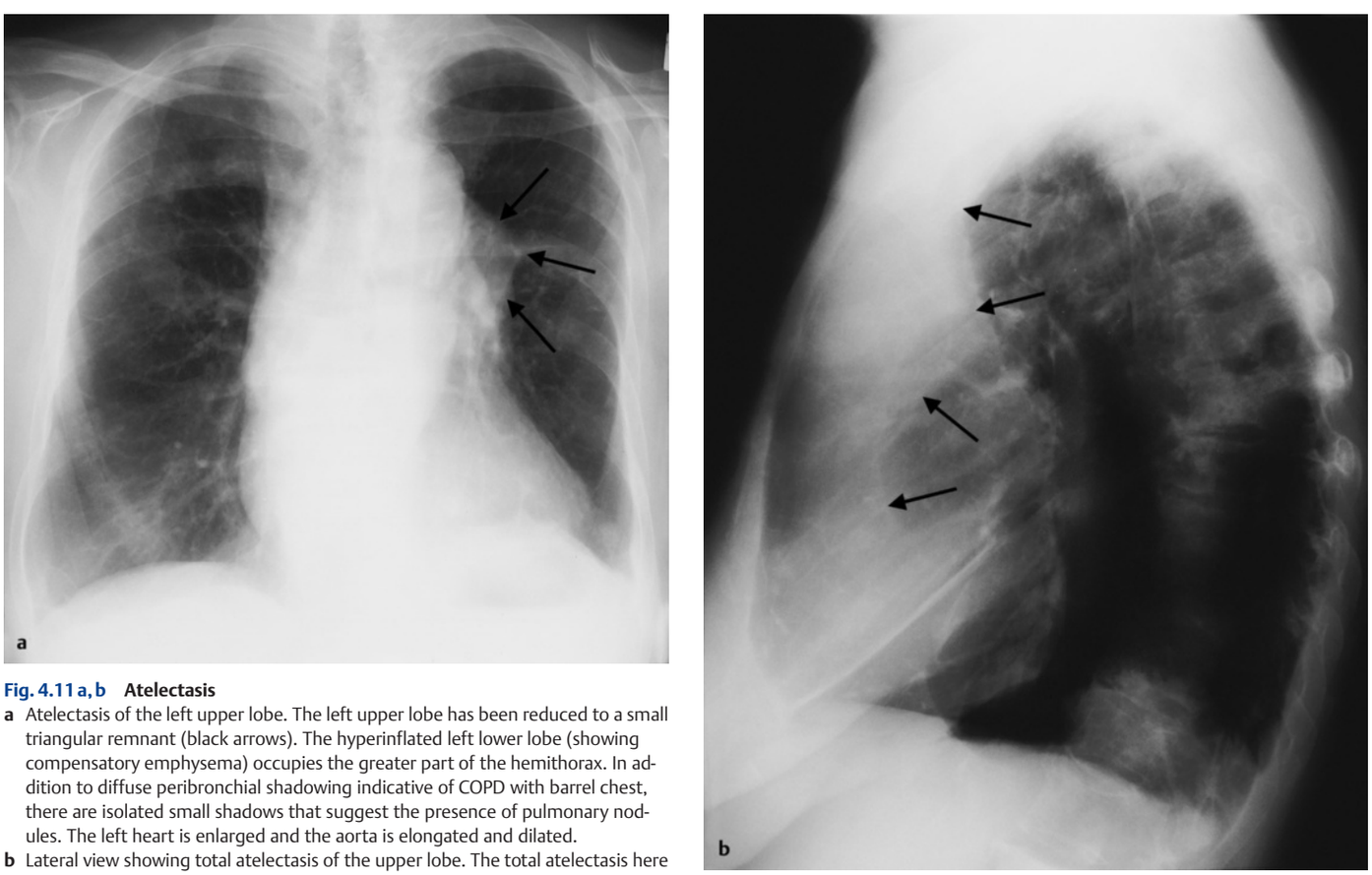

Fig. 4.11 a, b Atelectasis

a Atelectasis of the left upper lobe. The left upper lobe has been reduced to a small triangular remnant (black arrows). The hyperinflated left lower lobe (showing compensatory emphysema) occupies the greater part of the hemithorax. In addition to diffuse peribronchial shadowing indicative of COPD with barrel chest, there are isolated small shadows that suggest the presence of pulmonary nodules. The left heart is enlarged and the aorta is elongated and dilated.

b Lateral view showing total atelectasis of the upper lobe. The total atelectasis here appears as a radiodense retrosternal band (black arrows) that is easily missed. The radiolucent retrosternal space is completely overshadowed. Diffuse osteoplastic metastatic activity is observed with eburnation of individual vertebral bodies.

Excursus: Hilar Anatomy

Extrabronchial growth of a central bronchial carcinoma is directly detectable as disruption of normal hilar anatomy. The complex summation shadowgram of the hilum on a conventional radiograph is highly variable. This makes the diagnosis of a disease process located there very difficult in borderline cases, and their interpretation requires a lot of experience on the part of the radiologist. Occasionally one can accurately judge the size of calcified lymph nodes where they do not contribute to the border of the shadow. In an adult they can measure up to 3 cm without producing the typical picture of polycyclic thickening of the hilum. We feel this should not lead to the diagnostic fatalism that often prevails in such cases, because even significantly smaller changes can be detected when they occur at favorable locations.

The hilar shadow is the summation of the following structures:

- Pulmonary artery and its main branches
- Pulmonary veins
- Parts of the heart shadow
- Aorta, superior vena cava, azygos vein
- Pericardium
- Main and lobar bronchi
- Lymph nodes

Analysis of the hilar shadow focuses on two basic elements:

- Pulmonary arterial tree
- Bronchial tree

The analysis should begin with the lateral view (**Fig. 4.13**).

Lateral View

Step 1

The anatomic landmark is the broad, nearly vertical radiolucent band of the trachea. At its caudal end it merges with the main bronchi. The right main bronchus is often indistinct and rapidly darkens along its distal course. The left main bronchus is usually well visualized as a round circumscribed radiolucency. The anterior border of the tracheal band is readily recognizable by the fine undulating irregularities of its contour produced by the individual cartilage rings.

Step 2

The left branch of the pulmonary artery courses posteriorly in a tight arc above the round radiolucency of the left main bronchus. The right pulmonary artery is imaged end-on and appears as an anterior oval density slightly farther caudad.

The hilum resembles the hand of someone scratching his head in confusion: The index finger is the left pulmonary artery, the second metacarpal is the right pulmonary arterial trunk, and the rest of the hand is the heart (**Fig. 4.12**).

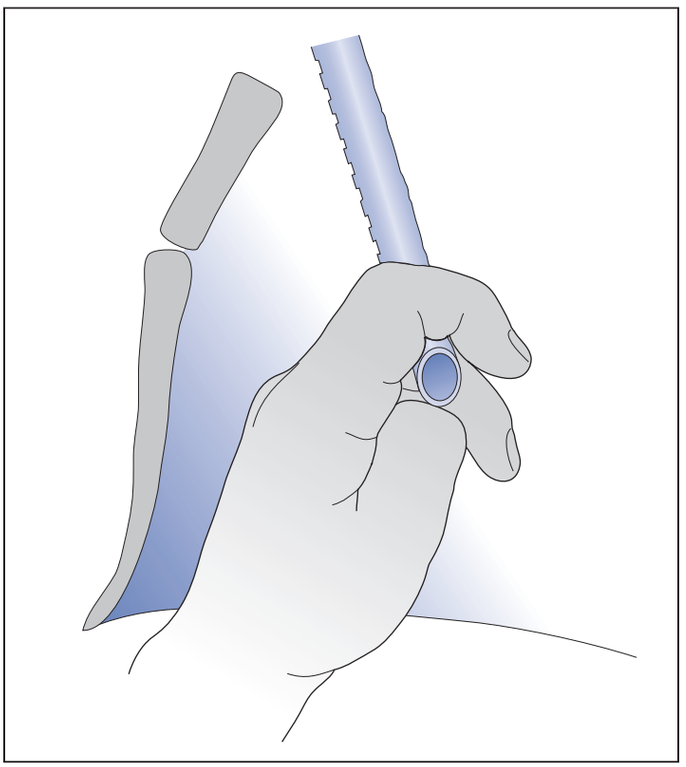

Fig. 4.12 **The lateral view of the hilum resembles a hand.**

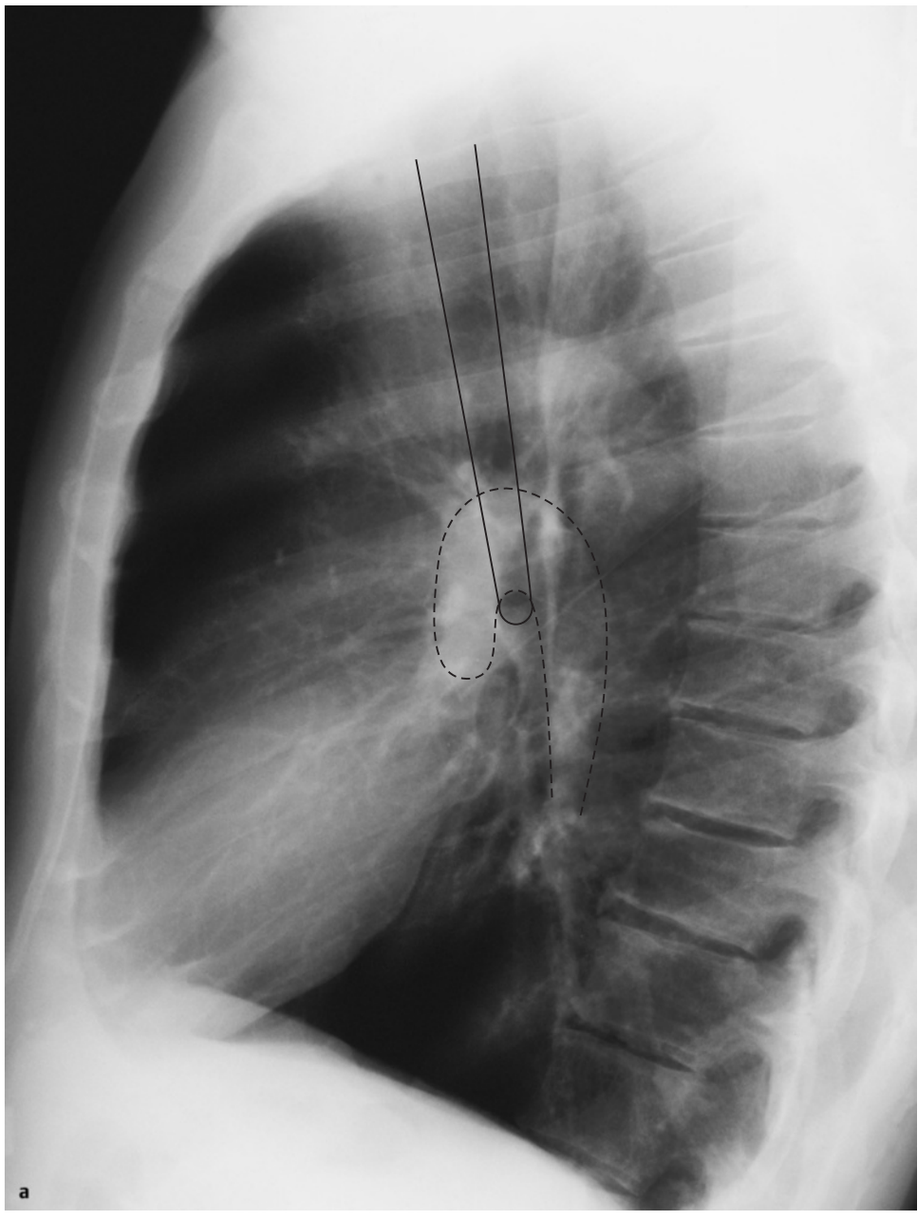

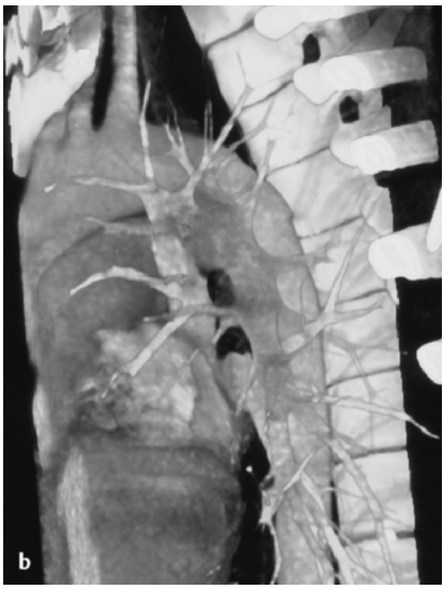

Fig. 4.13 a, b **Hilar anatomy**
a Lateral view with lines drawn to shown the tracheal band and the left and right main pulmonary arteries (dashed line).
b 3D CT reconstruction.

Posteroanterior View

The hilum is visualized less clearly on the posteroanterior radiograph (**Fig. 4.16**) than on the lateral film.

Left Hilum

The first step in analysis is to distinguish the left pulmonary artery from the aortic arch (aortic knob) to define what is known as the aortopulmonary window. The aortic arch and the left pulmonary artery are separated by an indentation. A protrusion into this aortopulmonary window regularly corresponds to pathology at this site (**Fig. 4.14**). Especially in adolescents, the arch of the pulmonary artery is particularly prominent (this is thought to be due to a physiologic jet effect). Yet even in these cases, a single arc defines the border above the left main bronchus; the contour is not polycyclic. The inferior lobe vessels of the left side are largely obscured by the left heart silhouette, although they become visible when the patient is rotated into the left anterior oblique (LAO) position.

Right Hilum

The right pulmonary artery (forming a precarinal oval on the lateral view) is not visible on the posteroanterior radiograph as it is completely obscured by the ascending aorta. The first right hilar structure to appear slightly caudal to the arch of the left pulmonary artery is the bifurcation of the right pulmonary artery into the common trunk of the superior lobe arteries and the intermediate artery. The intermediate artery has a maximum width of 1.6 cm. It is a fingerlike radiolucent band that courses caudally parallel to the middle bronchus and forms the greater part of the right hilum (**Fig. 4.15**).

We may therefore conclude that the analysis of the right hilum depends significantly on the examination of the structures of the bronchial tree. Unexposed radiographs are of little help here.

The bronchial system can usually be identified on digital images without any problem. First identify the radiolucent band of the trachea (slightly less than 2 cm wide) and trace it caudally as far as the carina. The spindle-shaped shadow visible directly in the angle between the right main bronchus and the trachea is the azygos vein. The dense structures visible above the origin of the right upper lobar bronchus correspond to the right superior lobe arteries. The density lateral to the caudally adjacent radiolucent structure (right middle bronchus) is the intermediate artery.

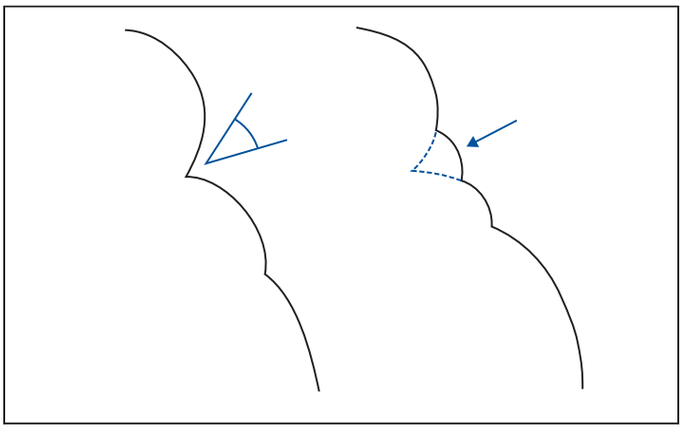

Fig. 4.14 Aortopulmonary window. There is normally an acute-angled indentation (∠) between the aortic arch and the left pulmonary artery. Any concavity at this site (arrow) should initially be regarded with suspicion.

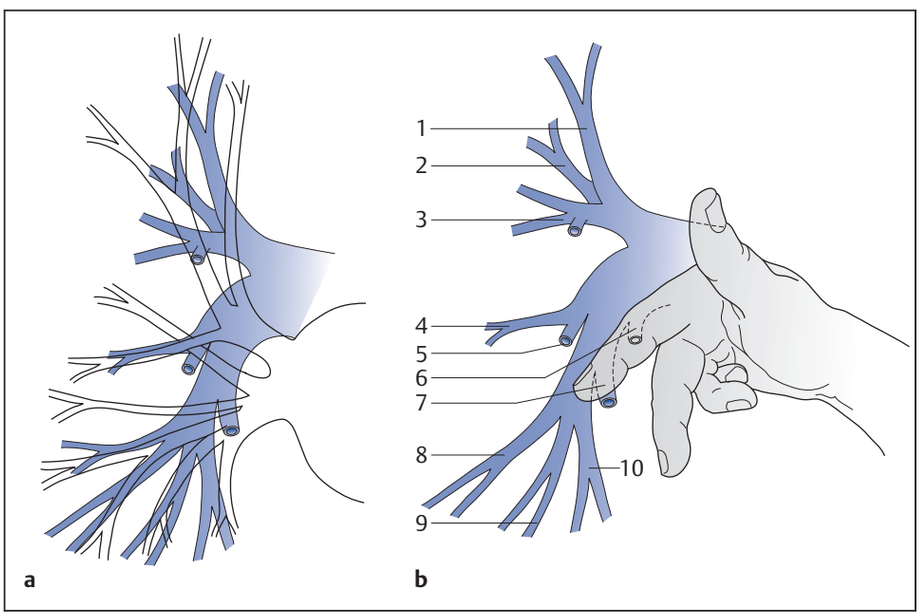

Fig. 4.15 a, b Right pulmonary arterial tree.
a Summation diagram of the pulmonary arteries (blue) and the pulmonary veins (transparent).
b Anatomy of the right pulmonary arteries.

1 Apical upper lobe
2 Posterior upper lobe
3 Anterior upper lobe
4 Lateral middle lobe
5 Medial middle lobe
6 Apical lower lobe
7 Medial basal lower lobe
8 Lateral basal lower lobe
9 Anterior basal lower lobe
10 Posterior basal lower lobe

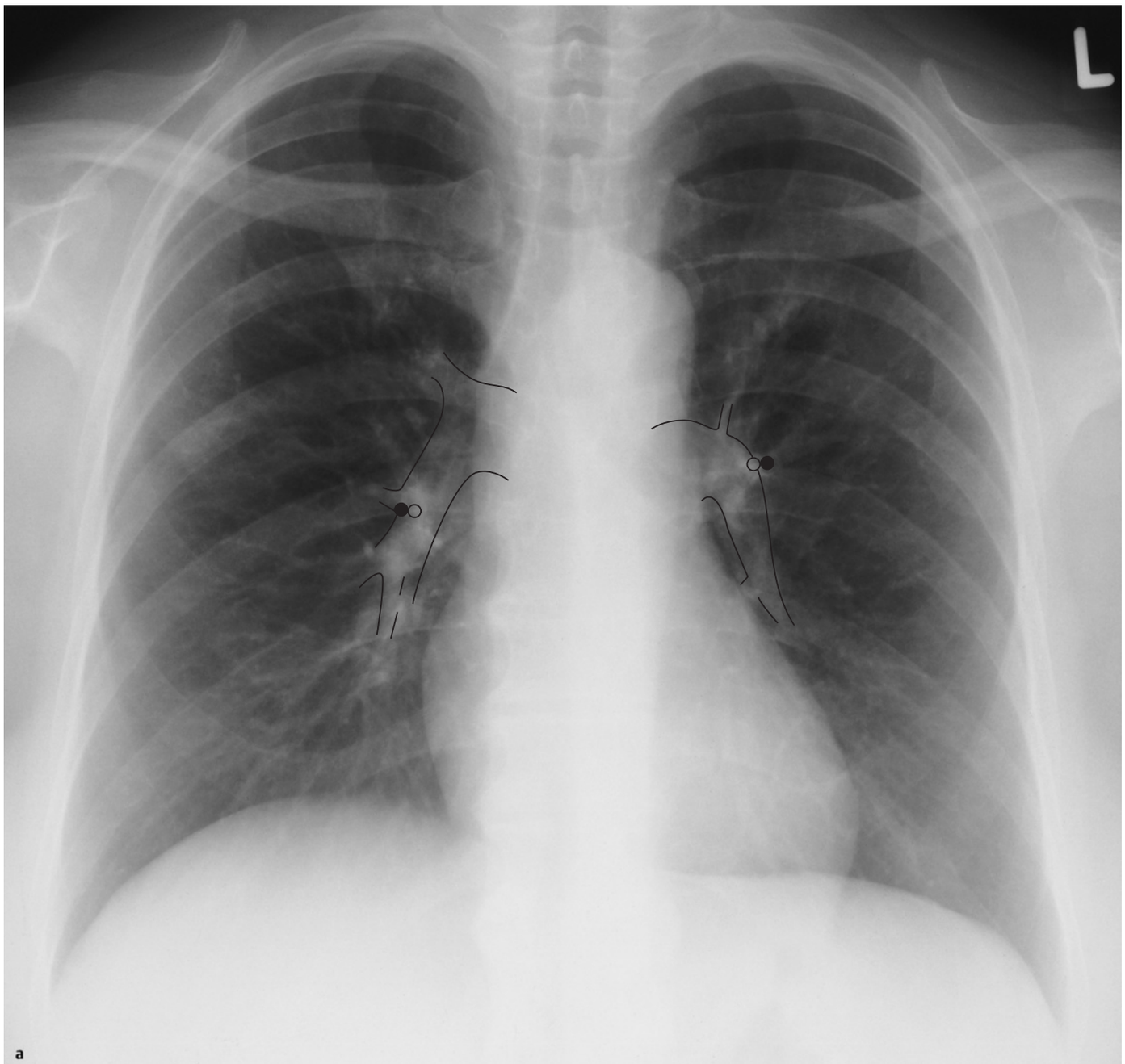

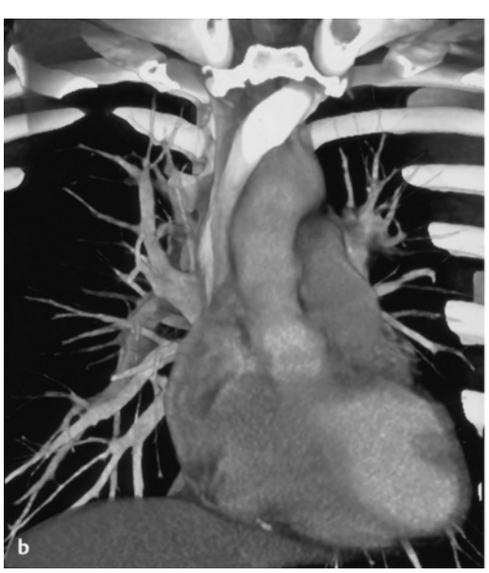

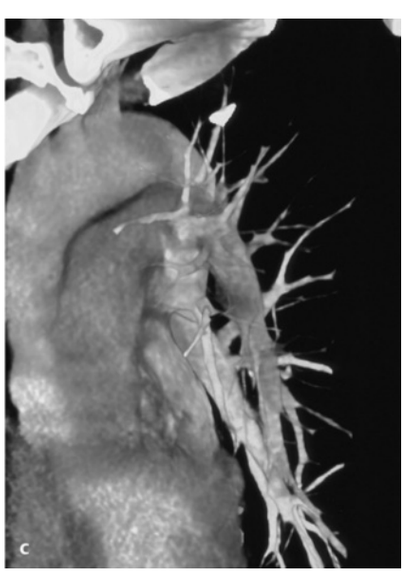

Fig. 4.16 a–c **Hilar anatomy**
a Posteroanterior view with the pulmonary arteries outlined.
b, c 3D CT in frontal (**b**) and parasagittal (**c**) reconstruction.

Simulated Central Bronchial Carcinoma

Plain Chest Radiograph

A polycyclic hilar contour should prompt the following questions before it is attributed to enlarged lymph nodes or a central mass:

- Was the film obtained in improper rotation?
- Is the view obscured by large pulmonary veins imaged end-on?
- Are there signs of COPD with obstructive barrel chest and increase of overall lung markings?
- Is there an abrupt change in caliber toward the periphery?

The basic elements of the hilum, i.e., the pulmonary arteries and bronchial tree, are normally clearly defined. However, overlying pulmonary veins (and there are many) can obscure these structures. One should be alert to these diagnostic pitfalls, which can simulate enlarged lymph nodes or a central tumor. Caution is required where the eccentric course of the superior pulmonary vein overlies the upper anterior portion of the oval of the right pulmonary artery. This vein often produces what appears to be a polycyclic contour at this site (**Fig. 4.18**). The left hilum often appears prominent in adolescents because the pulmonary valve can exhibit a physiologic jet that leads to dilatation of the left pulmonary artery (**Fig. 4.19**). Simple thickening of the pulmonary arteries in pulmonary arterial hypertension as in COPD (see Chapter 2, "Chronic Bronchitis") should not cause any significant diagnostic problems as generalized thickening of pulmonary arterial structures is observed in this case (**Fig. 4.20**)

The following strategy is helpful in differentiating masses from pulmonary arterial hypertension: Genuine polycyclic structures are invariably composed of multiple arcs. This means they have multiple centers at which their density will be greatest. Generalized hilar thickening differs in that density decreases toward the periphery. The center invariably shows the highest radiodensity (**Fig. 4.17**).

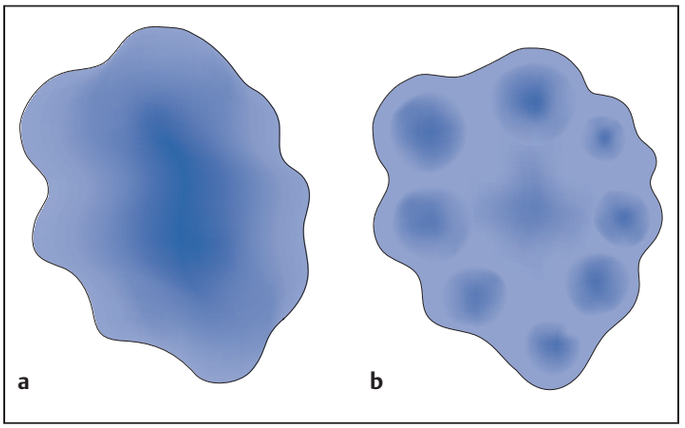

Fig. 4.17 a, b **Hilar thickening.** Differentiating generalized hilar thickening (**a**) from causes such as pulmonary arterial hypertension from polycyclic thickening (**b**) from causes such as enlarged hilar lymph nodes.

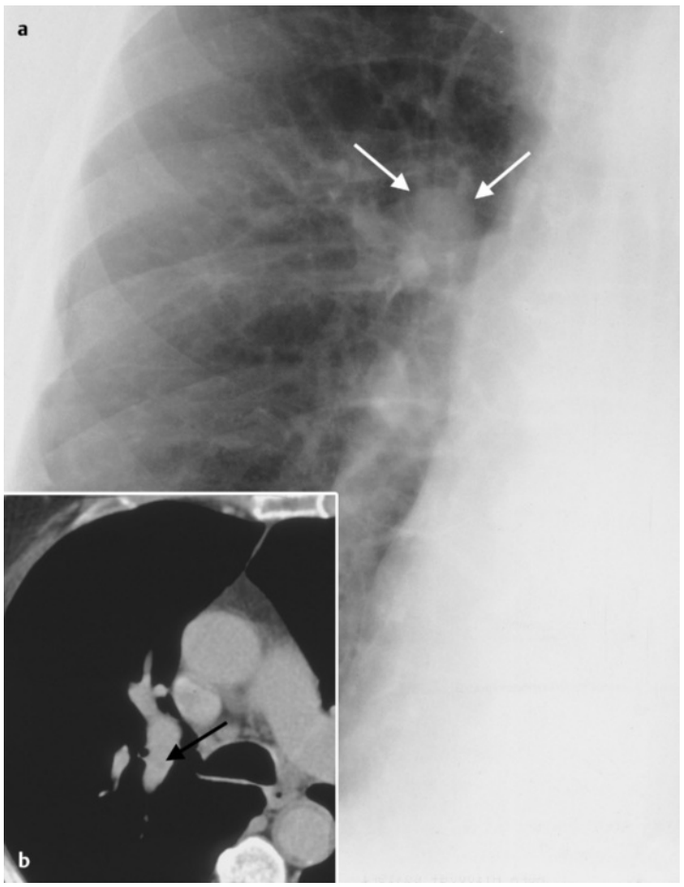

Fig. 4.18 a, b **Atypical course of the right superior pulmonary vein.**

a The posteroanterior view in this 64-year-old man with severe COPD shows a round mass slightly less than 2 cm in diameter at the origin of the right upper lobar bronchus (white arrows). The mass has a smooth peripheral border. Other findings include marked peribronchial shadowing and generalized hilar thickening in pulmonary arterial hypertension. Obstructive barrel chest.

b CT scan showing the atypical course of one of the right superior lobe arteries. The density is caused by a dilated posterior superior pulmonary vein (black arrow) coursing posteroanteriorly across the bifurcation of the anterior and posterior segmental bronchi.

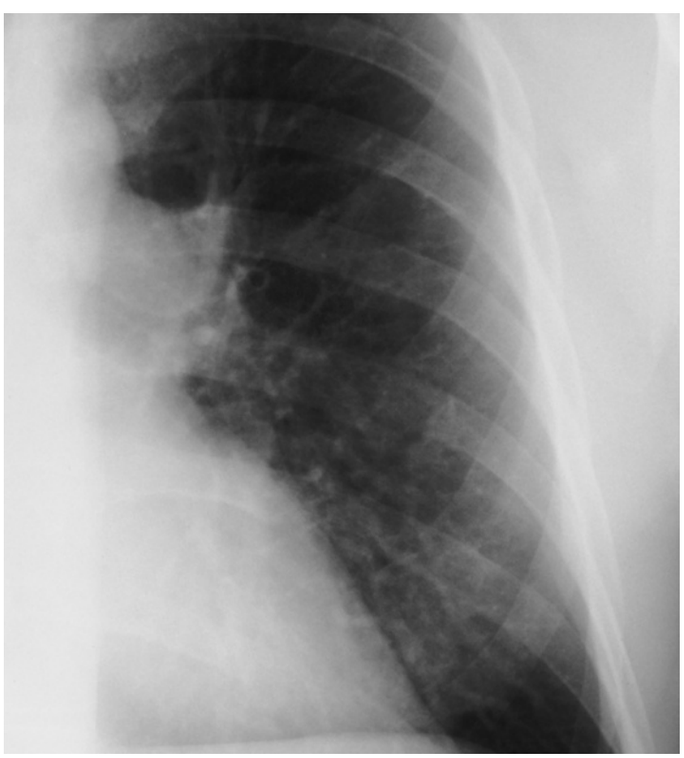

Fig. 4.19 **Jet in an adolescent (posteroanterior view).** Prominent left pulmonary artery. There is no protrusion into the aortopulmonary window. The left pulmonary artery exhibits a smooth border and normal taper.

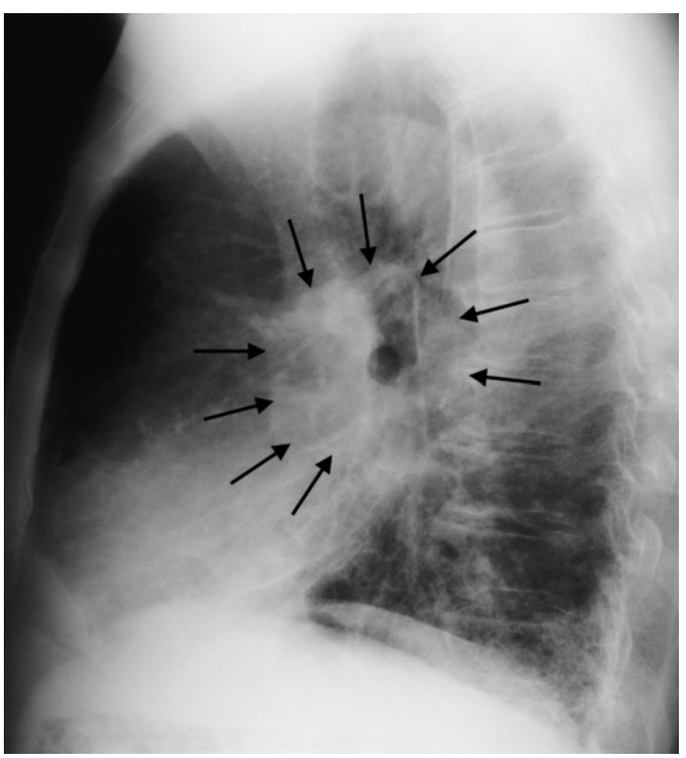

Fig. 4.20 **Significant thickening of all hilar structures in pulmonary arterial hypertension.** Findings on a preoperative chest radiograph of a 79-year-old male smoker. There is diffuse peribronchial shadowing in a finely nodular pattern. Areas of basal fibrosis are beginning to show honeycombing. There is global heart enlargement without signs of decompensation. The entire hilum is homogeneously thickened (black arrows). **Caution:** The thickened structures are always densest at the center.

Computed Tomography

Although the unobstructed visualization on CT of the chest eliminates many of the diagnostic pitfalls of conventional radiography, certain findings can simulate a central bronchial carcinoma. Such phenomena include:

- A pseudomass at the bifurcation of the right pulmonary artery into the common trunk of the superior lobe arteries and the intermediate artery (**Fig. 4.22**)
- Endobronchial mucus accumulations (**Fig. 4.23**)
- Carnified central pneumonia
- The confluence of the atrial veins in the presence of pericardial evaginations (**Fig. 4.21, Fig. 4.24**)
- Left superior pulmonary vein partially coursing through the mediastinum
- Duplication of the superior vena cava
- Large pleural effusion with a subpulmonary component extending into the center (**Fig. 4.25**)

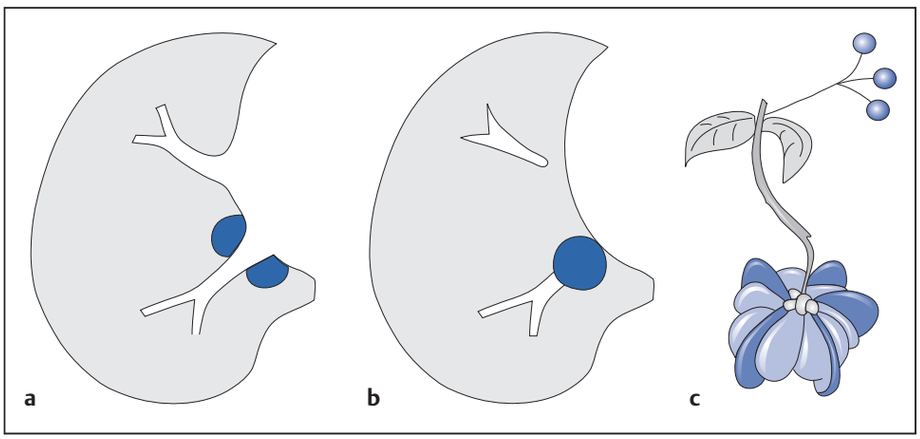

Fig. 4.21 a–c The "biretta" figure of the atrial venous confluence. Pericardial evaginations surrounding the atrial venous confluence (**a**) are common findings, especially in the right lower field. A partial volume effect on the next slice below the reconstruction can produce what appears to be a round focal lesion (**b**). The shape of the pericardial evaginations occasionally resembles a clerical biretta or the flower of the spindle tree (**c**).

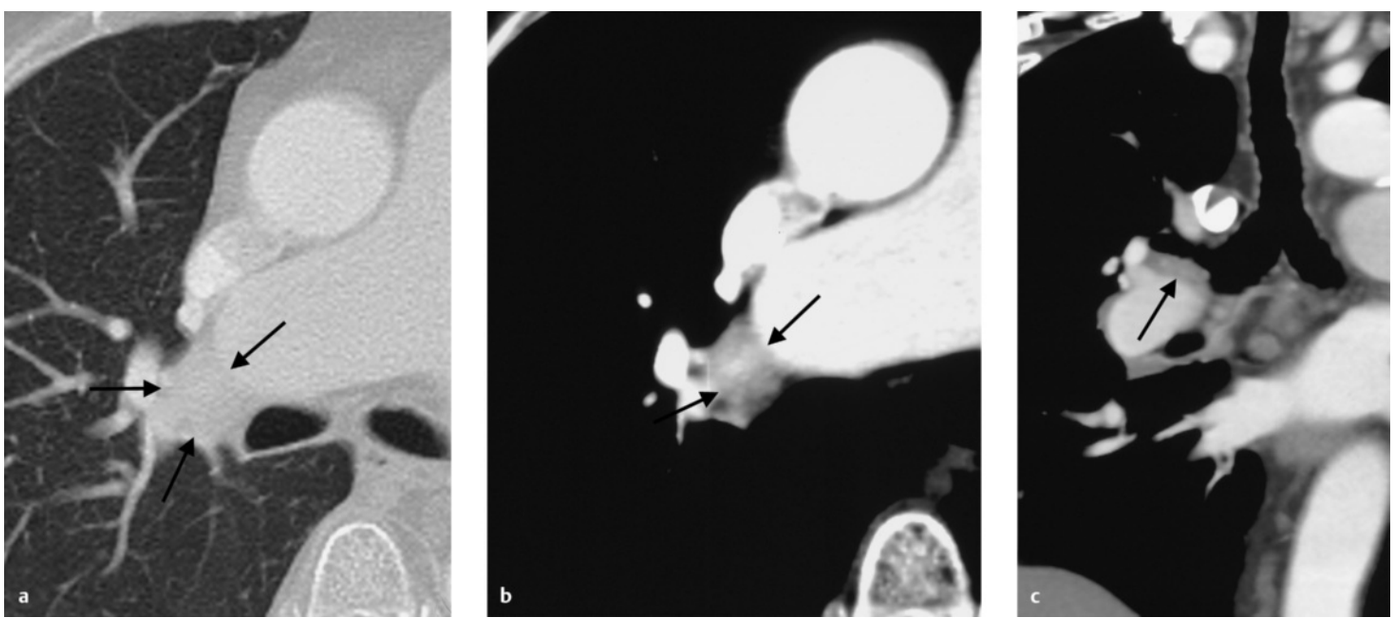

Fig. 4.22 a–c Pseudomass at the bifurcation of the right pulmonary artery. The axial view at the bifurcation of the right pulmonary artery shows what appears to be a mass 2 cm in diameter with the density of soft tissue (**a, b**, black arrows). 3D reconstruction (**c**): the pseudomass corresponds to soft tissue normally located above the right intermediate artery (black arrow).

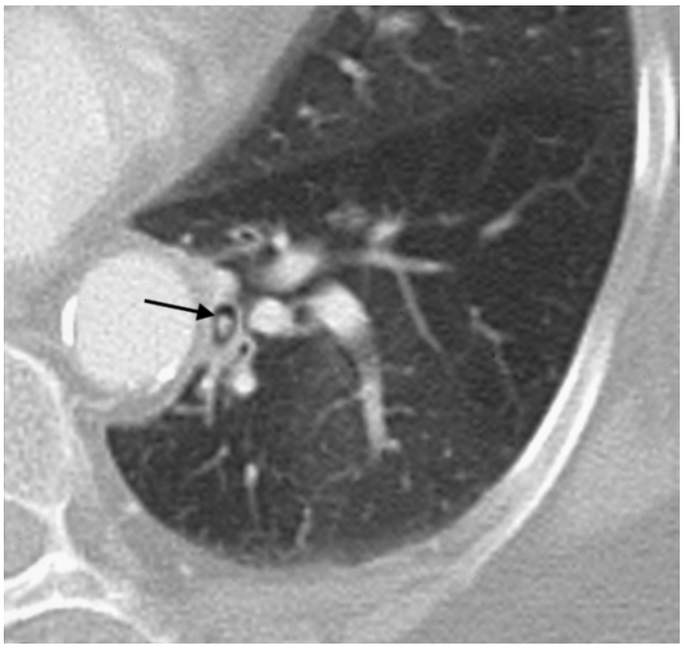

Fig. 4.23 Endobronchial mucus accumulation. In the bronchus of segment 6, there is a formation of soft-tissue density (black arrow) corresponding to a mucus inclusion.

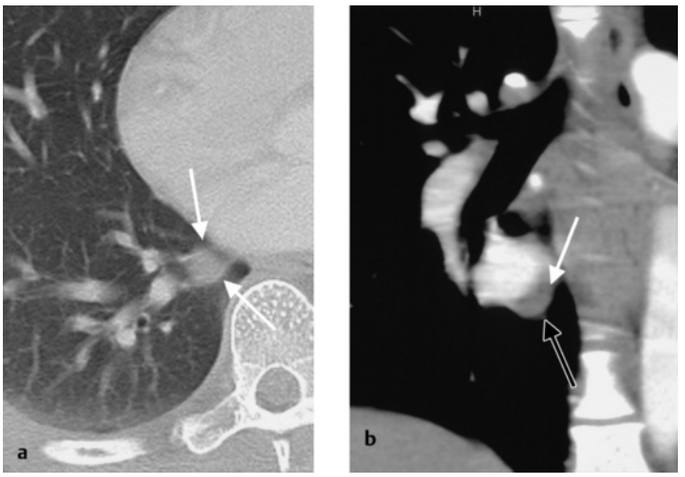

Fig. 4.24 a, b Pseudomass at the pericardial evagination at the entry of the right inferior pulmonary vein ("biretta figure"). The evagination surrounding the vein can resemble a central mass on the axial view (arrows).

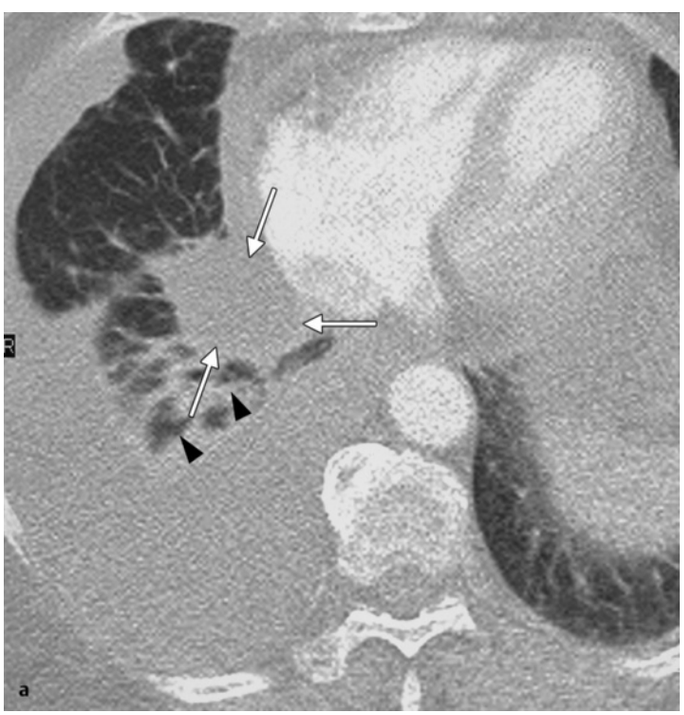

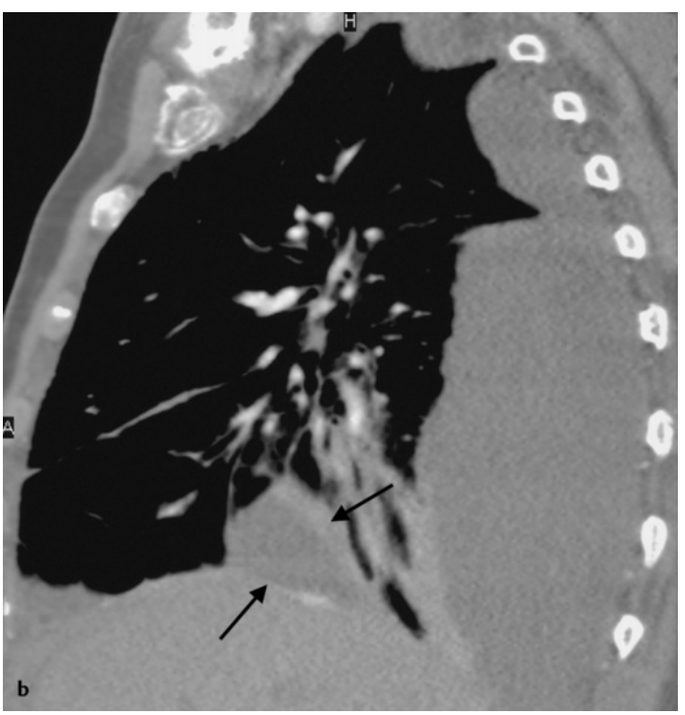

Fig. 4.25 a, b Central pleural effusion

a Large effusion of unknown origin on the right side. Presence of blood suggests malignant etiology. CT demonstrates what appears to be a large central mass in the lower lobe (white arrows).
Caution: The hypoventilation (black arrowheads) is clearly attributable to the effusion and not the apparent central mass.

b 3D CT reconstruction. In addition to the large posterior pleural effusion, the sagittal reconstruction shows a subpulmonary component of the effusion (black arrows) that mimics a central mass.

Direct Signs

Contour deformities of the hilar structures can be caused by (**Fig. 4.26**):

- Arcuate protrusions
- Local thickening
- Polycyclic margins
- Streaky shadowing

With the first three items, one should first exclude benign causes of hilar thickening such as pulmonary arterial hypertension or a physiologic jet in the left pulmonary artery in younger patients. Additional diagnostic studies are indicated in the absence of any signs of such causes.

Protrusion

The most common direct sign of a central bronchial carcinoma is a circumscribed arcuate protrusion of the hilum. This can lead to a polycyclic form (**Fig. 4.27**) or to asymmetrical extension of the hilum in an unusual direction.

Hilar Streaky Densities

Streaky densities in or around the hilum require special attention (**Fig. 4.28**). These are signs of distraction of pulmonary architecture or local infiltration of the lymph vessels.

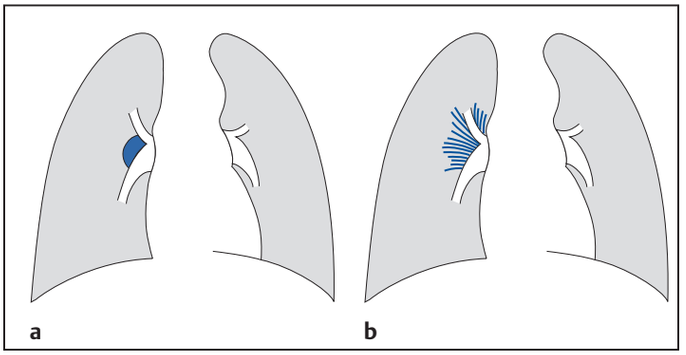

Fig. 4.26 a, b **Diagram of contour deformities.** Hilar contour deformities can be classified as protrusions (**a**) or streaky perihilar shadowing (**b**).

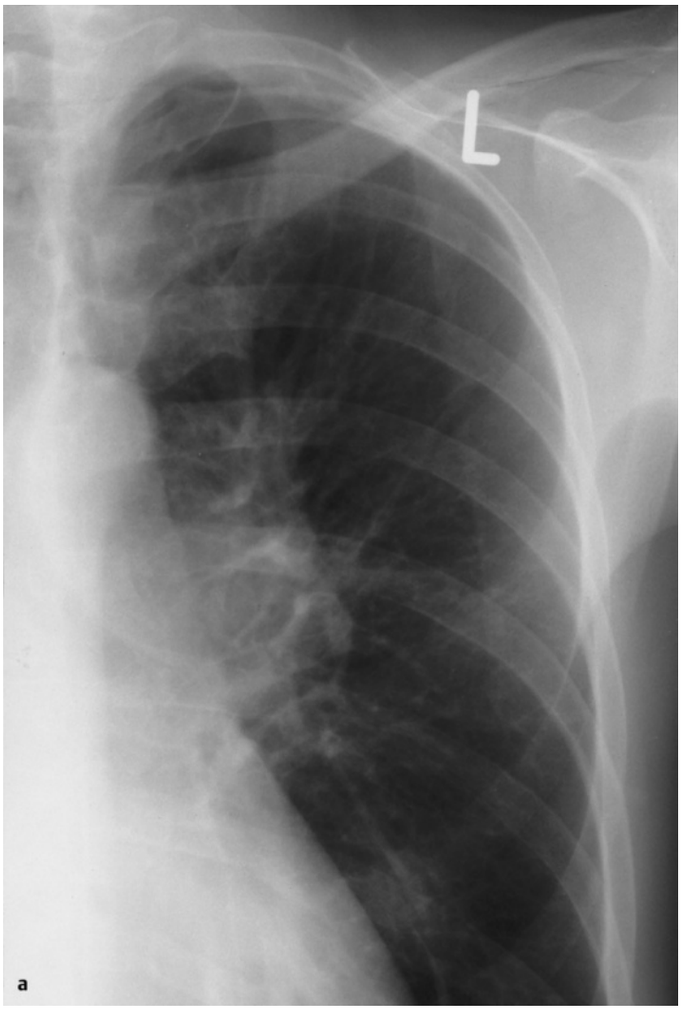

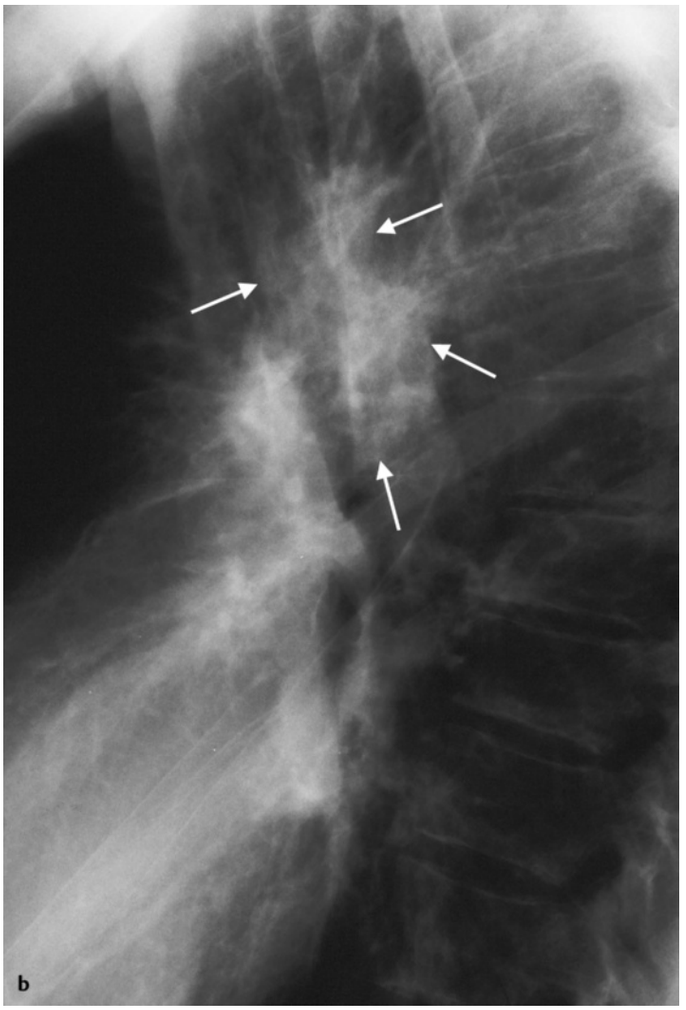

Fig. 4.27 a, b **Direct visualization of a left central bronchial carcinoma.**

a Obvious polycyclic contour of the left hilum in a 52-year-old man. Severe smoker's bronchitis.

b Lateral view. Asymmetric shift in the cranial border of the hilum in the vicinity of the left pulmonary artery. There is now no single point of maximum density but multiple peripheral epicenters (white arrows).

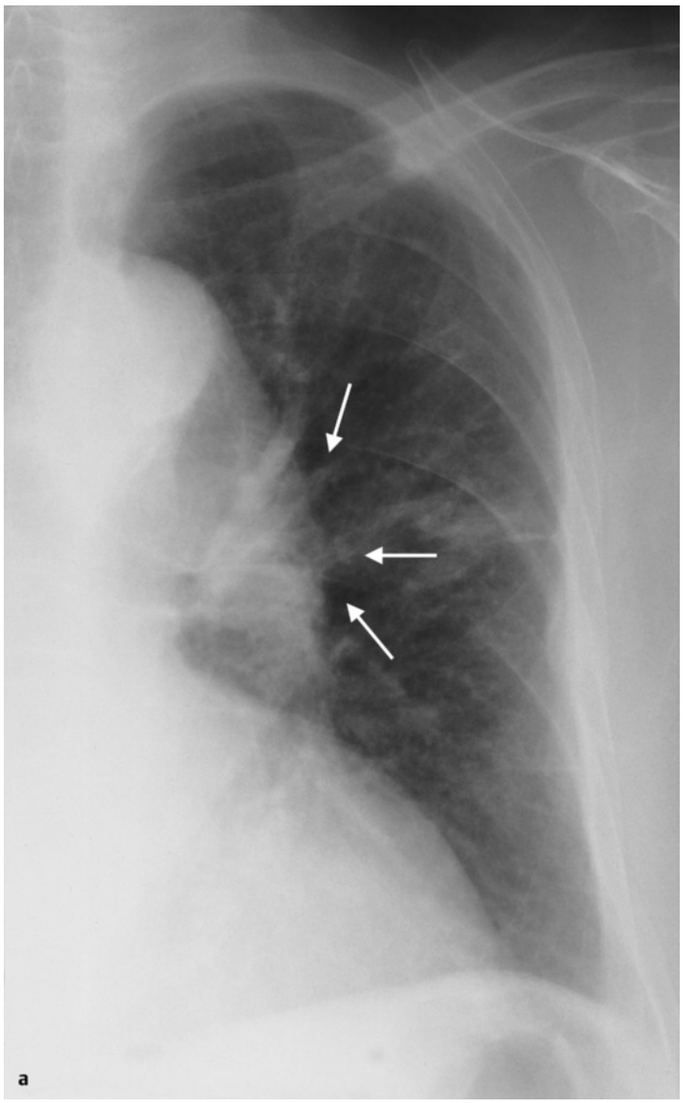

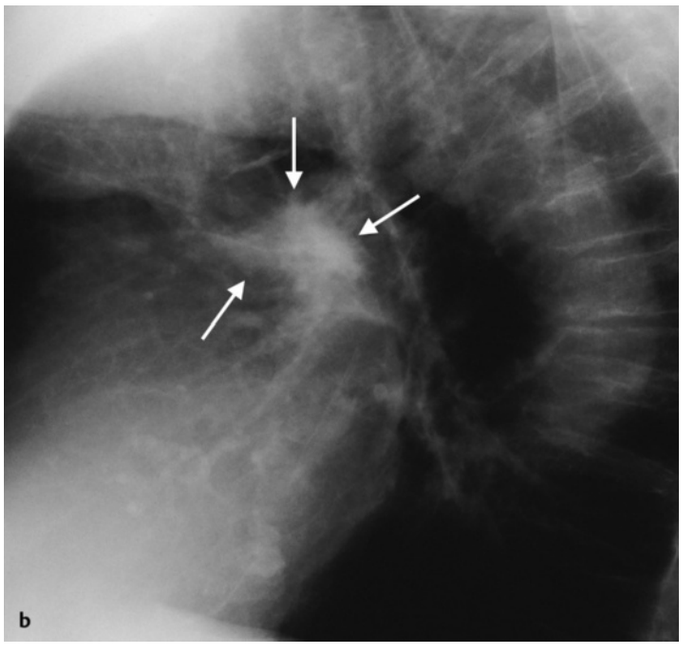

Fig. 4.28 a–c Direct visualization of a left central bronchial carcinoma with perihilar streaky densities (detail enlargement).

a The posteroanterior view shows a conspicuous radial pattern of perihilar shadowing on the left side (white arrows). Aortic dilatation.

b On the lateral view there is an asymmetrical density on the pulmonary trunk with small white streaky spiculations (white arrows).

c CT image. The left central tumor located between the pulmonary arteries (black arrow) and superior pulmonary vein (white arrow) reveals itself on the contrast-enhanced CT reconstruction as a less dense focal lesion with streaky radiating spiculations (black arrowheads).

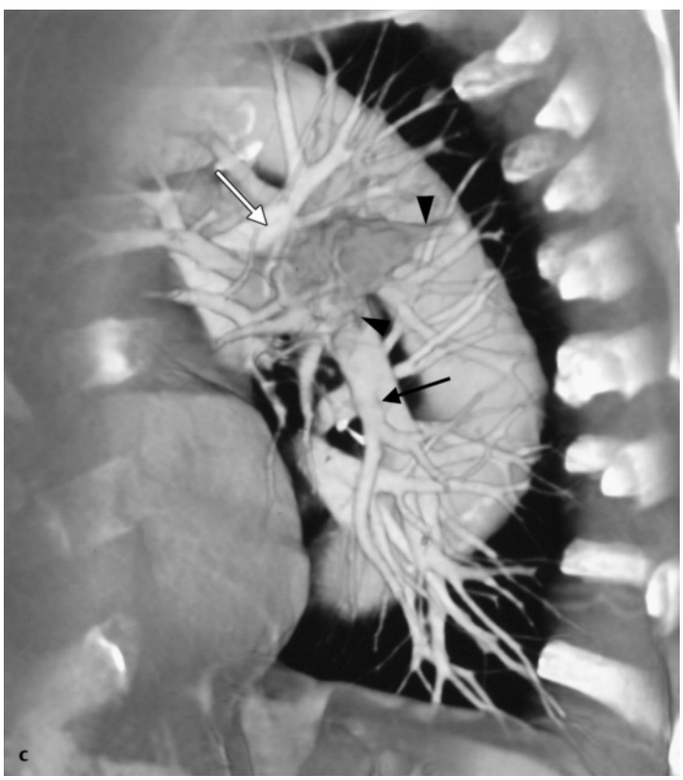

Peripheral Bronchial Carcinoma

Detection of Focal Lesions

Peripheral bronchial carcinoma arises in the segmental bronchi and their branches. Alveolar cell carcinoma occurring in the terminal bronchi and alveoli is discussed separately due to its distinctive features (see p. 190). Spread is primarily centripetal along the bronchi into the hilar and mediastinal lymph nodes. A different, centrifugal type of spread breaches the margin of the lung and progresses beyond it (Pancoast tumor).

The first step, which forms the basis for detecting a peripheral bronchial carcinoma, is that the observer establishes that a *focal density* is actually present in the pulmonary parenchyma and is not attributable to an artifact, superimposed external object, or anatomic variant. Familiarity with the numerous diagnostic pitfalls (**Fig. 4.29**) is essential to avoid unnecessary diagnostic studies. Whereas the radiation involved in an additional chest radiograph may be viewed as relatively harmless, a superfluous CT examination must be regarded far more critically. However, if after consideration of all the diagnostic pitfalls listed in **Table 4.3**, doubt remains as to the intrapulmonary location of the lesion, then these modalities are indicated.

The pitfalls listed in **Table 4.3** do not pertain to the incorrect *interpretation* of an intrapulmonary focal lesion (for example, classifying a postinfectious focal lesion in the upper lobe as malignant), but only to the detection of the lesion itself. In the following section we distinguish three separate errors:

- Incorrectly assuming the presence (**Fig. 4.30**) of a peripheral bronchial carcinoma (false-positive)
- Missing the tumor (false-negative; **Fig. 4.31**)
- Failing to classify the finding as malignant (also false-negative)

Recent studies have shown that false-negative evaluations are more often due to misinterpreting the finding than to missing it.

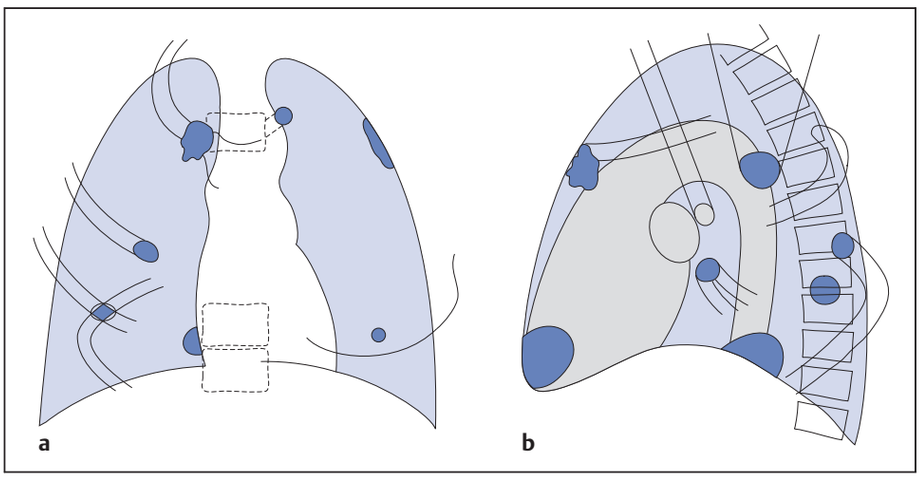

Fig. 4.29 a, b Diagnostic pitfalls: Detection of peripheral focal lesions on the posteroanterior (a) and lateral (b) radiographs. Anterior rib ends and intersections, nipple shadows, costotransverse joints, lateral spondylophytes, diaphragmatic hernias, and other structures can contribute to misinterpretation.

Table 4.3 Diagnostic pitfalls of intrapulmonary focal lesions

Posteroanterior View	Lateral view	
▶ First sternocostal joint ▶ Costotransverse joint (especially II–IV on the left) ▶ Lateral spondylophyte ▶ Anterior rib ends ▶ Intersection of anterior and posterior ribs	▶ Sternocostal joints ▶ Costovertebral joints ▶ Lateral spondylophytes ▶ Caudal end of the scapula	Bony
▶ Nipple shadows ▶ Diaphragmatic hernia	▶ Diaphragmatic hernias ▶ Pleuropericardial calluses ▶ Venous confluence at the left atrium	Other

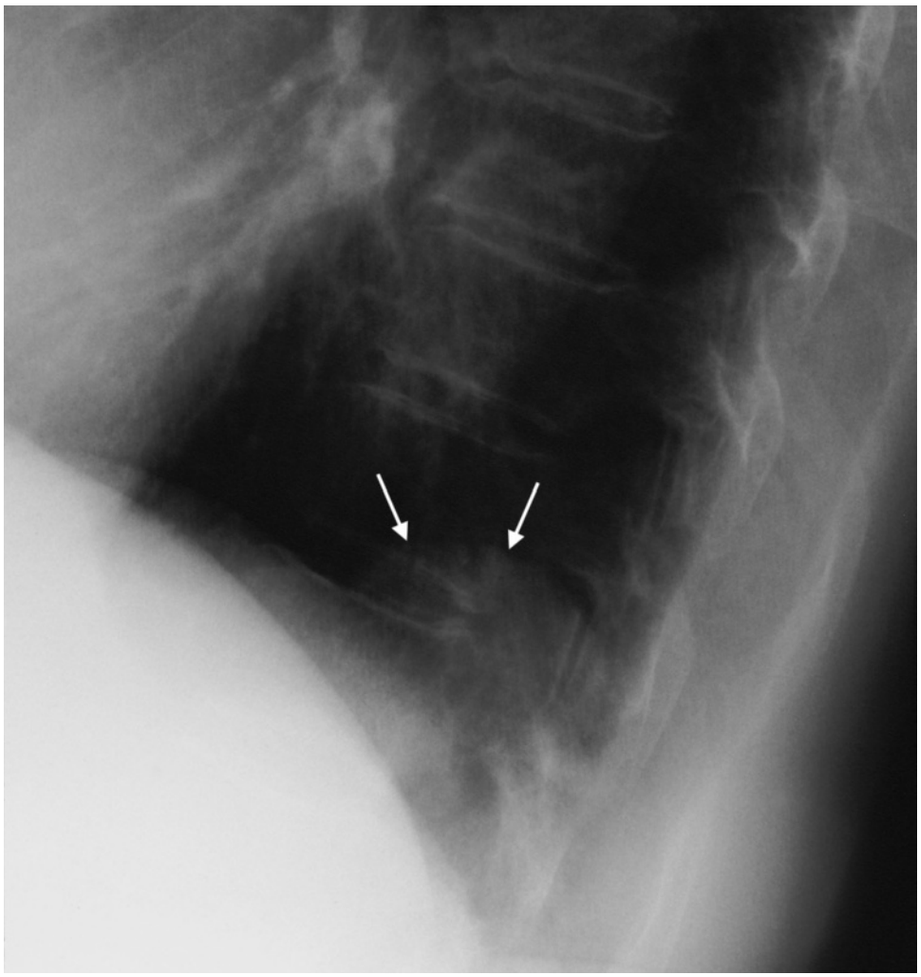

Fig. 4.30 Diaphragmatic hernia simulating a peripheral focal lesion. A smoothly demarcated mass measuring 4 cm (white arrows) is seen near the diaphragm in the left lower lung field.

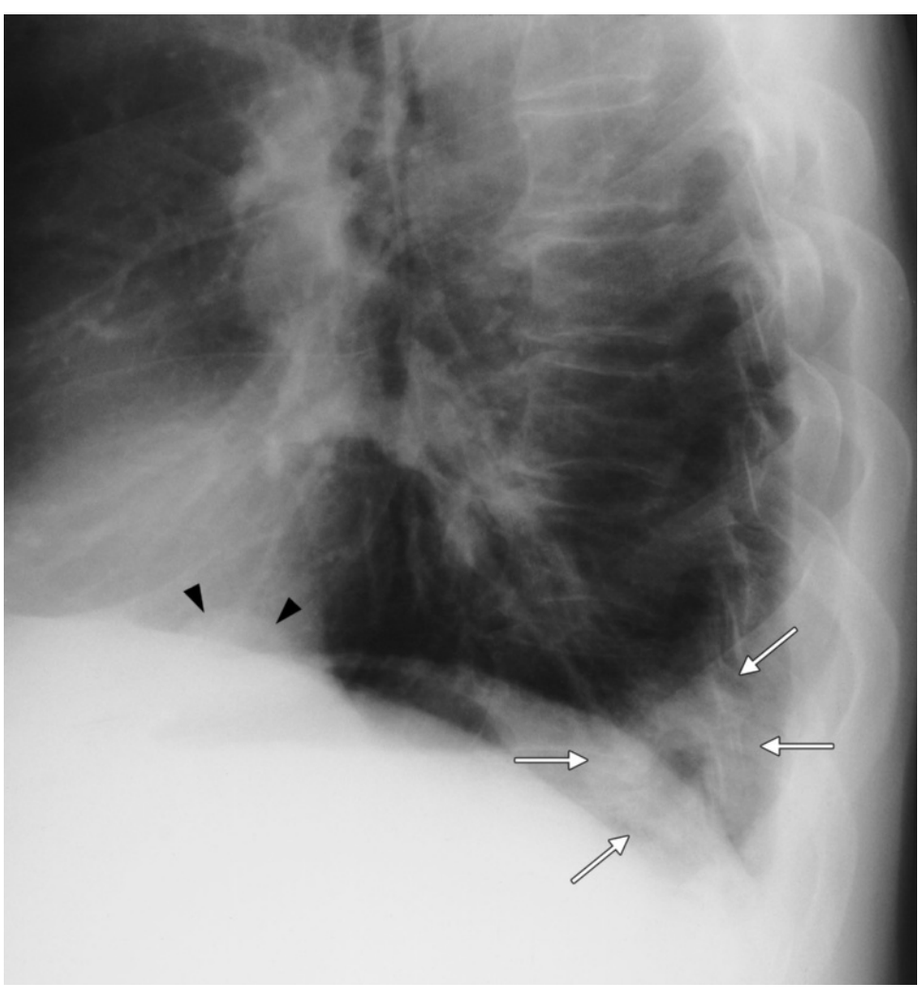

Fig. 4.31 Masked lesion in the posterior costophrenic angle. The posterior margin of the 11th thoracic vertebra, the 11th and 12th facet joints, and the 11th costotransverse joint almost completely obscure the 4-cm lesion (white arrows). A 2.5-cm peripheral focal lesion in segment 9 (black arrowheads) is also difficult to recognize because it resembles a small diaphragmatic hernia.

False-Positive Findings

Misinterpreting the lamellar ossifications of the osteochondral junction of the first rib (**Fig. 4.33, Fig. 4.34**) is regarded as a typical beginner's error. While this may be largely true, evaluation is not always a trivial matter. We know of several cases involving false-negative evaluations of peripheral focal lesions at this location (**Fig. 4.35**). Comparative examination of the contralateral side can aid in avoiding the tragic pitfall of such a misinterpretation. Does it also show such strange ossifications? Previous studies are also helpful. Have the calcified findings remained constant over time?

Less often the **costotransverse joints** of the upper thoracic spine can simulate intrapulmonary focal lesions. Such cases usually involve the left paramediastinal region on the posteroanterior radiograph.

One common cause of false-positive findings is misinterpretation of circumscribed shadows caused by the **ends of the ribs** (**Fig. 4.36**) or by the **intersection of two ribs** or a **rib and a vascular structure.** Precise analysis then identifies the figure, which occasionally is not round but often ellipsoid or even rhomboid.

Nipple shadows are usually sharply demarcated on the posteroanterior radiograph (air–soft tissue interface). They typically occur in the fifth intercostal space. Identification is facilitated by symmetrical contralateral findings.

Spondylophytes on the lateral radiograph (**Fig. 4.37**) can simulate focal lesions and masses of significant size. Such pseudotumors typically occur in the middle and lower thoracic spine and are projected onto the overlying posterior portions of the lung. The center of the respective density characteristically lies over the intervertebral space (**Fig. 4.32**).

On the lateral view the inferior pulmonary veins are often imaged end-on close to their mouths, especially in the middle segments of the lower lobes. They can produce figures resembling focal lesions. On the posteroanterior view, blood vessels imaged end-on can easily be misinterpreted as focal lesions close to the hilum, especially in the presence of central venous congestion or pulmonary arterial hypertension.

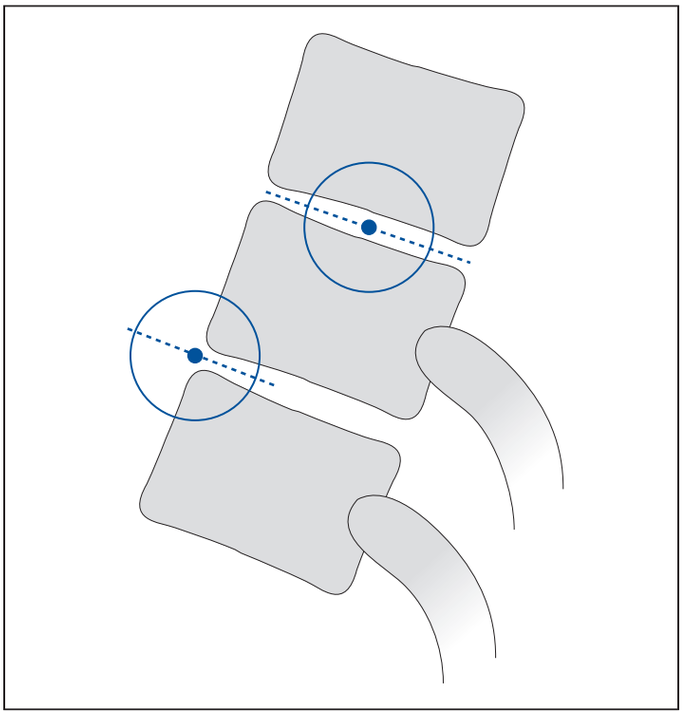

Fig. 4.32 Schematic diagram of the appearance of the lateral spondylophyte. The center of the round shadow caused by a lateral spondylophyte invariably lies at the level of the intervertebral space.

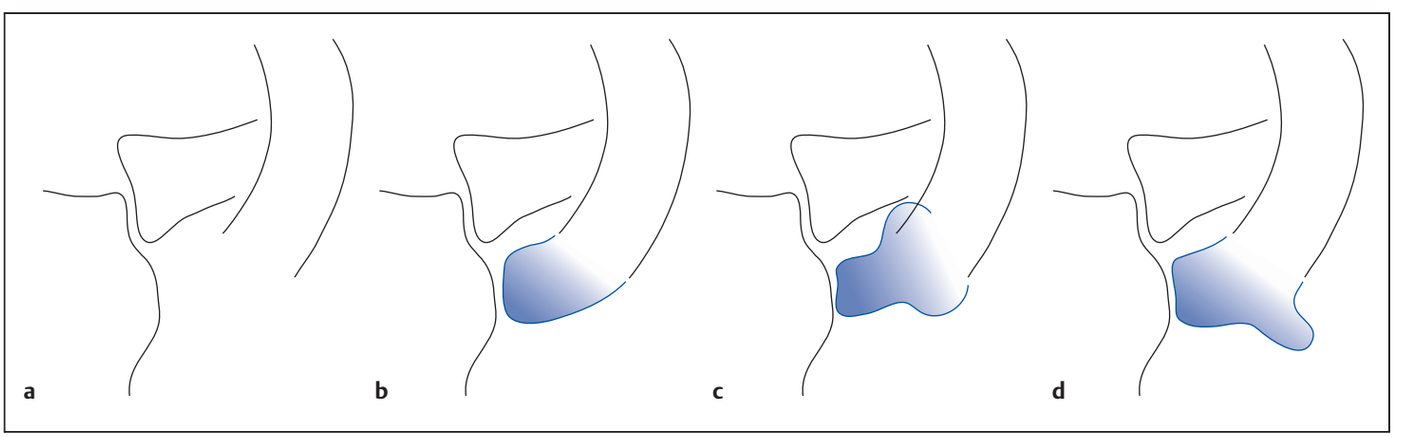

Fig. 4.33 a–d Appearance of the first sternocostal joint and the osteochondral junction of the first rib. The medial end of the first rib is highly variable. It can gradually disappear (**a**), ossify to produce particularly dense rib ends (**b**), exhibit polycyclic expansions (**c**), or show caudal spurs (**d**).

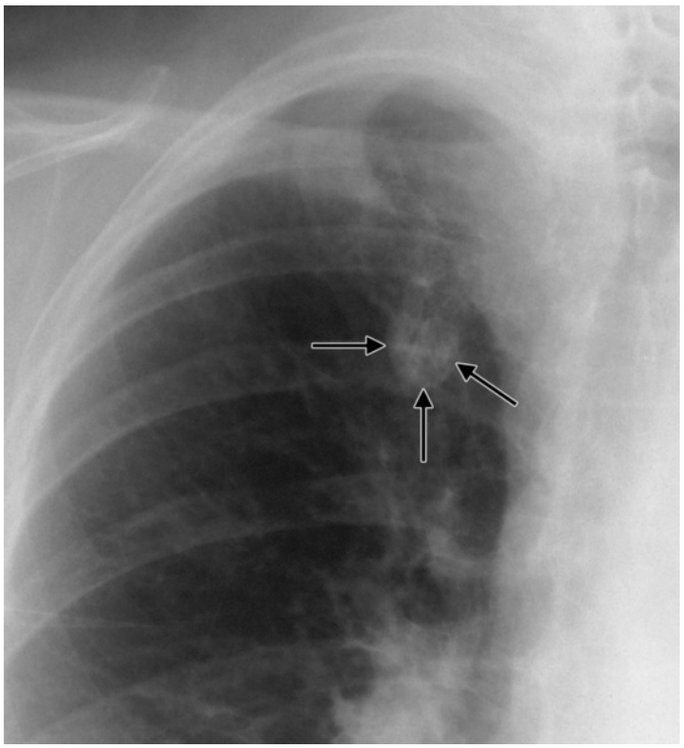

Fig. 4.34 Peripheral focal lesion simulated by atypical ossification of the osteochondral junction of the first rib. The relatively dense shadowing on the inferior margin of the first rib (black arrows) is sharply demarcated only over two-fifth of its circumference.

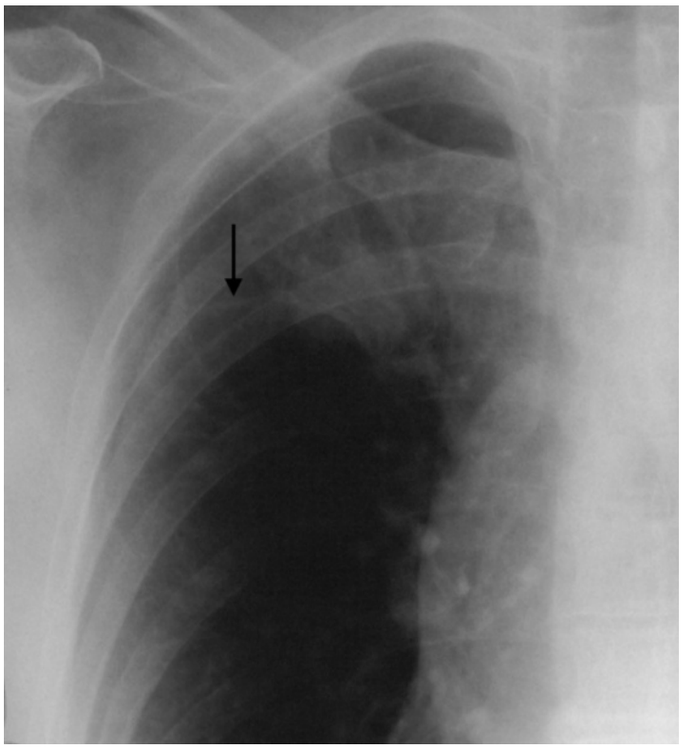

Fig. 4.35 Bronchial carcinoma masked by the first rib. Findings include a carcinoma 2.5 cm in diameter in the right upper lobe and conspicuously small platelike areas of hypoventilation extending laterally from the focal lesion (black arrow).

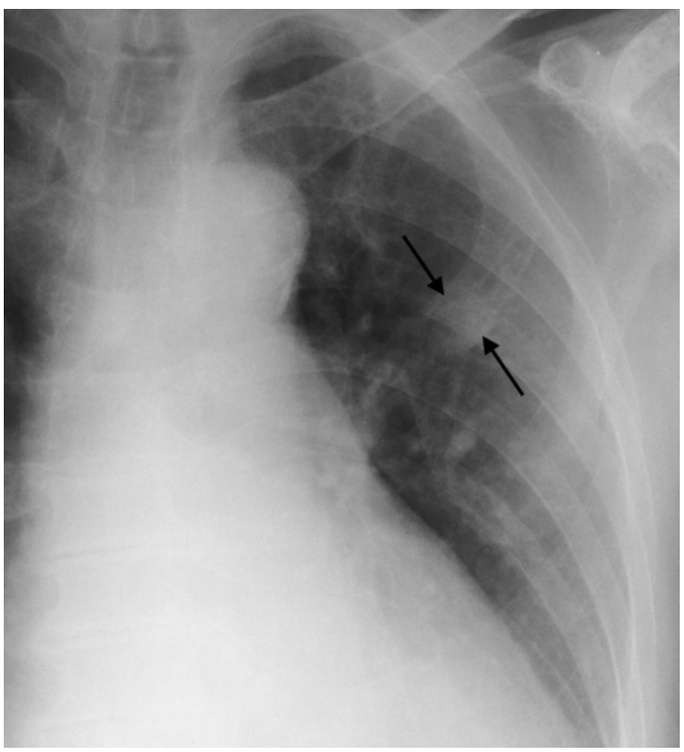

Fig. 4.36 Peripheral bronchial carcinoma in the left lung, obscured by a rib. A focal lesion 15 mm in diameter (black arrows) is seen at the intersection of the shadows of the first and sixth ribs.

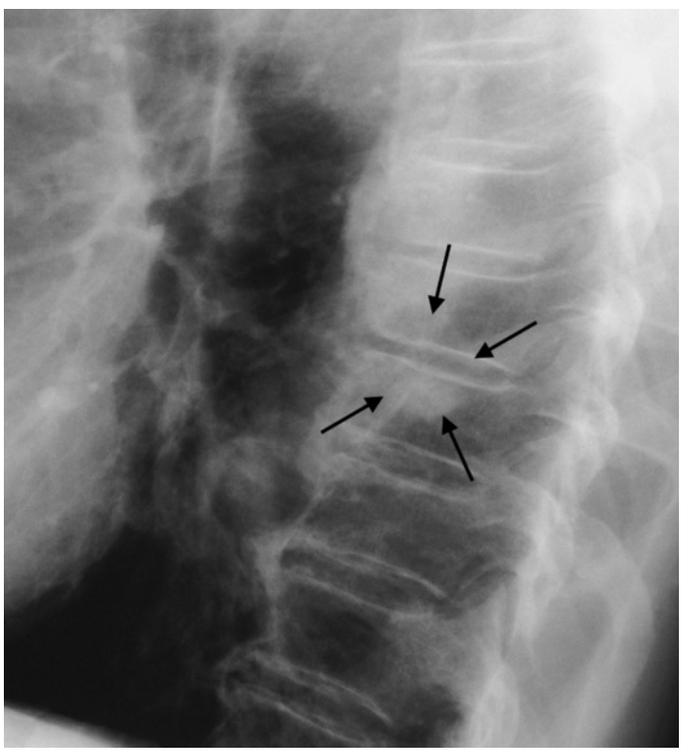

Fig. 4.37 Focal lesion simulated by lateral spondylophytes. There are severe degenerative changes in the spine with a lateral spondylophyte between the T8 and T9 vertebrae (black arrows).

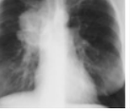

False-Negative Findings

The changes discussed in the previous section cannot only simulate a focal lesion, they can also lead the examiner to misinterpret a genuine lesion as simulated one. This especially applies to changes in the upper lung field classified as “postinfectious” or “indurated,” particularly in the presence of apical indurations (**Fig. 4.38**). The conventional radiograph also has its “blind spots” where intrapulmonary lesions can escape detection. These include the often overexposed retrosternal and the retrocardiac spaces on the lateral film. On the posteroanterior radiograph the posterior costophrenic angles are obscured by the diaphragm and represent additional blind spots. On the posteroanterior radiograph one should also pay attention to those parts of the left lower lobe that are obscured by the heart shadow (**Fig. 4.39**). Note that respiration can blur focal lesions close to the diaphragm beyond recognition.

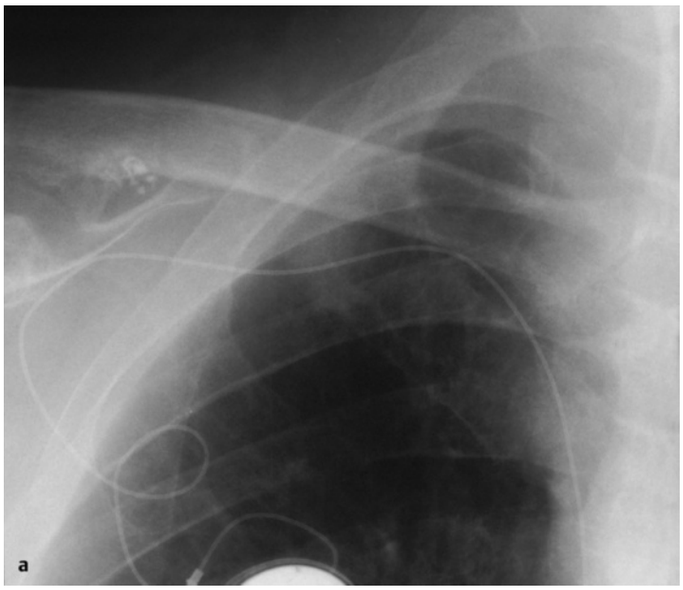

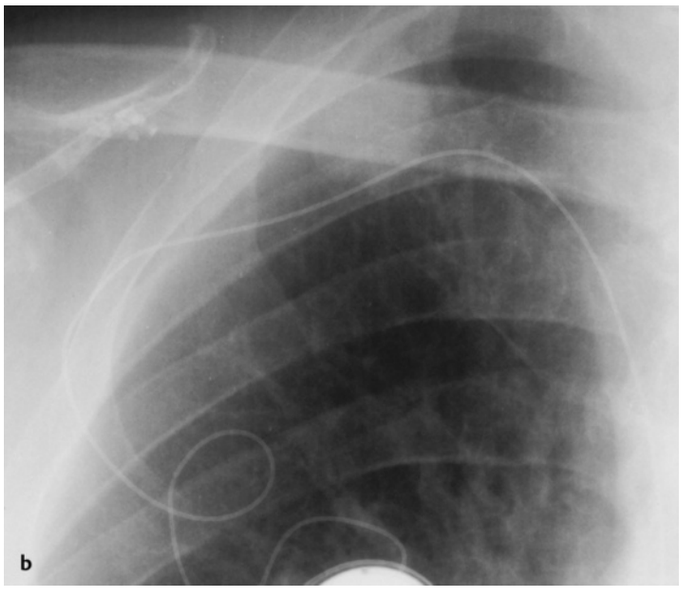

Fig. 4.38 a, b **The danger of misinterpreting a focal lesion as scarring.**

a The radiograph of this 91-year-old man with only moderate apical pleural thickening shows an irregularly shaped shadow 1.5 cm in diameter projected onto the anterior portion of the first rib. There are signs of chronic bronchitis with diffuse shadowing and pulmonary arterial hypertension. Surgery was contraindicated because of the patient's advanced age and severe ischemic cardiomyopathy.

b Follow-up examination 4 months later. There is increasing central congestion. The right apical mass has progressed significantly (now 2.5 cm).

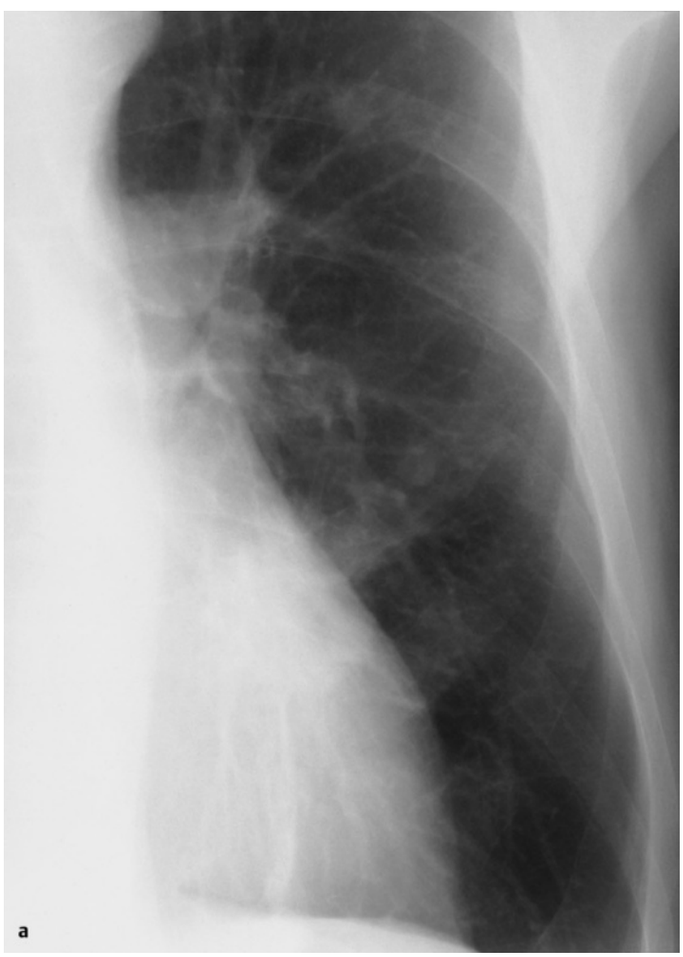

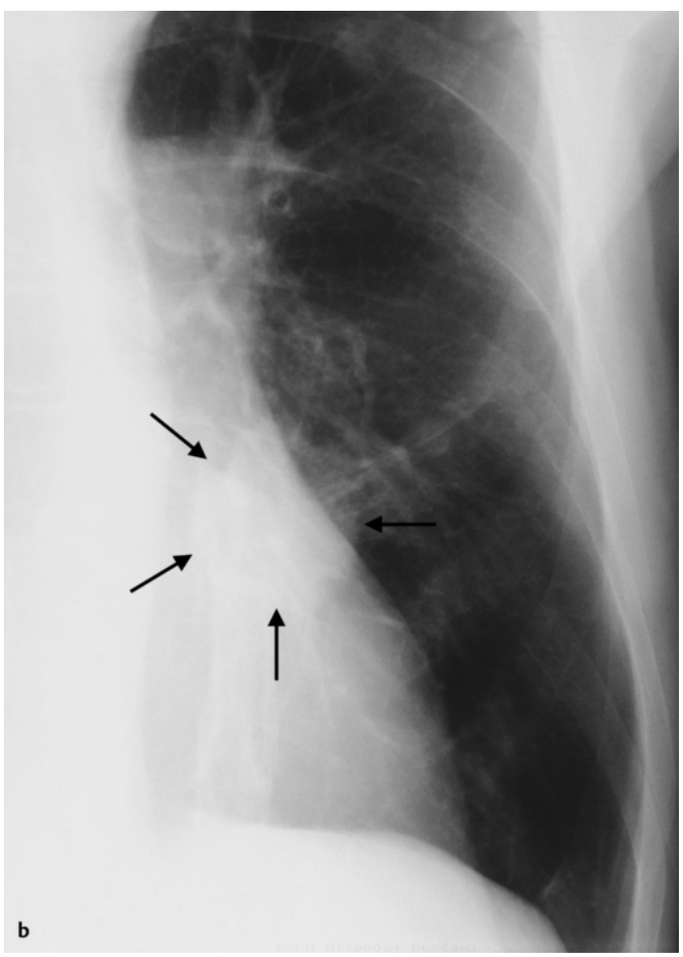

Fig. 4.39 a, b **Masking of an advanced retrocardiac mass.**

a Advanced COPD with emphysema and pronounced hila. The heart and aorta exhibit a hypertensive configuration without signs of decompensation.

b Follow-up examination 10 days later in a slightly different projection (slight rightward rotation). A 4.5-cm retrocardiac mass with a corona radiata and hypoventilation peripheral to it in the posterobasal segment of the lower lobe was almost completely masked on the previous study. Now it is partially visible (black arrows).

Evaluation of Focal Lesions

Focal lesions, especially solitary ones, often pose an insoluble diagnostic problem for both conventional radiography and CT. While it is possible to define morphologic criteria for a focal lesion and specify the probability of its being malignant, a definitive diagnosis can only be made by histologic examination. The following section discusses the criteria for classification as malignant or benign and the reactions in adjacent tissue.

Malignancy or benignancy:

- Location
- Shape
- Size
- Calcifications
- Liquefaction

Reactions of adjacent tissue:

- Pleural reactions
- Perifocal emphysema
- Ground-glass opacification

Comparison with any available previous images is helpful and often better than any supplementary imaging studies. The reason this is often not done is often simply a matter of inertia. (Ask: "Have you ever ...?" Obtain: "Where are you ...?" Telephone: "We have a patient who was in your care ... years ago ...").

Figure 4.40 shows a diagnostic flowchart. Growth documented on follow-up studies is diagnostic. However, one should not wait for such findings without first ordering an additional CT scan.

With "quarterly follow-up," one may encounter explosive growth (**Fig. 4.41**), and the tumor may suddenly progress from operable to inoperable. Even where there is no apparent growth, a slowly progressive tumor cannot be excluded. Only lack of growth over a period of 2 years can be evaluated as a certain sign of benignancy.

The previous discussion cannot apply to CT findings of small pulmonary nodules less than 1 cm in diameter. Due to the frequency with which modern spiral CT detects such focal findings, it is not possible to order histologic examination of every small nodule. Follow-up imaging studies are indicated instead. This puts us in the diagnostic dilemma of having to fall back on follow-up examinations at relatively brief intervals (6 weeks).

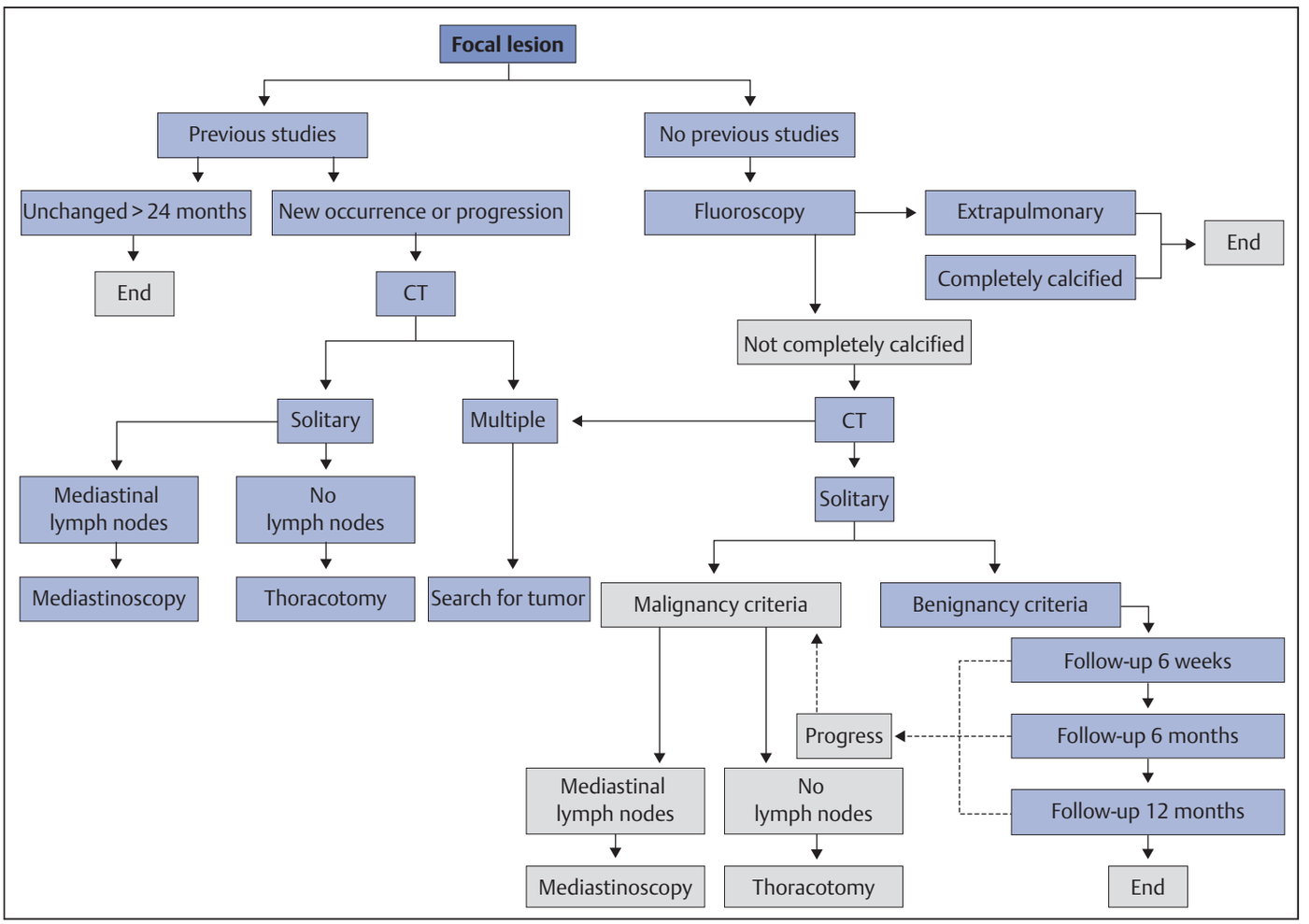

Fig. 4.40 Flowchart of diagnostic procedure for focal lesions.

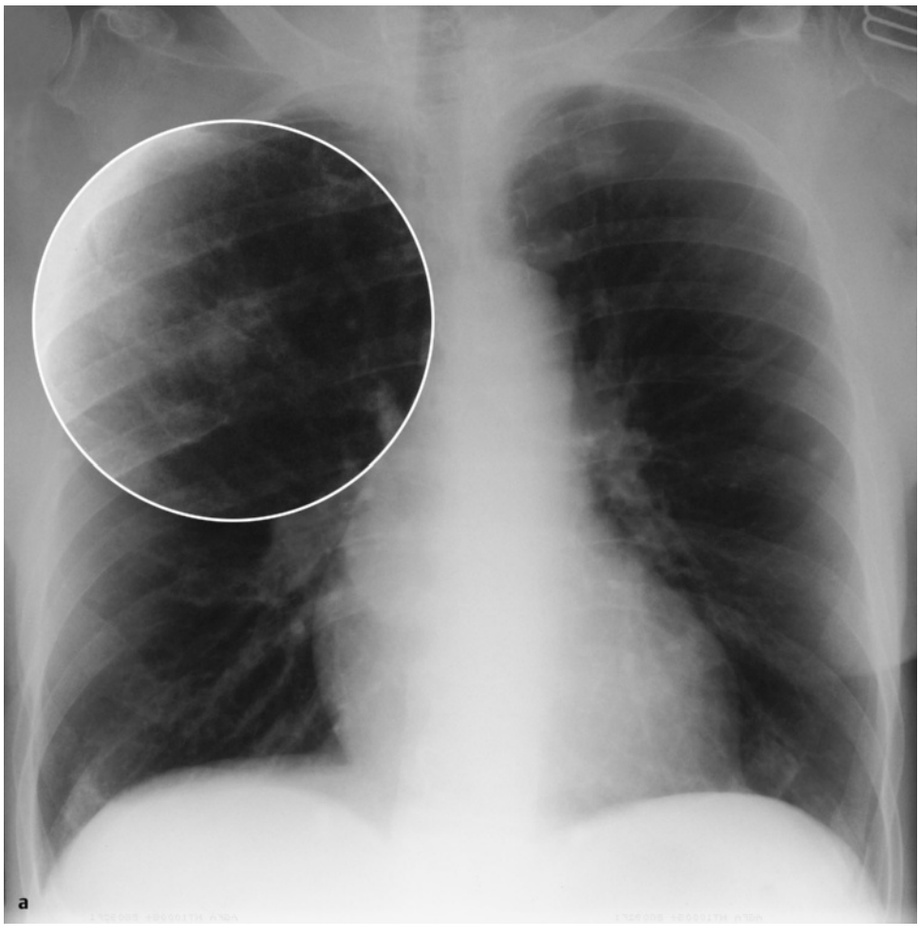

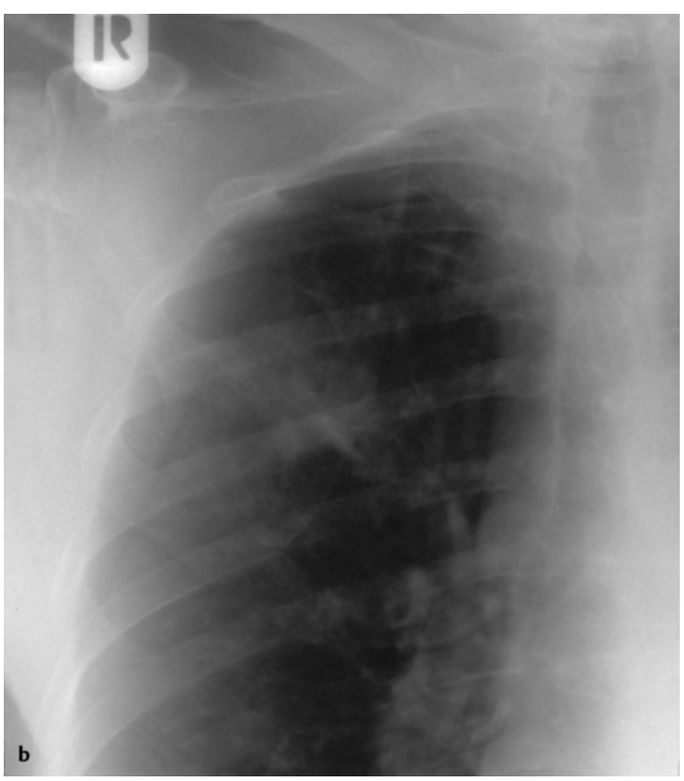

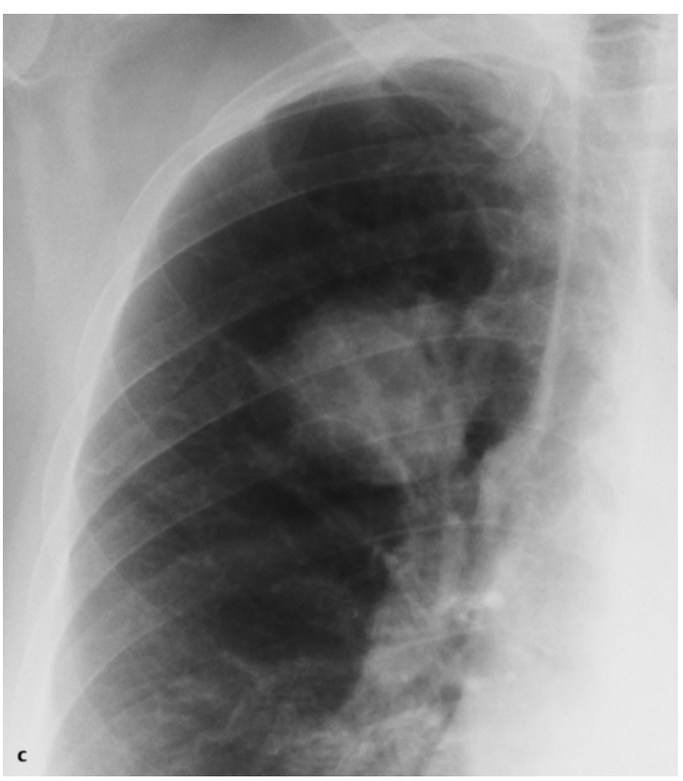

Fig. 4.41 a–c Spontaneous growth of a peripheral bronchial carcinoma.

a Faint focal lesion in the right upper lung field misinterpreted as a summation shadow of the fifth posterior and third anterior right ribs. Slightly obstructive barrel chest with diffuse peribronchial shadowing.

b Follow-up examination 6 months later. Without comparison with the previous studies, the faint nodular shadow in the right upper lung field looks less suspicious due to its relatively hard scarlike streak. It was misinterpreted as a post-infectious change.

c Follow-up examination after a further 4 months. The further course of the disorder was characterized by an exponential increase in growth with massively increased volume in only 4 months and ipsilateral lymph node involvement.

Note: The 66-year-old woman underwent complete tumor excision (R0) and today is in good health.

Location

The location of a focal lesion is a weak, purely statistical criterion. It is listed here only for the sake of completeness. The number of malignant changes with focal lesions is highest in the middle lobe. Benign focal lesions (postinfectious changes) predominate in the upper lung fields.

Size

In contrast to gastrointestinal diagnostic imaging (the larger the lesion, the higher the probability of malignancy), the actual size is of secondary importance in evaluating a pulmonary lesion. However, it is very important for the prognosis of a confirmed malignancy. In general, the rule is that tuberculomas do not exceed 3 cm. Tumors exceeding 6 cm without signs of pneumoconiosis have a high probability of malignancy. Progressive growth is diagnostic; refer to the previous section.

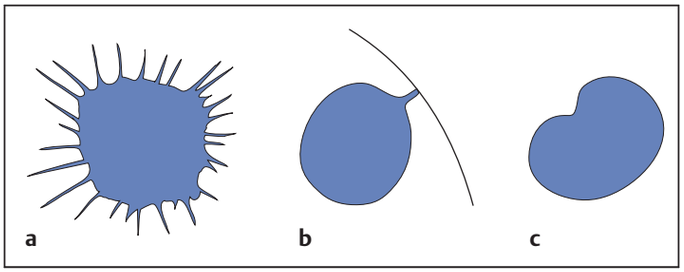

Fig. 4.42 a–c **Signs of malignancy in peripheral focal lesions.** Shapes that suggest malignancy include a corona radiata (**a**) with its radiating spicules, a fingerlike pleural extension (**b**), and Rigler dimpling (**c**).

Shape

The initial radiologic morphology of peripheral bronchial carcinoma is a circumscribed density of variable shape that can usually be classified under the generic term of intrapulmonary focal lesion. Small carcinomas (< 2 cm) initially show an ill-defined contour in most cases and do not appear uniformly round. The smooth, round shape with a relatively sharply defined border is more often observed in intrapulmonary metastases, which do not often occur as isolated lesions.

Extensions into the surrounding tissue can be caused by lymphangitis carcinomatosa. The septal thickening in lymphangitis carcinomatosa is accompanied by nodular swelling. The length of the extensions radiating from the focal lesion is significant. In tumors these are usually short spicules that taper toward the periphery and extend randomly in all directions, forming the corona radiata (**Fig. 4.43**). Long, thin extensions with hyperinflated areas between them are more consistent with scarring. A fingerlike extension into the pleura can be misinterpreted as benign scarring. Pleural involvement of peripheral focal lesions can be evaluated far better on CT (**Fig. 4.44**).

Central dimpling (Rigler sign) is another sign of malignancy. However, it is not diagnostic as it can also occur in tuberculomas (**Fig. 4.45**). The schematic diagram in **Fig. 4.42** summarizes the signs of malignancy.

Leo George Rigler (* 1896 Minneapolis, † 1979 Los Angeles): Student of Gösta Forssell; professor of radiology at the University of Minnesota and the University of California in Los Angeles; executive director of the Cedars-Sinai Medical Center.

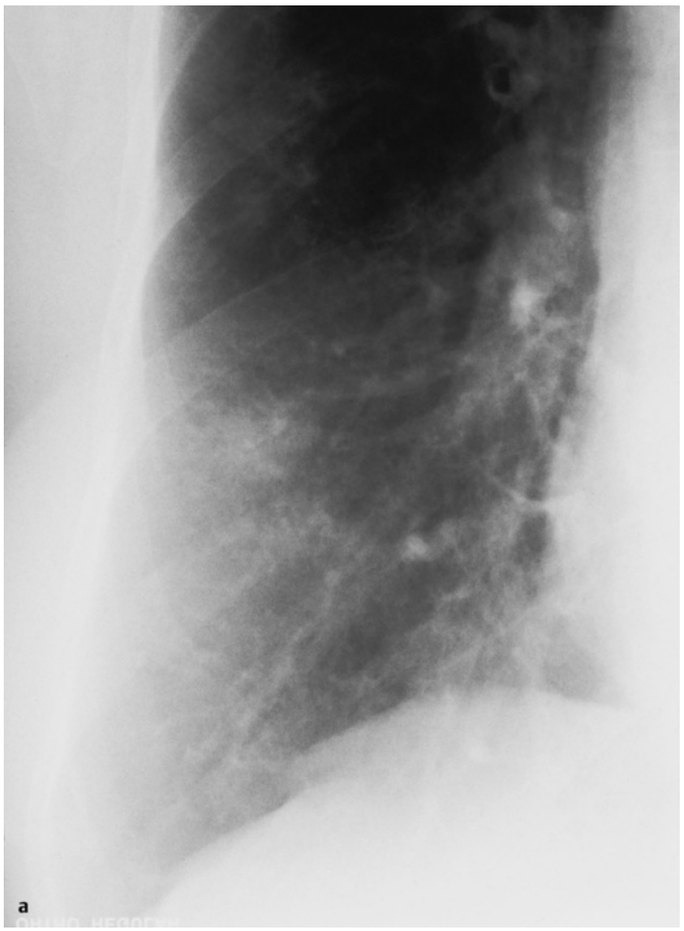

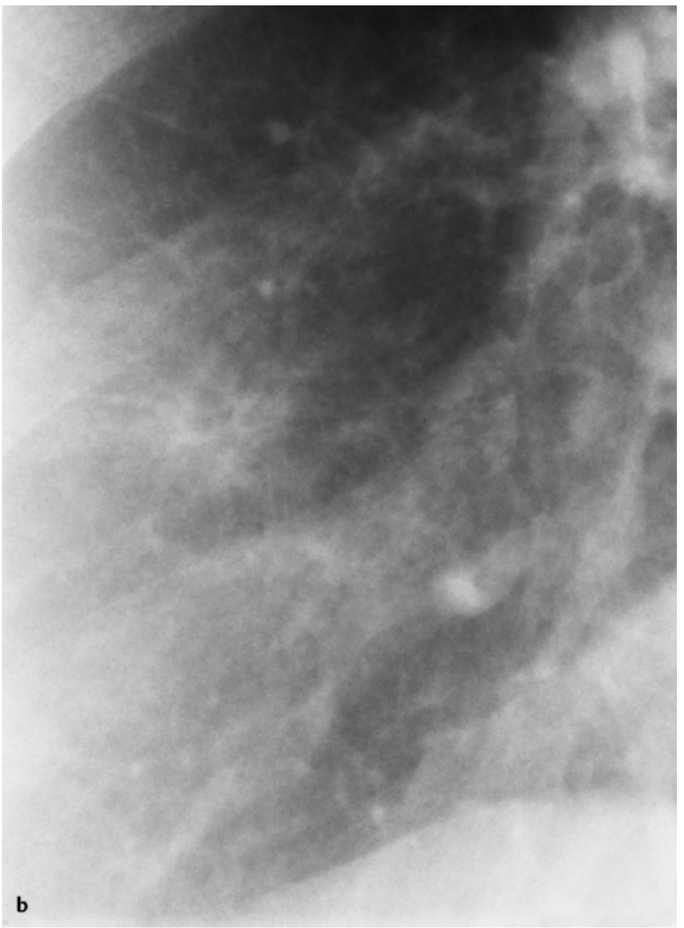

Fig. 4.43 a, b Corona radiata in a bronchial carcinoma.

a Faint focal lesion 1.5 cm in diameter in the lower lobe.

b Only the spot films obtained after fluoroscopy show the lesion to be malignant by clearly demonstrating a corona radiata.

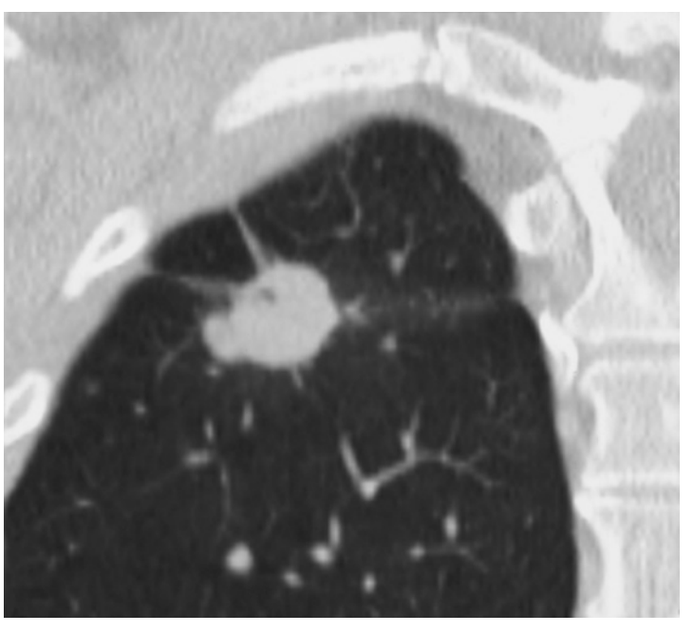

Fig. 4.44 Fingerlike pleural extension in a peripheral bronchial carcinoma. CT visualizes an evagination of the tumor, not a scar (the extension has its base on the tumor).

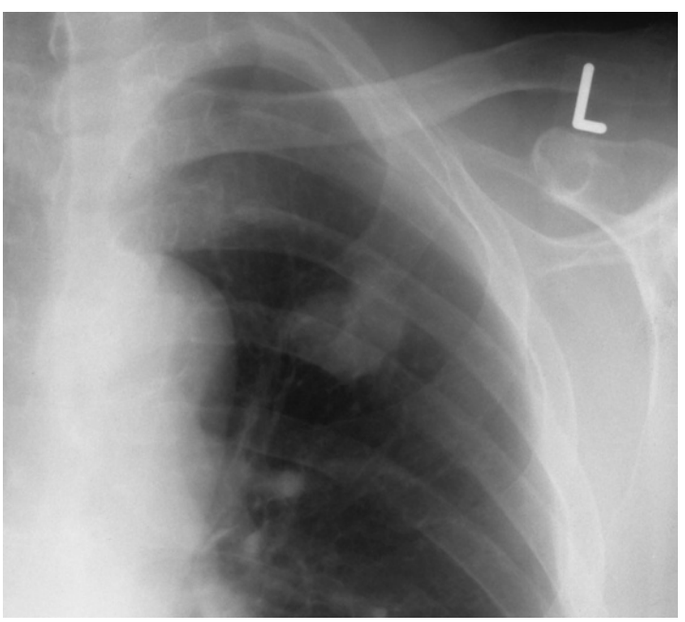

Fig. 4.45 Peripheral bronchial carcinoma showing a Rigler dimple. The 3-cm lesion projected on the anterior second left rib exhibits a distinct cranial indentation. The aortopulmonary window is clear without signs of lymph node involvement.

Calcification (Fig. 4.46)

Calcifications are significantly less distinct and more difficult to analyze on hard-radiation images than on fluoroscopy. CT clearly visualizes the pattern of calcification. Calcification in a lesion is primarily an indication of an inflammatory process that has run its course (**Fig. 4.47**). In spite of this, the literature describes malignancies with calcifications representing cell detritus. Metastases of osteosarcomas are an exception, as they regularly exhibit calcific inclusions indicative of new bone formation. Benign patterns of calcification include the central, diffuse, concentrically layered or popcornlike calcification (hamartoma, **Fig. 4.48**) of a focal lesion. Especially in calcifications occurring in an eccentric location and exhibiting a speckled pattern, a malignant process cannot be excluded. The combination of fatty components and calcifications within a lesion suggests a mixed tumor (teratoma).

Liquefaction

Liquefaction within a lesion is often evaluated as a sign of benignancy, although it can also occur in malignant lesions (especially squamous cell carcinoma). Liquefaction characteristically occurs in a peripheral location of the mass. The cavities are not completely cleaned, have residual septa (stroma remains intact), and exhibit fissured walls of irregular thickness (**Fig. 4.49**). We observe cases of cavitation with expectorated metastases relatively often. These findings closely resemble emphysematous bullae or drained cavities. In a differential diagnosis, their thicker halo distinguishes them from the former and their diffuse distribution from the latter (**Table 4.4, Fig. 4.50**).

Table 4.4 Differential diagnosis of pulmonary liquefaction

- Focus of bacterial infection (staphylococci)
- Tuberculosis
- Primary tumor (especially squamous cell carcinoma)
- Expectorated metastases
- Rheumatoid nodules

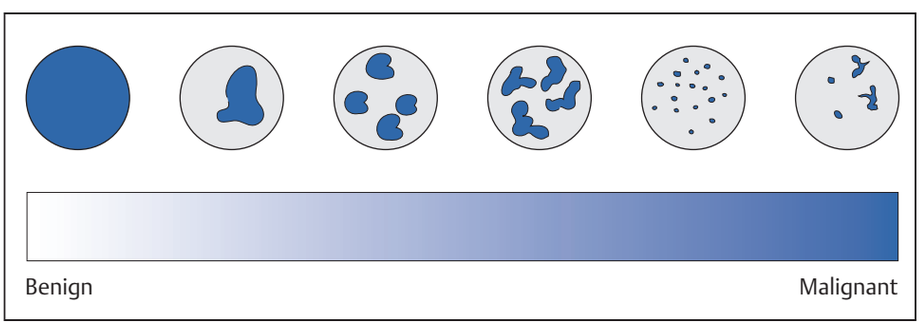

Fig. 4.46 Calcification patterns in peripheral focal lesions. Whereas completely calcified lesions are a relatively reliable sign of benignancy, finely nodular irregular calcifications (calcified cell detritus) suggest malignancy.

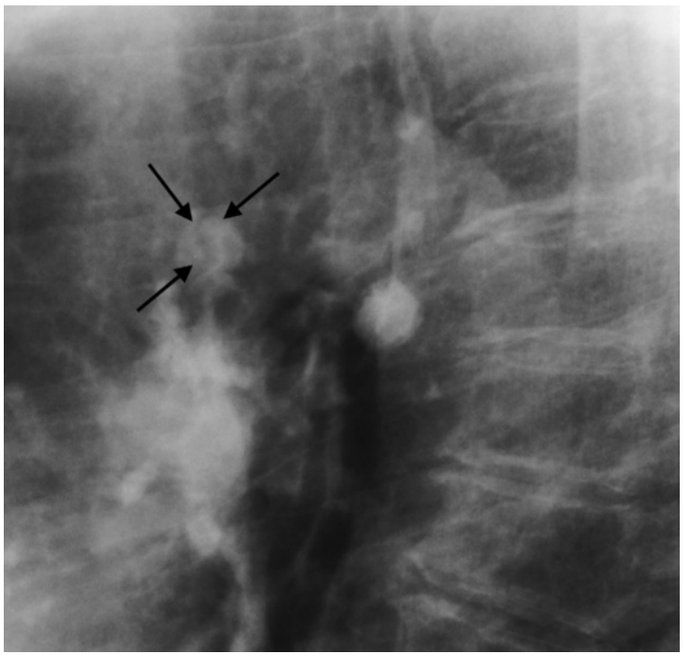

Fig. 4.47 Completely calcified tuberculoma. Smoothly demarcated 10-mm calcified focal lesion projected on the aorta. This corresponds to a slightly smaller paratracheal calcification of lesser radiodensity (black arrows). Evaluation: Postinfectious peripheral calcification with a central lymph node (calcified Ghon complex).

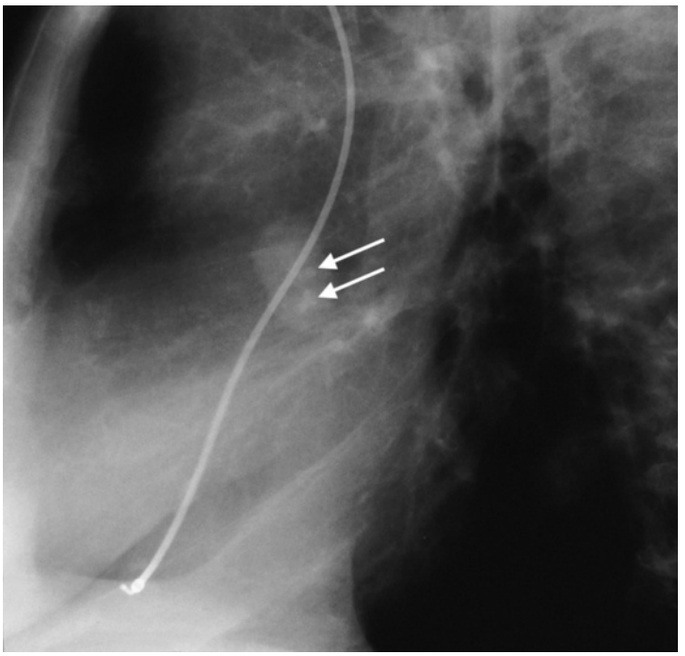

Fig. 4.48 Coarse calcifications in hamartoma. Smoothly demarcated ellipsoid lesion of relatively high radiodensity in the middle lobe showing a few coarse calcifications (white arrows).

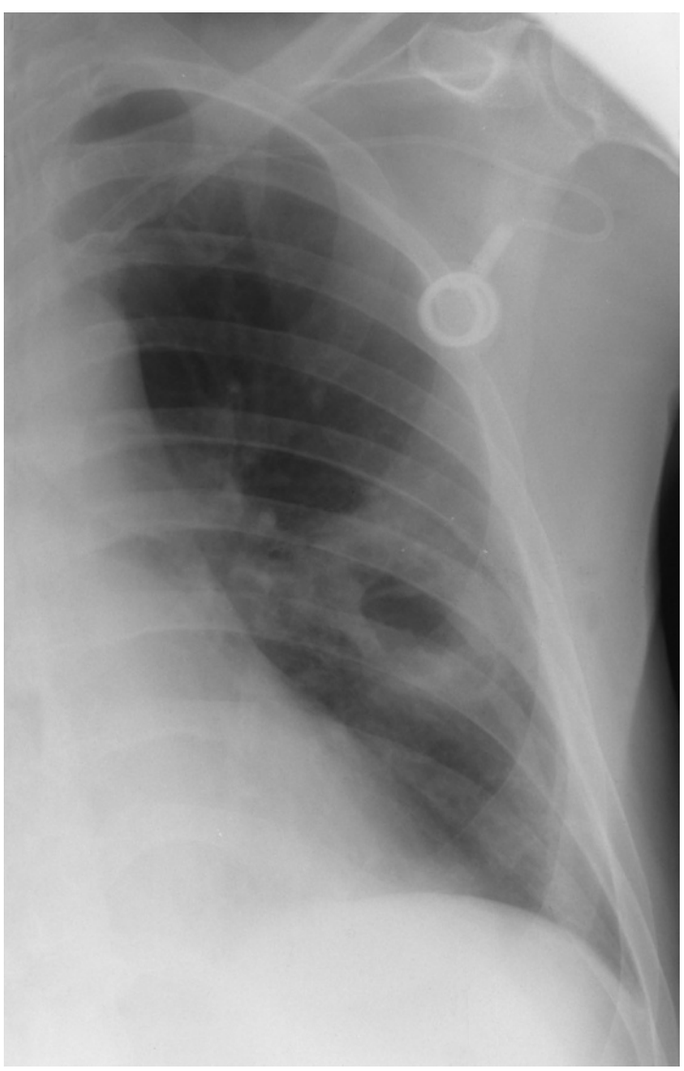

◀ **Fig. 4.49 Liquefying squamous cell carcinoma of the left lower lobe.** Ill-defined mass 5 cm in diameter with a large asymmetrical, partially expectorated area of liquefaction. Radiograph obtained after implantation of a venous port prior to chemotherapy.

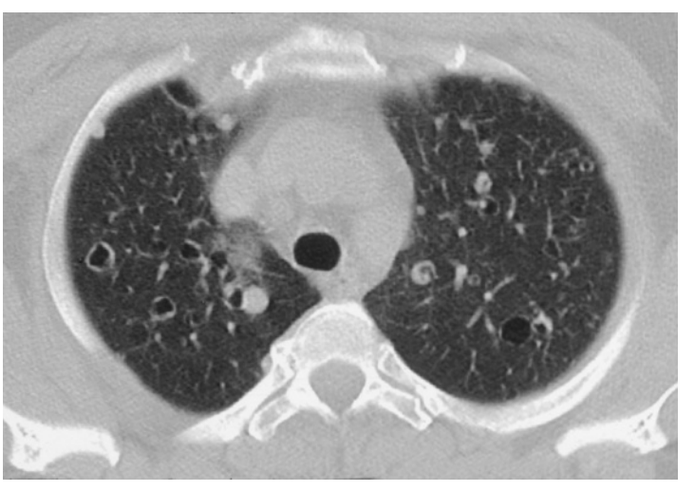

Fig. 4.50 Dislodged, partially expectorated metastases. This scan of a woman with diffuse pulmonary and mediastinal metastatic disease shows numerous lesions in the upper lung fields, some liquified and expectorated and appearing as "bullae."

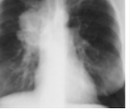

Perifocal Emphysema

Benign focal lesions on CT often exhibit circular perifocal emphysema indicative of shrinkage in the vicinity of scarring (**Fig. 4.51**).

It is dangerous to confuse this phenomenon with the presence of a peripheral malignancy within an area of preexisting emphysema (**Fig. 4.52**).

Ground-Glass Opacities

Ground-glass opacities are often signs of perifocal hemorrhage. In these cases the pathologic process has affected vascular structures. Such findings can occasionally be observed in certain benign processes such as aspergillosis (**Fig. 4.53**). However, these opacities are also signs of intra-alveolar tumor spread and are thus crucial findings demonstrating the presence of alveolar cell carcinoma (**Fig. 4.54**).

Pleural Reactions

Pleural reactions (localized, encapsulated, or diffusely spreading pleural effusion) only appear in malignant processes where the pulmonary lesion has direct pleural contact. Broad contact is the result of local infiltration. Larger pulmonary processes can impair lymph drainage, leading to what are usually discrete accumulations of pleural fluid. In addition to the focal lesion, reticular septal shadowing is also observed in the vicinity of the lesion. Differential diagnosis from lymphangitis is difficult on the basis of radiologic findings (no nodules, improvement under diuretic therapy). Larger pleural effusions in the presence of malignant lesions suggest pleural carcinomatosis.

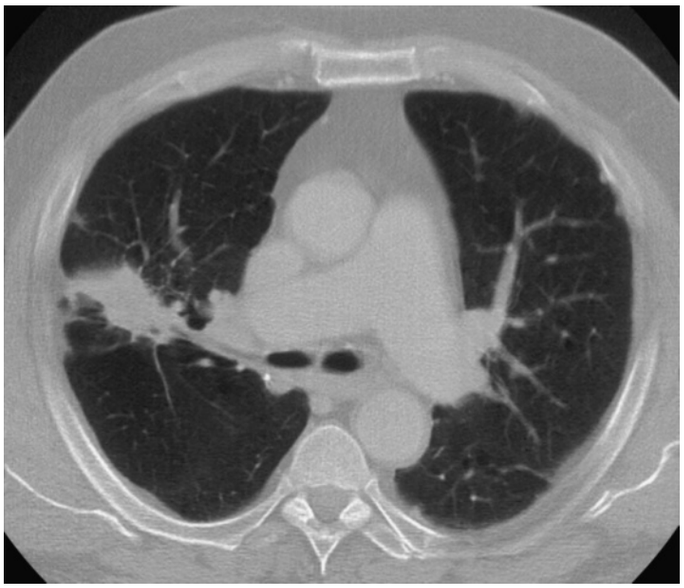

Fig. 4.51 Perifocal emphysema indicative of a benign lesion. The patient is a 65-year-old miner with known anthracosilicosis. Findings include a fibrotic mass 4 cm in diameter in the right middle lung field. The significant perifocal emphysema is a sign of benignancy.

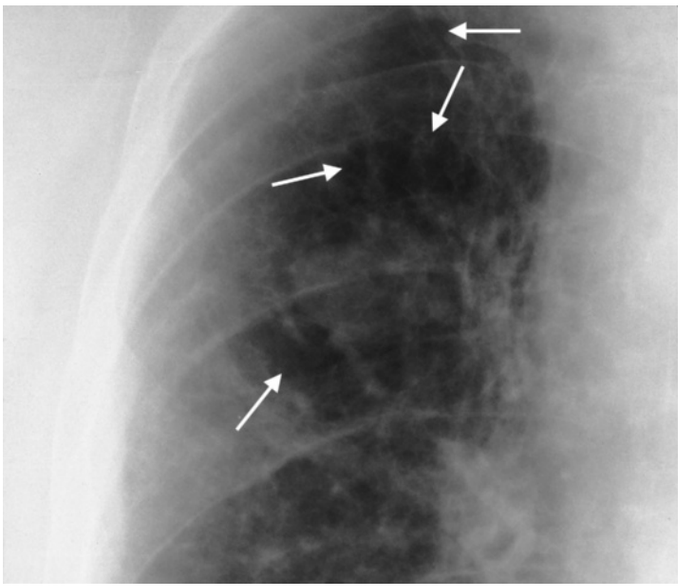

Fig. 4.52 Peripheral malignancy in preexisting emphysema (detail enlargement). There is an ill-defined lesion in the right upper lobe measuring 3 cm in diameter. The perifocal hypertransradiancy (white arrows) must not be misinterpreted as belonging to the patient's preexisting severe emphysema.

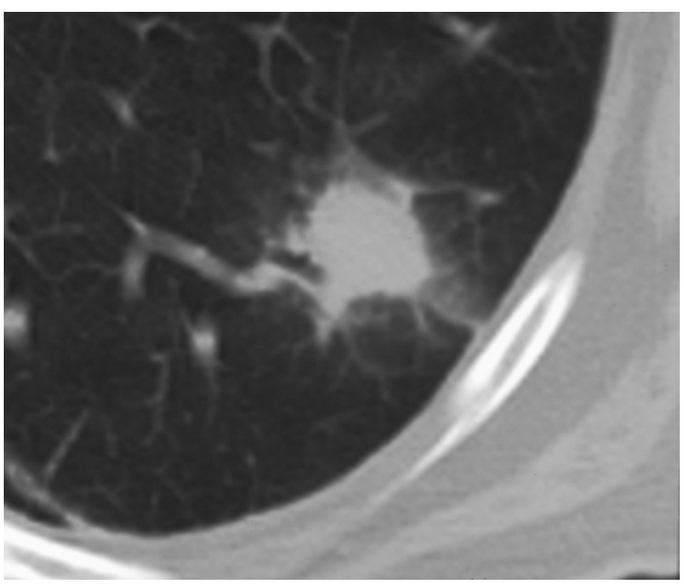

Fig. 4.53 Ground-glass perifocal opacity. Findings include a solid lesion with tiny extensions and a ground-glass halo consistent with perifocal hemorrhage. Invasive aspergillosis was confirmed on autopsy.

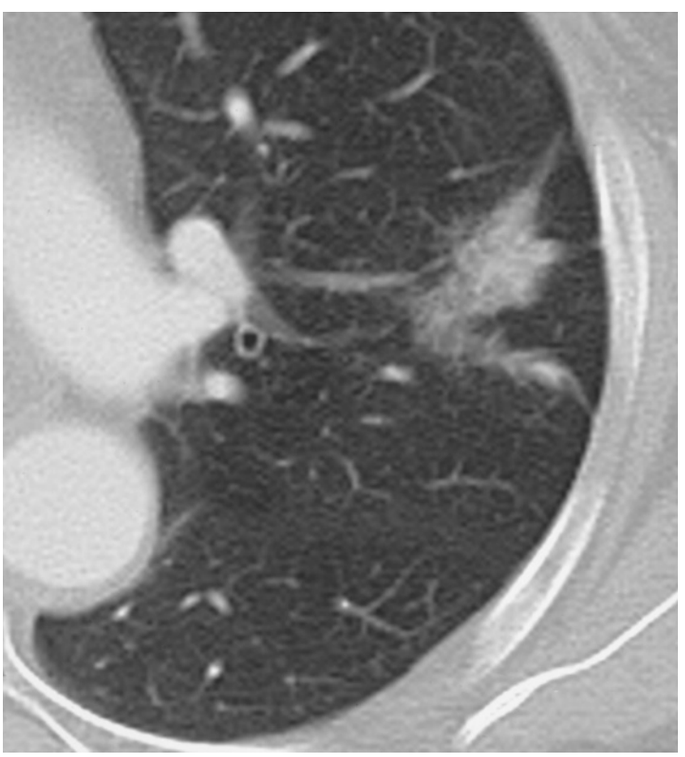

Fig. 4.54 Perifocal ground-glass opacification in alveolar cell carcinoma. The perifocal pattern is a sign of intra-alveolar spread.

CT Staging

Computed tomography is superior to conventional radiography in detecting focal lesions and facilitating their description and classification. Despite all opinion to the contrary, CT also represents a significant advance in preoperative staging and postoperative tumor management. Determining the extent of tumor spread (staging) is crucial to the choice of further treatment in non–small-cell bronchial carcinomas (**Table 4.5**):

- **T1 tumors** are easily resectable peripheral focal lesions less than 3 cm in diameter or endobronchial tumors of the lobar bronchi that have not invaded the main bronchi (**Fig. 4.56**).
- **T2 tumors** are also easily resectable peripheral focal lesions but more than 3 cm in diameter and without infiltration of the extrapulmonary structures (**Fig. 4.57**), or they are endobronchial tumors at a minimum distance of 2 cm to the carina.
- **T3 tumors** infiltrate the chest wall (**Fig. 4.55, Fig. 4.58**), mediastinum, diaphragm, or pericardium without invasion of important structures (heart, central vessels, trachea) so that resection appears feasible under certain conditions.
- **T4 tumors** are inoperable due to their infiltration of unresectable structures, or they exhibit pleural carcinomatosis or a malignant pericardial effusion. The classic example of an inoperable lesion is a Pancoast tumor that has invaded the apical thoracic cage, causing rib destruction (**Fig. 4.59**).

Table 4.5 Therapy of the various tumor stages in non–small-cell bronchial carcinoma

Stage	TNM	Therapy
IA	T1N0M0	Resection
IB	T2N0M0	
IIA	T1N1M0	
IIB	T2N1M0	
	T3N0M0	
IIIA	T1N2M0	Neoadjuvant combined radiation and chemotherapy and resection
	T2N2M0	
	T3N1M0	
	T3N2M0	
IIIB	T1N3M0	Radiation therapy, chemotherapy
	T2N3M0	
	T3N3M0	
IV	M1	Chemotherapy

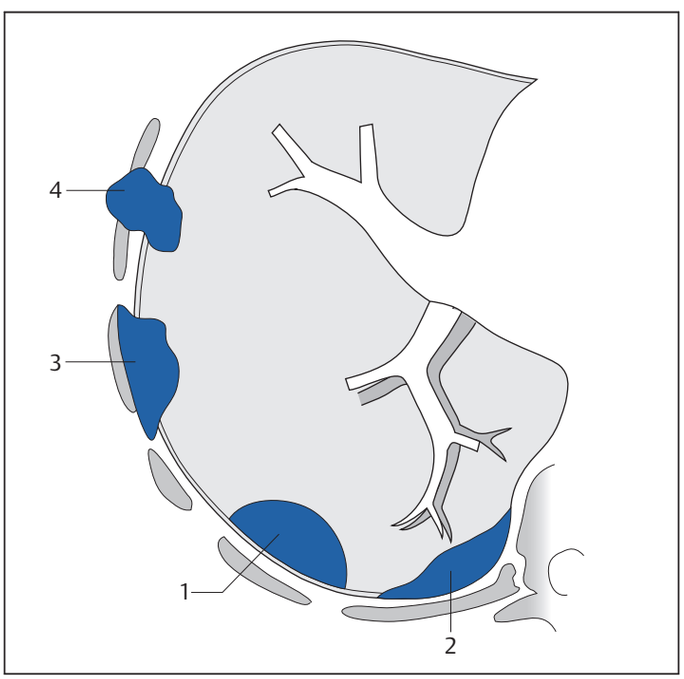

Fig. 4.55 CT criteria of chest wall infiltration. A peripheral tumor with more than 3 cm of pleural contact (1) and a lesion spreading to the pleura over gentle arc (2) can be regarded as moderately specific signs of chest wall infiltration. Displacement of extrapulmonary fatty tissue (3) and rib destruction (4) are regarded as definite signs.

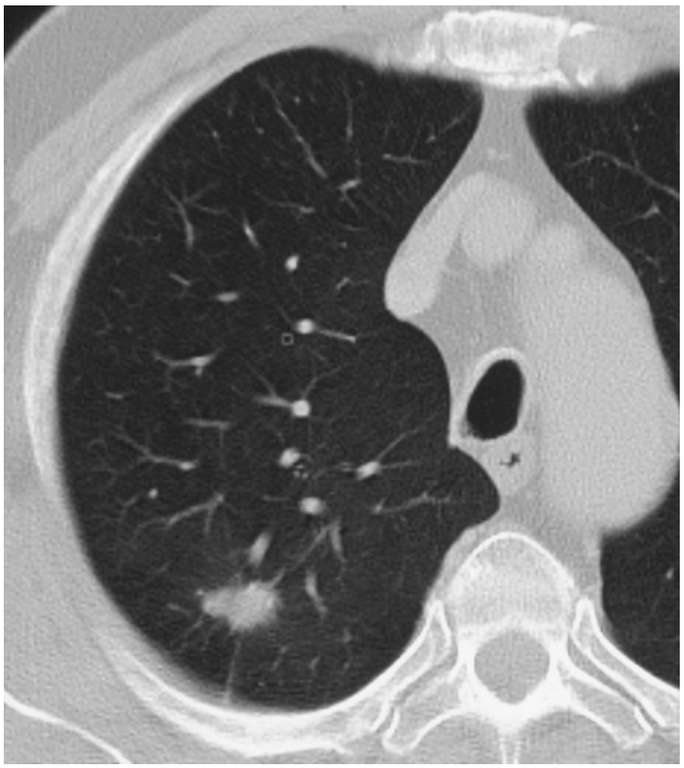

Fig. 4.56 **T1 carcinoma.** Surgically confirmed peripheral bronchial carcinoma measuring slightly less than 2 cm in the posterior segment of the upper lobe.

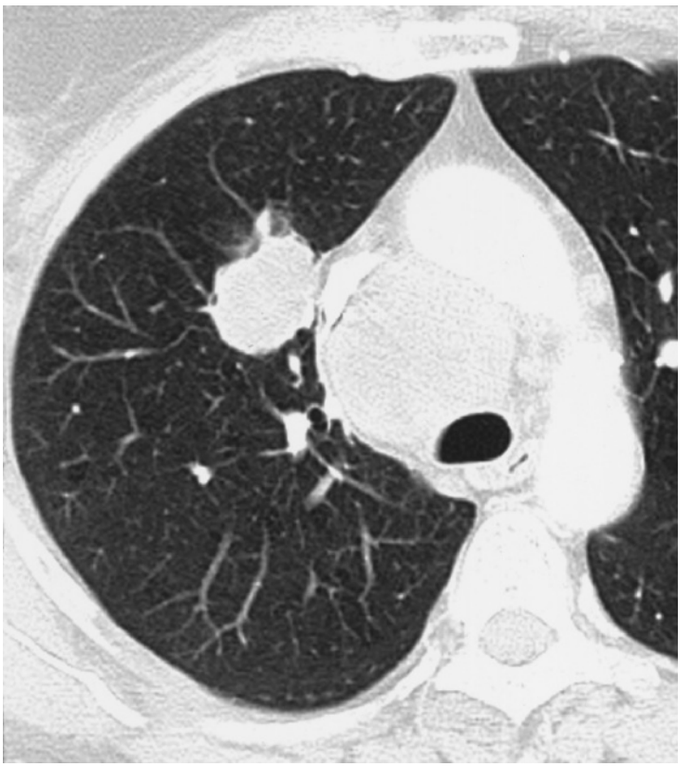

Fig. 4.57 **T2 carcinoma.** The CT scan shows a bronchial carcinoma measuring over 3 cm in diameter in the central right upper lobe. The tumor is in contact with the mediastinum but has not infiltrated it. Severe ipsilateral and contralateral lymph node metastases (N3) are present; this is stage IIIB disease (radiation therapy and chemotherapy).

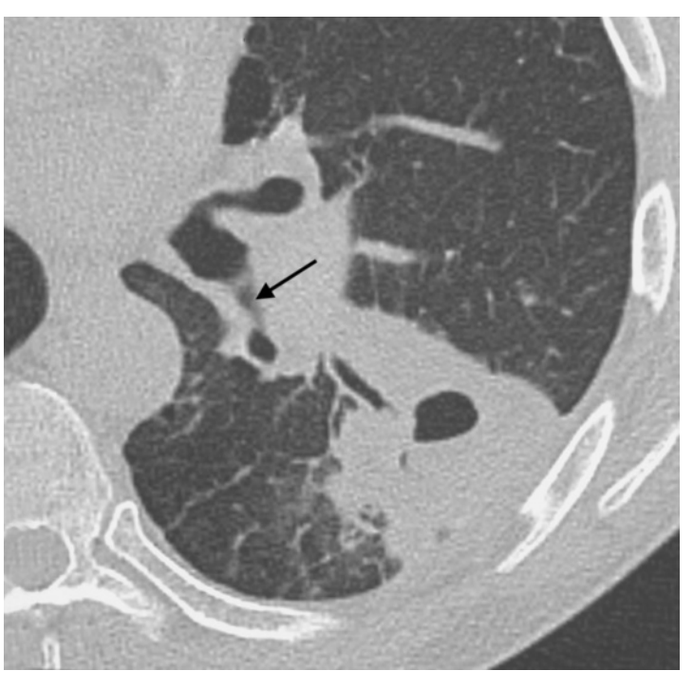

Fig. 4.58 **T3 carcinoma.** The patient is a 47-year-old male smoker with a liquefying 6-cm peripheral bronchial carcinoma showing broad pleural infiltration. The tumor has spread along the bronchovascular bundle toward the center as far as the lower lobar bronchus (black arrow), of which the origin is narrowed.

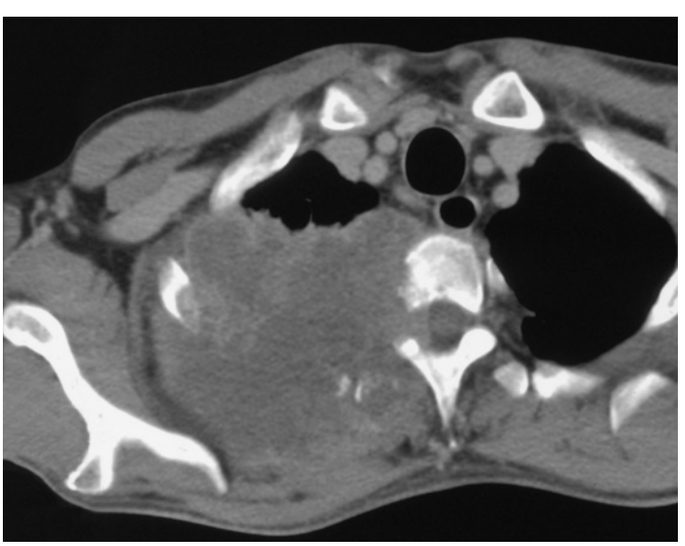

Fig. 4.59 **Pancoast tumor (T4).** The patient is a 38-year-old man with advanced apical bronchial carcinoma that has breached the chest wall. There is broad infiltration of the thoracic spine with spread into the spinal canal. The tumor has invaded the posterior and lateral chest wall, spreading through the musculature of the back and into the axilla.

Alveolar Cell Carcinoma

Alveolar cell carcinoma (also known as bronchioloalveolar carcinoma) represents a special case among the primary malignant processes of the lung. It is characterized by unique pathologic findings (see "Notes on Pathology"), and its radiologic forms and clinical course are different from those of other tumors. Notably, a relatively high percentage of patients with this carcinoma are nonsmokers.

Radiologic findings in alveolar cell carcinoma are neither consistent nor unequivocal; but certain signs considered in conjunction with appropriate clinical findings suggest the presence of this disease entity.

Radiographic signs include:

- Isolated peripheral nodules
- Area consolidation resembling pneumonia
- Circumscribed ground-glass opacities
- Rarely, multiple lesions

An isolated peripheral, usually ill-defined focal lesion should be evaluated as early-stage disease or as a mixed form with adenocarcinoma (**Fig. 4.60**). However, typical findings in classic alveolar cell carcinoma include area consolidations that resemble pneumonia but are slowly progressive, do not respond to antibiotics, and lack the clinical signs of pneumonia (**Fig. 4.61**). In the beginning these shadows are usually of low density, occasionally with a ground-glass appearance. They occasionally resemble multiple faint acinar shadows joined together. The shadows increase in density over time, occasionally evolving into dense consolidations covering entire lobes and showing an air bronchogram (**Fig. 4.61b**).

Notes on Pathology

Alveolar cell carcinoma is now regarded as a subgroup of the adenocarcinomas. Its relatively slow, minimally invasive growth sets it apart from the other bronchial carcinomas. Histologic findings include a single layer of well-differentiated tumor cells lining the alveolar walls like wallpaper and preserving the pulmonary interstitium. A clear distinction should be made between this classic form and mixed forms with adenocarcinoma. These mixed forms exhibit a combination of invasive growth and lining of adjacent alveoli. Their prognosis is poorer and varies with the proportion of invasive tumor component.

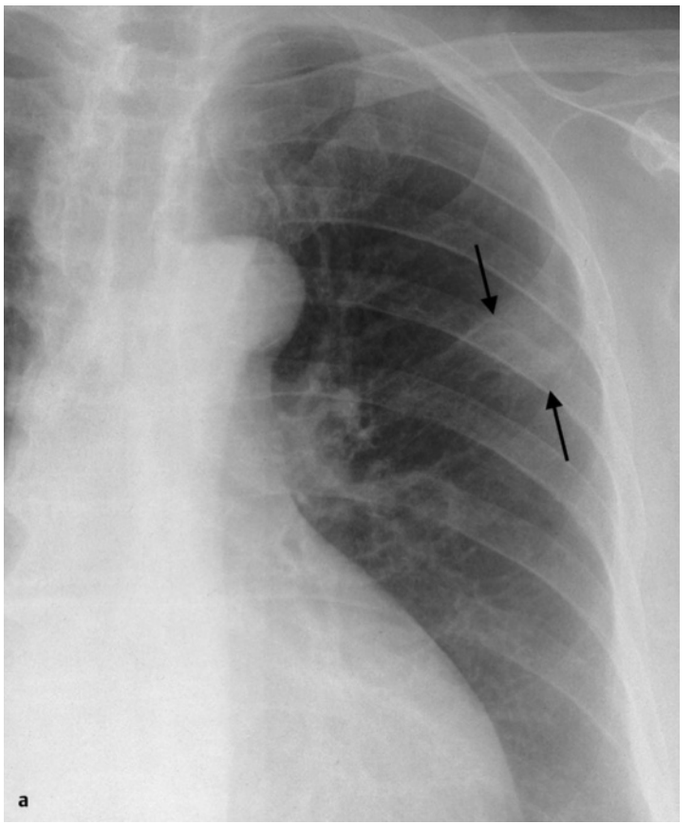

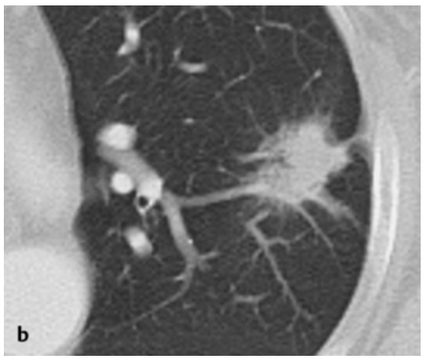

Fig. 4.60 a, b **Alveolar cell carcinoma as a peripheral focal lesion.**
a In the left upper lung field there is a faint shadow 3 cm in diameter (black arrows) showing minimal growth compared with previous examinations.
b CT reveals a solid lesion with spicules suggestive of malignancy (corona radiata), a fingerlike pleural extension, and an ill-defined border due to ground-glass perifocal halo.

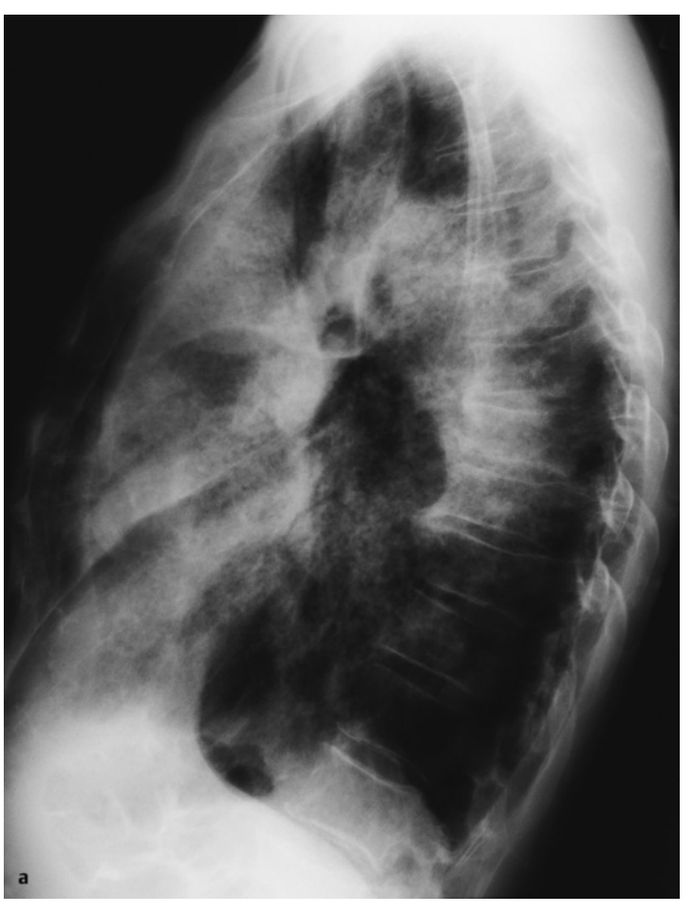

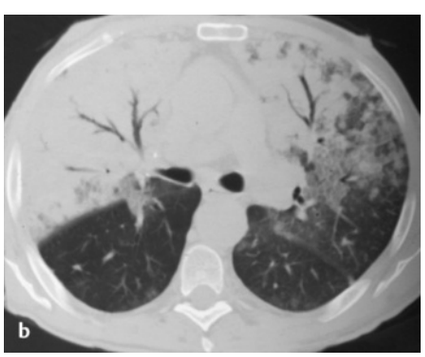

Fig. 4.61 a, b **Alveolar cell carcinoma of the pneumonia type.**
a Ground-glass opacification mixed with finely nodular acinar densities is seen in both upper lobes and the lingula. The cardiac borders are no longer visible. No effusion. Obstructive barrel chest.
b CT reveals advanced consolidations in both upper lobes with an air bronchogram in the right lung (findings here are typical of lobar pneumonia). Pronounced ground-glass infiltrates in adjacent tissue give the left lung a less tightly consolidated structure.

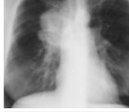

Review Case 1

The patient is a 78-year-old man with a long history of smoking and chronic bronchitis (Fig. 4.62). He has been admitted with swelling of the upper extremity and head. The tentative diagnosis is angioneurotic edema. No fever. Cough is worse than the chronic cough reported.

Question 1

How do you evaluate heart size and cardiac compensation? (Previously discussed in Chapter 1.)

Question 2

How do you evaluate the pulmonary parenchyma? Are there chronic changes consistent with the clinically known COPD? (Previously discussed in Chapter 2.)

Question 3

What finding prompts you to immediately look at the lateral film? (This chapter.)

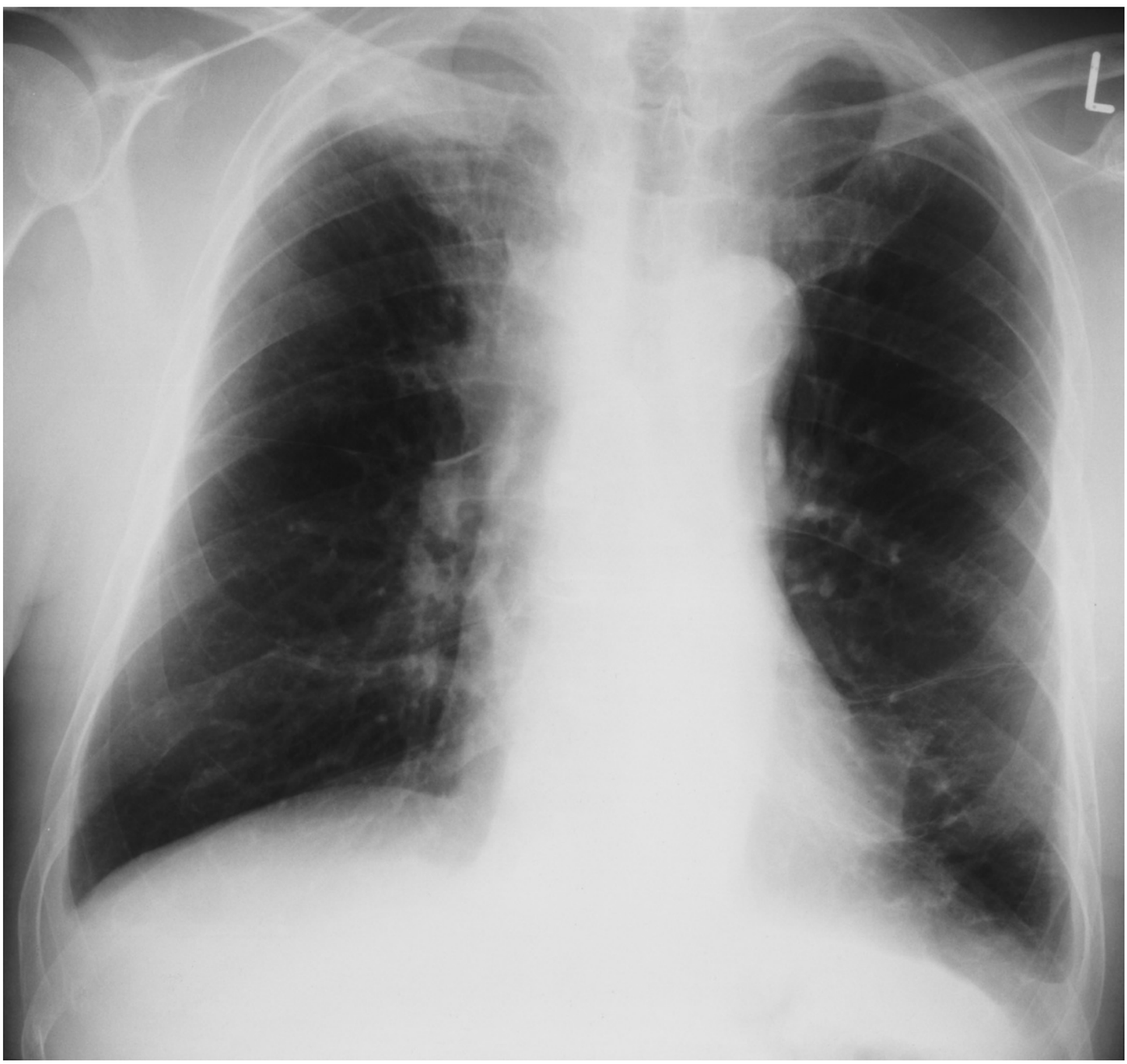

Fig. 4.62 Chronic cough, now with acute swelling of the upper extremity.

Answer

Heart size is normal with elongation and sclerosis of the aorta. There is diffuse peribronchial shadowing. A streaky reticular pattern is seen in the left lower lung field and perihilar centripetal shadowing in the right upper lobe, which shows the onset of volume loss (with a discrete cranial shift of the right horizontal fissure). Bilateral apical pleural thickening and shadowing of the costophrenic angles. The posteroanterior view shows widening of the mediastinal band. The pretracheal oval lacks a distinct cranial border on the lateral film (**Fig. 4.63**)

Clinical and radiologic diagnosis: Advanced right central bronchial carcinoma that has invaded the mediastinum, with congestion in the superior inflow tract. Patient died 7 days later.

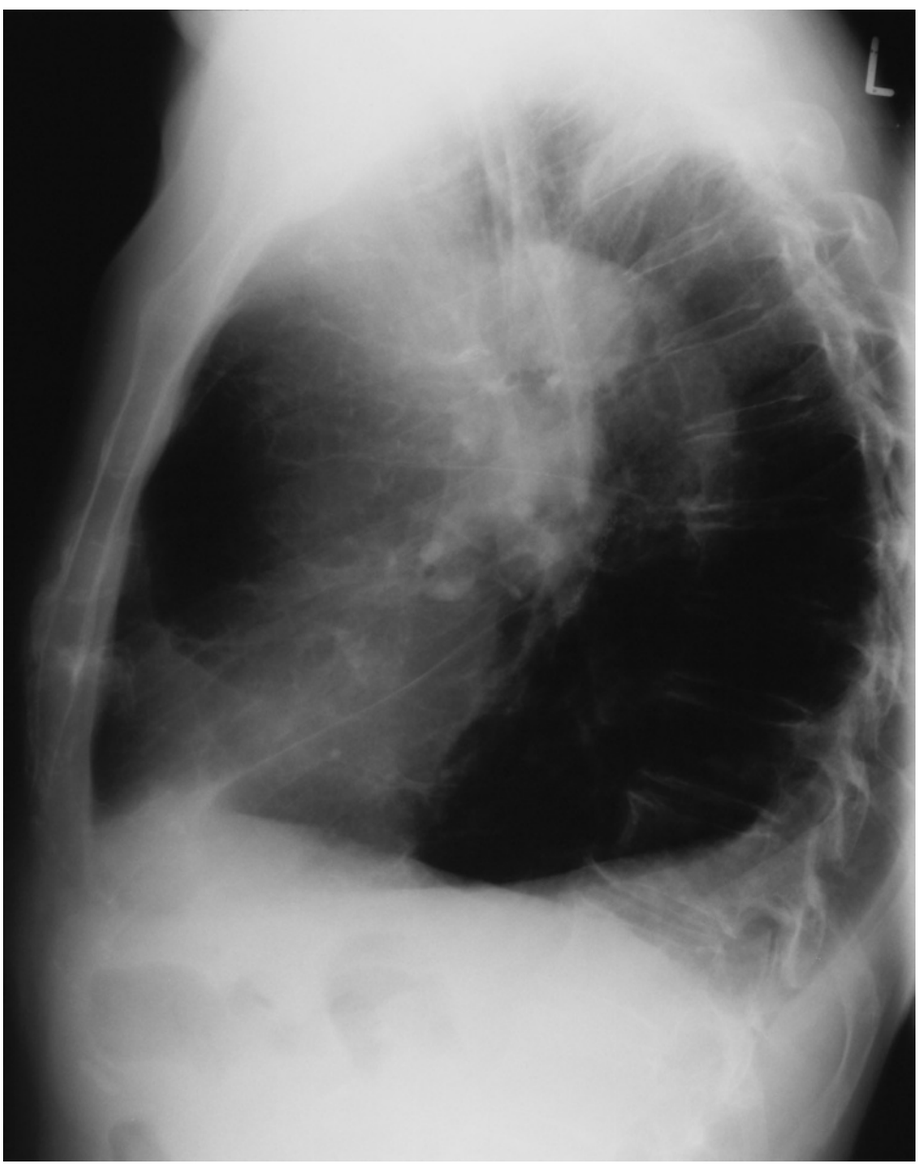

Fig. 4.63 Lateral view of Fig. 4.62. The hilum is significantly thickened and the cranial border of the pretracheal oval (right pulmonary artery) has been obliterated. The anterior upper mediastinum shows diffuse shadowing. The left costophrenic angle is thickened and there is a pleural effusion on the right side.

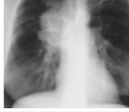

Review Case 2

Routine chest radiograph (Fig. 4.64) in a 76-year-old man prior to cardiac catheterization.
History of many years of smoking.

Question 1

How do you evaluate heart size and cardiac compensation? (Previously discussed in Chapter 1.)

Question 2

How do you evaluate the pulmonary parenchyma? Are there chronic changes consistent with the clinically known COPD? (Previously discussed in Chapter 2.)

Question 3

What finding prompts you to immediately request further diagnostic studies? (This chapter.)

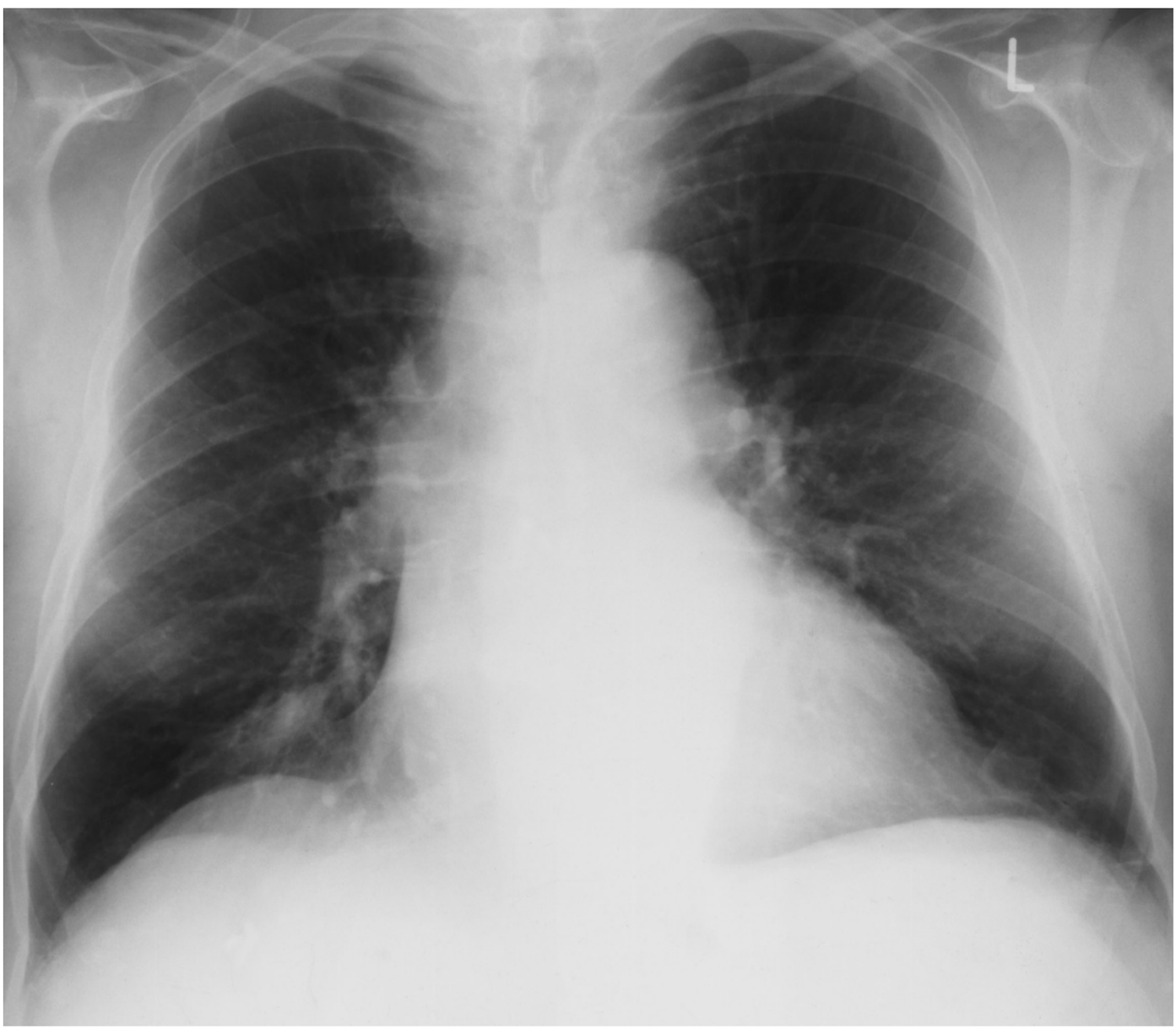

Fig. 4.64 Routine chest radiograph in a male chronic smoker prior to cardiac catheterization.

Answer

Answer to question 1: Left heart enlargement with moderate congestion in the pulmonary veins. There is no acute decompensation.

Answer to question 2: Shadowing as in chronic bronchitis. The obstructive barrel chest and pronounced pulmonary arteries are consistent with this.

Answer to question 3: There is a faint focal lesion in the third right anterior intercostal space (**Fig. 4.65**).

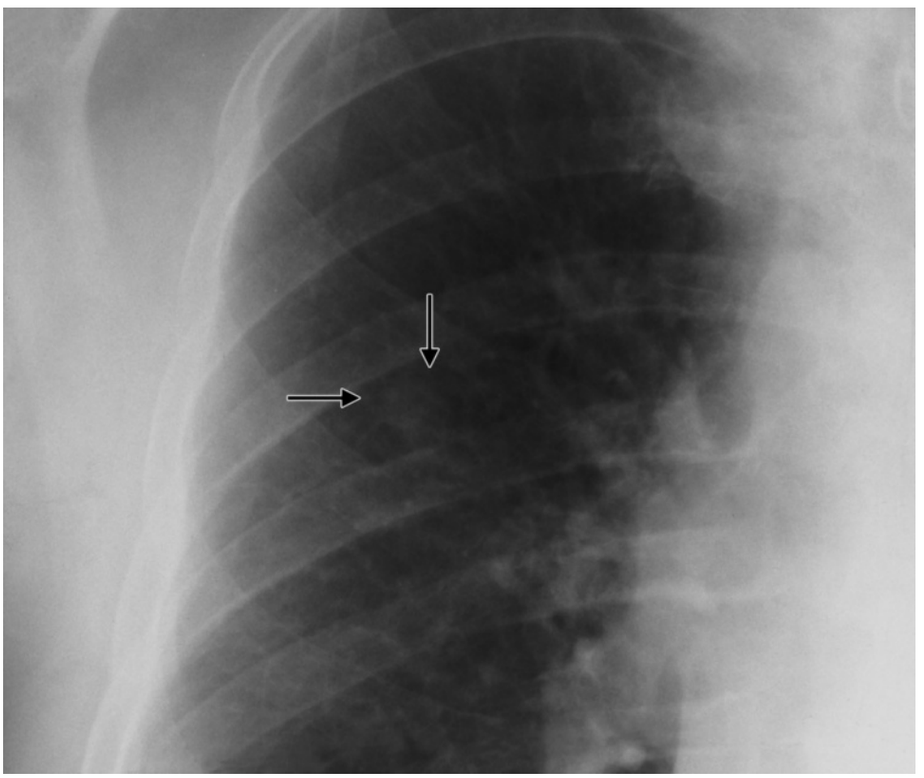

Fig. 4.65 Detail enlargement of Fig. 4.64 with the focal lesion marked (black arrows).

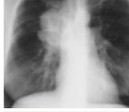

Review Case 3

The patient is a 62-year-old woman admitted to the emergency room with acute coronary syndrome (Fig. 4.66). Clinical angina pectoris, no fever, chronic but unproductive cough (long history of smoking).

Question 1

Find the intrapulmonary focal lesion.

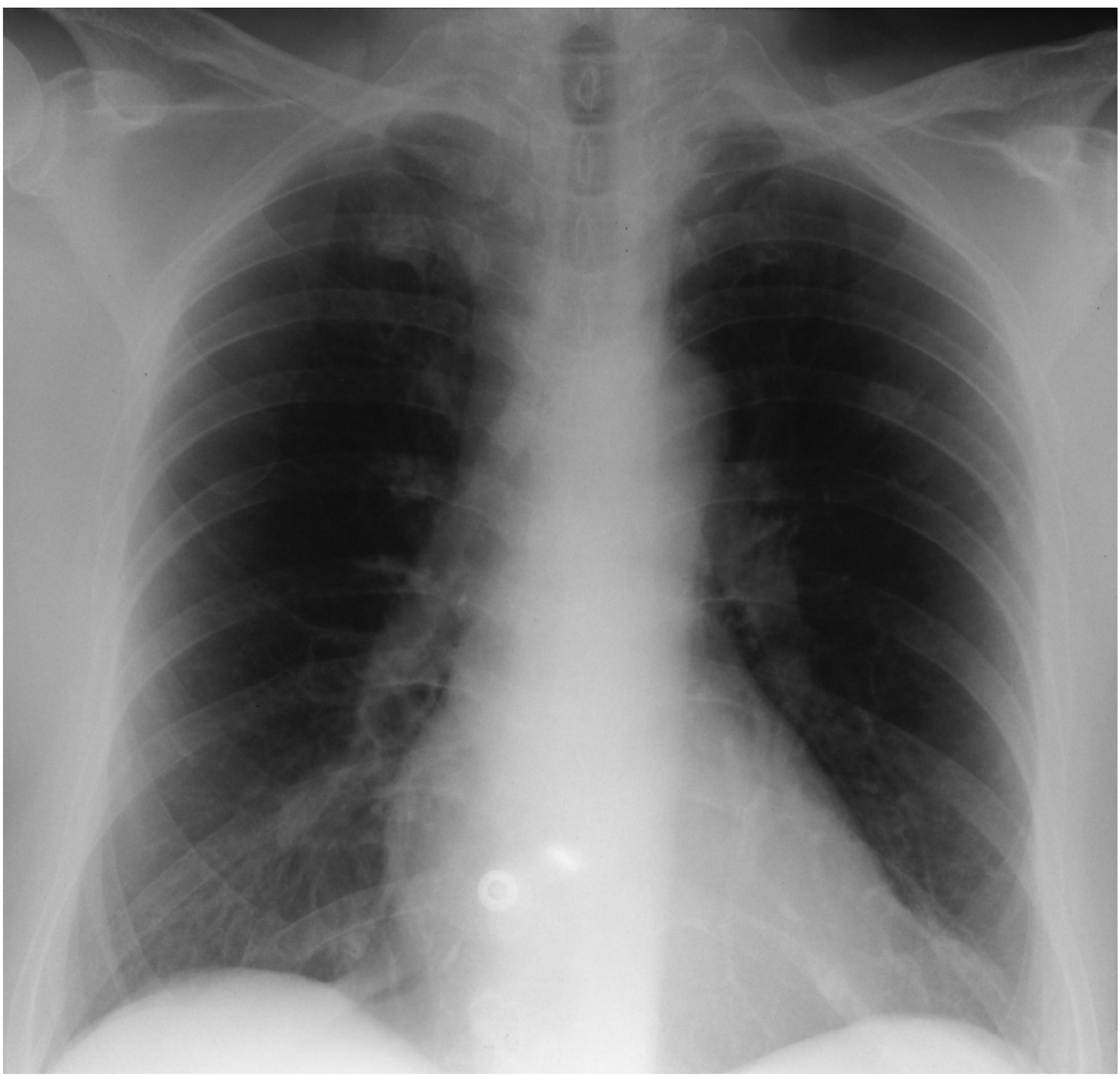

Fig. 4.66 Acute coronary syndrome in a female chronic smoker.

Answer

Clear signs of chronic bronchitis are present with obstructive barrel chest, but there is no area consolidation. A faint focal lesion approximately 13 mm in diameter is present in the left upper lung field. It is partially masked by the posterior portion of the sixth rib.

The follow-up films in two planes (**Fig. 4.67**) obtained with the patient standing clearly show the lesion in the anterior segment of the left upper lobe. The CT scan (**Fig. 4.67c**) supported the tentative diagnosis of peripheral bronchial carcinoma. The lesion was resected; the patient has been in postoperative care for 3 years without any signs of recurrence or metastasis.

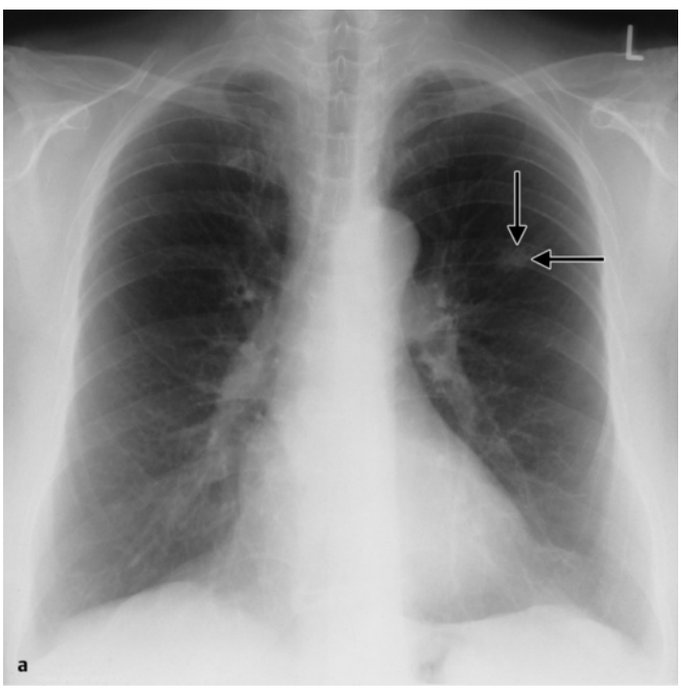

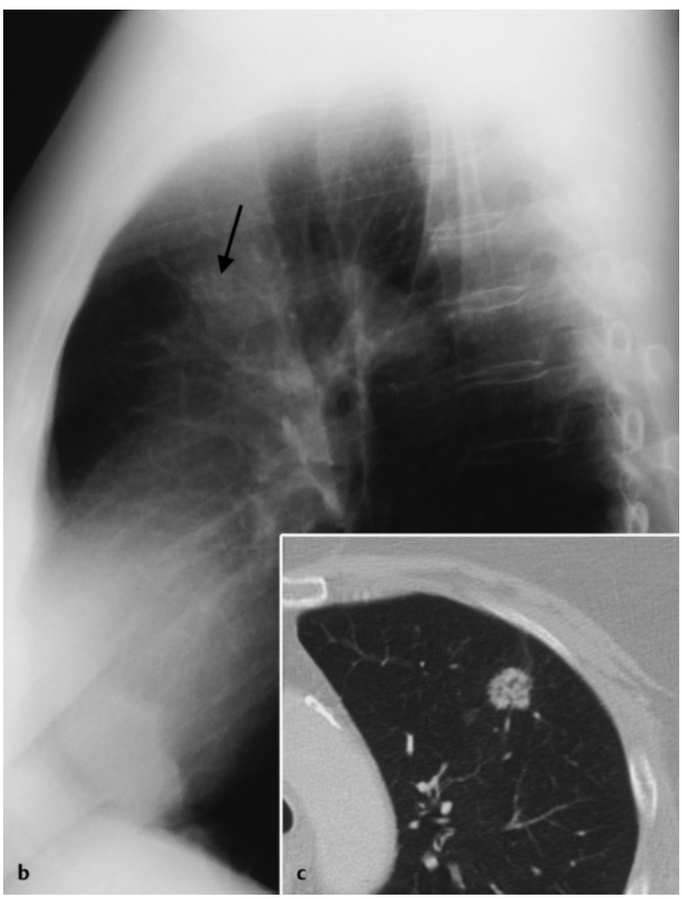

Fig. 4.67 a–c **Follow-up films in two planes obtained with the patient standing (a, b) and CT scan of the left upper lung field (c).** A faint focal lesion (black arrows) is projected on the sixth posterior rib. On the lateral film (**b**) it is projected onto the anterior upper lobe (black arrow). The CT scan (**c**) clearly shows signs of malignancy. The border is ill-defined with a fine corona radiata.

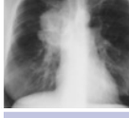

Review Case 4

The patient is a 72-year-old woman with a left hypernephroma. A plain chest radiograph (Fig. 4.68) was obtained as part of preoperative staging. The patient has a long history of smoking with chronic bronchitis and known coronary heart disease.

Question 1

How do you evaluate heart size and cardiac compensation?
(Previously discussed in Chapter 1.)

Question 2

What changes suggest chronic bronchitis?
(Previously discussed in Chapter 2.)

Question 3

What change suggests the presence of bronchial carcinoma?
(This chapter.)

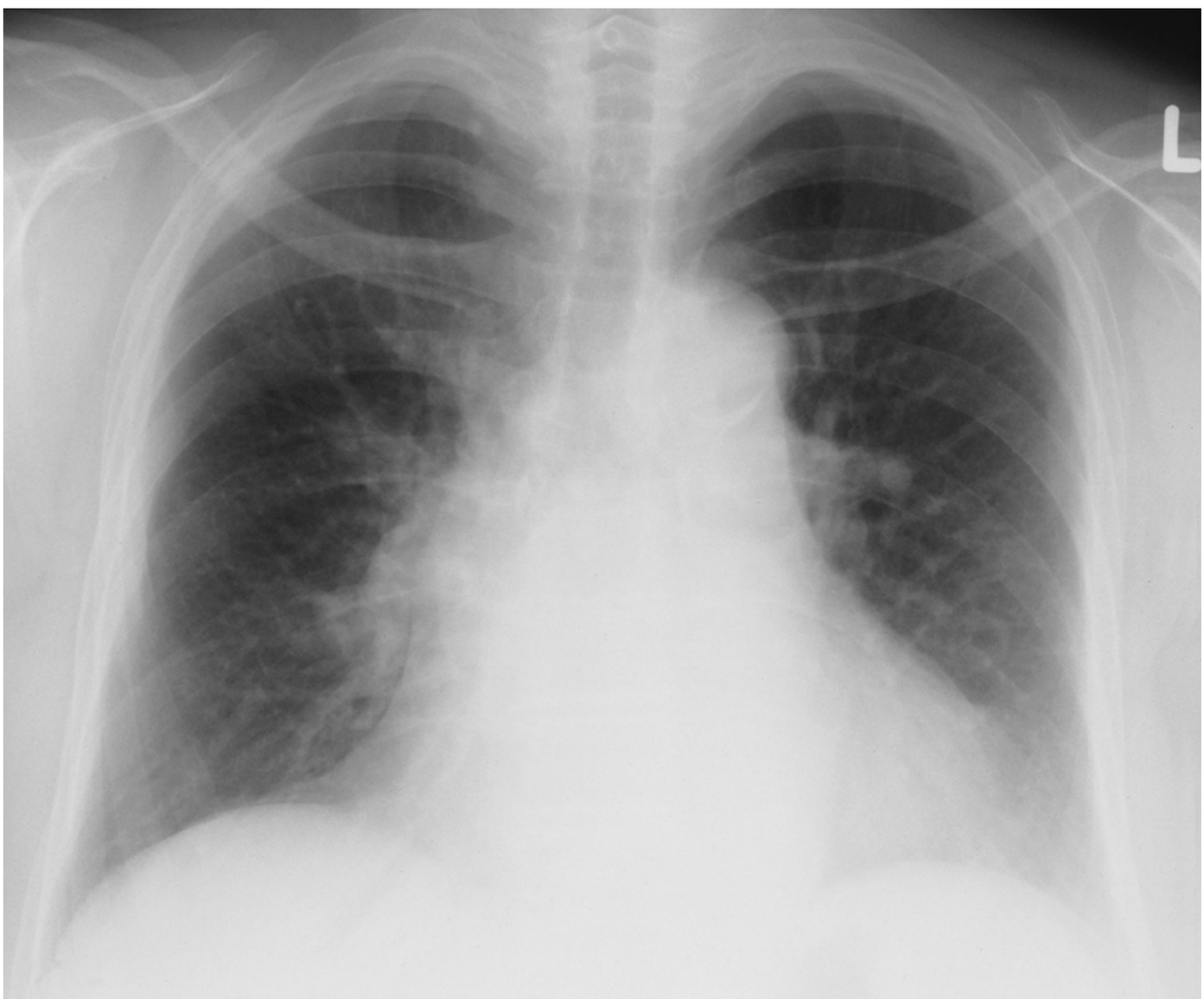

Fig. 4.68 Preoperative examination in the presence of a hypernephroma, coronary heart disease, and COPD.

Answer

Answer to question 1: The left heart is moderately enlarged (the long axis of the heart is longer than the width of the hemithorax). There are no signs of decompensation.

Answer to question 2: Diffuse shadowing is present with an obstructive chest type. However, inspiration is moderate on this posteroanterior radiograph.

Answer to question 3: Contour deformity of the right hilum is seen at the junction of the intermediate artery and lower lobar artery. The posteroanterior view shows atypical protrusion with a discrete platelike area of hypoventilation.

The CT scan performed immediately afterward (**Fig. 4.69**) shows the right central mass (black arrow) at the bifurcation of the intermediate artery. There is also a smaller focal lesion (white arrow) at the bifurcation of the third segmental artery, and the azygos lymph node is significantly enlarged (black arrowhead). Transbronchial biopsy confirmed the tentative diagnosis of bronchial carcinoma.

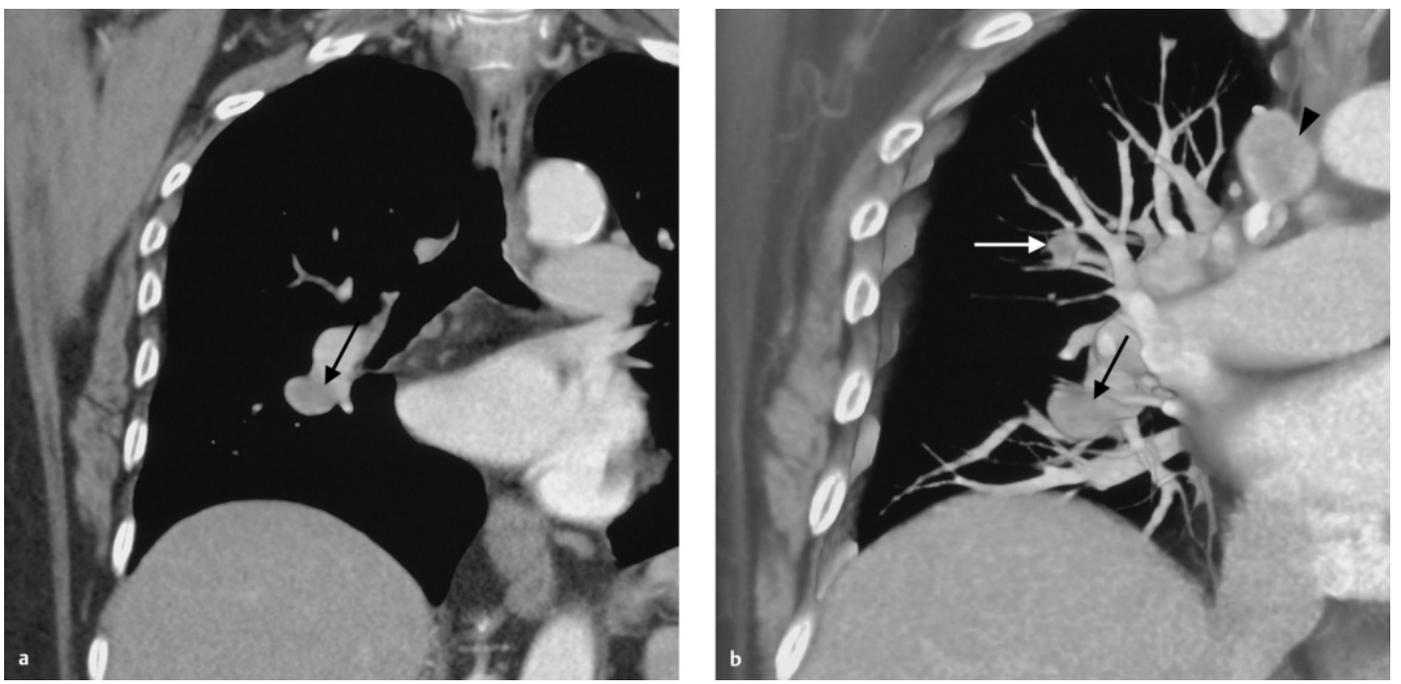

Fig. 4.69 a, b Central bronchial carcinoma in the right lung (CT scan of the patient in Fig. 4.68). The coronal soft-tissue reconstruction (**a**) and the 3D image of the right hilar vascular tree (**b**) both demonstrate a tumor at the bifurcation of the intermediate artery (black arrow). Another small lesion is located at the bifurcation of the third segmental artery (white arrow). Abnormal azygos lymph node (black arrowhead).

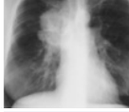

Review Case 5

The patient is a 70-year-old man presenting for cardiac catheterization for angina on exercise. History of many years of smoking.

Because the plain chest radiograph with the patient standing (**Fig. 4.70 a**) demonstrated a focal lesion in the right apical upper lobe, fluoroscopy (**Fig. 4.70 b**) was performed.

Question 1

What underlying disease of the pulmonary parenchyma is present?

Question 2

How do you evaluate the intrapulmonary focal lesion that has been demonstrated? What criteria suggest malignancy?

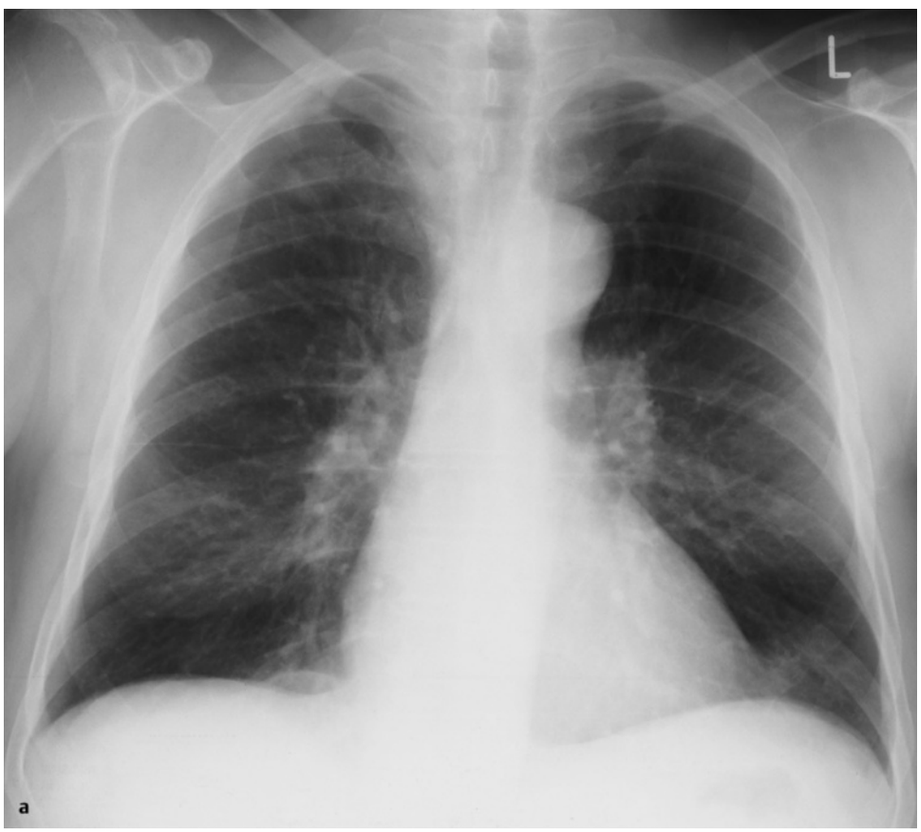

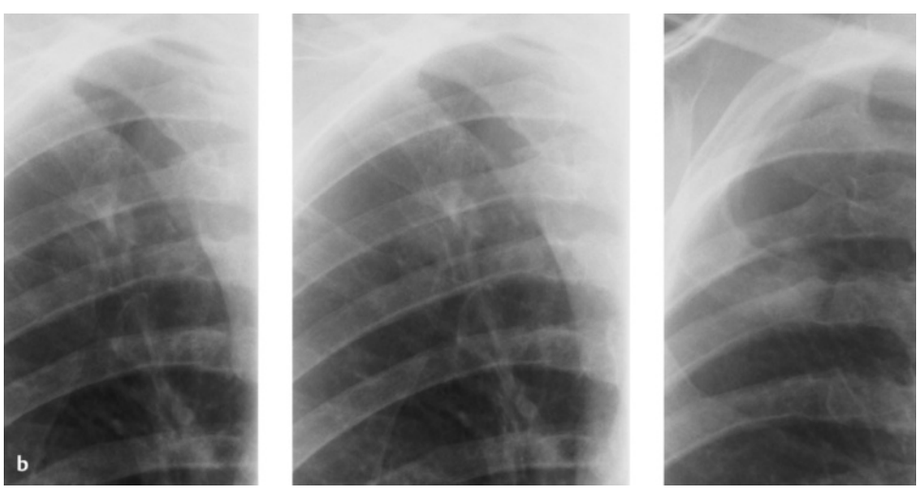

Fig. 4.70 a, b Plain chest radiograph of a male smoker prior to cardiac catheterization (a); fluoroscopy examination of the same patient (b).

Answer

Answer to question 1: Diffuse interstitial shadowing and obstructive barrel chest consistent with chronic bronchitis. The heart and aorta exhibit a hypertensive configuration without signs of decompensation.

Answer to question 2: The faint focal lesion 20 mm in diameter in the right upper lobe shows an obvious indentation of its lateral border (Rigler dimpling).

CT demonstrates the Rigler dimple (**Fig. 4.71 a**) and a fingerlike pleural lesion (**Fig. 4.71 b**). The axial slices show an obvious corona radiata (**Fig. 4.71 c**). With three criteria of malignancy present, this lesion is most probably a peripheral bronchial carcinoma.

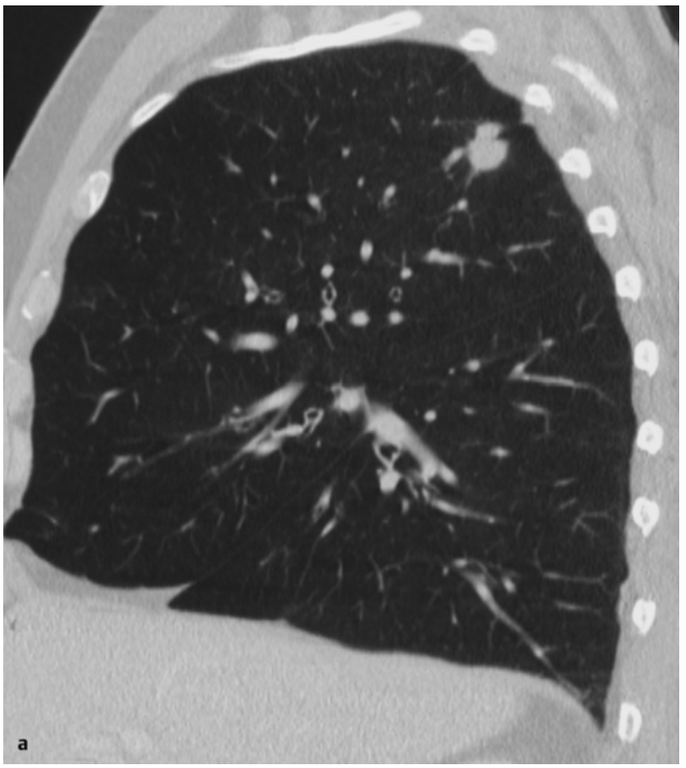

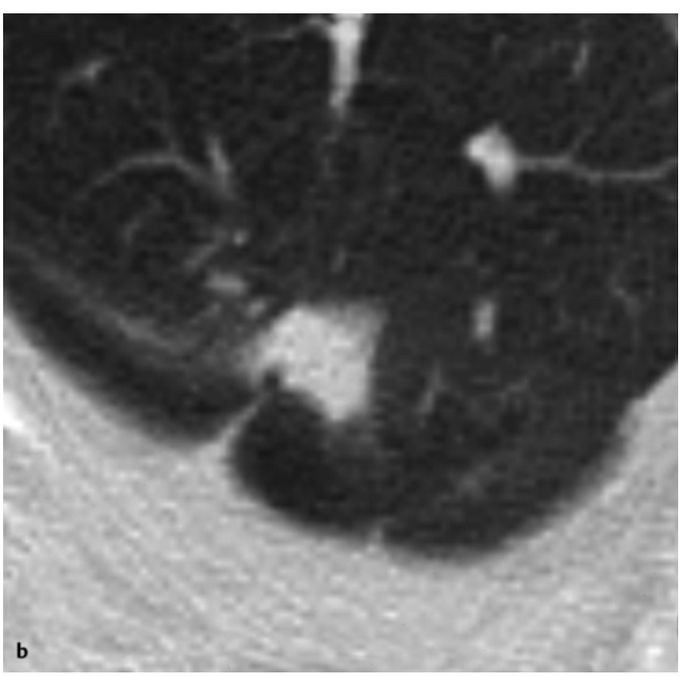

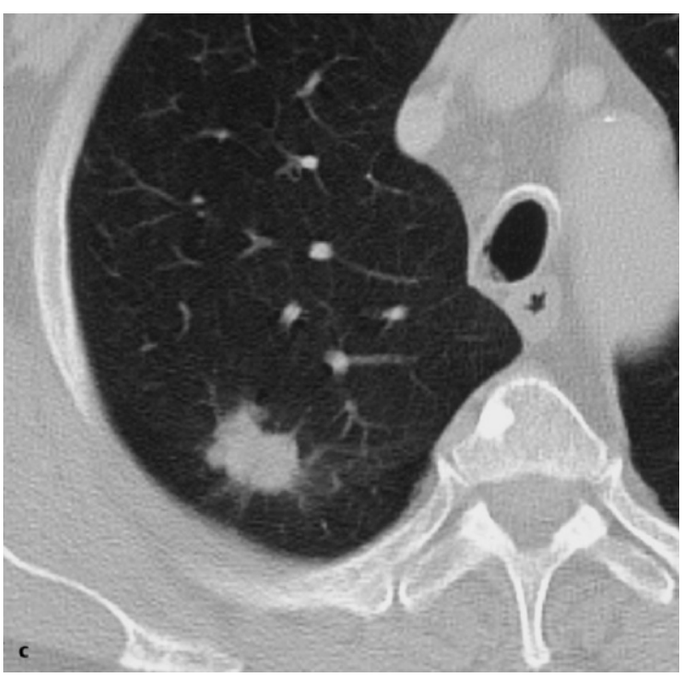

Fig. 4.71 a–c **CT findings in the patient in Fig. 4.70.** Signs of malignancy include Rigler dimpling (**a**), a fingerlike pleural extension (**b**), and corona radiata (**c**).

5

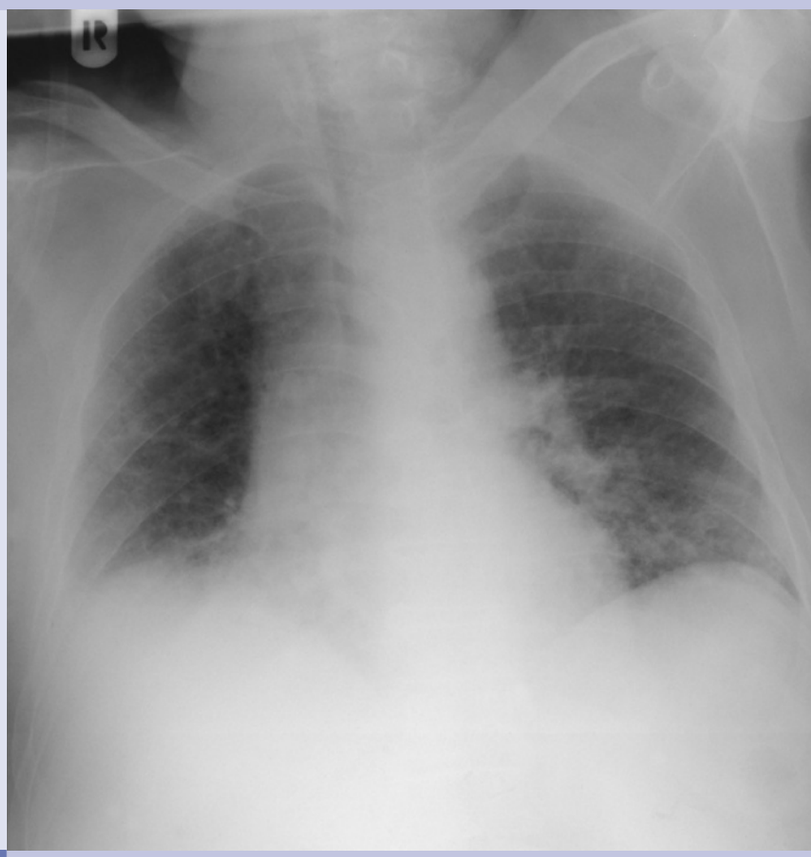

Fibrosing Lung Disease

General

The pulmonary interstitium is the space between the alveolar walls, which represent the actual functional pulmonary parenchyma. It forms the basic structure of the lung. The basic substance of the interstitium consists of proteoglycans synthesized by fibroblasts and a network of elastic collagen fibers, which account for up to 20% of the dry mass of the lung. Many lung diseases with a wide range of etiologies activate reactions that lead to inflammation of the interstitium with secondary scarring (fibrosis) (**Fig. 5.1**). As a result, many processes progress to fibrotic healing stages that are then indistinguishable even on histologic examination, not to mention on diagnostic imaging studies (**Fig. 5.3**).

Thus, various disorders eventually lead to pulmonary fibrosis by the common pathophysiologic mechanism of proliferation and activation of fibroblasts. These cells then produce excessive amounts of proteoglycans and collagen fibers. This reaction is physiologically limited; the fibroblasts die by apoptosis as the inflammation heals. However, chronic inflammations or conditions that perpetuate these processes can lead to increasing thickening of the interstitium, resulting in impaired gas exchange. Compliance is also decreased, leading to a restrictive ventilation defect. Advanced cases show fibroblastic invasion of the alveoli with development of fibrotic focal lesions (**Fig. 5.2**).

We first have to answer these questions:

- What signs suggest the presence of an interstitial process leading to fibrosis?
- More generally: What suggests that interstitial processes are present at all?
- Even more generally: What is the interstitium on the radiograph?

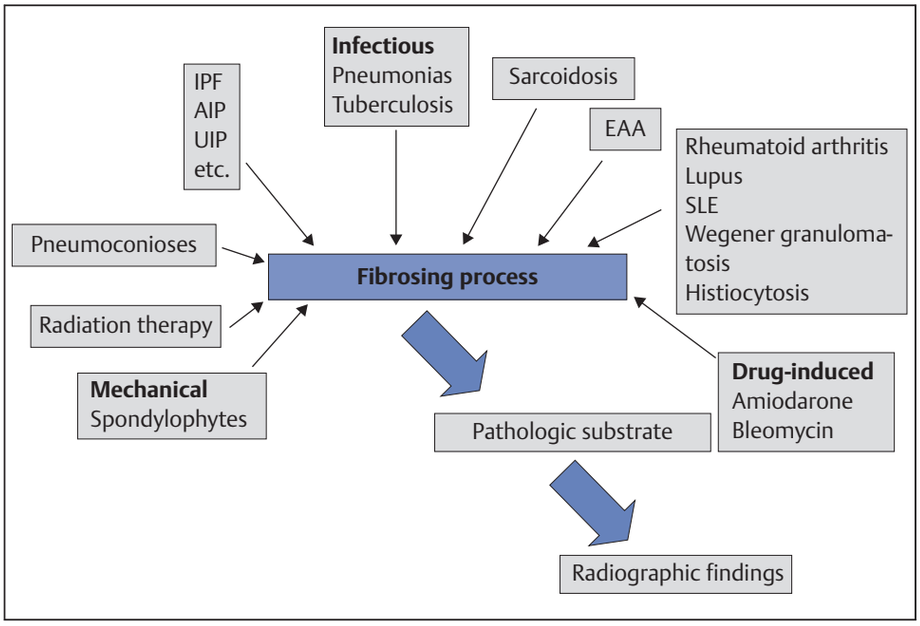

Fig. 5.1 The range of etiologies of pulmonary fibrosis. A variety of causes can activate fibrosing processes that then produce similar radiographic findings

AIP: Acute interstitial pneumonia
EAA: Extrinsic allergic alveolitis
IPF: Idiopathic pulmonary fibrosis
SLE: Systemic lupus erythematosus
UIP: Usual interstitial pneumonia

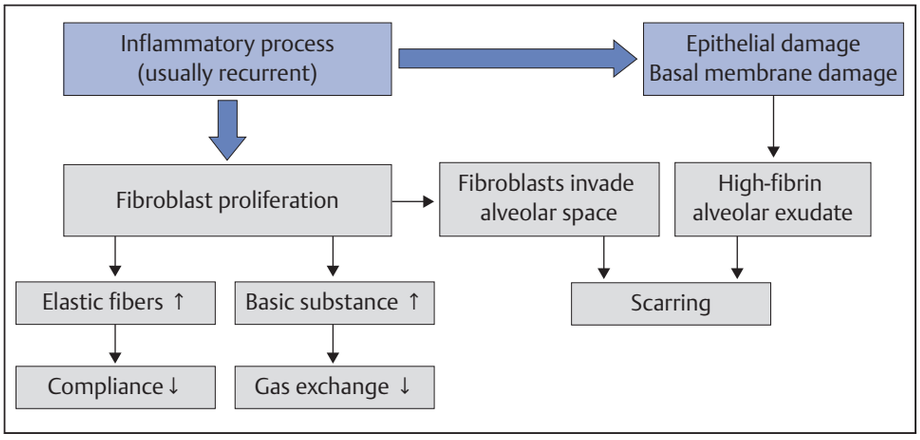

Fig. 5.2 Pathologic mechanism of pulmonary fibrosis.

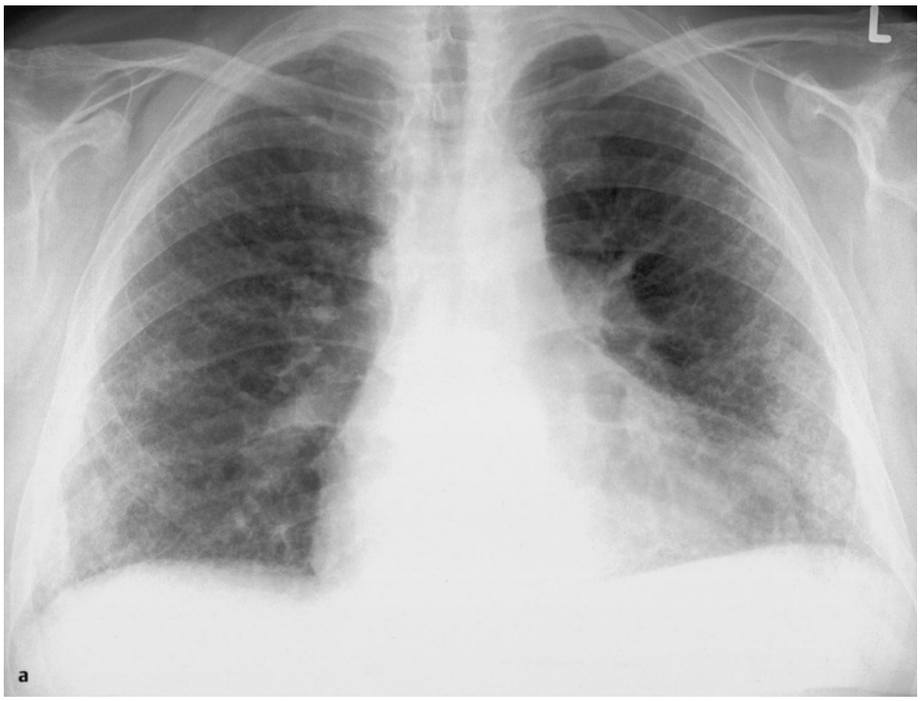

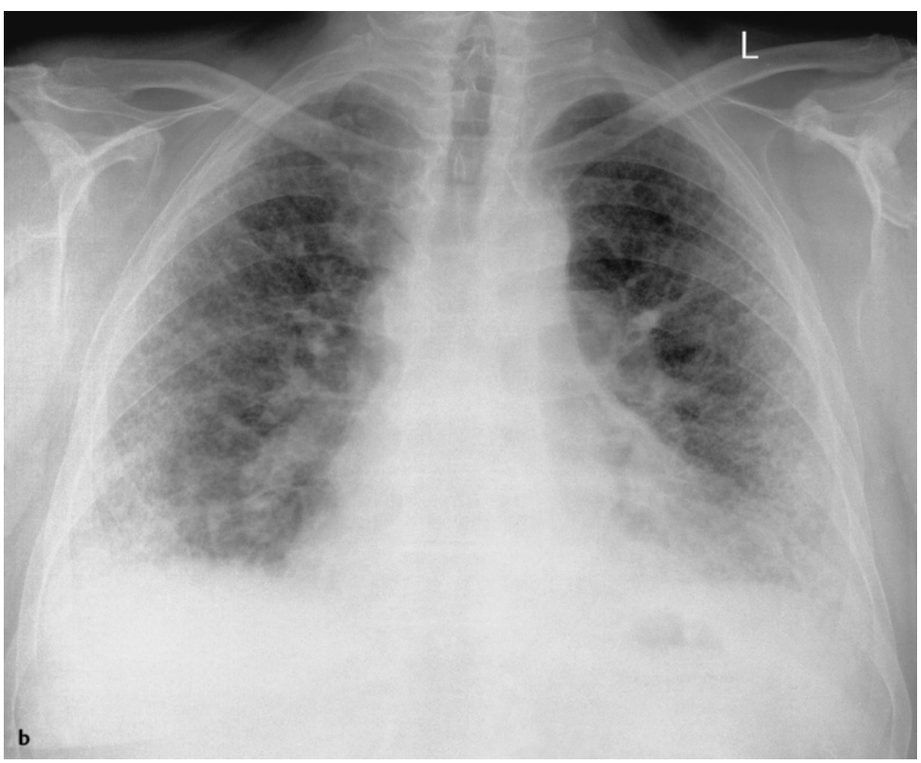

Fig. 5.3 a, b **Restrictive ventilation defect in idiopathic pulmonary fibrosis.**

a Findings include pronounced interstitial shadowing primarily in the mantle of the lung, and a high-riding diaphragm on both sides in broad contact with the heart.

b The follow-up examination 18 months later shows increased shadowing with initial blurring of the diaphragm. Other findings include further thickening of the pulmonary arteries, right heart enlargement, and widening of the upper mediastinum indicative of the onset of cor pulmonale.

Interstitial changes are discrete because of the much smaller volume of intervening tissue (**Fig. 5.5**) than in the alveolar spaces (**Fig. 5.4**). In fact, some authors go so far as to question whether it is possible to identify exclusively interstitial processes on chest radiography at all. However, there are in fact phenomena that indicate the presence of such changes. Direct comparison of alveolar and interstitial signs is particularly helpful (**Table 5.1**). Streaks, lines, and small focal lesions 2–3 mm in diameter (even in a miliary distribution pattern) are regarded as typical interstitial findings (**Fig. 5.6**). In granulomatosis, these findings exhibit relatively uniform size. They are sharply demarcated and only lose their sharp definition as their size increases (alveolar compression). The proliferation and thickening of the reticular pulmonary shadowing, which can even progress to a coarse weblike pattern, is attributable to a connective tissue reaction. Fine honeycombing is regarded as relatively typical. In contrast to alveolar processes (**Fig. 5.7**) the interstitial patterns are slow to change. Congestive interstitial pulmonary edema is an exception to this rule.

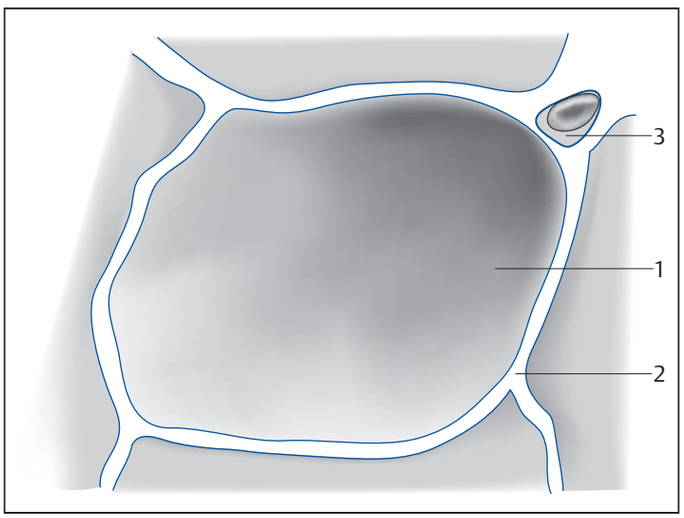

Fig. 5.4 Schematic diagram of the alveolar space. The air-filled space of the alveoli (1) surrounded by the alveolar walls and interstitial septa is far larger than the interstitial space (2). Capillary with erythrocyte (3).

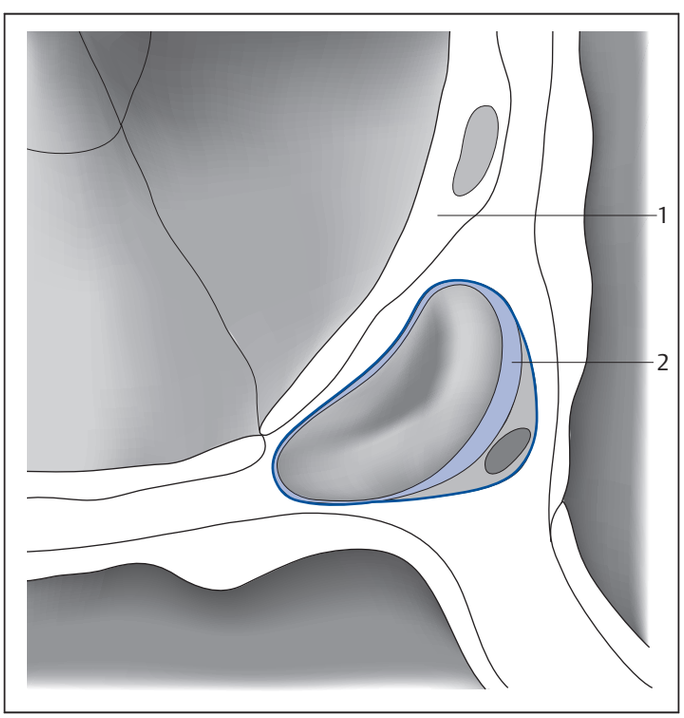

Fig. 5.5 Schematic diagram of the interstitial space. The space between the alveolar walls (pneumocytes [1], functional cells) is referred to as the pulmonary interstitium. It is filled with collagen. Blood vessels (2) and lymph vessels course through this space.

Table 5.1 Alveolar and interstitial signs

Alveolar	Interstitial
Acinar foci (5–10 mm)	Small nodules (2–3 mm)
Ill-defined	Sharply demarcated, uniform
Gradual transition to normal findings	Streaky and linear densities
Tendency to become confluent	Sharply demarcated
Area consolidation	Miliary
Air bronchogram	Honeycombing
Alveolar air pattern	
Butterfly pattern	
Rapid development	Slow development

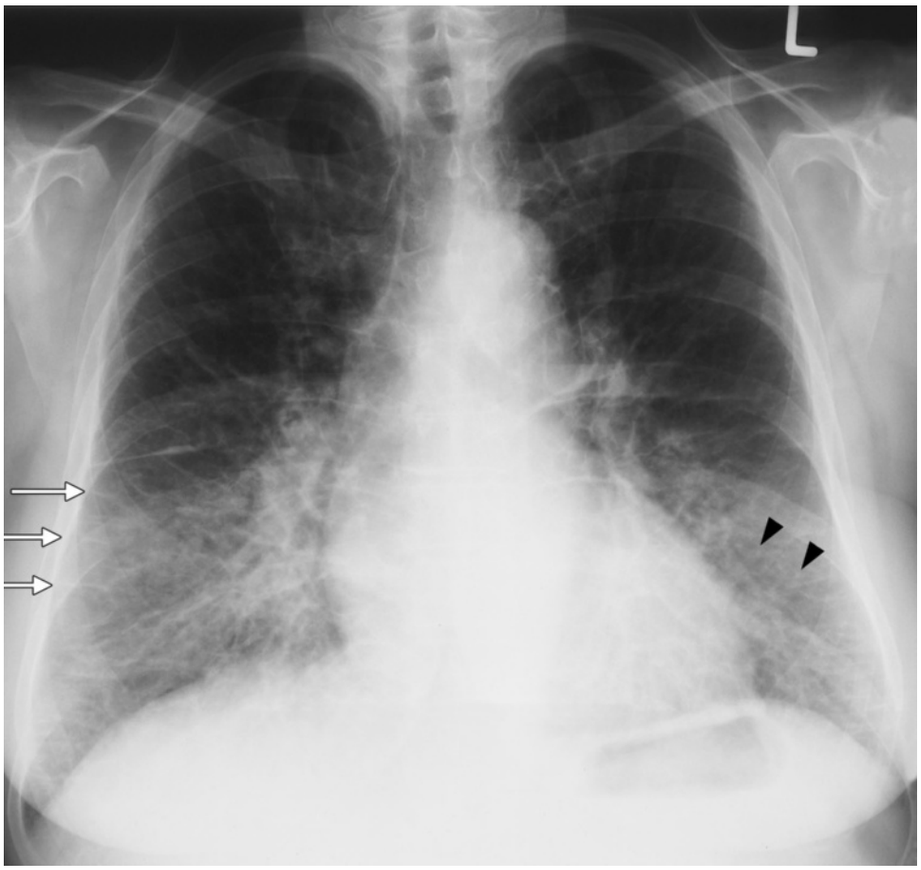

Fig. 5.6 Interstitial pattern in a cardiac pulmonary edema. In addition to pronounced Kerley lines (white arrows) and thickening of the right horizontal fissure due to onset of effusion, findings include acinar nodules (black arrowheads) beginning in the basal segments. Here, only the Kerley lines represent the interstitial pattern. The (discrete) acinar nodules represent onset of alveolar edema.

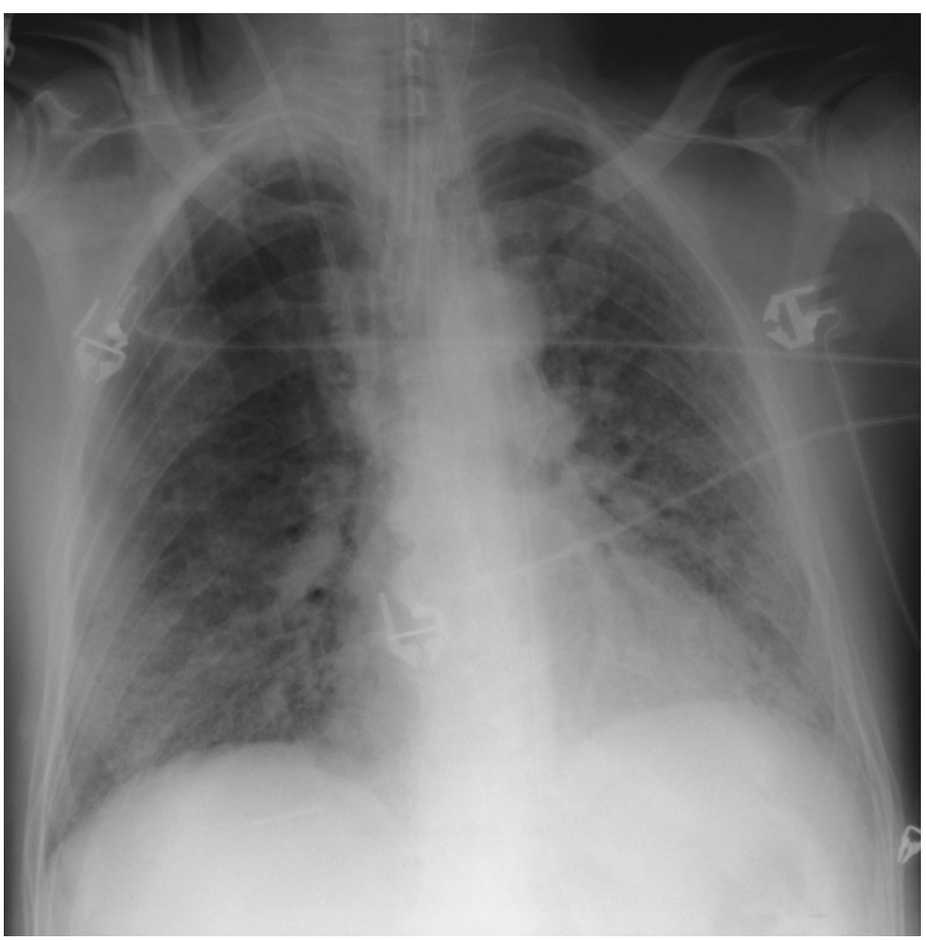

Fig. 5.7 Alveolar shadows in alveolar proteinosis. Alveolar proteinosis may be regarded as a classic example of an alveolar process. The patient is a 56-year-old man who has had a flulike infection and is now presenting with severe respiratory failure. Findings in the intubated patient include bilateral diffuse ground-glass opacities. Heart size is normal. CT demonstrated pathognomonic findings of a leaf pattern, and lavage produced the typical milky exudate.

Idiopathic Pulmonary Fibrosis

Idiopathic pulmonary fibrosis (IPF) is classified as an idiopathic interstitial pneumonia (**Table 5.2**). It is the most common of this group of disorders of uncertain pathogenesis. Idiopathic pulmonary fibrosis and its acute variant (acute interstitial pneumonia, AIP) also have the worst prognosis.

Radiologic signs of idiopathic pulmonary fibrosis on the chest radiograph include:

- Ground-glass opacities
- Reticular shadowing
- Disseminated small nodules
- Progressively reduced depth of inspiration
- Honeycombing
- Pronounced findings in the mantle of the lung

The most important criterion for the **differential diagnosis** of idiopathic pulmonary fibrosis from secondary fibrosis in chronic emphysematous bronchitis is the progressive reduction in the depth of inspiration (see **Fig. 5.3**). Decreased compliance leads to a restrictive ventilation defect with a progressively high-riding diaphragm and the picture of a "small lung." The picture of severe fibrosing bronchitis differs in that it is characterized by a barrel chest deformity. The signs occur in varying severity over the course of the disorder. Diffuse ground-glass opacities of the basal and central segments that blur the vascular structures and pulmonary borders tend to occur early (**Fig. 5.8**) and in the acute form of the disease. CT detects them in a significantly higher percentage of cases. The onset of fibrosis is marked by fine reticular shadowing in the basal lung segments. This pattern increasingly spreads through the periphery of the lung. Irregular streaky densities and nodular changes occur in the further course of the disorder. The pattern becomes coarsely reticular (**Fig. 5.9**).

The honeycombing that occurs only in advanced cases is regarded as a typical finding. This pattern is created by a circumscribed cluster of bullae measuring 1 to 10 mm in diameter. These clusters show a predilection for the posterobasal segments (**Fig. 5.9b**). Note that even advanced cases show neither effusion nor cardiomegaly with signs of congestion such as Kerley lines. However, this picture is often masked by intercurrent infections.

Notes on Pathology and Clinical Findings

Progressive inflammatory processes tending to produce fibrosis of the pulmonary parenchyma (interstitial and alveolar components) that are not the result of extrinsic noxious agents such as pneumoconiosis, extrinsic allergic alveolitis (see below), radiation therapy, etc. or systemic diseases such as scleroderma or systemic lupus erythematosus are classified as idiopathic pulmonary fibrosis (IPF). A further subdivision is still controversial. The Katzenstein classification has recently been expanded by an ATS/ERS study group (**Table 5.2**). This system differentiates the following forms:

- Acute form (AIP), corresponding to what was once known as Hamman–Rich disease
- Desquamative form with hypercellular alveolar exudate and highly uniform distribution (DIP)
- A form with a highly irregular distribution of changes and dense focal accumulations of collagen in the interstitium, known as the usual form (UIP or IPF)
- A nonspecific type with diffuse, homogeneous thickening of the alveolar septa: nonspecific interstitial pneumonia (NSIP)

However, various groups (Scadding, Turner–Warwick) have postulated that DIP and UIP may be only different stages of the same disorder, IPF.

Idiopathic pulmonary fibrosis is a disorder typically occurring in advanced age, significantly more often in women than in men. The disorder begins with slight, nonspecific symptoms such as a dry cough that responds poorly to cough medications and dyspnea on exercise. Symptoms progress insidiously over a period of months. Auscultatory findings include inspiratory basal rales. Clubbed fingers occur in up to 50% of all cases. The pulmonary function examination usually shows a purely restrictive ventilation defect. The course of the disease is fatal within 3–5 years in the majority of cases. Only about one-third of patients respond to therapy with steroids or immunosuppressives.

Table 5.2 Classification of the idiopathic interstitial pneumonias

Katzenstein (1998)	ATS/ERS (2002)
Usual interstitial pneumonia (UIP)	Usual idiopathic pulmonary fibrosis (IPF)
Acute interstitial pneumonia (AIP)	Acute interstitial pneumonia (AIP)
Nonspecific interstitial pneumonia (NSIP)	Nonspecific interstitial pneumonia (NSIP)
Desquamative interstitial pneumonia (DIP)	Desquamative interstitial pneumonia (DIP)
Respiratory bronchiolitis-interstitial lung disease (RB-ILD)	Respiratory bronchiolitis-interstitial lung disease (RB-ILD)
Bronchiolitis obliterans with organizing pneumonia (BOOP)	Cryptogenic organizing pneumonia (COP)
Lymphoproliferative disease (LPD)	Lymphoid interstitial pneumonia (LIP)

ATS, American Thoracic Society; ERS, European Respiratory Society.

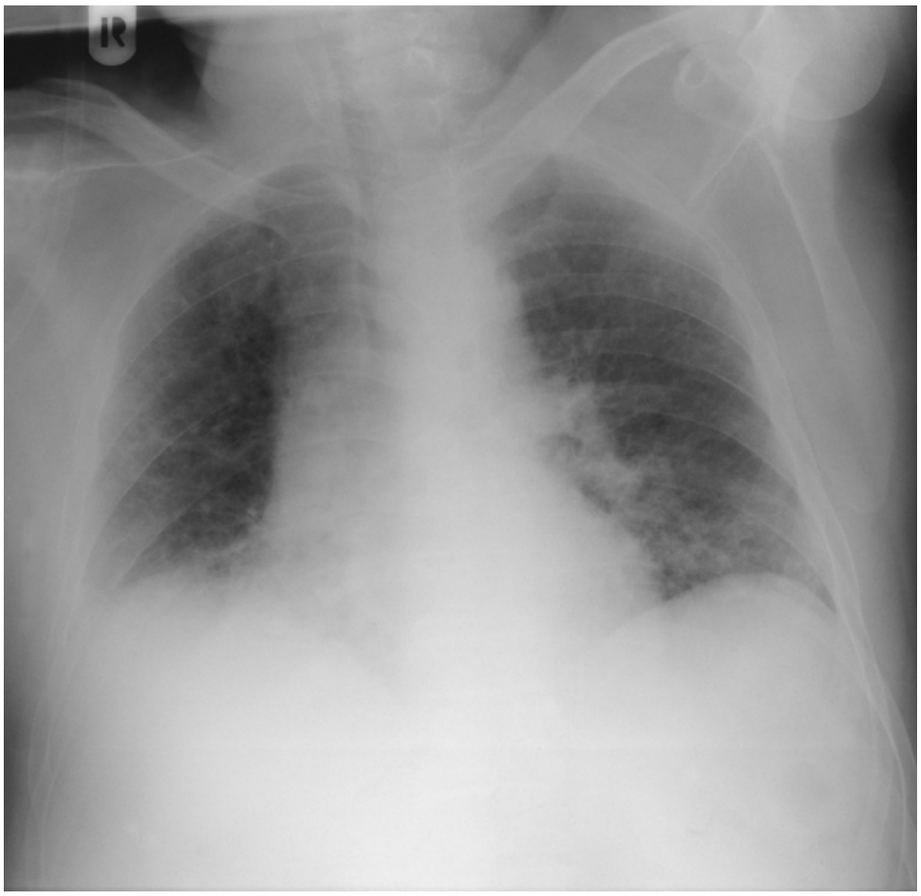

Fig. 5.8 Reduced depth of inspiration in idiopathic pulmonary fibrosis. The patient is a 66-year-old woman presenting with dyspnea on exercise. Diffuse shadowing is seen primarily in the basal segments, which also show hypoventilation and a high-riding diaphragm on both sides. The basal segments exhibit relatively "soft" ground-glass opacities.

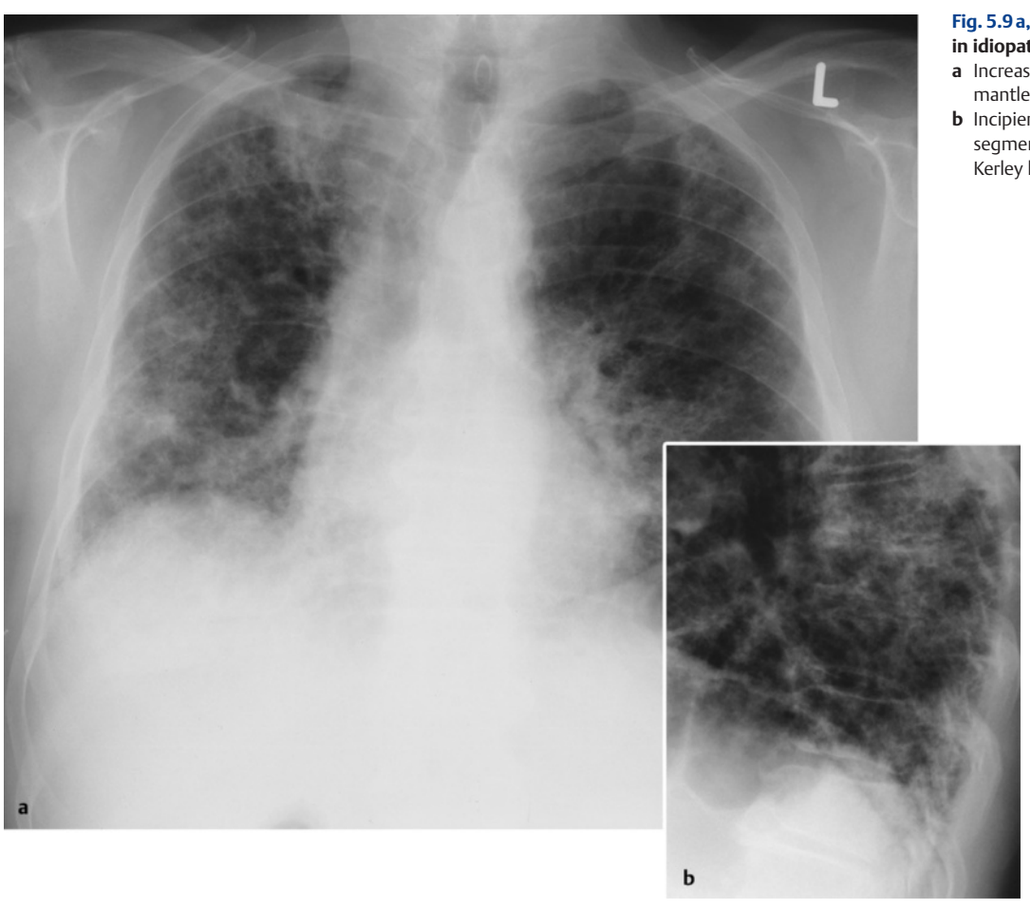

Fig. 5.9 a, b Reticular pattern and honeycombing in idiopathic pulmonary fibrosis.

a Increasing pulmonary restriction primarily in the mantle and basal segments of the lung.

b Incipient honeycombing is seen in the posterobasal segments. There are no effusions and hardly any Kerley lines.

On the **CT scan,** signs of idiopathic pulmonary fibrosis (**Fig. 5.10**) include increased intralobular and interlobular shadowing with a mantlelike distribution of septal thickening more pronounced in the lower lung fields, isolated nodules, linear densities parallel to the pleura, hyperinflated secondary lobules that can produce an arcade pattern, honeycombing, mosaic perfusion, and secondary changes (pulmonary arterial hypertension, right heart strain, etc.).

The intralobular shadowing (**Fig. 5.11**), the occurrence of fine nodular changes, linear densities parallel to the pleura (**Fig. 5.12**), hyperinflated secondary lobules, occasionally with mosaic perfusion (**Fig. 5.13**), bronchiectasis adjacent to areas of scarring (**Fig. 5.14**), and signs of right heart strain are all nonspecific findings. They can also occur in COPD or secondary to pneumonia. However the mantlelike distribution, which primarily involves the basal segments and is particularly well demonstrated on CT, is highly suggestive of idiopathic pulmonary fibrosis. Findings of subpleural arcades (**Fig. 5.15**) or honeycombing (**Fig. 5.16**) are essentially diagnostic of the restrictive process.

CT can provide more information about the activity of the fibrotic process than the plain chest radiograph. The fundamental consideration in this context is that the acute process causing the fibrosis (for example, in acute interstitial pneumonia) usually manifests itself as an alveolar pattern with blurring and ground-glass attenuation, whereas the scarring appears as a network of sharply defined markings (**Table 5.3**).

Lymph node enlargement is inconsistent with idiopathic pulmonary fibrosis. The diagnosis should be reconsidered where such findings occur in the hilum or mediastinum (sarcoidosis? lymphangitis carcinomatosa?). Pleural effusions are other findings that are not attributable to pulmonary fibrosis but can occur in the presence of heart failure.

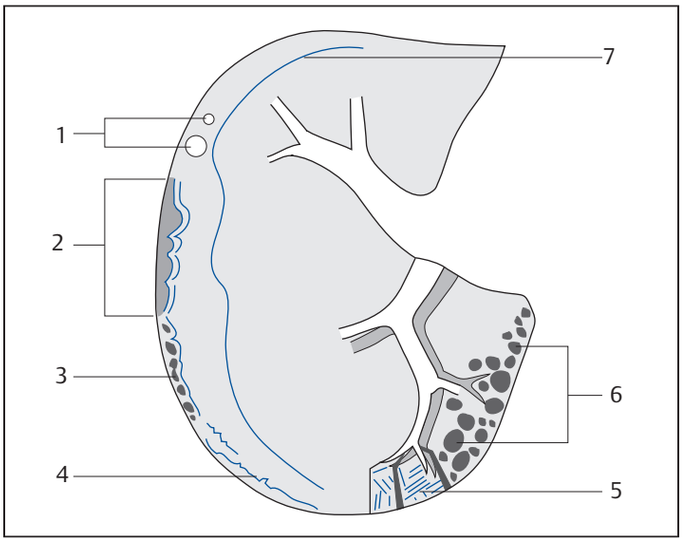

Fig. 5.10 Diagram of the CT signs of a fibrosing pulmonary process.
1 Isolated nodules
2 Arcades
3 Subpleural bullae
4 Linear densities parallel to the pleura
5 Thickened septa and interlobar fissures
6 Honeycombing
7 Peripheral location (mantle of the lung)

Table 5.3 Course of interstitial disorders

Acute "-itis"		Scarring		Destruction
Ill-defined	→	Sharply defined	→	Honeycombing
Ground-glass attenuation		Lines		Bullae
		Network		

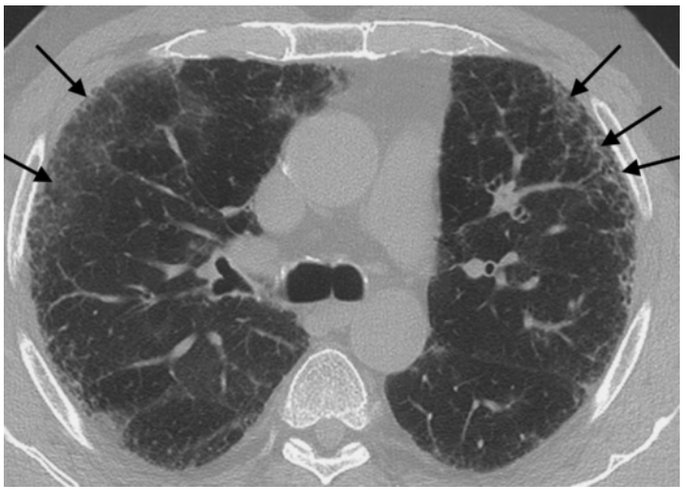

Fig. 5.11 Intralobular shadowing in idiopathic pulmonary fibrosis. The intralobular shadowing (black arrows) shows a mantlelike distribution.

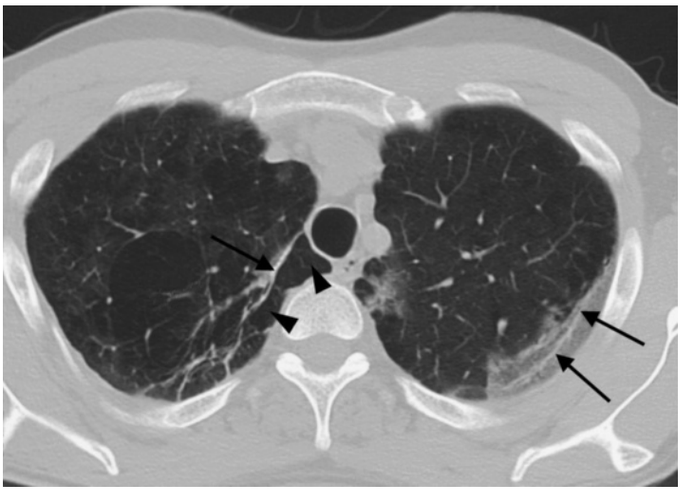

Fig. 5.12 Linear densities parallel to the pleura in idiopathic pulmonary fibrosis. In addition to ground-glass opacities in the left apical mantle, there are linear densities (black arrows) parallel to the pleura with hyperinflation of the subpleural portions of the lung (black arrowheads).

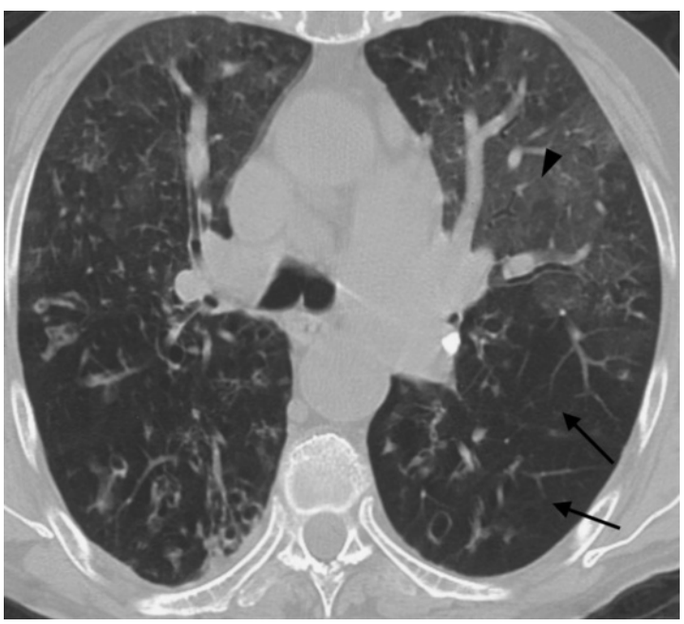

Fig. 5.13 Mosaic perfusion. The patient has severe COPD with advanced emphysema (increased lung volume, peribronchial shadowing, and isolated areas of mucus-filled bronchiectasis). In addition to hyperinflated areas visible as hypodensities (black arrows), findings include hyperperfused areas of higher density showing ground-glass attenuation (black arrowhead).

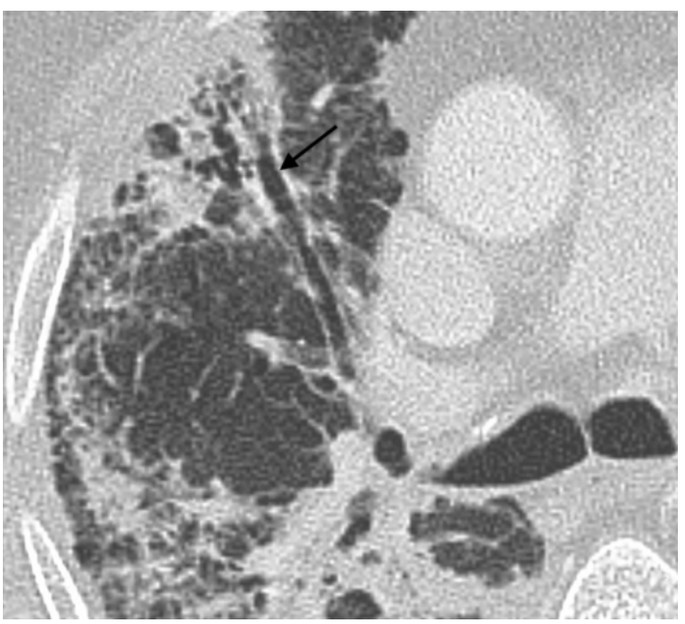

Fig. 5.14 Signs of shrinkage in a fibrotic area. Bronchiectasis (black arrow) and bronchiolectasis indicative of shrinkage of the peripheral area of scarring are nonspecific findings. However, in the context of other findings they can be evaluated as a sign of pulmonary fibrosis.

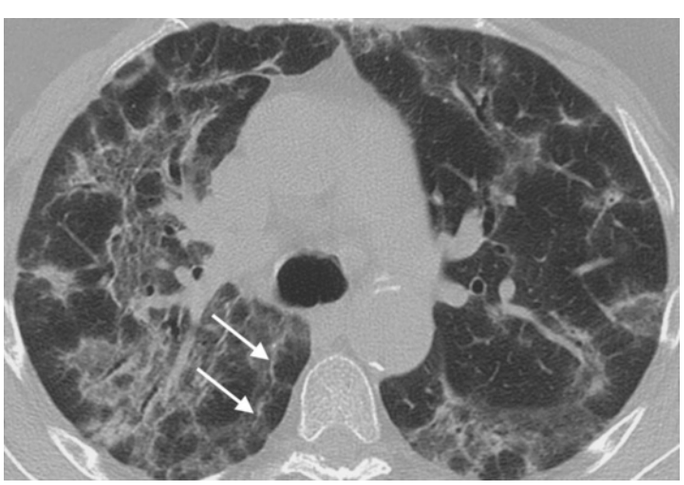

Fig. 5.15 Arcade pattern indicative of pulmonary fibrosis. Findings include significantly hyperinflated secondary lobules, shrinkage of the subpleural pulmonary tissue, and linear densities (white arrows) parallel to the pleura. Here, an arcade pattern is present.

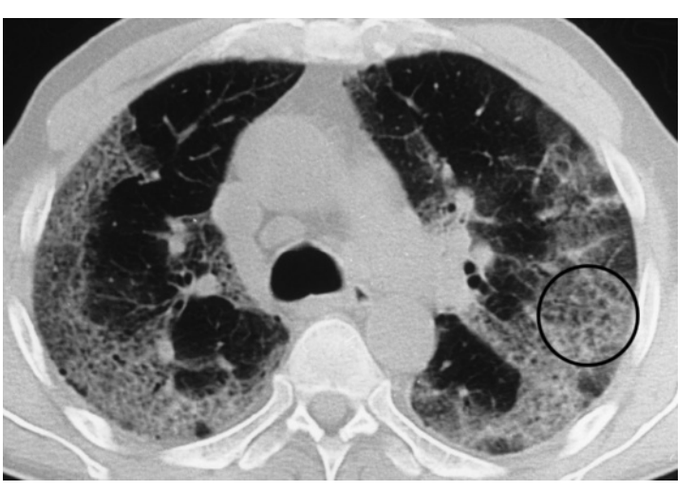

Fig. 5.16 Honeycombing in acute interstitial pneumonia. Extensive consolidations in the mantle of the lung with a significant loss of volume and finely bullous honeycombing (circle).

Acute Interstitial Pneumonia, Hamman–Rich Disease

As early as 1935 Hamman and Rich described a variant of pulmonary fibrosis with a fatal fulminant course in which the fibrotic transformations occurred within the space of a few weeks or months as in a time-lapse film sequence (**Fig. 5.17**).

Radiographic signs of acute interstitial pneumonia (AIP) include pronounced ground-glass opacities and progressive reduction in the depth of inspiration with severe septal thickening and fine honeycombing typically occurring simultaneously in a rapidly progressive course. In addition to extensive ground-glass opacities in the mantle of the lung (**Fig. 5.17 b**), Hamman–Rich disease shows septal thickening with hyperinflation of the smallest adjacent alveolar spaces at a very early stage. A fine honeycombing pattern of pulmonary changes rapidly appears even while ground-glass opacities are still present. The ground-glass opacities remain visible as volume loss progresses and architectural distortion increases. CT visualizes the arcadelike pattern of idiopathic pulmonary fibrosis in the mantle of the lung (**Fig. 5.17 d).**

In Hamman–Rich disease (acute interstitial pneumonia), ground-glass opacities (signs of activity) can often be demonstrated alongside honeycombing (signs of defects).

Differential Diagnosis of Idiopathic Pulmonary Fibrosis

The most important entity to consider in the differential diagnosis of idiopathic pulmonary fibrosis (idiopathic interstitial pneumonia) is a severe form of **chronic emphysematous bronchitis.** This differential diagnosis must be made almost daily in clinical practice and is not always a trivial matter. The crucial distinguishing criterion is whether an obstructive pulmonary disorder or a primarily restrictive ventilation defect is present. Signs suggesting obstructive disease include the presence of an emphysematous barrel chest with a high-riding diaphragm, widened intercostal spaces, etc. (see Chapter 2).

Difficult cases to interpret include those where the chronic bronchitis and obstruction are accompanied by factors leading to reduced inspiration, such as ascites, overhydration, or respiratory failure with intercurrent infiltrates. There are also borderline cases in which only the further course of the disorder permits definitive diagnosis. For example, hypoventilation is more rapidly progressive in idiopathic pulmonary fibrosis.

Pulmonary fibrosis in **scleroderma** closely resembles idiopathic pulmonary fibrosis, although the abnormal findings are rarely as extensive. Cutaneous changes are the crucial distinguishing feature in a differential diagnosis. Esophageal widening is a common finding indicative of systemic involvement.

Fibrosis secondary to **tuberculosis** is more or less localized and is easier to distinguish. Findings often include a stellate configuration of very dense fibrotic strands. The changes show a predilection for the upper lung fields. They are asymmetrical and can lead to significant destruction of pulmonary tissue with shrinkage. Compensatory emphysema is often observed in such cases. Associated findings include calcification (tuberculomas and hilar lymph node involvement) and calcified indurations of the pleura.

Lymphangitis carcinomatosa is not associated with any destruction of normal pulmonary architecture. The intralobular and interlobular septa are thickened and occasionally show nodular swelling. Pleural effusion indicative of impaired lymph drainage is a common finding here that is rarely seen in idiopathic pulmonary fibrosis.

The fibrotic changes in sarcoidosis, extrinsic allergic alveolitis, and pneumoconiosis are discussed on pages 214, 222, and 234.

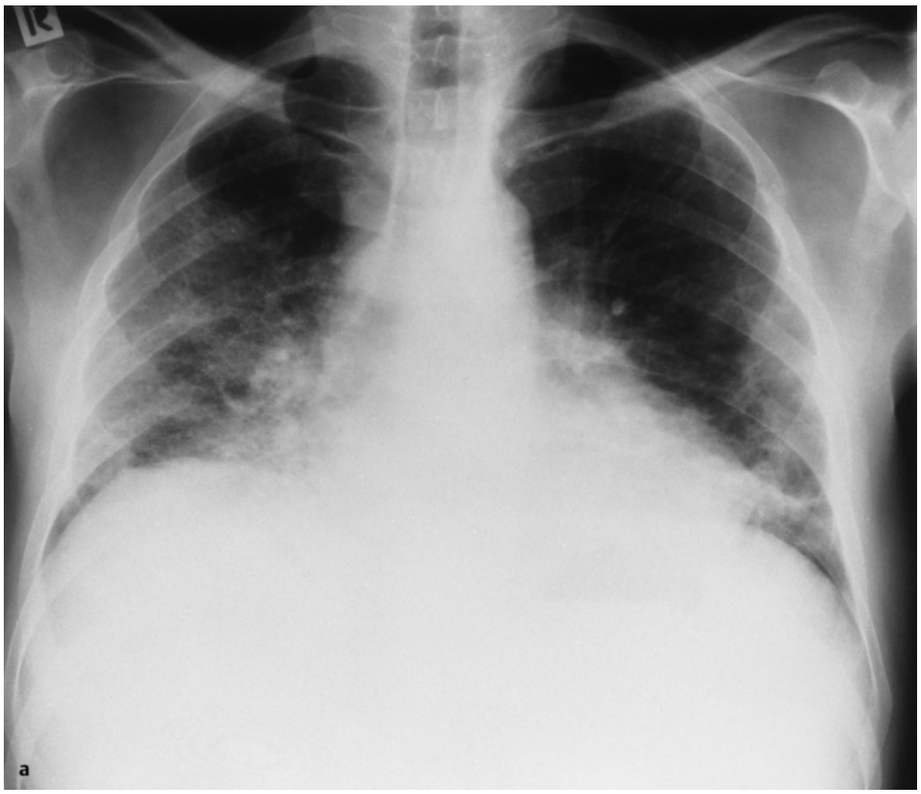

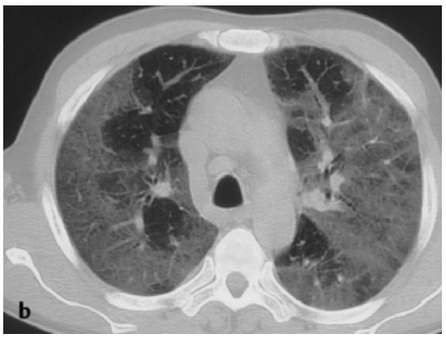

Fig. 5.17 a–d **Acute interstitial pneumonia**

a Interstitial shadowing is seen in the basal and peripheral areas. Depth of inspiration is significantly reduced, and the heart is in broad contact with the diaphragm. There is no cardiac decompensation.

b The CT scan performed at a relatively early stage of the disorder shows significant ground-glass opacities primarily in the mantle of the lung. Findings are strikingly symmetrical. No pleural effusion.

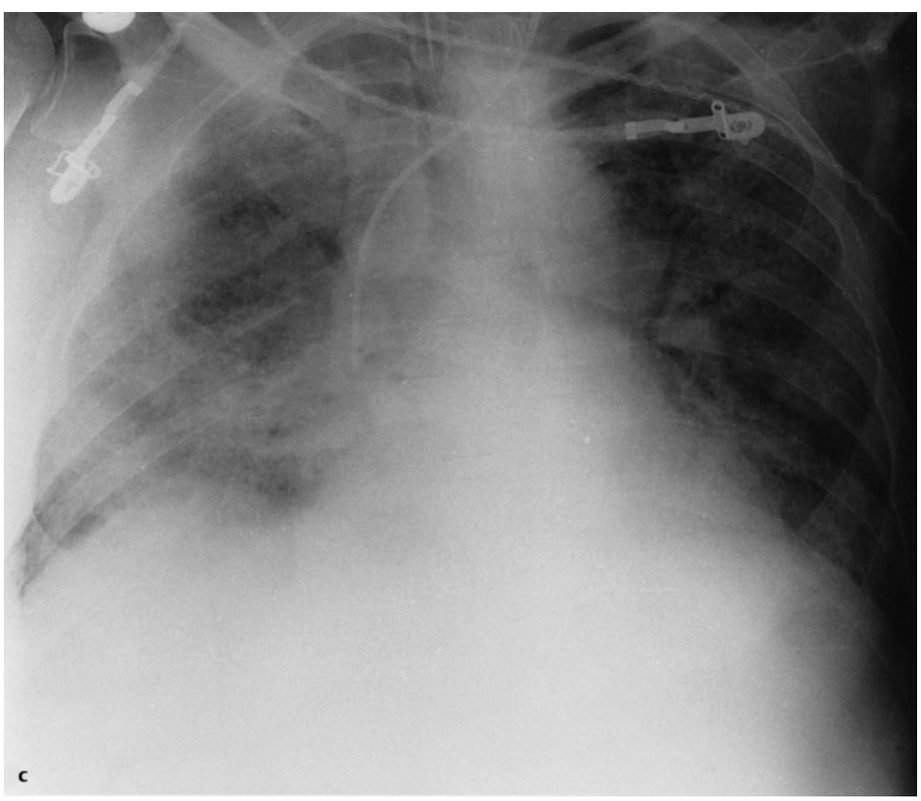

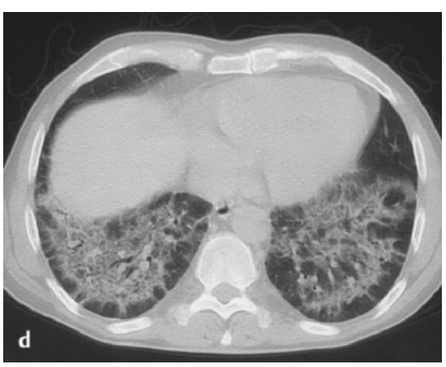

c, d The further course of the disorder is rapidly progressive. Two weeks later, the patient's condition has massively deteriorated. Large areas of ground-glass attenuation have developed in both lungs. The patient is intubated. No effusion. Shrinkage in the basal segments has led to detectable areas of subpleural hyperinflation (**d**) exhibiting an arcade pattern. The patient died a few days later.

Sarcoidosis

Hardly any other intrinsic disorder displays such a variety of symptoms as this generalized occurrence of granulomas of epithelioid cells, giant cells, and lymphocytes. Initially described as a skin disease, the disorder was later named after Boeck.

The many clinical symptoms and synonyms (sarcoidosis, Besnier–Boeck–Schaumann disease, Boeck disease) are matched by numerous radiographic signs. As a result, the disorder has been called the "chameleon of pulmonary diagnostic medicine" (**Fig. 5.18**).

Despite the broad palette of radiologic findings, some relatively typical pictures can be identified. Accordingly, the initial diagnosis of pulmonary sarcoidosis is usually made on the basis of incidental radiologic findings, such as on a routine examination prior to employment. In addition to raising initial suspicion, conventional radiography is also an important modality for evaluating the course and activity of sarcoidosis. To a lesser extent, it is also useful in differential diagnosis. This latter application is primarily the domain of CT.

After earlier classification systems, the **system of sarcoidosis staging described by Wurm** (1958) has gained general acceptance (**Fig. 5.19**). According to this classification system, three stages are differentiated on the basis of the chest radiograph. Stages II and III are further subdivided. Recently a five-stage classification system (stages 0–4) has come into widespread use (**Table 5.4**). These stages are also defined on the basis of the plain chest radiograph.

Regardless of the various staging systems, the following section will discuss the relevant radiographic signs in these three groups:

- Radiographic signs of hilar involvement
- Radiographic signs of pulmonary involvement
- Radiographic signs of irreversible pulmonary involvement (fibrosis)

Table 5.4 Radiographic staging in sarcoidosis

Stage	Findings
0	Normal findings
I	Lymphomas
II	Lymphomas and parenchymal involvement
III	Parenchymal involvement only
IV	Fibrosis

Notes on Pathology and Clinical Findings

The pathologic substrate of sarcoidosis granulomas consists of nodules of loosely organized epithelioid cells with or without Langerhans cells. Older granulomas hyalinize, although no central caseation occurs as it does in tuberculosis. The etiology of sarcoidosis remains unclear. Formerly, the consensus was that sarcoidosis was closely related to tuberculosis on the basis of the similarity of the pathologic substrates. Sarcoidosis was even thought to represent an abortive benign stage of tuberculosis, a "productive sarcoid form" (manifestations of sarcoidosis often resolve quickly in the presence of florid tuberculosis). However, after the Second World War sarcoidosis came to be regarded as a symptom with multiple etiologies. Today, Uehlinger's concept of sarcoidosis as a nonspecific hyperergic form of reaction, the morphologic equivalent of an antigen–antibody reaction, has gained general acceptance.

Only syphilis and tuberculosis are comparable to sarcoidosis in terms of the variety of its symptoms with their unpredictable progress, exacerbation, and latency periods. Theoretically, any organ could be affected. Yet aside from skin manifestations, the usually insidious symptoms primarily involve the lymph nodes, eyes, and lungs. Pulmonary involvement in particular often remains clinically silent and is only discovered by chance. The cutaneous sarcoids (lupus pernio, butterfly rash) are regarded as cosmetically disfiguring. Often the differential diagnosis of lymph node swelling that has persisted for years will lead to further diagnostic studies.

In contrast to other generalized afflictions, the complete absence of pain in combination with at most minimal general symptoms (fatigue, loss of appetite, weight loss, subfebrile temperatures) are diagnostic in the presence of extensive examination findings. The relative benignancy of the symptoms in most affected patients contrasts sharply with isolated serious clinical courses involving blindness, severe pulmonary fibrosis, cerebral processes producing the picture of a brain tumor, and the occasional sudden cardiac death.

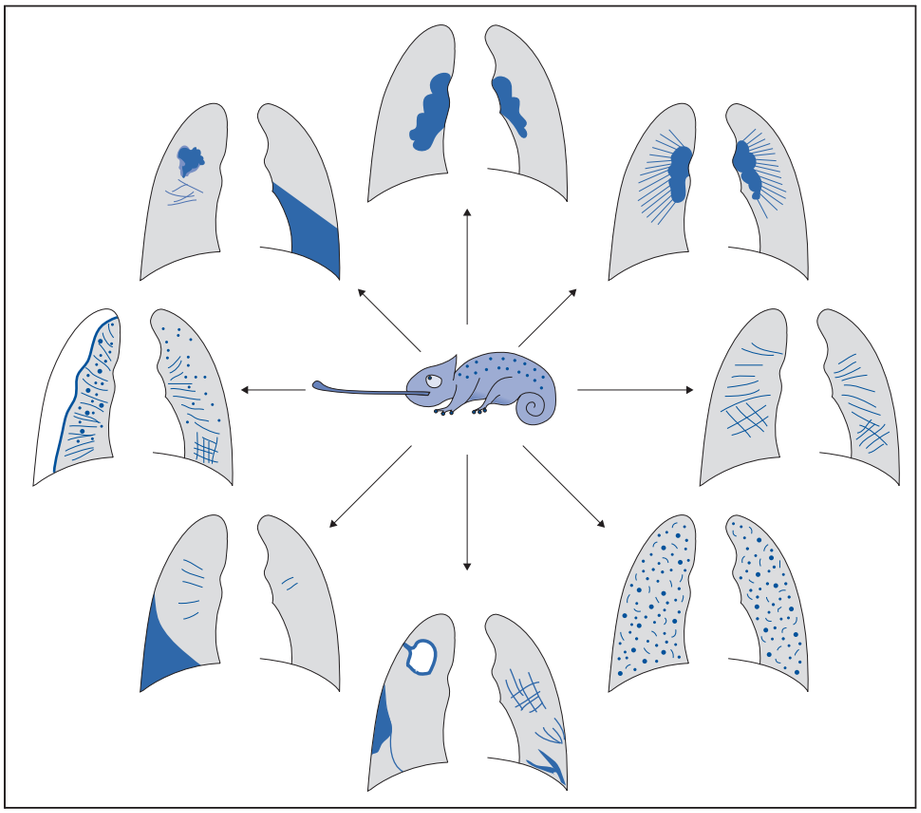

Fig. 5.18 Sarcoidosis, the "chameleon of pulmonary diagnostic medicine." Hardly any other disorder exhibits such radiographic variation. The broad spectrum of findings includes peripheral and hilar masses, atelectasis, miliary patterns, liquefaction, pleural effusion, pneumothorax, fibrotic pulmonary membrane, and combinations of these findings.

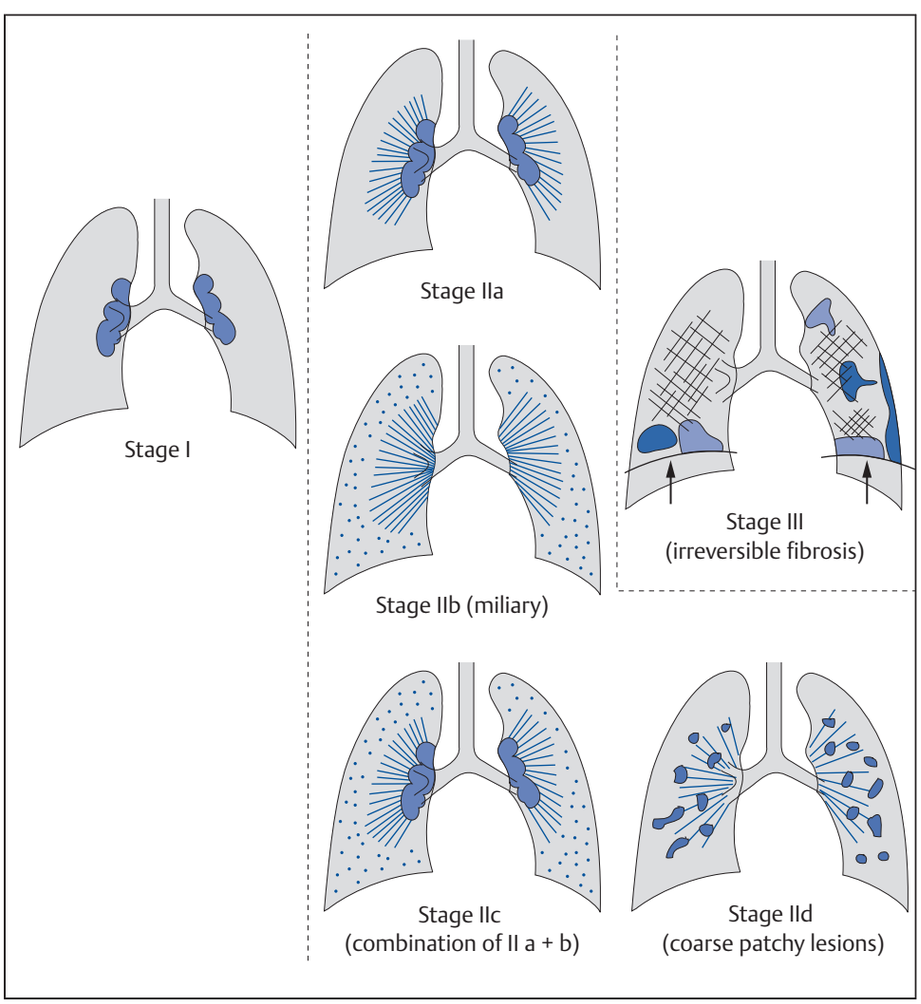

Fig. 5.19 Wurm's classification of the radiographic stages of sarcoidosis. The classification system described by Wurm includes three stages. Stage I is characterized by enlargement of isolated hilar lymph nodes; stage III shows signs of irreversible tissue destruction (distraction, shrinkage with reduced depth of inspiration, fibrotic areas, etc.). Stage II is divided into four substages. Stage II a shows a combination of hilar thickening and perihilar streaky densities; stage II b shows perihilar streaky densities with miliary nodules. In contrast, stage II d shows coarse patchy parenchymal involvement.

Hilar Involvement (Stage I)

Hilar involvement in sarcoidosis (approximately corresponding to stage I according to Wurm) shows the following radiologic features:

- Hilar thickening
- Usually bilateral and symmetrical findings
- Radiolucent band along the mediastinum
- Demarcated cardiac border

Characteristic findings in stage I according to Wurm include a bilaterally symmetrical pattern of hilar lymph node enlargement. The affected nodes can be massively enlarged. This usually symmetrical bilateral involvement of lymph nodes leads to a widened mediastinum with a polycyclic, sharply demarcated contour.

Differential diagnosis from a lymphoma or bronchial carcinoma (**Fig. 5.20**) requires attention to the peculiarities of lymph node involvement in sarcoidosis. One relatively characteristic finding is a narrow radiolucent band between the hilum and mediastinum (enlarged lymph nodes in the hilum but not those located in the azygoesophageal recess, **Fig. 5.21**). A strip of fat is often visible between the lymph nodes and the mediastinal structures. Unilateral hilar lymph node enlargement is rare, occurring in less than 10% of all cases. The lymph node involvement rarely leads to bronchial compression and almost never to atelectasis. This is only observed in endobronchial sarcoidosis. Calcifications are occasionally detectable in the enlarged lymph nodes. These calcifications persist after the swelling of the lymph nodes has receded, creating eggshell calcification figures (**Fig. 5.22**) that can imitate silicosis. A unilateral pleural effusion is rarely observed in stage I. Such cases usually exhibit a clinical Löfgren syndrome.

The **further course** of stage I can exhibit:

- Spontaneous healing within 3–12 months
- Persistence of radiologic findings over several years without any significant changes
- Transition to a chronic form with perihilar fibrosis
- Transition to stage II

The radiologic appearance of the **chronic form** with perihilar thickening is characterized by increased blurring of the massively enlarged hila with streaky radiating spiculations and compensatory emphysema. This process corresponds to a transition directly from stage I to stage III.

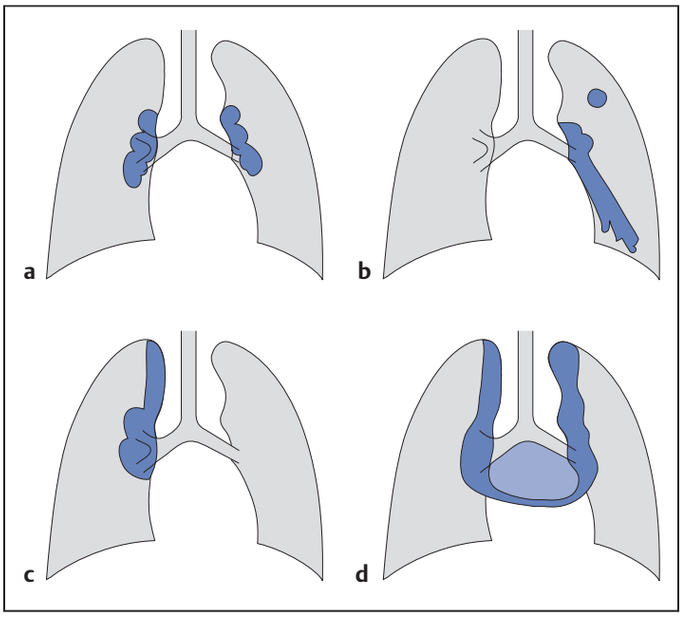

Fig. 5.20 a–d Differential diagnosis of hilar lymphomas.
a Sarcoidosis.
b Epituberculosis.
c Bronchial carcinoma.
d Hodgkin lymphoma.

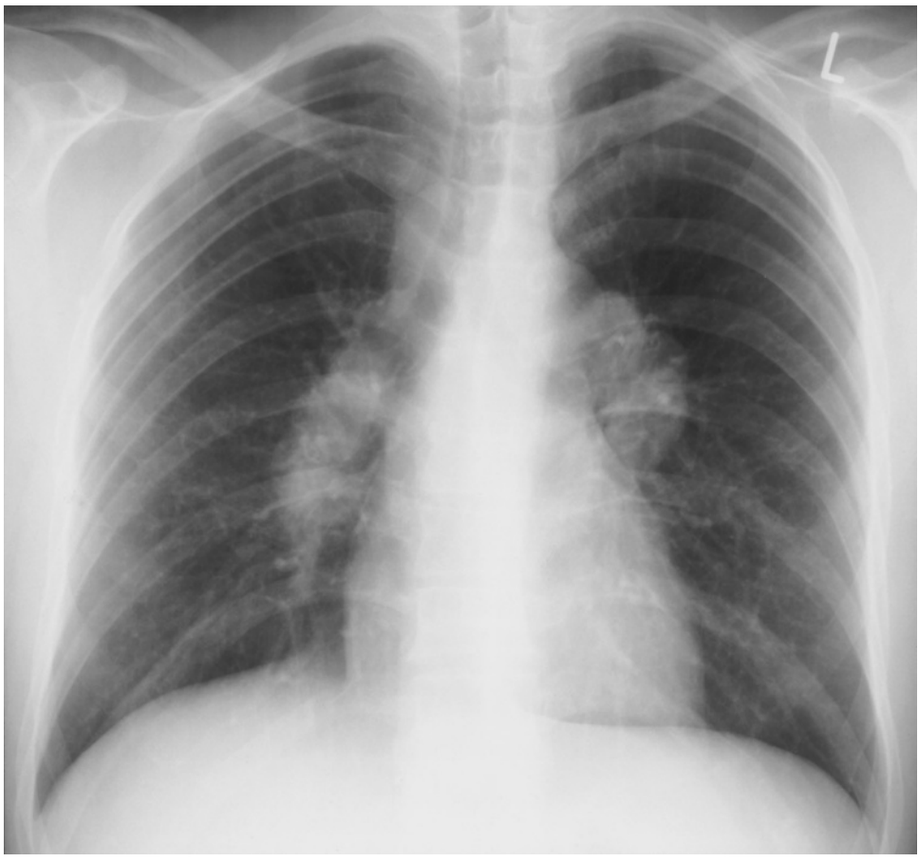

Fig. 5.21 Bilateral hilar lymph node enlargement in stage I sarcoidosis. Massively enlarged hilar lymph nodes on both sides in this 38-year-old man were incidental findings on a routine preoperative chest radiograph. The patient is clinically asymptomatic. The left cardiac border and right cardiomediastinal silhouette (radiolucent band along the mediastinum) are clearly visualized.

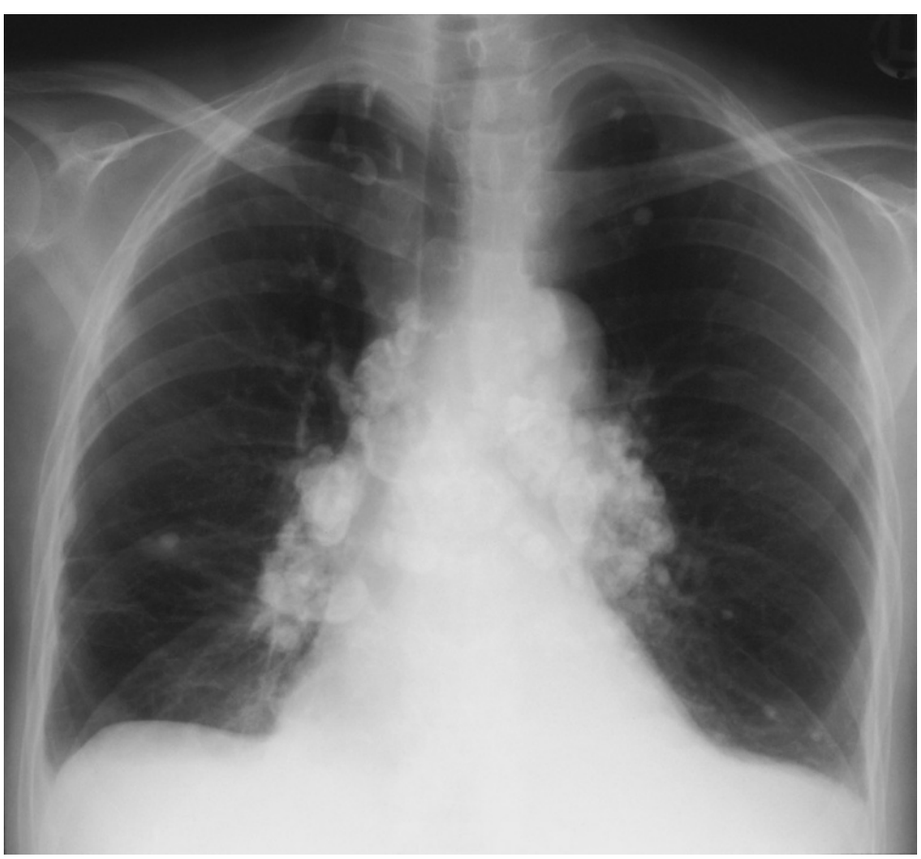

Fig. 5.22 "Eggshell hila": residual findings of bilateral hilar lymphomas in sarcoidosis. The patient is a 54-year-old woman. Follow-up radiograph obtained after cardiac decompensation in the presence of coronary heart disease and renal insufficiency requiring dialysis. The patient has a history of sarcoidosis many years previously. The effusions in the costophrenic angles are residues of the recent cardiac decompensation.

Pulmonary Involvement (Stage II)

Involvement of the pulmonary parenchyma on the plain chest radiograph defines stage II according to Wurm's classification system. The disease process spreads by lymphatic or hematogenous dissemination or by direct extension, producing focal granulomatous lesions. Often accompanied by remission of the central lymph node involvement, this spread shows the following pattern:

- Diffuse finely to coarsely nodular pattern (hematogenous)
- Diffuse finely to coarsely reticular pattern (lymphatic)
- Butterfly pattern of perihilar streaky densities (direct extension)
- Irregular coarsely nodular parenchymal involvement

Pulmonary changes are usually reticular at first. Nodular changes begin to appear during the further course of the disorder. These occur primarily in the central region and in the middle field, showing a predilection for the right lung.

The *diffuse fine-to-coarse nodular pattern* shows a typical peribronchial/perivascular configuration. This is only faintly visible on conventional radiographs (**Fig. 5.24**, detail), but clearly demonstrated on CT (**Fig. 5.23, Fig. 5.25**). Irregularities of the bronchial wall can be signs of granulomas in the bronchial mucosa.

The nodules in sarcoidosis can show the following configurations:

- Perilymphatic-peribronchovascular
  - Interlobular
  - Subpleural
- Random

This latter pattern can also include miliary forms (**Fig. 5.26**).

Purely nodular patterns or mixed pictures with a diffuse reticular pattern can occur. These patterns may include all types of linear shadows such as Kerley lines, especially the irregular type C lines. Kerley lines caused by sarcoidosis typically occur in the presence of a normal-sized heart without signs of redistribution or mediastinal widening indicative of interstitial edema. They show no postural movement. A perihilar streaky density is often observed (**Fig. 5.27**). The coarsely nodular parenchymal involvement results from the confluence of individual acinar shadows (**Fig. 5.28**).

Unusual findings in stage II pulmonary sarcoidosis include:

- Larger (occasionally isolated) nodules
- Liquefaction
- Pleural effusion

These findings usually occur in elderly patients. Here the "chameleon of pulmonary diagnostic medicine" again reveals its variability, and findings can be misdiagnosed as suspected pulmonary metastases or as bronchial carcinoma where isolated nodules or areas of liquefaction are present.

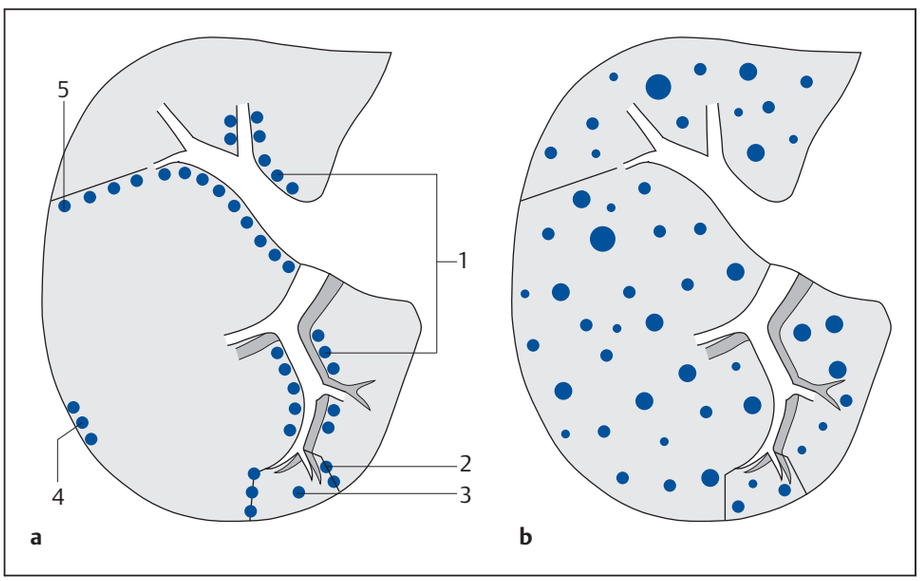

Fig. 5.23 a, b Schematic diagram of the spread of finely nodular changes in sarcoidosis.
a Bronchovascular-perilymphatic.
1 Peribronchovascular
2 Interlobular
3 Centrilobular
4 Subpleural
5 Perilymphatic
b Random.

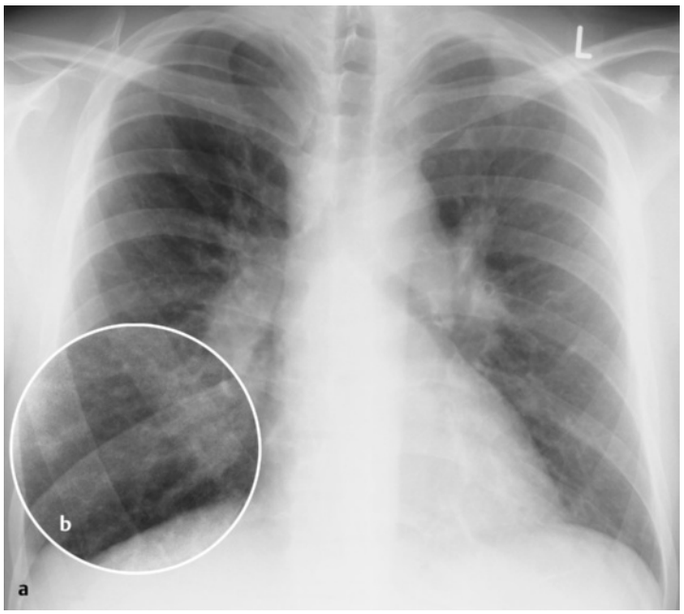

Fig. 5.24a, b **Pulmonary and hilar involvement in stage IIa sarcoidosis.**
a The patient is a 26-year-old man with clinically suspected Reiter syndrome, fever, and joint pain. Significant bilateral hilar thickening especially on the right side, with blurring of the central vascular structures. Diffuse shadowing, more nodular than reticular.
b Bronchovascular shadowing is faintly visible on the conventional radiograph (detail). The nodules are arranged sequentially like a string of pearls.

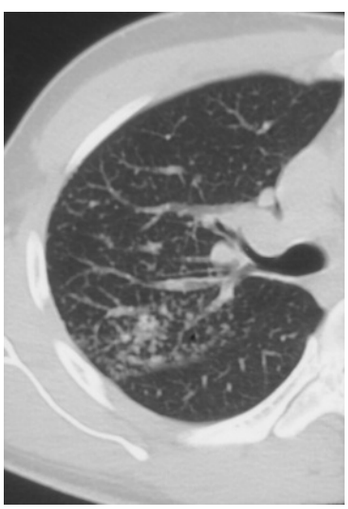

Fig. 5.25 **Bronchovascular distribution of the nodules.** A peribronchovascular configuration of small nodules is clearly visible in the posterior segment of the right upper lobe.

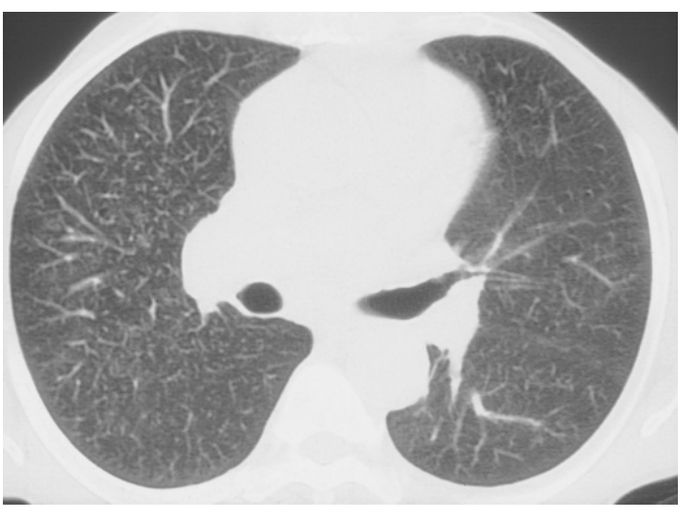

Fig. 5.26 **Miliary picture of finely nodular shadowing in stage IIb sarcoidosis.**

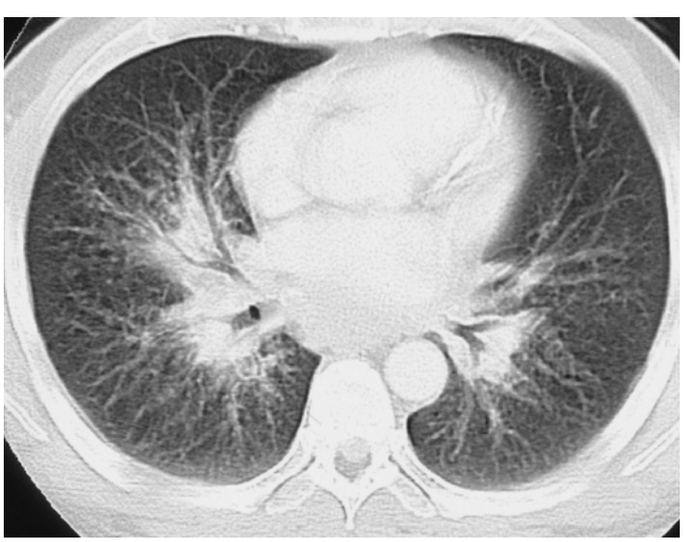

Fig. 5.27 **Streaky pattern of perihilar shadowing in stage IIa sarcoidosis.** Findings include significantly thickened hila and marked peribronchovascular shadowing. Streaky perihilar spiculations are present, creating the impression of a corona.

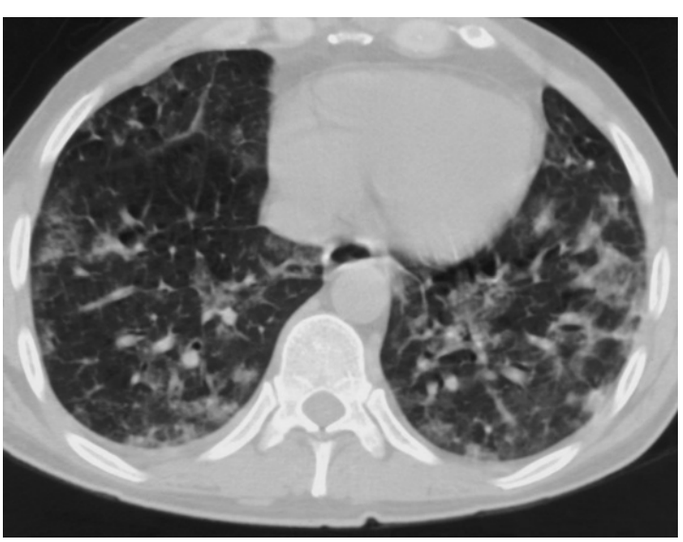

Fig. 5.28 **Coarsely nodular parenchymal involvement in stage IId sarcoidosis.** In addition to a faintly visible bronchovascular nodule, findings include focal lesions in both lower lung fields forming confluent area consolidation. No septal changes or effusion.

Fibrosis (Stage III)

Whereas the changes in stage II are reversible, stage III is defined by the occurrence of irreversible fibrotic changes in the pulmonary parenchyma. It is not possible to cleanly separate the two stages as the transition between them is not sharply defined. This is reflected in the many mixed pictures of beginning fibrosis in the presence of persisting granulomatous foci. Under steroids the granulomatous changes of stage II should resolve within 6 weeks. Changes persisting after this period are attributable to fibrotic processes.

The **fibrotic changes** include:

- Streaky densities from scarring
- Massive fibrosis
- Compensatory emphysema
- Bronchiectasis
- Bullae, cavities
- Pneumothorax

The ground-glass attenuation mentioned previously is usually indicative of fibrosis of the alveolar wall, similar to that occurring in interstitial pneumonia or interstitial pulmonary fibrosis (**Fig. 5.30**). The widely held opinion that ground-glass opacities should invariably be evaluated as signs of activity does not hold true with sarcoidosis. The attenuation may be a sign of chronic fibrotic thickening of the alveolar wall, or it may be attributable to an inflammatory alveolar reaction (**Fig. 5.29**).

Bands that are in contact with the hilum are often present in the middle and upper fields. These can lead to lung distortion. Large areas of scarring are found at the confluence of adjacent granulomas. Honeycombing can also occur adjacent to large bullae of emphysema associated with scarring. Localized fibrosis with bronchiectasis and hyperinflation of adjacent lung segments is a rather common finding.

The radiologic signs of the resulting fibrotic complications (pulmonary hypertension, cor pulmonale) are discussed in the respective chapters.

Pneumothorax (**Fig. 5.31**) is occasionally observed. Its relationship to the staging of the disorder is not clear. Some authors evaluate this as a sign of stage II.

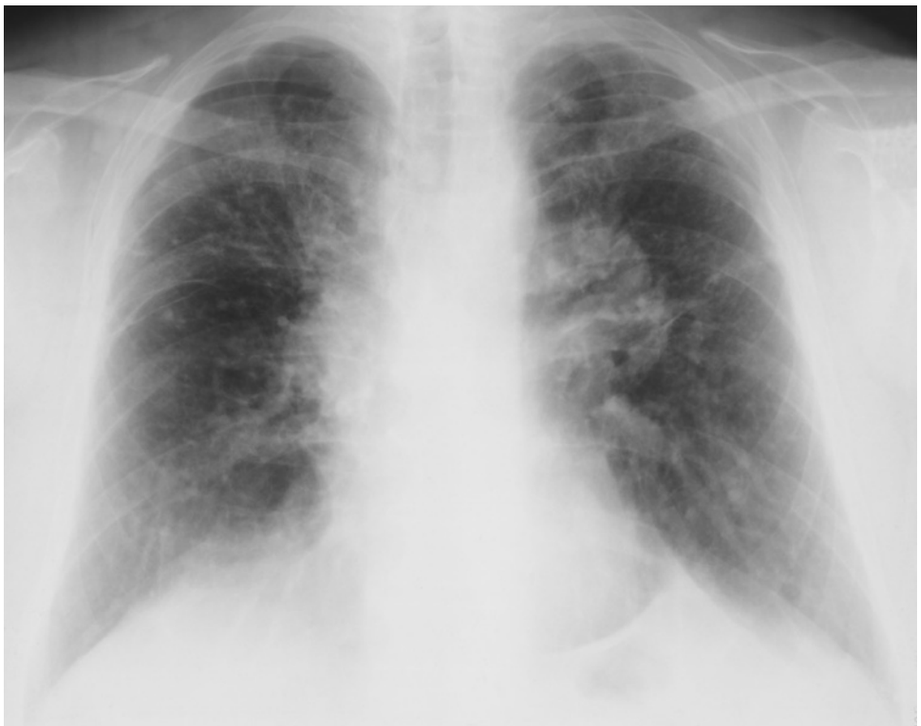

Fig. 5.29 Severe fibrotic transformation of the lung in sarcoidosis. In the presence of confirmed lymph node involvement there is clear evidence of scarring of the pulmonary parenchyma. Both hila are cranially displaced. The upper lobes show shrinkage with bullae and streaky parenchymal bands.

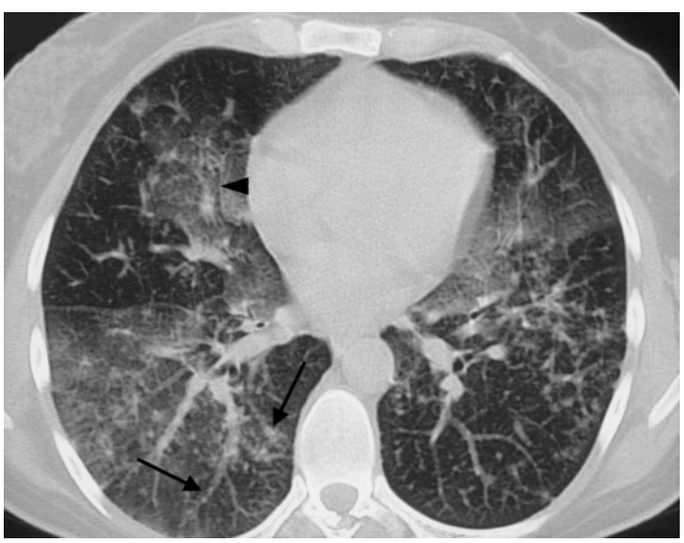

Fig. 5.30 Ground-glass opacities consistent with thickening of the alveolar wall in stage II–III sarcoidosis. In addition to peribronchovascular nodules (black arrows) indicative of stage II disease, hypoventilated areas are present bilaterally with dilatation of the small airways (black arrowhead) and ground-glass opacities consistent with alveolar wall fibrosis.

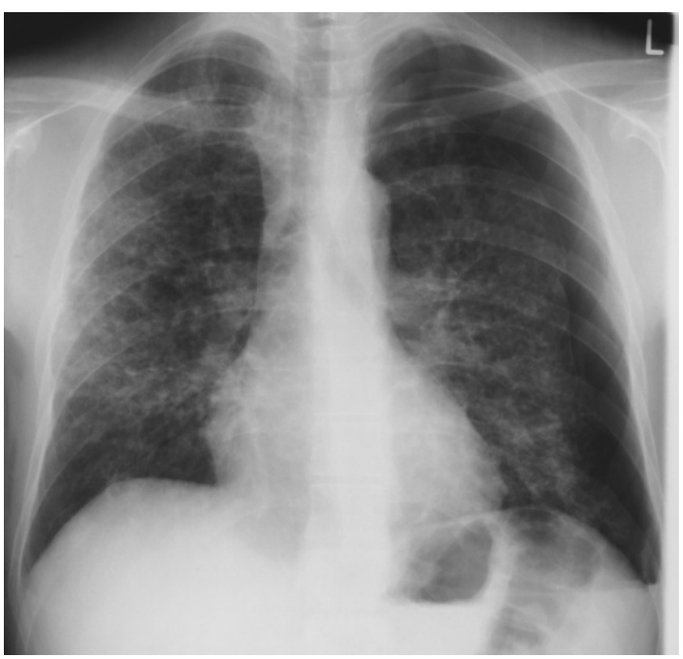

Fig. 5.31 Pneumothorax in sarcoidosis. The patient is a 29-year-old man presenting with dyspnea. Significant pneumothorax is present with a small associated effusion on the left side. Other findings include extensive bilateral nodular and reticular shadowing. Histologic diagnosis is pulmonary sarcoidosis.

Pneumoconiosis

General

Pneumoconiosis is a collective term to refer to abnormal pulmonary changes resulting from the inhalation and deposition of dusts. A distinction is made between pneumoconiosis and those pulmonary changes that result from hypersensitivity reactions caused by dusts (extrinsic allergic alveolitis, such as farmer's lung). The most important forms of pneumoconiosis in the strict sense are:

- Silicosis caused by quartz dust (also including anthracosilicosis, a form of pneumoconiosis from mixed dust)
- Asbestosis

The other forms of pneumoconioses caused by hard dusts (berylliosis, stannosis, etc.) are indistinguishable on the basis of radiologic findings.

ILO Classification

The International Labor Office (ILO) last issued a **classification** of pneumoconioses in 2000. The classification is based on plain chest radiographs and permits a systematic description of radiographic findings. It defines pneumoconiosis findings without evaluating clinical symptoms or data on pulmonary function.

Technical Quality

Image quality is graded according to a 4-point scale from 1–4 (good to unacceptable).

Small Opacities (**Fig. 5.32**)

Shape and size:

- *Round shadows* are classified according to their diameter as:
  - p (< 1.5 mm)
  - q (1.5–3 mm)
  - r (3–10 mm)
- *Irregular nodules* are classified as:
  - s (< 1.5 mm)
  - t (1.5–3 mm)
  - u (3–10 mm)

Distribution (**Fig. 5.33**): The classification is based on an estimate of the shadow concentration by comparison with standard films. Main categories include:

- 0 = Absence of small opacities.
- 1 = Isolated opacities; normal pulmonary markings are visible.
- 2 = Normal pulmonary markings are partially obscured.
- 3 = Normal pulmonary markings are obscured.

A second number specifies which category might also come into consideration as an alternative. For example, "0/1" means "normal, but may be grade 1," and so on.

Large Opacities (**Fig. 5.34**)

Large opacities are classified as categories A, B, or C according to their number and size:

- A = Isolated focus or summation of large foci up to 5 cm in diameter.
- B = Foci are larger than category A, but in summation smaller than the right upper lobe.
- C = The summation of the foci is larger than the right upper lobe.

Pleural Findings (**Fig. 5.35**)

Pleural thickening is classified as follows:

- Type: diffuse or circumscribed
- Site: right or left
- Maximum margin width, size, and shape (pleural plaques? calcifications?)

Other

An opportunity is provide to list additional findings such as cor pulmonale, honeycombing, or emphysema.

Notes on Pathology

The dust is absorbed via the airways. Large particles are trapped by the respiratory epithelium. The size of dust particles that can pass into the alveoli is estimated at 1–5 µm. There is a linear relation between quantity, time to onset of effect, and pulmonary reaction. After inspiration of the fine dust, it is phagocytosed in the alveoli by macrophages that can be expectorated (dust cells). A small part enters the pulmonary interstitium via the macrophages, primarily in the peribronchiolovascular region. Another part of the dust is removed by the lymph system and transported and deposited in the regional lymph nodes and pleura. The absorbed crystal spikes lead to destruction of the macrophages by a mechanism that is not fully understood. Their disintegration is thought to be the cause of the proliferation of reticular collagenous tissue. The histologic substrate of silicosis is a concentric layered nodule with perifocal emphysema. Findings include a hypercellular granuloma traversed by hyaline bands and transformed into a hypocellular nodule measuring approximately 2 mm in diameter. Conglomeration leads to large accumulations and finally to indurations.

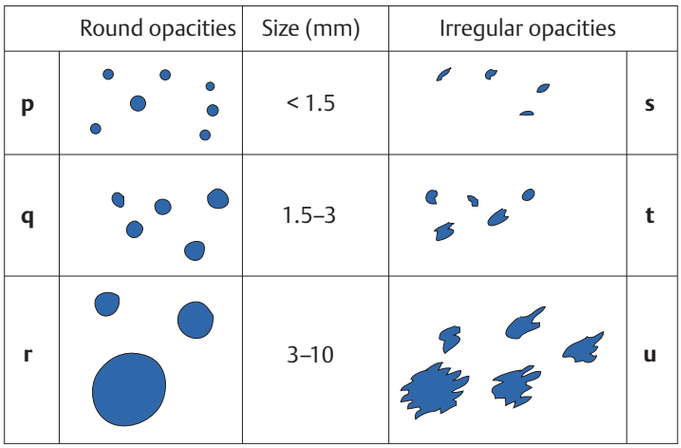

Fig. 5.32 Small opacities according to the ILO classification. Small opacities are classified according to their shape (round, irregular) and their size (< 1.5, 1.5–3, 3–10 mm).

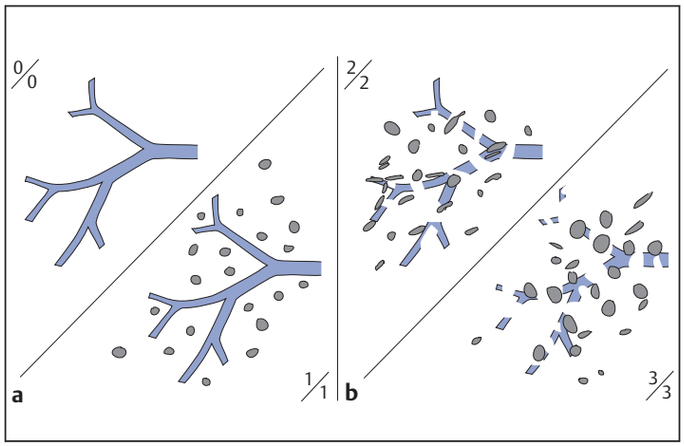

Fig. 5.33 a, b Distribution of small opacities according to the ILO classification. The size of the nodule is classified according to the visibility of the normal pulmonary markings. In main categories 0 and 1, pulmonary markings are still readily visible (**a**), whereas in distribution categories 2 and 3 normal pulmonary anatomy is obscured (**b**).

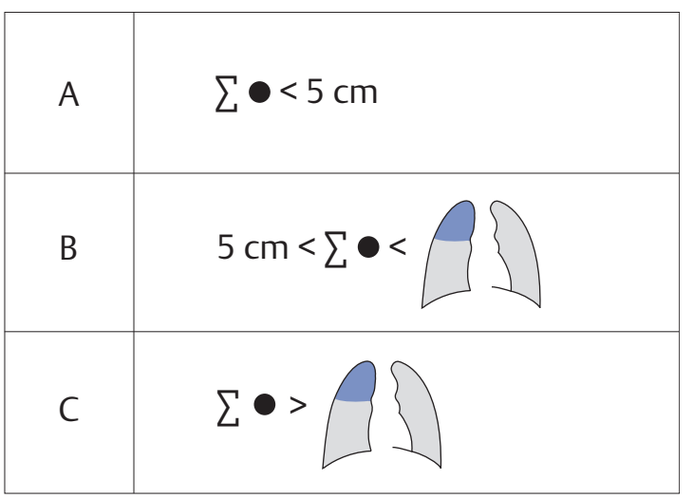

Fig. 5.34 Large opacities according to the ILO classification. In category A the entire area of the large opacities is less than 5 cm, in category B it is less than the right upper lobe, and in category C it is greater than the right upper lobe.

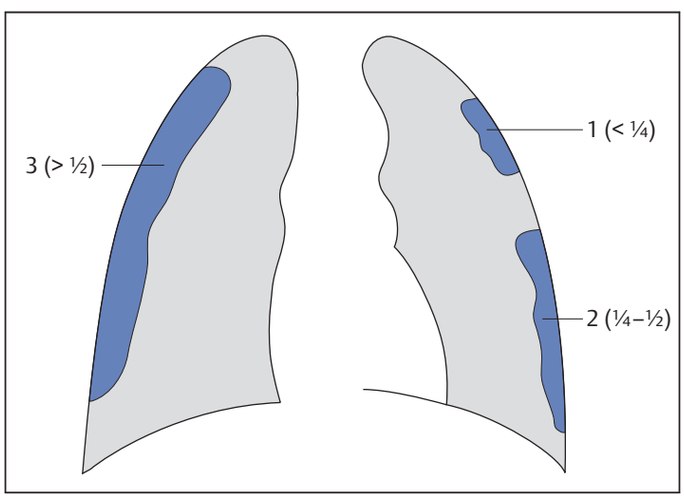

Fig. 5.35 Pleural findings according to the ILO classification. Category 1 shows an extent of pleural thickening less than one quarter of the length of the pleura.

The following section explains the ILO classification in greater detail based on a few examples.

Examples of "Small Opacities"

- **Figure 5.36** is an example of the presence of small opacities. Round opacities are classified as category p, q, or r. In this 72-year-old foreman who worked in an underground mine for over 30 years, findings primarily include tiny opacities less than 1.5 mm in diameter.
- **Figure 5.37** is an example of small irregular opacities. These opacities are not round and are classified as category s, t, or u. In this case, the patient is a 65-year-old miner who worked underground for 35 years and has clinically severe dyspnea. The radiograph shows numerous irregular opacities of categories t and u in the right middle lung field.

Examples of "Distribution"

- **Figure 5.39** shows a distribution of category 2/2 in a detail enlargement. The vascular architecture is significantly obscured in the left lower lung field. A small round opacity of category q is also demonstrated.
- In **Fig. 5.38** distribution is significantly broader and the underlying vascular architecture is completely obscured (distribution category 3/3). Very fine nodular shadowing and scarring with tissue distortion are also present.

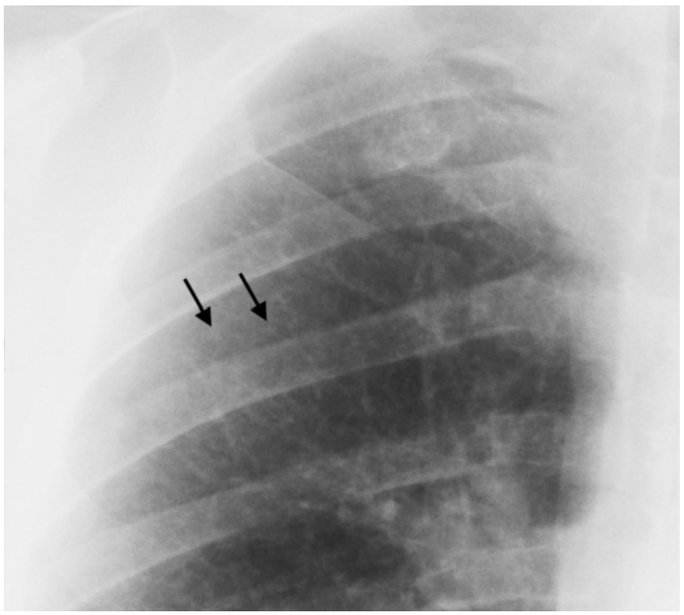

Fig. 5.36 Small opacities, category p (black arrows).

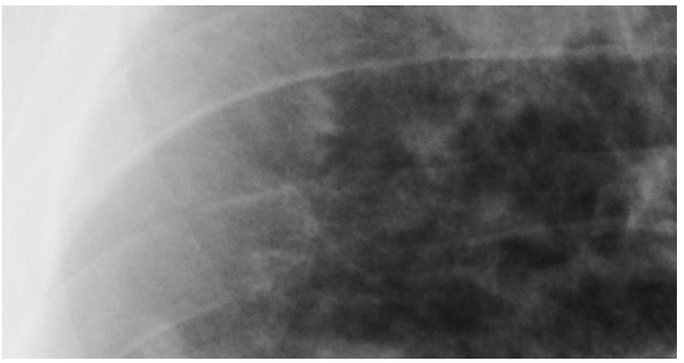

Fig. 5.37 Irregular opacities, category t and u.

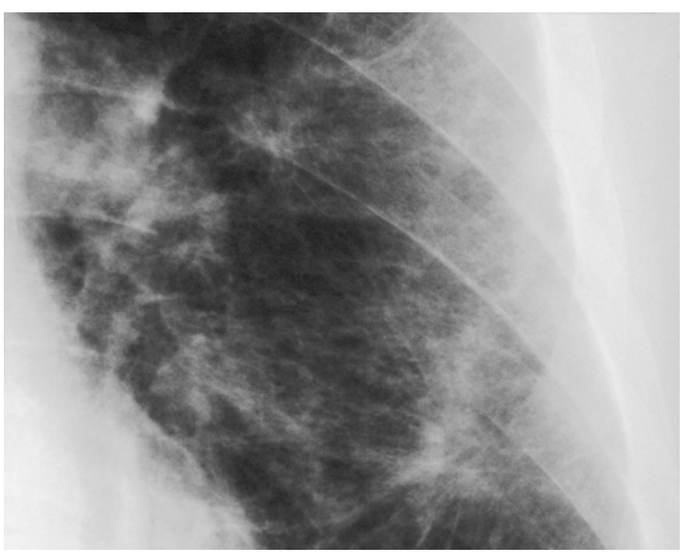

Fig. 5.38 Distribution of small nodules, category 3/3.

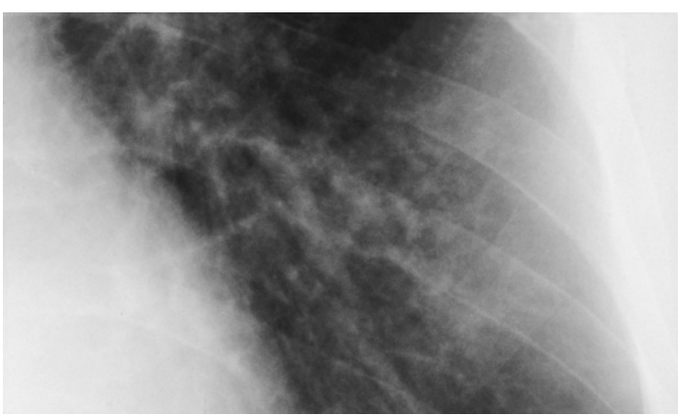

Fig. 5.39 Distribution of small opacities, category 2/2.

Examples of "Large Shadows"

- **Figure 5.40** shows a large shadow of category A; it is smaller than 5 cm and lies in the left upper lobe. A perifocal radiolucent halo consistent with shrinkage is visible. This is an important finding that distinguishes it from a malignancy.
- **Figure 5.41** shows a large shadow of category B in an 86-year-old miner who worked in an underground mine for 33 years. The patient shows severe emphysema and dyspnea at rest in the presence of coronary heart disease (unfortunately most miners were extremely heavy smokers in addition to their occupational exposure). The mass in the right upper lung field no longer falls under category A as it is larger than 5 cm. However, it is smaller than the area of the right upper lobe and therefore belongs to category B. These foci represent progressive massive fibrosis and can often increase in size. As a result, the differential diagnosis of this disorder from a bronchial carcinoma arising from a scar can occasionally be difficult.

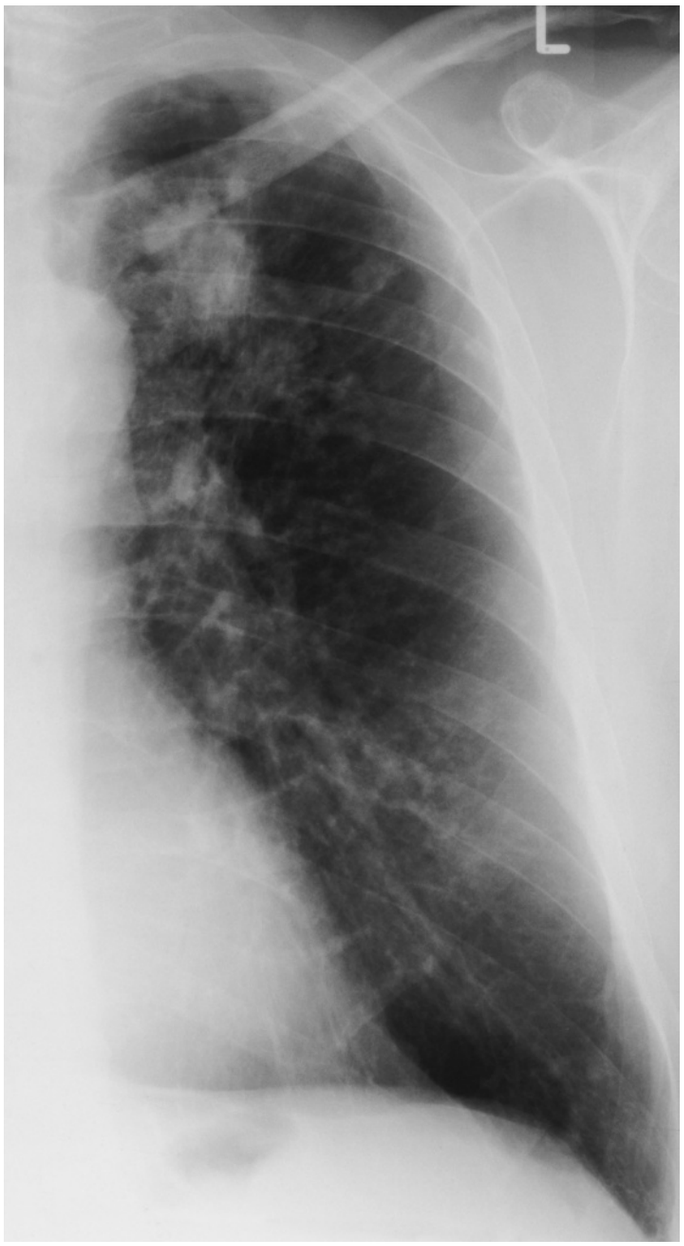

Fig. 5.40 Large shadow, category A.

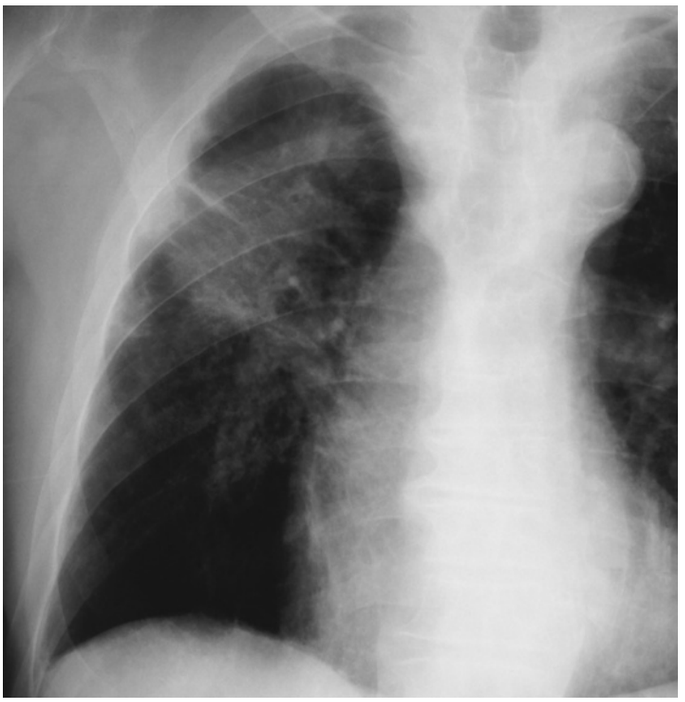

Fig. 5.41 Large shadow, category B.

Silicosis

Diagnosis

"The diagnosis of silicosis is made on the basis of the radiograph in the presence of an appropriate occupational history."
(German Federation of Commercial Professional Associations)

Earlier the diagnosis of silicosis was strongly influenced by an appropriate **occupational history** or the health insurance fund, or at least the radiologist's attention was drawn to early changes consistent with the disease. Today the situation is more complex, as the classic occupational history of mining has been superseded by industrial metal processing. We may assume that a large number of cases of inhalational damage due to silicosis are misinterpreted as emphysematous bronchitis caused by cigarette smoking.

Do not forget to investigate the patient's occupational history.

The basic examination in suspected silicosis involves conventional chest radiographs obtained with hard radiation. Radiographic signs of silicosis include:

- Occurrence of small, sharply demarcated round opacities (p, q, r according to the ILO classification) showing a predilection for the upper lung fields and perihilar region.
- Lesions become confluent, forming massive fibrosis with perifocal radiolucencies.
- Liquefaction can produce black sputum (melanoptysis).

The small nodules in simple silicosis (sandblasters and stonemasons) are typically relatively sharply demarcated, creating a picture resembling grain kernels or pellets (**Fig. 5.42**). In anthracosilicosis (miners) the nodules are less sharply defined. Here the predilection for the upper lung fields creates a picture resembling snow flurries (**Fig. 5.43**). The radiolucencies around the massive fibrosis (**Fig. 5.44a**) are the result of two processes: "migration" of the nodules toward the conglomerate mass, "cleaning" the vicinity; and emphysema associated with scarring (**Fig. 5.44b**).

The term "snow flurry lung" (**Fig. 5.43**) may require some explanation for those accustomed to warmer climates: In a snowstorm, you can make out individual snowflakes if you look down or straight ahead. But if you look up, you will only see the white cloudy sky (the foci become confluent).

Notes on Clinical Findings

Many process materials used in industrial production, especially quartz, contain crystalline silicates. The extraction and processing of these materials can produce dust that can cause silicosis. Hazards exist in mining, construction, the ceramics industry, the metal industry, and foundries.

Silicosis exhibits three essential courses:

- Acute silicosis from massive exposure (as in tunnel construction), leading to invalidity within months
- Accelerated course over a period of a few years
- Chronic course after a variable duration of exposure from 15 to 30 years

All these forms are characterized by the clinical triad of dyspnea, cough, and expectorate. Physical examination findings include noisy breathing and abnormal sounds on percussion. A restrictive ventilation defect is present in the advanced stage.

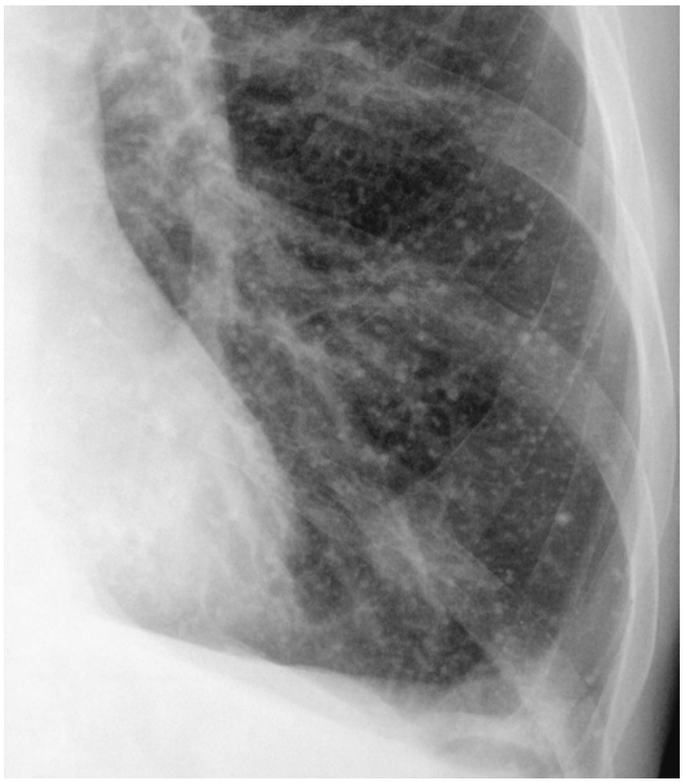

Fig. 5.42 Pelletlike silicosis in a 59-year-old male scissors sharpener. The detail enlargement of the left lower lung field shows primarily q opacities with very high radiodensity (distribution 2/2) and severe emphysema.

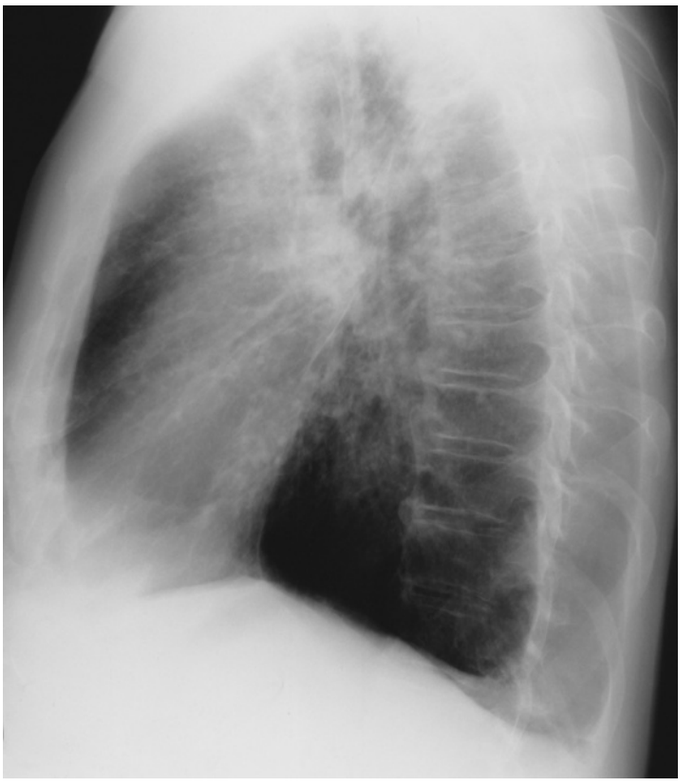

Fig. 5.43 "Snow flurries" in anthracosilicosis. The patient is a 65-year-old miner with advanced pneumoconiosis. The small opacities show an apicobasal decrease in intensity. Massive apical fibrosis is seen.

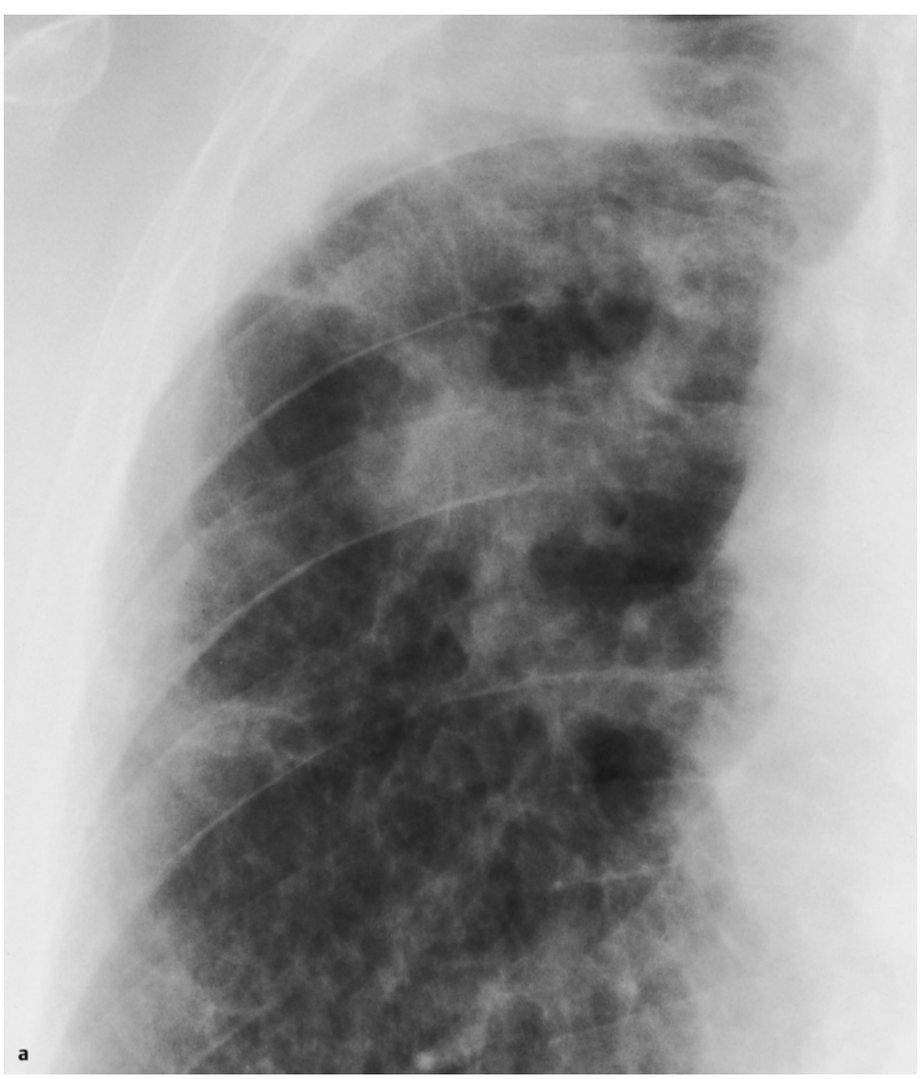

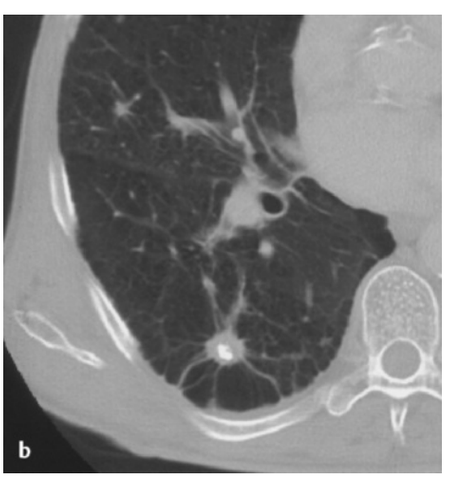

Fig. 5.44 a, b Radiolucency around the massive fibrosis. The patient is a 70-year-old miner with advanced anthracosilicosis (**a**). There is a distinct radiolucency around the large opacity (category A); otherwise the small opacities are diffusely distributed (distribution category 3). The CT scan (**b**) shows a focal lesion in the right lower lung field with significant perifocal emphysema.

Computed tomography can detect small *silicosis nodules* earlier than conventional radiography and can distinguish them from other disorders. The centrilobular subpleural location and predilection for the apical or posteroapical segments are characteristic of silicosis, as is its diffuse symmetrical distribution. CT can readily document *calcifications,* which are detectable in up to 30% of all cases, and can also detect *perifocal emphysema* due to irregular fibrosis around the respiratory bronchiole. Lesions larger than 4 cm show an irregular nonenhancing area with the shadow (**Fig. 5.47**) corresponding to *central necrosis.* These can occasionally be expectorated, creating large cavities. *Massive fibrosis* usually occurs symmetrically. These areas often show layering with high density in the dependent regions (dust deposits, **Fig. 5.48**). When these are expectorated, they produce the clinical picture of *melanoptysis* or black sputum (**Fig. 5.45**). It can be difficult to distinguish concomitant tuberculosis and bronchial carcinoma. It should be noted in this context that massive fibrosis can progressively enlarge (progressive mass fibrosis).

Progressive mass fibrosis can be compared with a vacuum cleaner. The material deposited in its center corresponds to the contents of the cleaner bag.

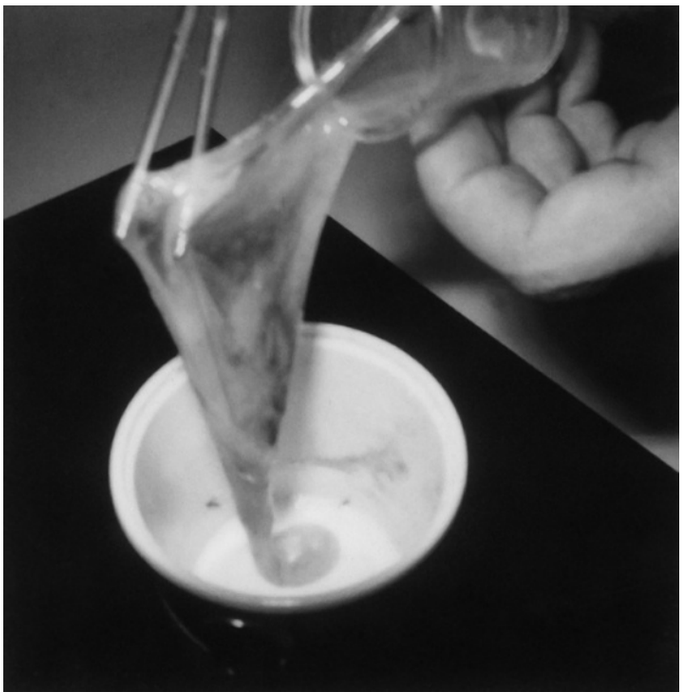

Fig. 5.45 **Black sputum (melanoptysis)**

On **MRI** (**Fig. 5.46, Fig. 5.49, Fig. 5.50**) progressive massive fibrosis shows the characteristic picture of layered foci. Its anterior portions (mucus accumulation with high protein content) appear hyperintense on T2-weighted images, and its dependent portions (silicates) appear hypointense on T1-weighted and T2-weighted images. Mass fibroses occasionally have contact with the hilum and pleura via spiculae. The pleura can appear dimpled, with formations isodense to fat appearing between the dimpled pleura and the chest wall. These formations might be caused by a local negative pressure (**Fig. 5.51**).

The clinical picture can be exacerbated by complications. These include disorders such as silicotuberculosis, carcinoma arising from scar tissue, and Caplan syndrome (combination of silicosis and rheumatoid arthritis, **Fig. 5.52**). Silicotuberculosis and Caplan syndrome are often associated with a severe course of the underlying disorder.

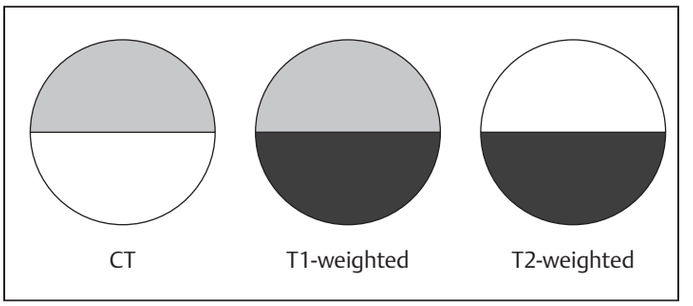

Fig. 5.46 **Schematic of CT density and MR signal intensity of massive fibrosis with dust deposits.**

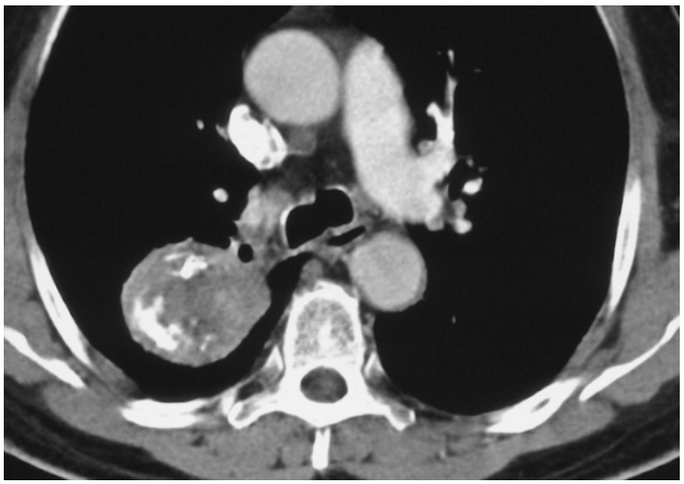

Fig. 5.47 Necrosis in the conglomerate mass. Calcifications in the conglomerate mass and central hypodensities after intravenous contrast administration are signs of central liquefaction.

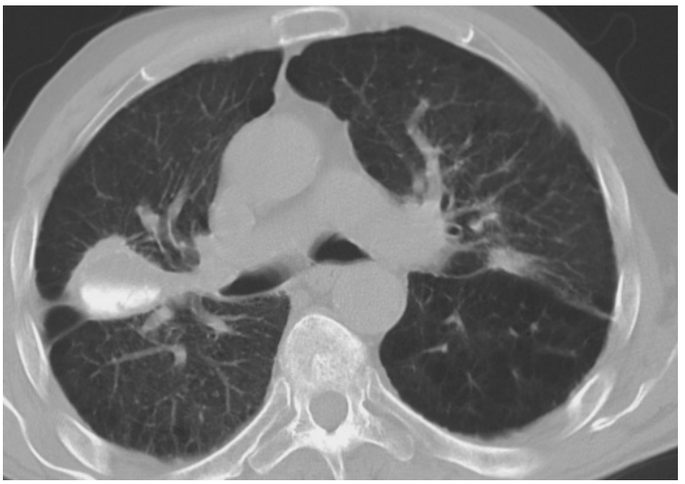

Fig. 5.48 Layering of the dust deposit in progressive massive fibrosis. Massive fibrosis is present in the middle field of both lungs. The right lesion measuring 4 cm in diameter shows a clearly visible fluid level with high density in the dependent areas.

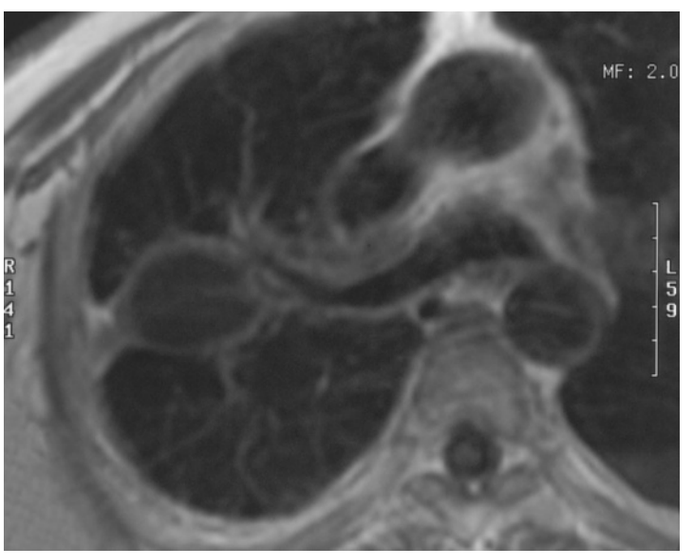

Fig. 5.49 T1-weighted image of massive fibrosis with dust deposit. On T1-weighted images the dependent dust deposit appears as a signal void, while the mucus fluid above it appears hypointense.

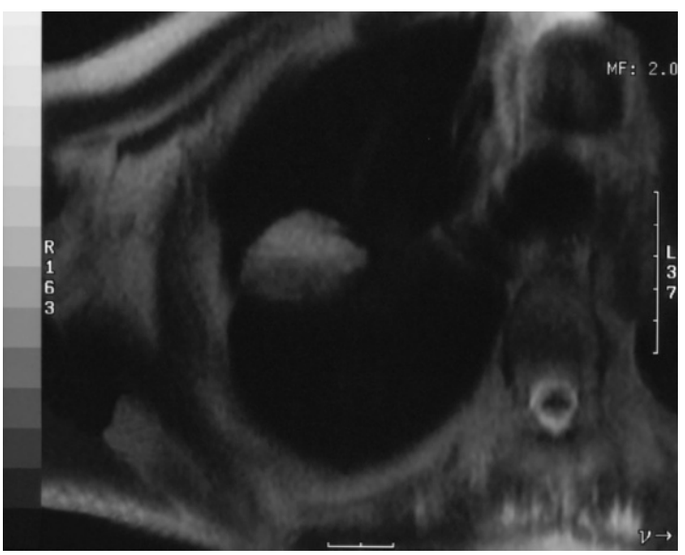

Fig. 5.50 T2-weighted image of massive fibrosis with dust deposit. On T2-weighted images the dust deposit appears unchanged as a signal void, while the mucus fluid above it now appears hyperintense.

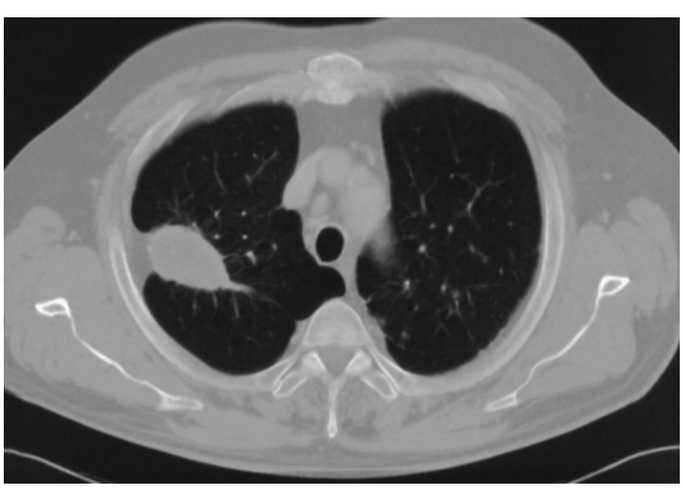

Fig. 5.51 Pleural contact in massive fibrosis. A fat-equivalent tissue formation is seen between the massive fibrosis and the chest wall with pleural dimpling. Note the severe emphysema.

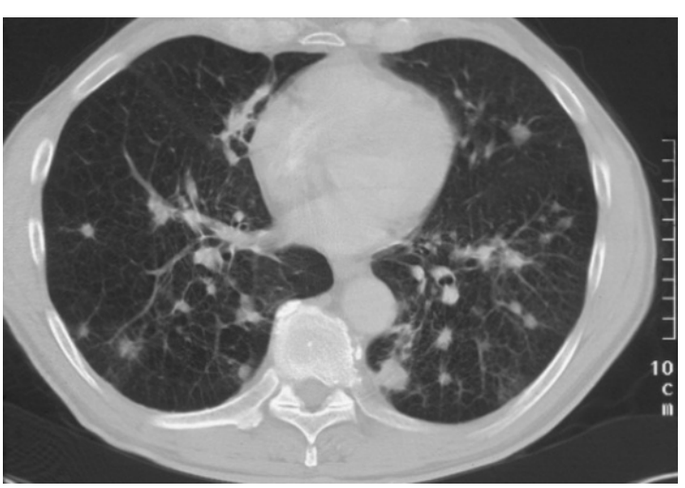

Fig. 5.52 Caplan syndrome. The patient is a 64-year-old miner who worked underground for 35 years. Severe rheumatoid arthritis. Numerous nodules are detected with perifocal emphysema and distraction of the pulmonary architecture. Bronchovascular contact is clearly demonstrated.

Asbestosis

Asbestosis is pulmonary fibrosis resulting from asbestos exposure. It should be distinguished from asbestos-associated pleural changes without pulmonary fibrosis.

Radiographic signs of pulmonary asbestosis include:

- Reticular shadowing especially in the basal and pericardial regions
- Irregular opacities (s, t, u according to the ILO classification)
- Absence of massive fibrosis
- Concomitant pleural plaques

Although the patient may already show clinical symptoms, radiographic findings in the early stages of pulmonary asbestosis are often discrete. Uncharacteristic shadowing will be observed especially in the middle and lower portions of the lung. The pericardial portions of the lungs are preferred, causing blurring of the heart shadow. In contrast to silicosis, findings in asbestosis generally include small irregular opacities (categories s, t, and u). Honeycombing may occur in severe cases. The massive fibrosis typical of silicosis is absent. The sensitivity and specificity of conventional radiographs are certainly higher with respect to asbestos-associated pleural disease. Findings of bilateral pleural calcifications are often the reasons for suspecting possible asbestos exposure.

Asbestos-Associated Pleural Disease

Whereas pleural involvement is the exception in silicosis, it is the rule in asbestosis.

Pleural plaques are the most common manifestation of asbestos exposure. Plaques can occur in any segment of the lung but show a predilection for the diaphragmatic pleura and spare the costophrenic angle. Pleural plaques (**Fig. 5.54**) appear as discrete punctate-to-linear plateaulike or diffuse areas of uniform pleural thickening. The characteristic finding is a table-mountainlike area of pleural thickening (**Fig. 5.53**). Pleural plaques can exhibit varying degrees of calcification (**Fig. 5.55**). Recurrent pleural effusions can be an early sign of asbestos-associated pleuritis. Rounded atelectasis may occasionally be present. It occurs at a peripheral location and shows a broad pleural base. Bronchi and blood vessels converge in an arc to enter the atelectasis in a fashion resembling the tail of a comet (**Fig. 5.56**). Fibrotic bands ("crow's feet") radiate into the surrounding parenchyma.

Notes on Pathogenesis and Clinical Findings

Asbestos (Greek ασβεστος, asbestos, unburnable) is any one of several minerals composed of long, flexible parallel fibers. Large winding (serpentine) white asbestos fibers are often trapped in the nasopharynx and upper respiratory tract. Smaller, rodlike hornblende asbestos fibers (amphibole or crocidolite), although longer than 5 µm, can travel distally as far as the alveoli because of their aerodynamic shape. Fibers longer than the diameter of the phagocytozing macrophages (> 25 µm) destroy the macrophages, initiating the process of fibrosis.

The malignant effect of pulmonary asbestosis is due to (1) the insidious clinical symptoms (minimal mucoid expectorate, stabbing or burning chest pain) with delayed occurrence of radiographic signs and (2) the often inexorable progression of the disease processes even after the patient has been removed from the causative dusty environment. Additionally, the duration of exposure is often significantly shorter than it is with silicosis, often no longer than 3–5 years.

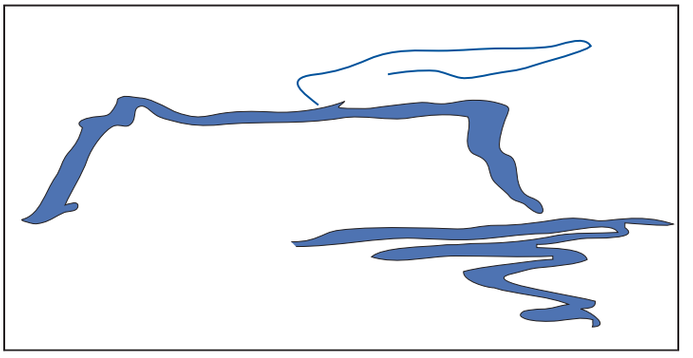

Fig. 5.53 Schematic diagram of the table-mountainlike configuration of pleural plaques from asbestos inhalation. (This image honors the physicians of Groote Schuur Hospital in Cape Town, South Africa, where the author had the privilege of staying while planning this chapter in November 2007.)

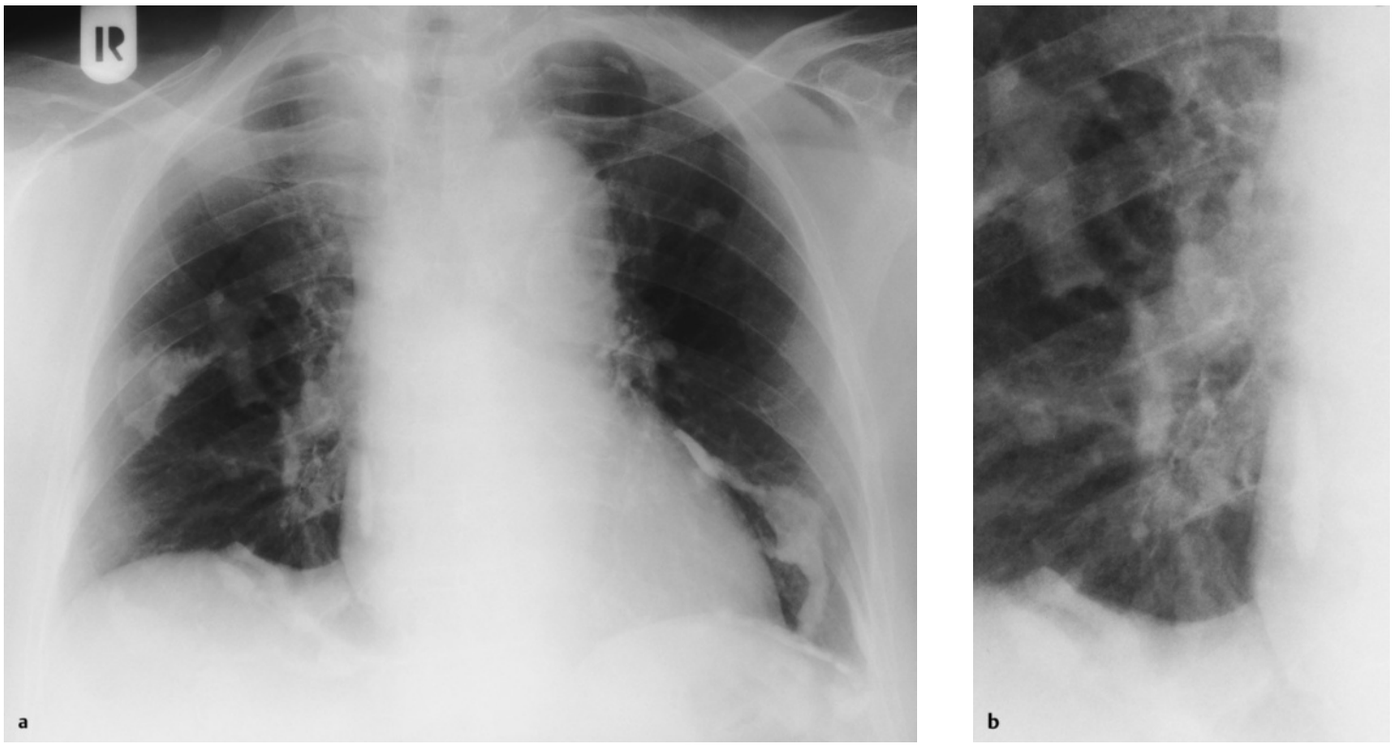

Fig. 5.54 a, b Pulmonary asbestosis and asbestos-associated pleural disease.

a In addition to bilateral pleural plaques, some bizarrely shaped, findings include predominantly central shadowing. Left heart enlargement without signs of decompensation, reduced caliber of the peripheral vessels, and poor inspiration are indicative of incipient restriction.

b The detail enlargement shows diffuse ground-glass attenuation of the paramediastinal tissue with gathering of some bronchi and vascular structures, leading to blurring of the central vascular structures.

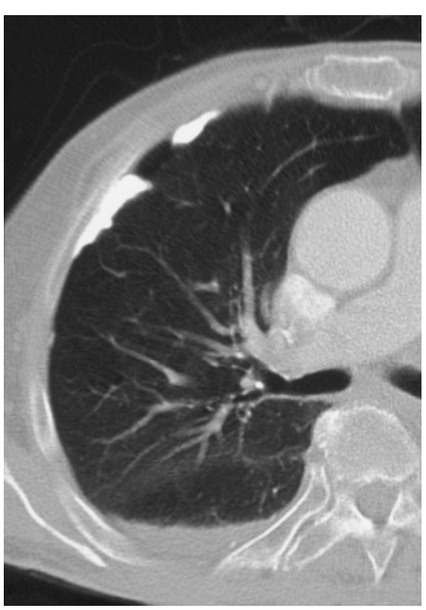

Fig. 5.55 Typical CT findings of asbestos-associated pleural plaques. In the right anterior region there are large pleural plaques showing table-mountain-like discontinuity with the adjacent normal areas of the pleura. Associated effusion, peribronchial shadowing, and noticeably severe tracheobronchopathia calcarea are also seen.

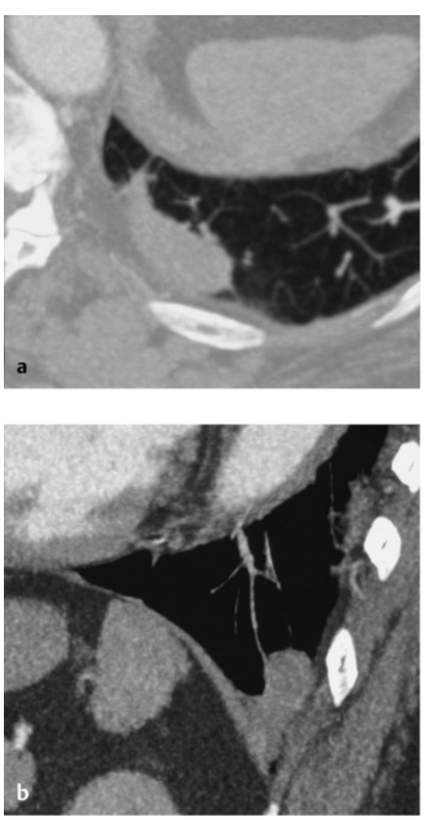

Fig. 5.56 a, b Rounded atelectasis in the left lower lobe. Findings include an elongated shadow resembling an eggplant on the axial reconstruction (**a**), which appears as a round shadow with a comet tail of converging vascular structures on the sagittal reconstruction (**b**).

Extrinsic Allergic Alveolitis

Extrinsic allergic alveolitis (EAA), or hypersensitivity pneumonitis, refers to a group of inflammatory pulmonary reactions caused by inhalation of various antigen substances (usually organic, less often inorganic). In contrast to drug-induced pulmonary fibrosis, the exposure is local, not systemic (**Fig. 5.57**).

Radiographic signs of extrinsic allergic alveolitis include:

- Symmetrical extensive shadows with normal heart size
- Ground-glass opacity
- Air trapping on CT
- Later, signs of fibrosis without predilection for the basal areas

When the first symptoms appear, the conventional chest radiograph shows faint symmetrical extensive densities that do not suggest underlying heart disease. The disorder can take one of several courses. When the diagnosis is not made, recurrent episodes usually lead to increasing fibrotic transformation of the lung (**Fig. 5.59**), a restrictive ventilation defect, pulmonary arterial hypertension, and cor pulmonale. Occasionally massive acute exacerbation will occur with alveolar edema that can progress to a "white lung" (**Fig. 5.58c**). When a timely diagnosis is made, changes can resolve rapidly under steroid therapy.

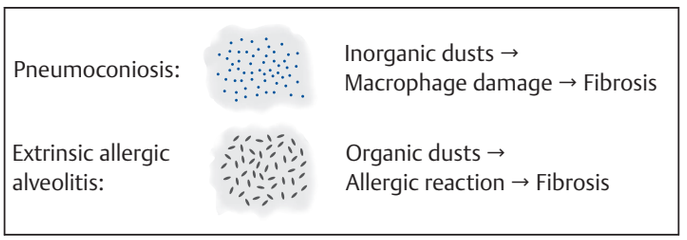

Fig. 5.57 Schematic diagram of the course of extrinsic allergic alveolitis (EAA) and pneumoconiosis. In pneumoconiosis inorganic dusts such as silicates lead to fibrosis due to their damaging effect on macrophages. In contrast, the fibrotic transformations in EAA occur as the result of an allergic reaction caused by organic materials.

Notes on Pathology and Clinical Findings

Histologic examination in extrinsic allergic alveolitis immediately after allergen contact shows perivascular granulocytic infiltrates. Edema is accompanied by interstitial infiltration by lymphocytes, plasma cells, and macrophages. Findings in the further course of the disorder include exudate with a high protein content and the presence of inflammatory cells in the alveoli. Recurrent exposure to the antigen leads to increasing collagen formation. The late stage is characterized by irreversible fibrosis with irregular transformation of the peripheral airways and alveoli and with confluent areas of scarring.

Many noxious agents can lead to extrinsic allergic alveolitis (**Table 5.5**). Inhalation of mildewed grain dust (farmer's lung) was the subject of the first such description. Bagassosis (from mildewed sugarcane fibers) and baker's lung (mildewed flour) are similar disorders. Bird breeder's lung is widespread. Note that there is a high proportion of nonsmokers among patients with extrinsic allergic alveolitis (up to 95%). This may be attributable to alteration of immune mechanisms in smokers, especially a reduction in serum antibody levels. As a result, extrinsic allergic alveolitis is rare in smokers.

Symptoms typically occur within 4–6 h after exposure. The symptoms (cough, mild fever, dyspnea) are initially nonspecific. However, the typical periodicity of their occurrence can provide valuable information. For example, patients with occupational exposure will be asymptomatic during vacations, whereas patients with bird breeder's lung will show improvement during hospitalization. Positive evidence of precipitating antibodies can be an important diagnostic sign. However, it can also be positive in healthy persons who show no symptoms of disease.

Table 5.5 Selected causes of extrinsic allergic alveolitis

Antigens	Antigen exposure	Entity
Thermophilic actinomycetes	Mildewed hay, grass	Farmer's lung
	Fungi	Mushroom worker's lung
	Bagasse	Bagassosis
	Contaminated water	Waterer's disease
Avian serum protein	Pigeons	Bird breeder's lung
	Parakeets	
Aspergillus and *Penicillium* species	Malt	Malt worker's lung
	Flour	Baker's lung
	Cheese	Cheese washer's lung
Sawdust extract	Wood	Logger's lung

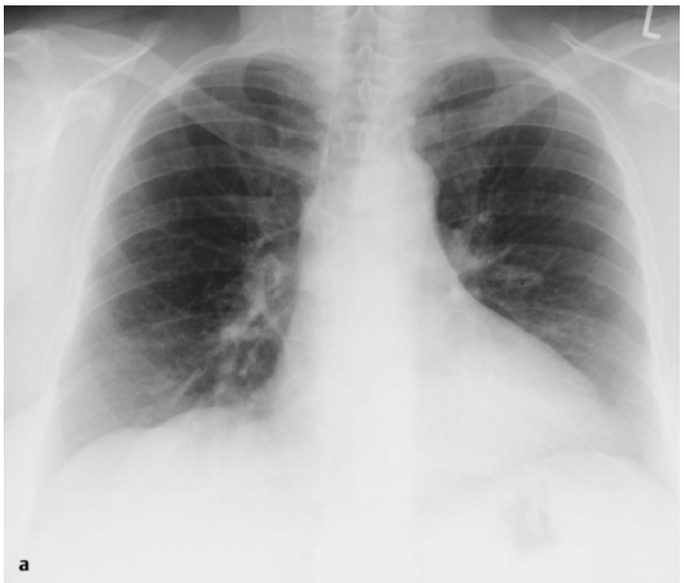

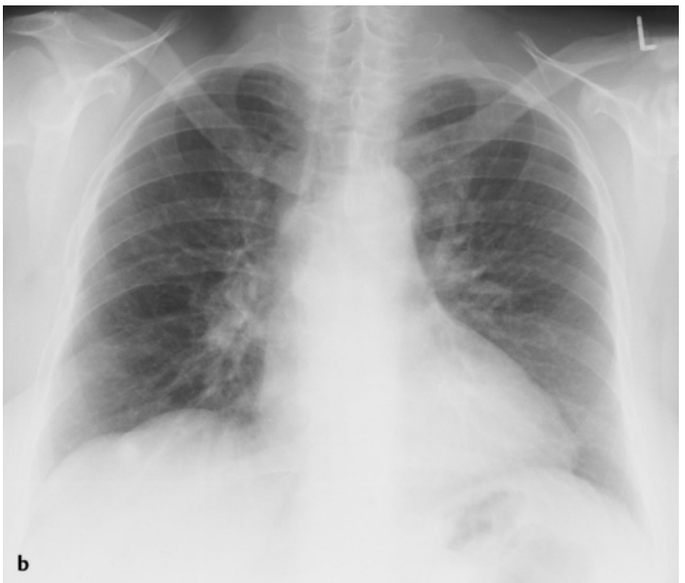

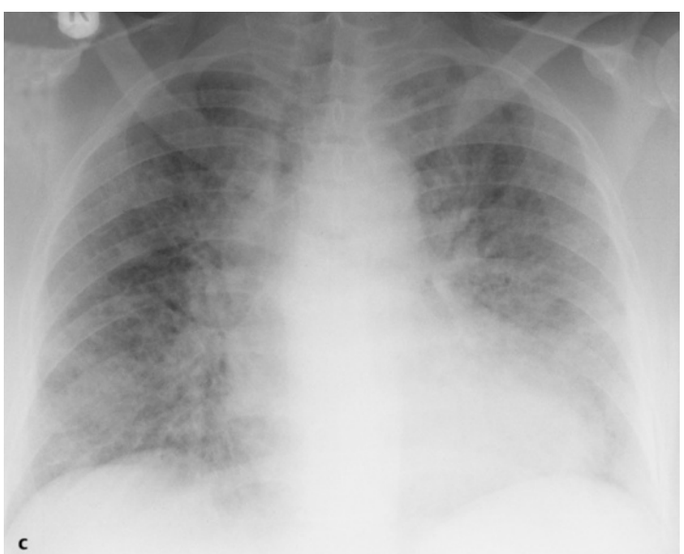

Fig. 5.58 a–c Course of extrinsic allergic alveolitis.

a A prior radiograph obtained 18 months before the onset of the disease shows left heart enlargement without signs of decompensation. There are no signs of infiltrates and no significant bronchitic shadowing.

b Faint opacity. Acute early stage with diffuse, finely nodular (acinar) shadowing that does not show a predilection for the apical or basal lung segments. There is only moderate peribronchial shadowing, no Kerley lines, no redistribution, and therefore no cardiac decompensation.

c Acute worsening with an incipient "white lung." Three days after the image **b** the patient is suffering from severe dyspnea. Radiographic findings now include severe diffuse shadowing with a partial air bronchogram. The contours of the diaphragm can be clearly traced into the posterior costophrenic recess. This excludes an effusion.

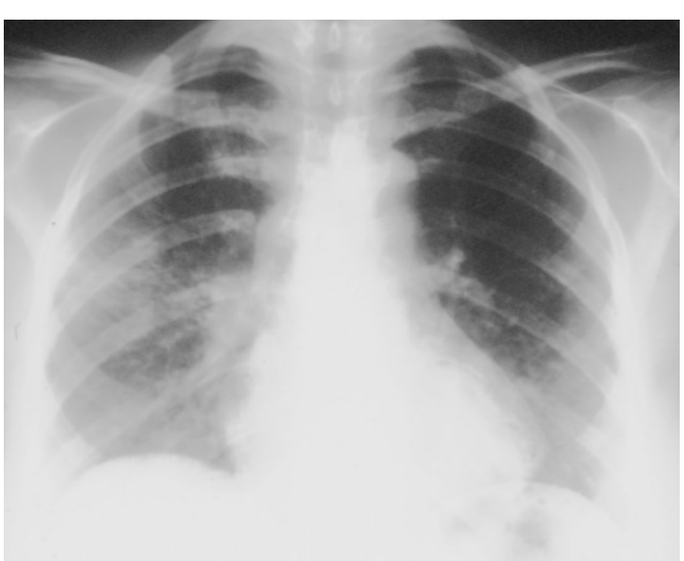

Fig. 5.59 Fibrotic pulmonary changes in EAA. The patient is a bird breeder with recurrent episodes of acute dyspnea and fever. Over the course of several years, the disorder has led to obstructive barrel chest, diffuse interstitial reticulonodular shadowing, and ground-glass opacities consistent with alveolar wall fibrosis.

The **CT scan** of the acute to subacute phase of extrinsic allergic alveolitis shows relatively characteristic findings:

- Ground-glass opacities
- Centrilobular predilection
- Sparing of the subpleural space
- Air trapping
- Absence of any basal and peripheral predilection

Ground-glass hyperdensities are initially visible as a result of the alveolar exudation. In the initial stage they show a predilection for the centrilobular space, sparing the peripheral portions of the secondary lobule (**Fig. 5.60, Fig. 5.61**). Notably, the ground-glass opacities also spare the subpleural space. Evidence of air trapping (**Fig. 5.62**) can be an important sign of the presence of extrinsic allergic alveolitis. Areas of air trapping appear hypodense. The normal architecture of the secondary lobule (honeycomb) can be preserved. With significant hyperinflation it takes on a round shape. Unaffected lung segments adjacent to the hyperinflated lobule usually show a significant increase in density similar to ground-glass opacities. Although air trapping can often be observed on inspiration, it can be missed when scans are regularly obtained in inspiration. As a result, one should make a point of obtaining additional scans in expiration. The fibrosing stage of extrinsic allergic alveolitis (**Fig. 5.63**) can also spare the subpleural space. This and the absence of the predilection for the basal segments seen in idiopathic pulmonary fibrosis are important criteria in the differential diagnosis of extrinsic allergic alveolitis from IPF.

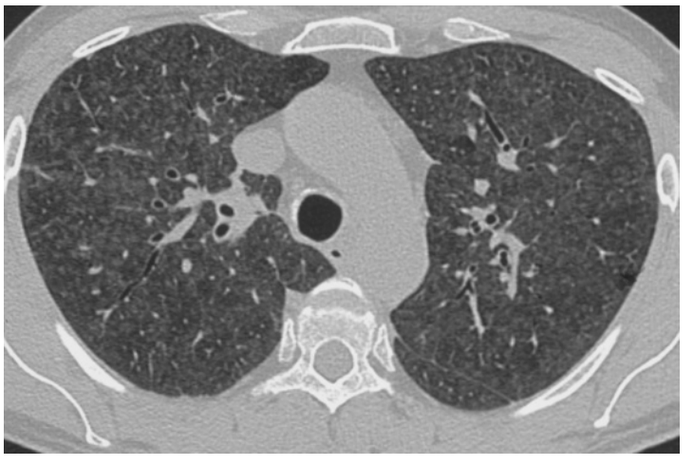

Fig. 5.60 Ground-glass and centrilobular opacities in EAA. The patient is a 47-year-old pigeon breeder presenting with fever and dyspnea. The plain chest radiograph shows diffuse shadowing. CT shows very finely nodular centrilobular ground-glass opacities beginning in the central region of the lung and largely sparing the periphery.

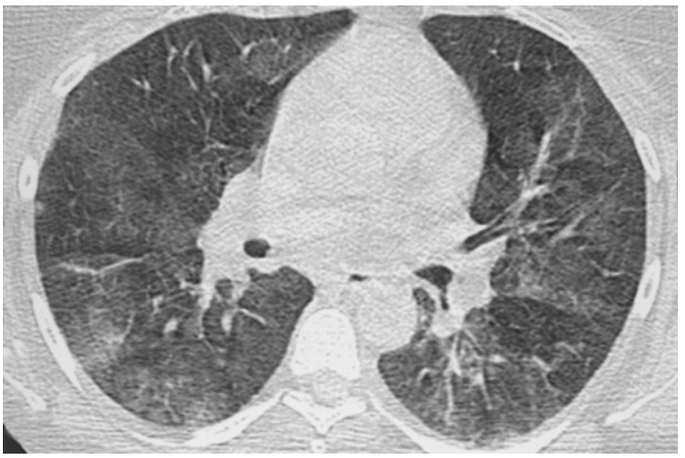

Fig. 5.61 Ground-glass opacities. The patient is a 32-year-old woman, owner of a parakeet, presenting with severe dyspnea. Findings include diffuse ground-glass opacities partially sparing the periphery with isolated unaffected subsegments.

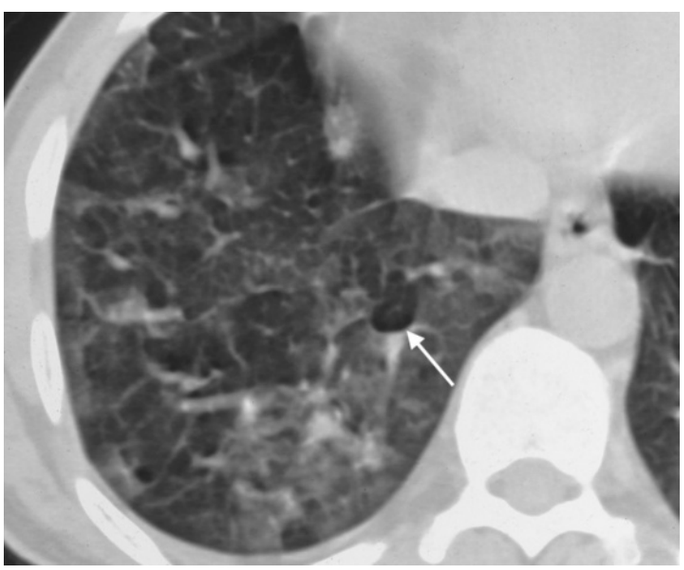

Fig. 5.62 Air trapping appears more pronounced on expiration. In the presence of significant motion artifacts from respiration (gull-wing appearance of the blood vessels), the image clearly demonstrates hyperinflation of isolated secondary lobules (white arrow) consistent with air trapping.

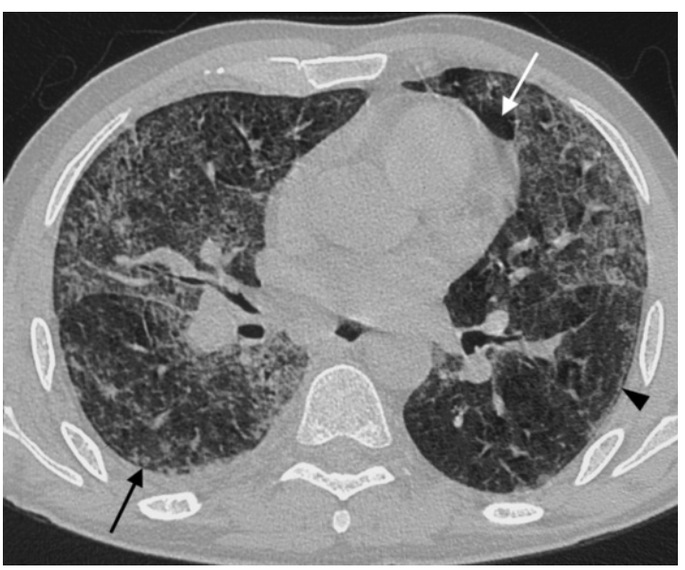

Fig. 5.63 Fibrotic changes secondary to EAA. The patient is a 51-year-old man, a pigeon breeder, with recurrent extrinsic allergic alveolitis. Findings include severe fibrotic transformation of the lung with interlobular and intralobular shadowing, micronodules (black arrow), subpleural bands of fibrosis (black arrowhead), and secondary hyperinflation with shrinkage (white arrow).

Radiation Pneumonitis and Fibrosis

Fibrosis secondary to radiation therapy is typically circumscribed and does not respect segmental and lobar boundaries but is distributed in the geometric shape of the irradiated field. The following forms are distinguished:

- Acute form (radiation pneumonitis)
- Radiation fibrosis

Acute radiation pneumonitis represents an acute inflammatory process presumably caused by damage to the surfactant-producing cells and accompanied by alveolar edema. The radiologic picture thus resembles that of surfactant deficiency, exhibiting the following findings:

- Ground-glass veil-like attenuation
- Blurring of vascular structures
- Hyperemia with no signs of heart failure

The edematous changes are largely limited to the irradiated field, although subacute findings can spread to adjacent areas (**Fig. 5.64**). The processes set in motion by the radiation therapy lead to fibrosis of the affected areas.

In the chronic stage of **radiation fibrosis** (**Fig. 5.65**, **Fig. 5.66**) conventional radiography and CT both show the typical signs of parenchymal fibrosis:

- Area consolidation
- Parenchymal bands
- Hyperinflation of adjacent areas with:
  - Bronchiectasis and bronchiolectasis
  - Subsegmental hyperinflation
  - Arcades
- Distracted pulmonary architecture

These findings occur in a circumscribed area in a distribution that does not respect segmental and lobar boundaries. They are relatively sharply demarcated. Radiation-induced fibrosis can occasionally exhibit characteristics of a mass (**Fig. 5.65**). This can complicate the differential diagnosis between radiation fibrosis and recurrence of the underlying tumor.

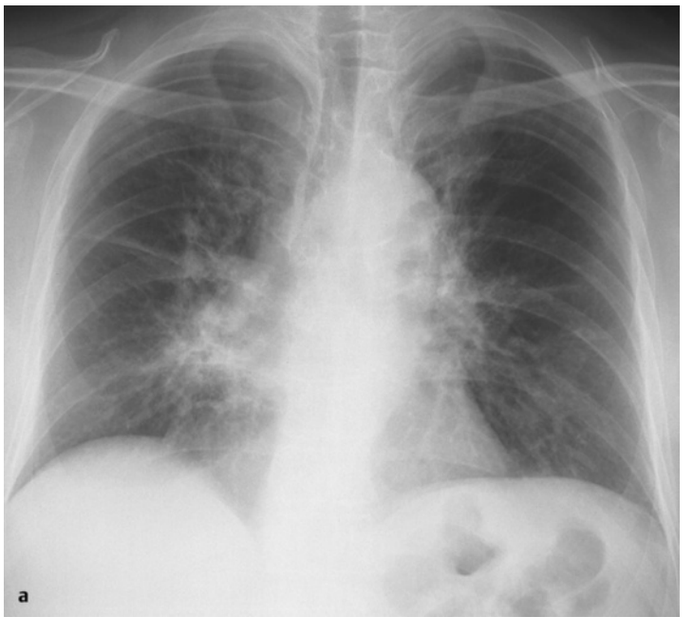

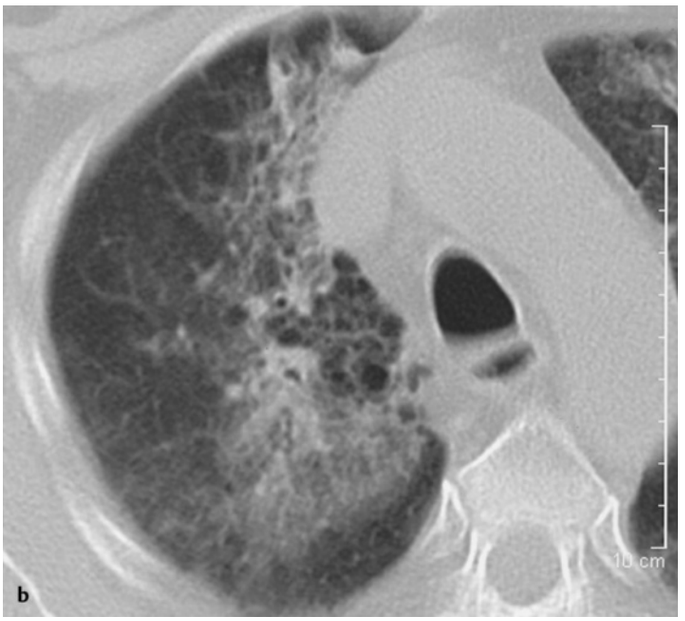

Fig. 5.64 a, b **Acute radiation pneumonitis**

a The patient is a 60-year-old man who underwent mediastinal radiation therapy for a bronchial carcinoma in the right lung. There is bilateral massive paramediastinal interstitial shadowing, more pronounced in the center. The proliferative vascular structures appear blurred. A discrete interlobar effusion is present on the right side. Heart size is normal.

b CT image. The scan shows a broad paramediastinal band of ground-glass attenuation with a relatively ill-defined border to normal tissue.

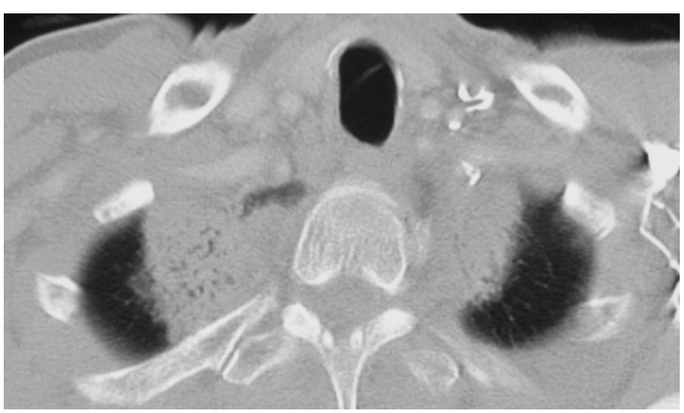

Fig. 5.65 **Post-radiation fibrosis exhibiting characteristics of a mass.** A Hodgkin patient who underwent radiation therapy according to the mantle field technique several years previously. Findings include solid-looking patches of fibrosis with bronchiolectasis that project beyond surrounding tissue.

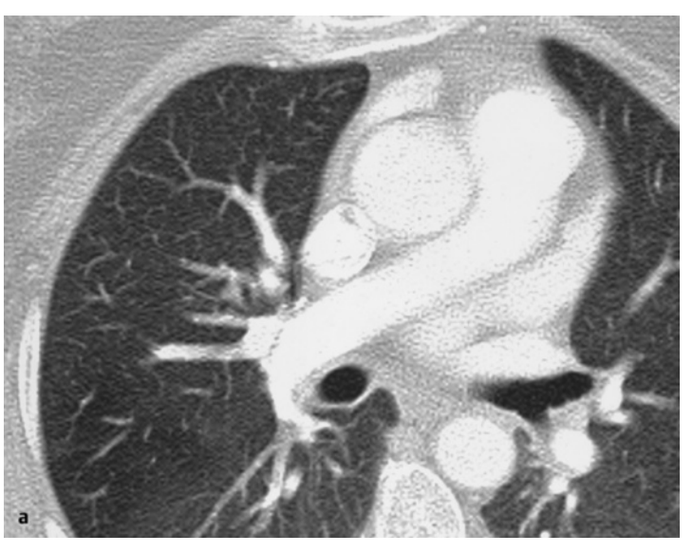

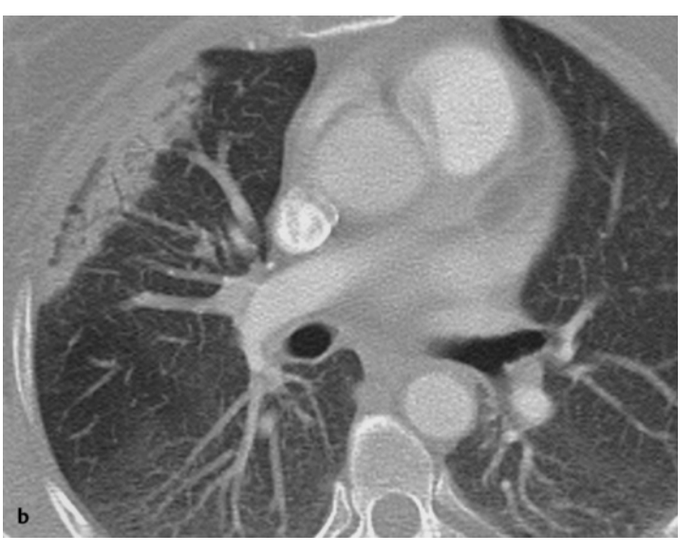

Fig. 5.66 a, b **Radiation fibrosis after tangential irradiation of the right breast.**

a The initial staging image does not yet show any fibrotic transformation in the right upper lobe. There are signs of chronic bronchitis with mild pulmonary arterial hypertension. No nodules suggestive of metastases are detected.

b Follow-up examination 6 months later. Following radiation therapy and subsequent radiation pneumonitis there is now a typical, sharply demarcated band of consolidation coursing tangentially to the irradiated field and not respecting anatomic boundaries. Other findings include an air bronchogram and small subpleural bullae indicative of shrinkage.

Drug-Induced and Pressure-Induced Fibrosis

Drug-Induced Fibrosis

The best known example of a medication that induces pulmonary fibrosis is amiodarone. However, there are many other pharmaceuticals that can also lead to fibrosing reactions (**Table 5.6**). The same distinction between the acute florid inflammatory reaction and the fibrotic residual state must be drawn in drug-induced fibrosis as in radiation fibrosis. It is now thought that these acute reactions represent severe damage to the basal membrane (diffuse alveolar damage), leading to adult respiratory distress syndrome (ARDS, **Fig. 5.67**). The acute stage begins within one week of administration of the chemotherapy agent. It is characterized by edema, hemorrhage, and hyaline membranes.

Radiologic findings include bilateral symmetrical ground-glass or denser shadows showing postural movement and representing the areas of highest concentration of the noxious agent. There are no signs of heart failure such as Kerley lines or effusions.

As in radiation fibrosis, the changes in drug-induced ARDS can eventually lead to a fibrosing process. However, this is by no means as inevitable as fibrosis secondary to irradiation.

Currently the most important pulmonary fibrosis induced by drugs other than chemotherapy agents is **amiodarone fibrosis.** The medication's long half-life poses a particular problem that requires early radiologic diagnosis (**Fig. 5.68**). Comparison with previous imaging studies is crucial to the detection of pathology in its early stages, which is an indication for immediate withdrawal of the medication. However, radiologic evaluation can be very difficult in the presence of emphysematous bronchitis due to the changes it frequently produces.

Table 5.6 Major pharmaceuticals that induce pulmonary fibrosis

Medication	Indication
Adriamycin	Chemotherapy agent
Amiodarone	Antiarrhythmic
Bleomycin	Chemotherapy agent
Cyclophosphamide	Chemotherapy agent
Busulfan	Chemotherapy agent
Gold	Antirheumatic agent
Methotrexate	Chemotherapy agent Antirheumatic agent
Mitomycin	Chemotherapy agent
Nitrofurantoin	Tuberculostatic agent
Penicillamine	Chelating agent
Taxane	Chemotherapy agent

Pressure-Induced Fibrosis

Mechanical forces acting on the pulmonary parenchyma can lead to reversible hypoventilation (compressive atelectasis) or hyperinflation. Such forces can also cause irreversible dilatation with loss of the alveolar wall (compensatory emphysema) and irreversible hypoventilation. The latter often occur in the form of local pressure-induced fibrosis. However, such findings are often overlooked or left out of the evaluation through lack of experience and uncertainty. Local mechanical fibrosis appears as narrow strands of consolidation:

- Adjacent to spondylophytes (**Fig. 5.69**)
- In aortic ectasia (**Fig. 5.70**)
- Predominantly in the basal lung segments

CT is the modality of choice for documenting these changes.

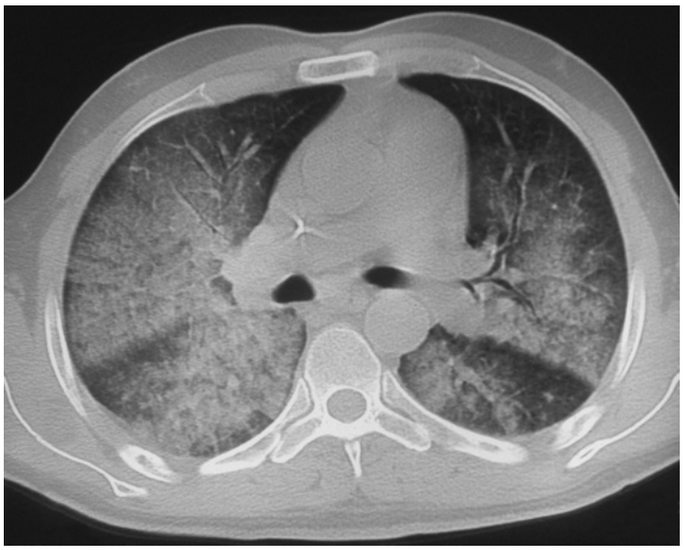

Fig. 5.67 Acute alveolar damage following high-dose chemotherapy (DAV treatment for acute myeloid leukemia). Symmetrical ground-glass opacities in the central region of the lung, increasing from anterior to posterior (up to the respective septa). No signs of congestion or effusion.

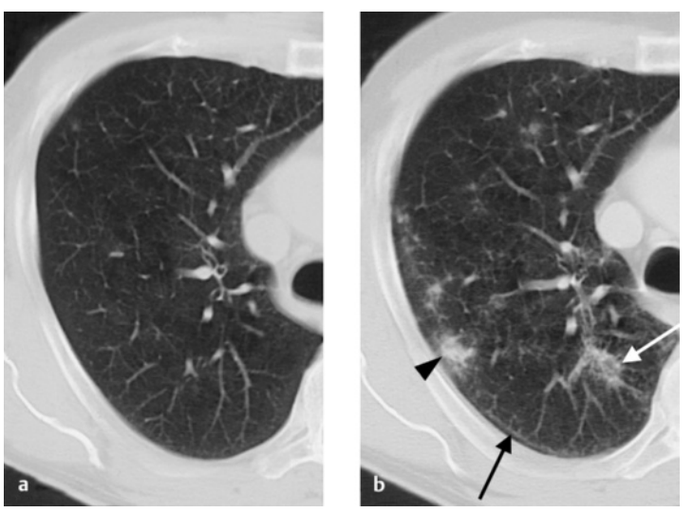

Fig. 5.68 a, b Amiodarone-induced fibrotic reaction.

a Pretreatment image of a 79-year-old man with COPD prior to beginning antiarrhythmic therapy with Cordarex (amiodarone). Obstructive barrel chest without area consolidation, diffuse, very finely nodular shadowing (respiratory bronchiolitis-interstitial lung disease).

b The follow-up examination 30 months later shows severe thickening of the interlobular fissures and intralobular septa, small areas of fibrosis (black arrowhead) with distracted pulmonary architecture (white arrow). Linear densities parallel to the pleura (black arrow) are also present.

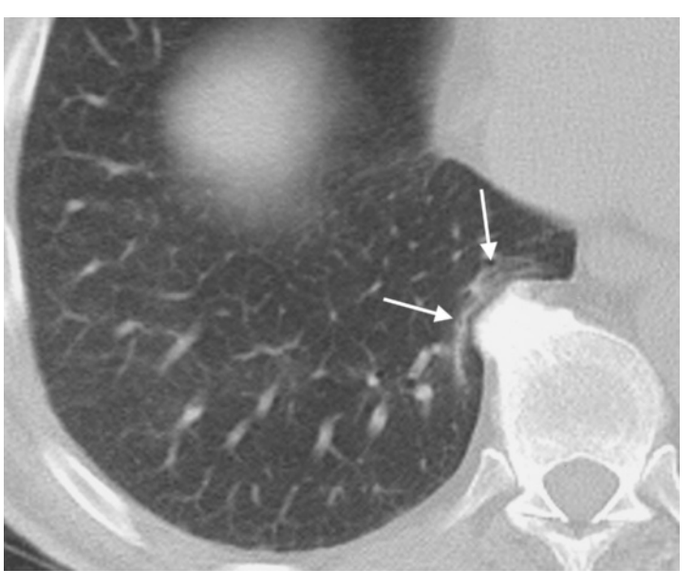

Fig. 5.69 Pressure-induced fibrosis. Fibrotic strand next to a lateral spondylophyte on the lower thoracic spine (white arrows).

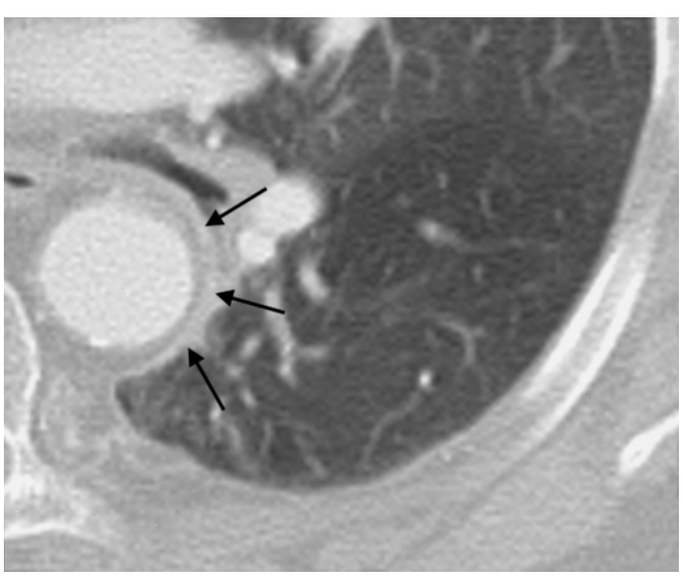

Fig. 5.70 Pressure-induced fibrosis. Para-aortic pressure-induced fibrosis in aortic ectasia (black arrows).

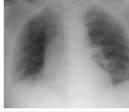

Review Case 1

The patient is a 45-year-old male smoker presenting with painful swelling of the ankles and fatigue. A plain chest radiograph was obtained to exclude pulmonary infiltrates in suspected parainfectious arthritis (Fig. 5.71).

Question 1

Are pneumonic infiltrates present?

Question 2

How do you evaluate the pulmonary parenchyma?
Are there signs of smoker's bronchitis?

Question 3

How do you evaluate the hilar structures?
Are there signs of a malignant process?

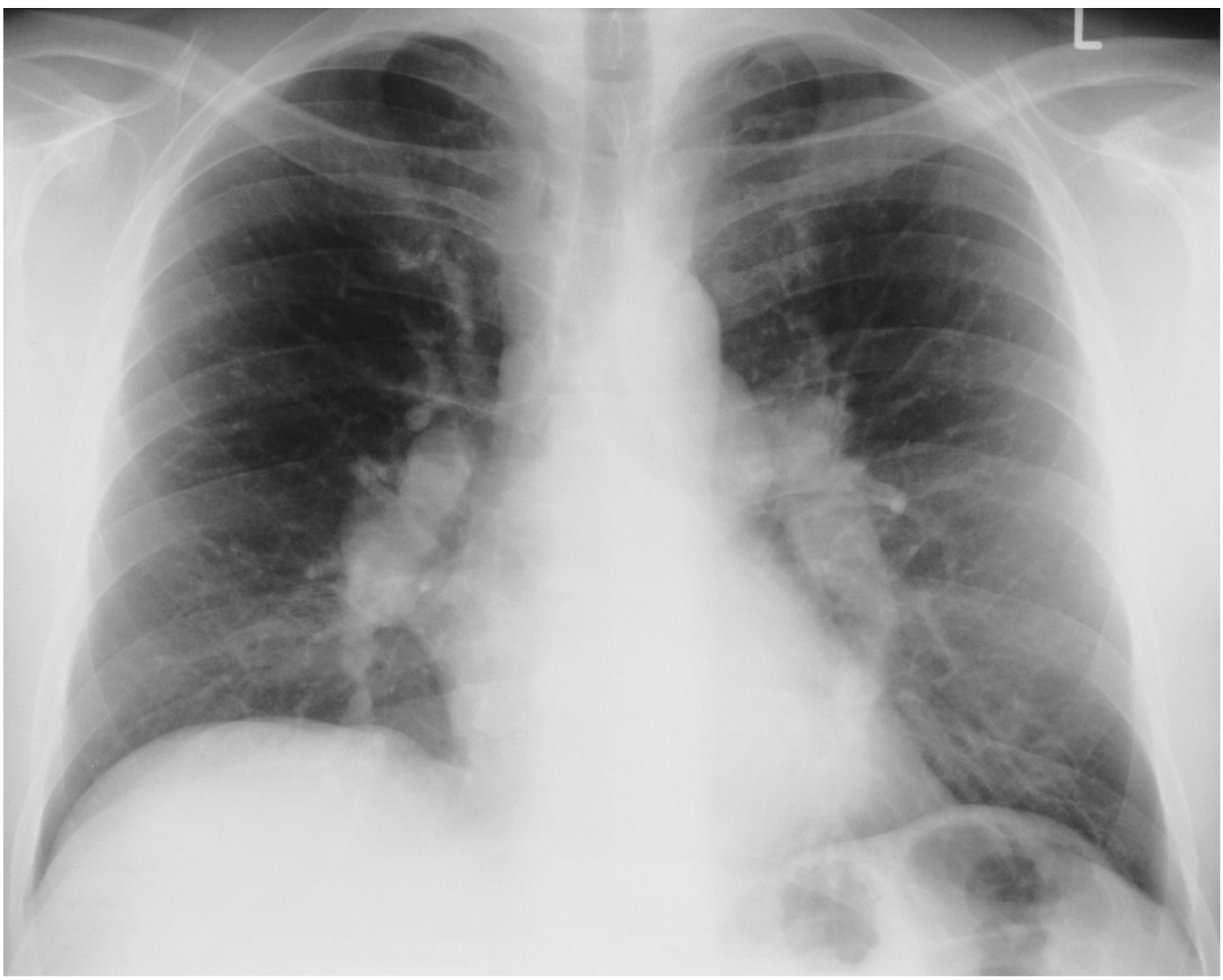

Fig. 5.71 Patient with arthritis

Answer

Answer to question 1: There is diffuse reticulonodular shadowing. Given the clinical findings of smoker's bronchitis, these changes most likely represent respiratory bronchiolitis-interstitial lung disease.

Answer to question 2: No pneumonic infiltrates are detectable.

Answer to question 3: The posteroanterior view clearly shows widened hila with a polycyclic contour and protrusion into the aortopulmonary window and azygoesophageal recess. The hilar masses are significantly less clearly defined on the lateral view (**Fig. 5.72**).

Evaluation: Pulmonary sarcoidosis with severe lymph node involvement. The pulmonary shadowing can be attributable to the chronic smoker's bronchitis. However, a differential diagnosis must consider incipient pulmonary involvement in the setting of stage II sarcoidosis. The clinical findings of painful swelling in the ankles are diagnostic of Löfgren syndrome.

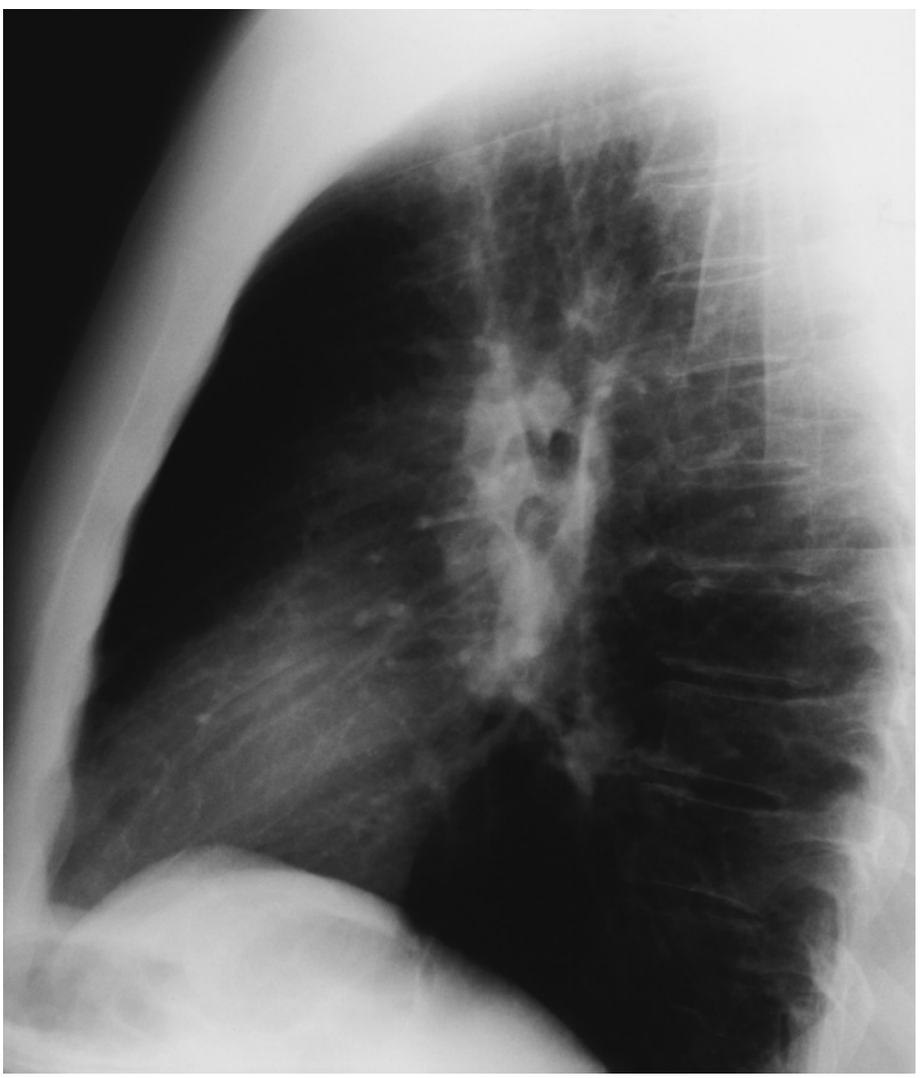

Fig. 5.72 Bilateral hilar lymphomas in sarcoidosis (lateral film of the patient in Fig. 5.71).

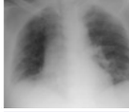

Review Case 2

The patient is a 44-year-old man. The chest radiograph was obtained during examination upon admission to the hospital to diagnose acute upper abdominal pain (Fig. 5.73).

Question 1

How do you evaluate heart size and cardiac compensation?

Question 2

If you assume there is no congestion, how do you evaluate the perihilar shadowing and the blurring of the hila?

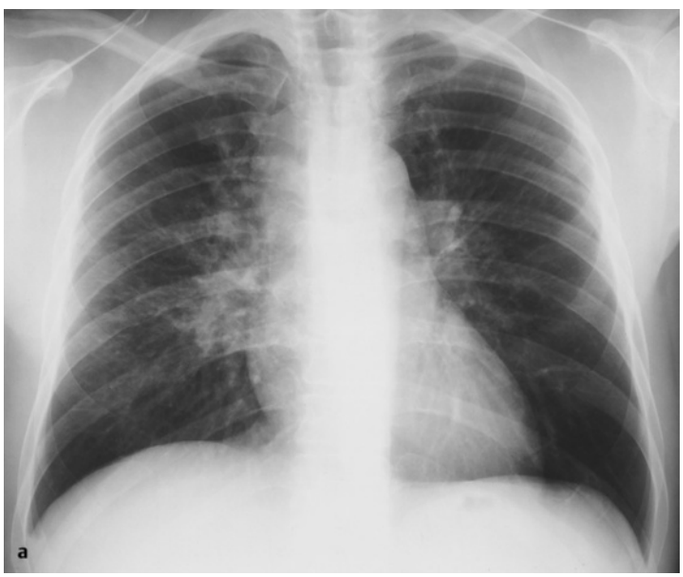

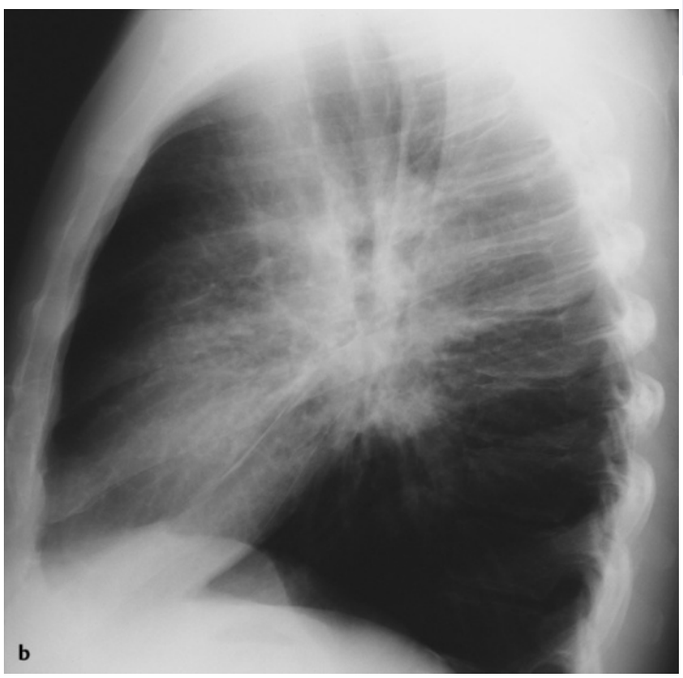

Fig. 5.73 a, b Routine radiographs of a patient with acute upper abdominal pain. No pulmonary symptoms.

Answer

Answer to question 1: Heart size is normal (large retrocardiac space; the width of the hemithorax is longer than the long axis of the heart). There are no signs of decompensation (no redistribution, no Kerley lines, no effusion).

Answer to question 2: The hila are moderately thickened, and streaky symmetrical interstitial shadowing is present primarily in the central compartment of the lung. A very finely nodular pattern is seen here too.

Evaluation: The CT scan performed immediately (**Fig. 5.74**) dramatically visualizes the bilateral perihilar reticulonodular shadowing causing blurring of the hila. The nodules lie primarily along the bronchovascular bundle. There are moderate bilateral hilar lymphomas and a significant infracarinal lymphoma. Mediastinoscopy confirmed sarcoidosis (stage II a according to radiographic findings).

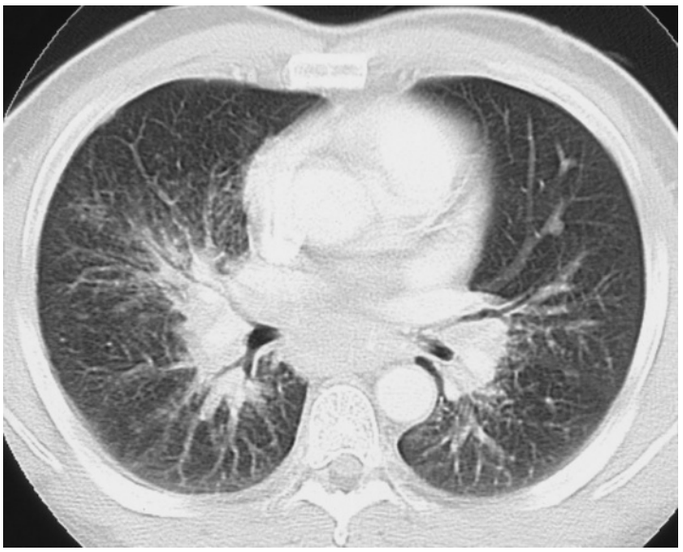

Fig. 5.74 CT scan of review case 2: perihilar shadowing with bronchovascular nodules in stage II a sarcoidosis.

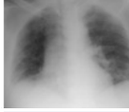

Review Case 3

The patient is a 51-year-old male nonsmoker presenting with recurrent attacks of fever with general malaise, cough, and increasing weakness. In his own words, he can hardly climb the stairs to his pigeon cages. The patient is upset that these symptoms invariably manifest themselves during his free time and especially on the weekends. As he works on an assembly line and is paid on a piecework basis, a psychologist suspected a burnout syndrome. The plain chest obtained during examination upon admission to the hospital shows severe interstitial shadowing with reduced volume at inspiration. A supplementary CT scan was then ordered.

Question 1

How do you classify the shadowing? How do you evaluate the circumscribed radiolucency in the apex of the left lung? (Fig. 5.75 a)

Question 2

How do you evaluate the activity of the shadows in the middle lobe? Are they more chronic or acute? What underlying disease do you suspect? (Fig. 5.75b)

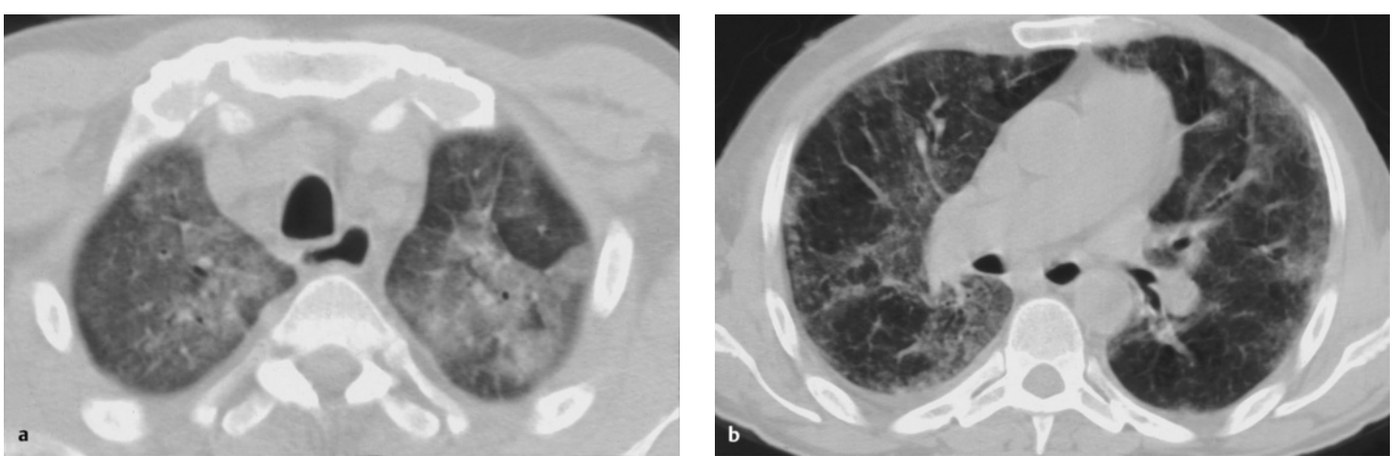

Fig. 5.75 a, b A 51-year-old nonsmoker with weekend attacks of cough and fever.

Answer

Answer to question 1: The apical changes detectable in both lungs are classified as ground-glass opacities because the underlying anatomic structure of the lung is visible through the shadows. The circumscribed radiolucency in the left apical lung (**Fig. 5.76**) corresponds to a dilated secondary lobule (concave border). This represents air trapping: acute hyperinflation with narrowing of the terminal bronchiole.

Answer to question 2: Most of the changes in the middle lobe are attributable to healed inflammatory processes with fibrotic transformation of the periphery of the lung. The few ground-glass opacities still detectable may represent alveolar wall fibrosis.

Evaluation: A new episode of advanced recurrent extrinsic allergic alveolitis in the presence of significant pulmonary fibrosis. In light of the typical history (exposure as an amateur pigeon breeder), findings may be classified as bird breeder's lung.

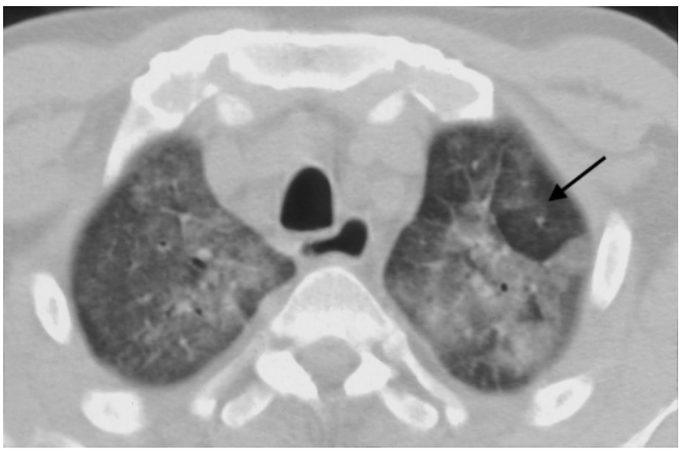

Fig. 5.76 EAA (bird breeder's lung) with air trapping (black arrow) and detectable fibrotic transformation.

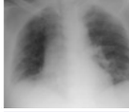

Review Case 4

The patient is a 66-year-old man with a history of general malaise and increasing dyspnea on exercise over the last few months. Symptoms have acutely worsened, with fever and severe dyspnea for the last 2 days (Fig. 5.77).

Question 1

Is the dyspnea on exercise caused by acute cardiac decompensation with left heart enlargement?

Hint

Inspiration?
Observe the right and left lungs separately.
Silhouette sign?

Question 2

How do you evaluate the pulmonary shadowing?

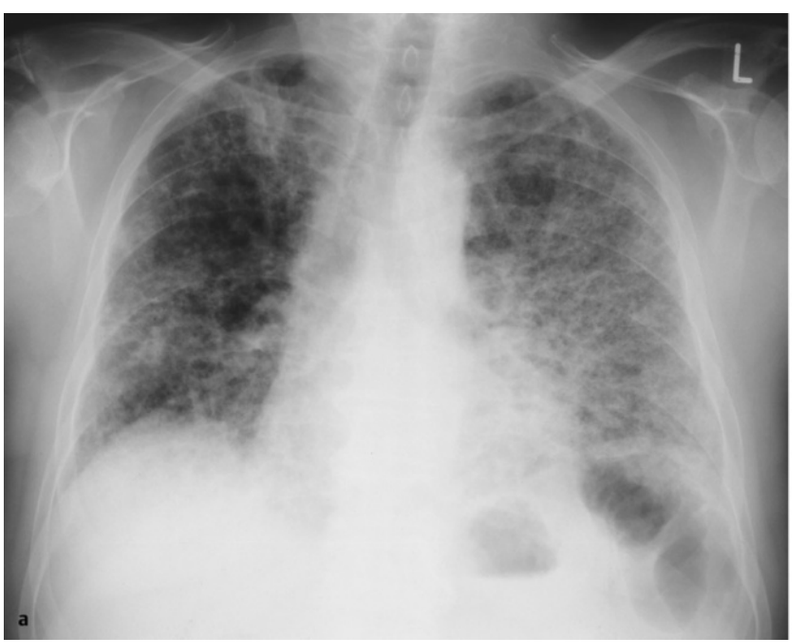

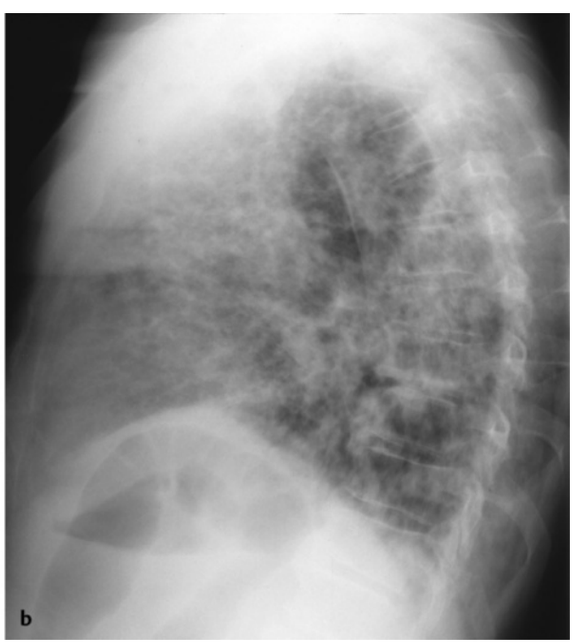

Fig. 5.77 a, b The patient has had increasing dyspnea on exercise over the last few months, now accompanied by fever.

Answer

Answer to question 1: With poor inspiration, the heart is in broad contact with the diaphragm but not enlarged (the long axis of the heart is less than half the width of the hemithorax). There is no cardiac decompensation (no Kerley lines or effusion).

Answer to question 2: There is extensive shadowing in the mantle of the lung, showing incipient basal honeycombing. There are area consolidations in the left lung with a silhouette sign involving the left cardiac border.

Evaluation: Comparison with a previous image obtained only a few days earlier (**Fig. 5.78**) is diagnostic of severe pulmonary fibrosis with intercurrent pneumonia.

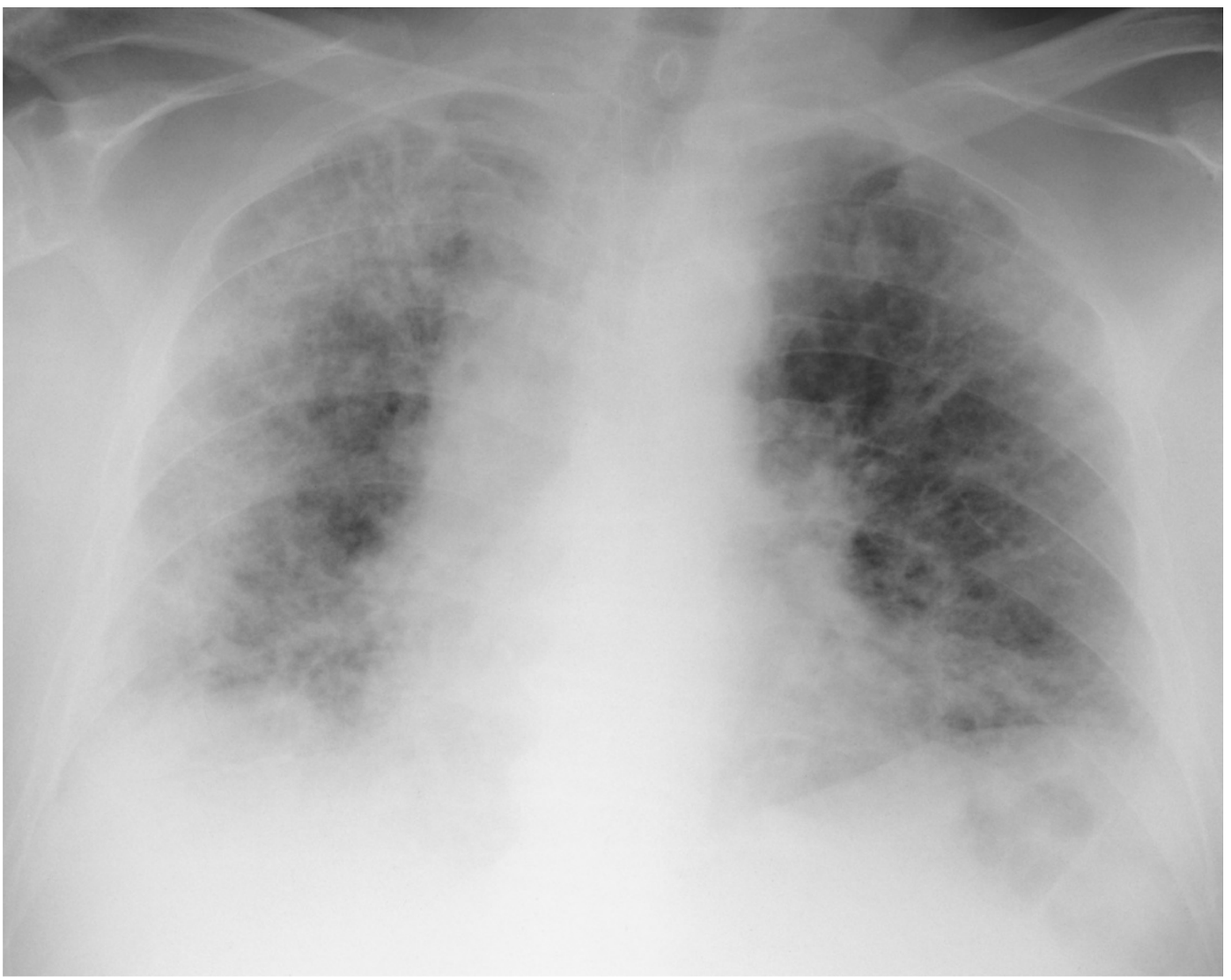

Fig. 5.78 **Previous image of the patient in Fig. 5.77.** Findings include shadowing in the mantle of the lung, decreased depth of inspiration, and beginning honeycombing with pulmonary fibrosis in the right basal region. The left diaphragmatic crus is still identifiable on this image.

6

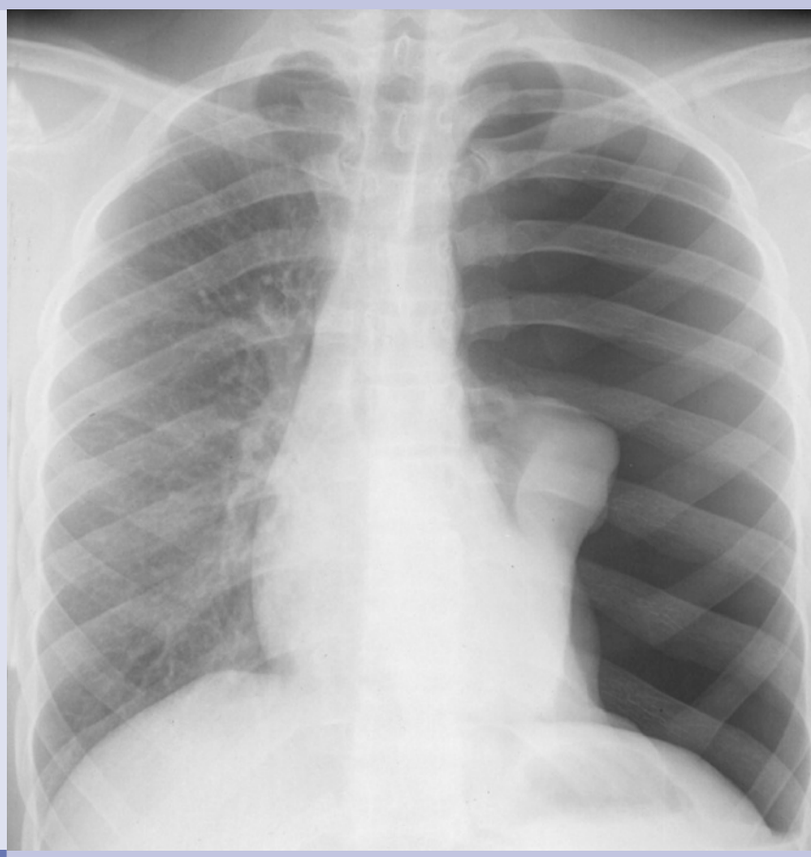

Pleura

General

Pathologic pleural changes often accompany disorders of the thoracic organs. Such changes were described early in the study of pulmonary disorders and have long been used in diagnosing underlying changes in the deeper regions of the chest. Honors for the description of attenuation phenomena by means of percussion belong to **Auenbrugger von Auenbrugg.** His work paved the way for Laennec's subsequent perfection of auscultation.

The physiologic pleura is only 1–2 mm thick. It consists of two layers:

- Visceral pleura
- Parietal pleura

The two layers are separated by a virtual space but normally lie in close contact with each other. The film of pleural fluid between them has a volume of a few milliliters (**Fig. 6.1**).

The pleura is indirectly visualized on **conventional radiographs** as follows:

- Where pleural tissue lies between air-filled spaces in the lungs (interlobar fissures, see below)
- Because of a "Mach effect" due to the abrupt change in radiodensity between the lung and adjacent soft tissue
- As the imaginary line connecting two ribs where the intercostal space is imaged tangentially (**Fig. 6.2**)
- As the border of a pleural effusion along the adjacent lung

The pleura can also be directly visualized where pathologic changes occur. These include:

- Thickening or calcification
- Pneumothorax (**Fig. 6.3**)

Leopold Auenbrugger von Auenbrugg (* 1722 Graz, † 1809 Vienna): Son of innkeeper, inventor of percussion, court physician to empress Maria Theresa. His book on sound attenuation laid the foundation for the physical examination of the chest organs.

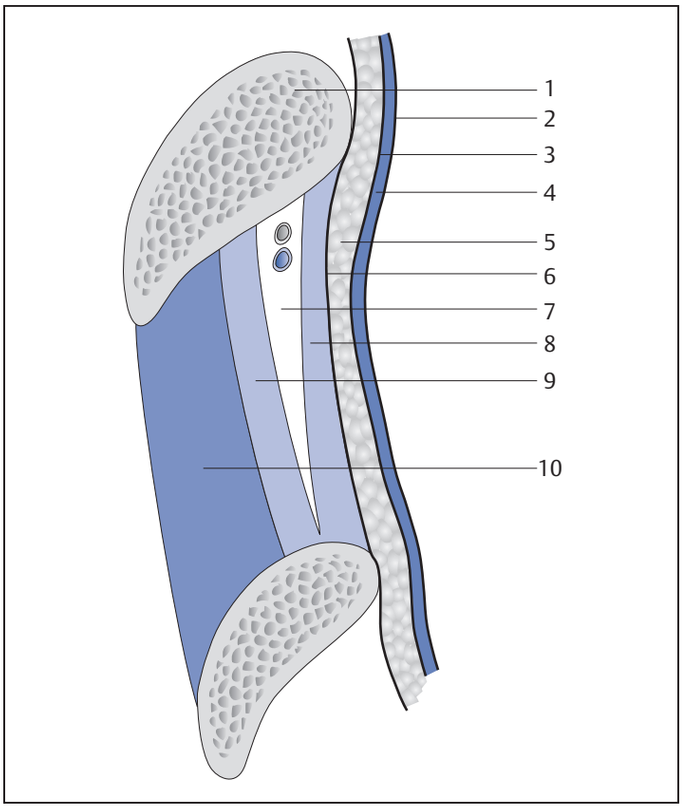

Fig. 6.1 Anatomic structure of the chest wall.
1 Rib
2 Visceral pleura
3 Parietal pleura
4 Pleural space
5 Extrapleural fat
6 Inner fascia of the chest wall
7 Intercostal space with fatty tissue and vascular structures
8 Internal intercostal muscle
9 Intermediate intercostal muscle
10 External intercostal muscle

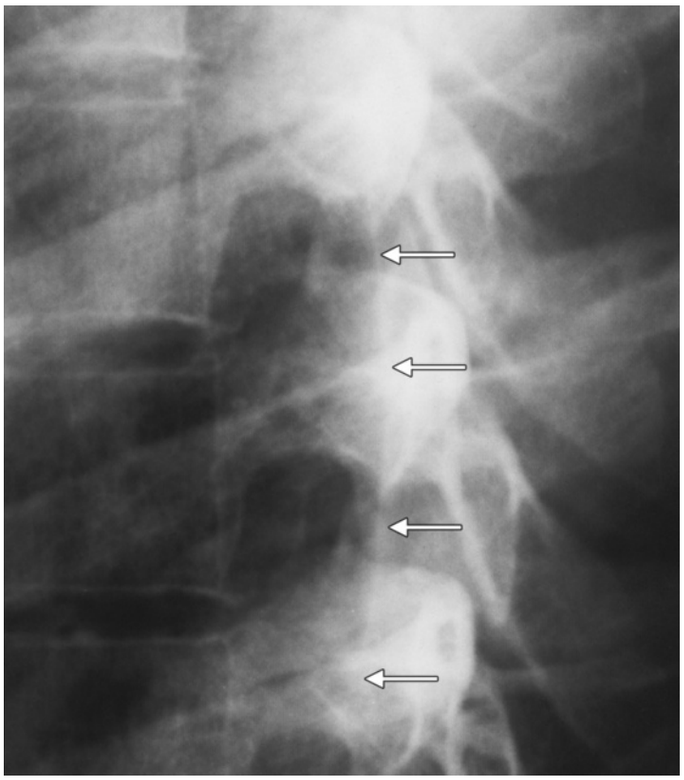

Fig. 6.2 Tangentially imaged pleura (detail enlargement of the chest radiograph). The posterior margin of the lung is marked by the line of the pleura (white arrows) coursing between rib arches.

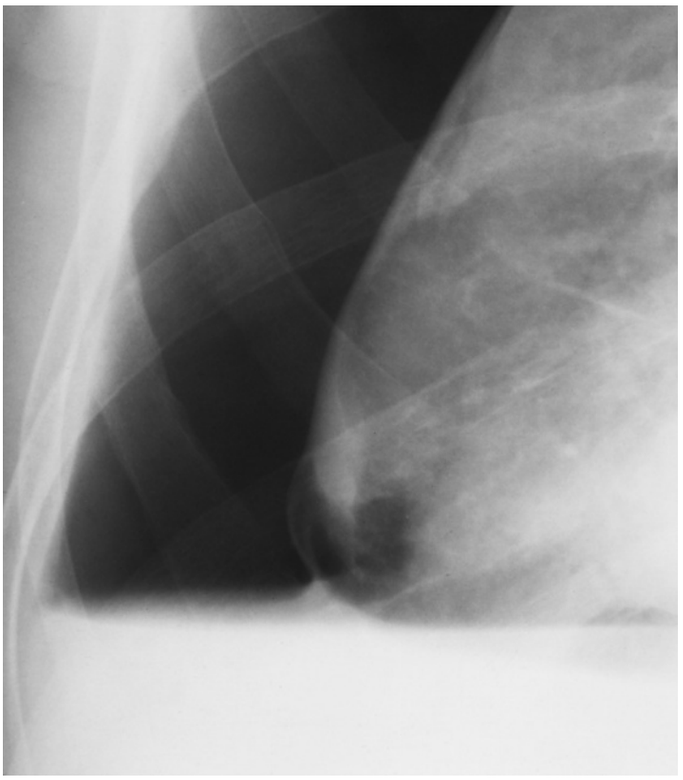

Fig. 6.3 Direct visualization of the visceral pleura in pneumothorax. Complete collapse of the right lung in pneumothorax with fluid accumulation. The visceral pleura can be identified along the partially collapsed basal segments of the right lung.

On **ultrasound studies** as well, the physiologic pleura is recognizable only because of an impedance mismatch between air-filled areas and the chest wall, which exhibits the acoustic impedance of soft tissue (**Fig. 6.5, Fig. 6.6**). Ultrasound can demonstrate the dynamics of the two separate layers of the pleura better than any other imaging modality.

Computed tomography directly visualizes the pleura as a fine band (**Fig. 6.7**). In pneumothorax with or without fluid accumulation and empyema, CT can also distinguish the visceral and parietal pleura from each other (**Fig. 6.8**).

Ultrasound and CT are clearly superior to conventional radiography in evaluating the pleural space. In the presence of clinical data ("But the patient has a pleural effusion on ultrasound"), one should be very careful with a plain chest radiograph that shows what appear to be normal findings (**Fig. 6.4**).

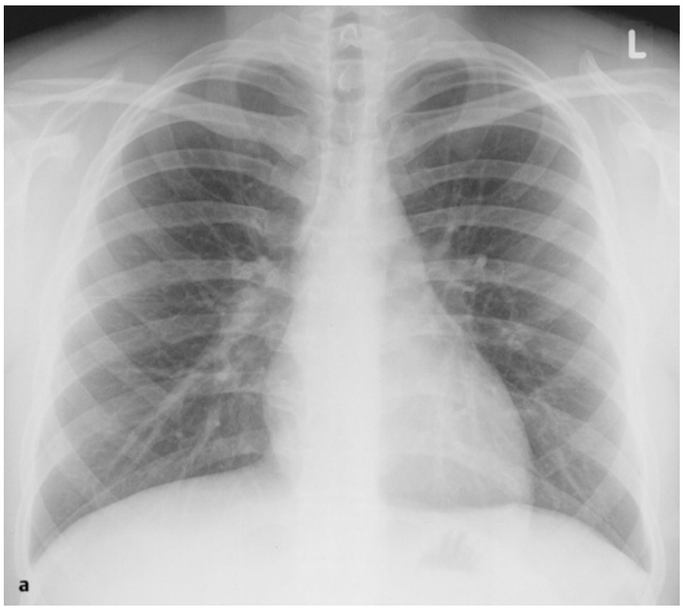

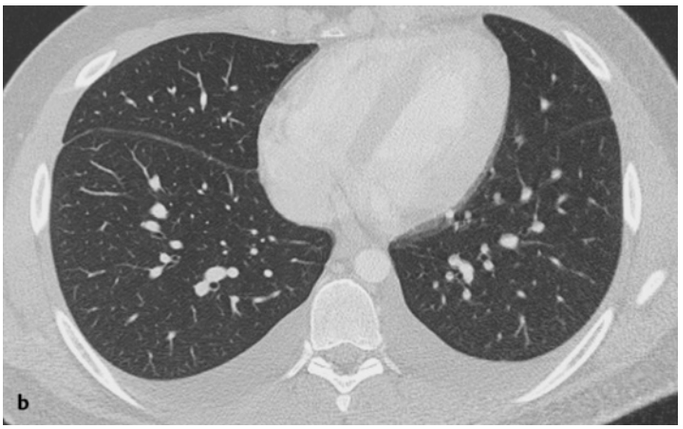

Fig. 6.4 a, b **Subpulmonary effusion**
a There is no evidence of the pleural effusion previously diagnosed on ultrasound.
b A CT scan performed the same day to exclude a pulmonary embolism confirmed the ultrasound findings.

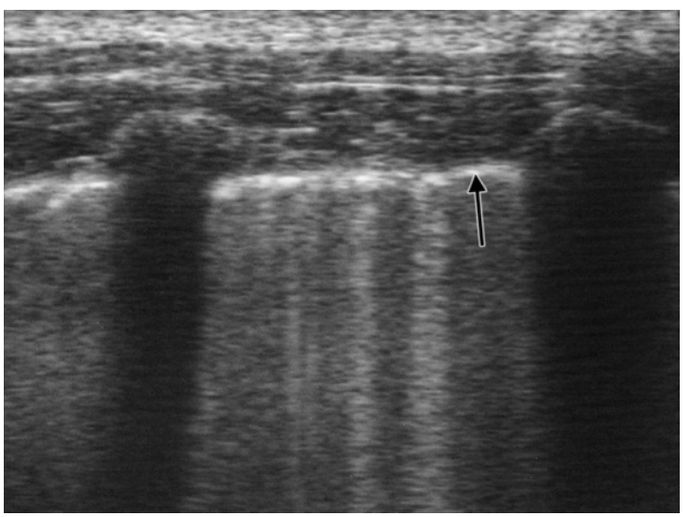

Fig. 6.5 **Ultrasound image of the pleura.** In the sagittal plane tangential to the ribs there is a streaky hyperechoic line along the impedance mismatch between the chest wall and the air-filled lung (black arrow).

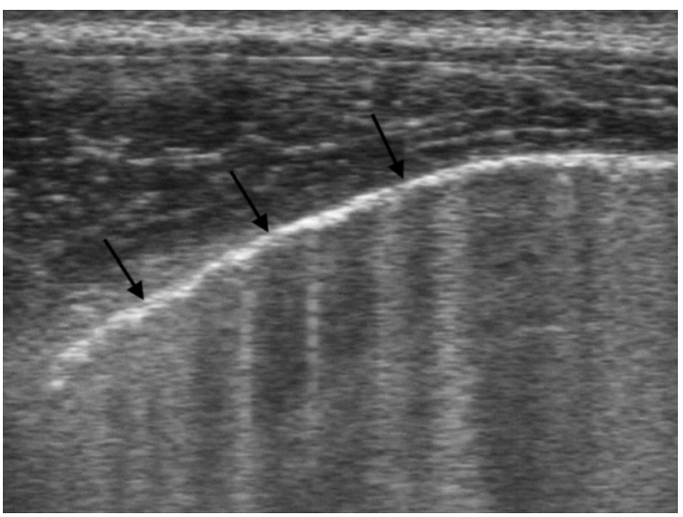

Fig. 6.6 **Ultrasound image of the pleura.** Unobstructed visualization of the pleural border (black arrows) in the intercostal plane.

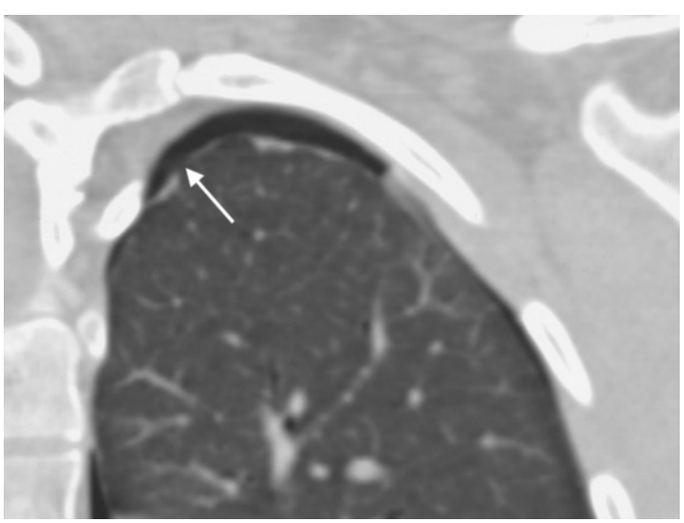

Fig. 6.7 **CT image of the visceral pleura in pneumothorax.** Discrete thickening of the visceral pleura in spontaneous apical pneumothorax. Tiny subpleural bullae (white arrow).

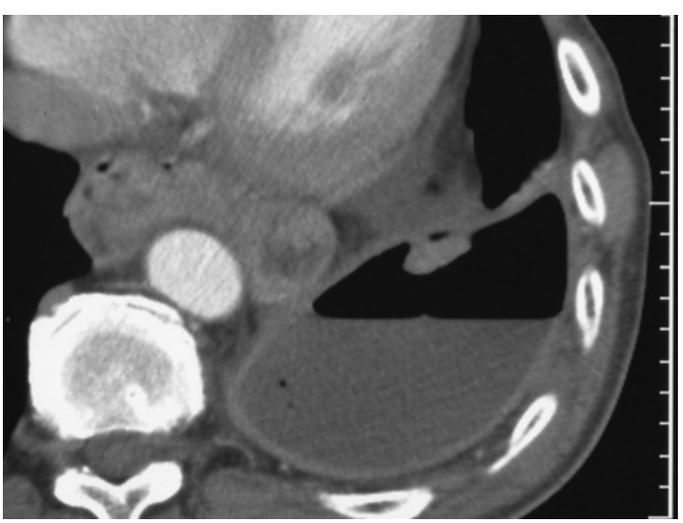

Fig. 6.8 **CT image of the thickened visceral and parietal pleura.** Pleural empyema already treated by aspiration and drainage; the thickened layers of the pleura can be differentiated because of the air inclusion.

The visible layers of the visceral pleura lying between the various pulmonary lobes are referred to as the **interlobar fissures** (**Fig. 6.9**).

The following fissures are regularly identifiable:

- Posteroanterior view: horizontal fissure of the right lung (**Fig. 6.11**)
- Lateral view: oblique and horizontal fissures (**Fig. 6.12**)

The interlobar fissures are also visible in the presence of various extra lobes:

- Azygos lobe (see Review Case 5, Chapter 1)
- Cardiac lobe

The pleura can also be visualized where an anterior pleural fold occurs (**Fig. 6.10**). This is present on the posteroanterior plain chest radiograph in ca. 20% of all patients examined (**Fig. 6.13**).

The anterior pleural fold corresponds to the zone of direct contact between the two lungs anterior to the upper mediastinum. The anterior pleural fold is readily detectable on conventional radiographs and CT images, especially in an emphysematous barrel chest (**Fig. 6.13b**). A posterior pleural fold similar to the anterior fold has been postulated. This posterior fold is not a clearly defined line, rather a zone between the medial borders of the posterior portions of the right and left lungs, which can approximate each other to a varying degree posterior to the aortic arch.

The visceral and parietal pleura are directly visualized on CT (see above). The horizontal fissure is occasionally difficult to identify. Note that there are fewer vascular structures in the pulmonary tissue adjacent to the horizontal fissure; this is comparable to the mismatch of vessels between the mantle of the lung and the central region of the lung.

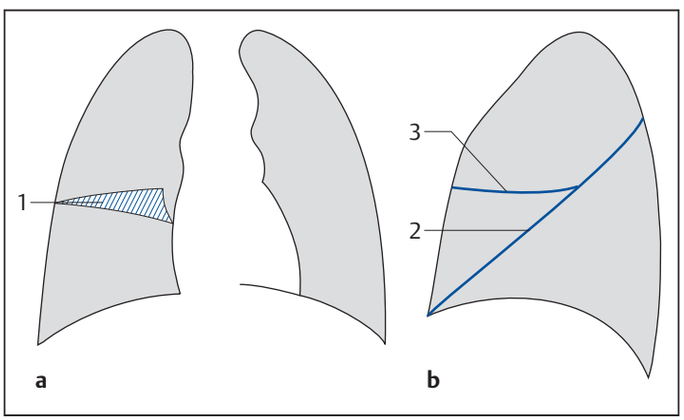

Fig. 6.9 a, b Schematic diagram of the various pleural folds visualized on the plain chest radiograph. The posteroanterior film (**a**) usually shows only the right horizontal fissure (1), the pleural fissure between the upper and middle lobes. In contrast, on the lateral film (**b**) the oblique fissures (2) of both lungs and the horizontal fissure of the right lung (3) are usually visualized.

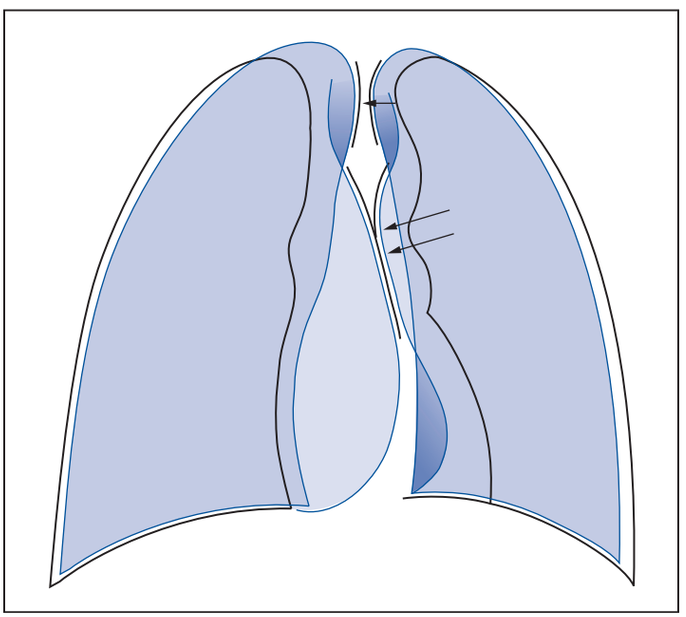

Fig. 6.10 Schematic diagram of the anterior and posterior pleural folds. The radiographic silhouette of the cardiomediastinal shadow does not correspond to the actual margin of the lung. There is an anterior area of contact between the lungs, which produces the radiographic figure of the anterior pleural fold (long arrows). The lungs are also nearly in contact posterior to the mediastinal shadow (short arrow).

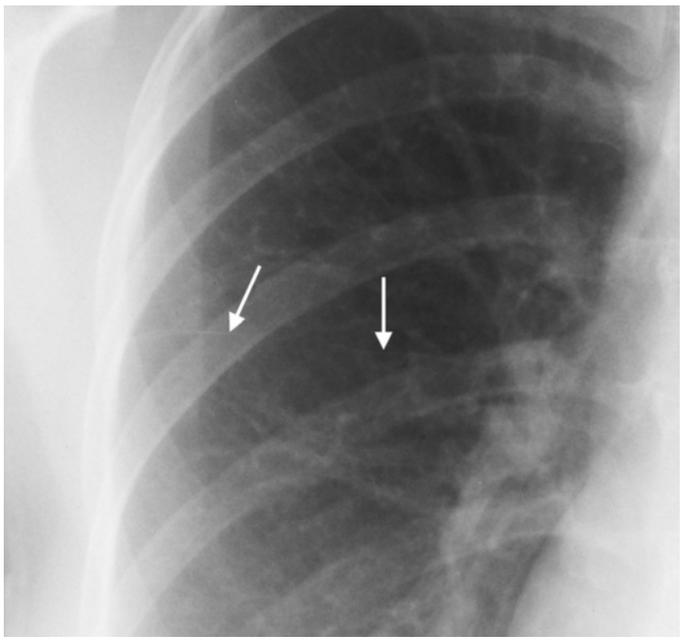

Fig. 6.11 Appearance of the horizontal fissure of the right lung on the posteroanterior radiograph. This 28-year-old woman shows normal findings for her age group. The horizontal fissure appears as a hairline shadow (white arrows).

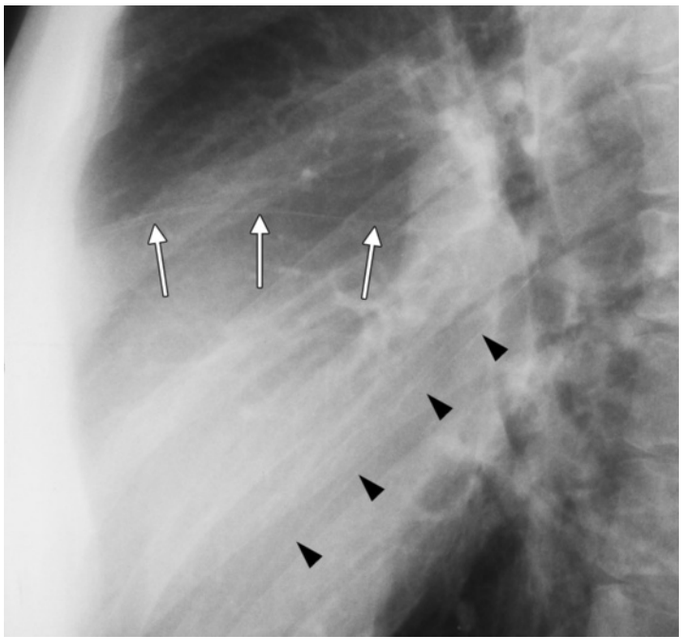

Fig. 6.12 The oblique fissures and horizontal fissure of the right lung on the lateral radiograph. This 32-year-old man shows normal findings for his age group. The oblique fissures (black arrowheads) and horizontal fissure (white arrows) appear as hairline shadows.

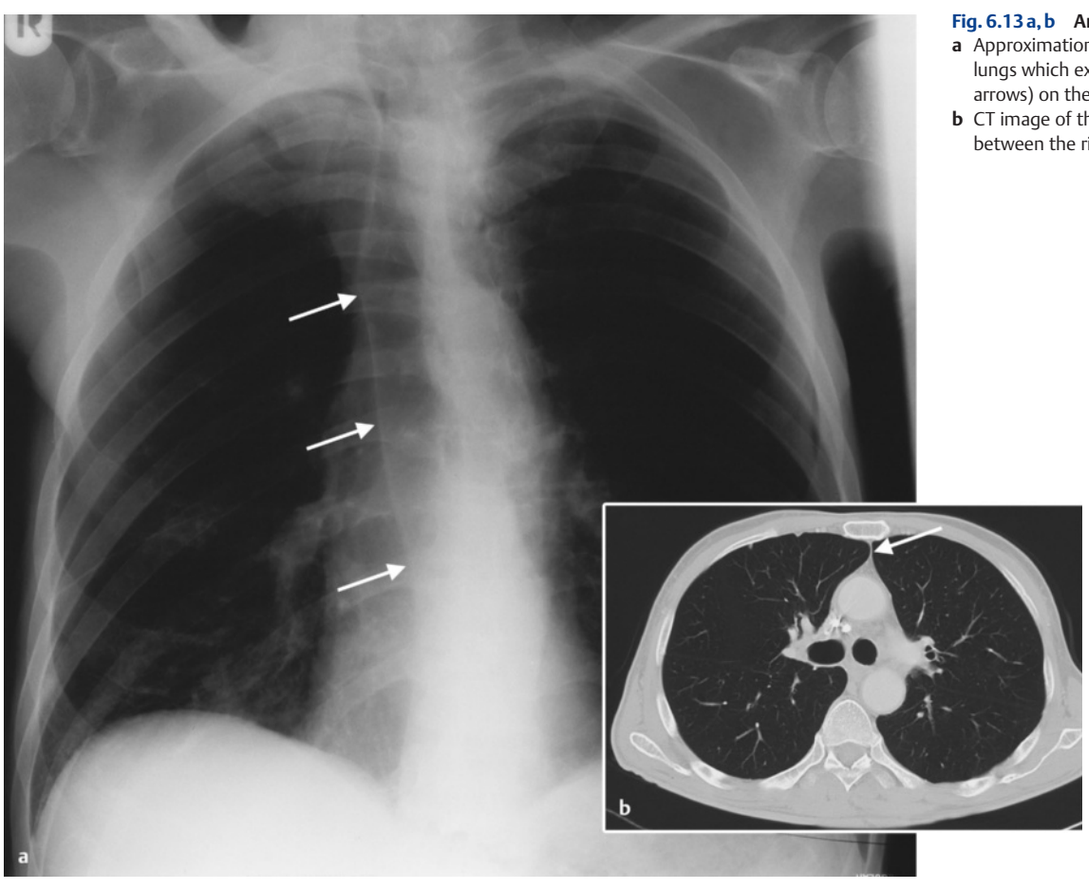

Fig. 6.13 a, b Anterior pleural fold

a Approximation of the pleura of the right and left lungs which extend into the mediastinum (white arrows) on the posteroanterior view.

b CT image of the extended anterior pleural fold between the right and left lungs (white arrow).

Pleural Effusion

The following forms of pleural effusion are distinguished on chest radiographs:

- Effusion in the costophrenic angle
- Interlobar effusion (**Fig. 6.14**)
- Subpulmonary effusion
- Loculated (encysted, encapsulated) effusion

Most often, and in the initial phases of the effusion, pleural fluid is observed in the posterior and lateral costophrenic angle (**Fig. 6.15, Fig. 6.16**).

Radiographic signs of this isolated effusion in the costophrenic angle include:

- Shadow in the costophrenic angle with an ascending lateral tip (meniscus sign)
- Larger effusion characterized by shadowing in the adjacent areas of the lung and vascular engorgement

The detection threshold for pleural fluid in the lateral costophrenic angle on the plain posteroanterior chest radiograph is between 150 and 200 mL. However, volumes up to 500 mL can be concealed behind the diaphragmatic domes. Significant volumes of fluid can be masked even in subpulmonary effusions (see **Fig. 6.4**). Where they occur unilaterally, they can simulate a high-riding diaphragm because the lung "floats" on the effusion and the lateral ascending shadow of the costophrenic angle is absent. The lateral view can demonstrate even volumes of less than 100 mL in the posterior costophrenic angle in a free flowing effusion. In this context, it is significant that the right costophrenic angle can be differentiated from the left one on the lateral view alone (see p. 260).

An interlobar effusion along the horizontal fissure often exhibits a lemon-shaped configuration; along the oblique fissures it tends to produce a spindle-shaped figure (**Fig. 6.17**). The encapsulated shape of the interlobar effusion (**Fig. 6.18**) can occasionally lead one to suspect a mass. However, this misdiagnosis is rare because of the effusion's typical location and shape ("lemon with a streak").

The Golden Lemon Award goes to the radiologist who interprets an interlobar effusion as a pulmonary tumor.

Encapsulated effusions result from pleural adhesions. Differential diagnosis from a pleural tumor is not difficult on CT.

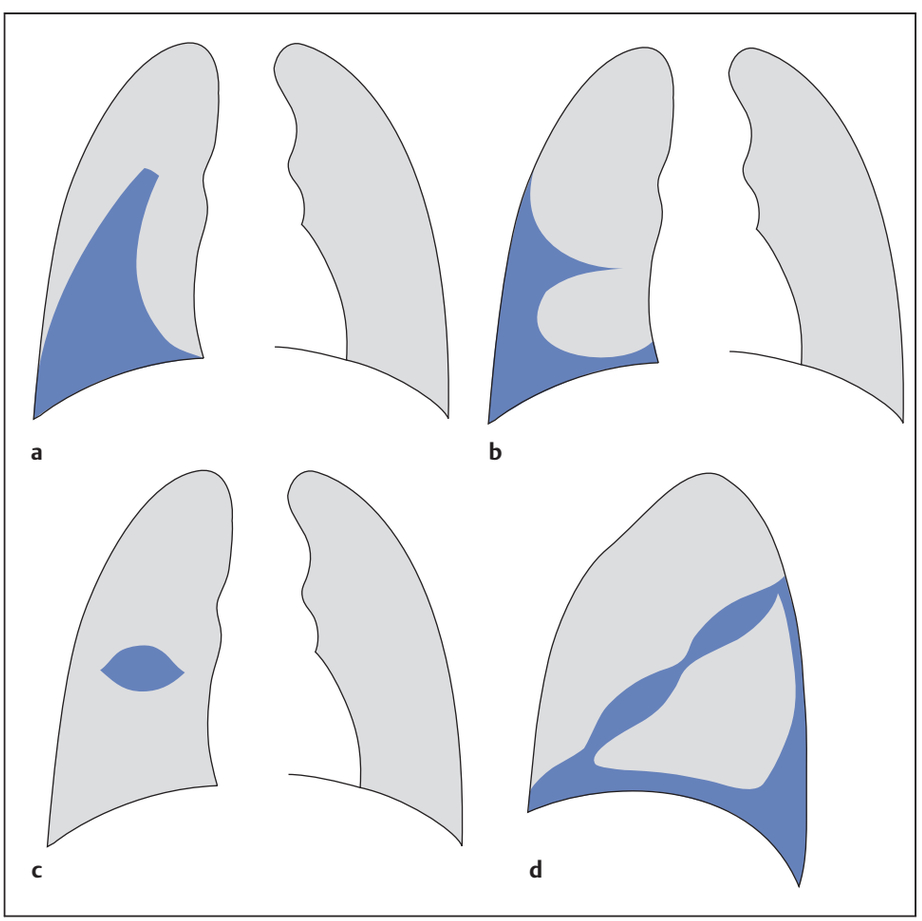

Fig. 6.14 a–d Forms of interlobar effusion.
a Effusion in the costophrenic angle and interlobar effusion in the oblique fissure of the right lung.
b Effusion in the right costophrenic angle and in the horizontal fissure of the right lung.
c Encapsulated interlobar effusion in the horizontal fissure of the right lung.
d Effusion in the costophrenic angle and interlobar effusion in the oblique fissure.

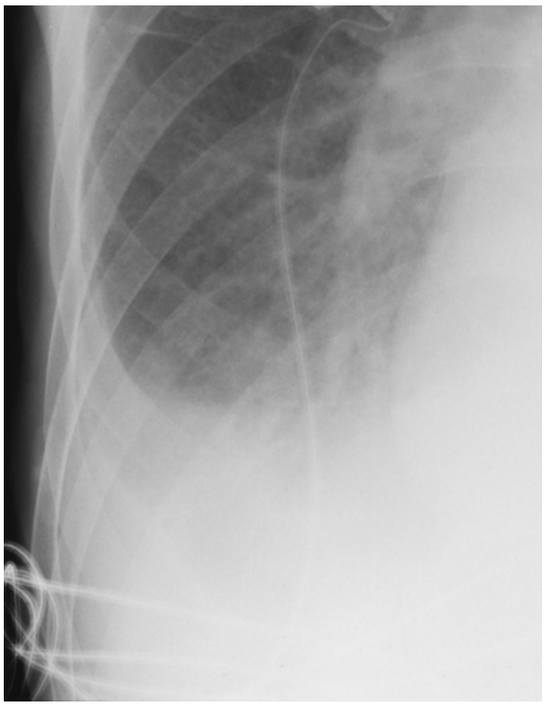

Fig. 6.15 **Meniscus sign.** Classic findings of a lateral ascending effusion in cardiac decompensation and alveolar edema.

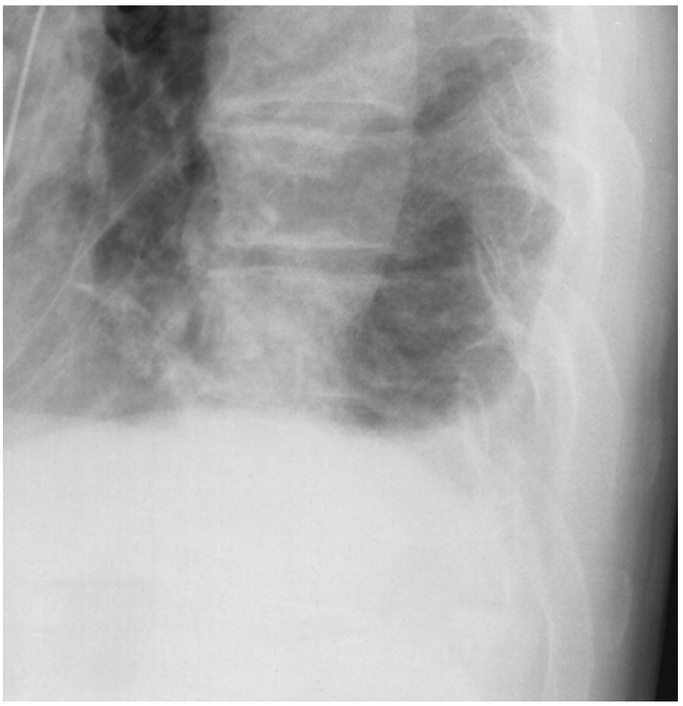

Fig. 6.16 **Effusion in the posterior costophrenic angle.**

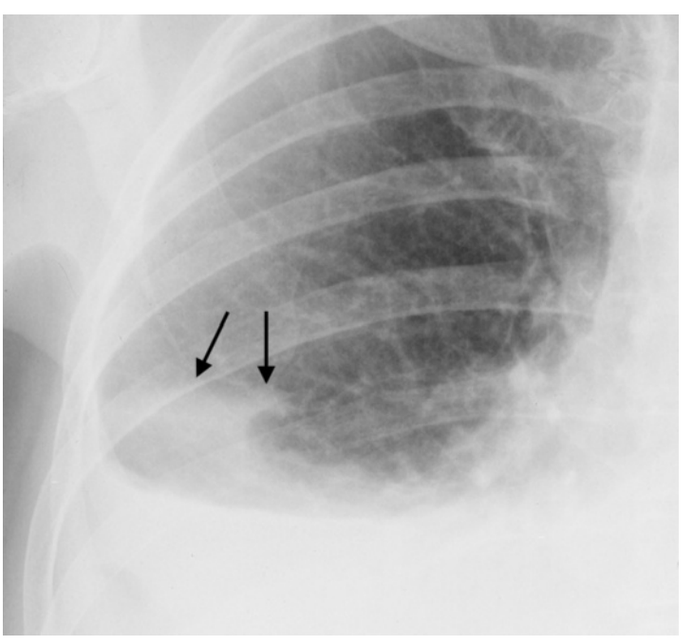

Fig. 6.17 **Interlobar effusion in the oblique fissure.** In addition to a large, partially subpulmonary effusion, a crescentic interlobar excursion of the effusion extends cranially into the oblique fissure of the right lung (black arrows).

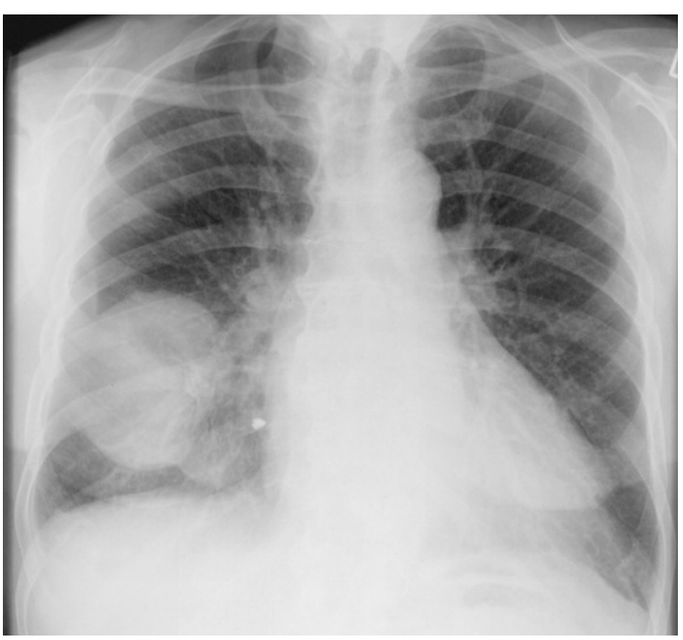

Fig. 6.18 **Interlobar effusion in the horizontal fissure of the right lung.** The effusion exhibits a typical lemon-shaped configuration. Do not confuse this with a pulmonary mass.

Excursus: Costophrenic Angle on the Lateral Film

Pleural effusions concealed in the posterior costophrenic recess and visible only on lateral films and processes lying posterior to the pleura and not visualized on the posteroanterior film occasionally raise the question of which side the pathology involves, right or left. Remarkably, the lateral chest radiograph alone is sufficient in most of these cases to determine whether it is the right or left posterior costophrenic angle and pleura that is involved.

Several diagnostic options are available to identify the side. For the sake of simplicity, all of the following specifications shall apply to the left lateral film:

Option 1: Using the Ribs for Orientation

- Identify the pleura corresponding to the respective ribs: The posterior line of the pleura passes through the apexes of the posterior rib arches (**Fig. 6.19, Fig. 6.21**).
- Answer the question: Are the ribs that belong to the respective pleural line
  - larger and slightly more blurred (far from the film)?
  - smaller and more sharply defined (close to the film)?
- Next, the pleural line identified as the left line (close to the film) or the right line (far from the film) is traced caudally as far as the respective costophrenic angle.

Option 2: Using the Stomach Bubble for Orientation

Where the stomach bubble is identifiable beneath a diaphragmatic crus (**Fig. 6.20, Fig. 6.21**), this crus should be regarded as the left one and traced posteriorly as far as the costophrenic angle.

Option 3: Using the Silhouette Sign between the Heart and Diaphragm for Orientation

The left diaphragmatic crus can only be traced as far as the posterior cardiac margin, the right one as far as the anterior chest wall (**Fig. 6.22**).

Note that all three of these criteria can rarely be evaluated simultaneously. However, one of them is almost invariably present.

The often quoted rule that "the right diaphragmatic crus is higher on the lateral film" is not correct.

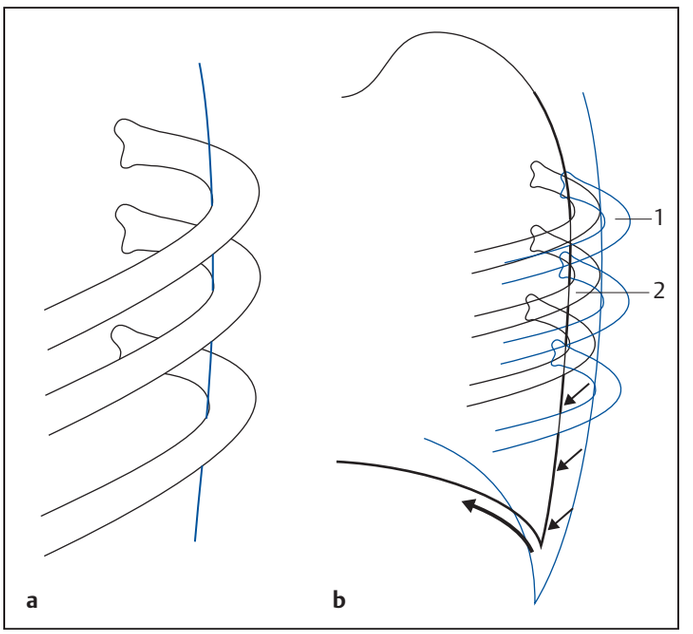

Fig. 6.19 a, b Schematic diagram of how to distinguish the right and left costophrenic angles on the lateral view. Using the ribs for orientation. The pleura passes through the apexes of the posterior rib arches (**a**). The respective ribs are analyzed as close to or far from the film (**b**) and the pleura is then traced caudally as far as the respective costophrenic angle.
1 Blurred, larger = far from the film = right
2 Sharply defined, small = close to the film = left

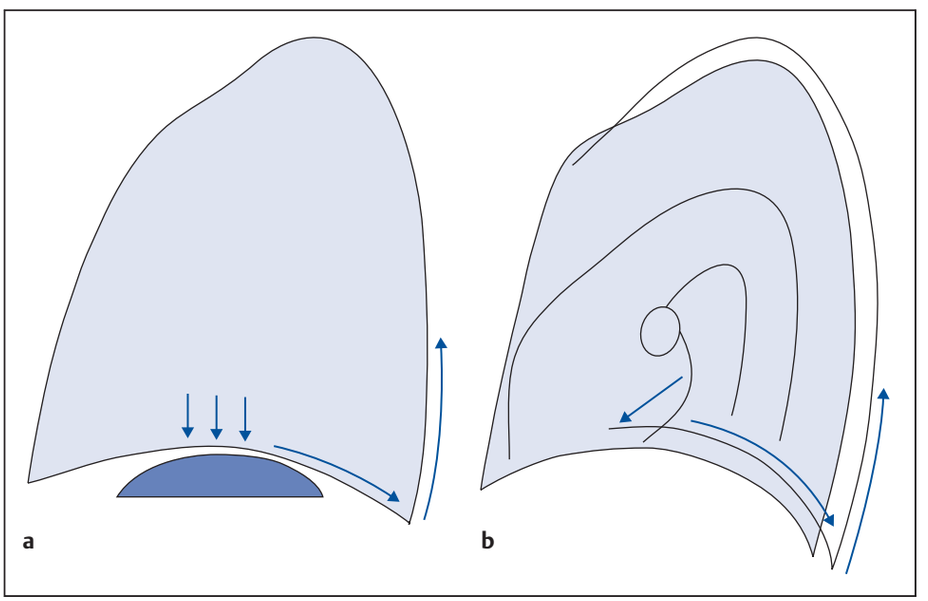

Fig. 6.20 a, b Schematic diagram of how to distinguish the right and left costophrenic angles on the lateral view. Use the diaphragm for orientation. Where the stomach bubble is identifiable beneath a diaphragmatic crus, this crus is considered the left one (**a**). The diaphragmatic crus that can only be traced as far as the cardiac shadow (**b**) is also considered the left one.

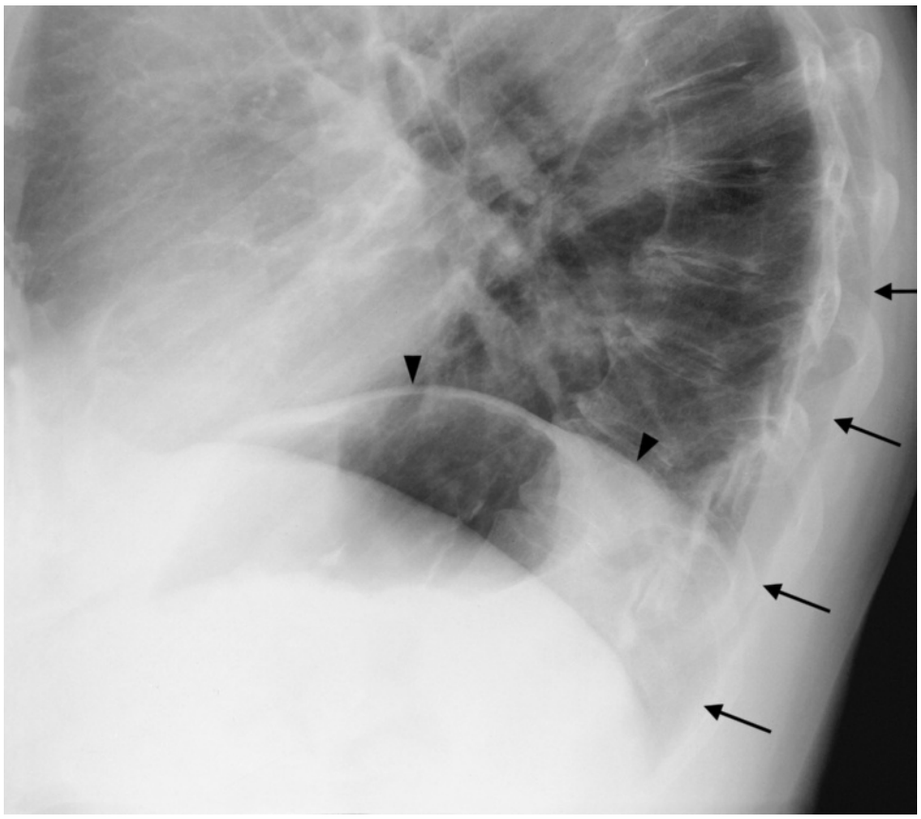

Fig. 6.21 Pleura in relation to the ribs. The pleura passes through the apexes of the posterior rib arches (black arrows) on the lateral radiograph. The pleura can be traced along the respective ribs (here the right ones) as far as the costophrenic angle. The diaphragmatic crus superior to the clearly identifiable stomach bubble is the left one (black arrowheads). This clearly defines the posterior costophrenic angle (patient with senile emphysema and gibbus).

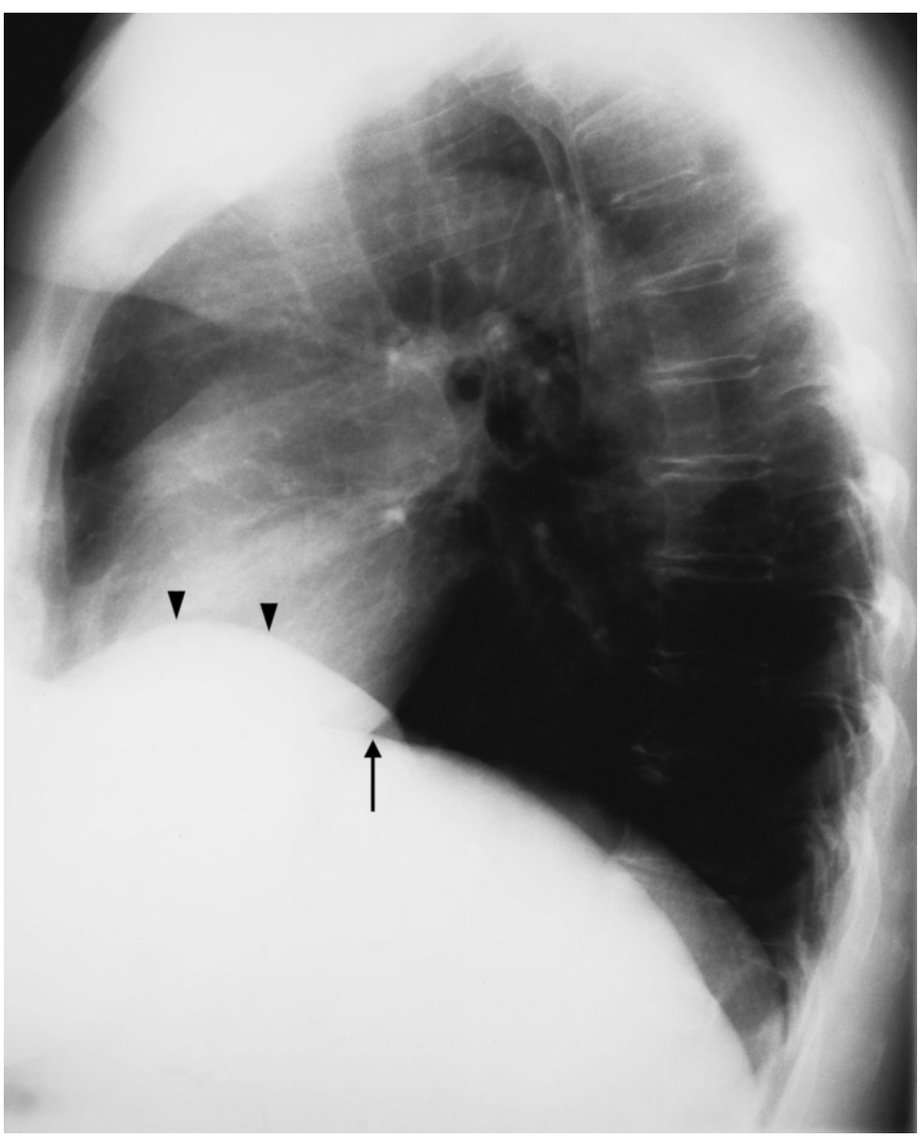

Fig. 6.22 Distinguishing the right and left costophrenic angles using the cardiac silhouette. The left diaphragmatic crus (black arrow) can only be traced as far as the posterior cardiac margin, the right one as far as the anterior chest wall (black arrowheads).

Distinguishing Effusion from Induration

Often it is not easy to distinguish an effusion from induration on the plain chest radiograph. The classic method repeatedly cited in the literature is to rotate the supine patient into the lateral position (**Fig. 6.23, Fig. 6.25**). Today this is rarely done, a major reason being to minimize the patient's exposure to ionizing radiation. Ultrasound is available practically everywhere and the examination can be readily performed with basic equipment. On CT the two can be differentiated directly by measuring density. The posterior shadow exhibits density values of less than 25 HU when caused by effusion. Indurations show higher density values or negative values where fatty components are present.

Distinguishing Effusion from Atelectasis

Effusion is often difficult to distinguish from atelectasis on radiographs obtained in the supine patient. Occasionally supplementary ultrasound or CT studies will be required. Plain chest radiographs can provide information about the cause of total opacification of the hemithorax (**Fig. 6.24, Fig. 6.26**):

- In atelectasis the mediastinum is displaced ipsilaterally toward the shadow.
- In a large pleural effusion it is displaced toward the contralateral side.

However, this simple rule is often hard to apply as hypoventilation and large effusion as a result of a central mass usually occur together. Definitive differentiation between effusion and atelectasis often requires a CT scan (**Fig. 6.26b**).

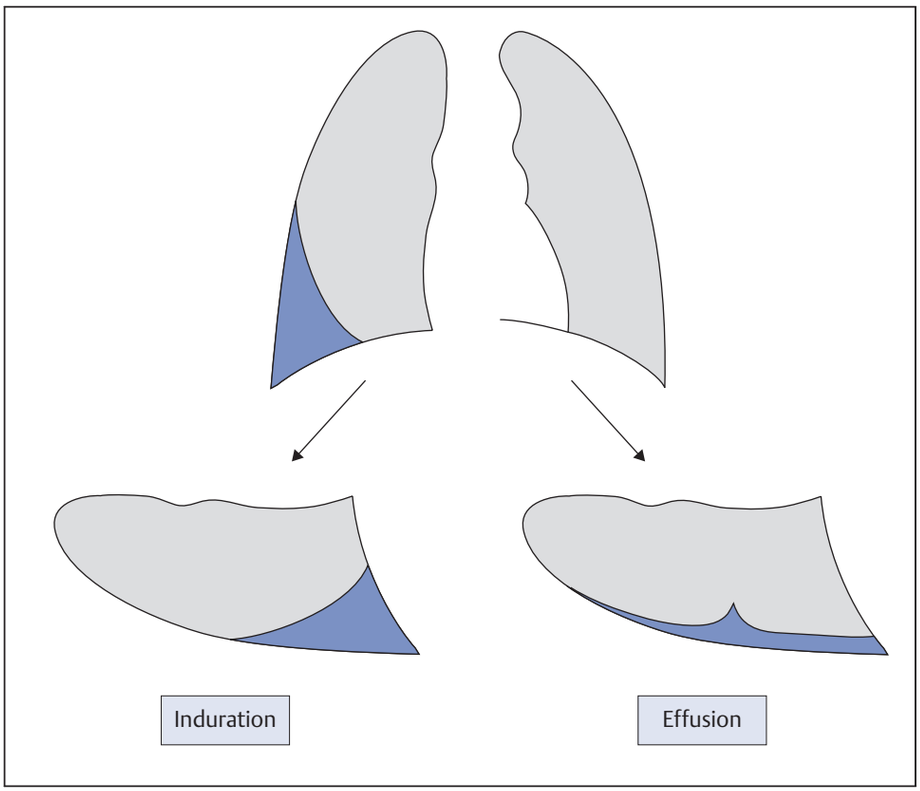

Fig. 6.23 Differentiating effusion from induration on the conventional radiograph. Placing the patient in the lateral position causes an effusion to drain to the lowest point, whereas an induration remains unchanged.

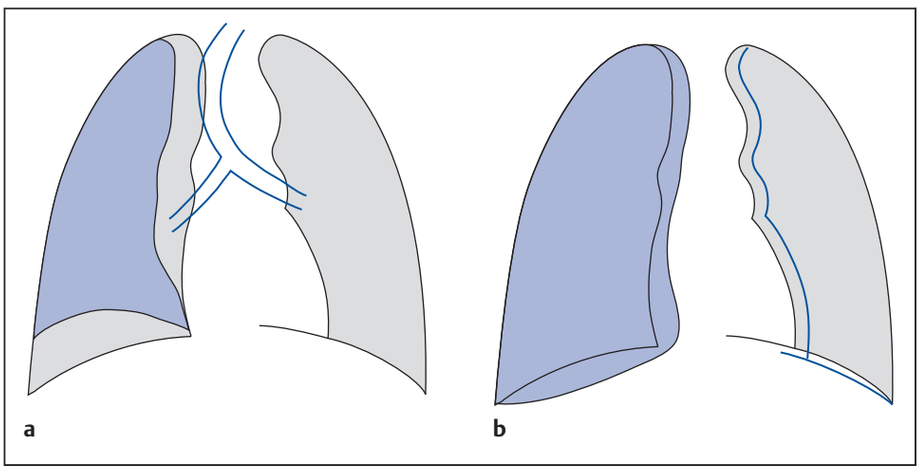

Fig. 6.24 a, b Differentiating effusion from atelectasis on the conventional radiograph. In total opacification of the lung due to atelectasis (**a**) the mediastinum and trachea are shifted ipsilaterally toward the pathologic finding, whereas in total opacification due to a large effusion (**b**) they are displaced contralaterally.

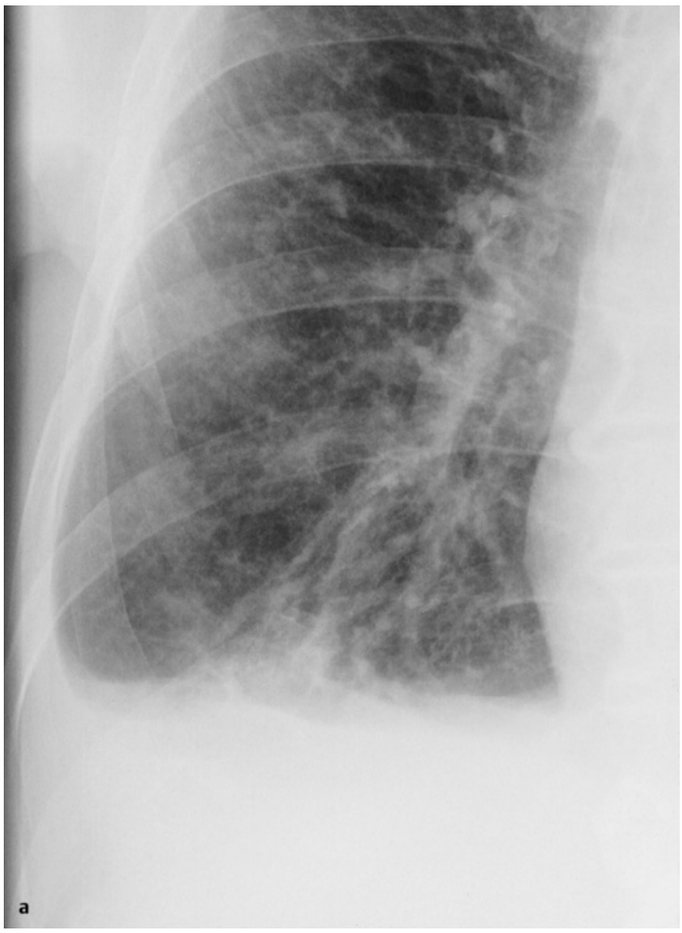

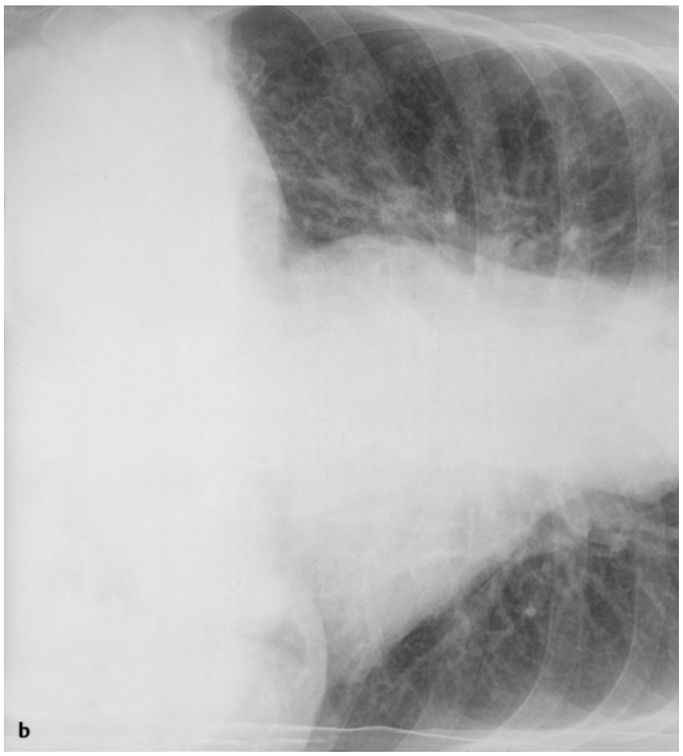

Fig. 6.25 a, b **Differential diagnosis of effusion from induration.** The right diaphragmatic crus cannot be identified on the posteroanterior radiograph (**a**). Placing the patient in the left lateral position (**b**) drains the effusion and the crus becomes clearly identifiable. There is now no silhouette sign, which is consistent with the tentative diagnosis of lower-lobe infiltrate.

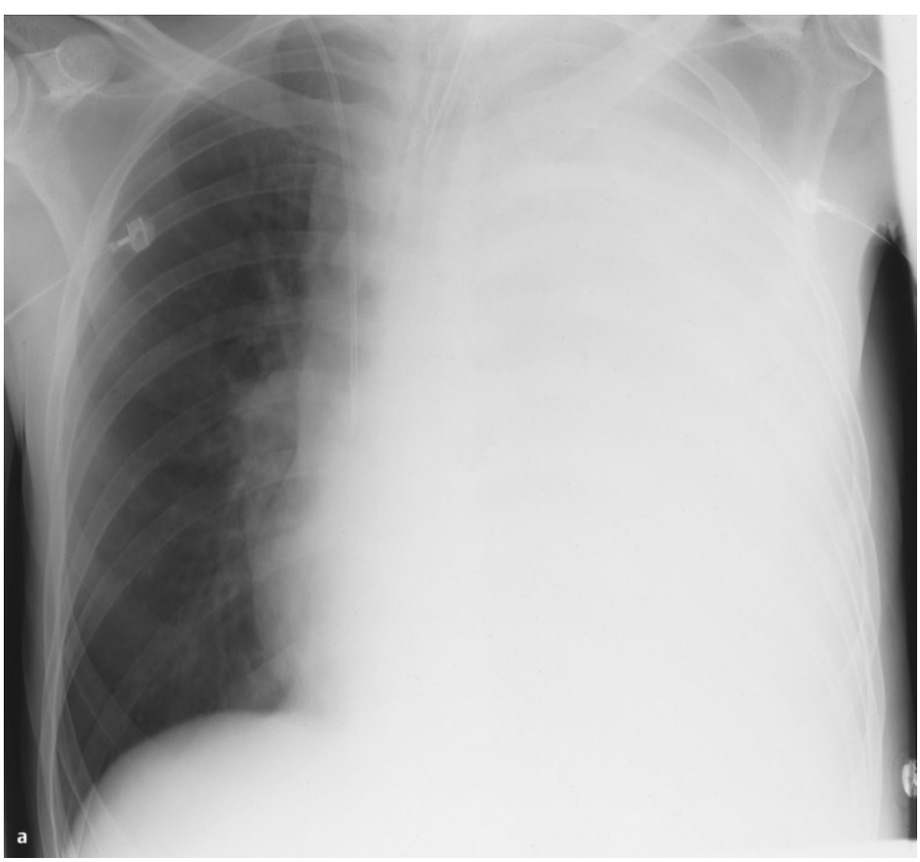

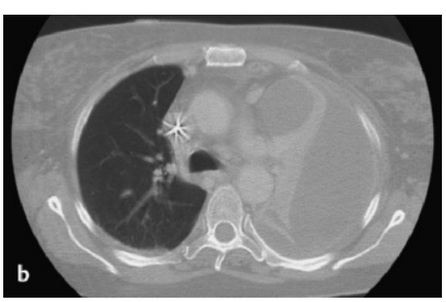

Fig. 6.26 a, b **Total opacification of the lung due to pleural effusion.**
a Massive effusion in the left lung is accompanied by rightward displacement of the mediastinum and compensatory hypervolemia in the right lung.
b CT can differentiate effusion from atelectasis.

Pneumothorax

Air dissecting between the layers of the pleura is referred to as pneumothorax (see "Notes on Pathology"). The ability to recognize pneumothorax is a crucial requirement for the radiologist on duty. Missing this condition is highly embarrassing for most radiologists, although this is of less importance than the actual danger to the patient as a result of a potentially life-threatening tension pneumothorax.

Radiographic signs of pneumothorax

- Direct signs:
  - Visceral pleura is visualized
- Indirect signs:
  - Increase in transradiancy
  - Absence of peripheral markings
  - Mediastinal emphysema

Visualization of the visceral pleura as a fine but dense linear shadow may be regarded as a direct sign of pneumothorax (**Fig. 6.28**). The apical pleura is often more clearly identifiable where indurations are present. This direct radiographic sign is often simulated by lateral skin folds in the supine patient (**Fig. 6.29**). Such folds are often created by more or less forcefully inserting the cassette under a bedridden patient (**Fig. 6.27**). The crucial criterion for distinguishing skin folds from pneumothorax is the absence of any pulmonary markings peripheral to the pleura in the case of pneumothorax (**Fig. 6.28**).

Especially in the supine patient, a slight anterior pneumothorax is not always easily detected. Indirect signs include a unilateral increase in transradiancy and a sharply demarcated mediastinum. Here, a differential diagnosis must exclude primarily unilateral emphysema (**Fig. 6.30**).

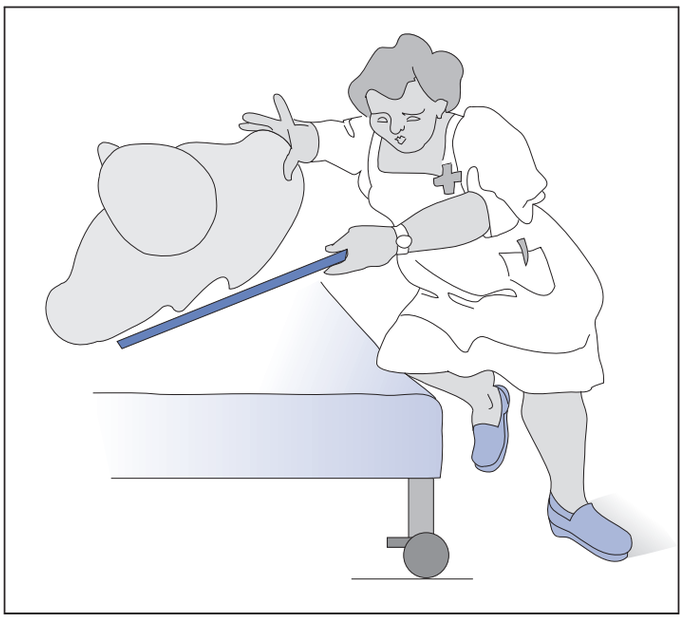

Fig. 6.27 **Why skin folds appear on supine radiographs.**

Notes on Pathology

Air between the layers of the pleura is referred to as pneumothorax (Greek πνεύμά [pneuma] = air, θώράξ [thorax] = breastplate). The lung is able to unfold in part because of a partial vacuum between the layers of the pleura which are separated by a thin film of fluid. Penetration of air into this space leads to the collapse of lung tissue. The following pathophysiologic types are distinguished:

- Open pneumothorax
- Closed pneumothorax
- Pneumothorax with a valve mechanism

Causes of **spontaneous** pneumothorax include:

- Idiopathic occurrence in young, slender persons
- Massive attacks of coughing
- Preexisting bullous pathology (such as paraseptal emphysema)
- Infant respiratory distress syndrome (IRDS)
- *Pneumocystis carinii* pneumonia
- Lymphangioleiomyomatosis
- Metastases

More often the condition results from the following **iatrogenic** and **traumatic** causes:

- Catheter placement
- Diagnostic aspiration of the lung (thoracentesis)
- Penetrating chest trauma
- Rib fractures
- Barotrauma

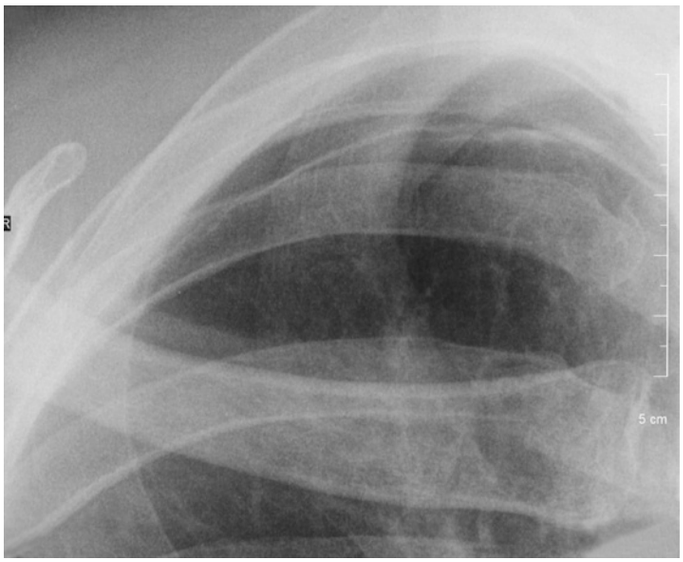

Fig. 6.28 **Line of the pleura in pneumothorax.** The visceral pleura is directly visualized as a fine, very dense linear shadow in pneumothorax in the apical right lung. Lung markings are visible central to the line of the pleura but are completely absent peripherally.

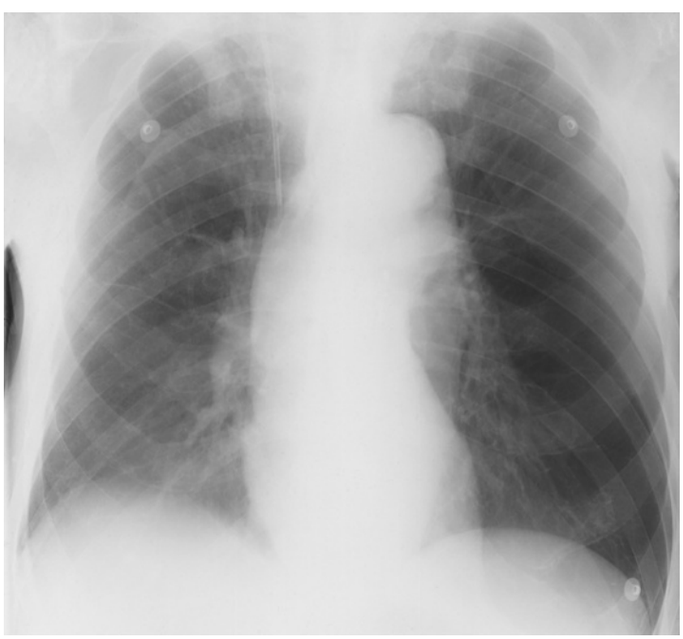

Fig. 6.30 **Differential diagnosis of a unilateral increase in transradiancy as a sign of pneumothorax.** The increase in transradiancy on the left side and the sharply defined cardiac border suggest pneumothorax. However, underlying unilateral pulmonary emphysema is present.

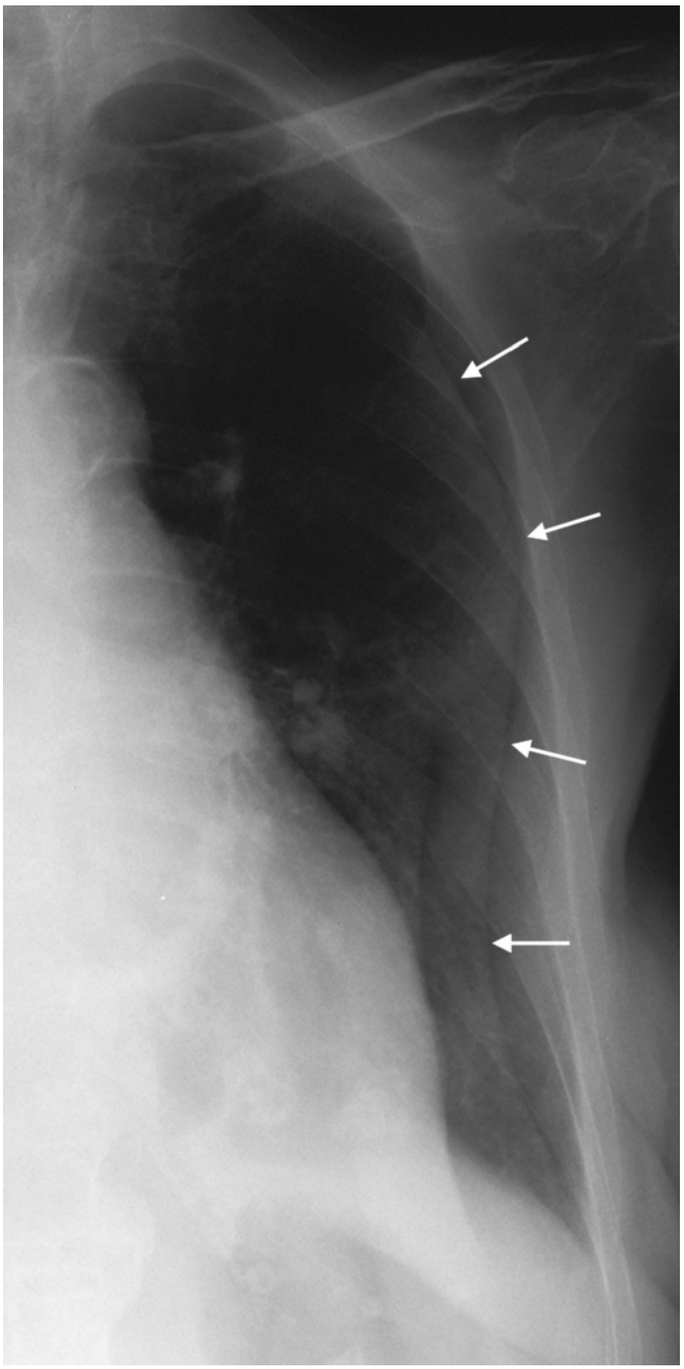

Fig. 6.29 **Findings simulating pneumothorax on a supine radiograph.** The difference in density caused by posterior skin folds creates a "Mach effect" simulating a pleural line (white arrows).

Mediastinal Emphysema

An elevated mediastinal pleura indicative of mediastinal emphysema can also be an indirect sign of pneumothorax. The full picture of mediastinal emphysema is characterized by:

- Streaky increases in transradiancy with a feathered appearance
- Visualization of the tracheal wall as in a double-contrast study
- Sharply defined cardiac border or aorta

Findings of mediastinal emphysema are highly suggestive of the presence of pneumothorax (**Fig. 6.31**). However, mediastinal emphysema can also be observed without pneumothorax in ruptures of the tracheal or bronchial wall (**Fig. 6.34**) or in pneumoperitoneum (**Fig. 6.32**).

Mediastinal emphysema caused by a pneumothorax can lead to pneumoperitoneum (without perforation of abdominal hollow organs; **Fig. 6.32**).

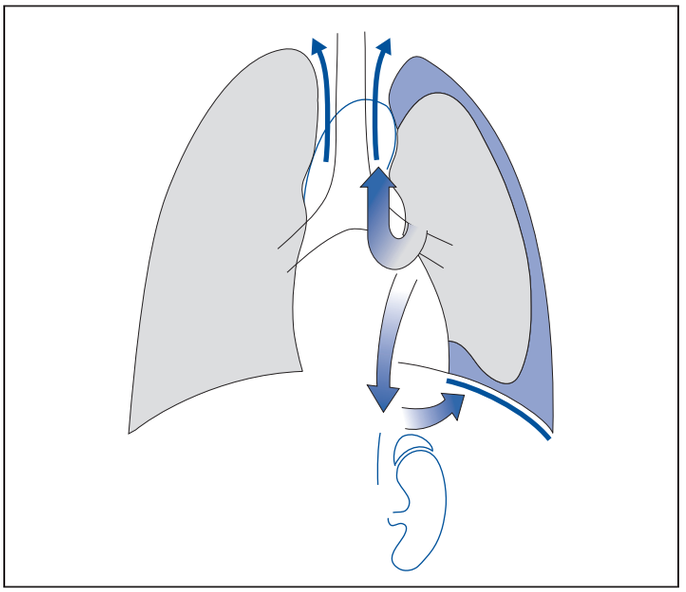

Fig. 6.31 **Relationship between pneumothorax, mediastinal emphysema, and retroperitoneal air.**

Tension Pneumothorax

Presence of a valve mechanism that opens the pleural space on inspiration and closes it on expiration leads to tension pneumothorax (**Fig. 6.33**). This involves:

- A unilateral increase in intrathoracic pressure
- Superior inflow tract congestion
- Entrapment of the inferior vena cava at the diaphragm with right atrial displacement and extensive compression of the affected lung

Radiologic signs of tension pneumothorax (**Fig. 6.35**) include:

- Contralateral mediastinal shift
- Low-riding ipsilateral diaphragm
- Extensive compression of the affected lung

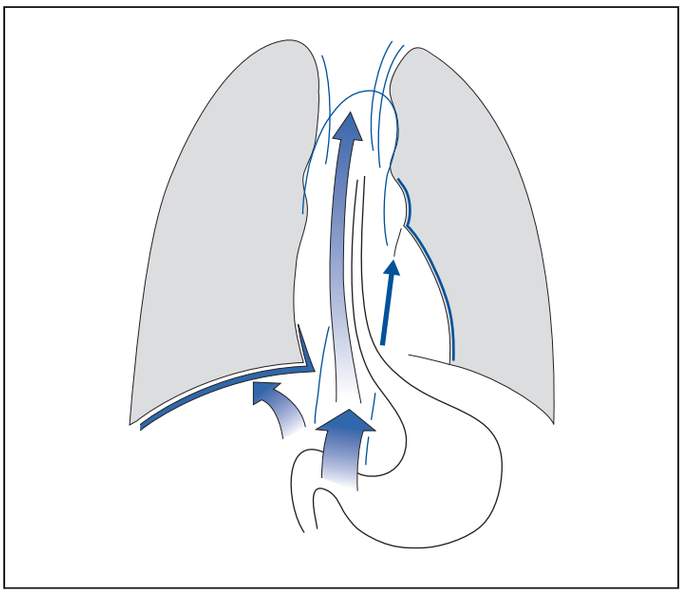

Fig. 6.32 **Relationship between free abdominal air secondary to perforation of a hollow organ and mediastinal emphysema.**

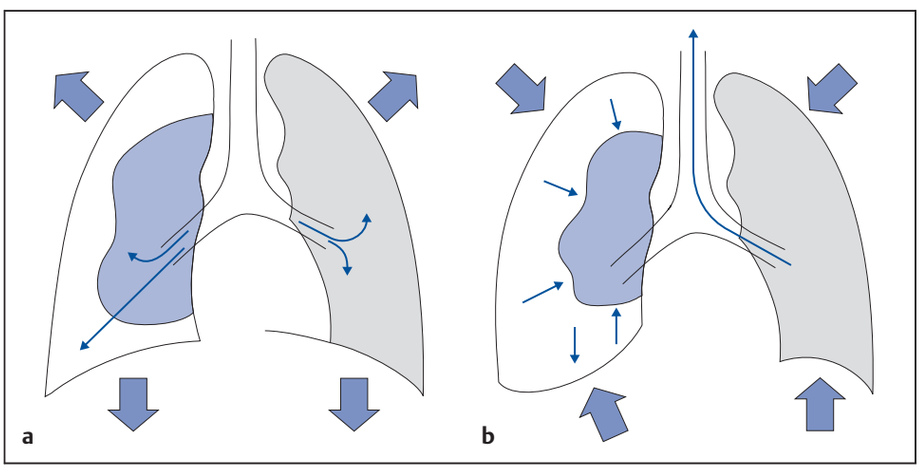

Fig. 6.33 a, b **Pathophysiology of tension pneumothorax.** A valve mechanism in which the pleura opens on inspiration (**a**) and leakage is sealed on expiration (**b**) leads to an increasing accumulation of inspired air and increasing pressure in the pneumothorax.

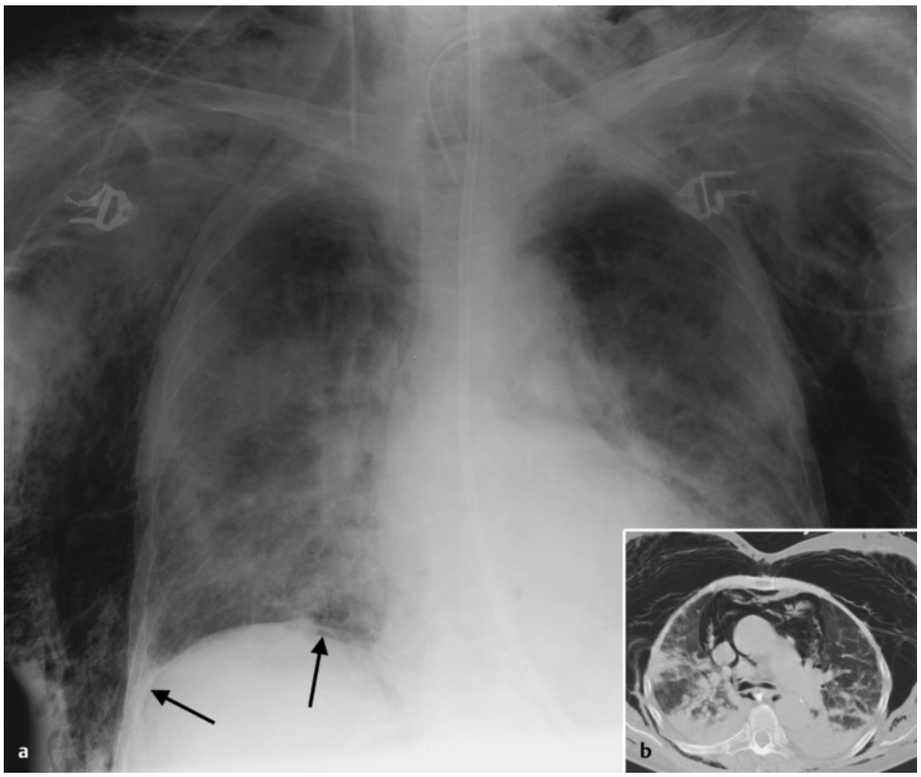

Fig. 6.34 a, b Mediastinal emphysema without pneumothorax.

a Massive skin and mediastinal emphysema and subphrenic free air (black arrows) secondary to tracheostoma. Both lungs are completely unfolded with a predominantly central pulmonary edema and bilateral basal infiltrates.

b CT confirms the lack of pneumothorax; both lungs are fully expanded. Feathered appearance of mediastinal emphysema.

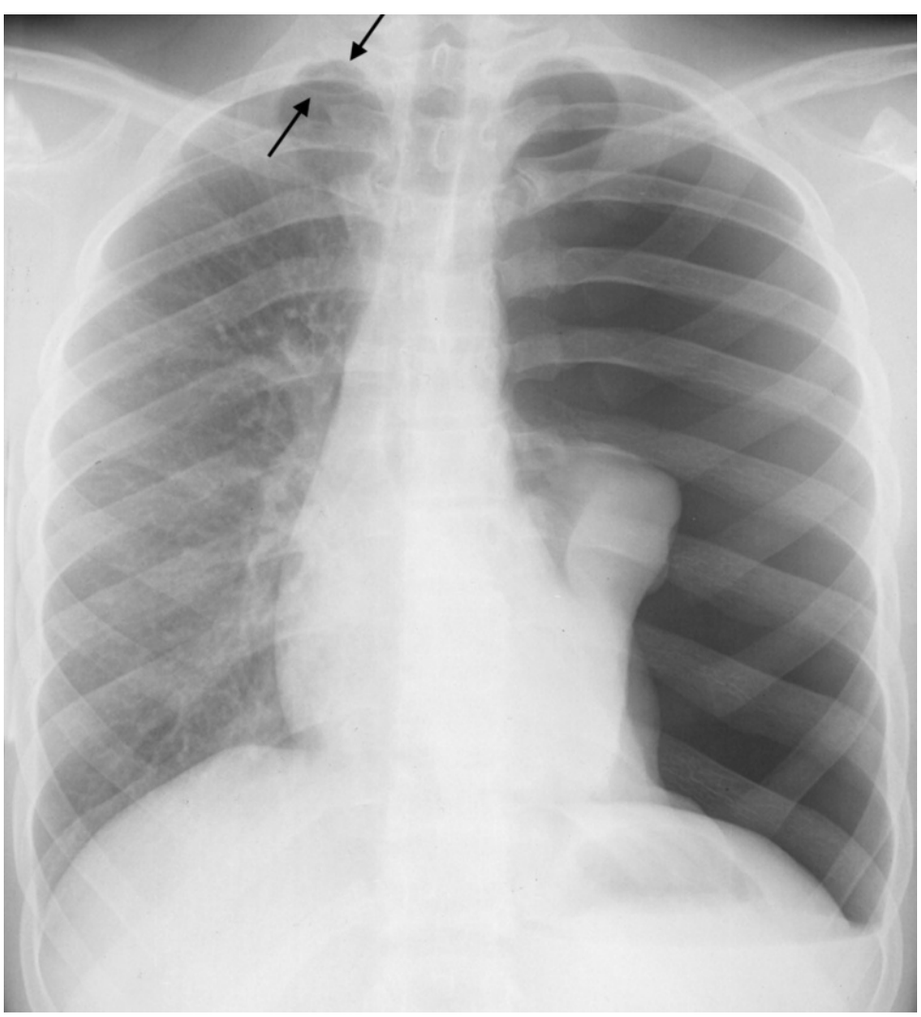

Fig. 6.35 Tension pneumothorax. Total collapse of the left lung, low-riding left diaphragm, and rightward mediastinal shift in tension pneumothorax on the left side. Compensatory hypervolemia in the right lung. Note the right apical bullae (black arrows).

Pleural Masses

Pleural masses occur in many thoracic processes and in the setting of metastatic disease.

Common **causes** include:

- Circumscribed indurations
- Pleural metastases
- Soft-tissue component of expansive osteolytic processes
- Hematoma

Less common causes are:

- Pleural mesothelioma
- Neurofibromatosis
- Fibrous dysplasia
- Coarctation of the aorta

The **Lenk rule** (**Fig. 6.36**) can be used to help differentiate a pleural mass from a peripheral pulmonary mass tangential to the pleura. This rule states that tangentially imaged processes arising from the pleura form an obtuse angle with the chest wall, whereas intrapulmonary processes adjacent to the pleura form an acute angle (**Fig. 6.37, Fig. 6.38**).

Metastases of primary malignant processes in the vicinity of the visceral and parietal pleura are significantly more common than primary pleural malignancies (pleural mesothelioma, see p. 270). A pleural effusion, which regularly occurs simultaneously, often severely compromises the quality of diagnostic information provided by the plain chest radiograph. Findings are then limited to nodular changes detectable at the edge of the effusion. In evaluating such images the radiologist can do little more than express a suspicion. Small pleural lesions can often be difficult to detect even on CT. The visceral pleura then shows irregularities and localized nodules. CT is clearly inferior to ultrasound in detecting masses in the parietal pleura within an effusion (**Fig. 6.39, Fig. 6.40**).

In neurofibromatosis, masses corresponding to schwannomas are observed in the intercostal spaces. These may also be visualized on conventional radiographs. Ectasia of the intercostal arteries occurring in coarctation of the aorta can also lead to misinterpretation of pleural masses. Doppler ultrasound findings of arterial flow murmur or contrast CT are diagnostic.

Robert Lenk (* 1885 Königliche Weinberge, Bohemia, Austria-Hungary, † 1966 Tel Aviv): Student of Guido Holzknecht, Vienna; emigrated in 1938 following the German annexation of Austria; professor of radiology in Tel Aviv; named honorary member of the German Radiography Society in 1961.

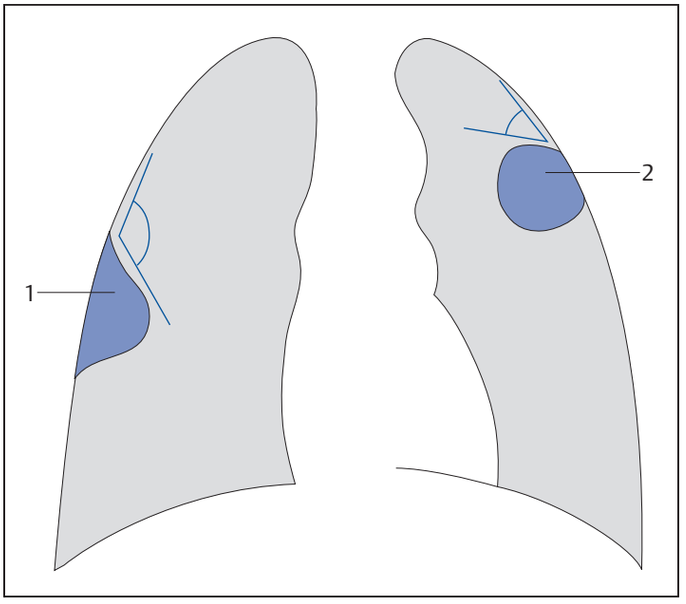

Fig. 6.36 Lenk rule. Pleural masses (1) form an obtuse angle with the adjacent pleura, pulmonary masses that infiltrate the pleura (2) form an acute angle with the adjacent pleura.

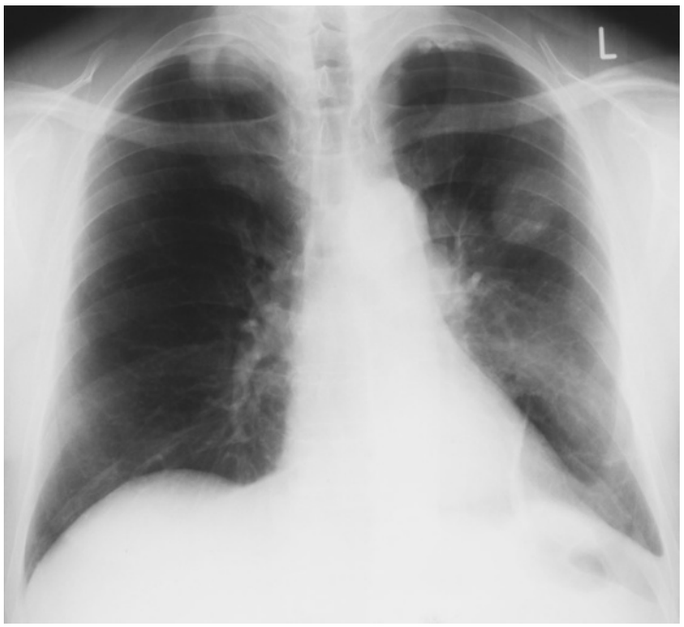

Fig. 6.37 **Pulmonary focal lesions with pleural contact.** Peripheral focal lesion in the right lung apex measuring 4.5 cm in diameter with broad pleural contact. An acute angle remains between the adjacent pleura and the focal lesion. Other focal lesions are present in the left middle and lower lung fields, some of them confluent. Apical pleural thickening and pleuropericardial thickening in the left lung.

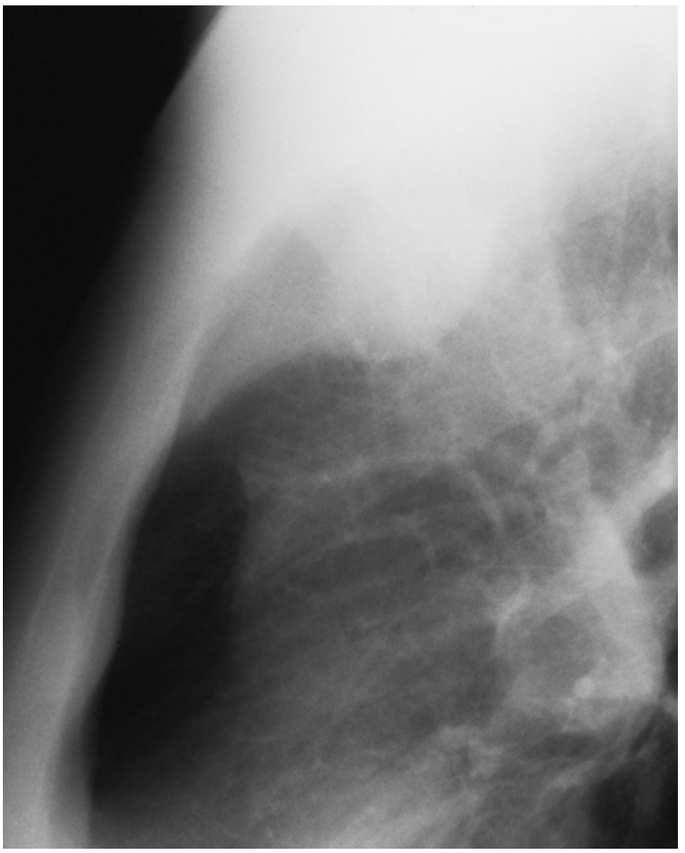

Fig. 6.38 **Pleural mass.** Retrosternal pleural mass 5 cm in diameter forming an obtuse angle with the adjacent pleura.

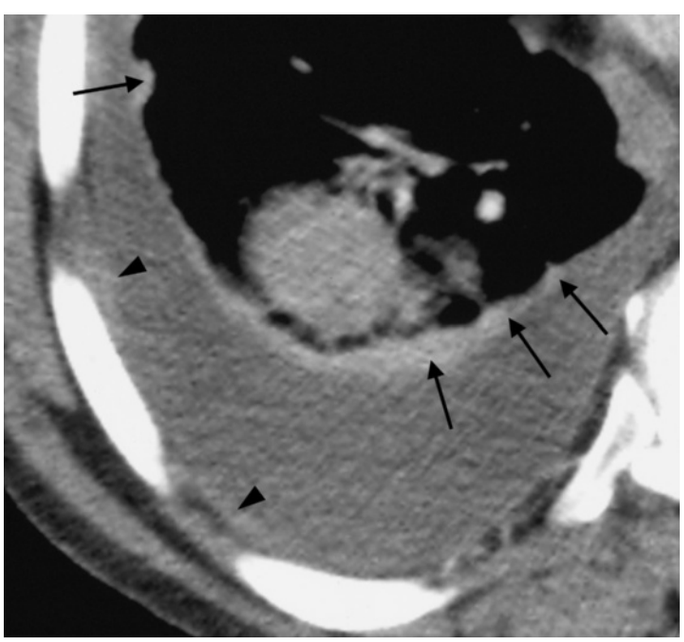

Fig. 6.39 **Pleural effusion on the right side in pleural metastatic disease.** CT shows a clearly nodular visceral pleura (black arrows) and faint thickening of the parietal pleura (black arrowheads).

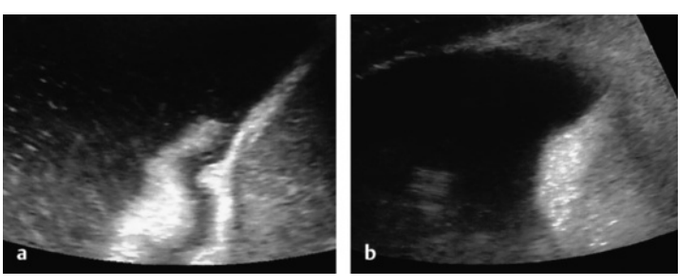

Fig. 6.40 a, b **Recurrent malignant pleural effusion secondary to breast carcinoma.**

a Diffuse hyperechoic pleural thickening with a circumscribed focal lesion is seen in the intercostal plane above the left thoracic outlet. Partial atelectasis of the left lower lobe is visible in the effusion.

b A diffuse plaquelike pleural mass is seen farther posteriorly.

Pleural Mesothelioma

Pleural mesothelioma is a primary malignant neoplasm arising from pleural tissue. It has a very poor prognosis, with a mean survival time of less than one year. Asbestos exposure is the crucial etiologic factor in the disease. For this reason, asbestos-associated pleural mesothelioma has been recognized as an occupational disease (German occupational disease 4105).

The radiographic signs of pleural mesothelioma (**Fig. 6.41**) reflect the pathologic circumstances of the disorder but on the whole are not very specific (see "Notes on Epidemiology and Pathology"). Findings on the **plain chest radiograph** include:

- Unilateral pleural effusion refractory to treatment and showing no signs of congestion
- Circumscribed pleural thickening (**Fig. 6.42**)
- Garlandlike pleural thickening
- Thickening of the oblique and horizontal fissures
- Unilateral reduction in lung volume
- Tethering of the lung (on fluoroscopy)
- Calcified pleural plaques may also be present
- Possible presence of rib destruction (**Fig. 6.42 b**)

CT can detect the circumscribed thickening of the parietal pleura and possible invasion of the chest wall earlier (**Fig. 6.43**). Findings normally include:

- Pleural effusion, possibly hemorrhagic
- Nodular pleural thickening
- Initially discontinuous, later coalescing to form a continuous plate
- Infiltration of the chest wall, diaphragm, pericardium
- Infiltration of the periphery of the lung
- Bone destruction

Notes on Epidemiology and Pathology

The current incidence of pleural mesothelioma is 1.1 per 100 000 persons. Because of the widespread prohibition of the use of asbestos fibers, a gradual decrease in the number of cases is to be expected over the next decades. Germany's central mesothelioma register in Bochum processed 168 cases in 1988, whereas 780 were reported in 2004. Incidence data (1973–1992) from the Surveillance, Epidemiology and End Results Program (SEER) in the USA suggested a peak in the annual number of mesothelioma cases for males at 2300 before the year 2000. The average age is 63 years. In patients younger than 50, another cause such as virus induction or nonoccupational asbestos exposure should be suspected.

Pleural mesothelioma arises from the mesothelial cells of the parietal pleura. Epithelial, sarcomatous, and mixed histologic subtypes are differentiated. The epithelial subtype is associated with more severe and often hemorrhagic effusion and appears to have a more favorable prognosis. In the further course of the disorder, the mesothelioma grows along the chest wall and encases the lung with a tumorous plate several centimeters thick. Invasion of the superficial pulmonary parenchyma can lead to fusion of the layers of the pleura with a retrograde effusion.

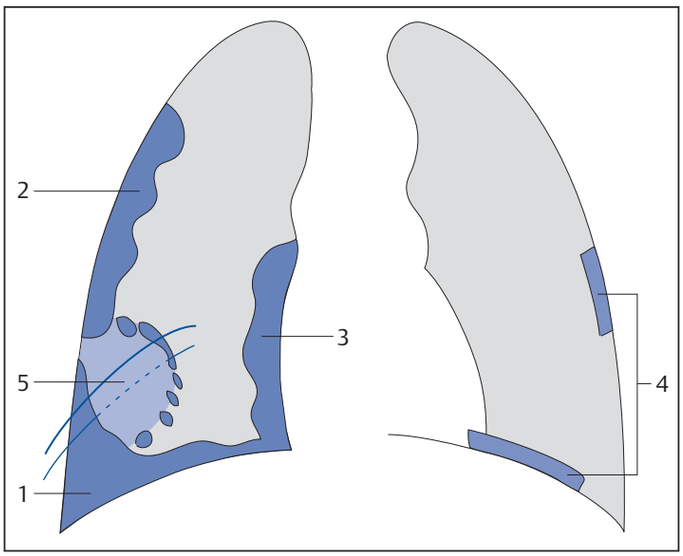

Fig. 6.41 Schematic diagram of radiographic signs of pleural mesothelioma.
1 Effusion
2 Garlandlike pleural thickening (tumor and partially encapsulated components of effusion)
3 Thickening of the mediastinal pleura
4 Calcified pleural plaques (sign of underlying asbestos exposure)
5 Bone destruction

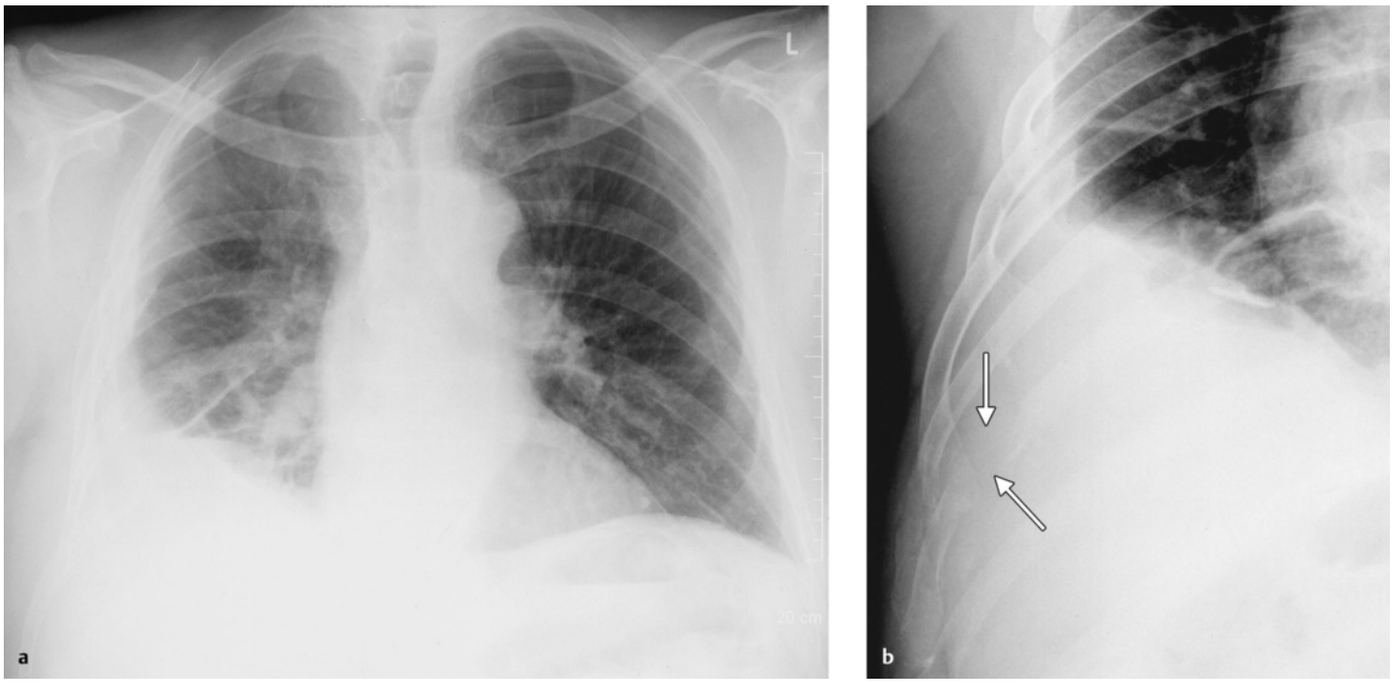

Fig. 6.42 a, b **Effusion in the costophrenic angle in pleural mesothelioma.**

a A meniscus shadow obscures the right costophrenic angle. Other findings include circumscribed pleural thickening. Significant hypoventilation of the right lower lobe is seen along with platelike dystelectasis and consolidation along the horizontal fissure of the right lung.

b The spot view shows circumscribed destruction of the lateral portion of the 9th rib (white arrows).

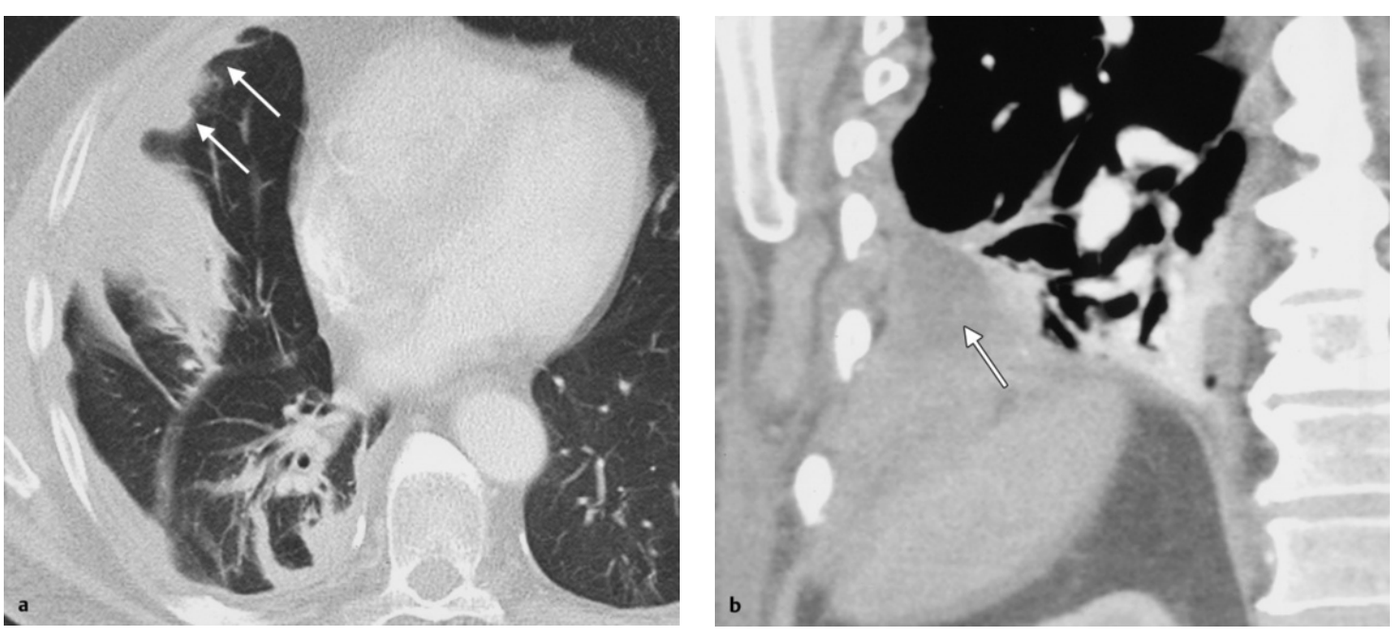

Fig. 6.43 a, b **Pleural mesothelioma with infiltration of the chest wall.**

a CT findings. The axial slice shows the typical garlandlike pleural thickening (white arrows) in addition to a larger supradiaphragmatic mass on the right side.

b The coronal reconstruction shows an extensive tumor isodense to soft tissue in addition to a slight, hypodense effusion (white arrow) within the shadow. The intercostal musculature and diaphragm can no longer be identified.

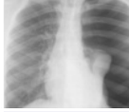

Review Case 1

The patient is a 93-year-old man with known cardiomyopathy. He was admitted to the hospital with dyspnea and chest pain. The supine chest radiograph (Fig. 6.44) was ordered by the emergency room physician to make the differential diagnosis between cardiac decompensation and pneumonic infiltrate.

Question 1

How do you evaluate the cardiac situation?
(Previously discussed in Chapter 1.)

Question 2

Are pneumonic infiltrates present?
(Previously discussed in Chapter 3.)

Question 3

Is a right-sided pneumothorax present?
(This chapter.)

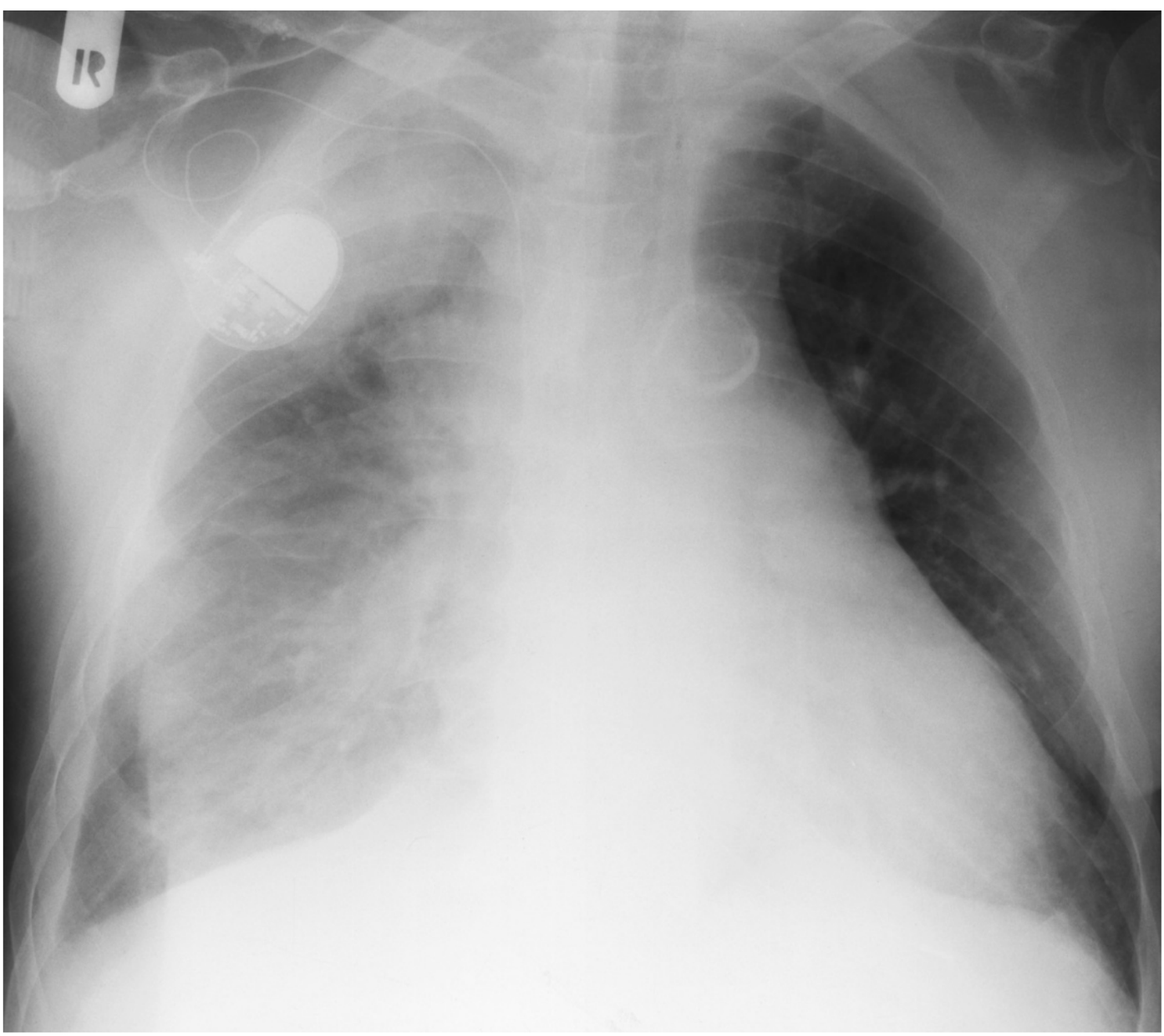

Fig. 6.44 Supine chest radiograph of a 93-year-old man with a long history of coronary heart disease and heart failure, now presenting with dyspnea.

Answer

Answer to question 1 (Fig. 6.45): The left heart is enlarged. Although the patient is rotated into the left anterior oblique (LAO) position, the long axis of the heart is still longer than the width of the hemithorax. Despite the right-sided effusion there is no decompensation. There are neither Kerley lines in the well visualized portions of the left lung, nor signs of redistribution.

Answer to question 2: There are several areas of shadowing in the right lung:

- In the central and peripheral upper lung field (most likely a tumor) (black arrows and black arrowheads)
- In the middle lobe (the right cardiac border cannot be identified)
- In the posterior basal segment of the right lower lobe (silhouette sign involving the farthest medial portion of the right diaphragmatic crus)

Answer to question 3: Right-sided pleural effusion but no pneumothorax. However, a linear medial shadow caused by a skin fold can cause confusion. Measuring up to 4 cm, this shadow (white arrows) courses caudally well past the border of the diaphragm.

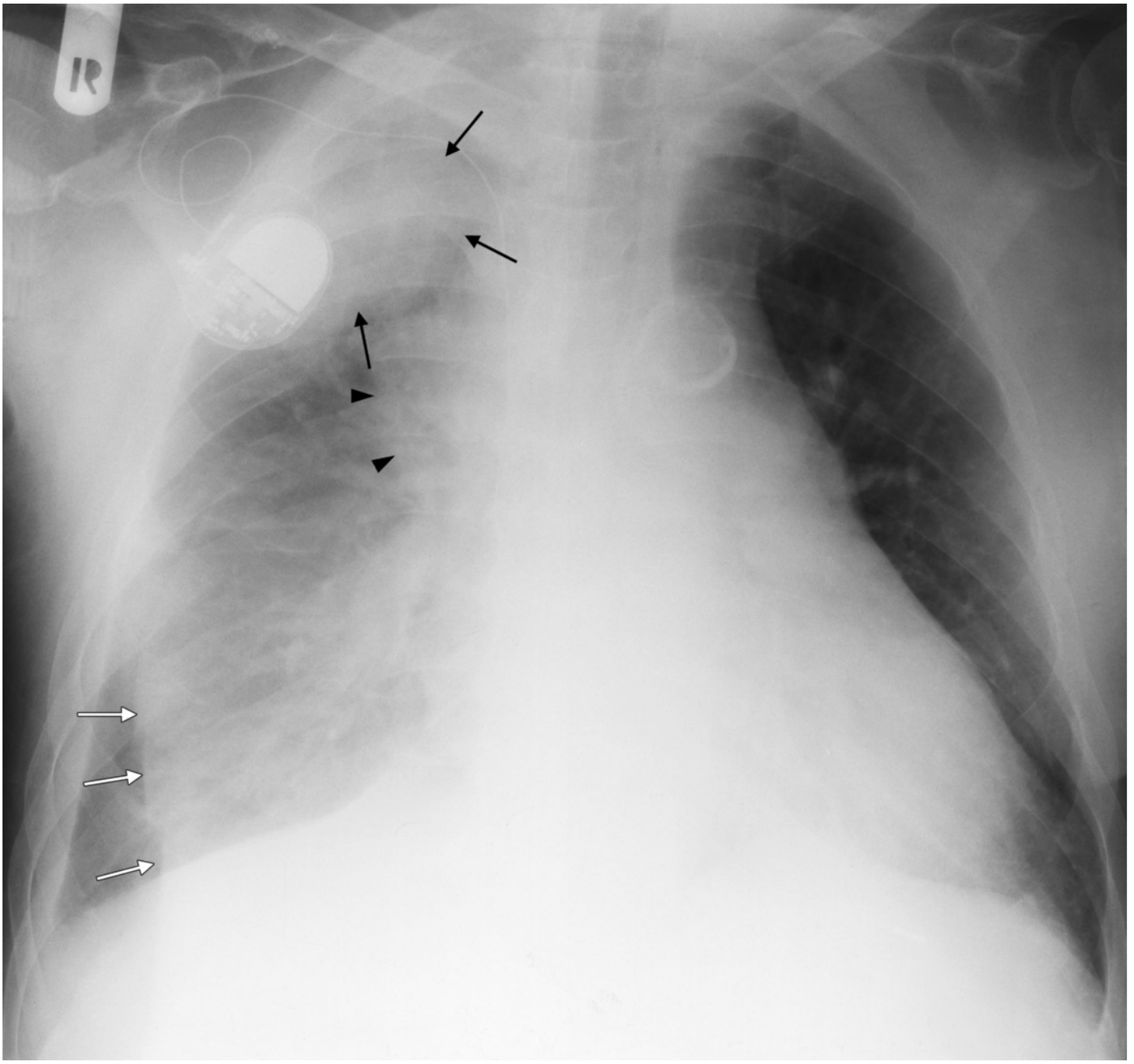

Fig. 6.45 The image in Fig. 6.44 with markings added. There is a mass in the right upper lobe (black arrows) measuring 8 cm in diameter and partially masked by the pacemaker. Findings also include massive involvement of the right hilum (black arrowheads) with poststenotic bronchopneumonia in the middle and right lower lobes and associated effusion on the right side.

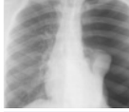

Review Case 2

The patient is a 62-year-old man with a right hypernephroma (Fig. 6.46).
Symptoms now include postoperative dyspnea secondary to right nephrectomy.

Question 1

Is cardiac decompensation present?
(Previously discussed in Chapter 1.)

Question 2

How do you evaluate the shadows in the right lung?
(Previously discussed in Chapter 4.)

Question 3

Why do you immediately inform the physician on duty in the intensive care unit? (This chapter.)

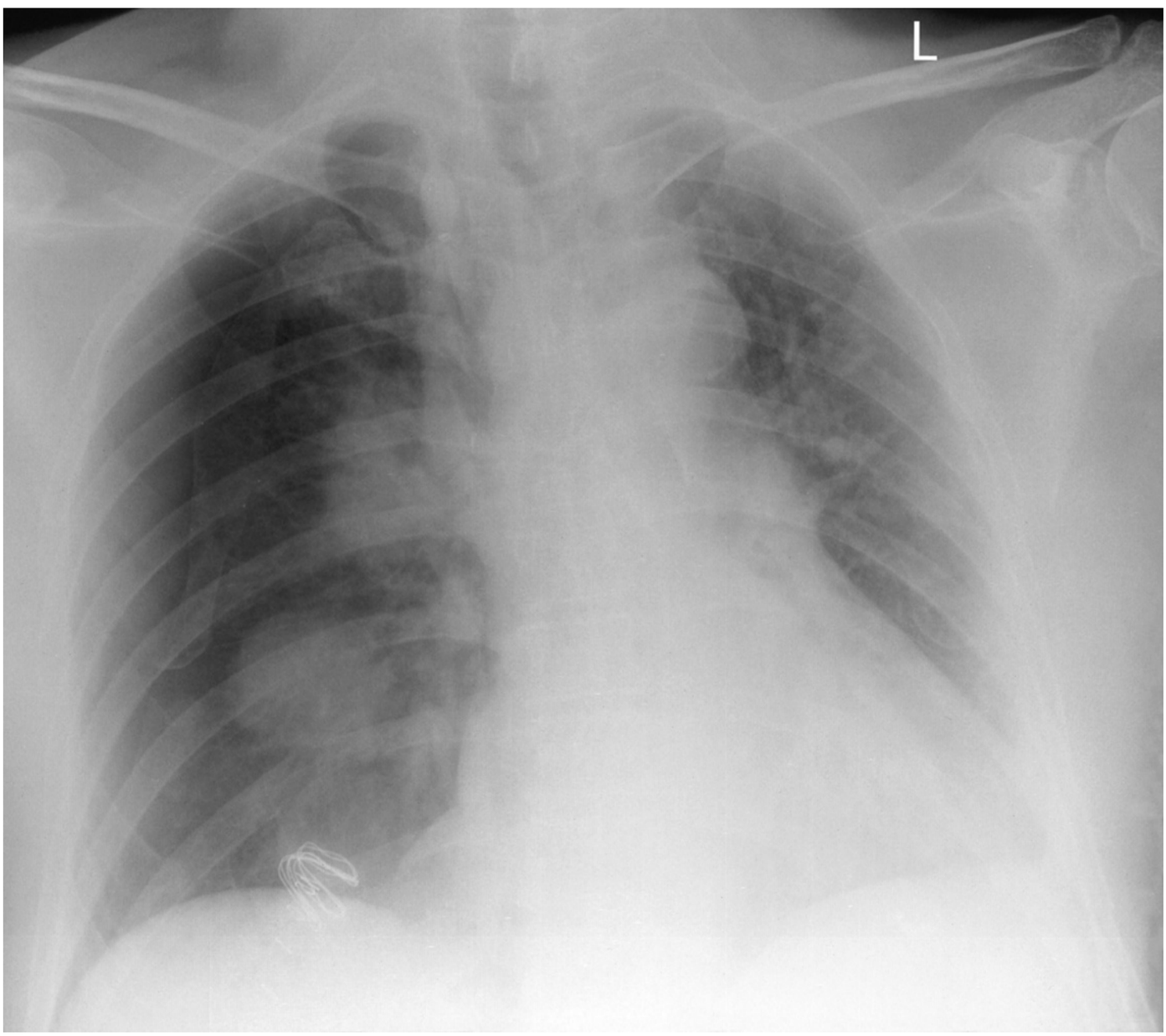

Fig. 6.46 Postoperative supine chest radiograph following right nephrectomy for tumor.

Answer

Answer to question 1 (Fig. 6.47): Although the chest is slightly obliquely positioned there is no gross decentering. The left heart appears enlarged (the long axis of the heart is longer than the width of the left hemithorax). The calcified elongated aorta exhibits a hypertensive configuration. The left lung shows compensatory hyperemia in response to the collapse of the right lung. However, there are no signs of edema (no Kerley lines or peribronchial cuffing). There is an effusion in the left costophrenic angle.

Answer to question 2: Other findings include a peripheral tumor 5 cm in diameter (black arrows) and an additional central mass (white arrows) in the collapsed right lung. The initial impression is one of a peripheral bronchial carcinoma with ipsilateral lymph node metastasis. However, closer examination reveals that the leftward shifted hilum does not lie in the center of what appears to be a central mass. This means there are probably two intrapulmonary lesions. The most likely explanation is that these are pulmonary metastases of the known hypernephroma.

Answer to question 3: There is a clearly defined pleural line in the right hemithorax (black arrowheads). The leftward shift in the trachea and heart and the low-riding right diaphragmatic crus are signs of a tension pneumothorax (**Fig. 6.47**).

Incidental finding: Left clavicular fracture.

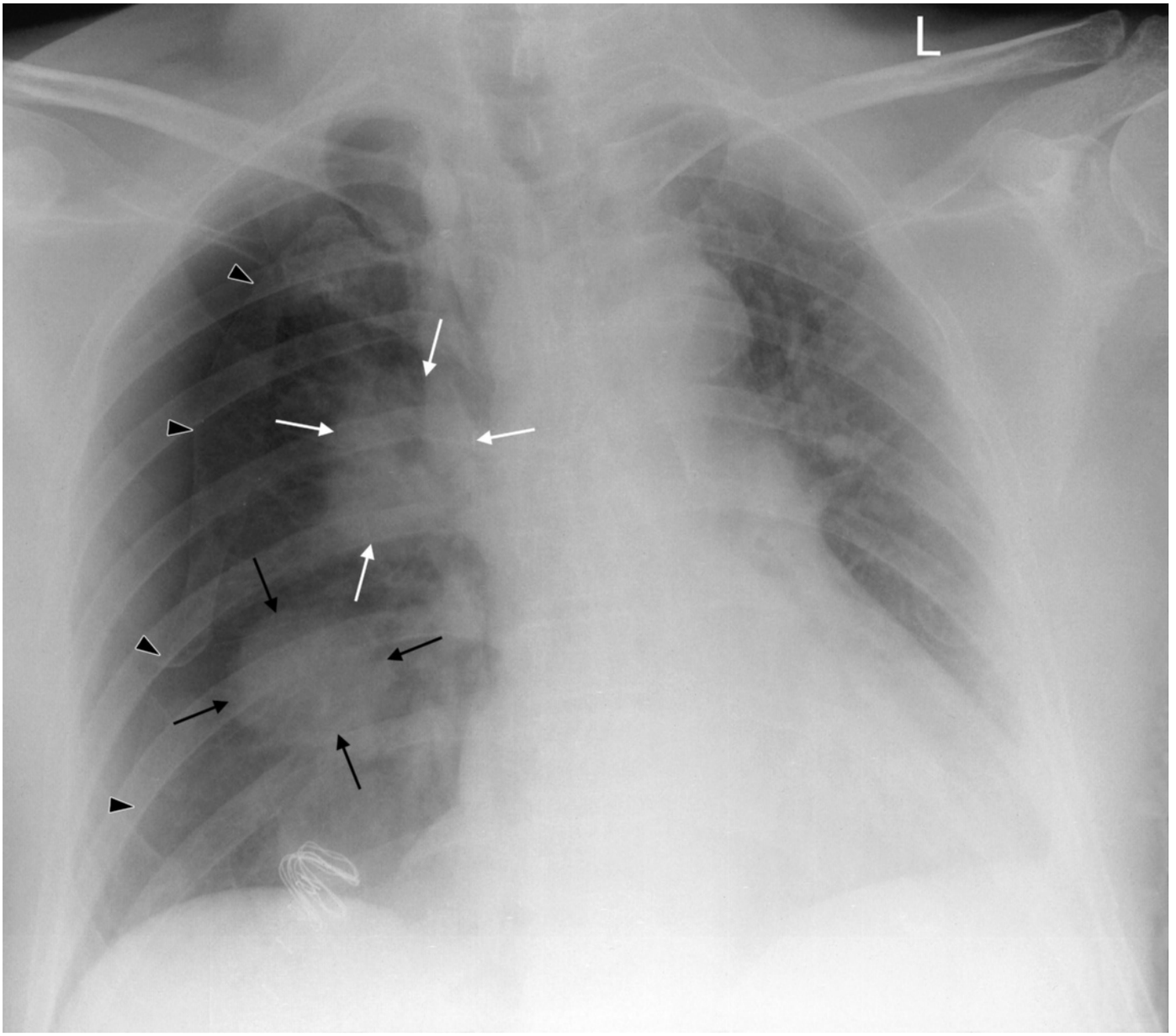

Fig. 6.47 Right-sided tension pneumothorax with contralateral mediastinal shift and contralateral compensatory hyperemia. Pulmonary metastases of a hypernephroma.

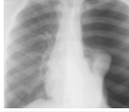

Review Case 3

The patient is a 66-year-old man with a history of many years of chronic bronchitis and a gastric carcinoma one year previously (Fig. 6.48). The patient suffered a "flulike infection" with severe pain in the left chest about 3 weeks previously. He now produces persistent purulent expectorate and has subfebrile temperatures.

Question 1

What changes suggest chronic bronchitis as documented in the history? (Previously discussed in Chapter 2.)

Question 2

How do you evaluate the findings in the left lower lung field? (Previously discussed in Chapter 3 and in this chapter.)

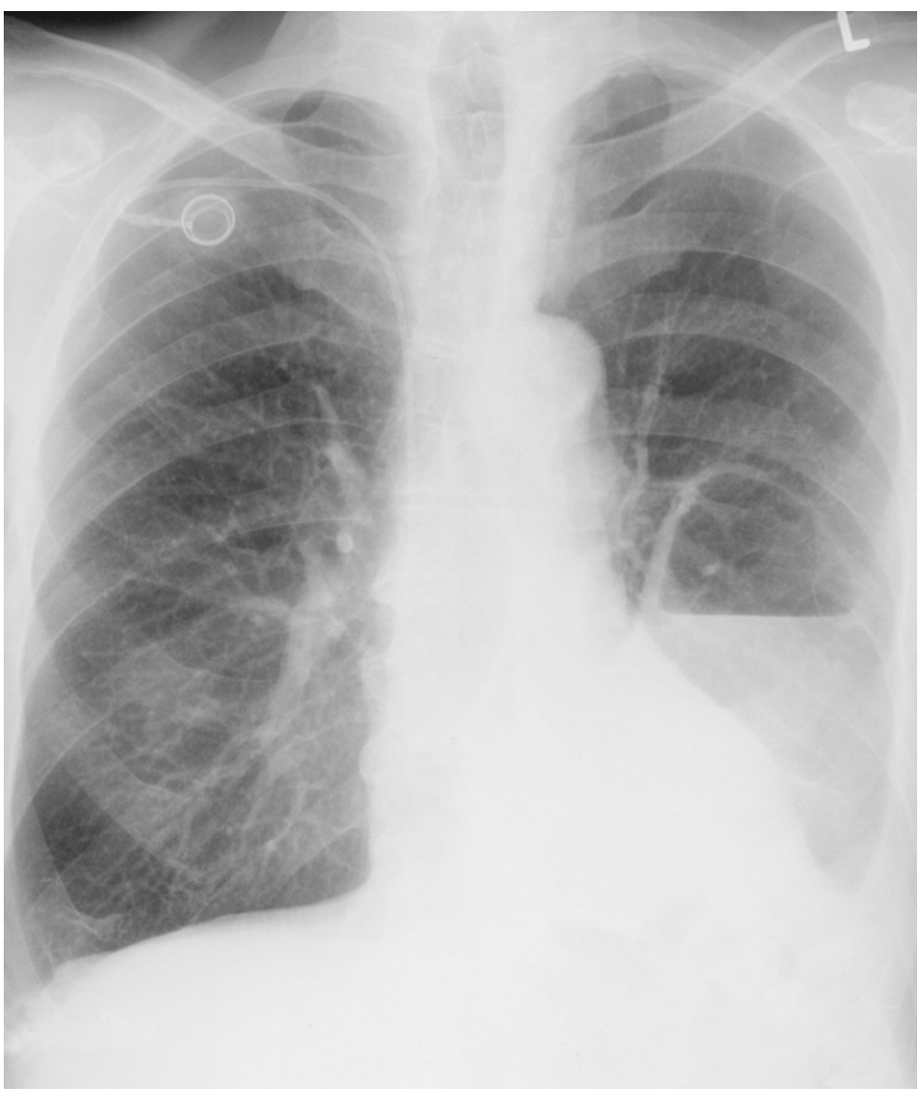

Fig. 6.48 Plain chest radiograph obtained because of persistent symptoms in status post pneumonia.

Answer

Answer to question 1: The barrel chest extending beyond the film and the obvious peribronchial and finely reticulonodular interstitial shadowing suggest chronic bronchitis.

Answer to question 2: Posterior encapsulated pneumothorax with fluid accumulation (**Fig. 6.49**). The left cardiac border is identifiable and the silhouette of the diaphragm is obliterated. The visceral pleura is clearly thickened. These findings and the patient's history suggest a pleural empyema. The CT examination (**Fig. 6.50**), which visualizes the thickening of the visceral and parietal pleura (black arrows), supports this tentative diagnosis. As no previous thoracentesis had been performed, the air inclusion must be evaluated as a sign of a pleurobronchial fistula.

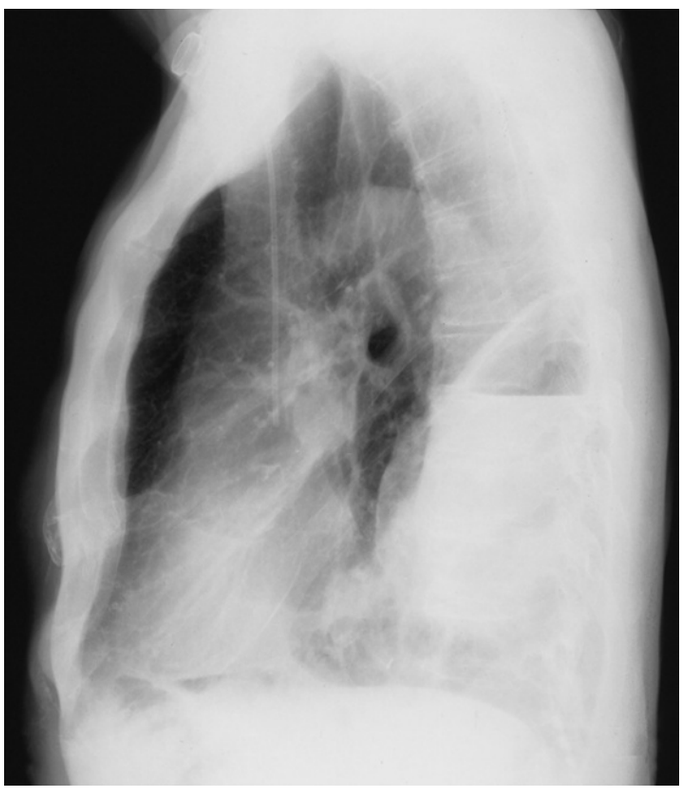

Fig. 6.49 **Lateral view.** Posterior encapsulated pneumothorax with fluid accumulation and noticeably thickened visceral pleura.

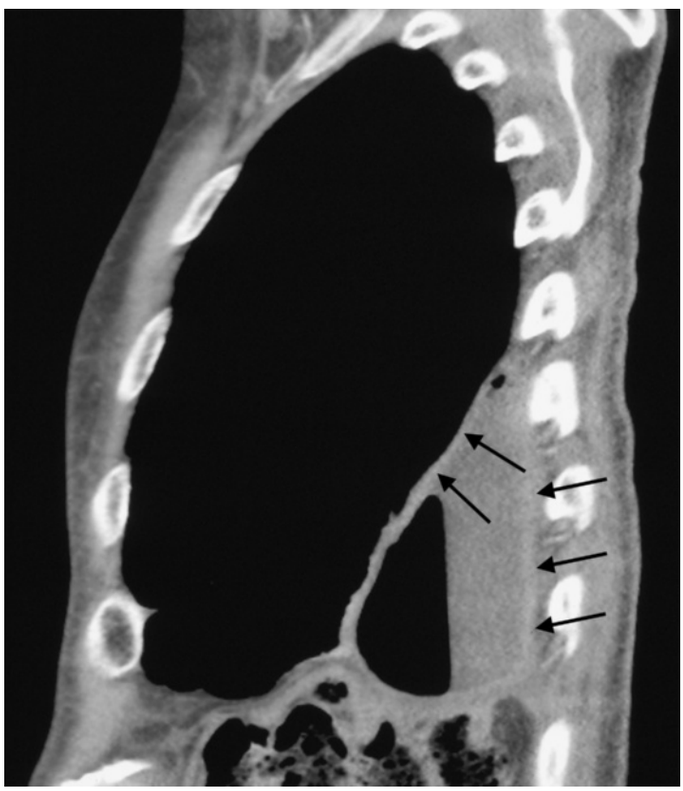

Fig. 6.50 **CT scan.** Thickening of the visceral and parietal pleura (black arrows).

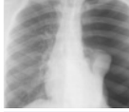

Review Case 4

The patient is a 54-year-old woman with increasing dyspnea. Clinically suspected cardiac decompensation is present. After the plain chest radiograph (Fig. 6.51), a supplementary CT scan was ordered in the presence of electrocardiographic signs of right heart strain to exclude a pulmonary embolism. This imaging study failed to demonstrate a pulmonary embolism but showed abnormal findings in the upper chest (Fig. 6.52).

Question 1

How do you evaluate the heart configuration?
Is cardiac decompensation present?
(Previously discussed in Chapter 1.)

Question 2

How do you evaluate the pleural changes?
Are they related to the cardiac situation?
(This chapter.)

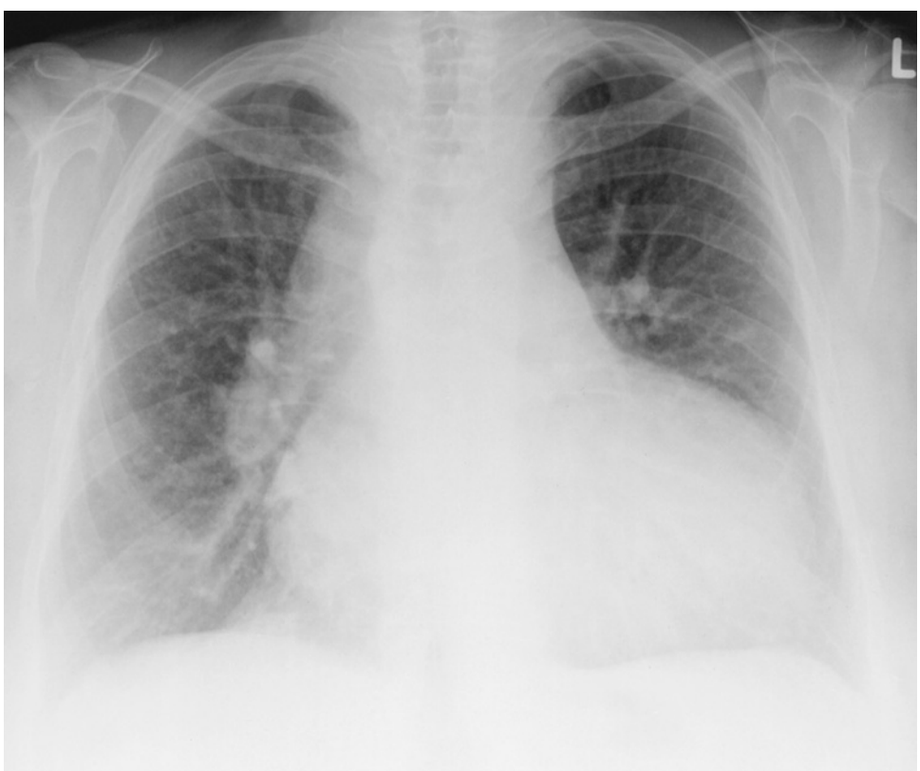

Fig. 6.51 Plain chest radiograph of a 54-year-old woman with increasing dyspnea.

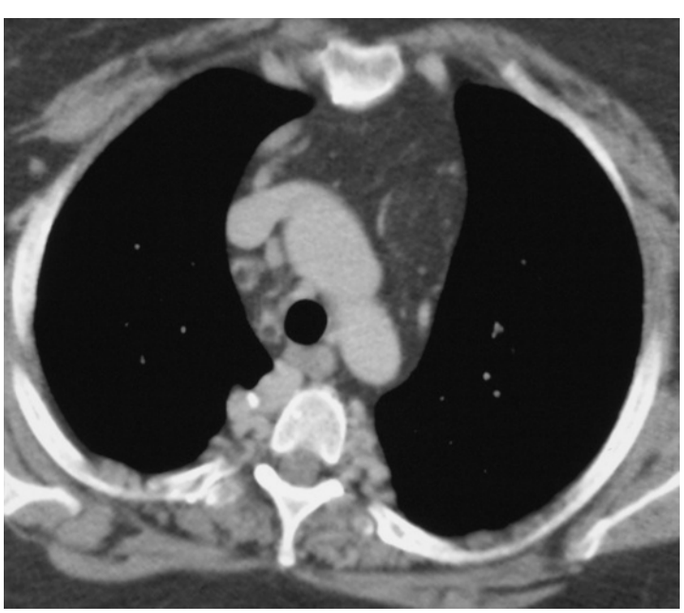

Fig. 6.52 The CT scan shows apical pleural masses of uncertain origin.

Answer

Answer to question 1: Findings include the picture of a pressure overload with significant enlargement of the left ventricle ("coeur en sabot" figure). There are no signs of acute decompensation. The noticeably slender descending thoracic aorta in the retrocardiac space and the widening of the right mediastinum (broad ascending aorta) together with the right apical garlandlike pleural thickening and faintly visible rib notching (**Fig. 6.53**) are indicative of the diagnosis.

Answer to question 2: The sagittal CT reconstruction (**Fig. 6.54**) confirms the tentative diagnosis of coarctation of the aorta with extensive collateral circulation via the intercostal arteries.

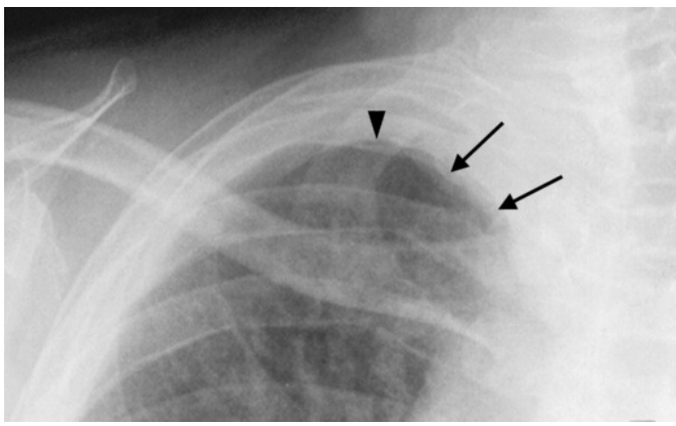

Fig. 6.53 Ectasia of the intercostal arteries in coarctation of the aorta. There is garlandlike thickening of the proximal portions of the ribs, decreasing from the center toward the periphery (black arrows). Rib notching (black arrowhead) is faintly visible.

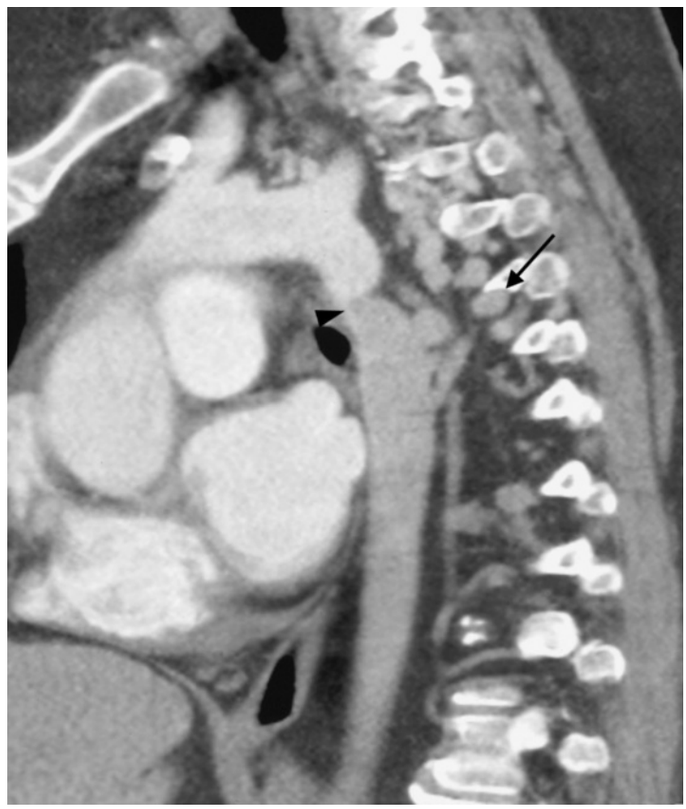

Fig. 6.54 Sagittal CT reconstruction. Ectasia of the intercostal arteries and rib notching (black arrow) are clearly visualized in coarctation of the aorta (black arrowhead).

Index

Page numbers in *italics* refer to illustrations or tables.

C

D

E

F

G

H

I

J

K

L